THE GEOLOGICAL SETTING, GEOCHEMISTRY AND GEOCHRONOLOGY OF HOST ROCKS TO HIGH–AND LOW–SULPHIDATION STYLE EPITHERMAL SYSTEMS OF THE EASTERN AVALON HIGH–ALUMINA BELT, EASTERN AVALON ZONE, NEWFOUNDLAND

GREGORY W. SPARKES

THE GEOLOGICAL SETTING, GEOCHEMISTRY AND GEOCHRONOLOGY OF HOST ROCKS TO HIGH- AND LOW -SULPHIDATION STYLE EPITHERMAL SYSTEMS OF THE EASTERN AVALON HIGH-ALUMINA BELT, EASTERN AVALON ZONE, NEWFOUNDLAND

by

©Gregory W. Sparkes, B.Sc. (Hons.)

A thesis submitted to the School of Graduate Studies in partial fulfilment of the requirements for the degree of Master of Science

Department of Earth Sciences

Memorial University of Newfoundland

OCTOBER 2005

St. John's

Newfoundland

ABSTRACT

The existence of well-preserved Late Neoproterozoic high- and low-sulphidation systems within the previously unseparated Manuels Volcanic Suite are hallmarks of the eastern Avalon high-alumina belt. These systems occur in a regionally extensive (15 x 1km) belt of hydrothermal alteration, located along the eastern margin of the Holyrood Horst, eastern Avalon Zone, Newfoundland. The contrasting formational environments of the pyrophyllite–diaspore-bearing high-sulphidation system and the auriferous colloform–crustiform chalcedonic silica + adularia ± calcite veins of the low-sulphidation system suggest a temporal or spatial break between the formation of the two systems. Both epithermal systems are hosted within a composite suite of predominantly felsic flows and ash-flow tuffs, which are locally intruded by rocks of the White Hills Intrusive Suite. The volcanic and plutonic rocks which host the epithermal systems are unconformably overlain by siliciclastic sedimentary rocks and associated mafic flows of the Wych Hazel Pond Complex. New U-Pb geochronology now permits the separation of older (625 to 614 Ma) and younger (ca. 585 Ma) intrusive units, older (pre-625 to 616 Ma) and younger (ca. 584 Ma) volcanic sequences, and provides time constraints on the development of the two epithermal systems.

U-Pb dating carried out during this study has bracketed the intrusion of the White Hills Intrusive Suite between 625 and 614 Ma, which demonstrates that, in contrast to previous models, this magmatic event is not associated with the herein defined 580.5 to 585 Ma formation of the high-sulphidation system. The geochemistry from this intrusive suite, however, indicates that the White Hills Intrusive Suite is closely related to the

ii

regionally extensive Holyrood Intrusive Suite. Feldspar porphyry, which is intrusive into the Wych Hazel Pond Complex, represents the youngest magmatic event exposed within the field area and is defined at 585 ± 5 Ma. This intrusion may represent a late stage magmatic pulse associated with the development of the regional epithermal systems, and is chemically distinct from the older intrusions of the White Hills Intrusive Suite.

The felsic volcanic succession hosting the high-sulphidation systems is now precisely defined at 584 ± 1 Ma. This sequence represents the younger Manuels Volcanic Suite, and can now be separated from the older (ca. 616 ± 2 Ma) White Mountain Volcanic Suite on the basis of new U-Pb geochronology and previously described intrusive relationships with the adjacent White Hills Intrusive Suite. Although these units represent a time span of ca. 40 Ma, both units display very similar arc-related trace-element geochemistry.

The base of the Wych Hazel Pond Complex is now dated at 582 ± 1.5 Ma, which is the time of the overall cessation in felsic volcanism within the region, and the onset of arc-collapse. This age provides the maximum limit for the development of the high-sulphidation system and also supplies the minimum age for the base of the sedimentary sequence.

New U-Pb zircon ages combined with previously known ages constrain the formation of the high-sulphidation system between 585 and 580.5 Ma. The maximum age limit for the low-sulphidation system is 586 Ma, combining this age with the fossil age of the unconformably overlying Cambrian succession restricts the formation of the low-sulphidation system between 586 and approximately 513 Ma.

ACKNOWLEDGEMENTS

TABLE OF CONTENTS

TABLES

FIGURES

PLATES

APPENDICES

CHAPTER 1:

INTRODUCTION

1.1 SYNOPSIS

The thesis area is located in the northeastern portion of the Avalon Peninsula, within an extensive zone of advanced argillic alteration (eastern Avalon high-alumina belt of Hayes and O'Driscoll, 1990) that is approximately 15km long and up to 1km wide. The geology of this part of the Newfoundland Avalon Zone is dominated by variably altered subaerial felsic volcanic and plutonic rocks, previously assigned to the Harbour Main Group and Holyrood Intrusive Suite (HIS), respectively (King, 1988a; Hayes, and O'Driscoll, 1990; O'Brien *et al.*, 1998, 2001; Figure 1-1). This region is host to well-preserved examples of pre-Cambrian high-sulphidation (pyrophyllite–diaspore) and low-sulphidation (chalcedonic silica ± adularia) epithermal systems, which exist in relatively close proximity (ca.1km lateral distance; *see*, O'Brien et al., 2001; Sparkes *et al.*, 2005). These epithermal systems are part of a much larger and complex, gold-mineralized magmatic arc system that extends the length of the eastern Appalachians, from eastern Newfoundland to the Carolina Slate Belt (see O'Brien *et al.*, 1998 and references therein). This broad belt of pre-Cambrian age magmatic rocks is metallogenically characterized by the presence of gold-bearing high-sulphidation-style epithermal systems, which are demonstrated or inferred to be pre-Cambrian in age (O'Brien *et al.*, 1996,1998; Dubé *et al.*, 1995). Despite the numerous examples of high-sulphidation-style epithermal systems throughout this belt (e.g. Brewer, Hope Brook,

1

PALEOZOIC

CAMBRIAN TO EARLY ORDOVICIAN
Adeyton and Harcourt Groups

LATE NEOPROTEROZOIC

Gabbro

UNSEPARATED SIGNAL HILL
AND ST. JOHN'S GROUPS

CONCEPTION GROUP

HOLYROOD INTRUSIVE
SUITE and related rocks

"HARBOUR MAIN GROUP"
(includes volcanic rocks of
ages between 730 Ma and
570 Ma)

● Epithermal system

● Low-sulphidation detritus

HARBOUR MAIN GROUP
Manuels Volcanic Suite
and Wych Hazel Pond
Complex.

AVALONIAN ROCKS

48° 00'

47° 00'

53° 00'

GROG POND

BERGS

STEEP NAP

St. John's

OVAL PIT MINE

Santana

Roadcut

Pastureland

COUNTRY PD.

Eastern
Avalon
High-
Alumina
Belt

James
Cove

Conception
Harbour

CONCEPTION BAY

WESTERN BLOCK

HOLYROOD HORST

EASTERN BLOCK

CENTRAL BLOCK

Hickey's Pd.-
Pt. Rosie

Long Hr

HOPE BROOK

Tug Pond

Kelstone

Manuels-
Grog Pd.

0   100
km

0   25
km

Figure 1-1: Simplified geological map of the Avalon Peninsula (modified from King,
1988a). Map shows the location of the eastern Avalon high-alumina belt
within the Avalon Zone. Shaded area on inset map shows approximate
distribution of "Avalonian" rocks, red dots and lines delineate epithermal
prospects and/or deposits (modified from O'Brien *et al.*, 1998).

Oval Pit mines), low-sulphidation-style epithermal systems have yet only been identified in the Avalonian rocks of Newfoundland. The best examples of the low-sulphidation systems are located on the eastern Avalon Peninsula.

Initial exploration studies in the thesis area date back to the early 1900's, and focused on pyrophyllite, which was used in the manufacturing of ceramic materials. Despite the fact that pyrophyllite is characteristic of advanced argillic alteration associated with auriferous high-sulphidation epithermal systems, it was not until the mid-1980's that gold was discovered within this area (Saunders, 1986). This discovery sparked an era of precious metal exploration within the region. Auriferous low-sulphidation epithermal veins were discovered within the high-alumina belt in the mid-1990's (O'Brien et al., 1997, 1998). Since that time the auriferous low-sulphidation veins have been the focus of intermittent exploration that is still ongoing in 2005.

One of the reasons that this exploration is still ongoing today is that both high- and low-sulphidation style epithermal systems have potential to host bonanza grade gold deposits. Examples of world-class auriferous high-sulphidation systems include Lepanto (Hedenquist et al., 1998), Rodalquilar (Arribas, A., et al., 1995) and Paradise Peak (Sillitoe, R.H., and Lorson, R.C., 1994). Elsewhere in the world, low-sulphidation-style banded chalcedonic silica ± adularia veins are host to bonanza grade gold deposits (e.g. Hishikari: Izawa, A., et al., 1990; Pajingo: Porter, R., 1988; and Midas: Goldstrand, P.M. and Schmidt, K.W., 2000).

The unique aspect of the high-alumina belt in comparison to other epithermal districts around the world is that these systems are not often preserved in old volcanic

terrains, as mineralization often occurs within 1-2km from the paleosurface. Several previous and ongoing geological studies have focused on the setting of the high-sulphidation system, genesis of the low-sulphidation veins, and the relationship between the two systems and gold mineralization in the high-alumina belt (Hayes, J. P., 1996; Mills, J., 1998; O'Brien *et al*., 1997, 1998, 1999, 2001). To date all known gold mineralization is associated with the low-sulphidation system or with processes (i.e. hydrothermal brecciation) with an assumed low-sulphidation affinity; no significant gold mineralization has been documented in the high-sulphidation system. The high-alumina belt contains several known occurrences of pyrophyllite ± diaspore (Mine Hill, Trout Pond, Dog Pond, and Oval Pit mine) and at least two known prospects of low-sulphidation veining (Bergs and Steep Nap prospects, which are within 1km of the Oval Pit mine). Several other examples of low-sulphidation systems occur elsewhere in the eastern Avalon Peninsula (e.g. Grog Pond, Country Pond prospects).

By definition, high-sulphidation systems are characterized by the mineral assemblages pyrophyllite-diaspore ± alunite and form from high temperature (200-300 °C), low pH (0-2) fluids that leach the surrounding host rock creating large alteration haloes (White and Hedenquist, 1995). Low-sulphidation systems consist of chalcedonic silica–adularia ± calcite, and form from low temperature, near neutral pH fluids and generally have less well-defined alteration haloes (Stoffregen and Alpers, 1987; Buchanan, 1981). As evident from other studies around the world, these two types of epithermal systems do not form in the same environment and therefore do not normally

exist in such close proximity (Hedenquist and Lowenstern, 1994; Sillitoe and Hedenquist, 2001; White and Hedenquist, 1995).

Historical interpretations of the geology in the region attributed the development of the advanced argillic alteration to the intrusion of the adjacent Holyrood Intrusive Suite (Papezik, 1978). More recent work has demonstrated that the advanced argillic alteration is hosted within a ca. 584 Ma volcanic succession and post-dates the intrusion of the adjacent 620 Ma Holyrood Intrusive Suite by ca. 40 Ma (O'Brien *et al.*, 2001). Consequently a more compositionally diverse intrusive suite (the White Hills Intrusive Suite) is thought to represent a younger magmatic event, which is associated with the formation of the advanced argillic alteration (O'Brien *et al.*, 2001).

1.2 LOCATION AND ACCESS

The area covered by this study is approximately 4.6km wide and 5.2km long and is located on N.T.S. 1N/07 and 1N/10. The field area covers the northern portion of the eastern Avalon high-alumina belt and is centered approximately 18km west-southwest of St. Johns, near the southern end of Conception Bay and the town of Conception Bay South. This area is easily accessible via route 2 off the Trans Canada Highway. All parts of the field area are readily accessible by way of the numerous roads in this region.

1.3 PURPOSE AND SCOPE

It is the focus of this thesis to determine the timing and relationship of the gold bearing low-sulphidation veins and associated breccias relative to the presumably barren high-sulphidation pyrophyllite-diaspore alteration. For this reason the northern portion of

the high-alumina belt was chosen for the focus of this thesis, with the main areas being the Berg's and Steep Nap prospects along with the region surrounding the Oval Pit mine (Figure 1-2).

This thesis attempts to determine the geochemical characteristics of the rocks that host both epithermal systems, along with their stratigraphic setting, and their environment of formation. Detailed field mapping, supplemented with petrography and geochemistry (some of which was collected during previous work by S.J. O'Brien), were utilized to try and establish the relationships between the two epithermal systems. Geochemistry was also utilized to investigate chemical anomalies in close proximity to low-sulphidation veins. These veins were the focus of several detailed studies, including structural measurements, petrographic study and ^{40}Ar-^{39}Ar geochronology.

Select lithological units from within the map were chosen for U-Pb geochronology based on recent mapping. New U-Pb data are combined with U-Pb ages determined from previous work and relative ages determined from detailed geologic mapping. With the new field and geochronological data an attempt will be made to determine 1) the relationship between the old intrusions and the young volcanic rocks, 2) the relationship between the old and young volcanic rocks, 3) the age of formation of both epithermal systems and 4) test the current hypotheses as to the heat source of the alteration.
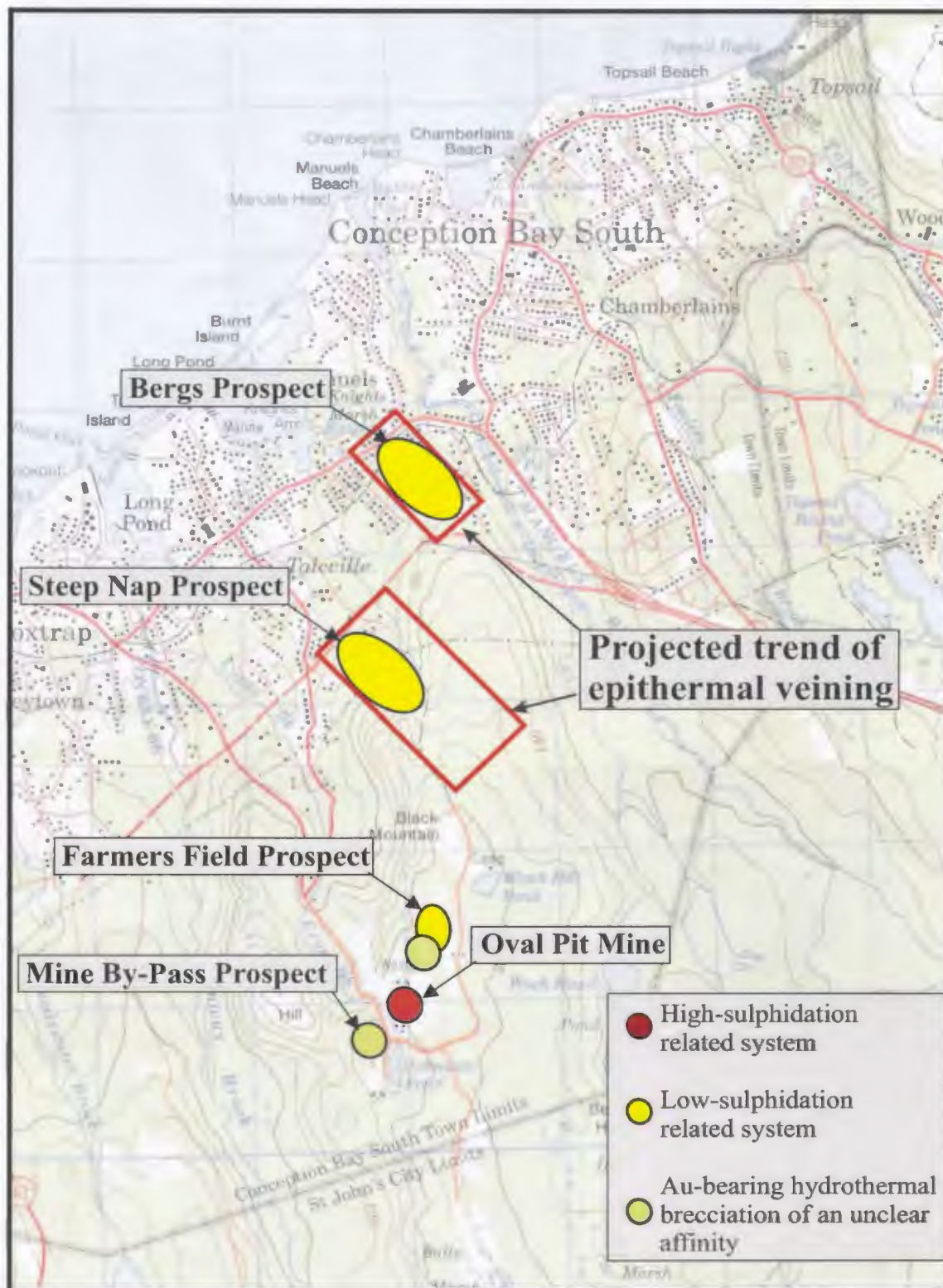
Figure 1-2: Map of epithermal prospects distributed throughout study area.

1.4 METHODS

1.4.1 Field Mapping

Field mapping was carried out on 1:12,500 scale air photos and/or photo enlargements for more detailed study. Mapping was conducted in late summer/early fall 2002, and in the summer of 2003. Sample sites and outcrop locations were recorded using a Garmin 12 GPS; all points where taken in Universal Transverse Mercator Projection, NAD 27 for Canada, Zone 22. These points were plotted on a base map using the GIS based program MapInfo. The base map was created by joining air photos together using Corel Photo Paint. An attempt was made to reduce the effects of photo distortion by joining center portions of overlapping photographs. The photo mosaic was registered using 31 control points taken from digital topographic data. It is recognized, however, that there is an offset of approximately 50m between the photo mosaic and the digital topography. This offset was corrected for by recording all outcrop locations on air photos in the field; the digital data was then shifted so that the GPS points plotted in the correct location.

In the beginning of this study, a large amount of data already existed for the proposed field area. Field and geochemical samples collected by S.J. O'Brien of the Newfoundland and Labrador Geological Survey were compiled into Excel spreadsheets and then put into the MapInfo database. Again, where field samples did not plot in the correct location, they were shifted to the proper location, which was recorded on air photos.

Samples collected in the field for whole rock geochemical analysis were cleaned of any weathered surfaces and labeled with GS-02-** or GS-03-**. Samples containing 02 were collected in late summer/ early fall of 2002, while samples labeled with 03 were collected in the summer of 2003. Geochemical samples were sent to the Department of Mines and Energy Geochemical Laboratory located in St. Johns, Newfoundland for preparation and analyses. Mineralized samples were either sent to Eastern Analytical in Springdale Newfoundland for gold fire assay, or Actlabs in Ontario for instrumental neutron activation analysis (INAA).

Unit descriptions for map units within the study area are compiled from 331 outcrop locations distributed throughout the thesis area. These descriptions are generated from observations in the field, the study of slabbed hand samples, and are further supplemented by petrographic study, where deemed necessary.

1.4.2 Geochemical Techniques

Rocks samples sent to the Geochemical Laboratory at the Department of Mines and Energy were analyzed by inductively coupled plasma-emission spectrometry (ICP-ES). This technique uses separate sample preparation procedures for major and trace element analysis. Major-element determinations, which also include the trace elements Ba, Cr, and Zr, utilize a lithium metaborate fusion technique. Ba, Cr, and Zr are included within the major-element preparation procedure because the more aggressive dissolution assures total digestion of the sample. Trace element preparation procedures involve a triple acid digestion technique, using concentrated hydrochloric, and hydrofluoric acids

and 1:1 perchloric acid. A more detailed description of analytical procedures can be found in Finch (1998).

Selected samples from the ICP-ES dataset were also submitted for extended trace element analysis at Actlabs. These select samples were submitted for the 4B2-std package, which uses a lithium metaborate/tetraborate fusion technique; the samples are analyzed by inductively coupled plasma mass spectrometry (ICP-MS). Several samples that were analyzed by both ICP-ES and ICP-MS were also submitted for X-Ray fluorescence (XRF) press pellet analysis at Memorial University of Newfoundland in order to identify any possible dissolution problems with the acid digestion technique.

A detailed alteration study that was carried out at the Steep Nap prospect utilized data supplied by a Portable Infrared Mineral Analyzer (PIMA) provided by IAMGOLD. PIMA analysis is a nondestructive technique that can be performed on hand samples or mineral powders. Samples are scanned and the PIMA measures the unabsorbed portion of the electromagnetic spectrum; the spectra is compared to that of known minerals and the analysis provides the best approximate of the minerals present. At the Steep Nap prospect this technique was used to identify the fine-grained alteration minerals developed adjacent to an area of well-developed colloform-crustiform chalcedonic silica–adularia ± calcite veining (refer to Chapter 5).

1.4.3 Geochronological Techniques

Geochronological samples collected for U-Pb dating were processed at Memorial University of Newfoundland and analyzed by Thermal Ionization Mass Spectrometry, which utilizes a Finnigan MAT 262V TI-mass spectrometer. Samples selected for ^{40}Ar-

[39]Ar dating underwent mineral separation at Memorial University of Newfoundland, and were then sent to the Geological Survey of Canada located in Ottawa. The Ar-Ar laboratory located at the Geological Survey of Canada uses a Merchantek 10W CO_2 laser, in conjunction with a VG3600 magnetic sector noble gas mass spectrometer.

Mineral processing for geochronological samples was conducted in the mineral separation laboratories located in the Earth Sciences Department. Samples were crushed and the heavy minerals were separated using various techniques, which include Wilfley table, heavy liquid separation, and magnetic separation (for a more detailed description of mineral separation procedures refer to Appendix A). After separation, zircon grains were hand picked under a microscope on the basis of grain morphology, clarity and abundance. The selected grains then underwent abrasion (cf. Krogh, 1982) followed by acid dissolution and ion exchange chemistry. After separation, U and Pb were then measured in the mass spectrometer. Data are reported using two sigma (2σ) uncertainties, and decay constants of Jaffey *et al*. (1971). Age calculations of concordant analyses are carried out using the weighted average of the $^{206}Pb/^{238}U$ ages of concordant points, while ages for discordant data are calculated using the weighted average of the $^{207}Pb/^{235}U$ ages; all ages are cited at the 95% confidence level.

1.5 REGIONAL GEOLOGY

The study area lies within the eastern part of the Avalon Zone; this region represents one of four major geologic subdivisions of the Appalachian Orogen present within Newfoundland (Williams, 1979). Bound to the west by the Dover-Hermitage Bay Fault, the Avalon Zone is the largest of the four zones, extending offshore approximately

250km across strike (Haworth and Lefort, 1979); this zone is largely comprised of Proterozoic age rocks that were once apart of, or formed close to, the ancient continent of Gondwana (Williams, 1964). The Avalon Zone consists of Neoproterozoic volcanic and plutonic rocks and associated sedimentary sequences related to arc-forming processes, unconformably overlain by a shale-rich cover sequence of Lower Paleozoic age (O'Brien *et al.*, 1997).

This region has undergone two periods of regional deformation, the "Avalonian Orogeny" of Lilly (1966), which occurred in the late Precambrian, and the "Acadian Orogeny" in the Silurian-Devonian (ca. 395 Ma; King, 1990). The effects of the Avalonian Orogeny have been described as enigmatic throughout the Avalon Peninsula (Hughes, 1970). More recent work has demonstrated the pre-Cambrian nature of the deformation within the current study area (O'Brien, 2002), more detailed descriptions of the pre-Cambrian deformation around the area of Conception Bay can be found in McCartney (1967) and Calon (1993). Aside from very localized shear zones, rocks of the eastern Avalon Peninsula lack high-grade deformation. The eastern most Avalon was affected less by the Acadian Orogeny, and displays prehnite-pumpellyite to lower greenschist facies metamorphism that is presumably related to that event (Rose, 1952; McCartney, 1967; Papezik, 1972, 1974). In contrast, folding, faulting, greenschist grade regional metamorphism and granitoid emplacement are attributed to the Acadian Orogeny in western sections of the Avalon Zone (O'Brien *et al.*, 1983).

1.5.1 Regional Geologic Setting of the Central Avalon Peninsula

Regionally the central Avalon Peninsula was subdivided into three discrete fault blocks that have been informally referenced as the western, central, and eastern blocks, which are separated by two major north-south trending fault zones (McCartney, 1969; Bruckner, 1969; Papezik, 1974; Figure 1-1). More recently this area has been further described and subdivided with the middle block being defined as the area bounded to the east by the Topsail fault, and to the west by the Peter's River fault (O'Brien *et al.,* 1997). For a more detailed description of the geology surrounding the central block the reader is referred to O'Brien *et al.,* 1997 and references therein. The central block, also known as the "Holyrood Horst", is located at the southern end of Conception Bay (McCartney, 1969). Felsic and mafic volcanic rocks previously assigned to the Harbour Main Group of Rose (1952), and intrusive rocks of King's (1988a) Holyrood Intrusive Suite are the predominant units within the horst structure.

Rocks assigned to Harbour Main Group form some of the oldest known units within the Holyrood Horst. These volcanic rocks consist of felsic and mafic flows and associated flow breccias, along with pyroclastic and ash fall deposits and locally intercalated sedimentary rocks. However, dated units within the Harbour Main Group span 160 Ma (ca 730 to 570 Ma), and have recently been further subdivided into more chronologically and regionally restricted units (O'Brien *et al.,* 2001a). Intruding into the Harbour Main group are gabbroic, monzonitic, and granitic bodies of the Holyrood Intrusive Suite (HIS), ranging from 640 Ma to 620 Ma. Many of these intrusions show

high-level characteristics such as tuffisite brecciation and numerous roof pendants of the Harbour Main Group.

On the eastern and western flanks, as well as in northwestern portions of the Holyrood Horst (Figure 1-1), the Harbour Main Group and the HIS are overlain by a thick sequence of marine siliciclastic sedimentary rocks known as the Conception Group (Rose, 1952). Contacts between the Conception Group and the Harbour Main Group are either tectonic or unconformable, while contacts with the Holyrood Intrusive Suite are both unconformable and intrusive. Deposition of the Conception Group generally corresponds with the cessation of volcanism within the Holyrood Horst, and predominantly consists of siliceous sedimentary rocks, which include conglomerate, tuff, agglomerate, tillite, and orthoquartzite (King, 1988a). Williams and King (1979) subdivided the Conception Group of the southeastern Avalon Peninsula into five formations that have been provisionally correlated, in part, with formations in central Avalon Peninsula (O'Brien *et al.,* 1997). The Conception Group is divided into an upper and lower sequence by the presence of a tillite, known in the both regions of the Avalon as the Gaskiers Formation (Williams and King, 1979). The lower Conception Group contains basal conglomerates that include granitoid rocks from the underlying Holyrood Intrusive suite. In one location on the eastern side of Holyrood Bay a tuff bed in the Conception, which overlies a basal conglomerate containing granitoid clasts, produced a U-Pb age of 621 +5/-4 Ma (Israel, 1998). Tuff beds from the upper Conception Group in the southeastern Avalon, although not in stratigraphic continuity with units dated near the

base of the Conception, give a U-Pb age of 565 ± 3 Ma (G.R. Dunning, 1998, unpublished data; King, 1988a).

Conformably overlying the Conception Group on the eastern side of the Holyrood Horst is the St. John's Group. The St. John's Group consists of interbedded grey to black shales and buff brown sandstones, and is interpreted by King (1990) as a pro-deltaic to shallow marine sequence. Overlying, and in gradational contact with the St. John's Group is the Signal Hill Group (King, 1988a). The Signal Hill Group is composed of red sandstones and conglomerates and is interpreted to represent an alluvial plain type environment (King, 1990). Clasts within the conglomerates are dominated by volcanic and plutonic material from adjacent, old arc-related sequences showing a period of major erosion and uplift.

The youngest sedimentary sequences found within the central Avalon are lower Paleozoic shale-rich units of Cambrian age. These shales unconformably overlie the underlying sedimentary rocks as well as the volcanic and plutonic rocks of the Harbour Main Group and Holyrood Intrusive suite.

1.5.2 General Geology of the Eastern Avalon High-Alumina Belt

Along the eastern portion of the Holyrood Horst is an area of hydrothermal alteration known as the eastern Avalon high-alumina belt (EAHB; Hayes and O'Driscoll, 1990; Figure 1-3). This region consists predominantly of subalkalic, calcalkalic, subaerial rhyolitic flows and ash-flow tuffs with minor alkalic to weakly subalkalic basaltic and pyroclastic material. The western margin of the high-alumina belt corresponds with the eastern limit of the Holyrood Intrusive Suite (HIS), which can be seen to intrude the

Study Area

Conception Bay

CAMBRIAN COVER

BERGS

STEEP NAP

WHITE HILLS INTRUSIVE SUITE

OVAL PIT MINE

MINE BY-PASS

MINE HILL

MINE HILL SHEAR ZONE

TOPSAIL FAULT

SANTANA

TROUT POND

ROADCUT

DOG POND

PASTURELAND ROAD

HOLYROOD INTRUSIVE SUITE

CONCEPTION GROUP

THOUSAND ACRE SHEAR ZONE

N

0   1000
metres

LEGEND

Early Paleozoic
Cambrian

Adeyton and Harcourt Groups
unseparated red, green and black shale with minor limestone

Late Neoproterozoic
Ediacaran

Conception Group
unseparated marine siliciclastic rocks

Wych Hazel Pond Complex
unseparated mafic volcanic rocks and terrestrial to marine sedimentary rocks; includes basal unit of red sandstone and brown breccia; minor unseparated feldspar porphyry

feldspar porphyry

diorite

Manuels and White Mountian Volcanic Suites
unseparated pyrophyllite-diaspore-sercite and silica-sericite alteration; protolith primarily flow-banded rhyolite, ash-flow tuff and tuff-breccia

unaltered, red to maroon, flow-banded rhyolite, ash-flow tuff and tuff-breccia

massive grey rhyolite

mafic volcanic flows & breccias

grey welded ash-flow tuff

White Hills Intrusive Suite
unseparated and variably altered (pyrite-silica) granite, monzonite and quartz-feldspar porphyry

Holyrood Intrusive Suite
quartz porphyritic to equigranular granite

Key
● Au vein or vein breccia
● Au-bearing breccia
○ Pyrophyllite ± diaspore
□ Base metals (Zn-Pb-Cu) ± Au
▬ Shear zone
⁄⁄ Fault (undifferentiated)
⁄ Depositional or intrusive contact
·-· Unconformity

Figure 1-3: Simplified distribution of regional units in the northern portion of the eastern Avalon high-alumina belt (from Sparkes *et al.*, 2005). Current study area outlined in white.

16

volcanic rocks of the high-alumina belt in several areas. Eastern boundaries of the high-alumina belt correspond to the regional structure known as the Topsail Fault (Figure 1-3). Volcanic rocks of the high-alumina belt form the previously unseparated Manuels Volcanic Suite (MVS), one of the six subdivisions of the Harbour Main Group proposed by O'Brien *et al*. (2001); this suite is the second youngest unit, and has been locally dated at 584 ±1 Ma (G. R. Dunning, unpublished data). Unconformably overlying the MVS are basal conglomerates of the Wych Hazel Pond Complex (WHPC). This unit is the youngest of the proposed subdivisions for the Harbour Main Group, and is primarily exposed in the eastern sections of the high-alumina belt, with a well-exposed unconformity at the Oval Pit mine (Figure 1-2).

Two known ages of volcanic activity exist within the high-alumina belt and includes a 616 ± 2 Ma welded ash-flow tuff and an altered flow-banded rhyolite, dated at 584 ± 1 Ma (G. R. Dunning, unpublished data). However, the majority of the volcanic rocks are thought to be the product of the younger volcanic event, as the dated 616 Ma event has a very restricted exposure within the current study area.

1.6 PREVIOUS WORK

Early geological investigations of the Avalon Zone began with J. B. Jukes in 1843, and were furthered by Murray and Howley (1881a), Walcott (1899) and Howley (1907). During this time a rough stratigraphy was developed and the distribution of regional-scale rock units was established with the publication of the first geological map of the Avalon (Murray and Howley, 1881b). Beginning in 1916, detailed geological mapping began on the eastern Avalon high-alumina belt, with the main focus being

around areas of argillic and advanced argillic alteration. From 1916 through to 1978 many people contributed to the knowledge base of the high-alumina belt; the main contributors include Buddington (1916), Vhay (1936), Dawson (1963), McCartney (1967), Keats (1970), and Papezik et al. (1978). For a more comprehensive listing of geological studies prior to 1978, the reader is referred to table1.1 in Hayes (1996).

Since the mid-1980's the eastern Avalon has been the focus of renewed detailed mapping and revision of stratigraphy (Table 1-1). It was not until the late 1990's when O'Brien *et al.* (1998) proposed a high-sulphidation origin for the pyrophyllite ± diaspore alteration that the formation of epithermal alteration in the Oval Pit mine was properly recognized. The most recent work in the area of the eastern Avalon includes regional scale mapping by King (1990), and ongoing mapping by O'Brien and Dubé (see O'Brien *et al.,* 1997, 2001 field guide etc.). Work carried out by S.J. O'Brien is part of a broader regional scale program that is focused on mapping the central part of the eastern Avalon. This work has established several new stratigraphic subdivisions within the central Avalon, and has outlined a preliminary chrono-stratigraphy supported by U-Pb dating (O'Brien *et al.,* 2001a).

Historically the high-alumina belt was recognized for its pyrophyllite deposits, and the regional scale argillic and advanced argillic alteration. However, since the mid-1980's the area has become the focus of intermittent gold and base metal exploration (Table 1.1). Since the discovery of low-sulphidation veins there have been ongoing studies to try and identify the timing and relationships between the high- and low-sulphidation epithermal systems and their relation to gold mineralization. In 2002 Rubicon Minerals Corporation began mineral exploration in the high-alumina belt. This

exploration resulted in a partnership between Rubicon Minerals Corporation and

IAMGOLD Corporation in an attempt to delineate the extent of auriferous low-

sulphidation veining in the Steep Nap area (Figure 1-2). At the time of thesis compilation,

exploration by Rubicon Minerals Corporation is still ongoing.

Table 1-1: Previous work carried out on the eastern Avalon high-alumina belt from 1986 to 2004 (Modified from Hayes, 1996).

Year	Author(s)	Contribution
1986	Lenters, M.H.	Mineral exploration, Esso Mineral Limited
1986	Saunders, P.	Mineral exploration, Apex Geological, Consultants Ltd.
1988	King, A.F.	Geological mapping of St. John's area, with stratigraphic revisions
1988	O'Driscoll, C.F., Collins, C.J. and Tuach, J.	Examination of alteration and proposal of epithermal style alteration system
1989	Hayes, J.P., and O'Driscoll, C.F.	1:12,500 mapping of epithermal alteration system
1990	Hayes, J.P. and O'Driscoll, C.F.	Description of setting and alteration within the EAHB
1991	Saunders, P.	Mineral exploration of the Dog Pond area
1994	Saunders, P. and Harris, J.	Mineral exploration of the Dog Pond area
1995	Pickett, J.W. and Jacobs, W.	Mineral exploration in Hennesseys Pond and Jakes Pond area
1996	O'Brien, S.J., and O'Driscoll, C.F.	Preliminary regional mapping of the central portion of the eastern Avalon
1997	Hayes, J.P.	Detailed study of the setting and genesis of the EAHB
1997	O'Brien, S.J., King, A.F. and O'Driscoll, C.F.	Preliminary results of 1:50,000 scale bedrock mapping of the central Avalon
1998	Mills, J.	Detailed analysis of the Steep Nap vein system
1998	O'Brien, S.J., Dubé, B., O'Driscoll, C.F. and Mills, J.	Geological summary of gold mineralization and associated hydrothermal alteration in Avalonian rocks

1999	Lewis, P.	Mineral Exploration, Fort Knox Gold Resources
1999	Mills, J., O'Brien, S.J., Dubé, B., Mason, R. and O'Driscoll, C.F.	Summary of results from detailed mapping of the Steep Nap vein system
1999	O'Brien, S.J., Dubé, B. and O'Driscoll, C.F.	Description of epithermal gold-silver mineralization in Newfoundland Avalonian belt and in eastern Avalon high-alumina belt
2001	Dubé, B., O'Brien, S.J., and Dunning, G.	Gold deposits in deformed terrains
2001	O'Brien, S.J., Dunning, G., Dubé, B., O'Driscoll, C.F., Sparkes, B., Israel, S. and Ketchum, J.	Revision of stratigraphy of central Avalon, along with new U-Pb geochronology
2001	O'Brien, S.J., Dubé, B. and O'Driscoll, C.F.	GAC-MAC guidebook summarized geology of the field area
2002	Sparkes, G.	Detailed description of two areas with breccia-hosted gold mineralization in EAHB
2002	O'Brien, S.J.	Description of the Berg's Prospect and basement cover relationships
2002	Sparkes, B.	Mineral exploration for Rubicon Minerals
2003	Sparkes, B.	Mineral exploration for Rubicon Minerals
2004	O'Brien, S.J. and Sparkes, G.	Bonanza-grade gold within the EAHB low-sulphidation system
2004	Sparkes, B.	Mineral exploration for Rubicon Minerals
2004	Sparkes G.W., O'Brien, S.J. and Dunning, G. R.	Setting and timing of epithermal alteration and gold mineralization, eastern Avalon Zone

1.7 PREVIOUS INTERPRETATIONS AND HYPOTHESES

Early studies along the eastern side of the Holyrood Horst noted the close spatial association between the advanced argillic alteration within the high-alumina belt and the adjacent granitic rocks of the HIS. These granitic rocks where originally thought to post-date the majority of the volcanic activity within the high-alumina belt (Rose, 1952;

20

McCartney, 1967, 1969; Hughes and Bruckner, 1971). Early investigations into the genesis of the advanced argillic alteration thus attributed the alteration to the intrusion of the adjacent altered granitic rocks of the HIS (Papezik, 1978). However, later investigations established the age of the HIS to be between 625 to 620 Ma, and that the volcanic succession hosting the Oval Pit mine post-dated the intrusion by approximately 40 Ma requiring a younger magmatic event for the formation of the advanced argillic alteration (O'Brien *et al.*, 2001a).

A suite of monzonite, granite and porphyry intrusions, referred to as White Hills Intrusive Suite (WHIS), was recognized by Sparkes *et al.* (2004). It is lithologically distinct, yet spatially associated with the eastern margin of the Holyrood Horst, and was interpreted to represent the younger magmatic event. This was supported by the numerous intrusive contacts between rocks of the WHIS and felsic volcanic rocks of the unseparated MVS (O'Brien *et al.*, 2001a). Several units from this assumed younger magmatic event have been selected for this study to determine the absolute age of the intrusions.

The felsic volcanic rocks of the MVS are unconformably overlain by siliciclastic sedimentary rocks, previously assigned to the Black Hill sequence or "mis-Conception" of Dawson (1963). These sedimentary rocks were later recognized as a lithologically distinct package that were deposited coevally with mafic volcanic rocks and have been incorporated into the regional-scale unit known as the Wych Hazel Pond Complex (WHPC; O'Brien *et al.,* 2001a). The unconformable contact between the felsic volcanic rocks and the overlying sedimentary rocks of the WHPC has been open to some debate regarding the temporal significance of the hiatus. The reason for the debate is that the

sedimentary rocks above the contact (best exposed in the open pit of the Oval Pit mine) contain conglomerate layers with altered detritus, while a basal conglomerate at the bottom of the sedimentary sequence is affected by silica–sericite–pyrite alteration. In previous work this contact has had various interpretations, it was originally thought to represent a significant break in time (Dawson, 1963), while others suggest that volcanism, alteration and sedimentation are relatively coeval (Hughes and Bruckner, 1971). The current view of the altered detritus contained within this sedimentary unit is that it demonstrates that the sequence affected by the advanced argillic alteration was uplifted and eroded prior to the deposition of the overlying sedimentary rocks.

CHAPTER 2:

DESCRIPTION AND DISTRIBUTION OF GEOLOGIC UNITS AND STRUCTURAL ELEMENTS

2.1 INTRODUCTION

The area surrounding Conception Bay South consists of gently dipping lowlands dominated by Cambrian age basal conglomerates and overlying shale and limestone successions, and more rugged terrain immediately to the south, consisting of Late Neoproterozoic volcanic and plutonic rocks. Topographically, the region varies from sea level in the lowlands to a maximum of 220m in the plateau region of the Oval Pit mine (Figure 2-1). Several well-defined valleys that are controlled by major structural boundaries divide the geology in the region. Good bedrock exposures occur in areas of higher elevation however these are generally lichen-covered; less bedrock exposure occurs in lowland areas. Numerous roadcuts and exposures due to rural development provide a good section across the northern portion of the study area. The region east of the Oval Pit mine and south of the Conception Bay By-Pass road, however, provides very little bedrock exposure, thus contacts are not as well defined in this area.

Geological units incorporated into this study have been briefly described by the authors O'Brien *et al.* (2001a). The informal nomenclature and grouping of units proposed within this thesis, where possible, have followed the informal nomenclature previously established (Table 2.1); this includes the recently proposed Manuels Volcanic Suite (MVS) and the Wych Hazel Pond Complex (WHPC), which embody the volcanic
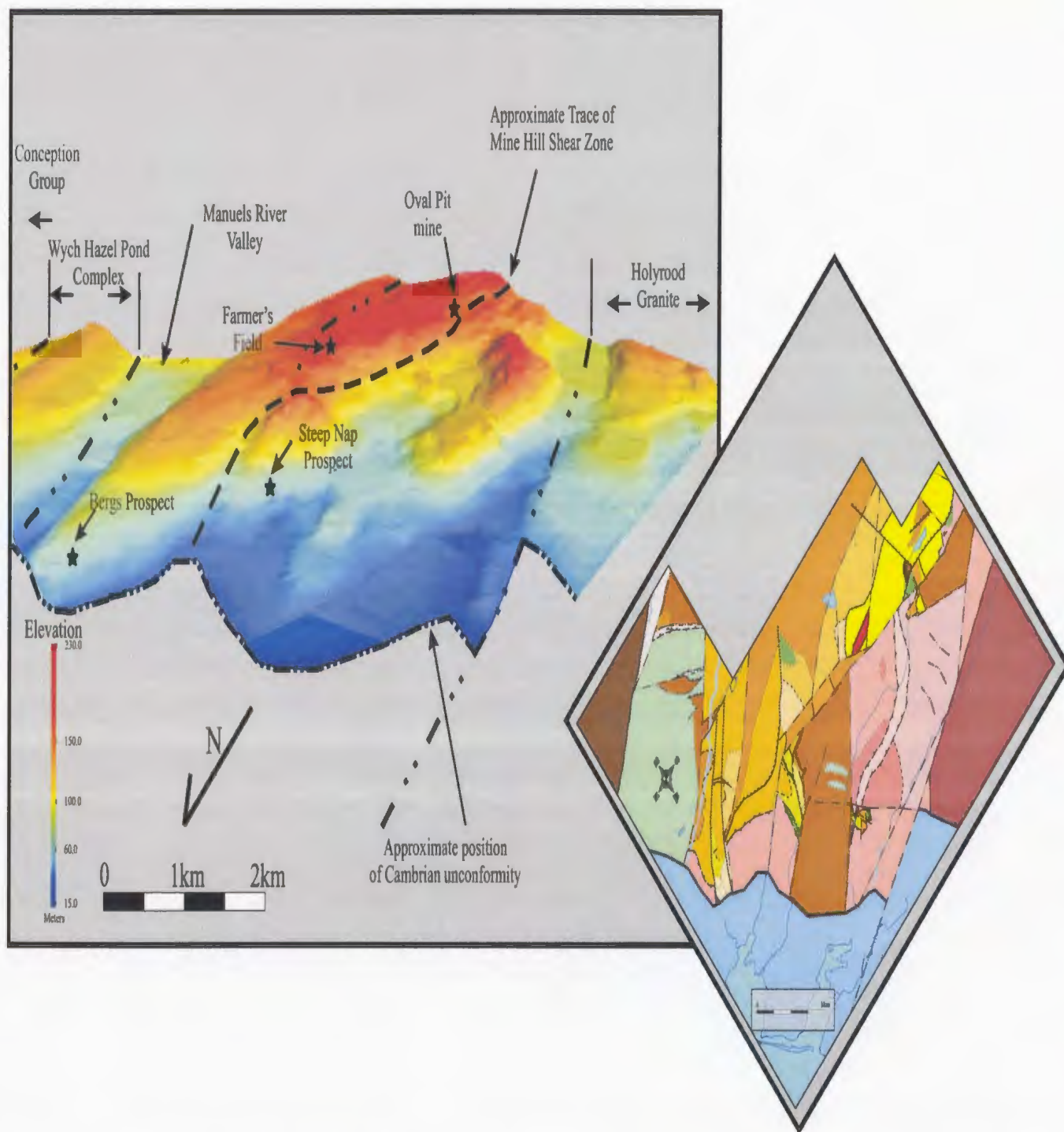
Figure 2-1: Elevation model of the study area viewed looking towards the southeast, with an inclination of 25 degrees above the horizon. Approximate position of major geological structures and epithermal prospects are shown.

Table 2.1: Table of Formations.

Era	Period	Major Subdivisions	Absolute Age or Age Range	Units
Early Paleozoic ~541 to ~513 Ma	Middle to Lower Cambrian	Adeyton and Harcourt Groups	541 to 513 Ma	Unit 24: Red and black siltstone and mudstone with interbedded grey limestone; locally massive, poorly sorted boulder conglomerate at base
Late Proterozoic pre-625 to 541Ma	Ediacaran	Erosional unconformity		
		Conception Group	ca 575 to 565 Ma	Unit 23: Unseparated marine siliciclastic sedimentary rocks
		Fault contact with Wych Hazel Pond Complex		
		Wych Hazel Pond Complex	582 to ca 575 Ma	Units 19 to 22: Intercalated marine sedimentary rocks and mafic volcanic rocks; includes lower unit of red siltstone and basal brown breccia; locally intruded by feldspar porphyry
		Erosional unconformity		
		Manuels Volcanic Suite	585 Ma	Units 9 to 18: Subaerial felsic volcanic rocks including flow-banded rhyolite and minor ash-flow tuff; contains minor mafic volcanic rocks
		Fault contact with White Hills Intrusive Suite (MHSZ)		
		White Hills Intrusive Suite	625 to 620 Ma	Units 6 to 8: Medium- to coarse-grained monzonite, granite and quartz–feldspar porphyry
		Fault Contact with Holyrood Intrusive Suite		
		Holyrood Intrusive Suite	620 Ma	Unit 5: Medium- to coarse-grained equigranular granite
		Intrusive contact with White Hills Intrusive Suite		
	Ediacaran and/or earlier	White Mountain Volcanic Suite	pre-625 Ma	Units 1 to 4: Subaerial felsic volcanic rocks including flow-banded rhyolite and minor lapilli tuff

and sedimentary rocks, respectively. The MVS and WHPC are here further subdivided on the basis of more detailed mapping carried out during this study.

Rock units in the study area range in age from greater than 625 Ma, which is the minimum age of the oldest volcanic rocks, to about 510 Ma. The latter is the age of the fossiliferous Middle Cambrian cover (Landing *et al.*, 1998). The boundary between the Lower and Middle Cambrian is currently defined at 513 ± 2 Ma by recent time scale studies (April 2005, <www.stratigraphy.org>; Howell, 1925; Bergstrom and Levi–Setti, 1978). Numerous contact relationships within the area allow for the separation and relative age determination of several major geological units. Similar geochronological complexities previously identified in the Harbour Main Group (O'Brien *et al.,* 2001a), have also become evident within the MVS; volcanic rocks within the study area range from pre-625 Ma to 582 Ma, spanning at least 43 Ma of volcanism. The complexity within the volcanic stratigraphy is not easily resolved because of the similar lithologic and geochemical (see below) nature of the felsic volcanic rocks spanning this time period.

2.2 GEOLOGY OF THE STUDY AREA

The western portions of the field area are dominated by granitic rocks of both the Holyrood Intrusive Suite (HIS; King, 1988a) and monzonite, granite and porphyry units of the White Hills Intrusive Suite (WHIS; Sparkes and O'Brien, 2004; Map 1). The central and southeastern regions of the map area consist of subaerial felsic volcanic rocks, previously assigned to the unseparated MVS (O'Brien *et al.*, 2001a). Eastern portions of the field area are dominated by marine siliciclastic sedimentary rocks and associated

26

mafic volcanic flows of the WHPC, which unconformably overlie the felsic volcanic rocks of the MVS (O'Brien *et al.*, 2001a). Cambrian age basal conglomerates and overlying siltstone and limestone successions dominate the northwestern lowlands of the map region. The Cambrian succession is unconformable upon the sedimentary rocks of the WHPC, volcanic rocks of the MVS and intrusive rocks of the Holyrood and White Hills intrusive suites (O'Brien *et al.*, 2001a; O'Brien, 2002).

2.3 UNIT DESCRIPTIONS

Significant amounts of hydrothermal alteration has affected both the volcanic and plutonic rocks in the field area. Where this hydrothermal alteration is relatively weak, relic primary textures can be used to identify the host rock. However, in areas of intense alteration where the original lithology cannot be identified, the rock unit is named in accordance with the alteration minerals present (e.g. silica–sericite alteration). It should be noted that sericite is used as a field term for soft, pale yellow to pale green, very fine-grained material that has been identified locally by X-ray diffraction (XRD). In most instances, the plagioclase and K-feldspar contents of intrusive rocks estimated from thin sections have been combined into "percent feldspar" due to identification difficulties caused by alteration. Estimated modal proportions of dominant mineral phases for the intrusive units are taken from stained thin sections only. To facilitate the following discussion, units are referenced to nine informally named geographical areas outlined in Figure 2-2. Unit numbers are assigned to each unit and represent a best approximation of ascending stratigraphic order. Map 1 (back pocket), shows the distribution of map units in the thesis area at a scale of 1: 10, 000.
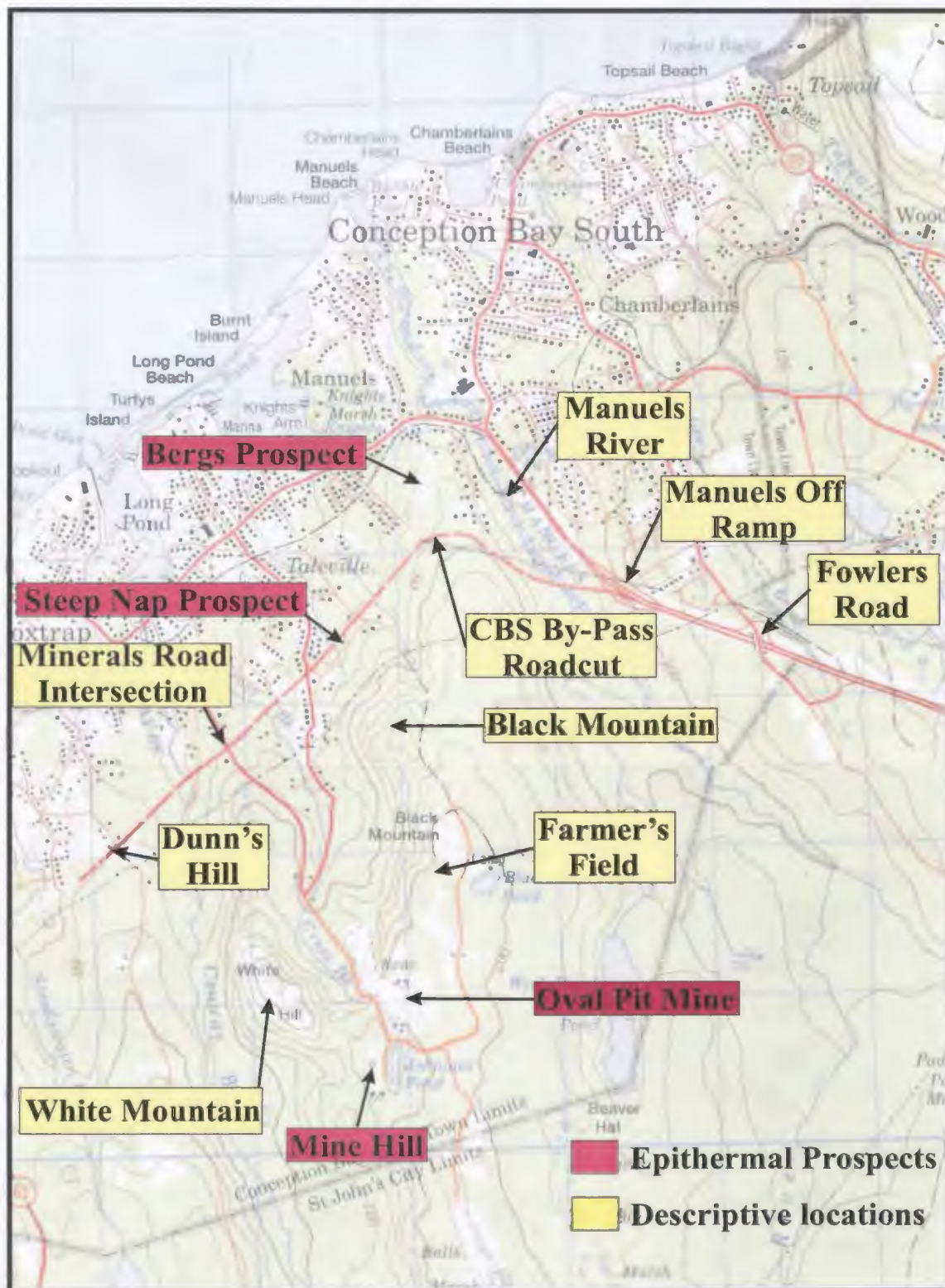
Figure 2-2: Distribution of areas described in text.

PROTEROZOIC ROCKS (pre-625–614 Ma)

2.3.1 White Mountain Volcanic Suite (WMVS)

The WMVS occurs in the northeastern portion of the map area and consists of subaerial volcanic rocks and associated volcaniclastic material previously grouped with the MVS (ca. 585 Ma). These volcanic rocks are lithologically similar to those of the MVS, however intrusive relationships between the WMVS and the WHIS demonstrate their pre-620 Ma age.

2.3.1.1 Unit 1: Moderately Feldspar-phyric, Fine, Flow-banded Rhyolite (Minerals Road Rhyolite)

LITHOLOGY AND PETROGRAPHY:

Unit 1 consists of moderately feldspar-phyric rhyolite, containing 2-4mm white feldspar crystals within a pale to dark purple, flow-banded and locally spherulitic groundmass. This unit is informally referred to as the Minerals Road rhyolite, and is best exposed in the area of Minerals Road Intersection, but also occurs as discrete outliers in the central and southern portions of the map area (Figure 2-3). The highly porphyritic nature of this unit is somewhat distinct, as other rhyolite units only develop very restricted porphyritic zones.

In thin section, 2-4mm sub- to euhedral phenocrysts of plagioclase, K-feldspar and minor quartz are supported within a very fine-grained groundmass. K-feldspar is the predominant phenocryst phase and is often identified by the presence of minor exsolution textures. Locally, patches of the groundmass consist of coarser-grained interlocking quartz crystals; however the majority of the groundmass is dominated by a
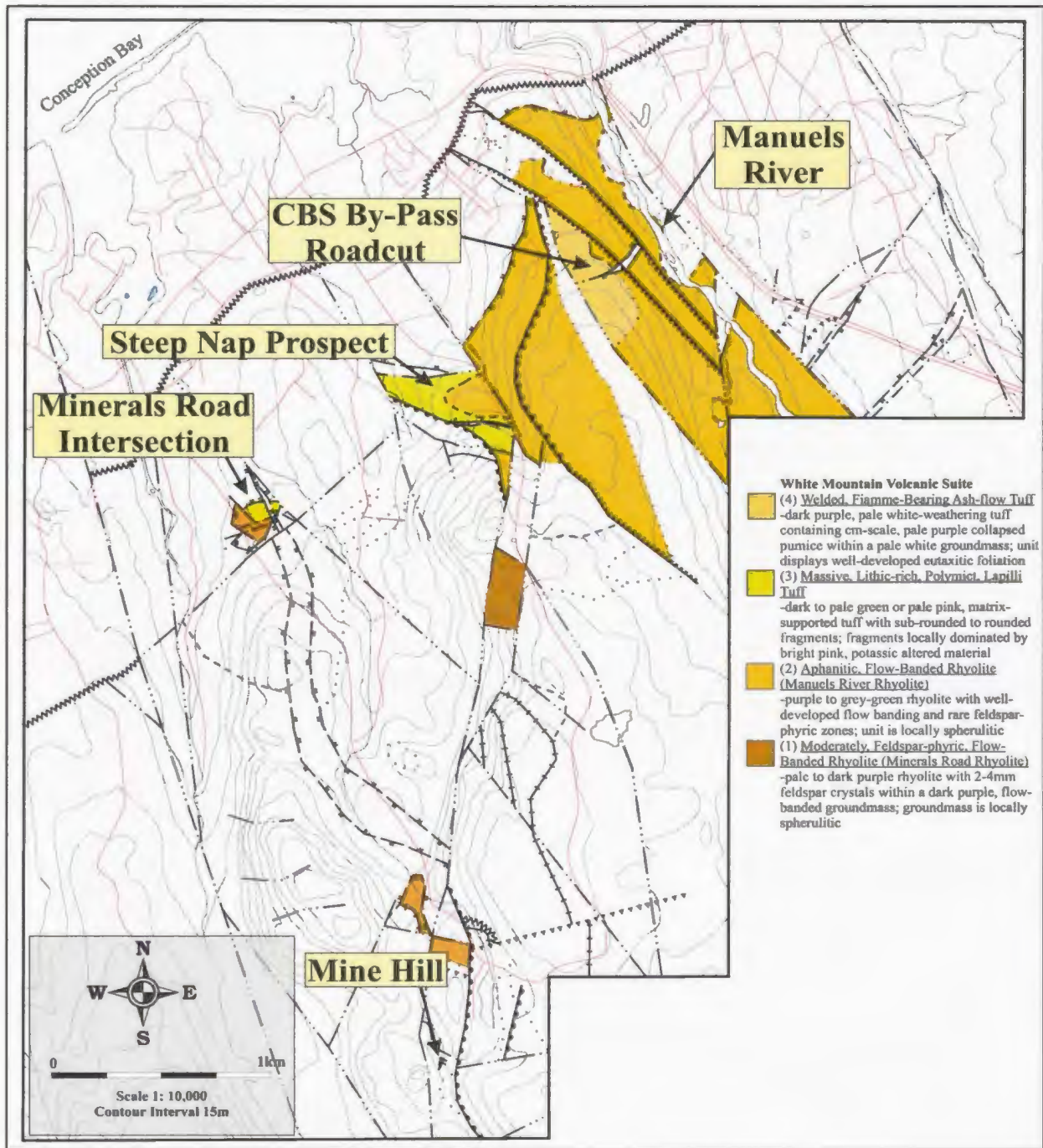
Figure 2-3: Distribution of the White Mountain Volcanic Suite, extracted from Map 1.

microspherulitic texture (evident from the radial extinctions within the groundmass; Plate 2-1), representing devitrification of the groundmass. Minor anhedral patches of a high-relief, third to fourth order birefringence mineral, thought to be titanite, is locally developed parallel to flow-banding. The feldspar phenocrysts are aligned in a weakly developed flow foliation, which is locally mimicked by the linear arrangement of the more coarse-grained quartz crystals within the groundmass. This unit displays a rare well-preserved granophyric texture (Plate 2-2).

In hand specimen, silica–sericite is the main alteration affecting this unit. Very localized sericite–chlorite alteration is seen along restricted fault zones in the area of Minerals Road Intersection. A small outlier of this unit located in the area of Mine Hill is host to advanced argillic alteration, which may be associated with the development of the high-sulphidation system (Figure 2-3). Thin sections from the Minerals Road Intersection contain minor sericite alteration developed parallel to the flow banding (generally <2%, but locally up to 5%); this is accompanied by minor chlorite–epidote alteration, in irregular patches within the groundmass and as fracture-filling material.

CONTACT RELATIONSHIPS:

In the White Mountain region, numerous rafts of feldspar-phyric rhyolite, which are thought to represent roof pendants of a volcanic carapace, are contained within granitic and porphyritic rocks of the WHIS (see below; Figure 2-2). These volcanic rocks are correlated with the feldspar-phyric flows of the Minerals Road Intersection on the basis of similar lithology and the close spatial association with the WHIS. All other contacts between Unit 1 and adjacent units are either tectonic or inferred.
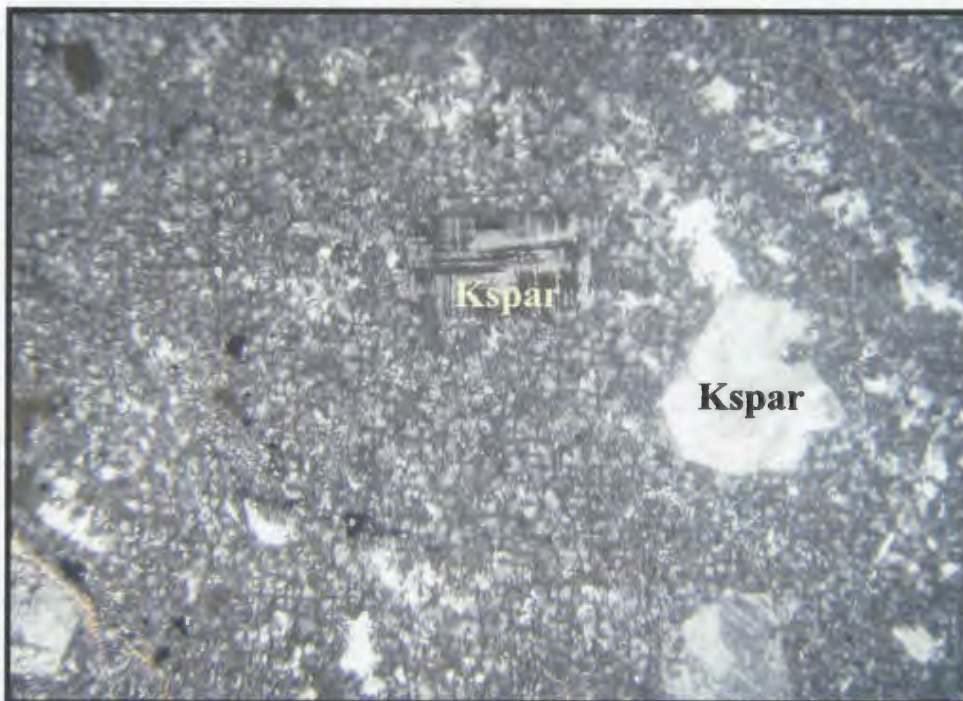
Plate 2-1: Flow-banded rhyolite containing K-feldspar phenocrysts in a fine-grained groundmass. Note the devitrification texture developed within the groundmass marked by the microspherulitic texture (Minerals Road Intersection; OB-01-36; XPL; FOV ~6mm; Kspar = K-feldspar).
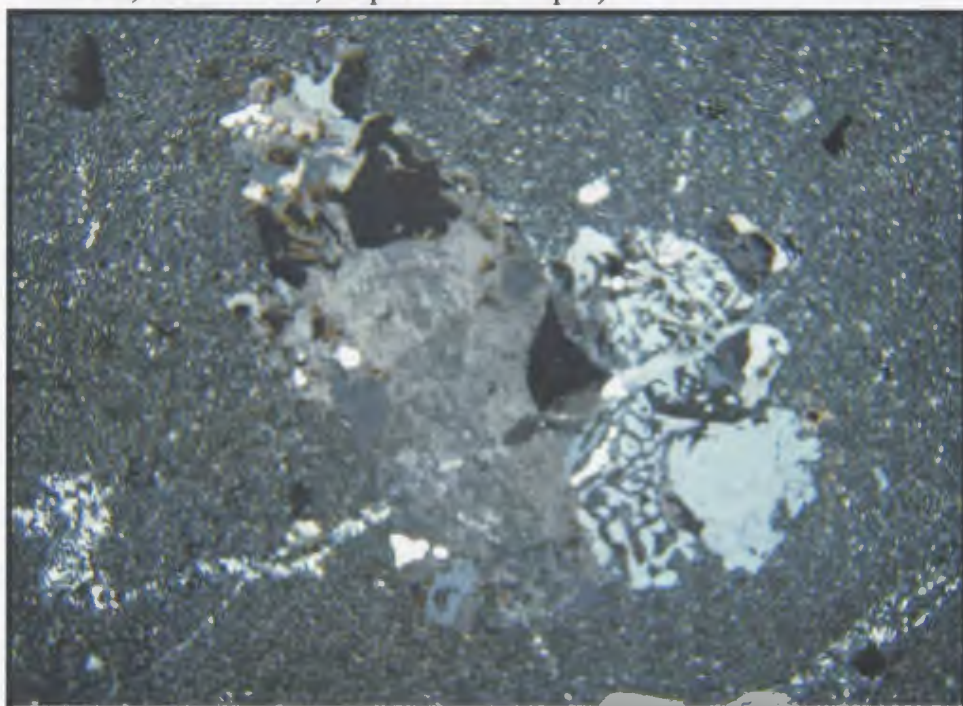
Plate 2-2: Well preserved granophyric texture within Unit 1 (White Mountain; OB-97-40; XPL; FOV ~ 4mm).

2.3.1.2 Unit 2: Aphyric, Flow-banded Rhyolite (Manuels River Rhyolite)

LITHOLOGY AND PETROGRAPHY:

Unit 2 consists of purple to grey-green, typically aphyric rhyolite, with well-developed flow banding and/or flow folds and rare weakly feldspar-phyric zones. This unit is mainly confined to the northeastern portion of the map area, and is exposed in areas along the Manuels River and CBS By-Pass roadcut (Figure 2-3). In outcrops along the CBS By-Pass roadcut, this unit has a massive, dark purple appearance and weak flow banding is visible on weathered surfaces. The unit is locally spherulitic, and has discrete zones of fine-grained disseminated pyrite associated with silicification in the area of the Bergs prospect; this alteration is locally anomalous in gold (sample GS-03-01; 74ppb Au). Unit 2 is host to numerous areas of hydrothermal brecciation and low-sulphidation veining, these features are most abundant in the area of the Steep Nap prospect (Figure 2-3). The breccias predominantly consist of angular to sub-rounded altered volcanic fragments in a dark red, hematite-rich matrix. Rare occurrences of a crackle breccia are also observed in the vicinity of the Steep Nap prospect. The crackle breccia is fragment-supported, with highly angular, 5-10cm diameter fragments, and open space infilling of comb-textured crystalline quartz, hematite, and chlorite (Plate 2-3). Other hydrothermal breccias in the area of the Steep Nap prospect are matrix-supported and typically contain chalcedonic silica vein fragments supported by a dark red hematite-rich matrix that locally contains minor pyrite; these breccias are also locally anomalous in gold (samples OB-03-11, OB-03-12, 398 and 640 ppb Au respectively).
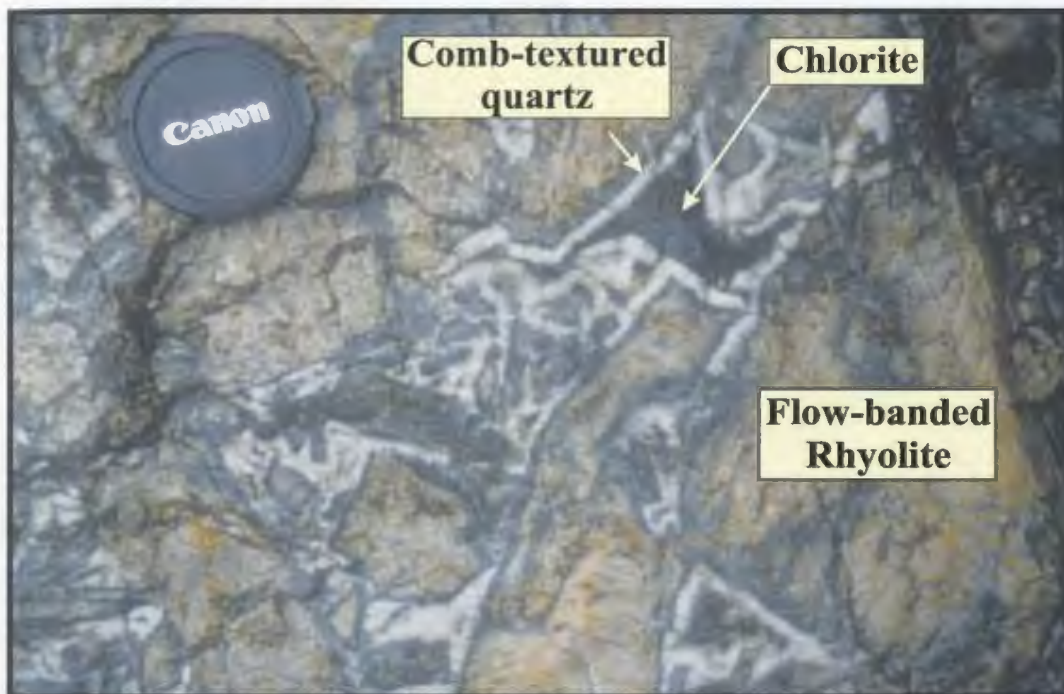
Plate 2-3: Highly angular, fragment-supported crackle breccia from the Steep Nap prospect (Photo courtesy of Sean O'Brien, Department of Natural Resources, Geological Survey).

Plate 2-4: Intrusive contact between Unit 2 and a fine-grained mafic intrusion (Manuels River; hammer is 60cm in length).

In the area of the Bergs prospect, Unit 2 appears to have a close spatial association with a fragmental volcaniclastic unit that has been highly silicified (Figure 2-3). The latter is white-weathering, grey-green on a fresh surface, contains 5-6cm subangular to angular, fragments of predominantly flow-banded rhyolite and is locally host to low-sulphidation-related quartz-hematite veinlets. This volcaniclastic rock has a very restricted distribution and is interpreted to be intercalated with the rhyolite.

Thin sections of the flow-banded rhyolite from the Steep Nap prospect reveal bands of alternating fine- and coarse-grained groundmass, along with local development of a microspherulitic texture. Thin sections from the area of the CBS By-Pass roadcut and Manuels River contain rare feldspar phenocrysts that show a weakly developed alignment, likely due to flow foliation. This foliation is further highlighted by the alignment of elongated quartz crystals within the groundmass. In both areas, thin sections reveal the presence of fracture-hosted titanite ± leucoxene, locally associated with minor quartz and chlorite within the fractures.

The unit is affected primarily by silica–sericite hydrothermal alteration, which is locally developed parallel to flow banding, along with minor chlorite and opaque minerals. In thin section, sericite is locally distributed throughout the groundmass (generally 2-3%), and chlorite is predominantly fracture hosted (not exceeding 5%). Macroscopic alteration is, for the most part, confined to areas of known epithermal veins and/or breccias, or very localized shear zones. An example of shear zone-related alteration is located along the eastern end of the CBS By-Pass roadcut, where relic pale

pink flow-banded rhyolite fragments that range from less than 1cm to greater than 10cm in diameter are contained within a pale green sericite–pyrite matrix.

CONTACT RELATIONSHIPS:

Unit 7 of the WHIS intrudes this unit in a number of areas, including along the Manuels River and the CBS By-Pass (see below). The flow-banded rhyolite is assumed to be overlain by a lithic-rich volcaniclastic rock (Unit 3), and the lower WHPC (Unit 19a; discussed below). Basaltic dykes, less than 1m wide, crosscut the unit in the area of the CBS By-Pass and Manuels River. In the latter area, 2-5m wide fine-grained mafic intrusions displaying sharp irregular boundaries with the adjacent flow-banded rhyolite (Plate 2-4).

2.3.1.3 Unit 3: Massive, Lithic-Rich, Polymict, Lapilli Tuff

LITHOLOGY:

Unit 3 is confined to the area around Minerals Road Intersection and the Steep Nap prospect (Figure 2-3). The lapilli tuff consists of a dark to pale green or pale pink matrix, which is host to abundant fragments of purple rhyolite, sub-rounded, light pink to white, coarse-grained granite and locally abundant fine-grained potassic altered material. The potassic altered material has a bright orange coloration and is the predominant clast at the Steep Nap prospect (Plate 2-5). The larger rhyolite fragments are porphyritic and locally display a dark purple core surrounded by a pale purple rim. Granite clasts show no evidence of chilling and are generally sub-rounded to rounded. Fragments are predominantly less than 1cm but reach upwards of 10cm in diameter and are

Plate 2-5: Lithic-rich, polymict lapilli tuff dominated by dark orange, potassic altered detritus. Note the unit is crosscut by banded chalcedonic silica-hematite veins of a low-sulphidation origin (Steep Nap prospect; scale is in cm).
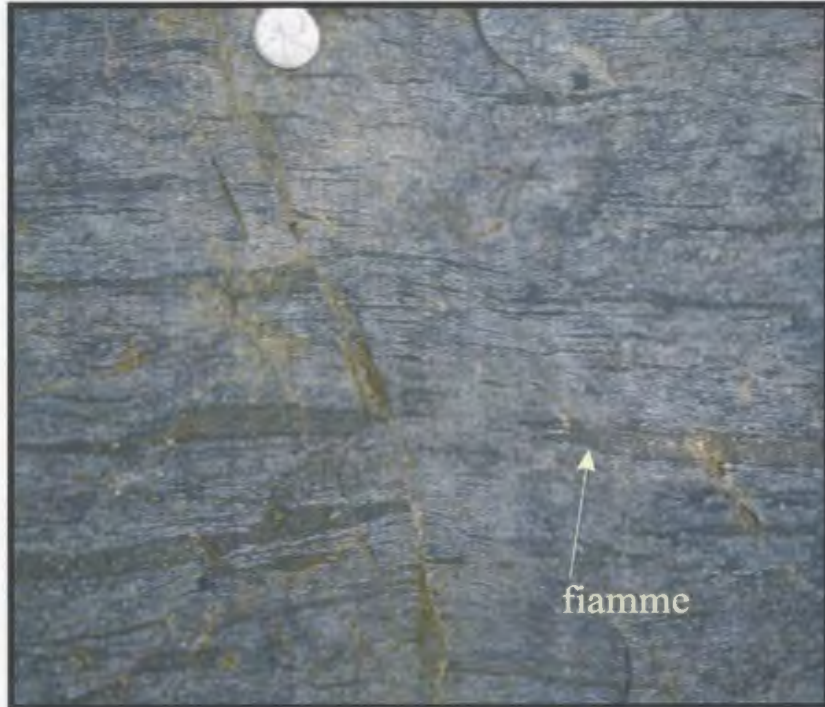
Plate 2-6: Welded, fiamme-bearing ash-flow tuff (Unit 4) with well-developed eutaxitic foliation (CBS By-Pass; Photo courtesy of Sean O'Brien, Department of Natural Resources, Geological Survey).

37

locally aligned in a poorly defined stratification. In the area of the Steep Nap prospect, this stratification appears to be relatively flat lying or very gently dipping.

Minor silicification as well as potassic and hematite alteration are developed within the tuff. The potassic alteration, which is fracture-hosted and has a pale pink coloration resembling adularia-rich alteration of the Steep Nap prospect, is associated with silicification in the area of Minerals Road Intersection. However, at the Minerals Road Intersection this alteration is barren with respect to gold. In the vicinity of Steep Nap, hematite is mobilized adjacent to hydrothermal veins, resulting in the formation of hematite haloes (Mills, 1998). Sericite and chlorite alteration are also pervasive throughout the unit. Relic sub-rounded to rounded fragments contained within a sericite–silica ± pyrite shear zone adjacent to the Steep Nap prospect are interpreted to be preserved features of Unit 3. The affinity of this alteration is not known, nor its timing relative to the low-sulphidation veining. The apparent absence of low-sulphidation veins within the alteration may indicate either that the alteration overprints the low-sulphidation veins or that the rheology of the altered host rock is such that it does not support vein development.

CONTACT RELATIONSHIPS:

At Minerals Road Intersection, the lapilli tuff is intruded by Unit 8 of the WHIS (see below) and a large (approximately 5m wide) basaltic dyke. In the region of the Steep Nap prospect, this unit is host to numerous banded crustiform-colloform chalcedonic silica ± adularia low-sulphidation veins and associated breccias. These breccias contain aphanitic flow-banded rhyolite fragments, which suggest Unit 3 overlies and contains

fragments of one of the underlying rhyolite units described above. Unit 3 is crosscut by several basaltic dykes that have a close spatial association with the development of low-sulphidation veins in the vicinity of the Steep Nap prospect. All other contacts with surrounding units are unexposed and therefore assumed or approximated.

2.3.1.4 Unit 4: Welded, Fiamme-bearing Ash-Flow Tuff

LITHOLOGY AND PETROGRAPHY:

Unit 4 contains pale purple weathering, centimeter-scale collapsed pumice within a pale white-weathering groundmass. Confined to the area of the CBS By-Pass, Unit 4 is dark purple on a fresh surface, and displays a well-developed eutaxitic foliation (Figure 2-3; Plate 2-6). The ash-flow has a moderate to steep northwesterly dip and is cut by several faults, which inhibit the estimation of a true stratigraphic thickness. However, an estimate of intact fault blocks suggests that the unit is on the order of tens of meters thick. The ash-flow contains localized zones of syn-volcanic brecciation, but no definitive evidence of any hydrothermal brecciation. The unit is moderately to strongly welded, and exhibits minor sericite–chlorite alteration. Several thin sections taken from east to west along the CBS By-Pass roadcut show an increase in the amount of compaction towards the east (Plate 2-7 and 2-8). In thin section, it is also evident that the unit contains rare feldspar crystals, and hairline veinlets containing quartz and titanite.

CONTACT RELATIONSHIPS:

This unit has a very restricted exposure and only occurs along the CBS By-Pass roadcut and several small wooded outcrops to the south. From this small amount of exposure, it appears that this unit is fault-bounded on all sides. Large-scale basaltic dykes

39

Plate 2-7: Photomicrograph of relatively uncompacted fiamme-bearing ash-flow tuff (CBS By-Pass roadcut; OB-01-011; PPL; FOV ~ 4.5mm).
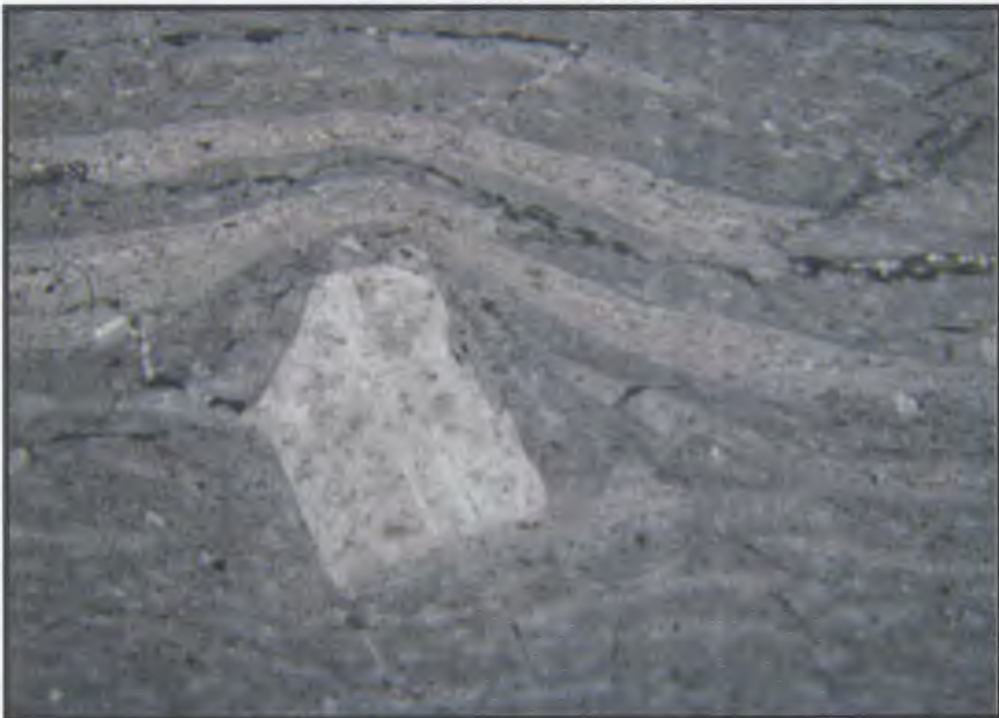
Plate 2-8: Photomicrograph of compacted fiamme-bearing ash-flow tuff (CBS BY-Pass roadcut; OB-01-008; PPL; FOV ~4.5mm).

(up to 7m wide) crosscut the unit and the ash-flow is apparently intruded by Unit 11 (see below), however due to the similar weathering of both units, the true nature of the contact is hard to determine.

2.3.2 Holyrood Intrusive Suite (HIS)

The HIS occupies the southwestern corner of the map area, and represents a much larger, homogeneous intrusion that forms the core of the Holyrood Horst. The HIS in the study area consists of one principle rock type, and has historically been interpreted as the source to the epithermal fluids responsibly for the development of the advanced argillic alteration within the study area.

2.3.2.1 Unit 5: Pink-White-Green Granite

LITHOLOGY AND PETROGRAPHY:

Pink–white–green, propylitized granite is the principal rock-type of the HIS exposed within the field area, which is confined to the southwestern corner of the Map 1 (Figure 2-4). Unit 5 is characteristic of the Holyrood Intrusive Suite's eastern margin in the northern part of the Avalon Peninsula (O'Brien *et al.,* 2001a) and is generally equigranular to quartz-phyric with sub-equal amounts of plagioclase, K-feldspar and quartz. Petrographic study shows this unit to consist of sub- to anhedral medium- to coarse-grained crystals of the above-mentioned minerals. The plagioclase typically displays albite twinning, and is affected by weak to moderate saussuritization. K-feldspar crystals display minor amounts of exsolution and show no evidence of twinning; the quartz crystals predominantly infill space between the two feldspars. Table 2-2 shows the
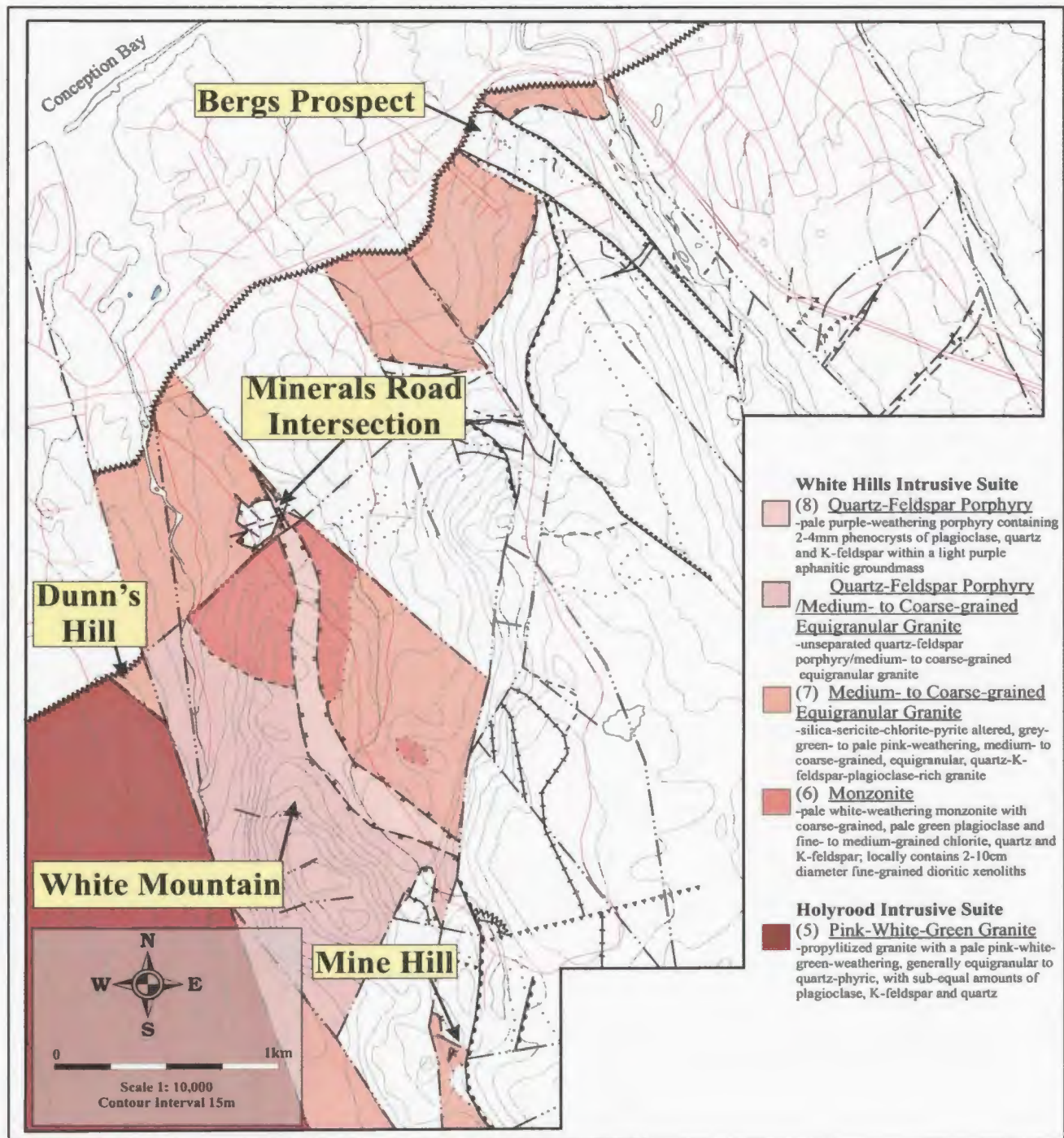
Figure 2-4: Distribution of the Holyrood and White Hills intrusive suites, extracted from Map 1.

modal proportions of the dominant mineral phases estimated from a stained thin section of typical Unit 5.

CONTACT RELATIONSHIPS:

The HIS intrudes the Hawke Hills Tuff (O'Brien *et al.*, 2001a) to the west and south of the Holyrood Horst (Figure 1-1). Its boundary with the WHIS in the eastern portion of the field area is a fault or inferred intrusive contact.

Table 2-2: Estimated modal proportions from a stained section of the pink–white–green granite (values are listed in % volume).

Sample #	Primary			Secondary		
	Plagioclase	K-feldspar	Quartz	Chlorite	Epidote	Carbonate
OB-97-039	24	30	35	8	2	1

2.3.3 White Hills Intrusive Suite (WHIS)

The WHIS is a new name proposed by Sparkes *et al.* (2005), for a suite of compositionally diverse intrusions that occur between the HIS and volcanic rocks previously assigned to the MVS.

2.3.3.1 Unit 6: Monzonite

LITHOLOGY AND PETROGRAPHY:

Unit 6 is largely confined to the western portion of the map area where it is intimately associated with other units of the WHIS (Figure 2-4). This unit is pale white-weathered and contains coarse-grained white to pale green plagioclase crystals supported by fine- to medium-grained dark green chlorite, white quartz and pale pink K-feldspar. The unit also contains distinctive fine-grained, dioritic xenoliths up to 10cm in diameter (Plate 2-9).

Plate 2-9: Fine-grained dioritic xenoliths contained within medium- to coarse-grained monzonite (Unit 6; Minerals Road Intersection).
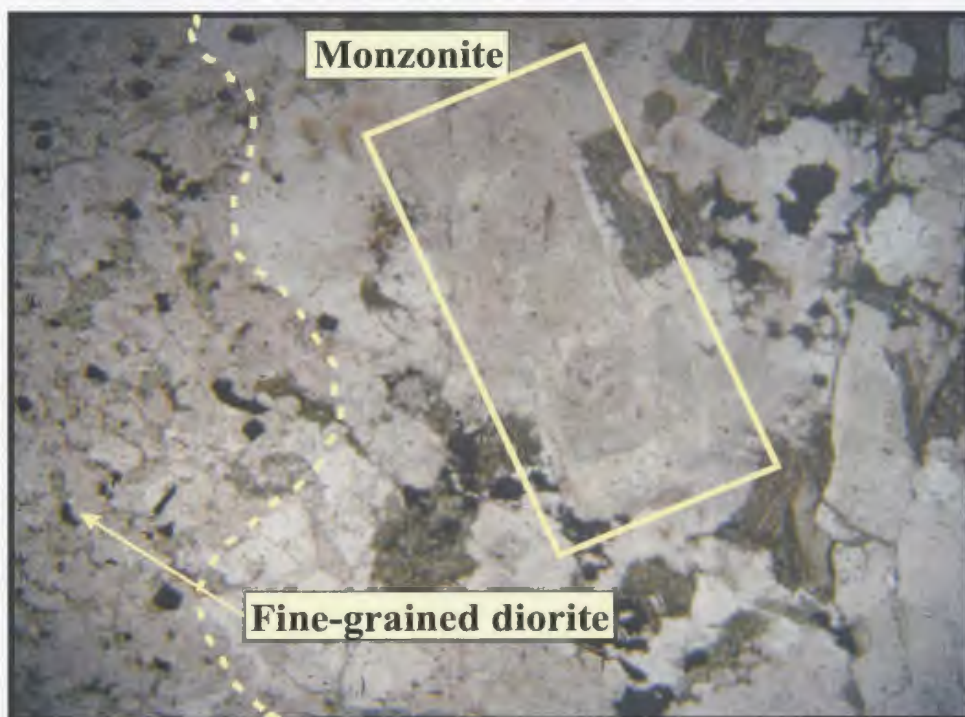
Plate 2-10: Photomicrograph of the contact between a diorite xenolith and Unit 6. The dashed line represents the approximated contact; note the subhedral plagioclase with a cloudy core outline in the rectangle (GS-02-81; PPL; FOV ~6mm).

In thin section, the unit typically contains medium- to coarse-grained, sub- to anhedral plagioclase crystals supported by a finer-grained groundmass of chlorite, quartz and minor K-feldspar. The plagioclase crystals contain albite-, Carlsbad- and pericline-twins and locally displays normal zoning, highlighted by preferential saussuritization of the central portion of the crystals. The zoning in the plagioclase, which is most prominent in plane-polarized light (due to the saussuritization), is a distinctive characteristic of this unit, not common to other units of the WHIS. K-feldspar does not everywhere display a dark pink color commonly characteristic in this unit. It is typically untwinned and exhibits local areas of cloudy dark pink coloration. Quartz crystals are dominantly anhedral and are intergrown with dark-green fibrous chlorite that displays a weak to moderate pleochroism. This chlorite is assumed to have completely replaced a primary mafic mineral phase since the chlorite often forms sub- to anhedral rectilinear pseudomorphs; it is assumed that the original mineral was biotite. Estimated modal proportions of the major mineral phases are contained within Table 2-3. This estimation is taken from four stained sections in order to properly identify the modal proportions of the plagioclase and K-feldspar.

Macroscopically this unit appears relatively unaltered, however, some alteration is visible in thin section. The main alteration that is presumed to be hydrothermal in origin is saussuritization of the plagioclase (Plate 2-10 and 2-11). Chlorite is also abundant throughout the groundmass and is associated with minor epidote and carbonate. This alteration is interpreted to represent the secondary alteration products of a mafic mineral(s). Minor evidence of biotite is locally preserved, which suggests this may be the

Plate 2-11: Photomicrograph of the contact between a diorite xenolith and Unit 6. The dashed line represents the approximated contact; note the subhedral plagioclase with preferential saussuritization of the central portion of the crystal outline in the rectangle (GS-02-81; XPL; FOV ~6mm).
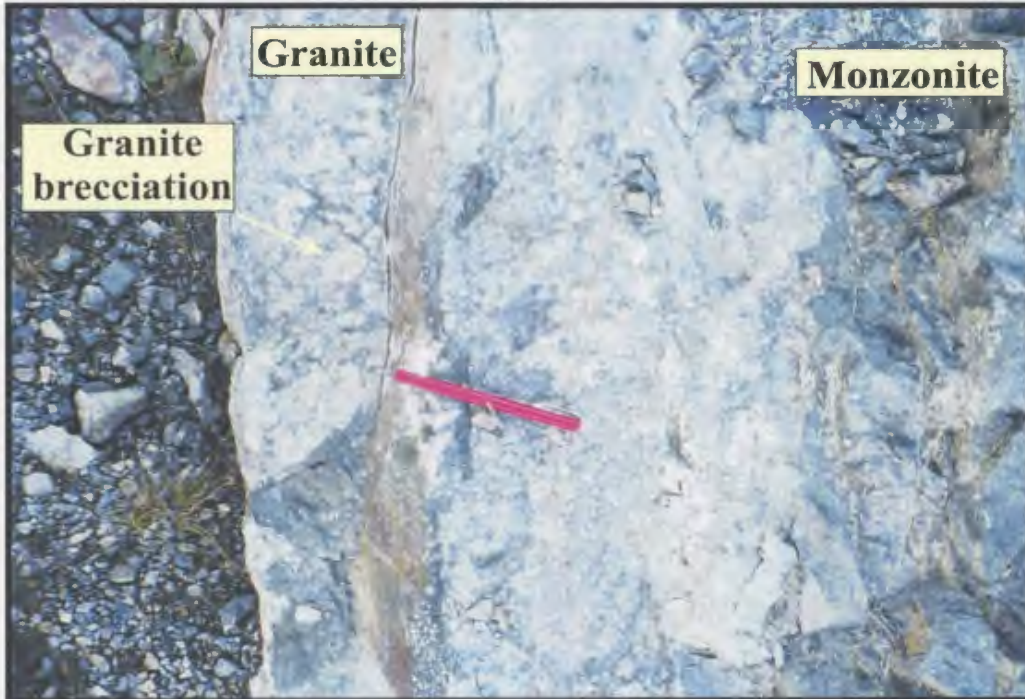
Plate 2-12: Intrusive contact between Unit 7 (left hand side) and Unit 6 (right hand side). Note characteristic brecciation of granite at the contact (White Mountain region).

mafic phase being replaced. A thin section containing both Unit 6 and a fine-grained dioritic xenolith reveals no apparent chilled margins between the two. The xenolith consists of fine-grained plagioclase surrounded by finer-grained opaque minerals, chlorite, minor carbonate and quartz.

Table 2-3: Modal proportions estimated from stained thin sections of the White Hills Intrusive Suite monzonite (values are listed in % volume).

Sample #	Primary			Secondary			
	Plagioclase	K-feldspar	Quartz	Chlorite	Epidote	Carbonate	Opaques
OB-97-024	63	3	10	20	2	1	1
OB-97-025	65	2	8	18	3	2	2
OB-97-057	70	1	8	15	4	1	1
OB-97-375	72	3	12	10	1	1	1

CONTACT RELATIONSHIPS:

Due to the small volume of exposed monzonite, contacts with adjacent units are typically unexposed and therefore inferred. Where the contact is exposed, Unit 7 intrudes Unit 6 and at the contact the granite becomes brecciated (Plate 2-12). Locally fine- to medium-grained aplite and granitic dykes (up to approximately 40cm in width) and fine-grained pale to dark brown-weathering mafic dykes (less than 1m in width) crosscut the unit. This field data suggests that this unit is the oldest unit of the WHIS. This inference is further supported by the lack of chemical differentiation and other chemical characteristics in relation to Unit 7 and Unit 8 (see Chapter 3).

2.3.3.2 Unit 7: Medium- to Coarse-grained Equigranular Granite

LITHOLOGY AND PETROGRAPHY:

Unit 7 granite mainly occurs in the western and northwestern portions of the map area (Figure 2-4). This unit occupies the greatest percentage of the WHIS and is considered to represent a single intrusion. Lithological variation is typically due to varying amounts of alteration, depending on the locality within the map area. The dominant phase of this unit is a medium- to coarse-grained, equigranular, quartz–K-feldspar–plagioclase-bearing granite. This unit predominantly has a grey-green- to pale pink-weathering, and has locally developed tuffisite brecciation (Plate 2-13). Locally Unit 7 is spatially associated with a fine- to medium-grained, chlorite-rich, intermediate intrusive phase that appears to comingle with the granite in the area of Minerals Road Intersection; Unit 7 also contains rare, fine-grained dioritic xenoliths (3-4cm in diameter) that closely resemble those observed in Unit 6. Rare outcrops of fine-grained, K-feldspar-rich Unit 7 occur in close proximity to outcrops of Unit 6 in the valley east of White Mountain (Figure 2-4).

In thin section, Unit 7 displays subhedral crystals of plagioclase displaying albite less commonly, periclinal twins, and minor exsolution (Table 2-4). Anhedral K-feldspar crystals, locally up to 4mm in length, show little or no evidence of twinning and commonly display exsolution features such as microperthite. Exsolution in both plagioclase and K-feldspar occur as lamellae and as irregular patches throughout the crystals. Most of the quartz mainly occurs as a late infill, forming anhedral crystals between the feldspars. However, the preservation of granophyric textures provides

Plate 2-13: Tuffisite brecciation developed in medium-grained equigranular granite of the White Hills Intrusive Suite (Manuels River; Photo courtesy of Sean O'Brien, Department of Natural Resources, Geological Survey).
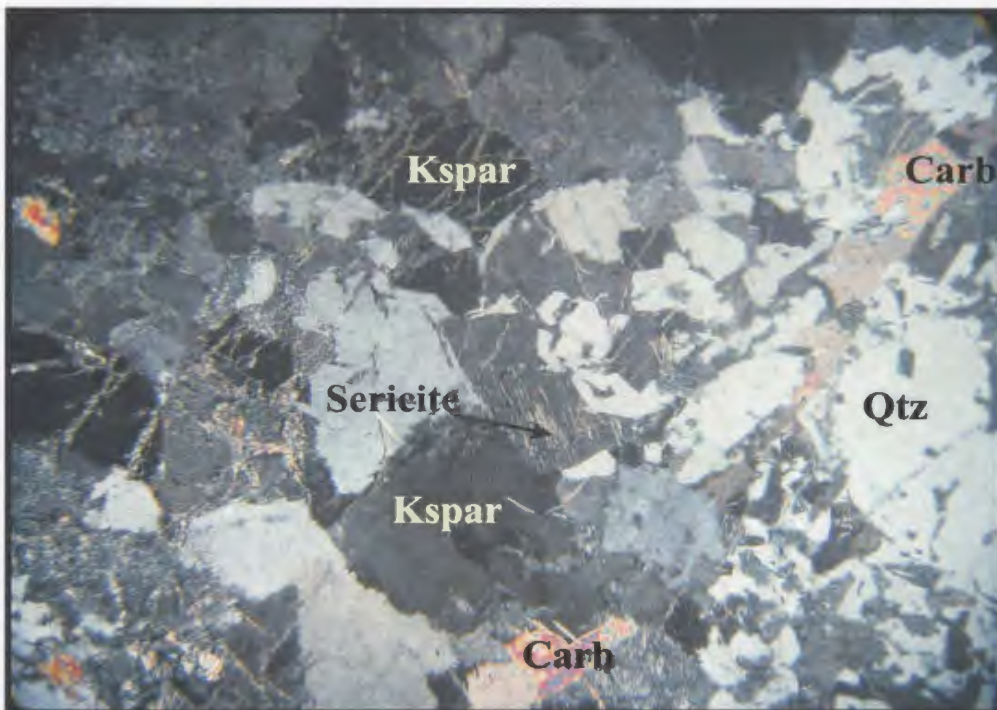
Plate 2-14: Altered granite adjacent to a cm-scale banded chalcedonic silica-hematite veinlet (Bergs prospect); note the fracture hosted sericite alteration and late stage carbonate (GS-02-44; XPL; FOV ~5.5mm; Kspar = K-feldspar, Qtz = quartz and Carb = carbonate).

evidence of co-crystallization of some quartz with K-feldspar. Alteration observed in thin sections is generally confined to micro-scale fracturing in most K-feldspar crystals (Plate 2-14), and local pervasive saussuritization of plagioclase produces a "peppered texture". Chlorite, often associated with sericite alteration, is generally confined to regions along grain boundaries, but rarely forms rectilinear shapes and is thought to be replacing primary biotite. Sericite (2-3%) and chlorite (2-5%) comprise the predominant alteration mineralogy within the CBS By-Pass region. Muscovite is very rare in thin section, and may or may not represent the remnants of primary mica within Unit 7.

In the region of Minerals Road Intersection (Figure 2-4), saussuritization is intense and plagioclase and K-feldspar can only be distinguished in stained thin sections. The feldspar crystals exhibit a dusty coloration due to saussuritization and appear to have been euhedral and zoned, but are now anhedral due to possible resorption. The feldspars are subhedral and coarse-grained (2-4mm) and are surrounded by later crystallized, finer-grained (<1mm) quartz and chlorite. The saussuritization is concentrated in the central portion of some of the crystals, possibly due to a weak compositional zonation. Locally, chlorite alteration (up to 6% modal chlorite) occurs with minor epidote; both are assumed to be replacing a primary mafic phase such as hornblende or biotite. Minor carbonate is also associated with the chlorite alteration.

Unit 7, in the vicinity of the Bergs prospect (Figure 2-4), is dominated by apple green silica–sericite alteration (Plate 2-15), while granite south of the Oval Pit Mine is rusty weathering and dominated by silica–pyrite alteration that can be traced for upwards of 4.6km south of Mine Hill. In the Bergs area Unit 7 is also affected by dark green

Plate 2-15: Silica-sericite-chlorite altered, medium-grained equigranular granite of the White Hills Intrusive Suite (CBS By-Pass roadcut; Photo courtesy of Sean O'Brien, Department of Natural Resources, Geological Survey).
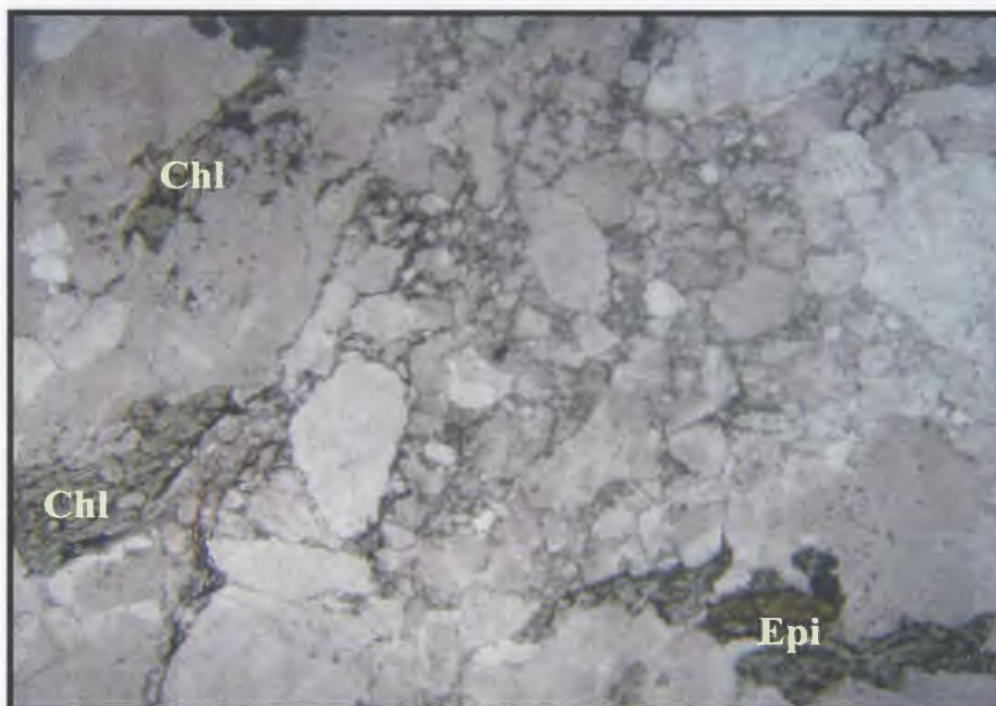
Plate 2-16: Photomicrograph of micro-scale brecciation possibly related to the development of low-sulphidation veins at the Bergs prospect; note chlorite (Chl) and epidote (Epi) alteration (GS-02-078; PPL; F.O.V. ~4mm; Bergs prospect).

chlorite alteration as well as a pervasive, micro-scale brecciation (Plate 2-16 and 2-17). Saussuritization affects the feldspar crystals while chlorite occurs both as sub- to euhedral crystals in the groundmass and within hairline fractures that crosscut Unit 7. The granite in that area generally contains between 5-8% modal chlorite and up to 8% modal sericite. In areas of intense hydrothermal alteration, the main mineral phases present are quartz, sericite, chlorite and rare coarse-grained K-feldspar (up to ~1cm in length), possibly representing potassic alteration. In the vicinity of Dunn's Hill (Figure 2-4), Unit 7 displays a style of alteration similar to that seen in the Bergs area, whereas granite outcrops immediately to the west of this area display a characteristic pink–white–green alteration, typical of the 620 Ma Holyrood Intrusive Suite (Unit 5; see section 2.3.2.1).

Table 2-4: Modal proportions estimated from stained thin sections of the White Hills Intrusive Suite granite (values are listed in % volume).

	Primary				Secondary				
Sample #	Plagioclase	K-feldspar	Quartz	Muscovite	Chlorite	Sericite	Epidote	Carbonate	Opaques
OB-97-017	20	32	40	1	2	3	0	0	2
OB-97-018	23	20	50	2	1	3	0	0	1
OB-97-026	31	22	35	1	3	2	2	3	1
OB-97-055	20	30	40	0	5	2	3	0	0
OB-97-221	37	20	38	0	3	1	1	0	0

CONTACT RELATIONSHIPS:

Numerous intrusive contacts exist between Unit 7 and adjacent country rocks. The granite at Bergs is host to large (up to approximately 1m) grey silicic pods of an unknown origin. In the adjacent Manuels River area, a large (approximately 2-4m) raft of fine-grained, pale purple rhyolite (Unit 2) is surrounded by intruding granite. A similar

52
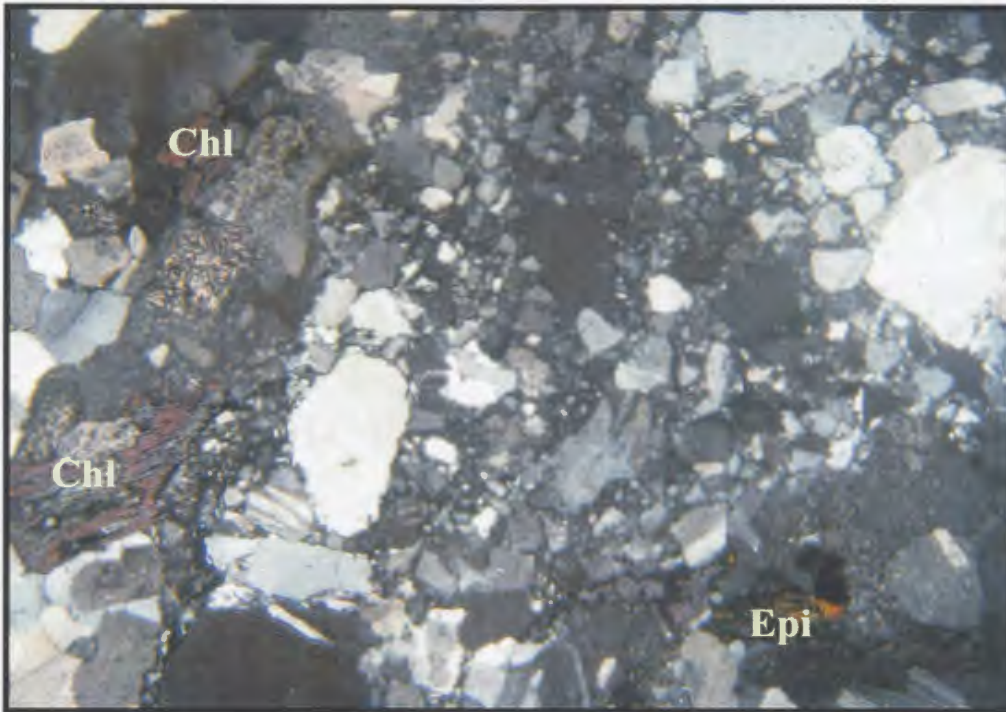
Plate 2-17: Photomicrograph of micro-scale brecciation possibly related to the development of low-sulphidation veins at the Bergs prospect; note chlorite (Chl) and epidote (Epi) alteration (GS-02-078; XPL; F.O.V. ~4mm; Bergs prospect).

Plate 2-18: Medium-grained granite of the White Hills Intrusive Suite (left hand side) becoming brecciated as it intrudes Unit 2 (right hand side; CBS By-Pass roadcut).

contact exists at Mine Hill, where a raft of fine-grained, silica-altered felsic volcanic rock (approximately 8m in length) is contained within silica-pyrite-altered granite (Figure 2-4). At White Mountain, numerous rafts of a pale-purple feldspar-phyric rhyolite (Unit 1) are contained within units of the WHIS.

Many of the contacts between Unit 7 and the surrounding country rocks result in brecciation of the granite, making it hard to decipher the true nature of the contact. In some areas, where Unit 7 is assumed to be intrusive, brecciated granite fragments appear to float in a matrix of the unit that is being intruded (Plate 2-18). This type of contact is observed in several locations (e.g. CBS By-Pass roadcut, Steep Nap prospect, and White Mountain; Figure 2-2), although its significance is unclear. Numerous fine-grained, brown-weathering, locally pyrite-bearing, basaltic dykes crosscut Unit 7. At the Bergs prospect, these dykes contain well-preserved evidence of rapid cooling as indicated by the presence of swallowtails within the feldspar crystals (Plate 2-19). Also at the Bergs prospect, Unit 7 is host to low-sulphidation-related, centimeter-scale, banded chalcedonic silica quartz-hematite veinlets, which are weakly anomalous in gold (sample GS-02-51; 27ppb Au).

2.3.3.3 Unit 8: Quartz–Feldspar Porphyry

LITHOLOGY AND PETROGRAPHY:

Unit 8 contains 2-4mm pale white plagioclase and pale pink K-feldspar crystals along with 3-4mm sub-rounded quartz crystals within a light purple aphanitic groundmass. The groundmass also contains dark green crystals of chlorite that are assumed to have replaced primary biotite (less than 1mm). The porphyry contains

Plate 2-19: Photomicrograph of a swallow-tail texture developed in a mafic intrusion within Unit 7 of the White Hills Intrusive Suite (Bergs prospect); note texture implies rapid cooling (GS-02-061; XPL; FOV ~1mm).
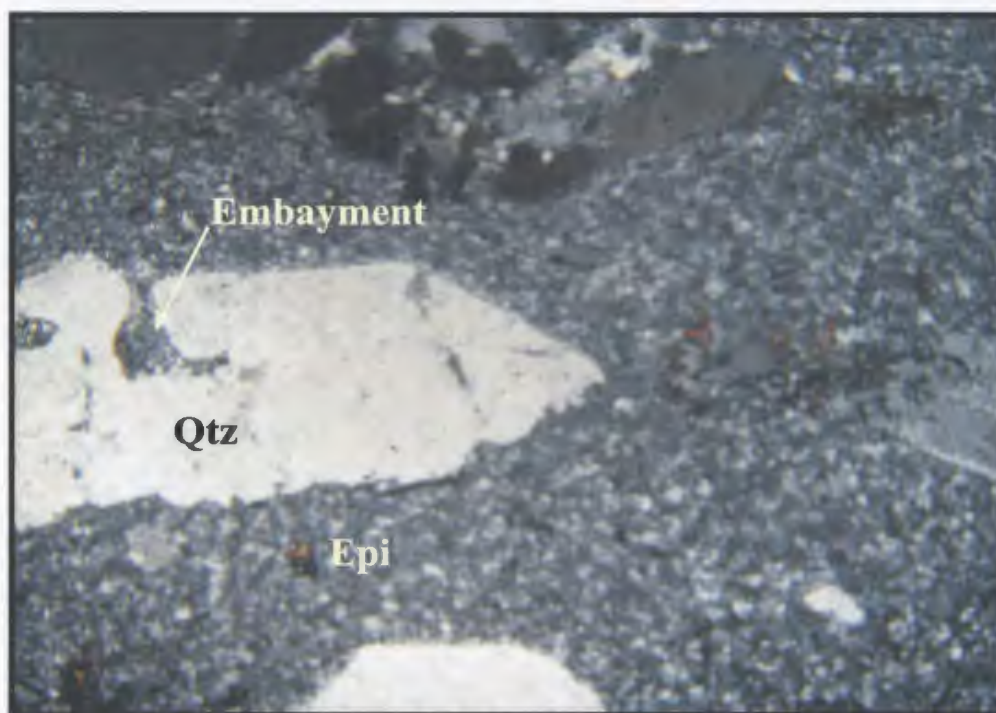
Plate 2-20: Photomicrograph of Unit 8 from the White Hills Intrusive Suite (Minerals Road Intersection); note embayments in the quartz phenocryst and epidote alteration hosted within the groundmass (OB-01-038; XPL; FOV ~6mm; Qtz = quartz and Epi = epidote).

between 40 to 60% phenocrysts, and locally takes on a granitic texture. Rare phenocrysts of pale white feldspar appear to be rimmed by pink K-feldspar, suggesting weak zonation in the feldspar phenocrysts. This unit is confined to the area of Minerals Road Intersection and the White Mountain region; Unit 8 is the most distinctive unit of the WHIS (Figure 2-4).

Thin sections from this unit contain anhedral to euhedral crystals of plagioclase and K-feldspar (up to 2-3mm in diameter) as well as anhedral, sub-rounded phenocrysts of quartz. The latter typically have ragged margins and display resorption textures (Plate 2-20). Unlike plagioclase, the K- feldspar crystals are untwinned and host exsolution textures. Plagioclase displays saussuritization that does not affect the K-feldspar crystals. Despite macroscopic evidence, zonation in feldspar crystals is rarely seen in thin section. The phenocrysts are contained within a very fine-grained groundmass that locally appears to develop devitrification textures similar to that seen in some of the volcanic rocks. Table 2-5 contains estimated modal proportions from three stained sections from Unit 8. Staining reveals that most of the K-feldspar content is contained within the groundmass, as the phenocryst phases are predominantly plagioclase and quartz.

Table 2-5: Modal proportions estimated from stained thin sections of the White Hills Intrusive Suite quartz–feldspar porphyry (values are listed in % volume).

	Primary				Secondary				
Sample #	Plagioclase	K-feldspar	Quartz	Muscovite	Chlorite	Sericite	Epidote	Carbonate	Opaques
OB-97-021	63	2	18	0	8	3	4	2	2
OB-97-027	50	4	29	2	5	5	3	1	1
OB-97-041	65	4	18	2	2	5	2	0	2

Although a pale green coloration within some of the plagioclase crystals (attributed to saussuritization) is evident in hand specimen, alteration within Unit 8 is generally only visible in thin section. Most sericite alteration is prevalent in the groundmass around feldspar crystals and generally has a patchy distribution throughout. Saussuritization is confined to the plagioclase, whereas patches of chlorite–epidote–carbonate alteration are confined to the groundmass.

CONTACT RELATIONSHIPS:

Unit 8 is locally intrusive into Unit 3, a volcaniclastic rock that contains fragments of both granite and porphyritic material in the area of Minerals Road Intersection. In this same region, and south along the eastern edge of White Mountain, Unit 8 is seen to crosscut Unit 7 in a number of places. This relationship confirms that this unit is the youngest intrusion of the WHIS. Unit 8 also crosscuts the same crystal-rich felsic volcanic rafts as the granite in the area of White Mountain. In the central part of White Mountain, Unit 8 and Unit 7 appear to comingle and could not be separated at the scale of this mapping. For this reason the two were combined into a single unit on Map 1. Mafic dykes (less than 1m wide) crosscut Unit 8 in several locations.

PROTEROZOIC ROCKS (585 Ma and younger)

2.3.4 Manuels Volcanic Suite (MVS)

The MVS was originally used to designate the volcanic succession east of the Holyrood and White Hills Intrusive suites and west of the regional Topsail Fault (Figure 1-2). The MVS is here modified to include those rocks east of the regional Mine Hill

Shear Zone (MHSZ) and west of the Topsail Fault (Figure 1-2). These rocks include subaerial, bimodal volcanic rocks with minor ash-flow tuff, and are mainly found in the area of the Oval Pit mine and the Bergs prospect.

2.3.4.1 Unit 9: Aphanitic Flow-Banded Rhyolite (Farmers Field Rhyolite)

LITHOLOGY

Based on intrusive relationships and geochronological data, two separate units of aphyric flow-banded rhyolite occur within the map area. These are Unit 2 (described above) and Unit 9 (described here). Unit 9 is confined to the region east of the MHSZ and south of the northwest-trending shear zone that separates it from Unit 2 (Figure 2-5). Similar to Unit 2, Unit 9 displays well-developed flow banding and/or flow folds with very localized development of porphyritic and lithophysae-bearing zones. This unit is dark purple with a pale white-weathering and is locally crosscut by areas of hydrothermal brecciation and quartz–hematite and/or "waxy" chalcedonic silica veinlets of a possible low-sulphidation affinity. The hydrothermal breccias within this unit contain pale white, sub-rounded to subangular, centimeter-scale silicified fragments supported by a dark red to purple hematite-rich matrix. Preservation of relic flow banding within the pyrophyllite–diaspore ore in the Oval Pit mine, and a close spatial association between this alteration and Unit 9 provide supporting evidence that this unit is the host to the high-sulphidation style epithermal alteration (Plate 2-21).

Locally Unit 9 is affected by patchy pale to bright pink potassic alteration that is associated with blotchy dark purple hematite. This potassic alteration is further associated with hematite-rich brecciation and minor disseminated pyrite along with banded silica–

Conception Bay

Bergs Prospect

CBS By-Pass Roadcut

Steep Nap Prospect

Minerals Road Intersection

Farmer's Field

Oval Pit Mine

Mine Hill Shear Zone

N
W—E
S

0 — 1km

Scale 1: 10,000
Contour Interval 15m

Manuels Volcanic Suite

(18) Hematite-Chlorite-rich Hydrothermal Breccia
-matrix supported, hematite-chlorite-rich breccia containing sub-rounded to subangular fragments of silicified rhyolite within a dark purple to green matrix; fragments generally 2-4cm in diameter

(17) Silica-Sericite-Pyrite-Pyrophyllite-Diaspore-Rutile Alteration
-pale white- to yellow-weathering alteration with varying proportions of silica-sericite-pyrite-pyrophyllite-diaspore-rutile

(16) Sericite-Silica ± Pyrite Alteration
-white- to pale yellow-weathering alteration with patchy pyrite development; alteration associated with prominent shear zones

(15) Mafic Volcanic/Intrusive Rocks
-fine-grained, dark brown- to dark green-weathering, moderate to weakly magnetic, locally amygdaloidal and plagioclase-phyric basalt

(14) Massive, Poorly-Sorted, Lithic-rich, Breccia
-matrix supported breccia containing sub-rounded to angular fragments of low-sulphidation vein material in a poorly sorted hematite-rich matrix

Silica Alteration
-pale white, pervasive silica alteration without pyrophyllite-diaspore-sericite (Bergs area)

(13) Dark Purple, Crystal-bearing, Ash-flow Tuff
-massive crystal-rich tuff, containing pale white mm-scale crystals within a dark purple, hematite-rich groundmass

(12) Grey-Green, Pyritic, Pumiceous, Crystal-bearing Ash-flow Tuff
-massive crystal-rich tuff, containing mm-scale white crystals, and cm-scale dark purple collapsed pumice fragments, in a dark green to grey groundmass; groundmass also contains minor fine-grained disseminated pyrite

(11) Pale Grey-Green, Moderately Porphyritic, Fine, Rhyolite
-light grey- to green-weathering rhyolite, mm-scale white feldspar crystals and fine-grained disseminated pyrite in a fine-grained groundmass

(10) Aphanitic, Massive Rhyolite/Polymict Lithic Volcanaiclastic Rock
-dark purple-weathering, massive volcanaiclastic containing subangular to sub-rounded fragments; fragments predominantly 5-10cm in diameter but locally up to 50cm

(9) Aphanitic Flow-Banded Rhyolite (Farmer;s Field Rhyolite)
-dark purple, pale white-weathering aphanitic rhyolite with local development of lithophysae

Figure 2-5: Distribution of the Manuels Volcanic Suite, extracted from Map 1.

59

Plate 2-21: Silica-sericite-pyrophyllite altered flow-banded rhyolite from within the Oval
Pit mine (Unit 9; Photo courtesy of Sean O'Brien, Department of Natural
Resources, Geological Survey).

Plate 2-22: Polymict lithic volcaniclastic rock (Unit 10) with a large block of silica-altered
material (outlined); note the other sub-rounded detritus contained within a
brown-weathering groundmass.

hematite–chlorite veinlets with anomalous gold (sample OB-03-16; 46ppb Au). This alteration occurs in the northwestern portion of the unit where it is spatially associated with a prominent structure separating volcanic and sedimentary rocks. In this region the alteration appears to increase westward with increasing proximity to the structure. In the area of the Oval Pit mine, Unit 9 is affected by intense silicification and sericite–pyrite alteration (Figure 2-5).

CONTACT RELATIONSHIPS:

Regional scale faults bound this unit along its western flank, as a result most major contacts are tectonic or unexposed; the remaining contacts with adjacent units are approximated or assumed as a result of poor exposure.

2.3.4.2 Unit 10: Aphanitic, Massive, Rhyolite/ Polymict Lithic Volcaniclastic Rock

LITHOLOGY

Spatially associated with Unit 9 is a volcaniclastic unit that is confined to the margins of the flow (Figure 2-5). This unit is dark purple, generally massive, and locally contains volcanic fragments. Lithic-rich variants of the Unit 10 contain subangular to sub-rounded fragments of crystal-rich and weakly flow-banded material (these are typically between 5-10cm in diameter), along with rare blocks of silica–sericite alteration (approximately 50cm in diameter; Plate 2-22).

Centimeter-scale quartz–hematite and/or "waxy" chalcedonic silica veinlets with weak banding crosscut this unit, and are locally associated with potassic-style alteration. Unit 10 is affected by silica–sericite alteration related to the high-sulphidation system and by more locally developed hematite-rich brecciation of unknown affinity. Minor chlorite–

pyrite alteration and local silica–sericite alteration is also developed within the vicinity of prominent shear zones.

CONTACT RELATIONSHIPS:

Unit 10 is spatially associated with, and interpreted to overlie, the Unit 9. This unit is in gradational contact with the main zone of advanced argillic alteration; all other contacts with adjacent units are either tectonic or inferred.

2.3.4.3 Unit 11: Pale Grey-Green, Moderately Porphyritic, Fine, Rhyolite

LITHOLOGY and PETROGRAPHY

Exposed only in the area of the CBS By-Pass, this unit is confined to rare meter-scale dykes (Figure 2-5). This rhyolite is light grey to light green, pale weathering and contains white millimeter-scale feldspar phenocrysts and minor amounts of fine-grained disseminated pyrite within a very fine-grained groundmass. In thin section, the rhyolite contains 2-3mm, subhedral K-feldspar crystals, with Carlsbad- and rare albite-twins. The groundmass contains lath-like quartz crystals along with fine-grained feldspar, chlorite and opaque minerals. Alteration is present throughout the groundmass and consists predominantly of chlorite, with minor patches of epidote and carbonate. Minor saussuritization is also evident within the feldspar crystals.

CONTACT RELATIONSHIPS:

Unit 11 is assumed to crosscut both Unit 2 and the fiamme-bearing ash-flow tuff (Unit 3). The unit is assumed to be truncated by a northwest-southeast trending shear zone at the eastern end of the CBS By-Pass roadcut. Locally, meter-scale mafic dykes crosscut the unit.

2.3.4.4 Unit 12: Grey-Green, Pyritic, Pumiceous, Crystal-bearing, Ash-flow Tuff

LITHOLOGY and PETROGRAPHY

This unit is limited to the area around the Bergs prospect (Figure 2-5). Unit 12 consists of a dark green to grey groundmass that supports white, 1-2mm feldspar crystals and pale purple collapsed pumice fragments. The unit also contains moderate amounts (less than 5%) of disseminated pyrite within the groundmass, and hosts very localized lithophysae-bearing zones.

In thin section, the unit contains sub- to anhedral feldspar crystals and/or crystal fragments up to approximately 4mm in length. The crystals are supported within a very fine-grained groundmass in which areas of texturally distinct quartz, consisting of fine-grained laths are preserved; these areas may represent recrystallized pumice fragments. The feldspars cannot be distinguished on account of the saussuritization, although the crystals display relic albite and Carlsbad twins. This alteration does not produce the typical "peppered" texture as seen elsewhere; instead, the alteration is patchy and unevenly distributed throughout the feldspar crystals. Chlorite is also present within the groundmass, and appears to be associated with the formation of the opaque minerals. In the vicinity of the Bergs prospect, Unit 12 is affected by silica–sericite alteration, adjacent to a major shear zone. Hydrothermal brecciation, and quartz–hematite veins crosscut the unit; these breccias contain angular fragments of host rock supported by a white quartz–hematite–chlorite-rich matrix (Plate 2-23).

Plate 2-23: Hydrothermal breccia developed within the grey-green, pyritic, pumiceous, crystal-bearing, ash-flow tuff (Unit 12; Bergs prospect).
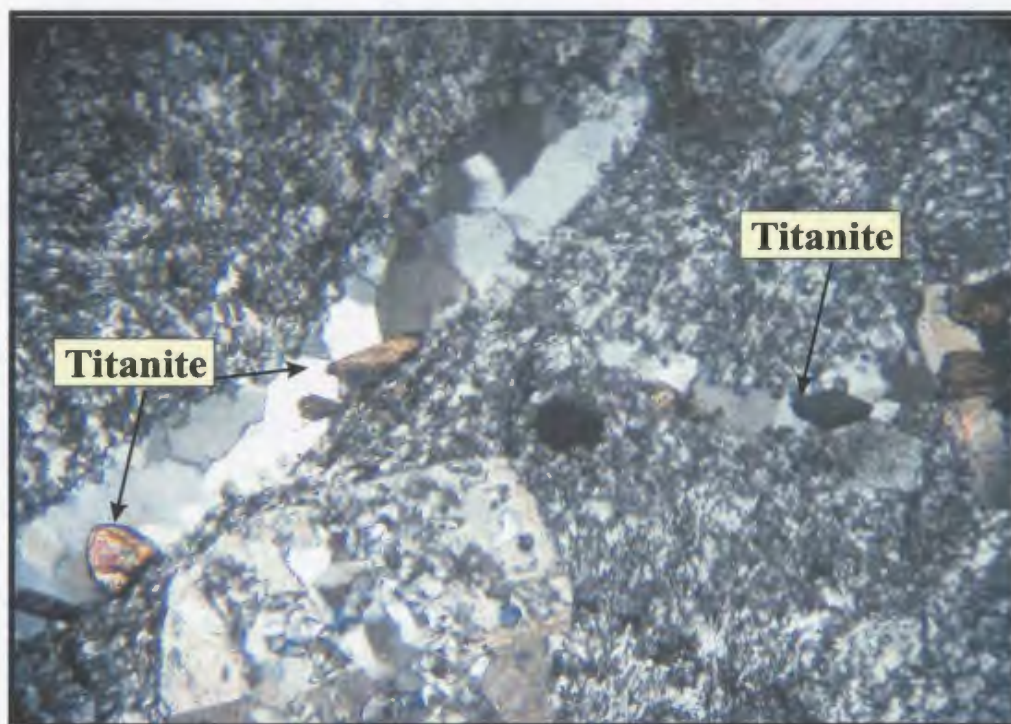
Plate 2-24: Photomicrograph of dark purple, crystal-bearing, ash-flow tuff crosscut by a titanite-bearing quartz vein. Note the patchy quartz developed within the feldspar phenocryst (Bergs prospect; GS-02-008; XPL; FOV ~6mm).

CONTACT RELATIONSHIPS:

The only exposed contact with this unit is an unconformable contact with Cambrian basal conglomerates that lie immediately to the north. All other contacts in this area are unexposed and are therefore inferred. The main distinguishing feature separating this ash-flow from Unit 13 (see below) is its color. Therefore it is probable that the two units are actually the same and/or represent two separate ash-flows from within the same sequence.

2.3.4.5 Unit 13: Dark Purple, Crystal-bearing, Ash-flow Tuff

LITHOLOGY and PETROGRAPHY

This unit is exposed immediately to the east of Unit 12 (Figure 2-5), and is distinguished mainly by the dark purple hematite-rich groundmass that supports pale white 1-2mm crystal and/or crystal fragments. Unit 13 is the main host to the low-sulphidation veins and associated breccias within the Bergs prospect (see section 5.3). Very localized mobilization of hematite occurs adjacent to the veins in some areas, causing the host rock to have a pale pink coloration.

In thin section, the unit contains sub- to euhedral plagioclase crystals, up to 4mm in length, with Carlsbad, albite and periclinal twins. Contained within these crystals are small irregular blebs of quartz that are interpreted to represent re-melting of the crystals. The feldspar crystals are supported within a fine-grained groundmass, which locally displays undulatory extinction and minor coarser-grained anhedral quartz crystals. Sericite has a patchy distribution throughout the rock. The groundmass is crosscut by hematite-filled hairline fractures and late crystalline quartz veins that contain fine-grained

euhedral crystals of titanite (Plate 2-24). The main form of alteration seen within this unit is silicification, this alteration is similar to that seen elsewhere in the vicinity of low-sulphidation veins.

CONTACT RELATIONSHIPS:

This unit is unconformably overlain by Cambrian basal conglomerates to the north, and is in tectonic contact with mafic volcanic rocks of the MVS to the east. All other contacts within the area are unexposed and are therefore inferred.

2.3.4.6 Unit 14: Massive, Poorly-Sorted, Lithic-rich, Breccia

LITHOLOGY

Unit 14 contains sub-rounded to subangular fragments ranging in size from less than a centimeter to approximately half a meter in diameter. These fragments weather proud from the poorly sorted, pale-weathering, nondescript matrix. The unit contains pale white sub- to euhedral feldspar crystals within a brecciated, sericite-altered, dark purple groundmass that supports angular, poorly sorted fragments of silica–hematite vein material. This unit is unique to the Bergs prospect and contains fragments of auriferous, banded chalcedonic silica up to 50cm in diameter and gold grades up to 7.75g/t (O'Brien and Sparkes, 2004; Figure 2-5; Plate 2-25). The unit is interpreted to represent a surficial hydrothermal eruption breccia (Hedenquist, personal communication, 2003; O'Brien and Sparkes, 2004).

Plate 2-25: Hydrothermal eruption breccia containing fragments of chalcedonic silica-hematite vein material; clasts locally contain up to 7.75g/t Au (Bergs prospect; Photo courtesy of Sean O'Brien, Department of Natural Resources, Geological Survey).
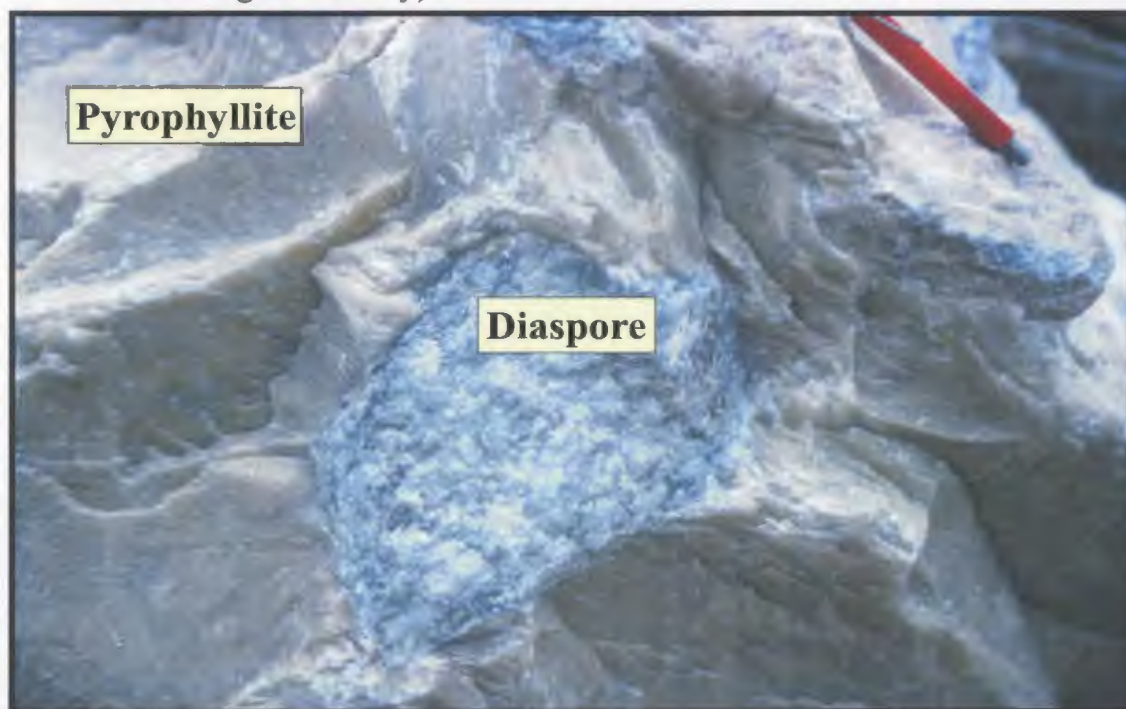
Plate 2-26: Pyrophyllite-diaspore alteration from within the Oval Pit mine (Unit 17; Photo courtesy of Sean O'Brien, Department of Natural Resources, Geological Survey).

CONTACT RELATIONSHIPS:

No contacts between this unit and surrounding rocks were observed. The abundance of tuff material incorporated into the breccia, and the close spatial association between the tuff and breccia, suggests that Unit 14 overlies Unit 13.

2.3.4.7 Unit 15: Mafic Volcanic/Intrusive Rocks

LITHOLOGY

This unit designates all mafic rocks within the study area that do not have a spatial association with the Wych Hazel Pond Complex (WHPC; see below). These mafic volcanic rocks are distributed throughout the map area as small discrete outliers of an unknown age (Figure 2-5). These volcanic rocks are generally fine-grained, dark brown- to dark green-weathering, moderately to weakly magnetic and locally amygdaloidal, with quartz infilling the amygdales. In the area of the Bergs and Steep Nap prospects, the mafic volcanic rocks contain millimeter-scale dark green phenocrysts, now pseudomorphed by chlorite (Figure 2-5). Near the vicinity of the Oval Pit mine, the unit contains phenocrysts of subhedral, pale white plagioclase and locally developed trachytic texture (1-2mm plagioclase laths). In the region of Minerals Road Intersection, this unit has a fragmental appearance, and consists of primarily mafic fragments within a dark purple fine-grained groundmass.

The main forms of alteration within this unit are chloritization and pyritization, with the latter locally causing a rusty coloration. In the area of the Bergs prospect this unit is host to banded chalcedonic silica veins and associated breccias. The main vein observed within the mafic unit contains <150ppb gold, while directly along strike to the

east, an exposure of what is assumed to be part of the same vein hosted within the crystal-rich tuff, contains gold-grades up to 600ppb. This relationship suggests that the host rock may have some influence on the gold-grades within the low-sulphidation veins. The mafic unit locally develops a moderate to strong cleavage adjacent to large-scale faults.

CONTACT RELATIONSHIPS:

All contacts with this unit are tectonic or unexposed, and since it is seen to host low-sulphidation veins, which are not observed cutting the WHPC, they are thought to be older. Consequently, these mafic volcanic rocks are assigned to the MVS.

2.3.4.8 Unit 16: Sericite–Silica ± Pyrite Alteration

This unit is localized along structural boundaries and large-scale shear zones and may or may not be related to the development of the main high-sulphidation alteration (Figure 2-5). The unit has a white-, pale yellow-, or green-weathering depending on the proportion of silica to sericite, with localized patches of rusty weathering, fine-grained, disseminated pyrite. Unit 16 locally affects Unit 3 in the region around the Steep Nap prospect, and frequently contains a strong penetrative fabric. In the region of the Steep Nap prospect, the alteration is also associated with very anomalous gold concentrations (samples OB-97-233, -433; 12 and 21ppb Au respectively).

2.3.4.9 Unit 17: Silica–Sericite–Pyrite–Pyrophyllite–Diaspore–Rutile Alteration

This alteration is associated with the main high-sulphidation occurrence at the Oval Pit mine (Figure 2-5). The very intense alteration results from extreme acid leaching of the host rock (see O'Brien *et al.,* 2001b GAC guide book; O'Brien *et al.,* 1998), often

obliterating any primary textures (Plate 2-26). Within the Oval Pit mine, rare primary

textures are still observed, these textures include flow banding and eutaxitic foliation;

such textures are the only clues to the actual host of the high-sulphidation alteration. This

alteration is fault bounded along the western margin and is in gradational contact with

Units 9 and 10 to the east and north. The gradational contact is drawn where primary

textures can no longer be distinguished from the alteration. This alteration is relatively

barren with respect to gold mineralization, however there are discrete zones with

anomalous gold values (<150ppb Au; OB-03-24, -25, -26), which is often associated with

gossan zones (a more detailed discussion of the alteration can be found in Vhay, J.S.,

1937; Papezik *et al.*, 1978; Hayes, J., 1996; O'Brien *et al.*, 1998, 2001).

2.3.4.10 Unit 18: Hematite–Chlorite-rich Hydrothermal Breccia

This breccia unit is best developed immediately north of the Oval Pit mine, where

it cuts the advanced argillic alteration (Figure 2-5). This unit contains a dark purple

hematite-rich matrix that supports pale white sub-rounded to subangular silicified

material less than 2-4cm in diameter. Similar style breccias are observed cutting the

advanced argillic alteration elsewhere in the field area, however these occur on a much

smaller scale and thus have not been shown in Map 1. Locally these smaller-scale breccia

bodies are associated with anomalous gold values (<1g/t; Hayes and O'Driscoll, 1989a).

In the vicinity of Mine Hill a well-developed chlorite-rich hydrothermal breccia is host to

minor gold mineralization and crosscuts silica-altered flow-banded rhyolite interpreted to

be related to the White Mountain Volcanic Suite (Plate 2-27). This breccia is somewhat

different from the hematite-rich breccia due to the abundance of chlorite and the higher

Plate 2-27: Chlorite-rich hydrothermal breccia with abundant silica-altered flow-banded rhyolite fragments. Breccia locally contains patches of disseminated pyrite within the matrix; this pyrite is locally associated with up to 1.8g/t Au (Mine Hill area).

Plate 2-28: Basal conglomerate of Unit 19a (Oval Pit mine). Note the detrital silica-sericite alteration (white clasts) within the pebble conglomerate.

concentrations of gold (up to 1.8g/t; O'Brien *et al.*, 1998; G. Sparkes, 2002). It is currently unknown whether this breccia is associated with the formation of the high-sulphidation system.

2.3.5 Wych Hazel Pond Complex (WHPC; Unit 19)

The WHPC of O'Brien *et al.* (2001a), designates those marine sedimentary rocks that are intercalated with mafic volcanic rocks within the study area. These sedimentary rocks mainly occur in the eastern map region, and locally unconformably overlie rocks affected by advanced argillic alteration. Rocks of the WHPC are locally intruded by syn-sedimentary feldspar porphyries in the northeastern portion of the map area, these porphyries represent the youngest preserved magmatism with the region.

2.3.5.1 Unit 19a: Lower Wych Hazel Pond Complex

LITHOLOGY

Most of the lower WHPC is exposed in the Oval Pit mine (Figure 2-6) and contains red, thin- to medium-bedded siltstone interbedded with medium- to thick-bedded, medium- to coarse-grained, red sandstone (Plate 2-28). Both the sandstone and the siltstone are inter-layered with pebbly, muddy-sandy to sandy oligomict conglomerate beds. Stratigraphically lower sections of the conglomerate are dominated by sub-rounded clasts exhibiting silica–sericite ± pyrophyllite alteration, but pass upwards into beds dominated by subangular to sub-rounded clasts of purple flow-banded rhyolite. The siltstone and sandstone units are interbedded with several pale yellow- to green-weathering, chloritic–sericitic, massive to medium bedded, pumiceous, lithic and ash-

Wych Hazel Pond Complex

(22) Fowlers Road Porphyry
-plagioclase-phyric, pale grey to green
aphanitic rhyolite; unit associated with local
development of a blocky peperite

(20) Amygdaloidal Basalt/
Hyaloclastite
-moderately vesicular, locally amygdaloidal
and pillowed dark purple basalt; associated
with hyaloclastite containing irregularly
shaped, dark purple basalt fragments in a
dark grey-green, fine-grained matrix

(19b) Upper Wych Hazel Pond
Complex
-thin- to medium-parallel-bedded,
moderately to strongly siliceous, pale to dark
green siltstone and interbedded medium- to
coarse-grained, subarkosic sandstone;
siltstone commonly displays soft sediment
deformation

(19a) Lower Wych Hazel Pond
Complex
-thin- to medium-bedded red siltstone;
locally interbedded with medium- to coarse-
grained red sandstone, pebbly conglomerate
and pale yellow, chloritic-sericitic, massive
pumiceous tuff

Figure 2-6: Distribution of the Wych Hazel Pond Complex, extracted from Map 1.

73

flow tuffs; one of these tuffs overlies the basal boulder conglomerate of the WHPC in the Oval Pit mine. Exposures of the basal boulder conglomerate within the mine displays silica–sericite–pyrite alteration and contain clasts of pre-incorporated alteration. The lower contact with the volcanic rocks is concealed by the late alteration (Plate 2-29).

Elsewhere, a rusty brown-weathering, poorly-sorted, pebble to boulder breccia overlies silica-altered rhyolite and granite belonging to the White Mountain Volcanic Suite and White Hills Intrusive Suite, respectively. This unit contains sub-rounded to angular clasts of silica altered flow-banded rhyolite, up to 50cm in diameter, and medium-grained granite. The relationship between the basal brown breccia and the interbedded pebble conglomerate, red siltstone, and very coarse-grained red sandstone, is unknown, however it is interpreted that the brown-weathering unit underlies the red siltstone and sandstone unit. In areas east of the Oval Pit mine the sandstone displays a buff brown-weathering, pale green on fresh surfaces, with abundant blocks and sub-rounded fragments of both felsic and mafic material (Plate 2-30).

This unit has been affected by only minor alteration as mentioned above. This alteration is only seen in the area of the Oval Pit mine and is attributed to the same alteration responsible for the development of the advanced argillic alteration as discussed in more detail below.

CONTACT RELATIONSHIPS:

Defined unconformable contacts exist between Unit 19a and Unit 1, Unit 2, Unit 9, and with intrusive rocks of the White Hills and Holyrood intrusive suites.
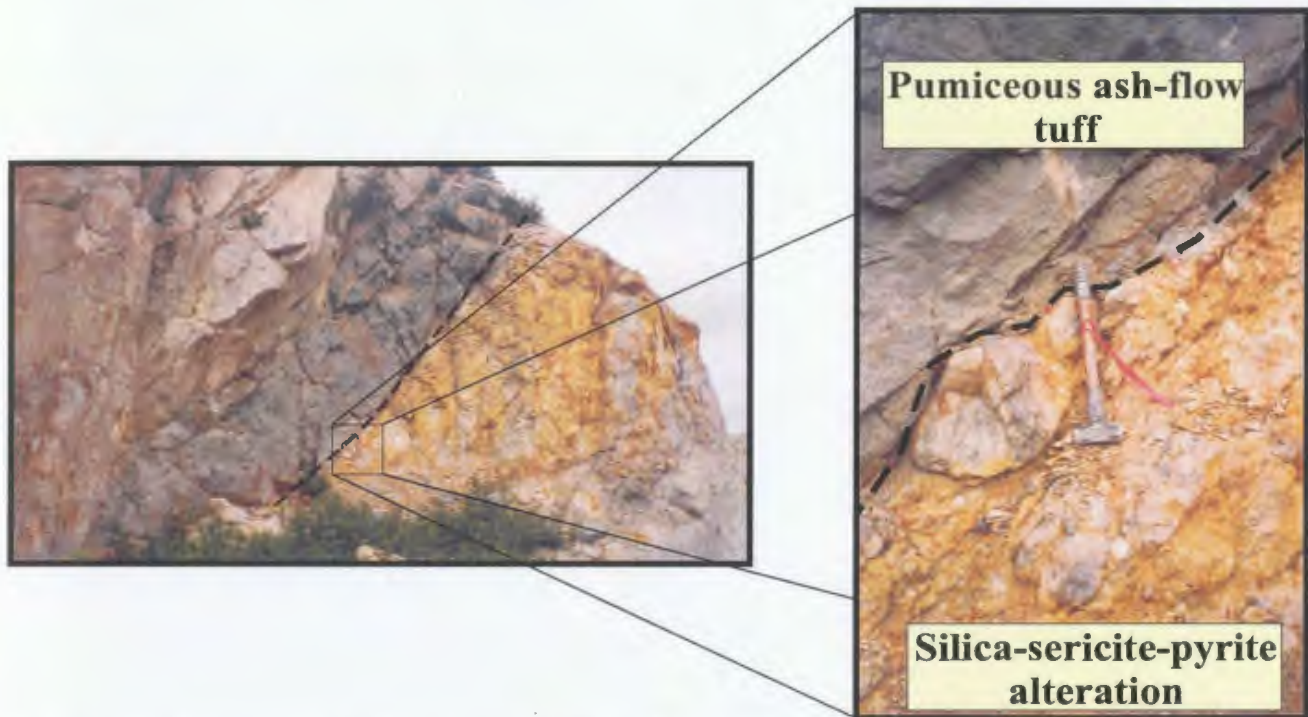
Plate 2-29: Pumiceous tuff overlying altered basal conglomerate (Oval Pit mine). The overlying tuff was sampled for geochronological study.

Plate 2-30: Basal conglomerate of Unit 19a (Manuels River). Note the unit contains detritus of both felsic and mafic volcanic material.

Nowhere is this unit seen to contain low-sulphidation veins, however it is crosscut by numerous mafic dykes that in turn have a close spatial relationship with the development of the low-sulphidation veins.

2.3.5.2 Unit 19b: Upper Wych Hazel Pond Complex

LITHOLOGY

Sedimentary rocks of the upper WHPC are predominantly confined to large, moderately to steeply southwesterly-dipping, down-dropped fault blocks in the eastern, central and southern areas of the region (Figure 2-6). This unit consists of thin to medium, light-weathering beds of pale to dark green, moderately to strongly siliceous siltstone. Bedding within the unit typically alternates between light and dark green, with local development of slump folds and microfaulting (Plate 2-31). The siltstone is often interbedded with dark green, thick to massive bedded, medium- to very coarse-grained subarkose sandstone. In the eastern section of the map area, the sandstone is very coarse-grained to granular, and locally contains large fragments of fine-grained, pale green, chert.

No evidence of any hydrothermal alteration is seen within the upper portions of WHPC. Thermal metamorphism is developed adjacent to basaltic dykes that intrude the unit. The sedimentary rocks also display thermal alteration adjacent to a feldspar porphyry unit (see below), which intrudes the upper WHPC in the area of Fowlers Road (Figure 2-6). Minor folding is evident within the unit, as observed within the Oval Pit mine, where the sedimentary rocks are preserved in a shallow southwest plunging syncline (O'Brien *et al.,* 1998).

Plate 2-31: Soft sediment deformation within Unit 19b (Oval Pit mine; Photo courtesy of
Sean O'Brien, Department of Natural Resources, Geological Survey).

Chlorite filled
amygdale
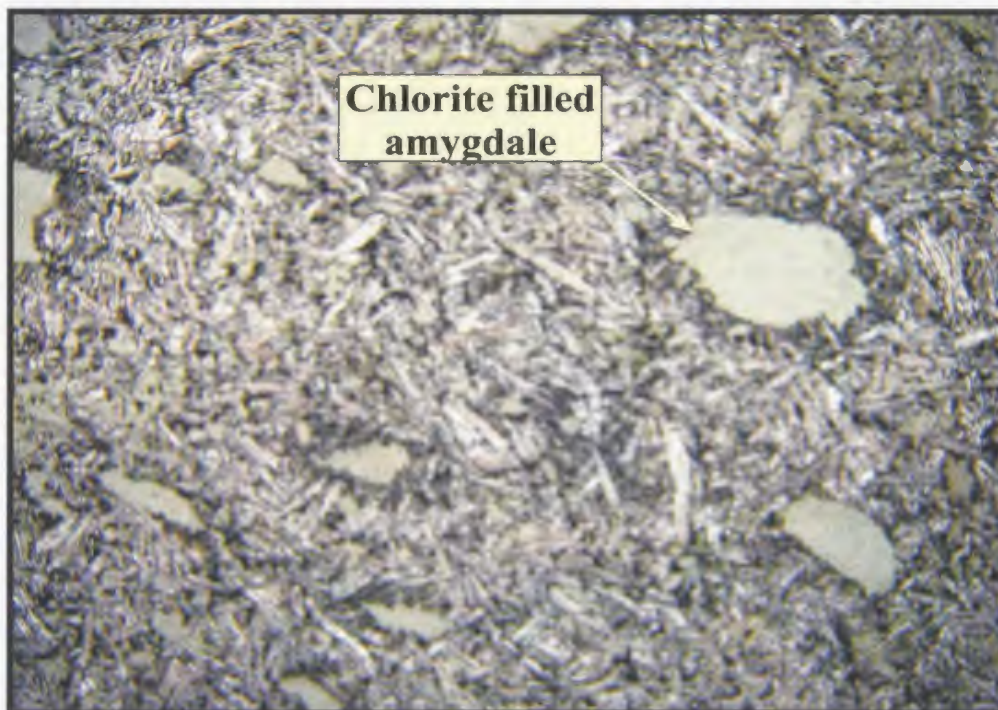
Plate 2-32: Photomicrograph of a basaltic dyke. The large crystals of chlorite appear to be
infilling amygdales (Manuels Off Ramp; OB-01-002; PPL; FOV ~4.5mm).

CONTACT RELATIONSHIPS

The upper WHPC is in gradational contact with the lower red siltstone and sandstone unit. In several areas, the upper WHPC is interbedded with mafic flows (see below), which are possibly fed by the mafic dyke swarm that locally crosscuts the sedimentary rocks (see below); all other contacts are tectonic or inferred.

2.3.5.3 Unit 20: Mafic dykes

LITHOLOGY and PETROGRAPHY

These dykes are observed throughout the study area and predominantly trend between NNW to ENE. They are dark green, fine-grained, brown-weathering, strongly to weakly magnetic and basaltic in composition. Locally the dykes contain subhedral phenocrysts, now pseudomorphed by dark green chlorite, within a pale green aphanitic groundmass. Overall widths of the dykes range from less than 20cm up to 8 meters. In thin section, the dykes display a well-developed trachytic texture with fine-grained, "ragged", subhedral plagioclase; very fine-grained anhedral epidote and opaque minerals make up most of the groundmass (Plate 2-32). Chlorite is interstitial to the above-mentioned minerals. Coarser-grained ragged chlorite may be replacing a primary mafic mineral(s) and minor sericite alteration is evident within the plagioclase. Some dykes are amygdaloidal, with chlorite, epidote and rare carbonate infilling the amygdales.

CONTACT RELATIONSHIPS

Contacts between basaltic dykes and adjacent wall rock are sharp and rarely tectonic. Local field relationships show that dykes in the area of the Oval Pit mine are post-alteration and pre-deformation (Plate 2-33).
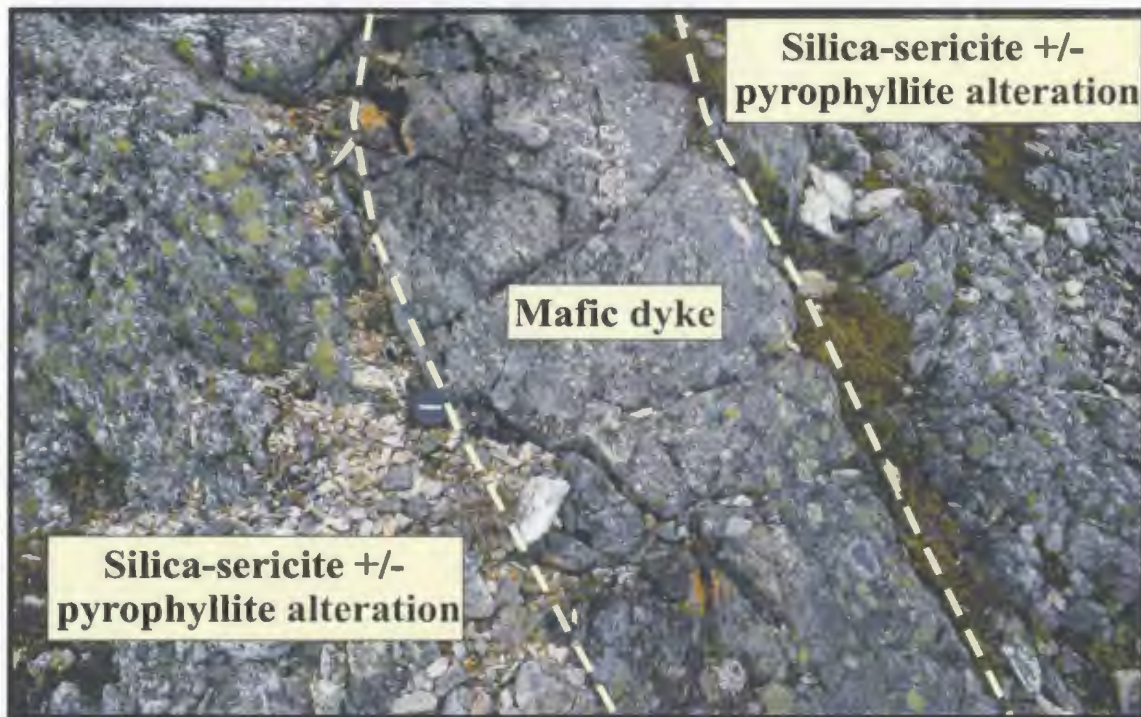
Plate 2-33: Pre-deformation, post-alteration mafic dyke crosscutting silica-sericite alteration (Mine Hill). Note lens cap near center of photo for scale (Photo courtesy of Sean O'Brien, Department of Natural Resources, Geological Survey).

Plate 2-34: Amygdaloidal pillow basalt developed within the Unit 19b (Manuels Off Ramp).

2.3.5.4 Unit 21: Amygdaloidal Basalt/ Hyaloclastite

LITHOLOGY and PETROGRAPHY

Dominantly confined to the northeastern portion of the field area, this unit represents the youngest period of mafic volcanism preserved in the map area (Figure 2-6). The basalt is moderately vesicular and locally amygdaloidal, rarely pillowed (with pillow forms up to 1.5m in diameter), dark purple, and fine-grained (Plate 2-34). Locally a trachytic texture with 1-2mm plagioclase laths is developed. This basalt is weak to moderately magnetic and locally plagioclase-phyric, with fractures locally infilled with light green epidote. In thin section, this unit consists of sub- to anhedral fine-grained plagioclase laths with intersertal anhedral fine-grained epidote, chlorite and opaque minerals (Plate 2-35). Locally quartz, carbonate and epidote infill amygdales.

The associated hyaloclastite contains irregularly shaped dark purple basaltic fragments, locally showing chilled margins and plastic deformation. These fragments are supported by a dark grey-green, fine-grained matrix containing fine-grained, subhedral crystals, now pseudomorphed by chlorite (Plate 2-36). Fragments range in size from less than 1cm up to 10 cm in diameter and in many cases are vesicular. Locally the unit contains light green, subangular cherty fragments (1-3cm in diameter).

CONTACT RELATIONSHIPS

The amygdaloidal basalt and hyaloclastite are interbedded with the sedimentary rocks of the WHPC. Locally the sedimentary rocks are thermally metamorphosed and have a dark red coloration in areas adjacent to basaltic flows.
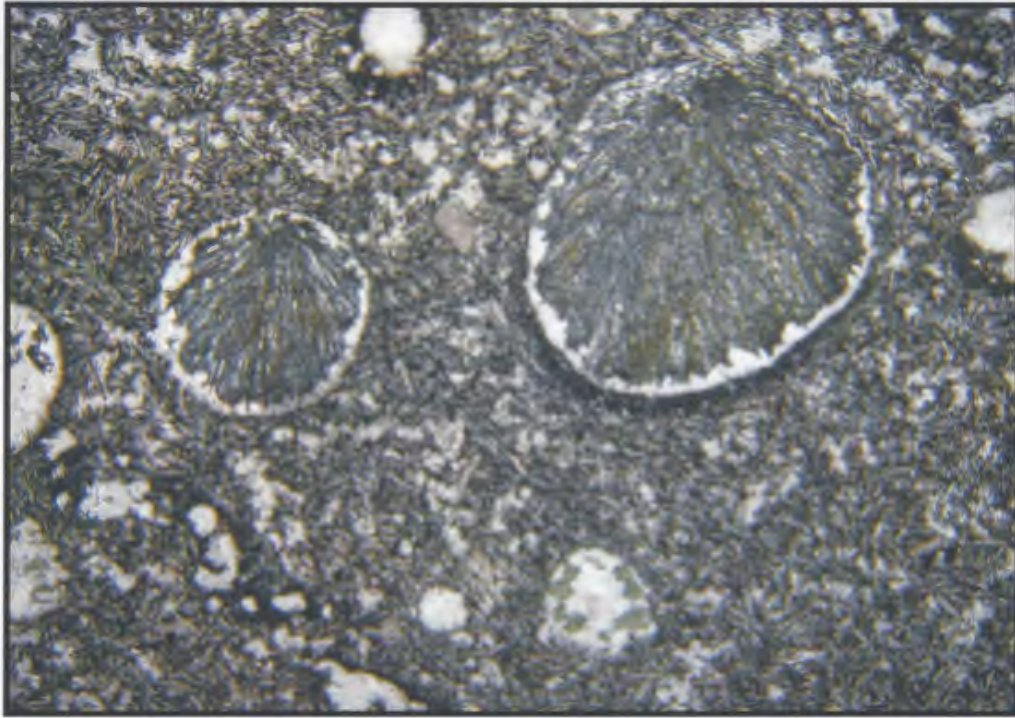
Plate 2-35: Photomicrograph of amygdaloidal basalt with quartz and epidote infilling the amygdales (Manuels Off Ramp; OB-01-003; XPL; FOV ~4.5mm).

Plate 2-36: Hyaloclastite associated with the amygdaloidal basalt (Manuels Off Ramp; Photo courtesy of Sean O'Brien, Department of Natural Resources, Geological Survey).

2.3.5.5 Unit 22: Fowlers Road Porphyry

LITHOLOGY

Restricted to the area east of the Manuels River, this unit represents the youngest known intrusive event within the field area (Figure 2-6). Unit 22 consists of 1-2mm white feldspar crystals within a pale green to grey aphanitic groundmass. This unit is brecciated at the contact with the upper WHPC, where it forms a blocky peperite consisting of angular porphyry fragments supported within a matrix of thermally altered, fine-grained siltstone (Plate 2-37). As a result of the alteration, the sediment is dark purple adjacent to the intrusion. The association of brecciation and thermal metamorphism of the sediment suggests that it was still unconsolidated at the time the porphyry intruded. Alteration within this unit is rare, very weak and consists of disseminated pyrite and minor silicification.

CONTACT RELATIONSHIPS

The feldspar porphyry is intrusive into with both the upper WHPC and associated mafic volcanic rocks. Most contacts, however, are tectonic or unexposed.

2.3.6 Conception Group (Unit 23)

Confined to the region east of Fowlers Brook Fault (Map 1; Figure 2-7), the Conception Group consists of medium to thick bedded, fine-grained, very siliceous, pale green- to grey-weathering siltstone. This unit is juxtaposed against Unit 19b by the Fowlers Brook Fault, which is sub-parallel to the regional-scale Topsail Fault.
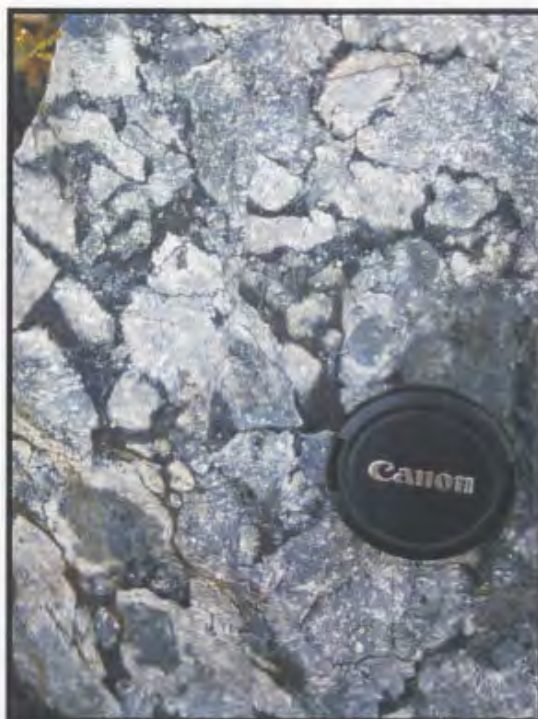
Plate 2-37: Brecciated Fowlers Road porphyry, note the interstitial dark red, thermally altered, fine-grained siltstone matrix (Fowlers Road).

Plate 2-38: Foliated, advanced argillic detritus in basal Cambrian age conglomerate (Bergs prospect; Photo courtesy of Sean O'Brien, Department of Natural Resources, Geological Survey).
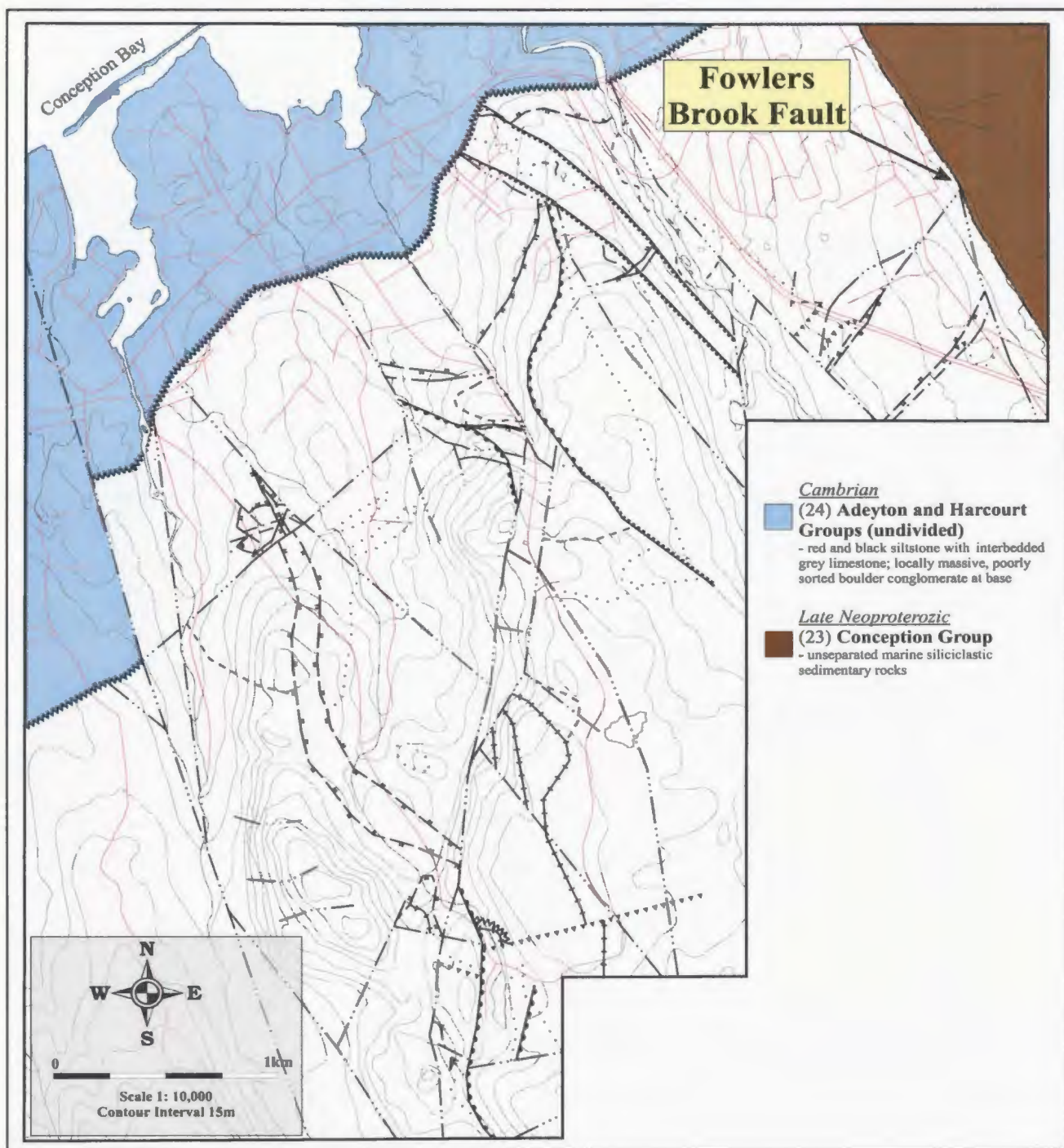
Figure 2-7: Distribution of the Conception Group and Cambrian age sediments, extracted from Map 1.

The relationship between the sedimentary rocks of the WHPC and the Conception Group is uncertain, as the term WHPC has only been applied to those sedimentary rocks west of the Topsail Fault. These two formations are very similar, with the main distinguishing feature being the close temporal association between sedimentary rocks of the WHPC and mafic volcanism.

PALEOZOIC ROCKS

2.3.7 Cambrian Sedimentary Rocks: Adeyton and Harcourt Groups (Unit 24)

Occupying the lower elevations in the northwestern regions of the map area are Cambrian age basal conglomerates consisting of a massive, poorly-sorted, locally clast-supported, boulder conglomerate, overlain by shale and limestone successions (Figure 2-7). Detritus within this unit ranges from sub-rounded to rounded clasts of volcanic and sedimentary material. Locally the conglomerate contains clasts of silica–sericite alteration, banded epithermal vein, and foliated sericite–silica alteration (Plate 2-38). The conglomerate is conformably overlain by grey-green and red thin- to medium-bedded siltstones, and locally interbedded limestone successions. This succession has been described in detail by McCartney (1967) and many others; and is not included in this study.

The Cambrian succession is the youngest unit preserved within the field area, and unconformably overlies many of the major geological units (See McCartney, 1967; O'Brien, 2002). This unit also provides the minimum age limit for the low-sulphidation vein system as well as the post mineral deformation with the region (see below).

2.4 STRUCTURAL GEOLOGY

This section provides a brief description of some of the main structural elements within the study area including bedding measurements from the WHPC, cleavage development within the region, prominent faulting, and the main orientations of hydrothermal veins within the Bergs and Steep Nap prospects. The work establishes a broad framework for low-sulphidation veins and high-sulphidation alteration in this area, provides first order observations of the main geologic features and provides some insight into the overall tectonic development and distribution of the geologic units.

2.4.1 Structural Data

BEDDING MEASURMENTS

Within the map area, four main fault-bounded blocks of the WHPC provide well-exposed bedding surfaces and sufficient exposure to obtain a general orientation of the isolated blocks. In the northern region of the map area, large packages of sedimentary rock belonging to the WHPC are located east of the Manuels River and in the area of Black Mountain, adjacent to the Steep Nap prospect. These two down-dropped fault blocks predominantly consist of thin- to medium-bedded siltstone of Unit 19b and produce a well-developed cluster of polar points for bedding measurements (Figure 2-8A and B). The two fault blocks of sedimentary rock located further south also show good clustering of polar points for bedding measurements, but these blocks also appear to have been affected by minor folding (Figure 2-8C and D). Regional scale folding is evident

86

A

--- 17%

--- 34%
(Max. = 50.00%)

Mean Principal Orientation = 131/69S
Mean Resultant dir'n = 222-65
Mean Resultant length = 0.89
(Variance = 0.11)
Calculated. girdle: 036/76E
Calculated beta axis: 306-14

B

--- 7%

--- 14%

--- 28%
(Max. = 37.50%)

Mean Principal Orientation = 088/33S
Mean Resultant dir'n = 178-34
Mean Resultant length = 0.95
(Variance = 0.05)
Calculated. girdle: 214/69W
Calculated beta axis: 124-21

C

--- 8%

--- 16%

--- 32%
(Max. = 35.71%)

Mean Principal Orientation = 131/44S
Mean Resultant dir'n = 221-38
Mean Resultant length = 0.81
(Variance = 0.19)
Calculated. girdle: 262/57N
Calculated beta axis: 172-33

D

--- 10%

--- 20%

--- 40%
(Max. = 45.45%)

Mean Principal Orientation = 052/34S
Mean Resultant dir'n = 131-32
Mean Resultant length = 0.87
(Variance = 0.13)
Calculated. girdle: 201/60W
Calculated beta axis: 111-30

Figure 2-8: Compilation on equal area projections (lower hemisphere) of bedding measurements from fault-bound blocks of the Wych Hazel Pond Complex (A= sediment in northeastern map region; B= sediment from Steep Nap region; C= sediment located within the Oval Pit mine; D= sediment from south of White Mountain).

87

from the polar points that define small girdles distal to the main cluster of data points. More directly observable evidence of folding of the WHPC is exposed at the Oval Pit mine, where the sequence is preserved in a shallow southwest plunging syncline (Map 1; O'Brien *et al.,* 1998).

The sedimentary rocks located within the Oval Pit mine have a calculated girdle of 262/57 N, whereas those immediately south of White Mountain have a calculated girdle of 201/60 W. Different structural orientations are observed between the various fault blocks and their corresponding position in relation to the Mine Hill Shear Zone (MHSZ). From the stereo plots it is evident that the mean principal orientation of bedding measurements for the Black Mountain and White Mountain regions (west of the MHSZ) are very similar, 088/33 S and 052/34 S, respectively. In contrast, the two packages of sedimentary rock located on the opposite side of the MHSZ have different mean principal orientations. The sedimentary rock within the Oval Pit mine has a mean orientation of 131/44 S, while the sediment east of the Manuels River has a mean principal orientation of 149/41 W. This contrast across the MHSZ suggest that the sedimentary rocks on opposing sides of the structure either 1) underwent different deformation, or 2) were once a part of a single synclinorium that has since been dismantled by later deformation. Figure 2-9 contains the data from all four sedimentary blocks from which it is interpreted that the polar points define a crude small girdle with an orientation of 264/59 N and a beta-axis of 174-31. This data is consistent with the sedimentary sequence once forming a shallow southward-plunging syncline, which has since been broken apart by extensional faulting.
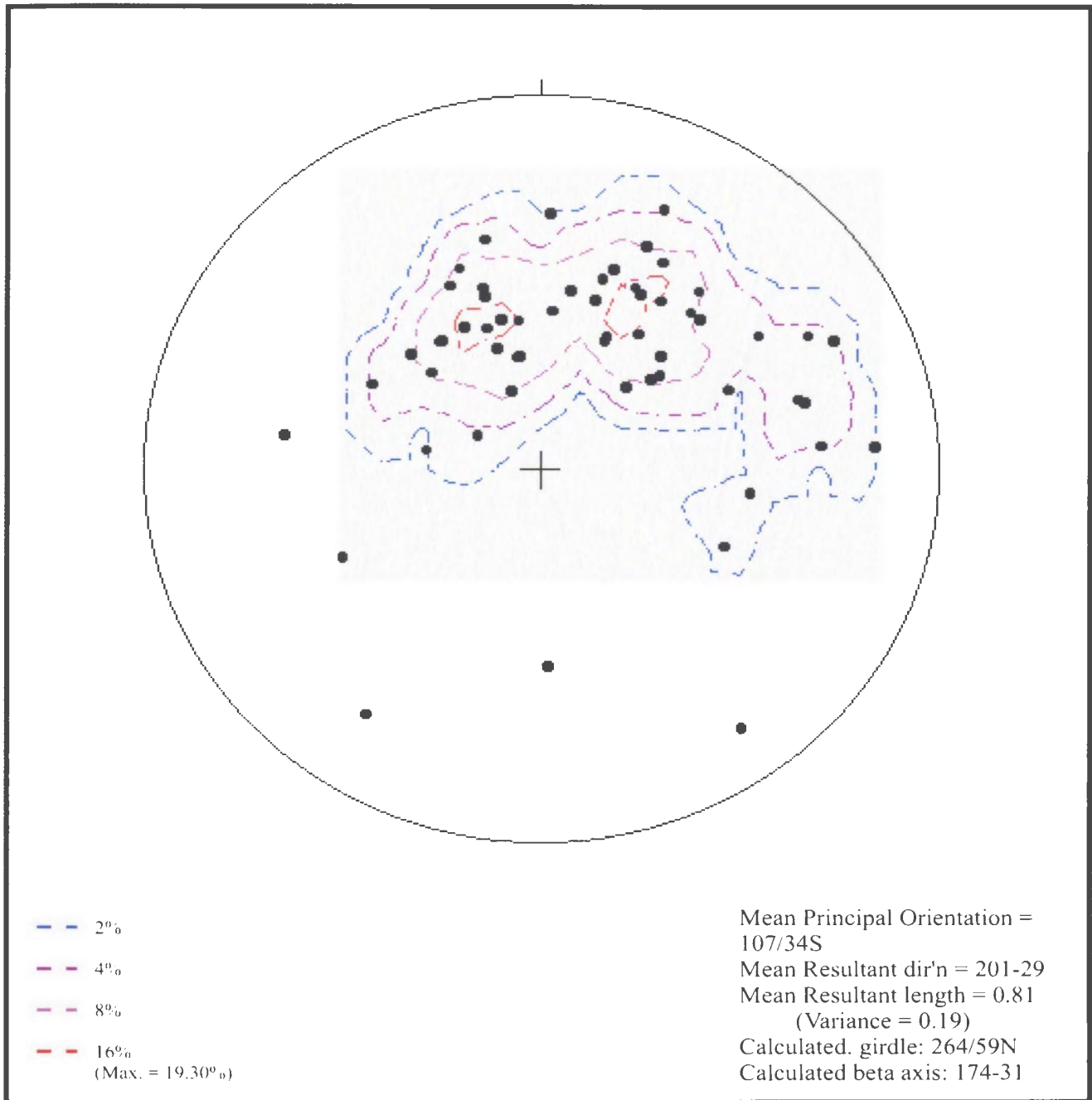
Figure 2-9: Compilation on equal area projections (lower hemisphere) of bedding measurements from all four fault-bounded blocks of the Wych Hazel Pond Complex. Note the combined measurements define a small girdle with an orientation of 264/59 N and a corresponding beta axis of 174-31.

2.4.2 Cleavage Measurements

Cleavage in the region around the Oval Pit mine and White Mountain is dominated by an E-W to NE-SW orientation (Figure 2-10A and B). A similar E-W cleavage is observed in the Steep Nap prospect, however in this area there is also a minor NW-SE trending cleavage (Figure 2-10C). In the northern portion of the field area, the E-W to NE-SW cleavage is again predominant but is also accompanied by a second, moderately dipping, N-S trending cleavage (Figure 2-10D). The above data indicates that the NE-SW cleavage is the main fabric developed within the field area and is locally associated with a locally developed NW-SE to N-S cleavage. The predominant cleavage may be associated with the N-S directed folding that is assumed to have affected the sedimentary rocks of the WHPC. The E-W directed cleavage possibly represents a later event associated with the development of the E-W oriented reverse-fault that offsets the alteration within the Oval Pit mine.

2.4.3 Fault Measurements

Figure 2-11 is a polar plot of fault measurements within the area of the Oval Pit mine, Steep Nap and the Bergs-Manuels Off Ramp regions. The field area contains a predominant E-W to NE-SW fault orientation, however at in the region of the Steep Nap prospect there is also a minor NNW-SSE trending fault set. More northern regions of the study area display N-S oriented faulting, which is the main regional trend and which may be related to the larger-scale Topsail Fault (Figure 2-11C).
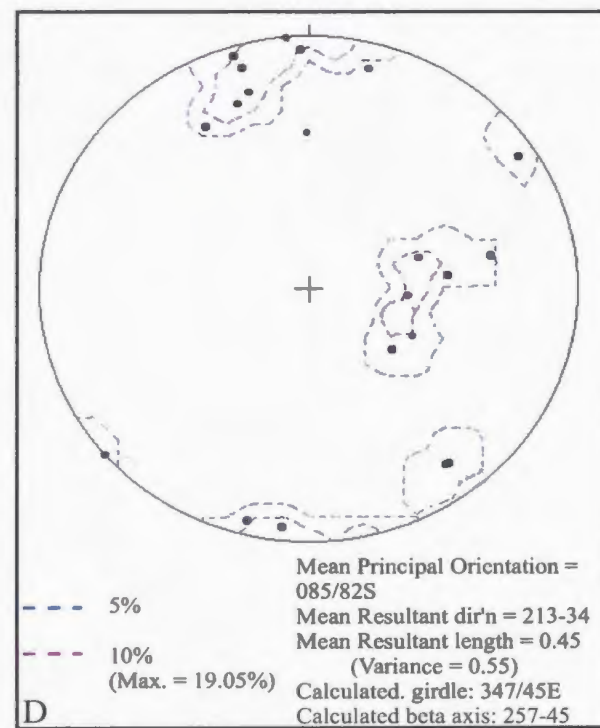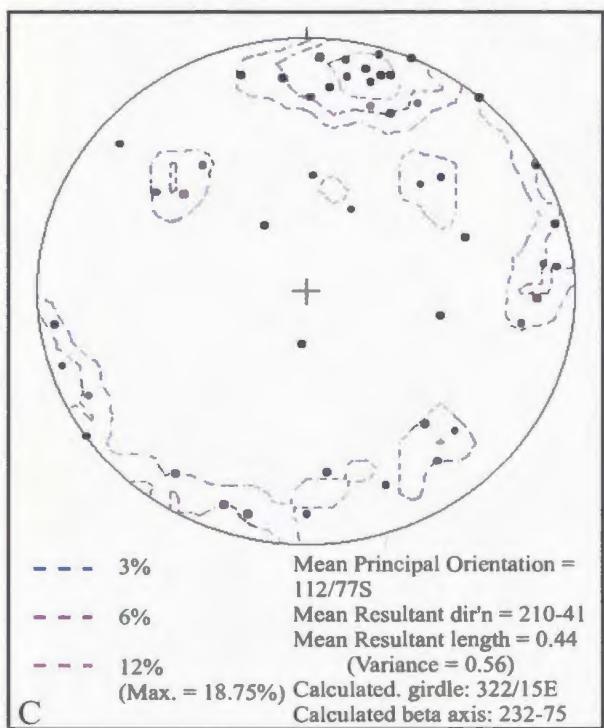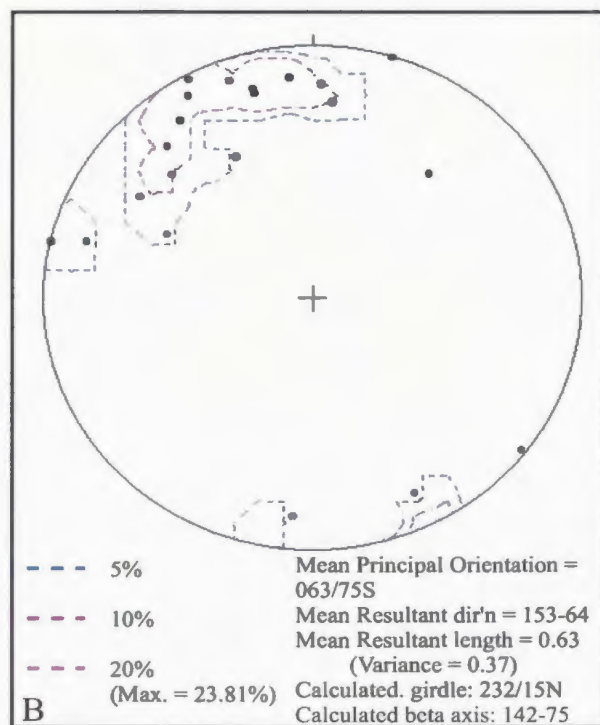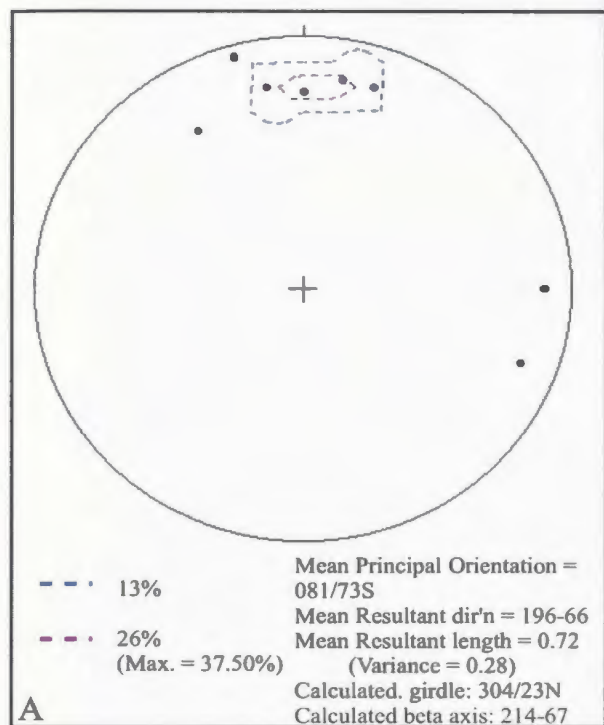
Figure 2-10: Compilation on equal area projections (lower hemisphere) of cleavage measurements from selected areas (A= White Mountain region; B= Oval Pit mine region; C= Black Mountain region; D= Bergs and Manuels Off-Ramp region).

Panel A legend:

- - - 15%

- - - 30%
(Max. = 42.86%)

Mean Principal Orientation
099/60S
Mean Resultant dir'n = 181-43
Mean Resultant length = 0.59
(Variance = 0.41)
Calculated. girdle: 302 32N
Calculated beta axis: 212-58

Panel B legend:

- - - 5%

- - - 10%
(Max. = 19.05%)

Mean Principal Orientation =
082/85S
Mean Resultant dir'n = 224-57
Mean Resultant length = 0.42
(Variance = 0.58)
Calculated. girdle: 332 15E
Calculated beta axis: 242-75

Panel C legend:

- - - 4%

- - - 8%
(Max. = 14.29%)

Mean Principal Orientation =
020/67E
Mean Resultant dir'n = 094-49
Mean Resultant length = 0.56
(Variance = 0.44)
Calculated. girdle: 216/24W
Calculated beta axis: 126-66

Figure 2-11: Compilation on equal area projections (lower hemisphere) of measured faults within the study area (A= Oval Pit mine region; B= Steep Nap region; C= Bergs and Manuels Off Ramp region).

2.4.4 Structural Elements in Relation to Low-Sulphidation Veins

In general, no regional structures are known to control the development of low-sulphidation veins. Locally developed structures may have some influence on their distribution, since in the region of the Steep Nap prospect, a NW-SE-trending sericite–silica shear zone appears to parallel the orientation of the main low-sulphidation vein. Figure 2-12 and 2-13 displays the principle orientation of hydrothermal veins in the Bergs and Steep Nap prospects, respectively. Vein orientations within the Bergs prospect are much more variable in comparison to veining within the Steep Nap prospect. This may be the result of the Bergs prospect forming at shallower crustal levels, which is also supported by the presence of surficial hydrothermal eruption breccias. The Steep Nap vein system displays a distinct NW-SE trend, which may have resulted from the influence of higher lithostatic pressures. Within the Steep Nap prospect the NW-SE trending faults may control the main development of the low-sulphidation veins, however this faulting is assumed to be a splay off the main N-S trending MHSZ. In the Bergs prospect the vein orientations do not show a good correlation with other structural measurements, however this veining is assumed to lie between two NW-SE trending shear zones. As a result the vein array observed at Bergs may represent extension occurring between the two shear zones.
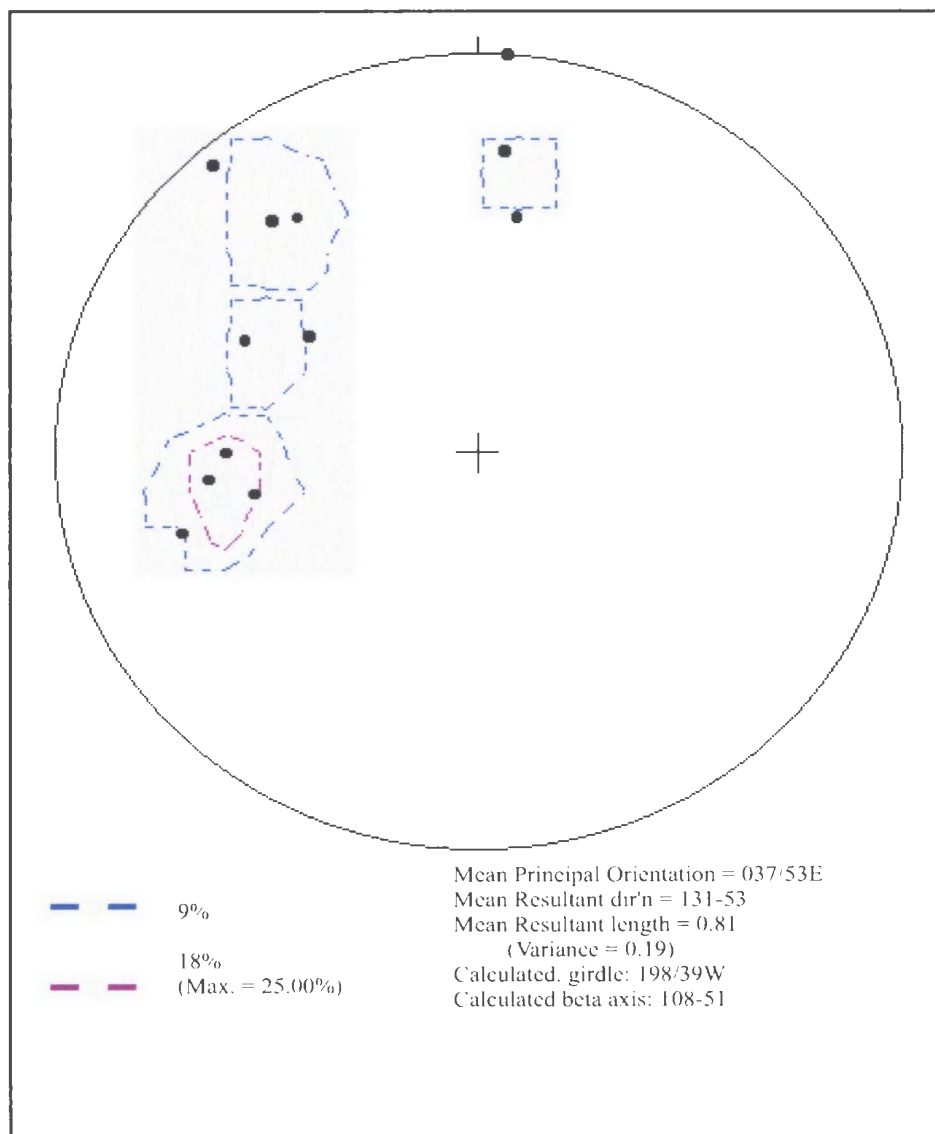
Figure 2-12: Compilation on equal area projections (lower hemisphere) of low-sulphidation-style veins (Bergs prospect).
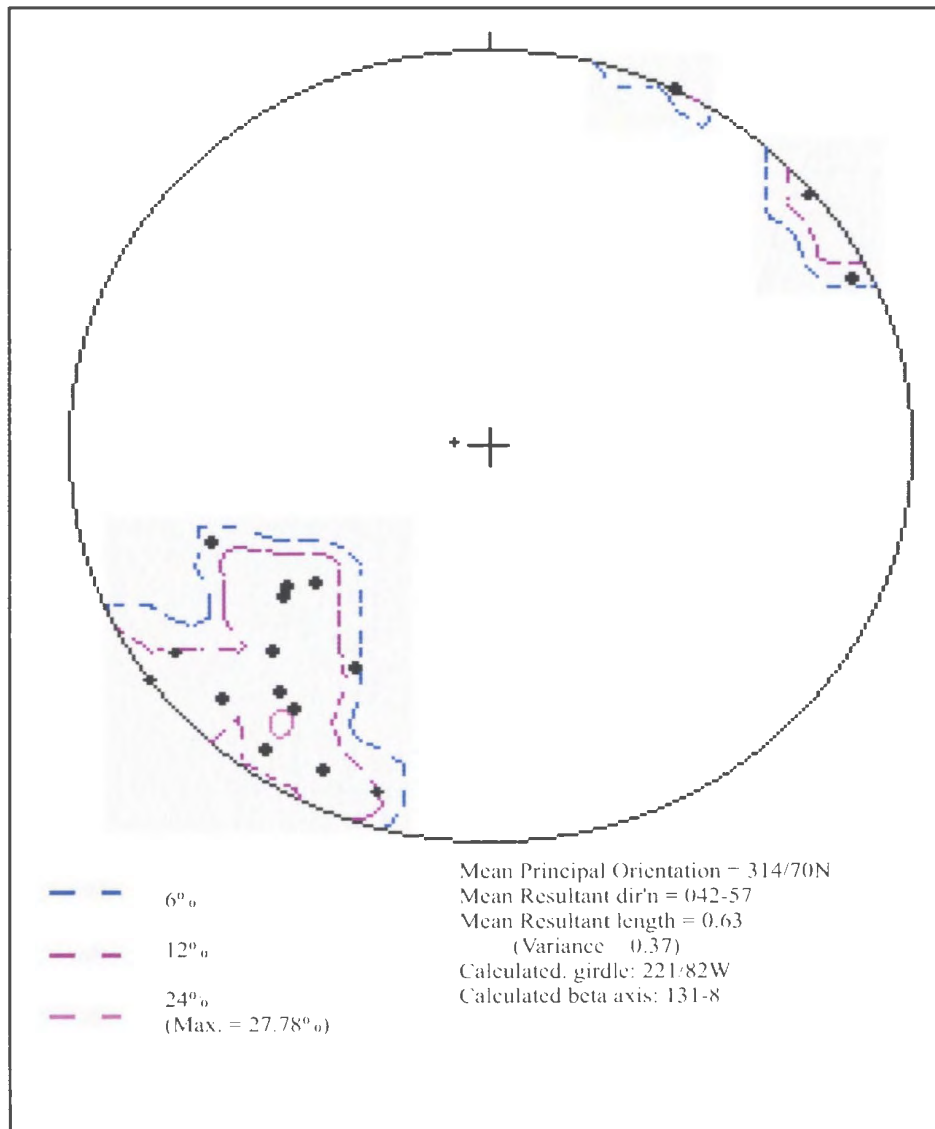
Figure 2-13: Compilation on equal area projections (lower hemisphere) of low-sulphidation-style veins (Steep Nap prospect).

2.5 SUMMARY

The area outlined in this study is dominated by Late Neoproterozoic plutonic rocks of the Holyrood and White Hills intrusive suites and volcanic arc-related rocks belonging to the previously unseparated Manuels Volcanic Suite. The area also includes siliciclastic sedimentary rocks of the Wych Hazel Pond Complex, which unconformably overlie the arc-related sequence. All of the above-mentioned units are unconformably overlain by a shallow dipping Paleozoic platformal cover.

The oldest known volcanic rocks within the region are included within the White Mountain Volcanic Suite. This unit is locally intruded by the White Hills Intrusive Suite, and develops chlorite-epidote alteration adjacent to these intrusions. Units contained within the WMVS host well-preserved examples of Late Neoproterozoic colloform-crustiform, chalcedonic silica, adularia ± calcite, low-sulphidation veins and associated breccias. Volcaniclastic rocks associated with this unit contain clasts of older plutonic and porphyritic material, presumably derived from pre-620 Ma intrusions. This unit may possibly represent the eastern equivalent of the Hawk Hills Tuff, which is intruded by the Holyrood Intrusive Suite along the western and southern margins of the Holyrood Horst (O'Brien *et al.,* 2000).

Intrusive rocks belonging to the Holyrood and White Hills intrusive suites occupy all of the western portions of the map area. Rocks of the WHIS include monzonite, granite and quartz–feldspar porphyry; these units contain numerous rafts of the WMVS, which are presumed to represent roof pendants of the overlying volcanic carapace. The presence of numerous volcanic rafts and the common development of tuffisite brecciation

suggest relatively shallow levels of erosion within the WHIS. Granitic units of the WHIS display localized silica–sericite–pyrite alteration but at this juncture, it is unclear whether this alteration is syn-magmatic or related to the younger epithermal alteration. Locally Unit 7 is affected by centimeter-scale banded chalcedonic silica veinlets of a low-sulphidation affinity. The boundary between the intrusive rocks of the WHIS and the younger volcanic rocks of the MVS is defined by the Mine Hill Shear Zone (MHSZ).

Volcanic rocks of the MVS include flow-banded rhyolite and lesser amounts of rhyolitic ash-flow tuff, volcaniclastic and mafic volcanic rocks. This volcanic sequence is host to the main pyrophyllite-diaspore deposit located at the Oval Pit mine and is the predominant host to the regionally developed advanced argillic alteration. The MVS is also host to auriferous low-sulphidation veins and associated breccias in the vicinity of Farmer's Field and the Bergs prospects. Data from the Bergs prospect show that the felsic volcanic rocks of the MVS hosting low-sulphidation veins generally contain higher Au-grades in comparison to veins hosted within mafic volcanic rocks.

Siliciclastic sedimentary rocks of the WHPC unconformably overlie and contain detrital alteration from the underlying high-sulphidation system in the vicinity of the Oval Pit mine. This unit consists of lower red siltstone with interbedded red sandstone and conglomerate, overlain by interbedded green siltstone, sandstones and associated mafic volcanic rocks. Unit 19a locally contains interbedded ash-flow tuffs layers, which locally overlie a silica–sericite–pyrite altered basal conglomerate at the base of the WHPC in the Oval Pit mine. The alteration affecting the base of this sedimentary sequence is attributed to late stage advance argillic alteration.

In eastern sections of the map region, feldspar porphyry intrudes green, thin-bedded siltstone of Unit 19b, representing the youngest magmatic event exposed within the study area. Upon intrusion into the sedimentary sequence the porphyry becomes brecciated, which suggests the sediment was unconsolidated at the time of intrusion. Unconformably overlying deformed rocks of the Holyrood and White Hills intrusive suites, MVS and WHPC are relatively undeformed Cambrian age basal conglomerates and overlying siltstone and limestone succession.

Volcanic and plutonic rocks within the region commonly lack strong penetrative fabrics, aside from shear zones developed within areas of advanced argillic alteration. Clasts within the conglomerates of Unit 19a lack the development of pre-incorporated fabrics, which implies that the deformation within the region post-dates the deposition of the sedimentary sequence. Foliated clasts of advanced argillic alteration within undeformed Cambrian basal conglomerates in the Bergs prospect provide an upper limit for the development of the deformation (O'Brien, 2002). Bedding measurements from the WHPC suggest that the unit underwent folding and subsequent extensional faulting to produce the present day distribution of the sedimentary units. This data is consistent with deformation observed within sedimentary sequences east of the Topsail Fault (King, 1990). The folding is interpreted to be associated with the development of the predominant NW-SE trending cleavage, which is present throughout the study area.

NW-SE trending normal faults are predominant throughout the region and are interpreted to coincide with a period of arc collapse. Locally NW-SE trending faults occur near the development of meter-scale low-sulphidation veins in the vicinity of the

Steep Nap prospect. These NW-trending structures are interpreted to be associated with the larger-scale MHSZ, which shares a close spatial relationship with the development of advanced argillic alteration on a regional scale. Low-sulphidation veins in the Steep Nap prospect display a predominant NW-trend, suggesting that the veins are influenced by some structural control. In the area of the Bergs prospect the low-sulphidation veins display more varied orientations. The variable vein orientations at Bergs, along with the presence of a surficial eruption breccia (O'Brien and Sparkes, 2004; Hedenquist, personal communication, 2004), suggest that the low-sulphidation veins formed at relatively shallow crustal levels in comparison to the Steep Nap prospect. The effects of folding on the distribution and orientation of the low-sulphidation veins is still not fully understood. Current structural data on vein orientations is very localized and does not indicate folding of the vein systems. However field evidence does indicate that the veins have undergone post-mineral deformation.

CHAPTER 3:

GEOCHEMICAL ANALYSIS

3.1 INTRODUCTION

Whole rock geochemical analyses were carried out on all major igneous rock units within the study area. This geochemistry was used to compare relatively unaltered samples with intensely altered samples of the same unit. Such comparisons demonstrate that the trace-elements Nb, Zr, Ti, Dy, and Y, from the ICP-ES dataset, remain immobile when subjected to extreme acid leaching in advanced argillic alteration zones within the map region. These immobile trace elements are used to characterize the volcanic units listed in Chapter 2, as well as demonstrate the various tectonic environments in which these units formed. Mobile elements are used with caution in characterizing the plutonic rocks within the region and immobile trace-element plots further support the interpretations of the units based on potentially mobile elements. The major-elements are used to show the effects and intensities of the various types of alteration. Due to the mobilization of several major-elements, trace-element chemistry is relied upon for the classification of major lithological units where possible.

In the following discussion, volcanic and plutonic rock units are described in groups of similar age and/or lithology. Primitive mantle-normalized spider diagrams (normalizing values from Sun and McDonough, 1989) are used in the comparison of various volcanic and plutonic units. These plots prove very useful in separating older and younger felsic intrusions, but are ineffective in segregating the older and younger

100

volcanic units. In addition to normative diagrams, X-Y plots and ternary diagrams are employed to test relationships between various units of the WHIS, as well as the chemical similarities between plutonic rocks of the White Hills and Holyrood intrusive suites. Select samples of both the volcanic and plutonic units were analyzed for rare earth-elements (REE) and other high field strength (HFS) trace-elements in order to try and identify chemical differences between the various units using elements not contained within the ICP-ES dataset. This REE data provided very little information that could not already be ascertained from the ICP-ES data.

In the region of the Steep Nap prospect, a detailed chemical analysis of wall rock adjacent to the main low-sulphidation vein demonstrates mobilization of light rare earth-elements (LREE). This mobility of the LREE was tested by three separate techniques, ICP-ES, ICP-MS and XRF. Each technique produced somewhat different concentrations for particular elements, however all techniques supported the depletion of LREE adjacent to the low-sulphidation vein.

As noted previously a large amount of geochemical data already existed for this area prior to the current study (unpublished data of S.J. O'Brien, Geological Survey of Newfoundland). Data presented below includes that collected by the author as well as existing unpublished Geological Survey data. Sample numbers beginning with "OB" are from the previously unpublished Geological Survey data, while samples beginning with "GS" were collected during this study. Samples analyzed by ICP-ES from the previous work and the current study were submitted to the same laboratory, located at the Department of Natural Resources Geochemical Laboratory, St. John's, Newfoundland.

Note, for ease of reference, tables of the geochemical data referred to in the following discussion are presented at the end of the chapter.

3.2 MAJOR-ELEMENT GEOCHEMISTRY

INTRODUCTION:

It is common knowledge that most major-elements are mobile when subjected to hydrothermal alteration. Although some samples in the following descriptions have undergone hydrothermal alteration, the units as a whole still retain major-element compositions similar to relatively fresh rock, except for a few anomalous intensely altered samples. Tables containing accuracy and precision data for the major-elements are in Appendix B.

3.2.1 Unit 5: Holyrood Intrusive Suite (HIS)

Exposures of the Holyrood Granite occupy the southwestern corner of the map area, however this portion of the granite is only a small part of a more regionally extensive granitic intrusion. The following description includes geochemical samples collected outside of the study area (provided by S. O'Brien of the Newfoundland Geological Survey) and therefore provides a more accurate geochemical average for the Holyrood Granite. From the analyses of thirty-eight samples the SiO_2 values range between 70.20 to 77.58 wt.% (mean 73.80 wt.%), K_2O between 3.07 to 5.07 wt.% (mean 4.00 wt.%), Na_2O between 3.58 to 4.71 wt.% (mean 4.08 wt.%), CaO between 0.06 to 1.79 wt.% (mean 0.68 wt.%), Al_2O_3 between 11.82 to 15.31 wt.% (mean 13.62 wt.%) and TiO_2 between 0.011 to 0.256 wt.% (mean 0.16 wt.%; Table 3-1). Despite weak propylitic

102

alteration (see section 2.3.2.1), the variation in the major-element geochemistry is attributed to regional primary compositional differences over the large area covered by the sampling.

3.2.2 White Hills Intrusive Suite (WHIS)

DATA:

Unit 6, Unit 7 and Unit 8 of the WHIS all share a close spatial and geochemical association. Three samples were analyzed from Unit 6, these samples contain SiO_2 values that range between 64.56 to 65.86 wt.% (mean 65.39 wt.%), K_2O between 2.61 to 2.78 wt.% (mean 2.68 wt.%), Na_2O between 4.07 to 5.10 wt.% (mean 4.42 wt.%), CaO between 1.66 to 3.17 wt.% (mean 2.23 wt.%), Al_2O_3 between 15.77 to 16.02 wt.% (mean 15.87 wt.%) and TiO_2 between 0.477 to 0.545 wt.% (mean 0.500 wt.%; Table 3-2). The consistency within the major-element geochemistry demonstrates that this unit is relatively unaffected by intense hydrothermal alteration.

In total twenty-five samples of granitic rock were analyzed from the WHIS. These samples have SiO_2 values ranging between 70.30 to 80.58 wt.% (mean 74.83 wt.%), K_2O between 0.17 to 5.43 wt.% (mean 3.81 wt.%), Na_2O between 1.46 to 7.27 wt.% (mean 3.78 wt.%), CaO between 0.05 to 1.05 wt.% (mean 0.33 wt.%), Al_2O_3 between 9.55 to 14.42 wt.% (mean 13.13 wt.%) and TiO_2 between 0.068 to 0.284 wt.% (mean 0.190 wt.%; Table 3-2). As noted previously, the granitic rocks of the WHIS have undergone variable amounts of hydrothermal alteration. This is indicated by SiO_2 values up to 80.58%, which is accompanied by the apparent dilution of the immobile major-elements such as Al_2O_3 and TiO_2 (e.g. sample OB-97-228). A second example of altered granite,

sample OB-97-171, contains anomalously high Na_2O (7.27 wt.%) and has been depleted in K_2O (0.17 wt.%), possibly representing some weak albite alteration.

A total of seven samples analyzed from Unit 8 contain SiO_2 values between 71.10 to 74.40 wt.% (mean 72.96 wt.%), K_2O between 3.06 to 4.03 wt.% (mean 3.44 wt.%), Na_2O between 4.05 to 5.13 wt.% (mean 4.58 wt.%), CaO between 0.36 to 1.02 wt.% (mean 0.73 wt.%), Al_2O_3 between 13.47 to 14.24 wt.% (mean 13.90 wt.%) and TiO_2 between 0.151 to 0.261 wt.% (mean 0.206 wt.%; Table 3-2). This unit is like Unit 6 in that it displays no field evidence of intense hydrothermal alteration. The lack of alteration is further supported by the uniform major-element chemistry of the porphyry unit.

INTERPRETATION:

X-Y plots of the major-element geochemistry displays an igneous trend between the less differentiated Unit 6 and the chemically similar Unit 7 and Unit 8 (Figure 3-1). The close grouping of Unit 7 and Unit 8 supports field relationships from the White Mountain region, whereby the two units become so intermixed that they could not be separated on the mapping scale employed in this project. Plutonic rocks of the WHIS display a calc-alkalic trend and plot in the peraluminous field of Maniar and Piccoli (1989; Figure 3-2 and 3-3). These major-element plots imply that Unit 7 and Unit 8 of the WHIS are differentiates from Unit 6. This is further supported by the geochronological data discussed in Chapter 4.
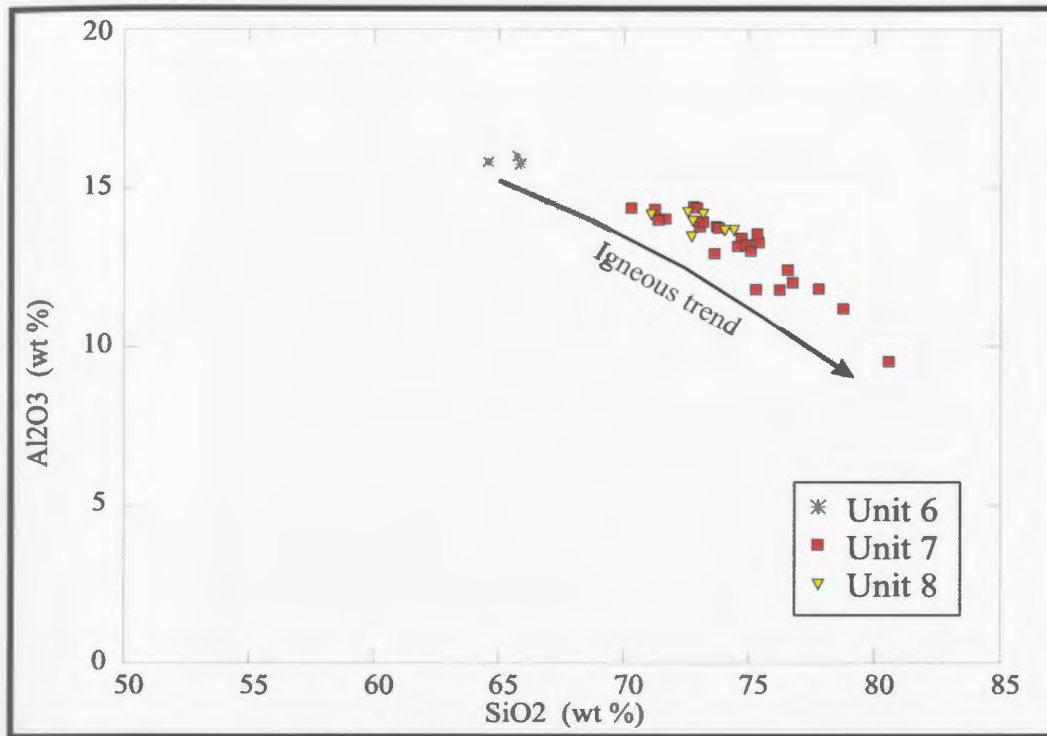
Figure 3-1: Major-element plot showing an igneous trend and increasing chemical differentiation in the White Hills Intrusive Suite. Note granite samples with anomalously high SiO₂ values are affected by alteration.
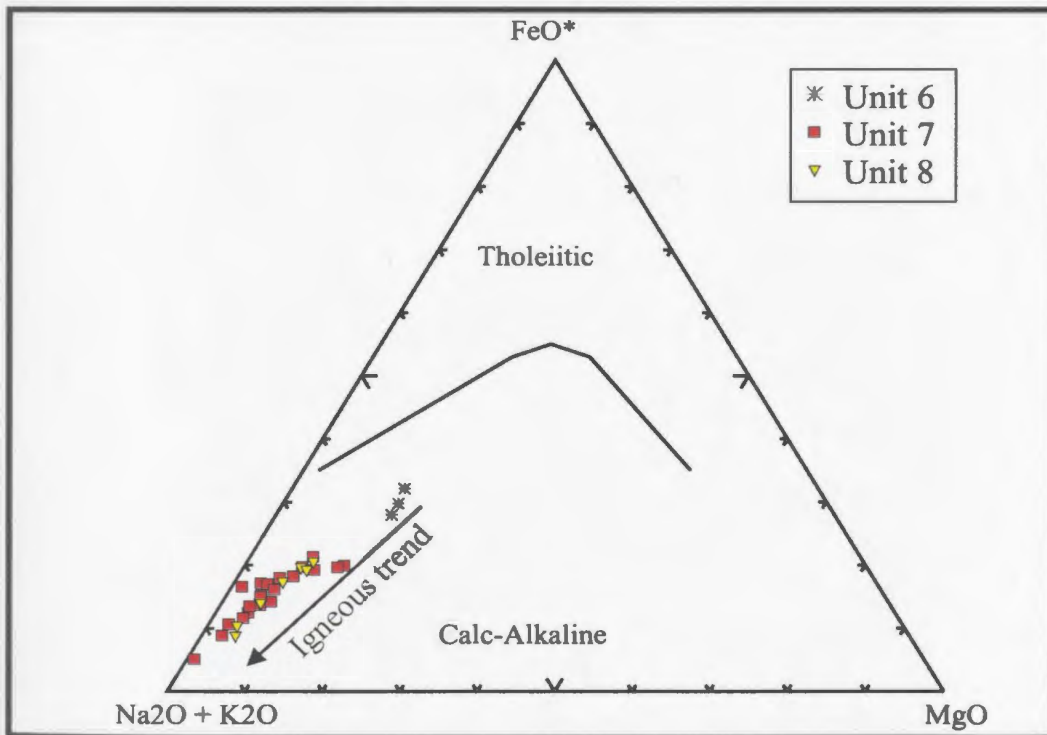
Figure 3-2: AFM diagram showing the calc-alkalic trend of the White Hills Intrusive Suite Boundary between the tholeiitic and calc-alkaline fields after Irvine and Baragar (1971).
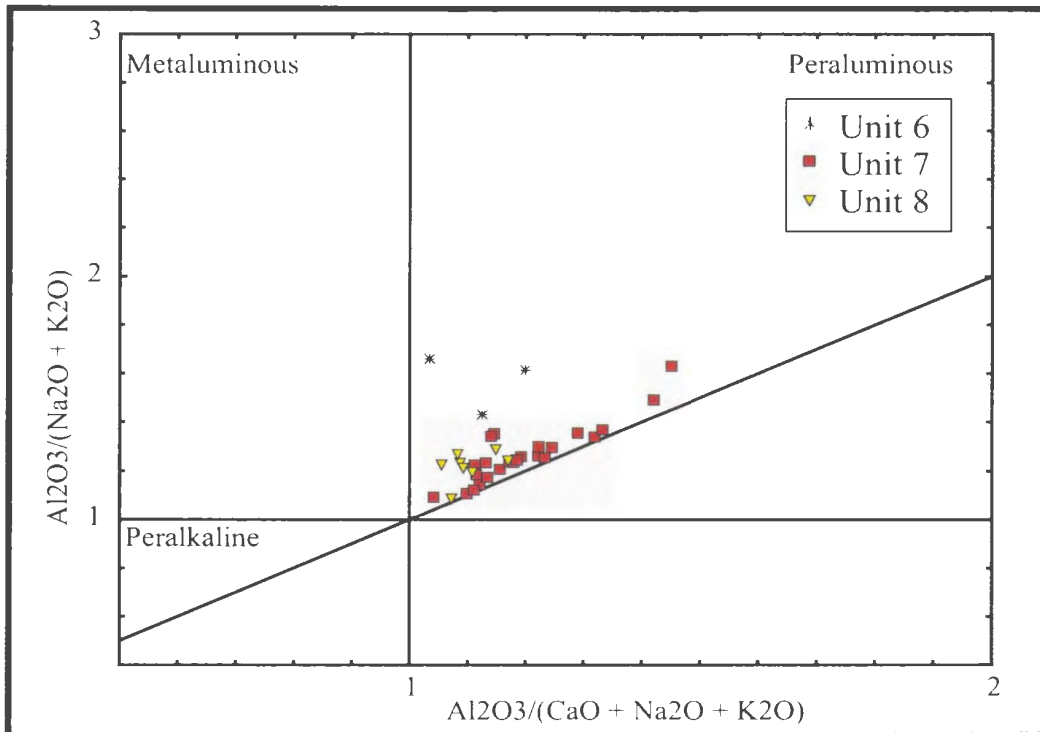
Figure 3-3: Alumina saturation diagram of Maniar and Piccoli (1989) showing the peraluminous nature of the White Hills Intrusive Suite.
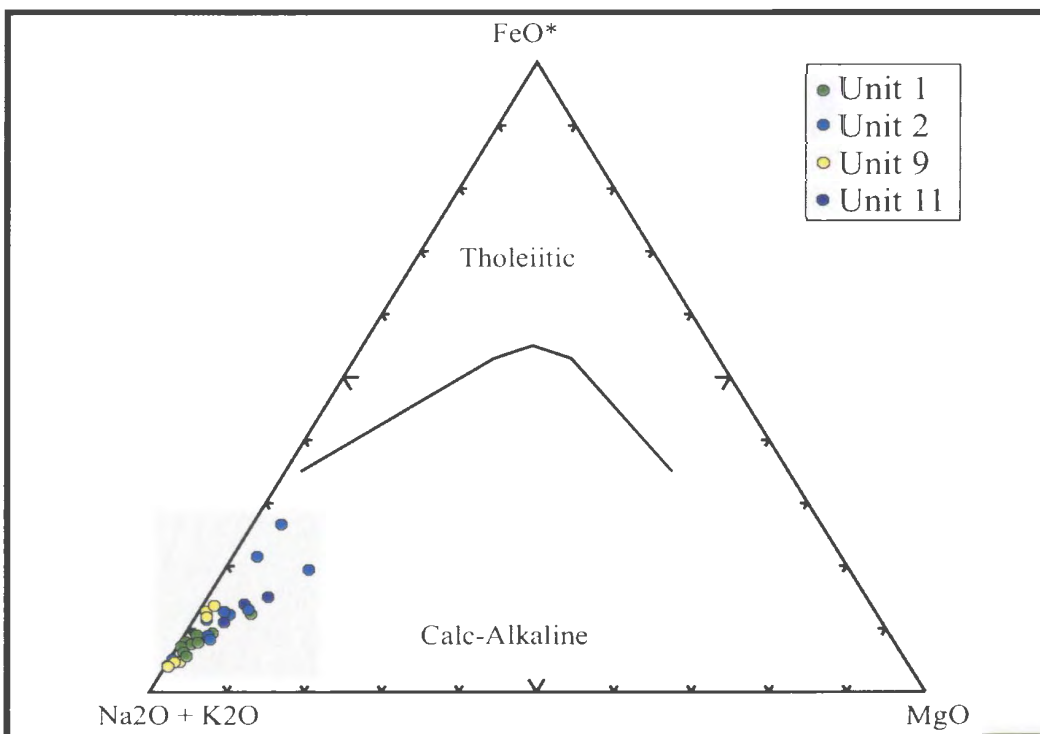
Figure 3-4: AFM diagram showing the calc-alkalic trend of rhyolite units within the field area. Note the three outliers of the Unit 2 may represent a less differentiated flow. Boundary between the tholeiitic and calc-alkaline fields after Irvine and Baragar (1971).

3.2.3 Unit 1 (Minerals Road rhyolite), Unit 2 (Manuels River rhyolite), Unit 9 (Farmer's Field rhyolite) and Unit 11 (Pale Grey-Green rhyolite).

DATA:

The lithological distinction between these groups is rarely reflected in the major-element geochemistry. In total nine geochemical samples were collected from the Unit 1, SiO_2 values range between 72.68 to 79.89 wt.% (mean 76.99 wt.%), K_2O between 0.10 to 8.80 wt.% (mean 4.94 wt.%), Na_2O between 0.72 to 6.68 wt.% (mean 3.46 wt.%), CaO between 0.08 to 0.21 wt.% (mean 0.13 wt.%), Al_2O_3 between 10.89 to 13.46 wt.% (mean 12.24 wt.%) and TiO_2 between 0.117 to 0.159 wt.% (mean 0.133 wt.%; Table 3-3). The minor silica alteration observed within this unit is reflected by the slightly elevated SiO_2 values that are common to many of the rhyolites within the region. This rhyolite is generally K_2O-rich in the area of Minerals Road Intersection, with the exception of a fine-grained aphanitic phase (sample GS-02-080). Two feldspar-phyric samples collected 1.2km to the east of Minerals Road Intersection are more sodic; this may be due to the effects of alteration within the samples or could possibly imply they are part of a different rhyolite succession (e.g. samples OB-03-18, -19).

A total of thirteen samples from Unit 2 show that SiO_2 value range between 67.87 to 81.41 wt.% (mean 75.33 wt.%), K_2O between 0.14 to 9.17 wt.% (mean 3.49 wt.%), Na_2O between 0.15 to 7.98 wt.% (mean 4.52 wt.%), CaO between 0.03 to 0.91 wt.% (mean 0.30 wt.%), Al_2O_3 between 10.50 to 16.19 wt.% (mean 13.13 wt.%) and TiO_2 between 0.087 to 0.780 wt.% (mean 0.277 wt.%; Table 3-3). The higher SiO_2 values (>78 wt. %) in this group correspond to samples taken in the vicinity of low-sulphidation

veining (samples OB-00-150, OB-01-006, OB-01-007 and GS-02-86) and may represent minor silicification in the area of the Steep Nap prospect. Several samples with somewhat lower SiO_2 values (< 70 wt.%) and slightly elevated TiO_2 and Fe_2O_3 values (samples OB-01-039, OB-01-040 and GS-03-096) may represent a less differentiated flow in the northeastern portion of the unit. The relatively unaltered samples of Unit 2 display sub-equal amounts of Na_2O and K_2O in comparison to the more K_2O -rich Unit 1. This chemical difference is attributed to the predominant aphyric nature of the Manuels River unit. Elevated K_2O in sample OB-03-061 (located near the Bergs prospect) may represent a sample of Unit 1, or it may also represent potassic alteration similar to that seen in samples from Unit 9 (e.g. sample OB-03-017; see below). No evidence of any pale to dark pink coloration, which is characteristic of potassic alteration, was noted within the sample; this supports its possible relation to Unit 1. The relatively similar geochemistry of both the Unit 1 and Unit 2 inhibit the distinction between the two units on the basis of major-elements.

Six samples analyzed from Unit 9 contain SiO_2 values ranging between 73.39 to 79.67 wt.% (mean 75.66 wt.%), K_2O between 0.15 to 9.93 wt.% (mean 5.58 wt.%), Na_2O between 0.38 to 7.61 wt.% (mean 2.99 wt.%), CaO between 0.02 to 0.27 wt.% (mean 0.14 wt.%), Al_2O_3 between 10.90 to 14.17 wt.% (mean 12.71 wt.%) and TiO_2 between 0.084 to 0.362 wt.% (mean 0.196 wt.%; Table 3-3). In the comparison of altered versus unaltered samples from the Oval Pit mine it can only be assumed that the rhyolite hosting the advanced argillic alteration is actually Unit 9. As mentioned above, localized potassic

alteration causes a pale to dark pink coloration in the rhyolite, and results in elevated K_2O

values (up to 9% K_2O; e.g. OB-03-017).

The fourth unit included within this group is Unit 11. Three samples analyzed

from this unit show SiO_2 values ranging between 69.57 to 76.48 wt.% (mean 73.45 wt.%),

K_2O between 1.34 to 4.80 wt.% (mean 2.89 wt.%), Na_2O between 4.70 to 6.20 wt.%

(mean 5.67 wt.%), CaO between 0.33 to 0.54 wt.% (mean 0.40 wt.%), Al_2O_3 between

12.63 to 15.29 wt.% (mean 14.24 wt.%) and TiO_2 between 0.267 to 0.434 wt.% (mean

0.343 wt.%; Table 3-3). Unit 11 shows no macroscopic evidence of major hydrothermal

alteration. This unit is more sodic than other rhyolite successions, which may be

attributed to the composition of the feldspar phenocrysts.

INTERPRETATION:

Data in Table 3-3 demonstrates that the rhyolites are similar chemically and show

only subtle variations in major-element geochemistry beyond that attributed to

hydrothermal alteration, although some of these rhyolites differ in age by at least 40 Ma

(see Chapter 4). This implies that similar sources for melts were tapped for upwards of 40

Ma and also indicate that the older and younger volcanic sequences are derived from

similar source regions. Plots of mobile major-elements from these units display a

significant amount of scatter, which may be related to the presence of more than one flow

within particular units (Figure 3-4) or may also be related to the effects of intense

hydrothermal alteration. However, some discrimination diagrams, such as the alumina

saturation diagram (Figure 3-5), can be utilized as both the altered and unaltered
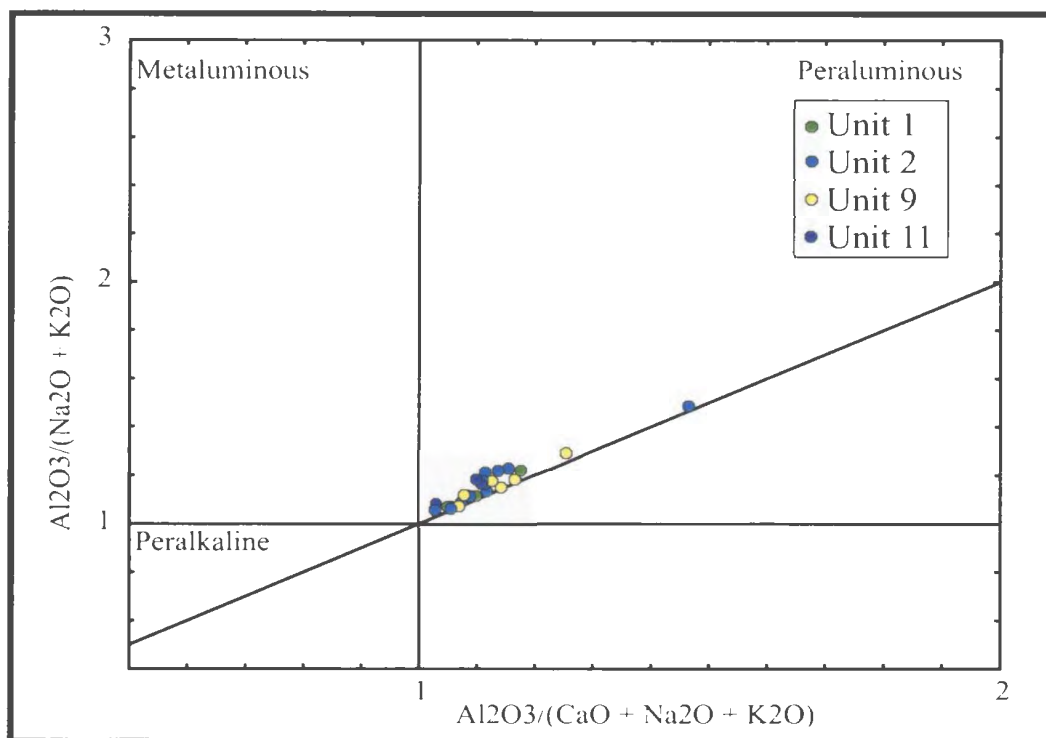
Figure 3-5: Alumina saturation diagram of Maniar and Piccoli (1989), displaying the peraluminous nature of rhyolites within the study area. Note the two outliers have both undergone moderate amounts of hydrothermal alteration.
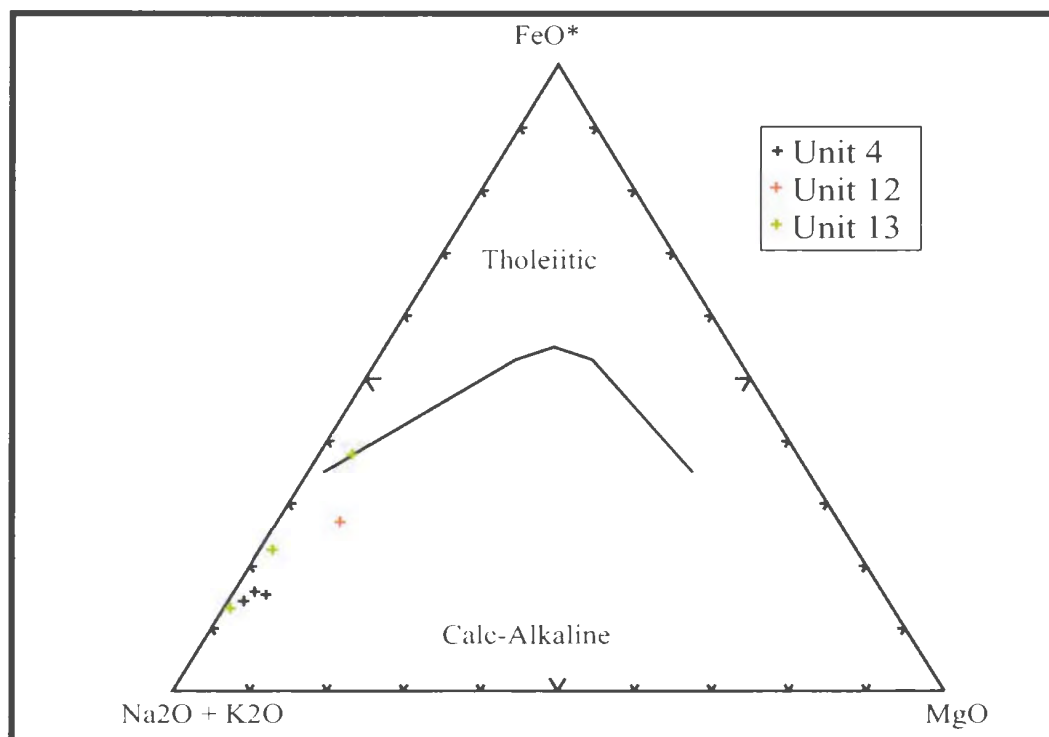
Figure 3-6: AFM diagram showing the calc-alkalic trend of ash-flow tuffs within the study area. The sample that plots on the boundary between the tholeitic-calcalkaline fields was collected adjacent to a low-sulphidation vein and has undergone hydrothermal alteration. Boundary between the tholeiitic and calc-alkaline fields after Irvine and Baragar (1971).

samples of the same unit plot within the peraluminous field, suggesting that the original units were indeed peraluminous. From this example it is evident that some major-element classification diagrams can still be used in classifying the different lithologies within the map area.

3.2.4 Ash-flow Tuffs (Units 4, 12 and 13)

DATA:

The data presented here are from three ash-flow tuff successions (Unit 4, 12 and 13), the latter two of which have a close spatial association. Two of the ash-flow tuffs have been dated (Unit 4 and 13; see Chapter 4), and differ by ca. 32 Ma. Four geochemical samples from the oldest, welded, fiamme-bearing ash-flow tuff (Unit 4), contains SiO_2 values between 72.58 to 74.22 wt.% (mean 73.60 wt.%), K_2O between 2.88 to 3.59 wt.% (mean 3.15 wt.%), Na_2O between 5.01 to 5.67 wt.% (mean 5.33 wt.%), CaO between 0.41 to 0.45 wt.% (mean 0.43 wt.%), Al_2O_3 between 13.82 to 14.11 wt.% (mean 13.95 wt.%) and TiO_2 between 0.332 to 0.353 wt.% (mean 0.341 wt.%; Table 3-4).

The second ash-flow tuff is a grey-green, pyritic, pumiceous, crystal-bearing, ash-flow (Unit 12). Only one sample was analyzed from Unit 12 and the data are given in Table 3-4. Unit 13 is a dark purple, crystal-bearing, ash-flow tuff. In total four samples were analyzed from this unit, SiO_2 values range between 64.62 to 74.32 wt.% (mean 70.84 wt.%), K_2O between 1.41 to 5.60 wt.% (mean 3.83 wt.%), Na_2O between 1.73 to 6.94 wt.% (mean 3.94 wt.%), CaO between 0.14 to 0.61 wt.% (mean 0.45 wt.%), Al_2O_3 between 10.65 to 14.68 wt.% (mean 12.72 wt.%) and TiO_2 between 0.417 to 0.677 wt.% (mean 0.576 wt.%; Table 3-4). Sample GS-02-087 was collected adjacent to a low-

sulphidation vein and is therefore more altered than the other three samples from this unit. Samples collected adjacent to low-sulphidation veins are often associated with silicification, however GS-02-087 displays a lower SiO_2 value in comparison to the other samples. This loss in SiO_2 is not understood, however it is noted that the percent total for this sample is only 89.16%, which may suggest analytical problems.

INTERPRETATION:

All three ash-flows are subalkalic, calc-alkalic and show little variation in their major-element geochemistry. The effects of hydrothermal alteration, however, can clearly be seen in the data. Unit 4 is relatively unaffected by hydrothermal alteration and the data is tightly grouped (Figures 3-6, 3-7 and 3-8). In contrast Unit 13 displays some scatter, which is attributed to the development of low-sulphidation veins and associated pyritization within the unit. The X-Y major-element plot (Figure 3-8) demonstrates a prominent distinction between the older and younger ash-flow tuff successions. One exception is sample GS-03-052 which is lithologically similar to Unit 13, yet plots near the older Unit 4. The analyzed sample came from an outcrop 1.7km south of the main area of Unit 13 and may not be related. It is noted that both the older and younger ash-flows contain veinlets and fractures hosting titanite ± leucoxene, which may have some effect on the TiO_2 values within these units. The geochemical difference between the older and younger units is also reflected in the trace-element data (see 3.3.4).
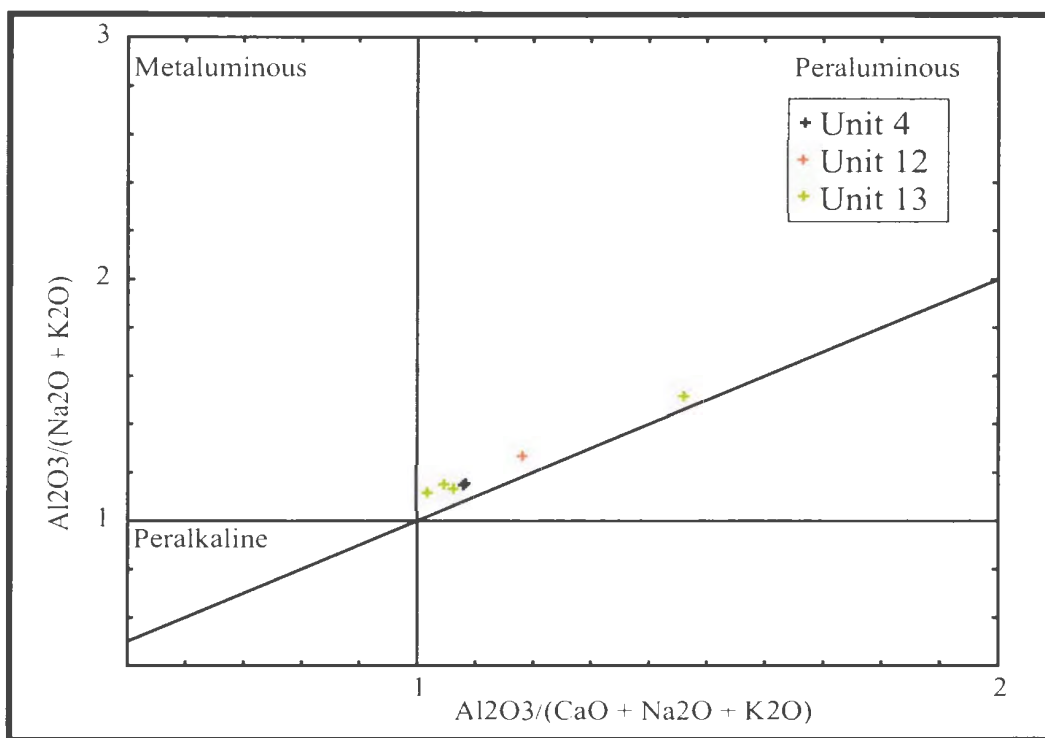
Figure 3-7: Alumina saturation diagram of Maniar and Piccoli (1989), displaying the peraluminous nature of the ash-flow tuffs. The outlier that plots furthest from the group has undergone hydrothermal alteration.
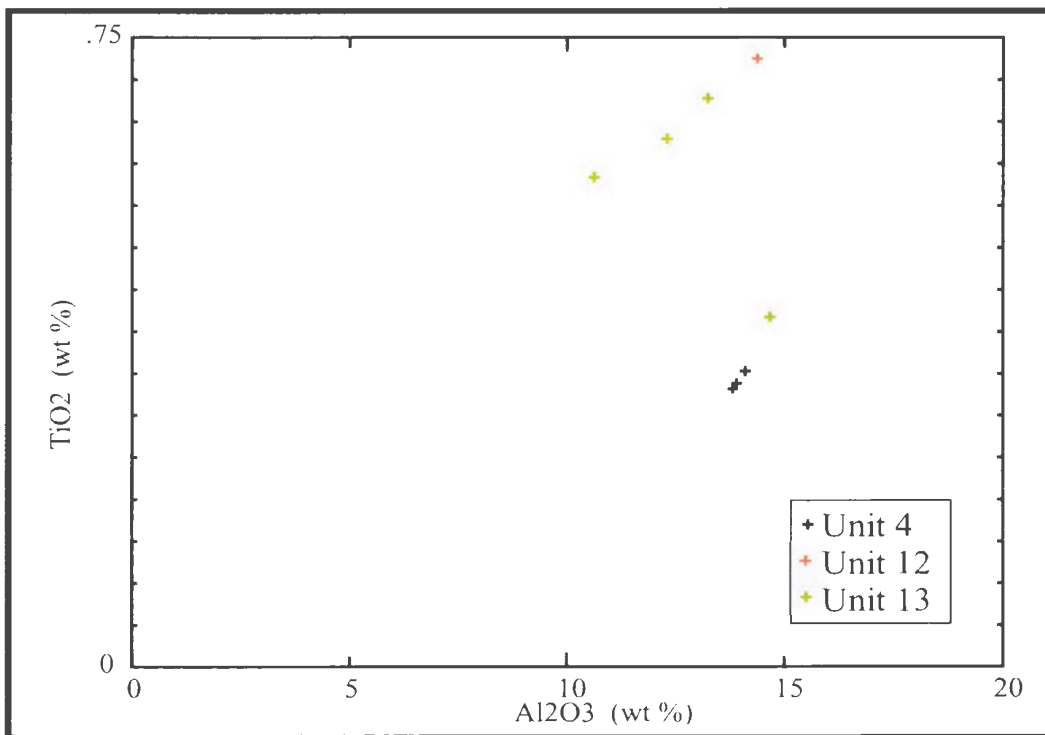
Figure 3-8: Major-element plot showing the distinction between the older Unit 4 and the younger Unit 13.

113

3.2.5 Mafic Rocks (Units 15, 20 and 21)

DATA:

Of the four samples analyzed from the mafic rocks of the Manuels Volcanic Suite (Unit 15), SiO_2 values range between 47.15 to 56.79 wt.% (mean 51.80 wt.%), K_2O between 0.14 to 3.59 wt.% (mean 1.67 wt.%), Na_2O between 0.98 to 7.79 wt.% (mean 4.70 wt.%), CaO between 1.17 to 4.47 wt.% (mean 2.52 wt.%), Al_2O_3 between 16.06 to 18.77 wt.% (mean 17.31 wt.%) and TiO_2 between 0.977 to 2.381 wt.% (mean 1.711 wt.%; Table 3-5). This group is chemically homogeneous, with the exception of samples near low-sulphidation veins (e.g. sample GS-02-10). It is unclear whether the enrichment in FeO, MgO and K_2O and depletion in Fe_2O_3 and Na_2O adjacent to the veins is solely the result of low- sulphidation veining.

Mafic rocks of Unit 21 are spatially associated and locally interbedded with sedimentary rocks of the Wych Hazel Pond Complex; six samples were collected from this unit and are shown to contain between 49.53 to 57.36 wt.% SiO_2 (mean 53.36 wt.%), between 0.19 to 3.36 wt.% K_2O (mean 1.12 wt.%), between 2.66 to 7.25 wt.% Na_2O (mean 5.52 wt.%), between 2.35 to 5.49 wt.% CaO (mean 4.43 wt.%), between 14.30 to 16.80 wt.% Al_2O_3 (mean 15.35 wt.%) and TiO_2 values between 1.203 to 2.091 wt.% (mean 1.557 wt.%; Table 3-5). Lithologically this unit is more uniform than Unit 15, and this is reflected in the homogeneity of its major-element geochemistry. This is in part due to the lack of epithermal alteration in this part of the WHPC.

Also included in Table 3-5 is the major-element geochemistry for mafic dykes that crosscut many of the units within the study area. In total fifteen samples were

collected, these samples are shown to contain SiO_2 values between 43.33 to 63.00 wt.% (mean 52.81 wt.%), K_2O between 0.57 to 5.44 wt.% (mean 2.34 wt.%), Na_2O between 0.40 to 6.44 wt.% (mean 3.61 wt.%), CaO between 0.50 to 7.47 wt.% (mean 2.85 wt.%), Al_2O_3 between 12.83 to 20.09 wt.% (mean 16.36 wt.%) and TiO_2 between 0.511 to 2.399 wt.% (mean 1.562 wt.%; Table 3-5).

INTERPRETATION:

The mafic dykes are subdivided into three groups: Unit 20a contains the majority of mafic dykes and generally displays tight clustering on major-element diagrams; Unit 20b plots within the metaluminous field on the alumina saturation diagram; Unit 20c is characterized by relatively high SiO_2 values (>60 wt%). These data indicate that several generations of dykes are included within the group; however no field evidence was found that would allow their chronological separation. The mafic dykes are all alkalic to weakly subalkalic and predominantly plot within the calc-alkalic field. Units 20a and 20b generally overlap, while Unit 20c separates from the other two groups of mafic dykes (Figures 3-9 and 3-10). Units 20a and 20c are distinctly peraluminous, while Unit 20b plots within the metaluminous field on the alumina saturation diagram.

In Figures 3-9, 3-10 and 3-11 the amygdaloidal basalt displays a closely grouped cluster, with alkalic, calc-alkalic and metaluminous affinities. In contrast, the mafic unit from the MVS displays significant amounts of scatter, is predominantly alkalic, and overlaps both the tholeiitic–calc-alkalic and metaluminous–peraluminous fields (Figures 3-10 and 3-11). From the above diagrams, no clear link can be implied between mafic
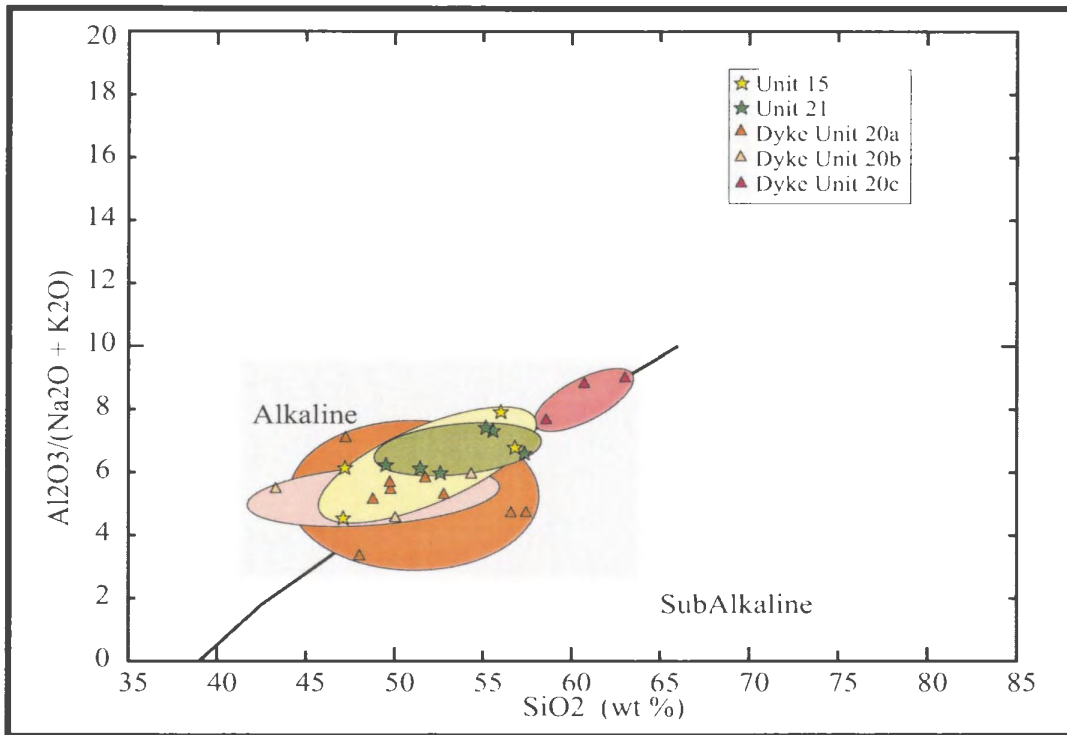
Figure 3-9: Major-element plot showing the alkalic to weakly subalkalic nature of the mafic rocks within the study area. Boundary between the alkaline and subalkaline fields after Irvine and Baragar (1971).
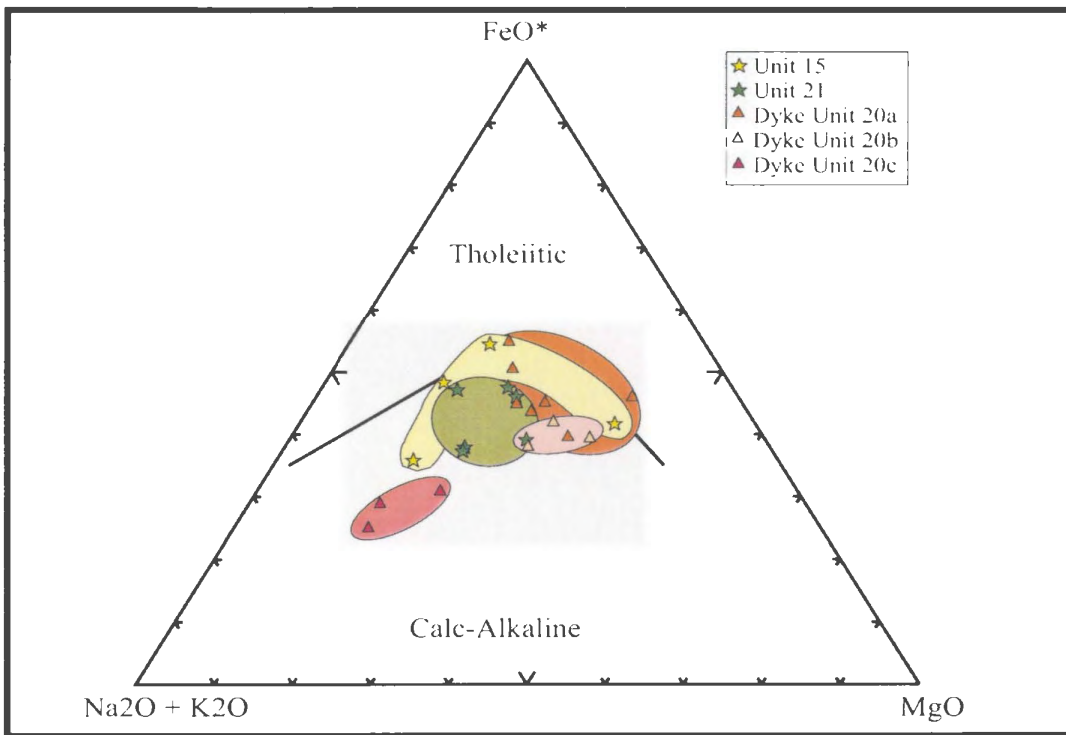
Figure 3-10: AFM plot for mafic rocks within the study area. Boundary between the tholeiitic and calc- alkaline fields after Irvine and Baragar (1971).
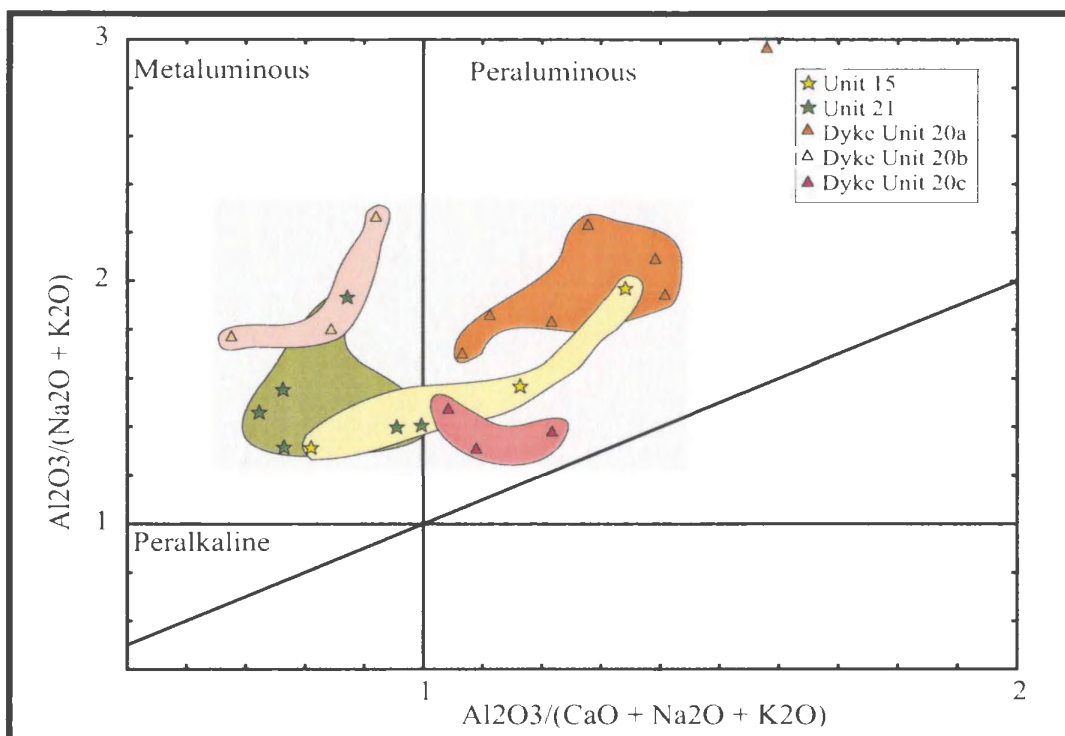
Figure 3-11: Alumina saturation diagram of Maniar and Piccoli (1989), displaying the metaluminous to peraluminous nature of the mafic rocks within the study area.
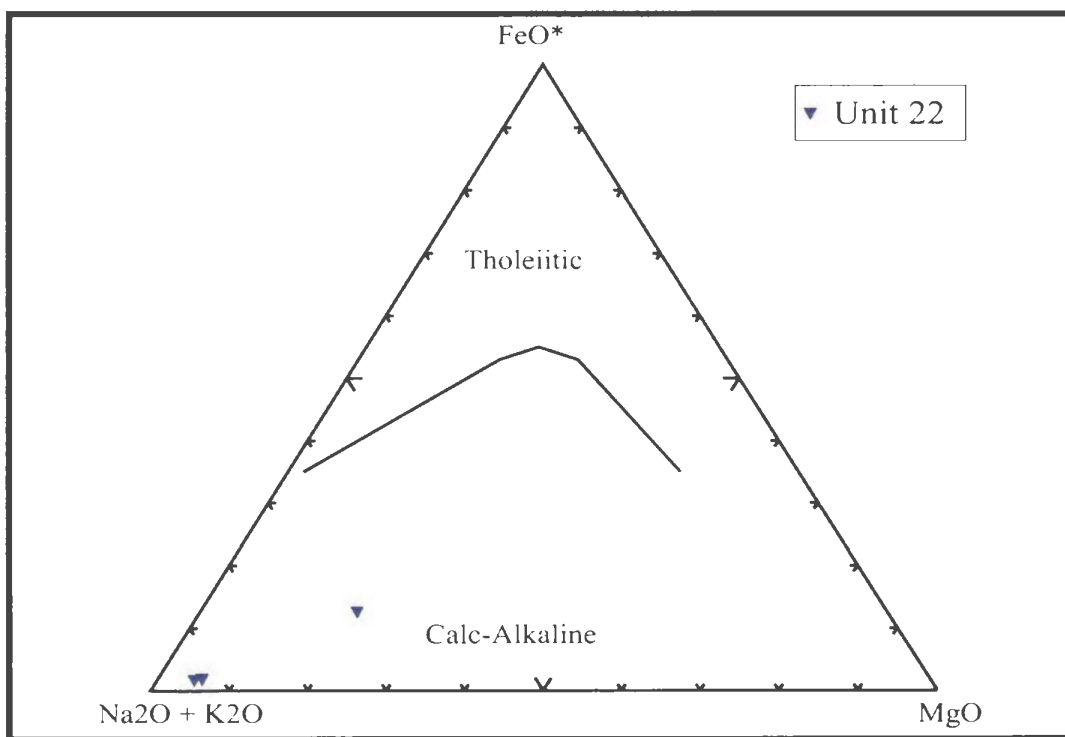
Figure 3-12: AFM plot showing the calc-alkalic nature of the Unit 22. Boundary between the tholeiitic and calc-alkaline fields after Irvine and Baragar (1971).

dykes and flows, although the alumina saturation diagram suggests the mafic dykes of Unit 20b may have a genetic relationship to the amygdaloidal basalt.

3.2.6 Unit 22: Fowlers Road Porphyry

This unit represents the youngest felsic magmatic event within the study area. Four samples collected from the porphyry unit contain SiO_2 values between 70.20 to 77.24 wt.% (mean 73.40 wt.%), K_2O between 0.40 to 9.59 wt.% (mean 3.29 wt.%), Na_2O between 1.10 to 6.14 wt.% (mean 4.51 wt.%), CaO between 0.09 to 0.31 wt.% (mean 0.21 wt.%), Al_2O_3 between 12.84 to 13.46 wt.% (mean 13.24 wt.%) and TiO_2 between 0.151 to 0.268 wt.% (mean 0.208 wt.%; Table 3-6). Unit 22 is subalkalic, calc-alkalic and plots within the peraluminous field on the alumina saturation diagram (Figure 3-12 and 3-13). This unit displays little evidence of any hydrothermal alteration aside from very localized pyritization (sample GS-02-77). It is therefore assumed that the chemical differences observed within Figures 3-12 and 3-13 are primary. These differences may imply that two separate pulses of magmatism exist within the eastern section of the map area. This will be further explored with the trace-element geochemistry in following sections.

3.3 TRACE-ELEMENT GEOCHEMISTRY

INTRODUCTION:

The samples described in this section were analyzed for the trace elements Cr, Zr, Ba, Mo, Zn, Pb, Co, Ni, Cd, Ti, V, Be, Nb, Cu, Dy, Sc, Y, Mn, Sr, La, Ce, Li and As. The accuracy and precision calculations for the trace-element data is given in Appendix C.
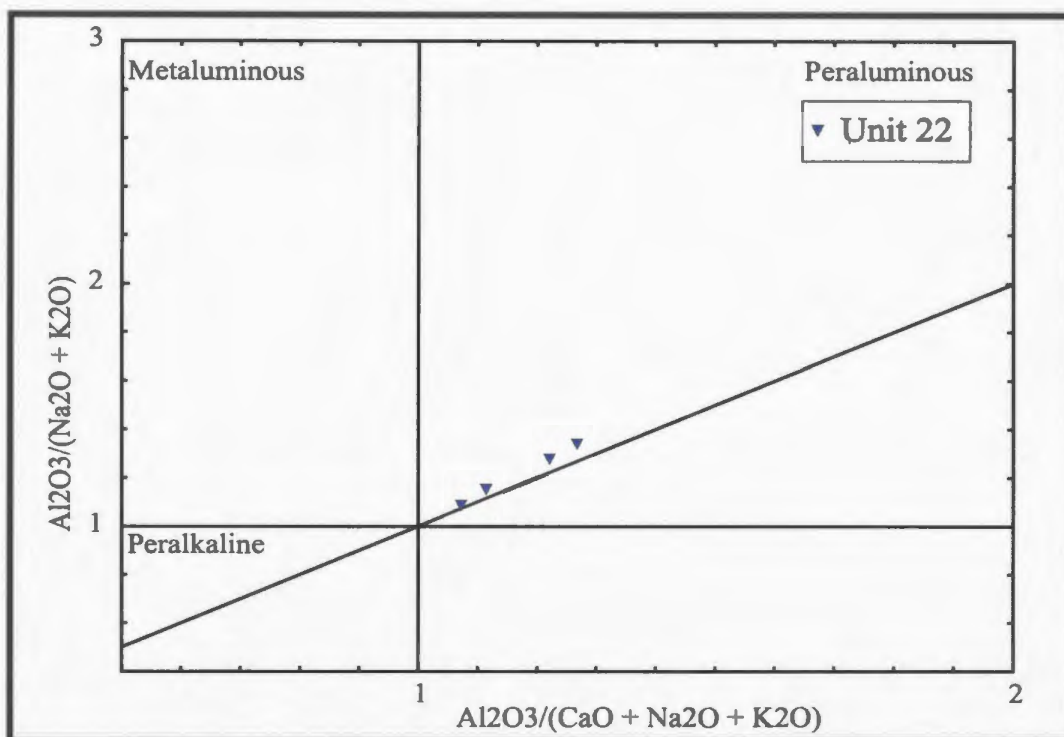
Figure 3-13: Alumina saturation diagram of Maniar and Piccoli (1989), displaying the peraluminous nature of the Unit 22.
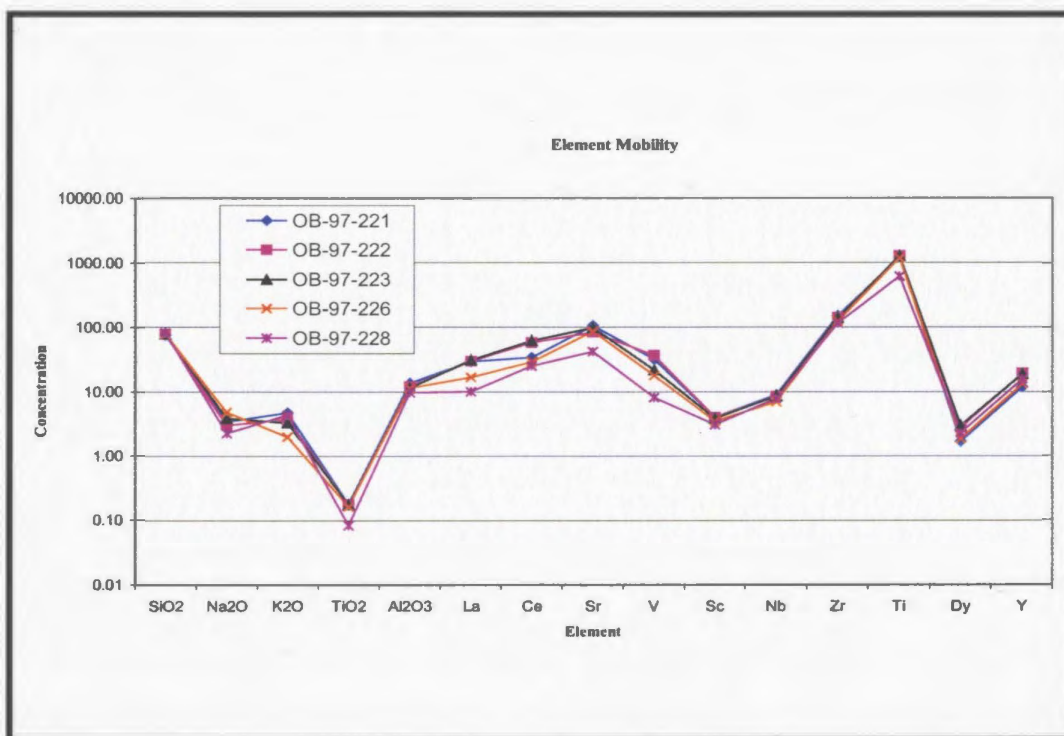
Figure 3-14: Diagram displaying immobility of the trace elements Nb, Zr, Dy, and Y; select major elements are also included to display the effects of alteration (trace element concentrations are given in ppm; major elements concentrations are in wt.%).

Note that, within the ICP-ES trace-element data tables Rb is not a standard analysis and is therefore not included for all samples. Ga data is available only for those samples analyzed in the year 1997.

HYDROTHERMAL ALTERATION:

Trace-element geochemistry was employed to characterize aspects of some of the hydrothermal alteration that is common to many of the rock units within the study area. Analyses were completed on altered and unaltered samples of the same unit in an attempt to identify those elements which remained immobile when subjected to intense hydrothermal alteration. These data were then used to characterize the main igneous units.

One such comparison employs five samples of Unit 7 from the WHIS. Samples OB-97-221, -222, -223, -226, and -228 were collected along the CBS By-Pass roadcut in a region of silica–sericite alteration (Table 3-7 and 3-8). The samples were collected approaching the alteration and therefore sample OB-97-221 is the least altered and sample OB-97-228 is the most altered. Intense silica–sericite alteration is first noted in sample OB-97-223; as alteration increases, primary igneous textures begin to disappear, ending in predominantly massive silica alteration. From Figure 3-14 it is evident that the immobile high field strength elements (HFSE) Nb, Zr, Ti and Y, the middle rare earth-element Dy, as well as the major-elements Al_2O_3 and TiO_2 are not affected by the alteration. One exception is the TiO_2 value for OB-97-228, which shows minor depletion; however it is noted that this is the most intensely altered sample. Also evident from this figure is the scatter imposed by the alteration within the LREE La and Ce, the low field

120

strength element (LFSE) Sr, the transition element V, and the mobile major-elements Na_2O and K_2O.

The second demonstration of element immobility is from the Oval Pit mine. In this region, the average of three relatively fresh samples of Unit 9 were compared to silica–sericite–pyrophyllite alteration (Table 3-9 and 3-10). It is noted that, while no primary textures remain in the intensely altered samples, it is assumed that these samples like those elsewhere in the Oval Pit mine, have a flow-banded rhyolite protolith. Figure 3-15 displays similar element behaviour to that seen in Figure 3-14 with the LREE displaying some scatter and the HFSE maintaining near constant element-element ratios. These altered samples represent the most intense alteration assemblages found within the study area, and therefore elements immobile within this alteration should be immobile elsewhere within the region. As evident from Figure 3-15, the altered samples do not maintain the exact concentrations of HFSE in comparison to the unaltered samples, but do maintain similar element-element ratios (Table 3-10). As indicated by Table 3-9 and 3-10, the altered samples within the Oval Pit mine contain elevated SiO_2 values which are accompanied by depletions in the immobile elements such as Al_2O_3, Nb, Zr, Ti, Dy and Y. No one factor appears to be responsible for this decrease in concentration. The similar element-element ratios of the immobile elements imply the depletions are not attributed to element mobility. Therefore, the decrease is taken as a combination of some dilution due to silicification and hydration associated with the advanced argillic alteration.

From the two examples listed above, the trace elements Nb, Zr, Ti, Dy and Y remain immobile in intense hydrothermal alteration and, therefore, these elements can be
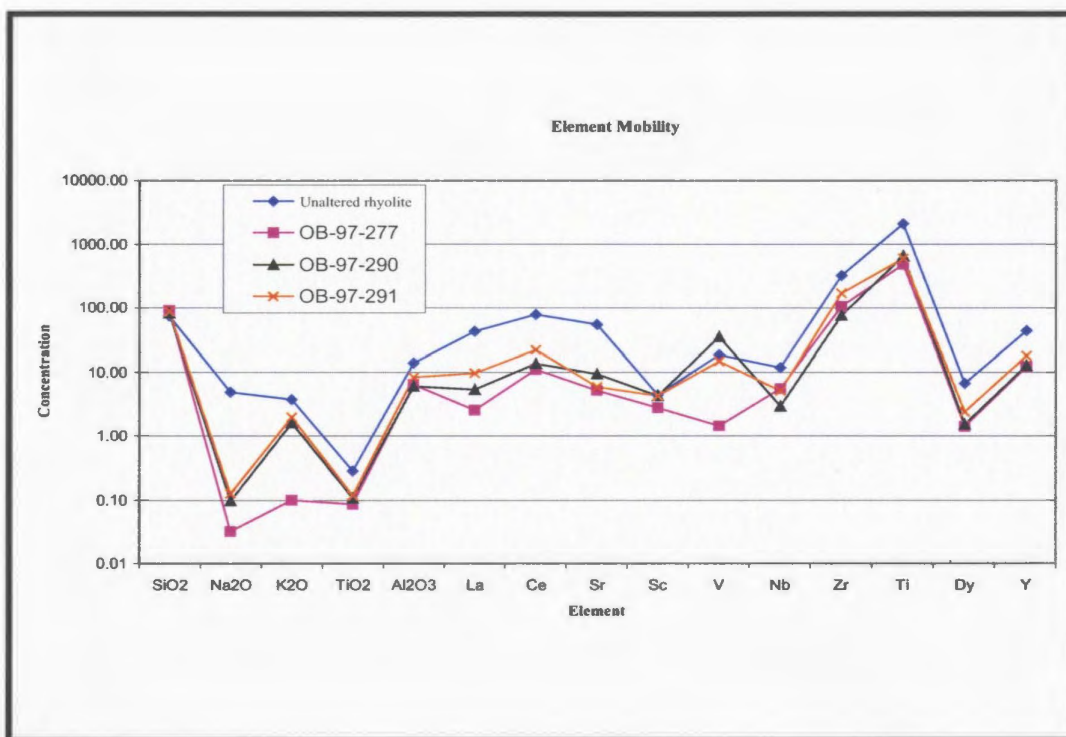
Figure 3-15: Diagram displaying immobility of the trace elements Nb, Zr, Dy, and Y; select major elements are also included to display the effects of alteration (trace element concentrations are given in ppm; major elements concentrations are in wt.%).
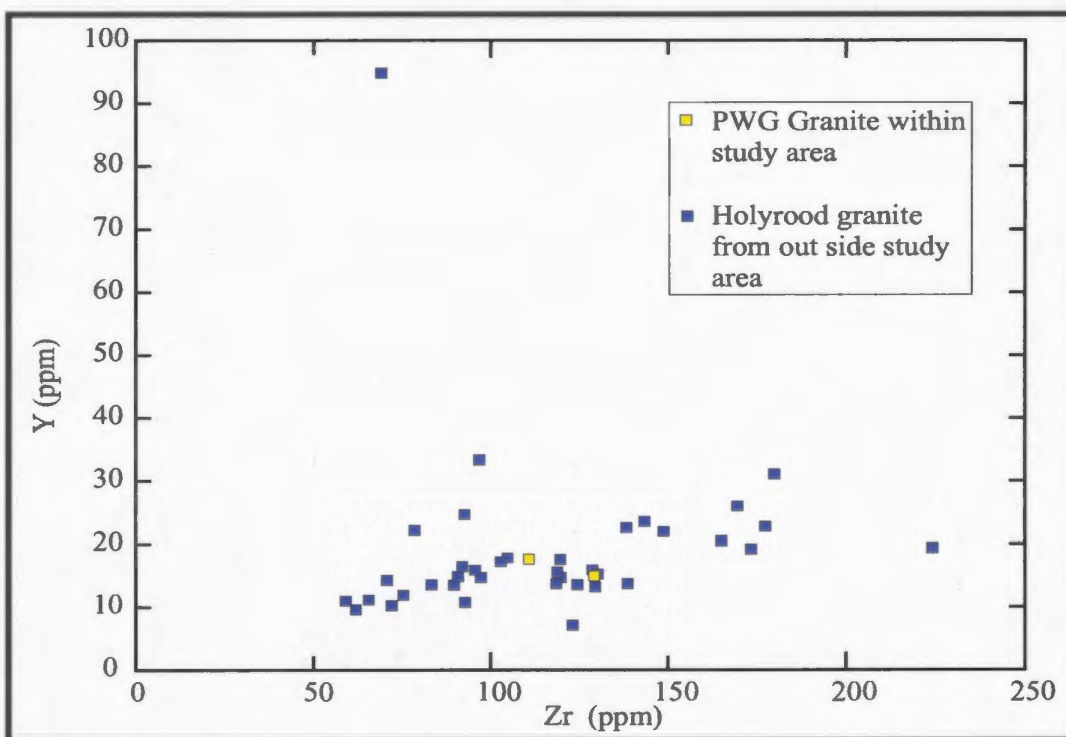
Figure 3-16: Immobile trace-element plot showing the chemical similarity between samples of pink-white-green granite within the study area and Holyrood Intrusive Suite samples outside of the study area.

used to characterize most of the geological units in the study area. In the following discussion these elements are also used to demonstrate whether other elements are immobile or mobile in altered samples. As pointed out previously, trace-element variations within the felsic volcanic rocks of distinctly different ages are very subtle. For this reason, some of the volcanic units are virtually indistinguishable. In contrast, the trace-element geochemistry is very effective in segregating older and younger intrusions.

3.3.1 Unit 5: Holyrood Intrusive Suite (HIS)

Trace-element geochemistry of the HIS is characterized by LREE enrichment and weak to moderately negative Nb, P_2O_5, TiO_2, Sc and V anomalies (Table 3-11; note for several of the samples P_2O_5 was not detected). Two samples of the HIS from within the study area plot within a cluster of HIS granite samples which represents the average chemistry of the main granitic intrusion within the Holyrood Horst (Figure 3-16; unpublished data from S. O'Brien). The similar chemistry of these samples is again highlighted in Figure 3-17. Figure 3-18 displays three representative samples of the HIS selected for extended trace-element analysis (Table 3-12). These three samples appear to have a very subtle concave pattern developed between the middle rare earth-element Tb and the heavy rare earth-element Lu. The Nb-Y tectonic plot of Pearce *et al*. (1984) shows that the granitic rocks of the HIS plot within the volcanic arc granite/syn-collisional granite field (Figure 3-19). From the above-mentioned figures it is evident that the trace-element geochemistry supports the link between PWG granite from within the study area and the regionally extensive HIS.
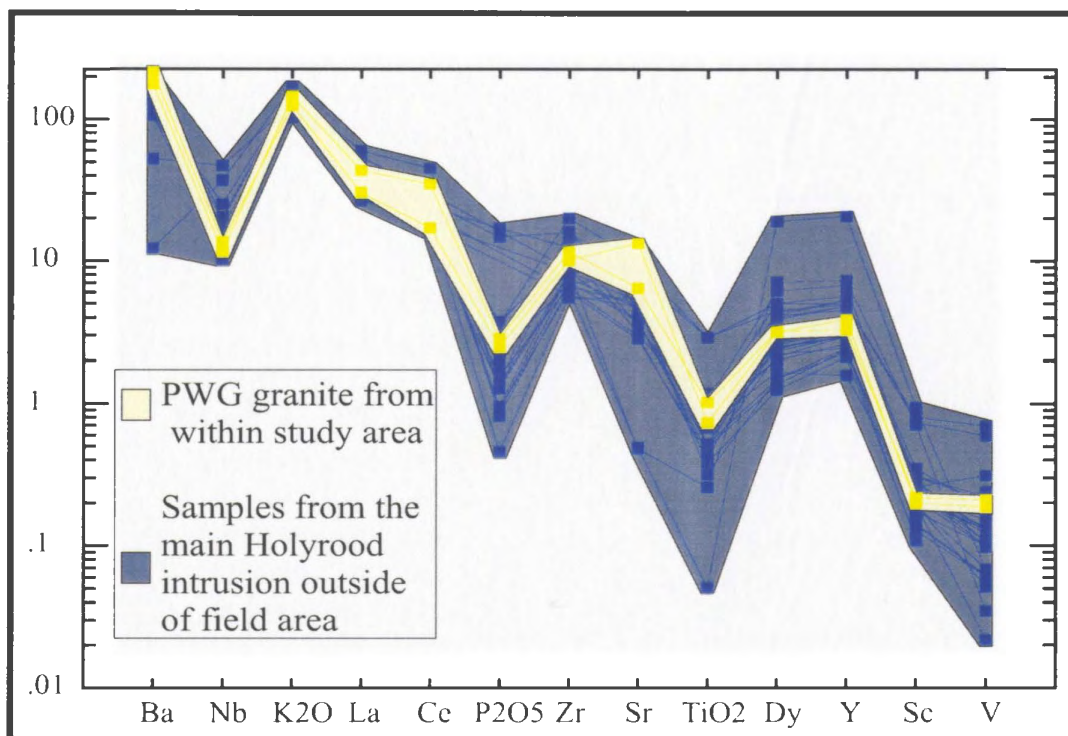
Figure 3-17: Spider diagram showing the chemical similarity of Holyrood granite samples from within the study area in comparison to the Holyrood Intrusive Suite outside of the study area.
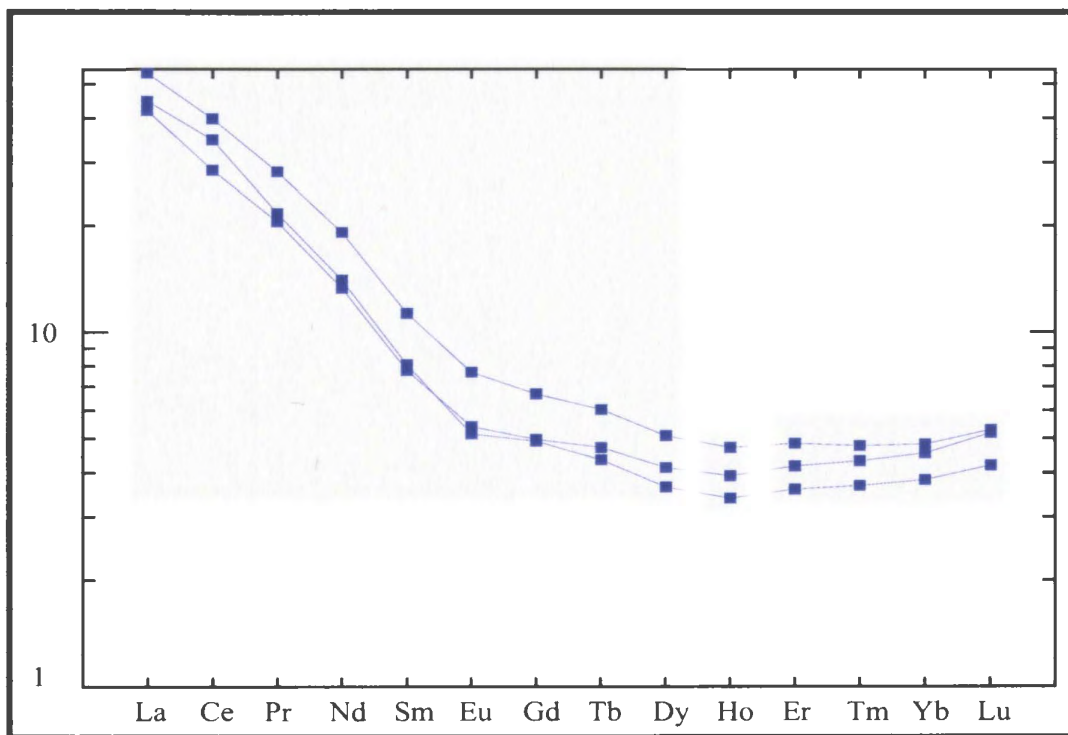
Figure 3-18: Primitive-mantle normalized REE spider diagram of three representative samples from the Holyrood Intrusive Suite.
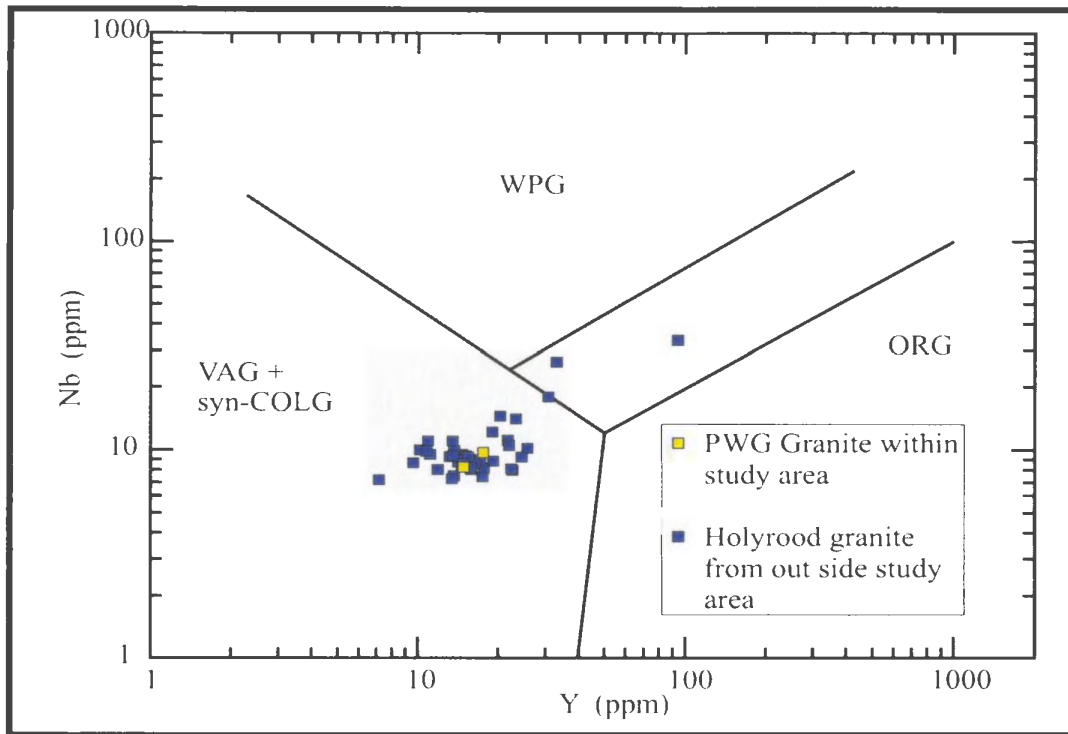
Figure 3-19: Nb-Y tectonic plot of Pearce *et al.* (1984) displaying the tectonic affinity of the Holyrood granite.
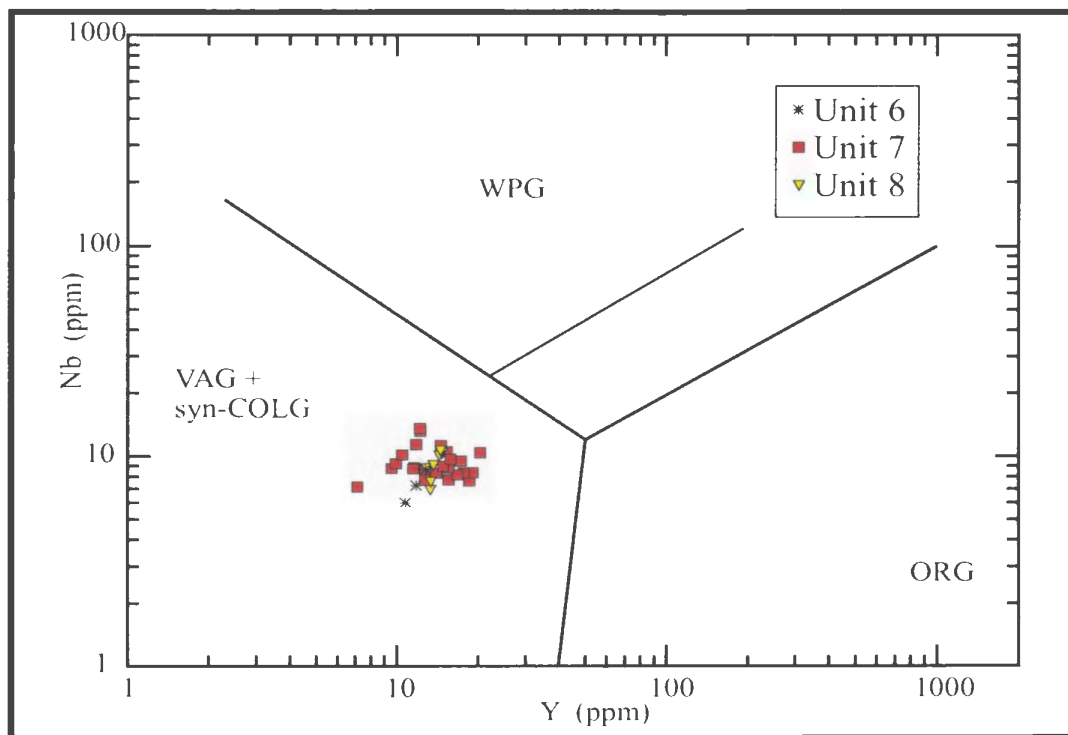
Figure 3-20: Nb-Y tectonic plot of Pearce *et al.* (1984) displaying the tectonic affinity of the White Hills Intrusive Suite.

3.3.2 White Hills Intrusive Suite (WHIS; Units 6, 7 and 8)

Rocks of the WHIS share many chemical similarities with rocks of the HIS. As with the HIS, rocks of the WHIS plot within the volcanic arc granite/syn-collisional granite field of Pearce *et al.* (1984; Figure 3-20). Unit 6 of the WHIS is characterized by a moderate enrichment in LREE and a positive Sr anomaly. The unit is also characterized by negative Nb, Sc and weakly negative P_2O_5 and TiO_2 anomalies (Figure 3-21; Table 3-13). Trace-element ratios of Unit 6 are consistent in both the immobile and mobile elements.

In Figure 3-22, Unit 6 from within the study area is compared to older (ca. 640 Ma) Woodford's monzonite from the western margin of the HIS (O'Brien *et al.*, 2001a; Table 3-14). From this figure, it is evident that the two units are chemically similar aside from the variable Zr values of the Woodford's Monzonite. The difference in Zr values may be the result of incomplete dissolution of the sample, or may also be the result of zircon fractionation. This comparison shows that the trace-element geochemistry is ineffective in segregating the older and younger monzonite units.

The granitic rocks of the WHIS are characterized by a moderate enrichment in LREE, positive to weakly negative V anomalies and negative Nb, P_2O_5, TiO_2 and Sc anomalies (Figure 3-23; Table 3-15). Outliers in some of the mobile trace-elements include sample OB-97-171, which is depleted in Ba, and K_2O, and samples OB-97-228 and OB-01-060, which are depleted in P_2O_5 (note P_2O_5 was not detected in sample OB-01-060). As mentioned previously, these samples have undergone intense hydrothermal
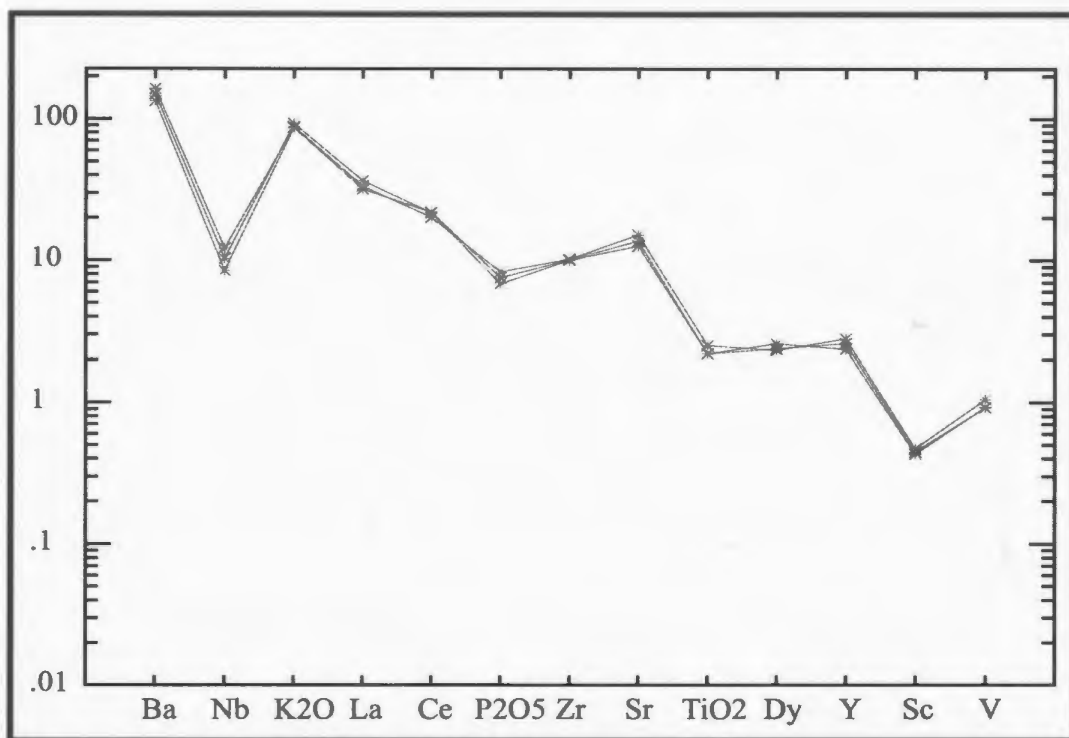
Figure 3-21: Primitive-mantle normalized spider diagram showing the chemical trends within Unit 6 of the White Hills Intrusive Suite.
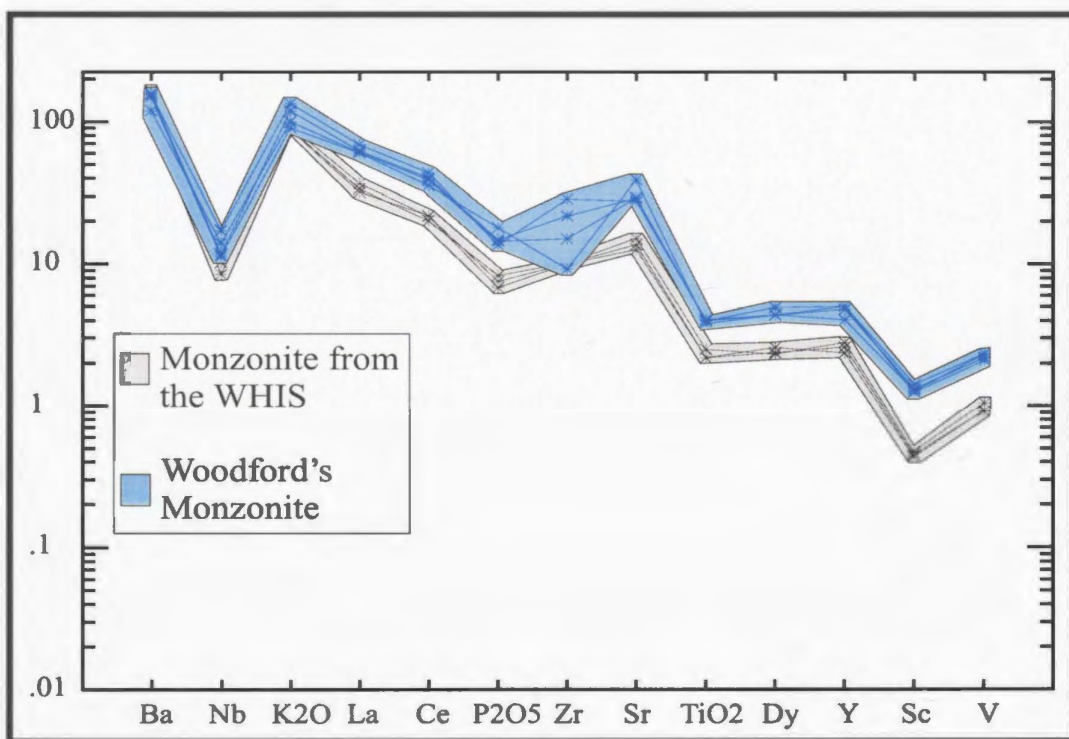
Figure 3-22: Primitive-mantle normalized spider diagram showing the chemical similarity between samples of monzonite from the White Hills Intrusive Suite in comparison to the Woodford's monzonite.
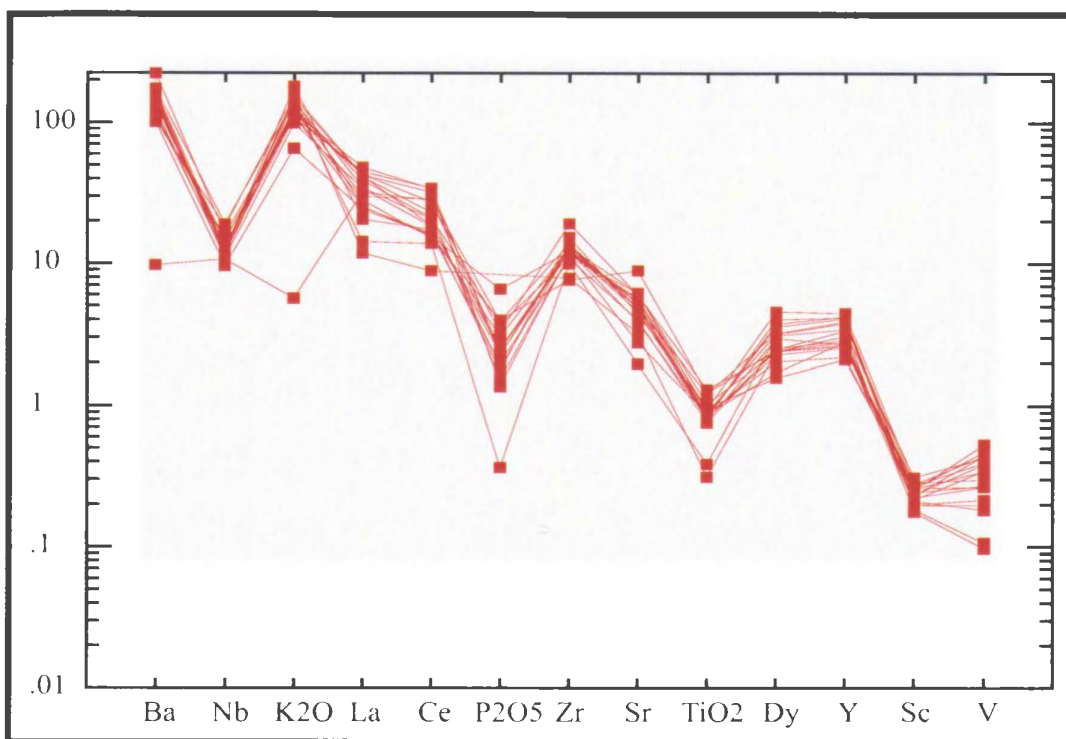
Figure 3-23: Primitive-mantle normalized spider diagram showing the chemical trends within Unit 7 of the White Hills Intrusive Suite.
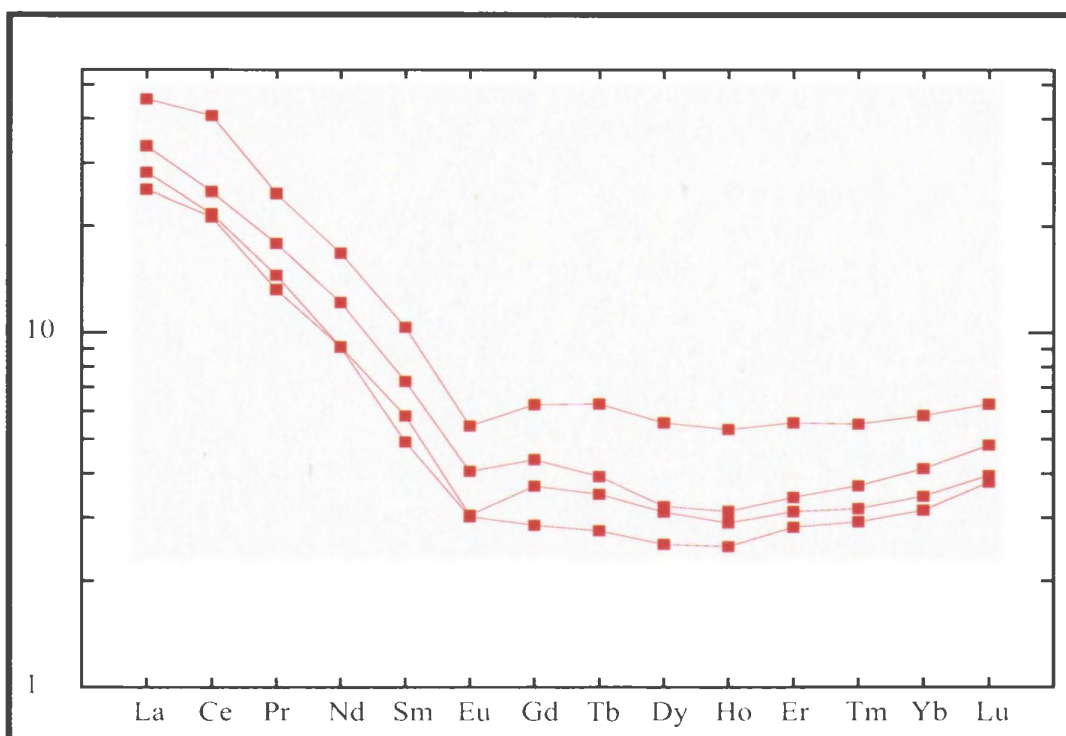
Figure 3-24: Primitive-mantle normalized rare earth element diagram of four representative granitic samples from the White Hills Intrusive Suite.

alteration, which can account for the loss of these mobile elements. The remaining depletions in relatively unaltered samples are attributed to chemical fractionation; this is because the depletions only affect compatible elements. The REE pattern of Unit 7 from the WHIS is very similar to that of the HIS, with the exception of a slight negative Eu anomaly in the WHIS (Figure 3-24; Table 3-16). Figure 3-24 displays a pronounced LREE enrichment and a similar concave pattern between the middle rare earth-element Tb and the heavy rare earth-element Lu. The minor variation in element concentrations between various samples of the WHIS (Figure 3-24) is attributed to alteration. The chemical trends displayed by the granitic rocks of the WHIS are indistinguishable from those of granitic rocks from the HIS (Figure 3-25). This geochemical similarity between the two units, combined with new geochronological data presented elsewhere in the thesis, suggests that the two units are cogenetic.

Unit 8 has chemical characteristics identical to those of Unit 7 from the WHIS (Figure 3-26; Table 3-17). The two units share a close spatial relationship in the area of White Mountain and their similar chemical characteristics support the proposed comagmatic relationship between the two units (Figure 3-27).

3.3.3 Minerals Road, Manuels River, Farmer's Field and Pale Grey-Green Rhyolites

The use of trace-element geochemistry alone is largely ineffective in segregating the various rhyolite units within the region. There are, however, minor chemical differences attributed to alteration that are specific to rhyolites of certain areas (Table 3-18). All of the rhyolitic units within the study area overlap the rhyolite and rhyodacite fields of Winchester and Floyd (1977; Figure 3-28). These units predominantly plot
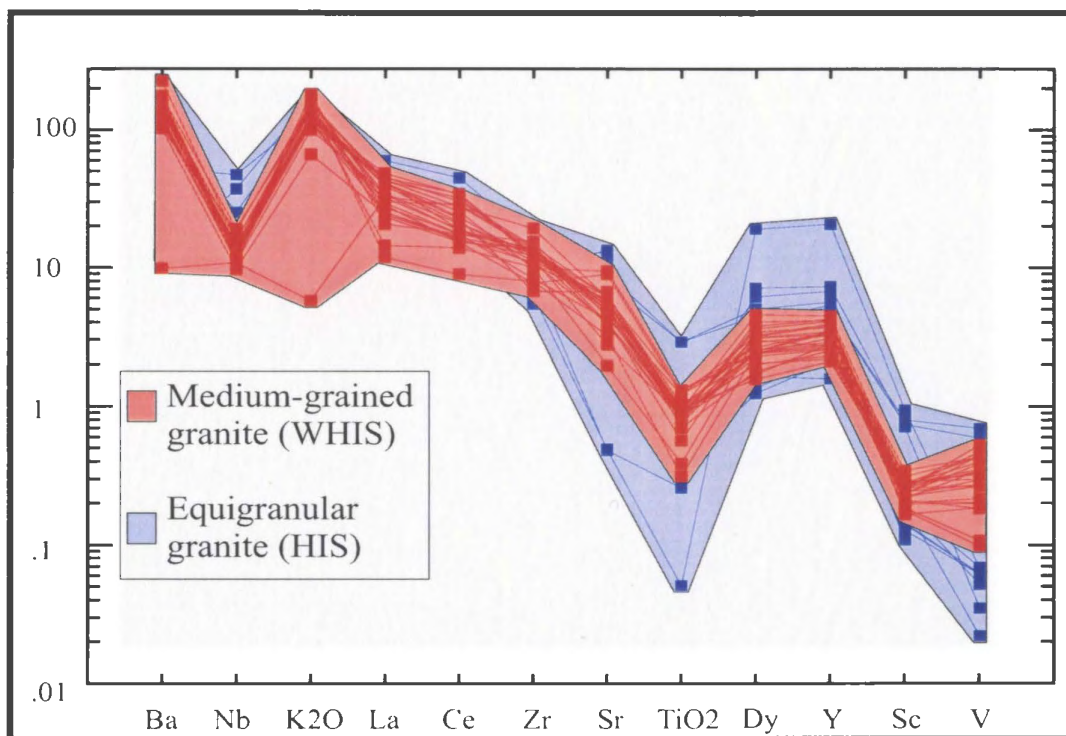
Figure 3-25: Primitive-mantle normalized spider diagram showing the chemical similarity between samples of granite from the White Hills Intrusive Suite in comparison to granite samples from the Holyrood Intrusive Suite.
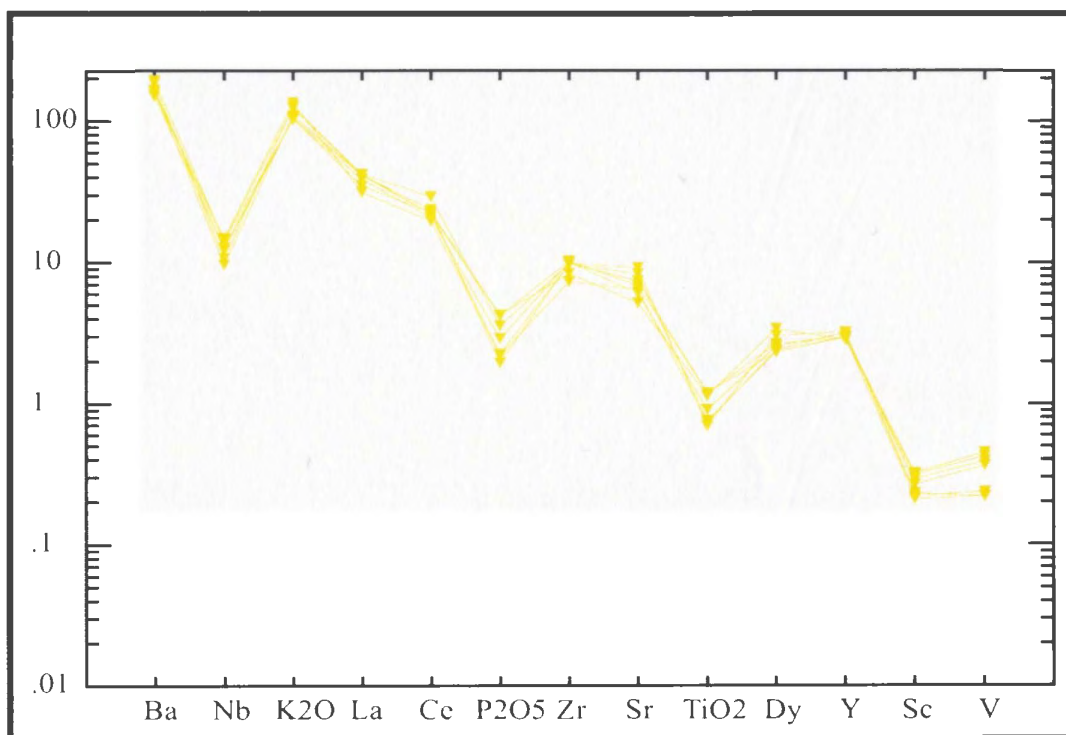
Figure 3-26: Primitive-mantle normalized spider diagram showing the chemical trends of Unit 8 (White Hills Intrusive Suite).

130
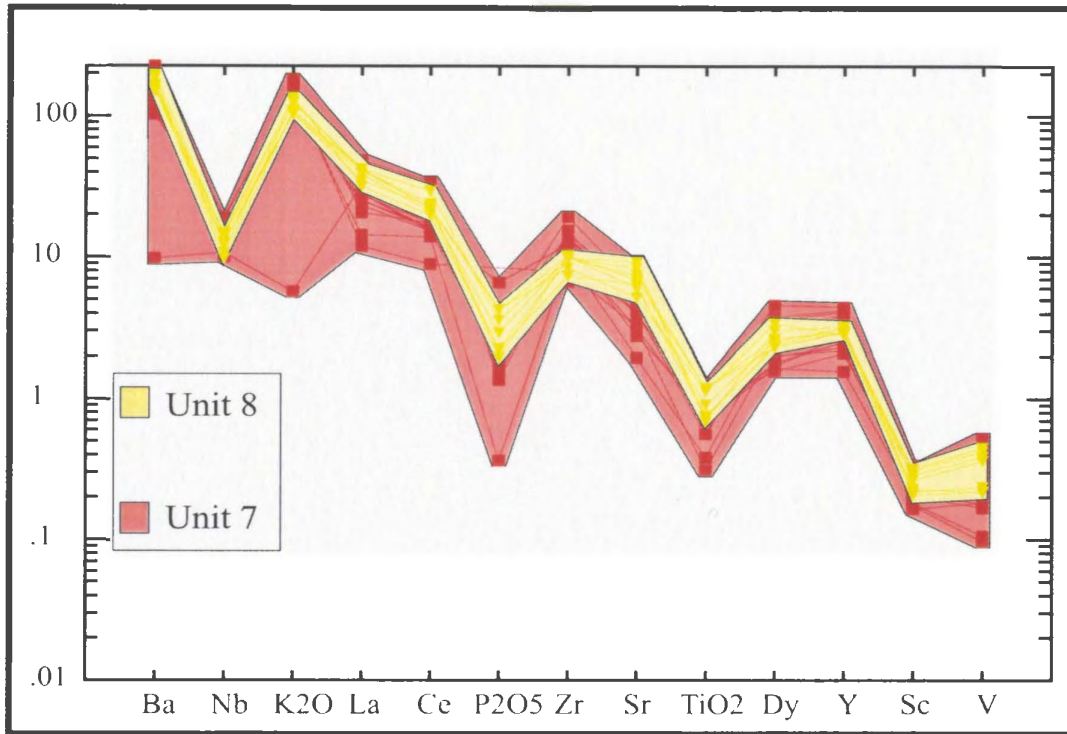
Figure 3-27: Primitive-mantle normalized spider diagram showing the chemical similarity between samples of Unit 8 and Unit 7 from the White Hills Intrusive Suite.
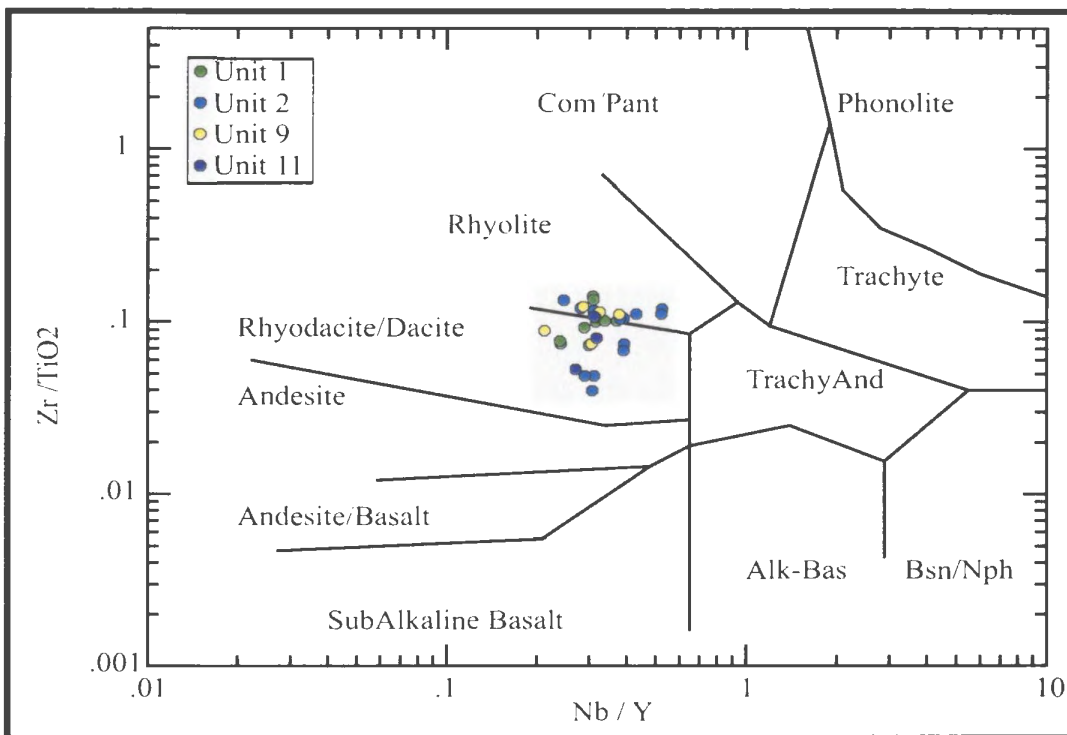
Figure 3-28: Trace-element discrimination diagram of Winchester and Floyd (1977) for rhyolite units within the study area.

within the volcanic arc field of Pearce *et al.* (1984; Figure 3-29) and display the characteristic negative Nb anomaly that is associated with arc-related volcanic rocks.

Unit 1 of the White Mountain Volcanic Suite displays a moderate enrichment in Ba and K_2O and depletions in Nb, Sr, TiO_2, Sc and V (Figure 3-30). Nb values are typically lower than La values except for sample OB-97-040, which has a Nb/La value > 1. This sample was collected from a volcanic raft within the WHIS and the loss in La is assumed to be the result of intrusion-related alteration. Sample OB-03-018 is depleted in Ba, and has less La and Ce in comparison to the other samples. This sample is altered and therefore the chemical differences are assumed to be the result of the alteration and not a primary feature. The depletion in the compatible elements Sr, TiO_2, Sc, and V are attributed to chemical fractionation as all of the samples have similar element-element ratios for these particular elements.

Unit 2 of the WMVS displays the same geochemical trends as Unit 1 however, several subtle chemical anomalies do exist that may represent regionally restricted zones of alteration and the presence of more than one flow within the unit. All of the samples collected within the region of the Steep Nap prospect are characterized by Nb/La ratios >1. The samples from the Steep Nap prospect (OB-00-150; OB-01-06, -07; GS-03-086) plot well below the La and Ce values in comparison to the other samples within the unit (Figure 3-31), however the immobile trace-elements of the altered samples display chemical trends identical to the rest of the unit. For this reason, the chemical anomalies are attributed to alteration, which may be associated with the nearby development of
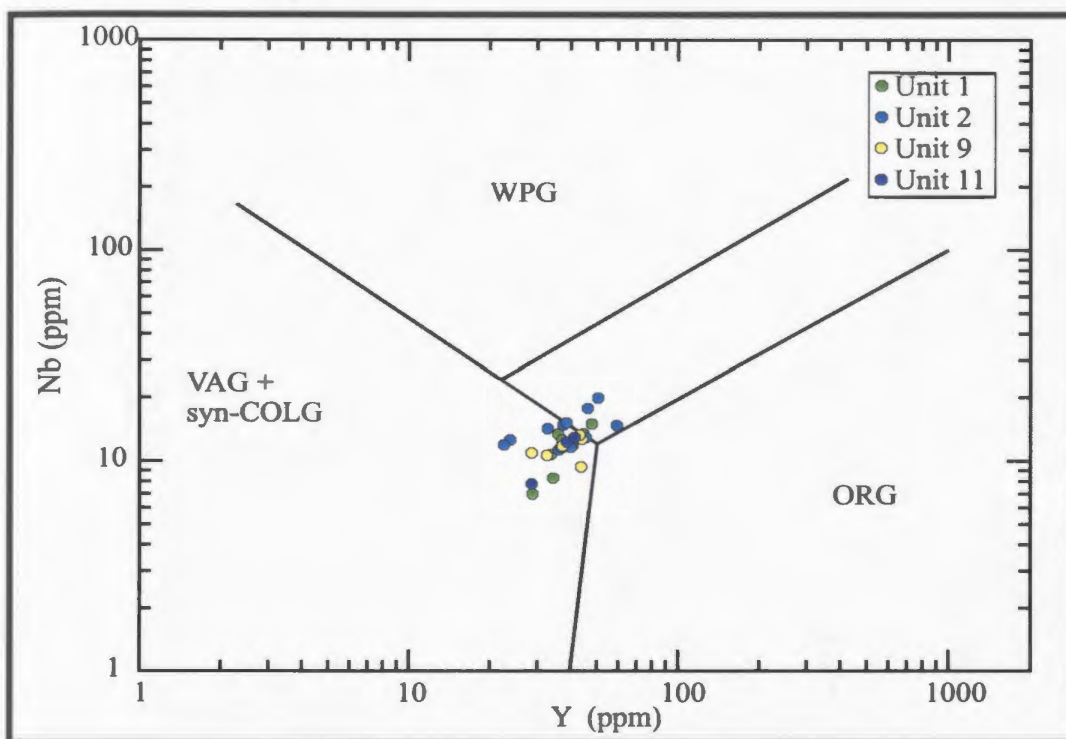
Figure 3-29: Nb-Y tectonic plot of Pearce *et al*. (1984) displaying the tectonic affinity of the rhyolite successions within the study area.
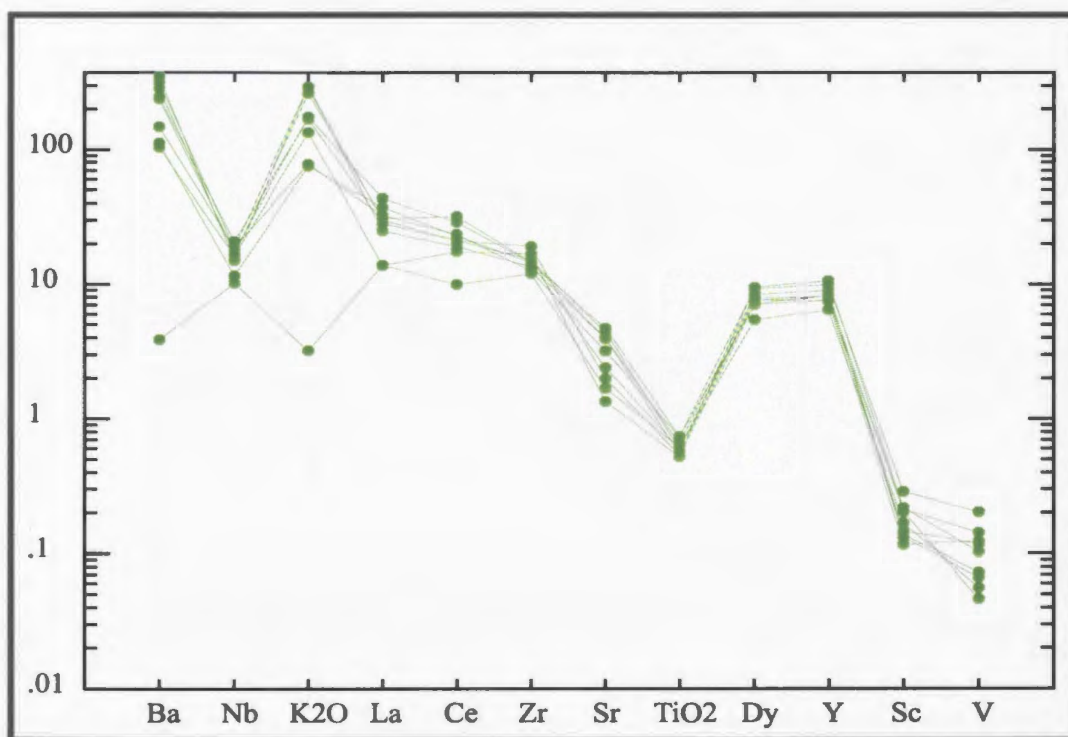
Figure 3-30: Primitive mantle-normalized spider diagram for Unit 1.
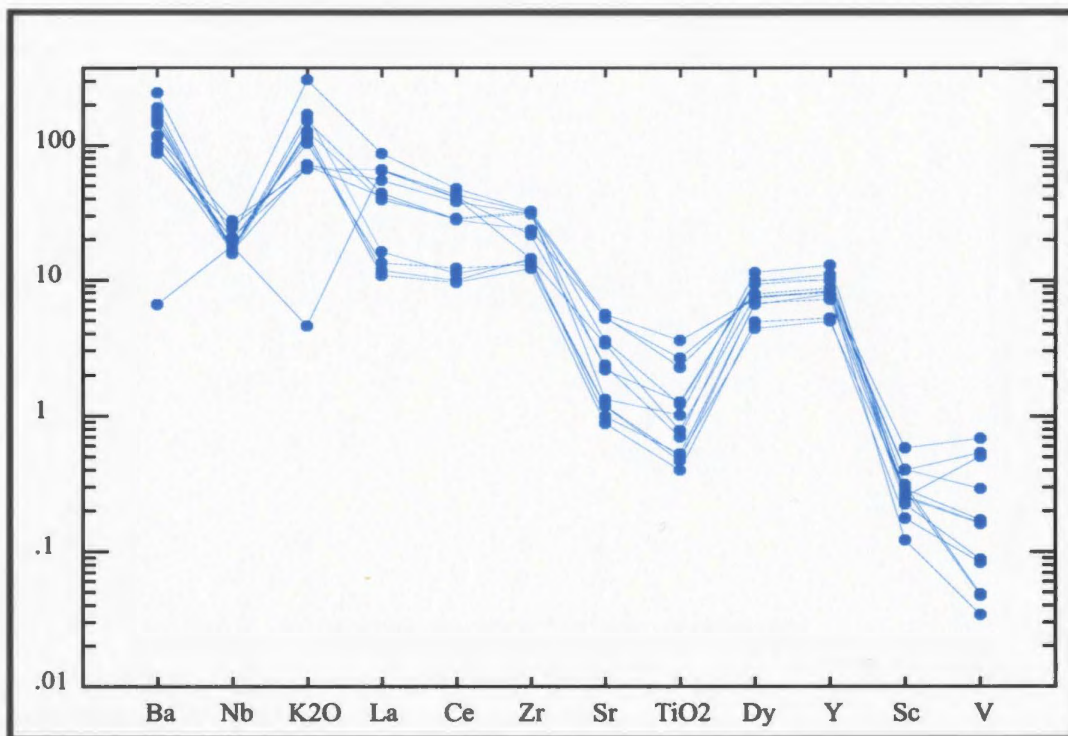
Figure 3-31: Primitive mantle-normalized spider diagram for Unit 2.
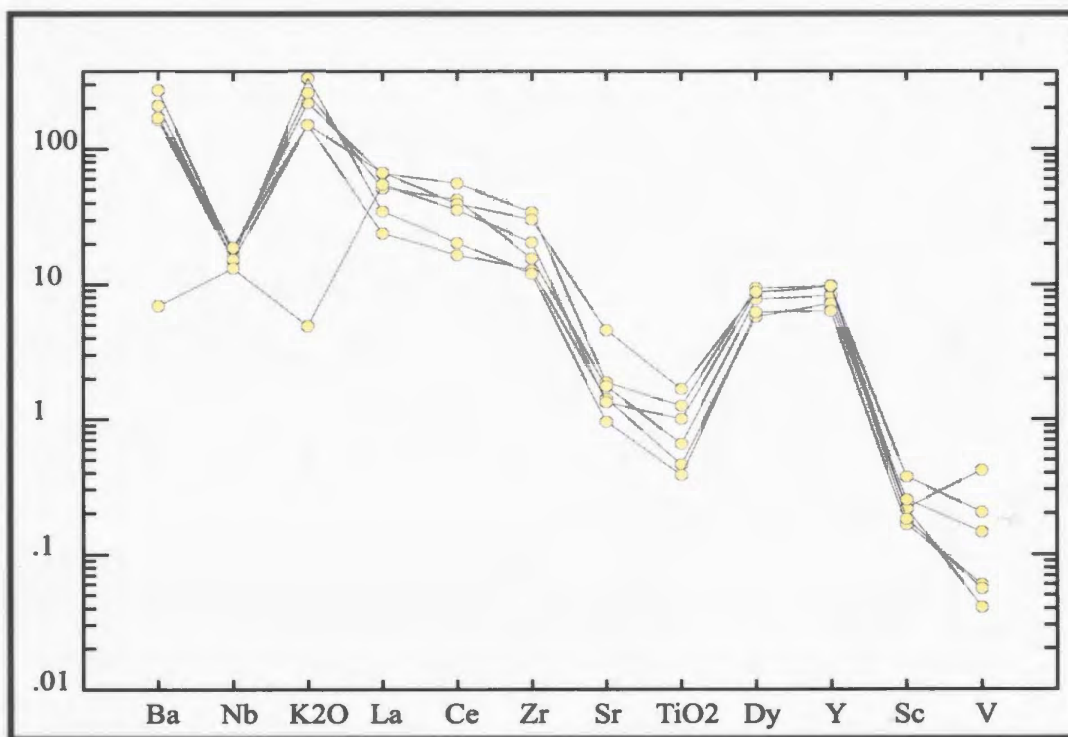
Figure 3-32: Primitive mantle-normalized spider diagram for Unit 9.

low-sulphidation veins. As mentioned in the major-element section, several of the samples from the northeastern portion of this unit have a somewhat distinct chemistry. These samples are characterized by anomalously high Ti/Zr ratios (>10) and corresponding elevated Zr/Nb ratios. Due to the lack of prominent hydrothermal alteration, these ratios are interpreted to represent primary geochemical differences. Therefore it is assumed that the chemical differences represent multiple flows within the unit. It is noted that the anomalously high TiO_2 values may be explained by fracture hosted titanite ± leucoxene, which is locally observed in thin section, but this does not account for the other variations noted in the major- and trace-element chemistry. Sample OB-03-013 is depleted in Ba and K_2O, which is similar to that seen in sample OB-03-018 of Unit 1. As is evident from the major-element geochemistry both samples are highly sodic and may share a common form of alteration.

Unit 9 of the MVS forms a fairly consistent grouping with no significant geochemical outliers. This is likely due to the fact that all the samples representing this unit are relatively fresh and altered samples within the advanced argillic zone were not sampled. Similar enrichments in Ba and K_2O and depletions in Sr, TiO_2, Sc and V, as seen in the other rhyolite units, are again evident within this unit (Figure 3-32). Sample GS-03-058 is depleted in Ba and K_2O and is associated with anomalously high Na_2O values.

The pale grey-green, porphyritic, fine, rhyolite (Unit 11) of the MVS is dominantly distinguished from Unit 2 by its porphyritic nature. Chemical characteristics of this unit include enrichments in Ba and K_2O and negative Nb, Sr, TiO_2, Sc and V anomalies (Figure 3-33). Sample OB-97-010 also has a weakly positive Ce

135
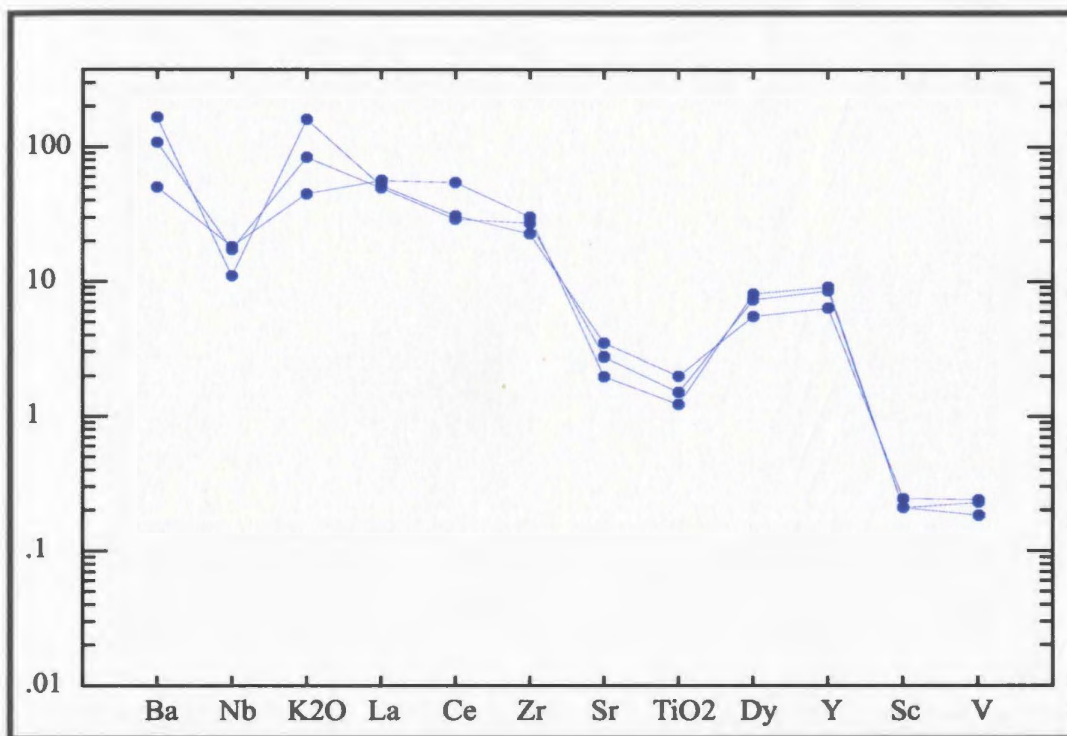
Figure 3-33: Primitive mantle-normalized spider diagram for Unit 11.
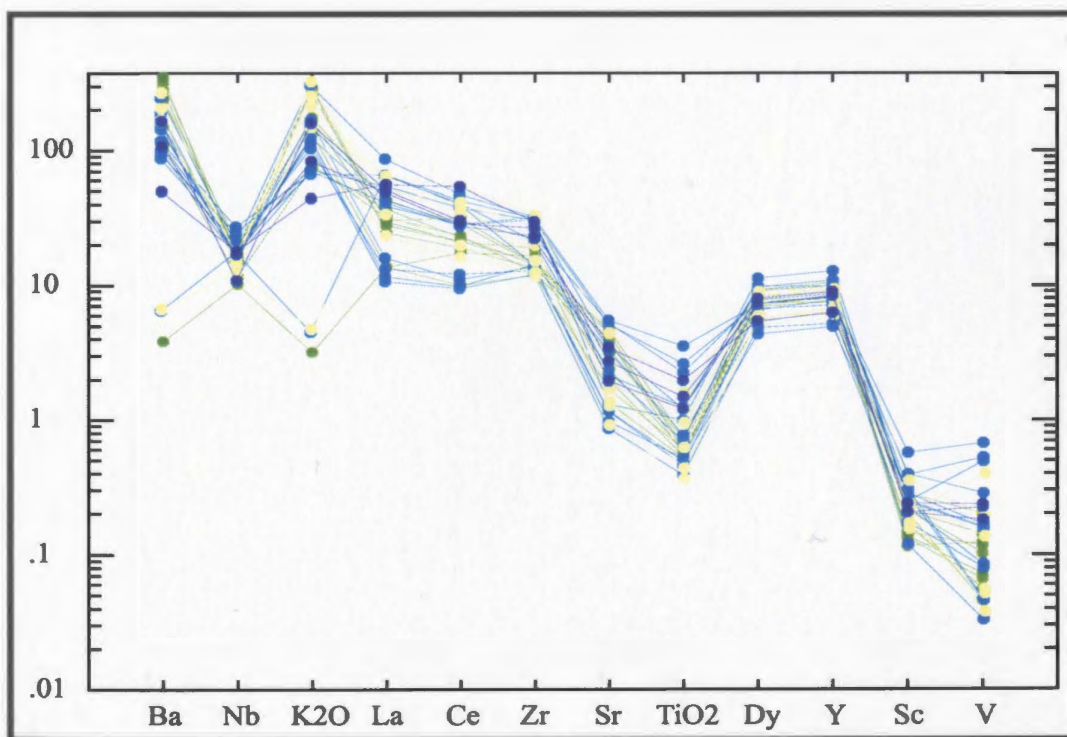
Figure 3-34: Primitive-mantle normalized plot comparing all four of the rhyolitic units from within the study area.

anomaly not seen in other samples from the unit. These samples all display similar lithological characteristics, with only minor amounts of alteration visible in thin section. This coupled with the compatible nature of Sr, TiO_2, Sc and V, suggests the observed depletions are due to chemical fractionation.

Although units 1 and 2 are at least 40 Ma older than Unit 9, the trace-element geochemistry of all three units are very similar (Figure 3-34). The trace-element geochemistry supports the view based on major-element data that there has been very little change in the source melting process over the 40 Ma time span of the rhyolite units.

3.3.4 Ash-flow Tuffs

The ash-flow tuffs within the region typically show the same geochemical trends as the rhyolite units described above (Table 3-19). These ash-flow tuffs plot within the rhyodacite field of Winchester and Floyd (1977; Figure 3-35) and fall within the same region as the rhyolites on the Nb-Y tectonic plot of Pearce *et al.* (1984; Figure 3-36). In Figure 3-37, all three ash-flow tuffs are combined due to their similar trace-element pattern. They are enriched in Ba and K_2O and depleted in Sr, TiO_2, Sc and V; Unit 4 is more depleted in V relative to other units.

A sample of wall rock from Unit 13 was collected adjacent to an auriferous low-sulphidation vein (sample GS-02-087) to test the effects of alteration. This sample is highly enriched in Ba and is depleted in La and Ce while the other trace-elements remain unaffected by the alteration. This mobility of the LREE (La and Ce) has been demonstrated in numerous areas, all of which occur in close proximity to the
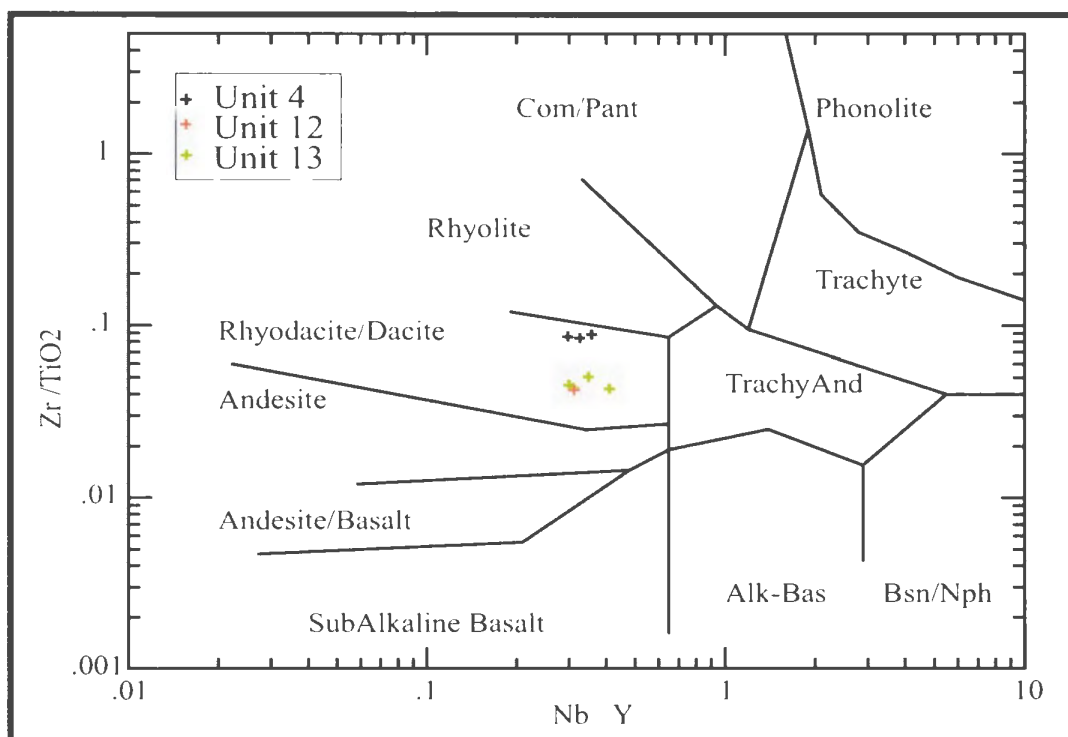
Figure 3-35: Trace-element discrimination diagram of Winchester and Floyd (1977), showing the rhyodacitic nature of the ash-flow tuffs within the study area.
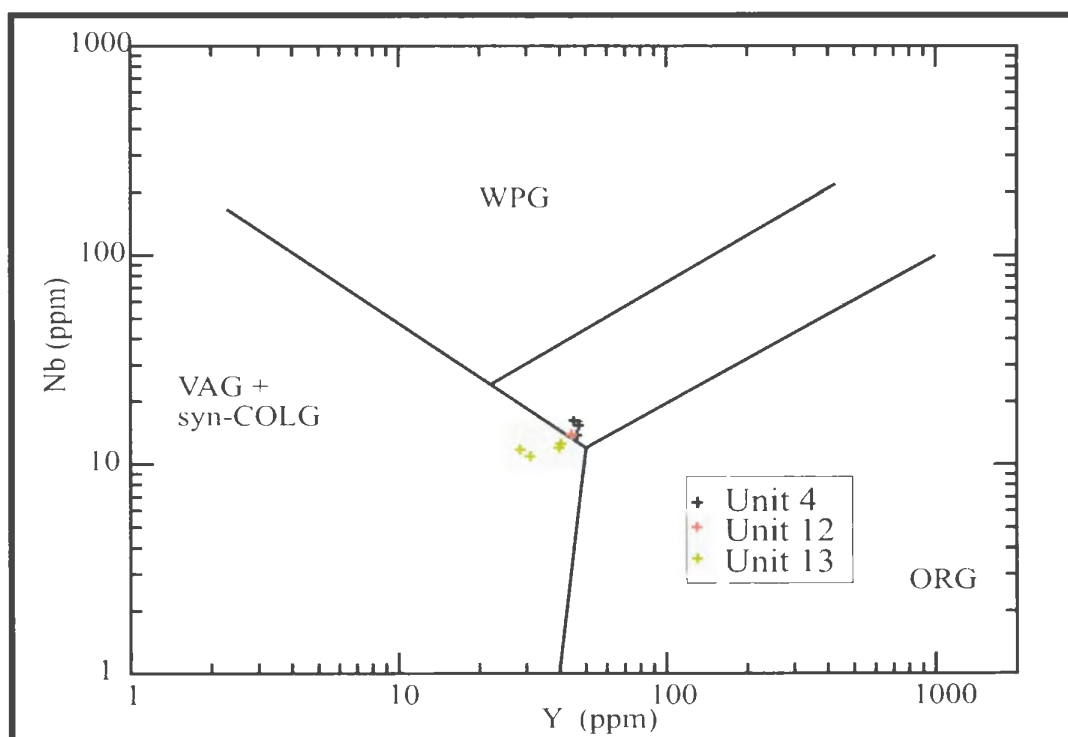
Figure 3-36: Nb-Y tectonic plot of Pearce *et al.* (1984) displaying the tectonic affinity of the ash-flow tuffs within the study area.
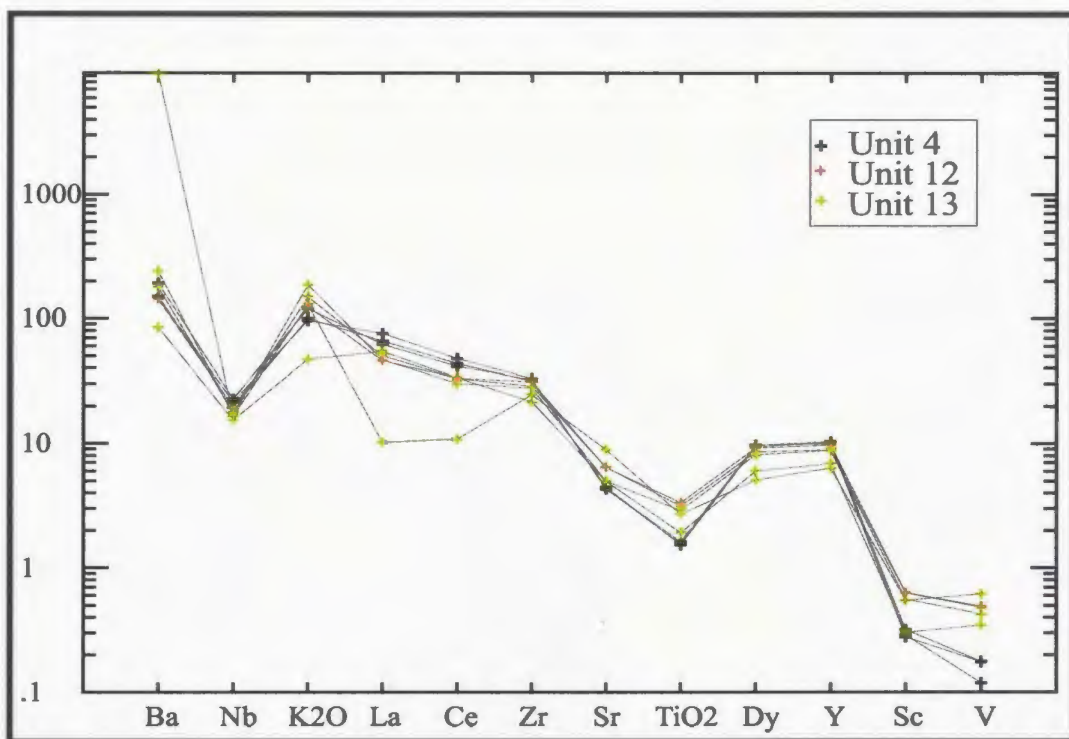
Figure 3-37: Primitive mantle-normalized spider diagram for ash-flow tuffs within the study area.
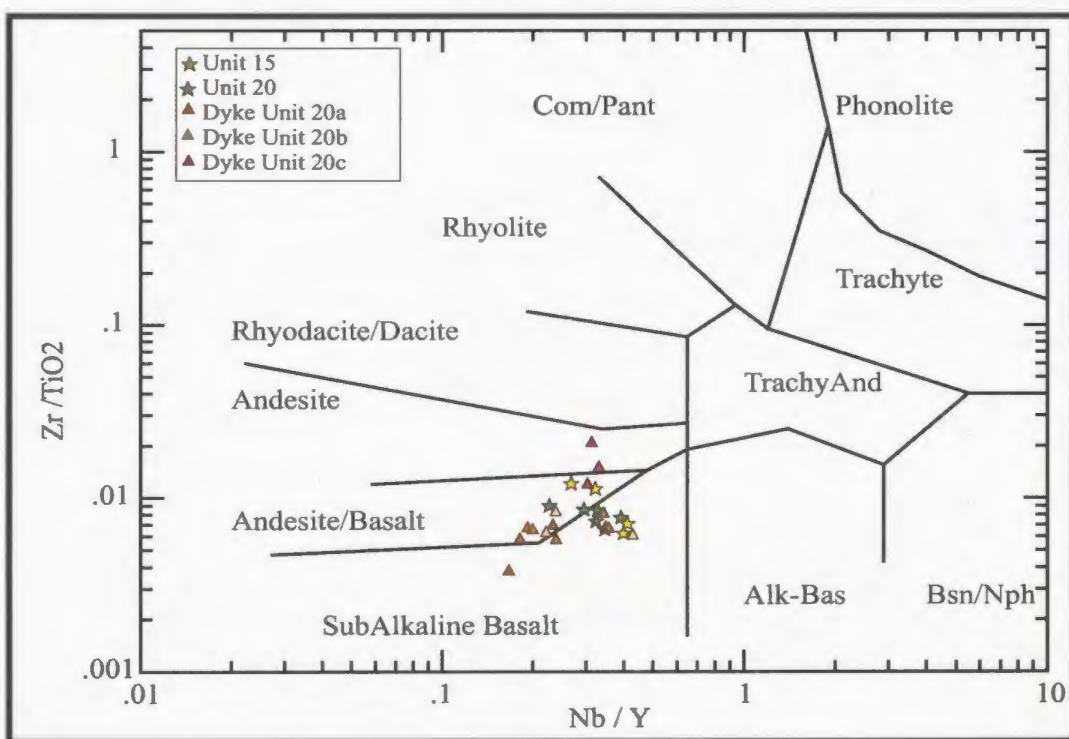
Figure 3-38: Trace-element discrimination diagram of Winchester and Floyd (1977) for mafic units within the study area.

development of low-sulphidation veins. Despite their age difference of 34 Ma, Unit 4 and Unit 13 have very similar trace-element patterns. Nevertheless they can be segregated by using element–element ratios, as indicated in Figures 3-35 and 3-36.

3.3.5 Mafic Units

Mafic units within the study area span the fields of andesite to subalkaline basalt on the Zr/TiO_2–Nb/Y discrimination diagram of Winchester and Floyd (1977; Figure 3-38). Although the mafic rocks of the MVS cluster within Figure 3-38, the trace-element pattern is highly variable, suggesting that this group contains more than one unit (Figure 3-39; Table 3-20). This is likely, given that this group incorporates all mafic flows and/or intrusions not associated with the WHPC. In general, this unit is enriched in Ba and K_2O and weakly enriched in Y and is also characteristically depleted in Nb, Sr and Sc. Samples GS-02-010 and GS-03-105 have similar element-element ratios for the immobile trace-elements and are therefore assumed to be related.

Samples OB-00-289 and GS-03-039 have contrasting element ratios and therefore may represent separate units. Sample OB-00-289 displays a minor enrichment in P_2O_5 and is deleted V with respect to the other samples. Sample GS-03-039 is depleted in Ba and K_2O, enriched in Na_2O and displays a minor depletion in P_2O_5 and a minor enrichment in Sr. Sample GS-02-010, which was collected in the vicinity of low-sulphidation veining, is the only sample with a Nb/La ratio >1. As discussed above, this chemical anomaly is attributed to the development of low-sulphidation veins and/or associated breccias. The development of low-sulphidation veins within the mafic rocks of the

140
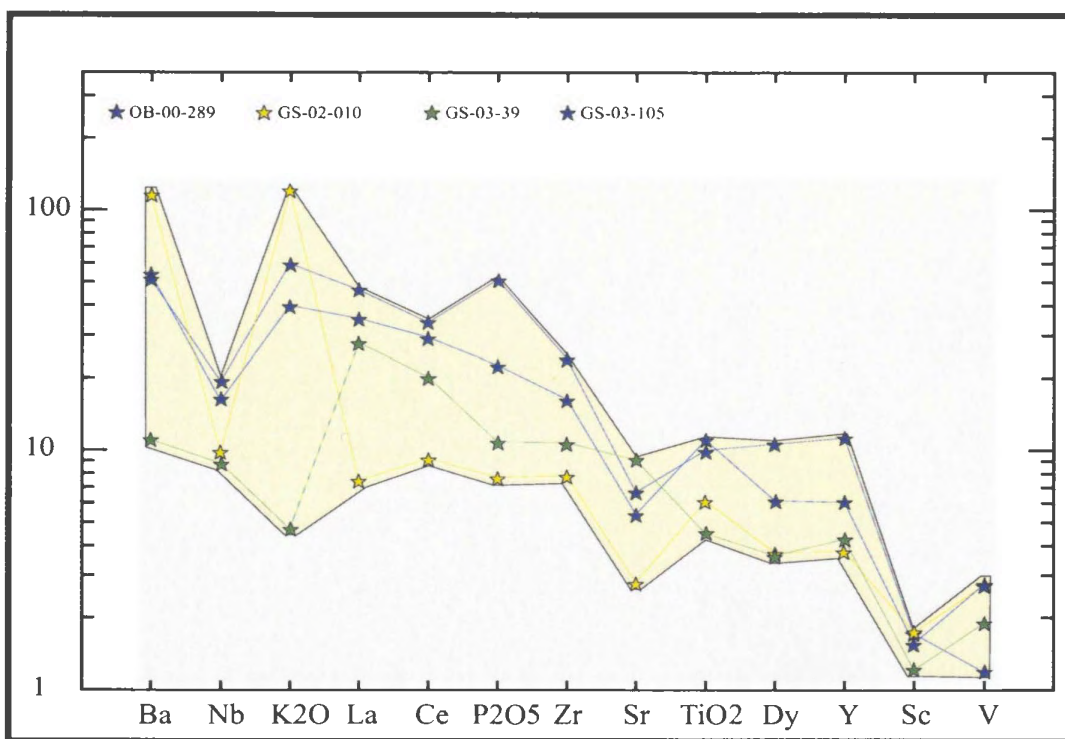
Figure 3-39: Primitive mantle-normalized spider diagram for mafic rocks of Unit 15.
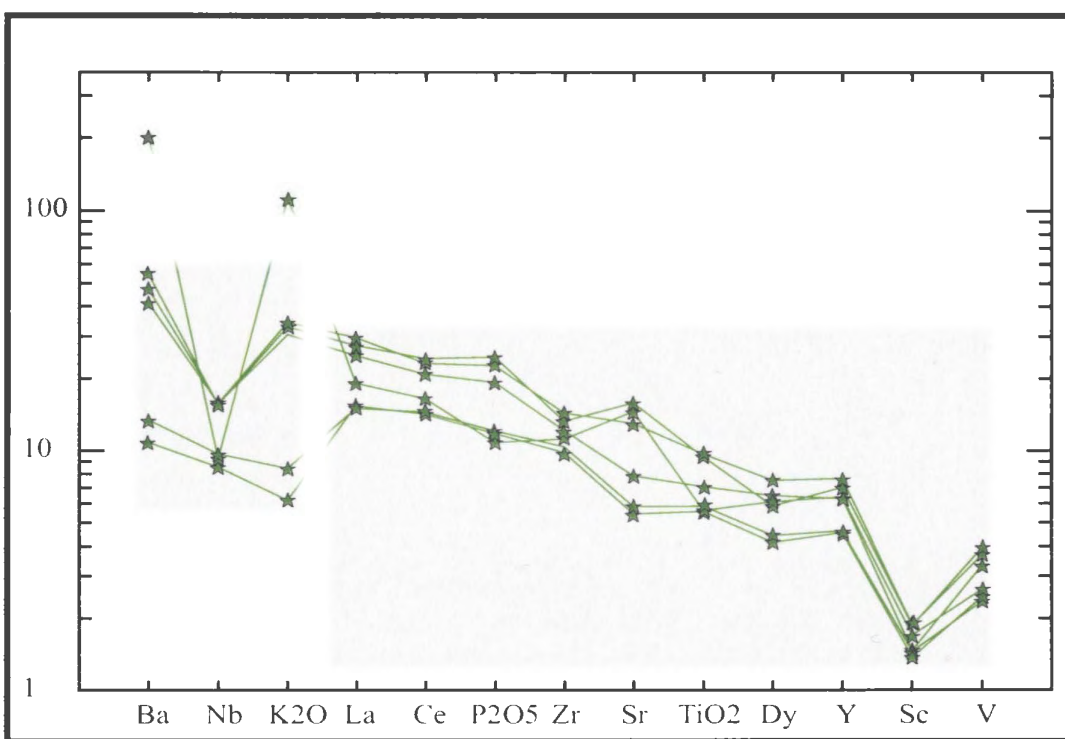
Figure 3-40: Primitive mantle-normalized spider diagram for mafic rocks of Unit 21.

141

MVS at the Bergs prospect is the only evidence of epithermal alteration identified within the unit. In the area of the Oval Pit mine the unit develops patchy pyritization, however this alteration is not suspected to be related to the development of the advanced argillic alteration.

The mafic volcanic rocks associated with the WHPC form a chemically homogeneous group, with only a minor amount of scatter developed within the mobile trace-elements (Figure 3-40; Table 3-20). This unit is characterized by enrichments in Ba, and less so, Y, and depletions in Nb and Sc. Sample OB-01-001 is highly enriched Ba, and also displays a positive Sr anomaly, along with depletions in P_2O_5, and TiO_2. Samples OB0-00-280, OB-01-003 and OB-01-004 display a minor enrichment in P_2O_5 and OB-00-280 is also enriched with Sr. The anomalous Ba concentrations are coincident with the corresponding high values of K_2O and those samples that are depleted in Ba are distinctly more sodic. As this unit is contained within the post-alteration WHPC these anomalies are not assumed to be associated with epithermal alteration. Aside from Nb, all other elements mentioned above are compatible and consequently, the differences in concentration are attributed to varying degrees of chemical fractionation.

The grouping of mafic dykes based on major-element geochemistry (section 3.2) is less obvious in the trace-element data. However, subtle variations do exist (Table 3-20). The larger group of dykes (Unit 20a) is characterized by varying degrees of Ba and K_2O enrichment and a slight enrichment in Y (Figure 3-41). These dykes also display negative Nb, Sr and Sc anomalies, as well as varying degrees of a negative Dy anomaly. Unit 20b (OB-01-002, OB-01-044, GS-03-124) displays a minor enrichment in Ba and
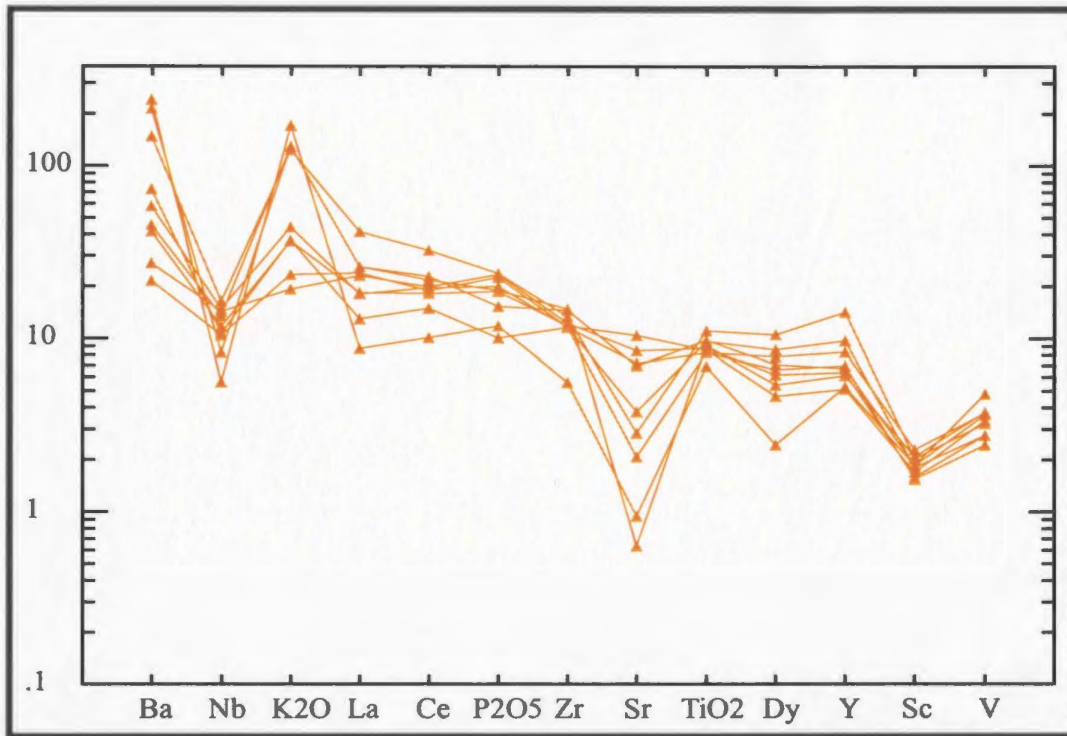
Figure 3-41: Primitive mantle-normalized spider diagram for mafic dykes in group 20a.
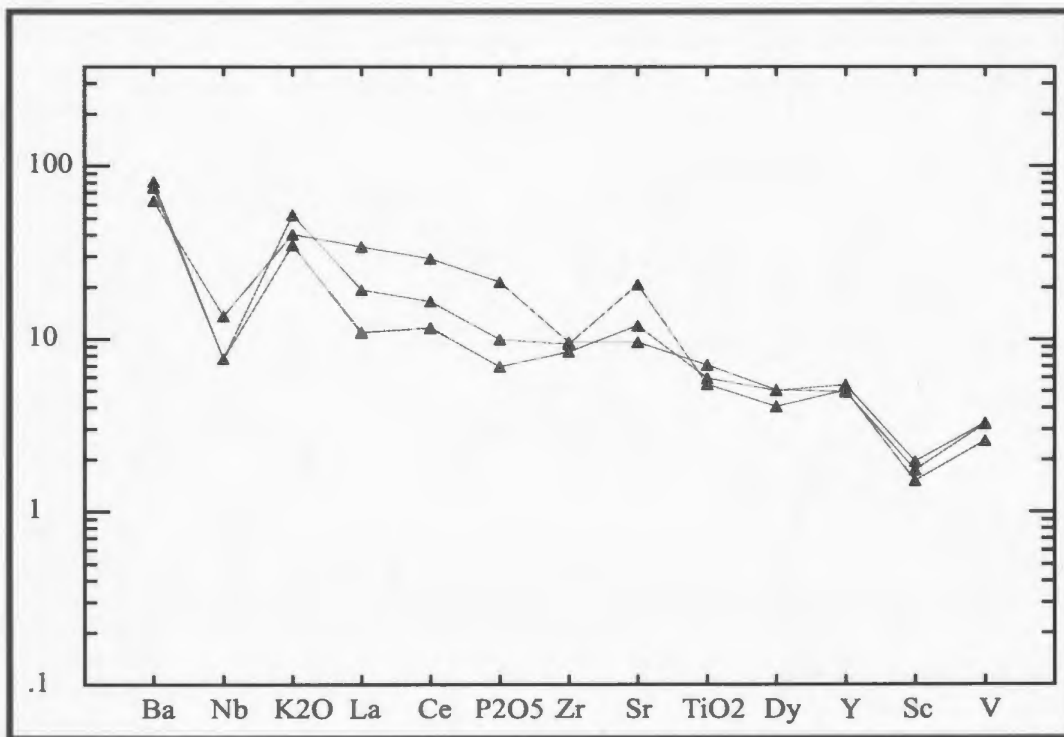
Figure 3-42: Primitive mantle-normalized spider diagram for mafic dykes in group 20b.

143

K_2O with two of the three samples also showing a strong Sr enrichment (Figure 3-42). As with the other group, this unit has pronounced negative Nb, Sc and minor Dy anomalies. Within this group, one sample has a minor depletion in La with respect to Ce, and two of the samples display a weakly negative P_2O_5 anomaly. The third group of mafic dykes (Unit 20c) is characterized by positive Ba and K20 anomalies and a weak enrichment in Sr and Y. This group also displays negative Nb, and Sc anomalies and minor depletions in P_2O_5 and TiO_2 (Figure 3-43).

Data demonstrate that several discrete chemical anomalies are characteristic for certain groups of mafic dykes. For example, Unit 20b is the only group that displays a strong enrichment in Sr. This may also provide further supporting evidence that this group of mafic dykes is related to the amygdaloidal basalt since it also is enriched in Sr.

Tectonic discrimination diagrams suggest that mafic units from the MVS and the WHPC originate in a volcanic-arc, or within-plate type setting (Figure 3-44). The discrimination diagram of Pearce and Norry (1979) also indicates that the volcanic rocks are influenced by continental crust as indicated by the elevated Zr/Y ratios (Pearce, 1983; Figure 3-45). Not all discrimination diagrams are as effective in classifying the mafic units as indicated by Figure 3-46. The predominant portion of the mafic units plot within the MORB–back-arc basin basalt field, while some of the more V-enriched samples plot within the overlapping fields of MORB–BAB and continental flood basalts. The mafic rocks of the MVS displays a considerable amount of scatter again suggesting the presence of more than one unit within the group.
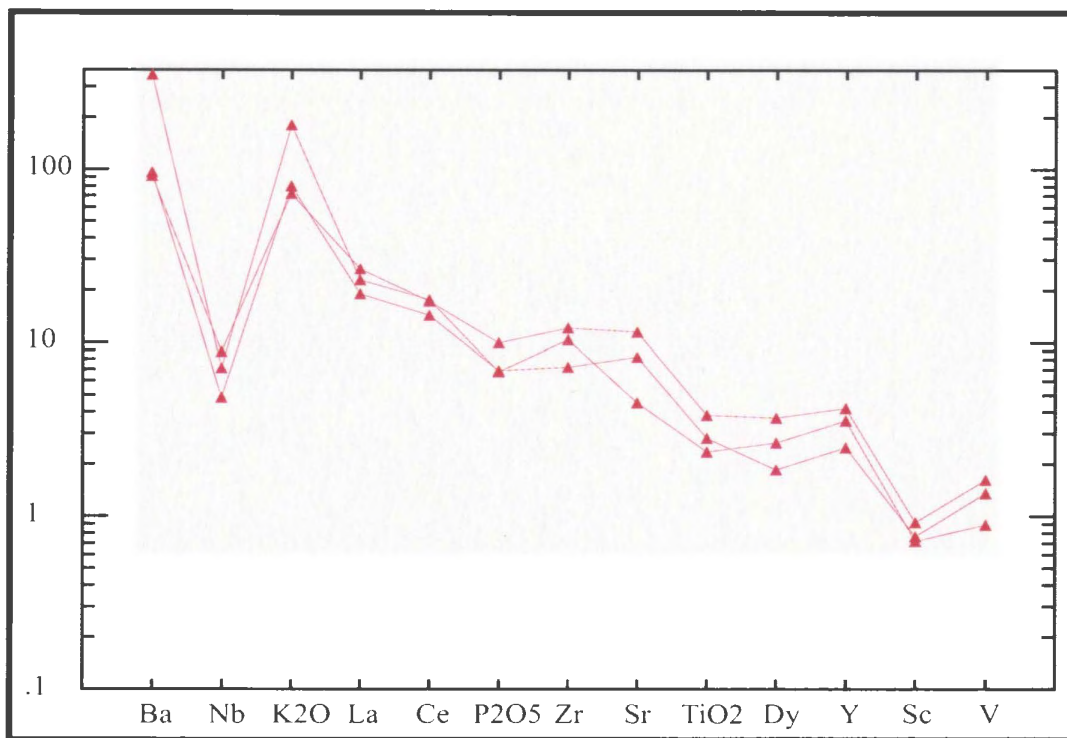
Figure 3-43: Primitive mantle-normalized spider diagram for mafic dykes in group 20c.
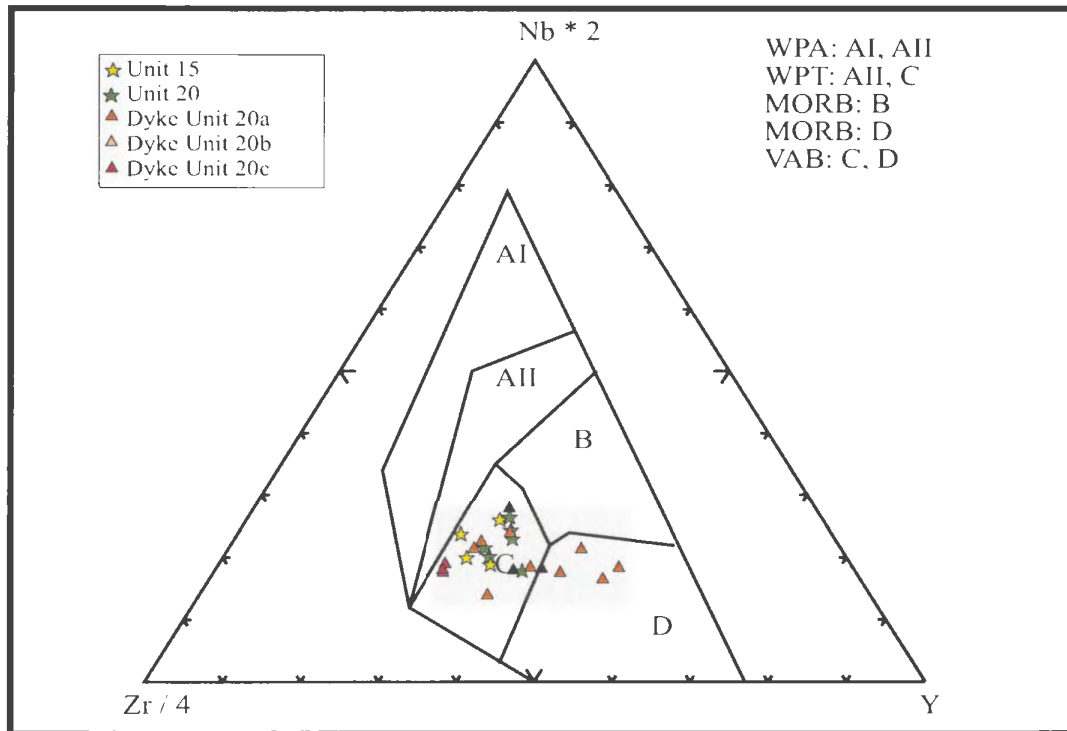
Figure 3-44: Discrimination diagram for basalts after Meschede (1986).
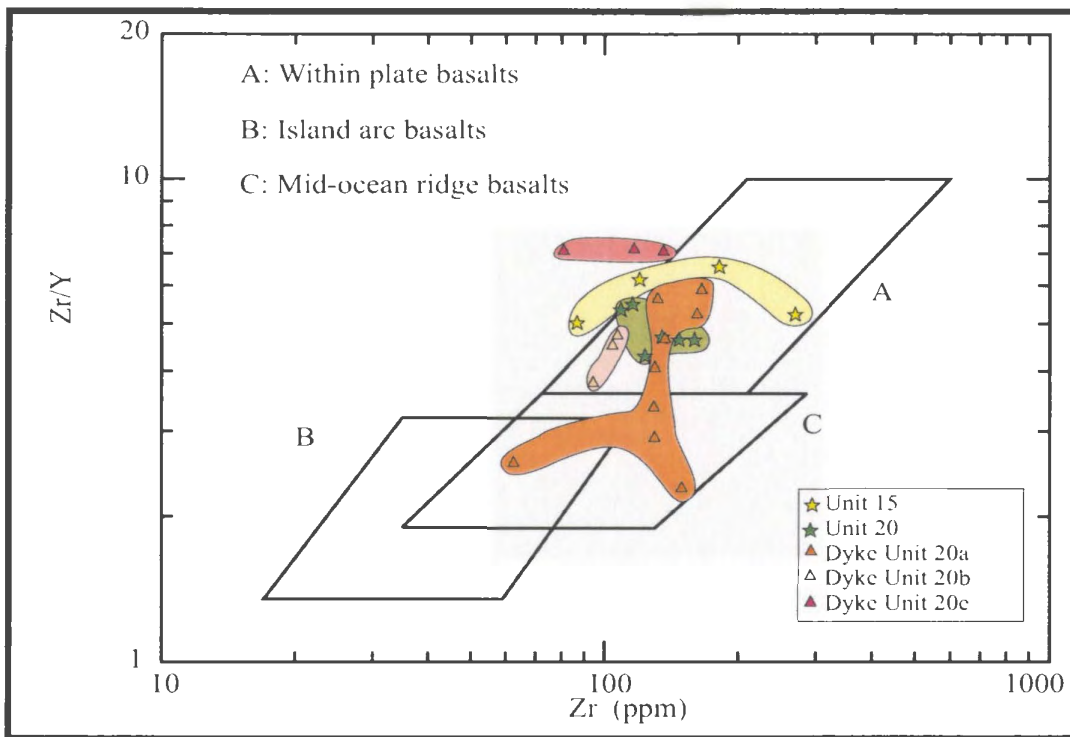
Figure 3-45: Tectonic discrimination diagram for basalts (after Pearce and Norry, 1979). Note the predominantly higher Zr/Y ratios (>3) of most of the mafic units, which suggests continental input into arc construction (Pearce, 1983).
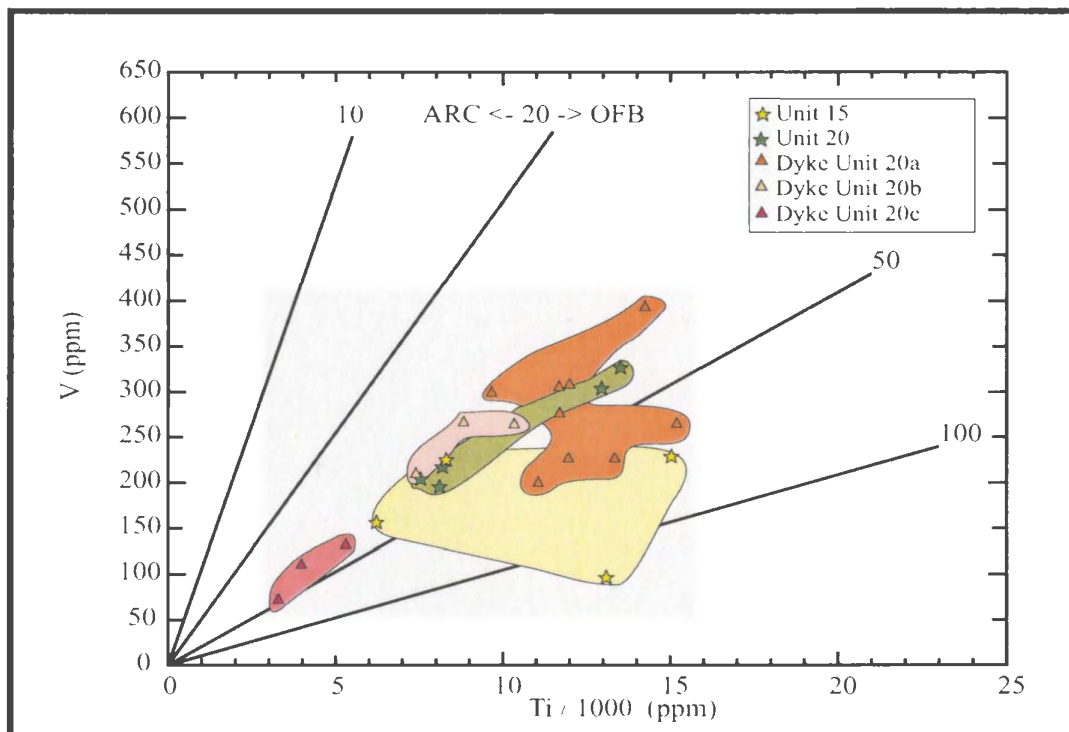
Figure 3-46: Ti-V discrimination diagram for basalts after Shervais (1982).

3.3.6 Fowlers Road Porphyry (WHPC)

Unit 22 represents the youngest known magmatic event within the high-alumina belt. This unit plots within the rhyolite field of Winchester and Floyd (1977; Figure 3-47). Two separate pulses of magmatism appear to be represented by the geochemistry, as mentioned in the major-element section (Table 3-21). The samples collected at Fowlers Road have enrichments in Ba and K_2O, and have less Zr than the samples collected approximately 1km to the west. The samples collected to the west of Fowlers Road are depleted in Ba and K_2O, and have slightly higher Zr concentrations. Aside from these minor chemical differences this unit displays uniform element-element ratios and only weak negative Nb anomalies (Figure 3-48). Unit 22 is chemically distinct from the older porphyry of the WHIS as it is enriched in Dy and Y, and depleted in Sr and V in comparison to Unit 8.

Trace-element geochemistry support the field data that suggest that Unit 22 may have been emplaced in a somewhat different tectonic environment. In contrast to Unit 8 of the WHIS, Unit 22 plots outside of the volcanic arc field (Figure 3-49). Field relationships supporting the assumption of a different tectonic environment include the fact that Unit 22 intrudes sedimentary rocks that unconformably overlie the majority of the volcanic units within the region. This suggests that Unit 22 intruded during basin infilling, which is thought to represent the beginning of arc-collapse.
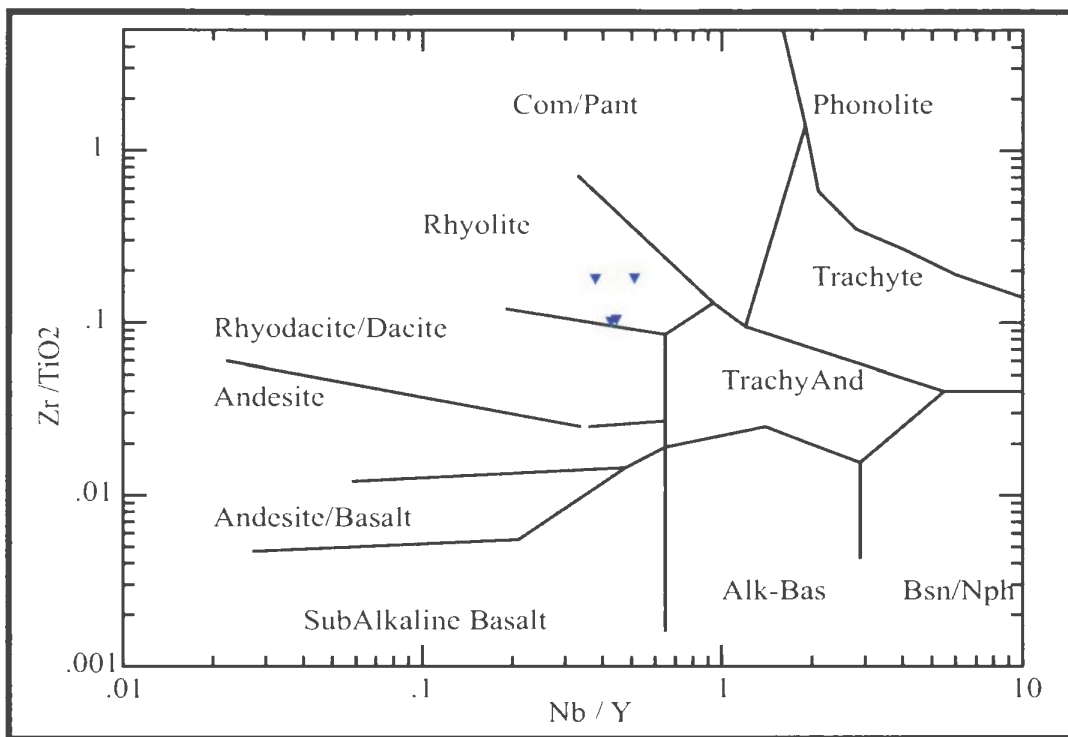
Figure 3-47: Trace-element discrimination diagram of Winchester and Floyd (1977) for Unit 22.
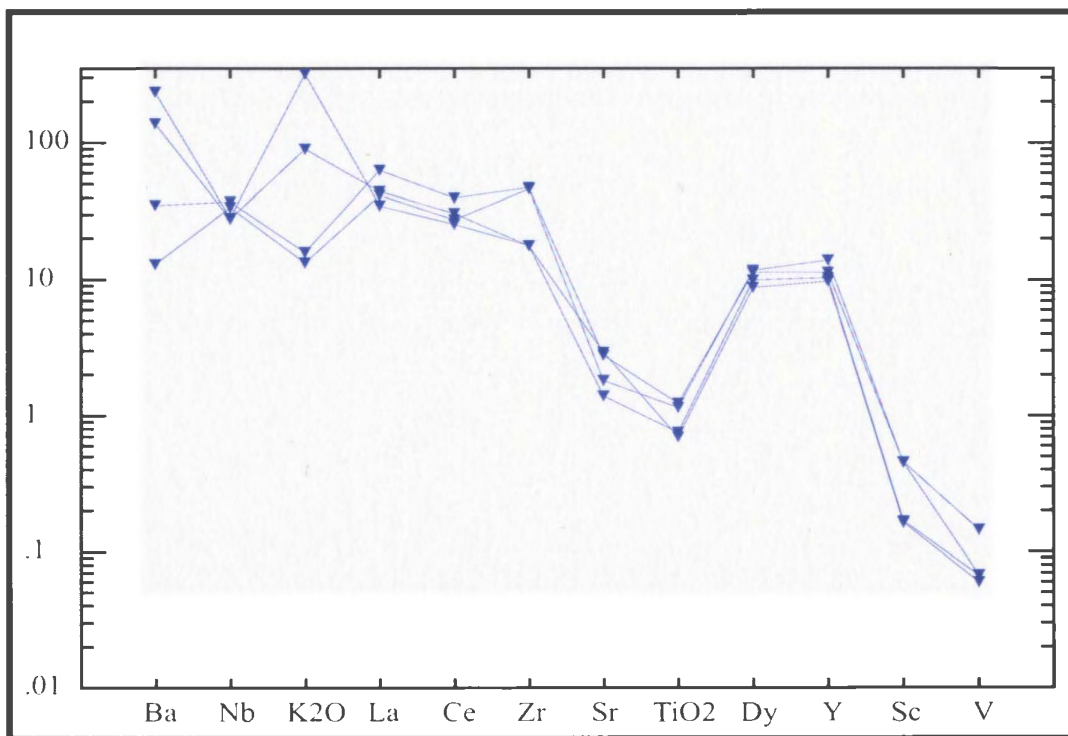
Figure 3-48: Primitive mantle-normalized spider diagram for Unit 22.
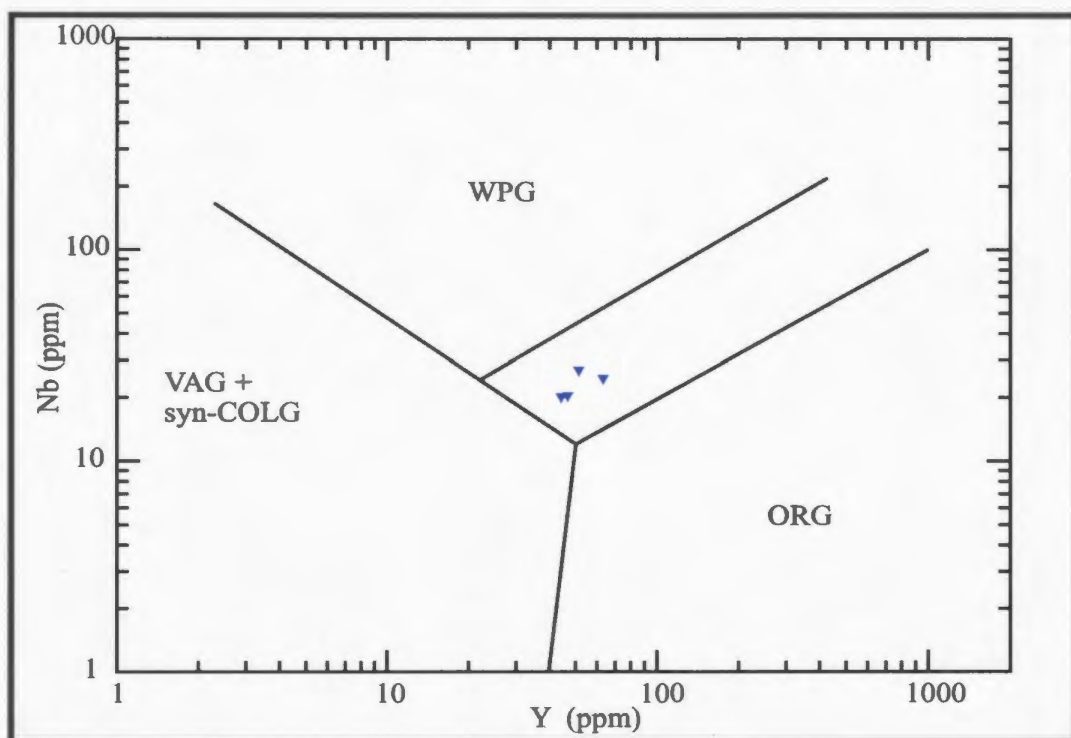
Figure 3-49: Nb-Y tectonic plot of Pearce *et al.* (1984) displaying the tectonic affinity of Unit 22.
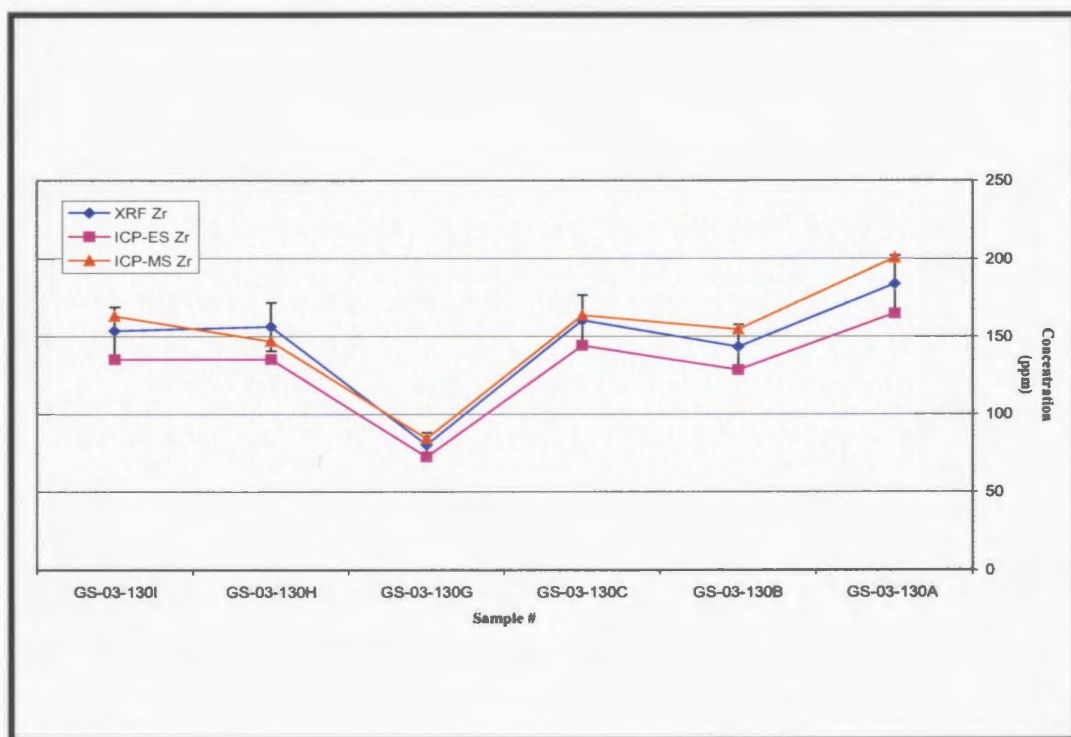
Figure 3-50: Comparisons of Zr values from the three different techniques used to analyze the lithic tuff.

3.4 LREE MOBILITY ADJACENT TO LOW-SULPHIDATION VEINS

3.4.1 Introduction and Sampling Strategy

The regional dataset described in the previous section showed some evidence of La depletion in areas of low-sulphidation veining. Given the potential significance for vein origin and mineral exploration, it was decided to investigate the phenomenon further. This was done by way of additional sampling in the region of the Steep Nap prospect, where a section of roadside outcrop provides an excellent cross-section through a 1.9m wide colloform-crustiform, chalcedonic silica–adularia ± calcite low-sulphidation vein, hosted by a polymict volcaniclastic unit (Unit 3; Plate 3-1 and 3-2). In order to investigate the mobility of elements adjacent to the hydrothermal vein, it was first necessary to determine the chemical homogeneity of the host rock. This test was necessary to prove that the variations in element concentrations are the result of hydrothermal alteration and not the effects of chemical heterogeneities within the host. To do this, two samples distal to the roadside outcrop and six host rock samples collected adjacent to the vein were analyzed for a complete ICP-ES package (Tables 3-22 and 3-23). The six samples of host rock collected at the roadside outcrop were also submitted for ICP-MS (extended trace-elements) and XRF analysis in order to compare the different datasets and identify any analytical problems (Tables 3-24 and 3-25; accuracy and precision of this data is given in Appendix D).

Samples of host rock were collected at 4m, 2m and 1m intervals on both sides of the vein (Plate 3-3). From west to east, the corresponding samples of host rock are GS-
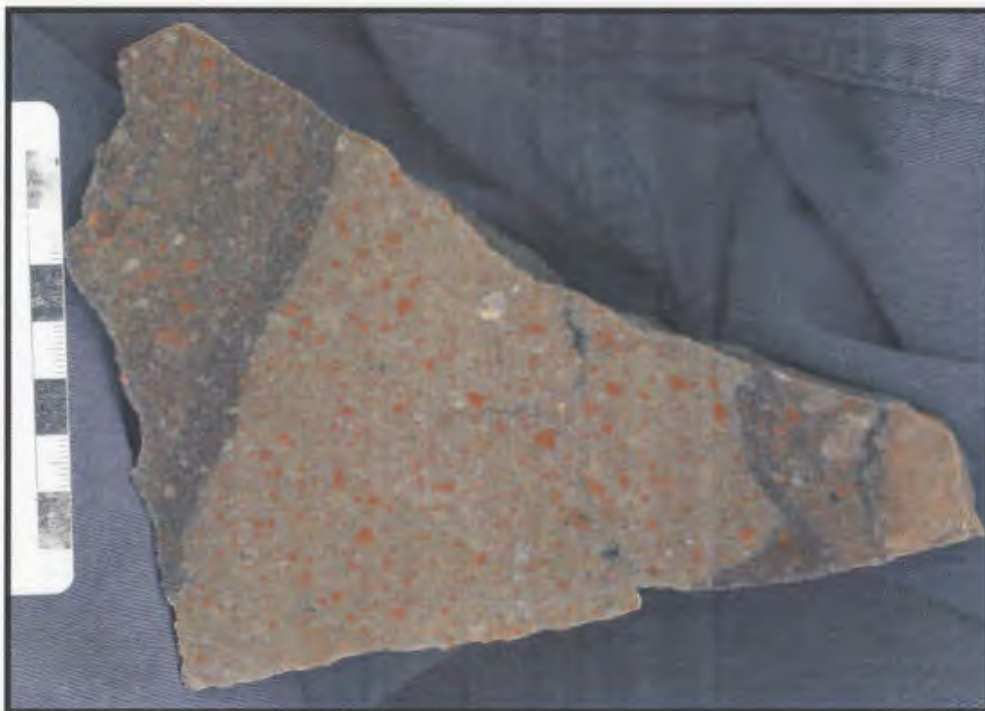
Plate 3-1: Representative hand sample of Unit 3 (Steep Nap prospect).
Note dark orange potassic altered material within the host rock.

Plate 3-2: Representative hand sample of Unit 3 (Steep Nap prospect).
Sample is crosscut by low-sulphidation-related quartz-hematite veins.
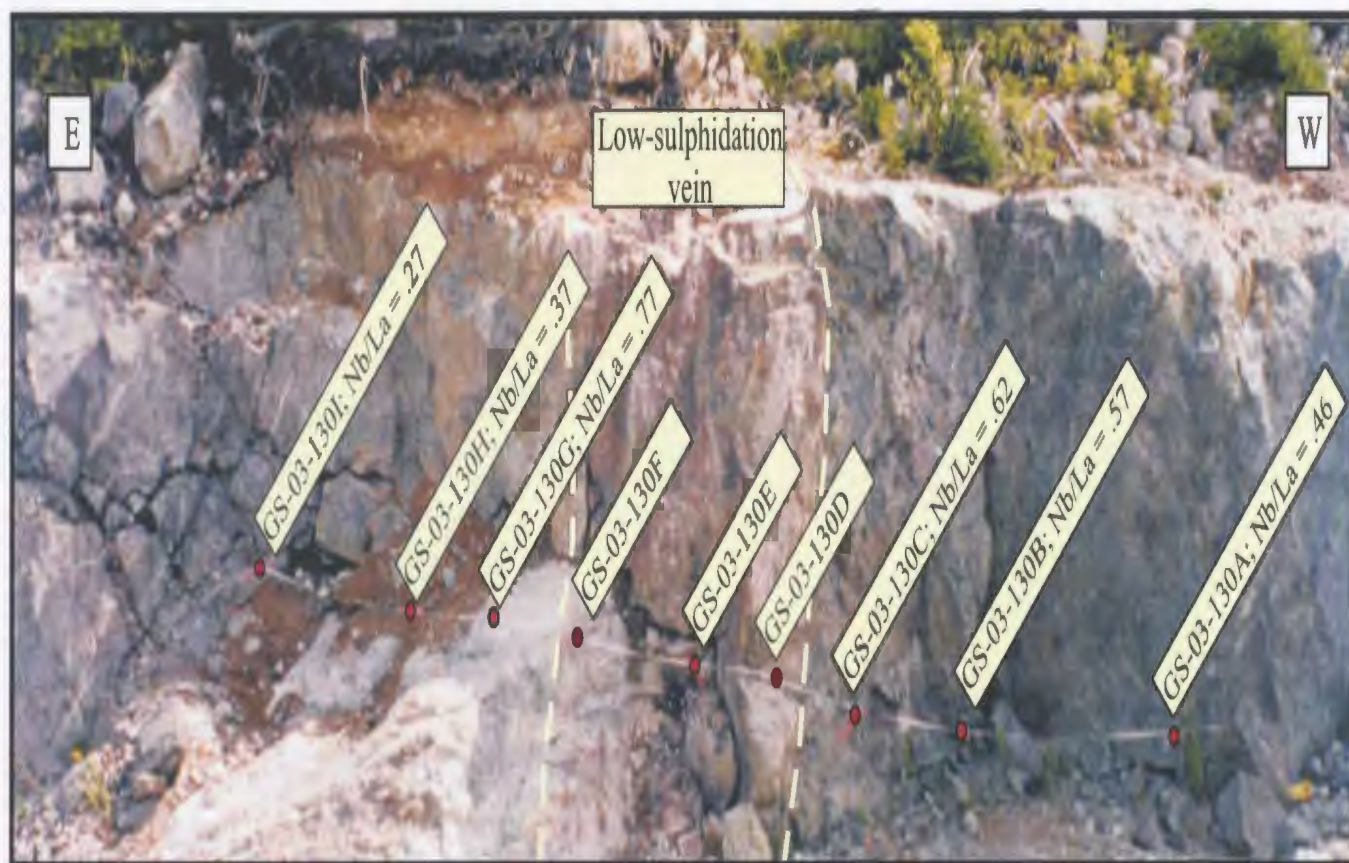
Plate 3-3: Photograph of the measured section carried out at the roadside outcrop with labeled sample locations (Steep Nap prospect).

03-130A, GS-03-130B, GS-03-130C, GS-03-130G, GS-03-130H and GS-03-130I. Three samples of vein material were also collected; they include two samples from the margin of the vein (GS-03-130D and GS-03-130F) and one sample from the central portion of the vein (GS-03-130E).

3.4.2 Comparison of Analytical Techniques

In comparing common elements from the various techniques, several discrepancies between element concentrations were noted. Significant differences, those being greater than 10%, existed between V, Ga, Y, Nb and Ce values measured by ICP-MS and by XRF techniques. From these elements V, Nb and Ce values from the ICP-MS data were consistently less than the XRF data, whereas the elements Ga, and Y values were consistently higher (Table 3-26). The ICP-ES dataset for the six host rock samples contains mostly major-element data, however it does contain the trace-elements Cr, Zr and Ba. In comparing the ICP-ES and the XRF data Fe_2O_3, MgO, CaO, TiO_2 and MnO had differences greater than 10%, as well as Al_2O_3 for 3 of the six samples. It is noted that for most of these samples the concentrations were often less than 1 wt.% (Table 3-27).

For the six samples of host rock the only common element between the ICP-ES and ICP-MS data was Zr. Five of the six samples displayed greater than 10% difference between the Zr values of the ICP-ES and ICP-MS data, with the ICP-ES data being consistently lower. In comparing the Zr values of the three different techniques it was evident that the differences in concentration between the XRF and ICP-ES and the XRF and ICP-MS data were less than 10%. Only when the data from the ICP-ES is compared

to the ICP-MS are the differences in Zr values greater than 10% (Figure 3-50). Appendix C and E shows that the ICP-ES and the ICP-MS datasets are internally consistent, however as shown above caution must be taken when comparing different analytical techniques. For the following discussion the Zr values from the ICP-MS dataset are chosen to be the correct values and are utilized in the corrections for alteration.

3.4.3 Chemical Homogeneity of the Polymict Lapilli Tuff (Unit 3)

Sample GS-02-085 was collected 100m to the south of the main vein and is distal (>10m) from any major hydrothermal vein development. Sample GS-03-100 was collected approximately 200m to the south of the main vein, which is located 1m from a major vein and breccia zone. Comparison of the two samples shows that the main immobile trace elements Y, Zr, Nb, and Dy all differ by less than 10%, which is chosen to be the acceptable analytical error (Figure 3-51). From this example, it is therefore assumed that the trace-element geochemistry of this unit is homogeneous even when sampled over a distance of a couple hundred meters.

Sample GS-02-085, taken to represent the least altered sample, was then compared to the two samples collected 4m from either side of the low-sulphidation vein. From this comparison it was determined that GS-03-130A was the least altered of the two samples, as the Al_2O_3 and Zr (the two main immobile elements used) values differed by <10% when compared to the relatively unaltered sample GS-02-085. Sample GS-03-130A also has a lower SiO_2 value (in comparison to GS-03-130I), thus showing less effects of silicification (Table 3-28). Although sample GS-03-130A is somewhat altered, it was chosen as the best representative of weakly altered host rock because a pristine
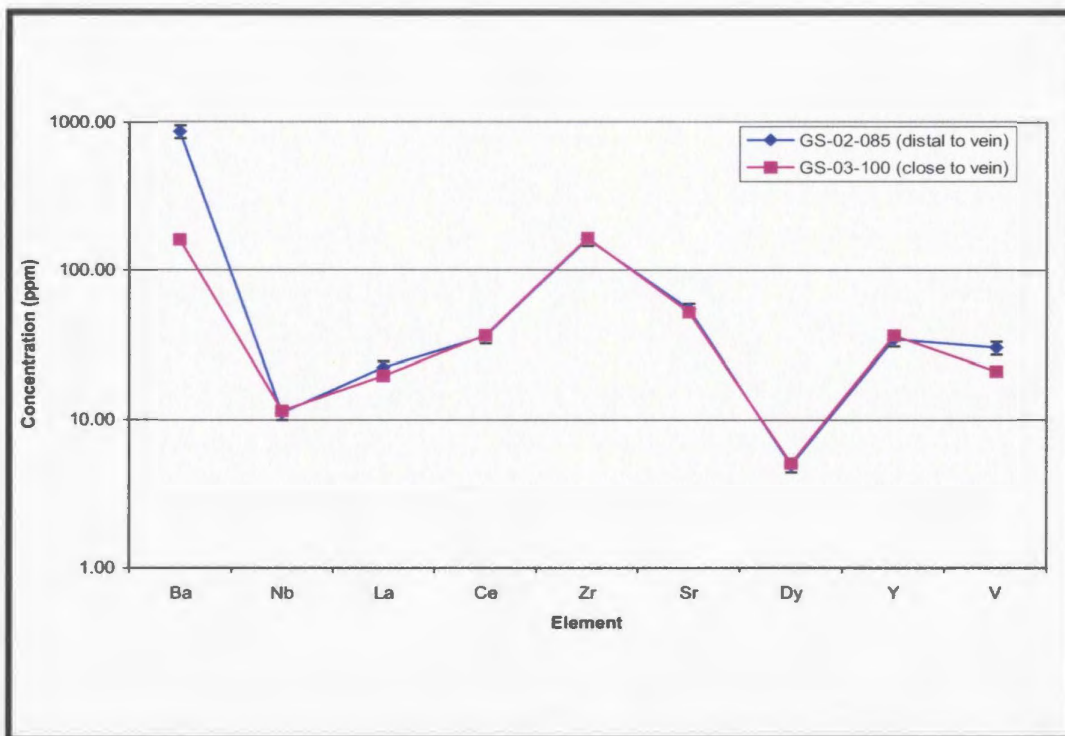
Figure 3-51: Comparison of the lithic tuff samples collected south of the main road outcrop. Note sample GS-02-085 contains a +/-10% error bar.
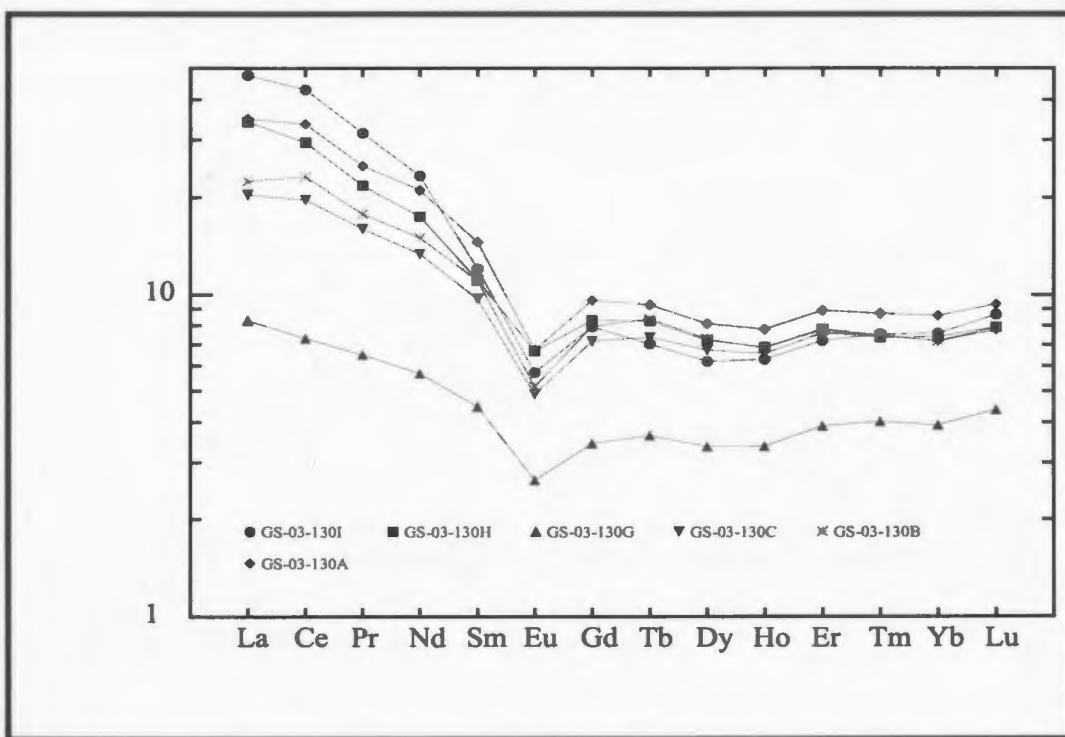
Figure 3-52: Primitive mantle-normalized REE patterns of the raw ICP-MS data from Unit 3.

sample of this unit is unavailable.

3.4.4 Element Mobility Adjacent to Low-Sulphidation Veining

In order to compare the mass gain/loss of the six host rock samples the effects of dilution due to alteration must be corrected for. This was done using the Zr values from the ICP-MS dataset. The Zr value of sample GS-03-130A, which is chosen to be the precursor, is divided by the Zr values of the altered samples thus providing a correction ratio for each sample. The geochemical data for each sample is then multiplied by this ratio to correct for any dilution effects created by the alteration (e.g. silicification; Barrett and MacLean, 1994). For ease of comparison the corrected element concentrations are then divided by the concentration of the same element in the precursor. This provides a ratio of altered vs. precursor for each element. Those elements with ratios >1 are enriched in comparison to the precursor, while those elements with ratios <1 are depleted with respect to the precursor (Figures 3-52 and 3-53).

From Figure 3-53, it is evident that the concentration of the LREE decreases with proximity to the vein. Samples GS-03-130I and 130A are the furthest from the vein and therefore have the highest concentration of LREE. In comparing individual samples to the unaltered precursor. It is evident that sample GS-03-130I has a ratio >1 for the elements La, Ce, Pr and Nd; this may reflect higher concentrations of these elements in the original sample with respect to the precursor or overcompensation due to the alteration correction. Sample GS-03-130C and GS-03-130G both show depletion in La, Ce, Pr, Nd, and Sm, whereas the values of Eu-Lu are all close to 1. This depletion
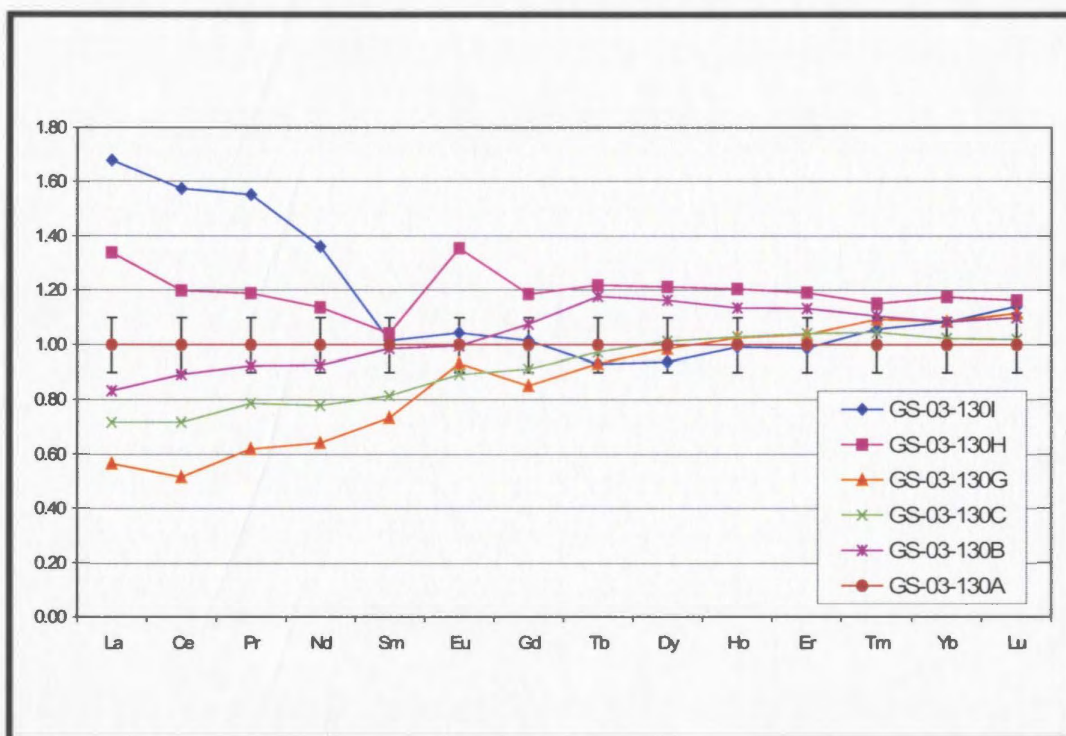
Figure 3-53: Corrected element concentrations for Unit 3 in comparison to the precursor (GS-03-130A). Note +/-10% error bar applied to precursor.

suggests that the LREE become mobile adjacent to the vein. It is also evident that this alteration halo is not symmetrical disposed since sample GS-03-130H does not show any depletion in the LREE and sample GS-03-130B, which is equidistant from the vein on its opposite side, does.

This evidence further supports the proposed link between the identified anomalies of Nb/La ratios >1 in rocks near the development of low-sulphidation veining (identified in the regional dataset). It is noted that although the rhyolite units within the region of the Steep Nap prospect have Nb/La >1, the volcaniclastic rock hosting the low-sulphidation veins does not. However, the Nb/La ratio of the volcaniclastic rock does increase with decreasing distance from the vein (Plate 3-3). La can be compared to other immobile elements to display the same end result. However caution must be taken as this anomaly was also identified in a single sample of volcanic rock intruded by Unit 7 in the area of White Mountain (Unit 1, sample OB-97-040).

3.5 SUMMARY

The geochemistry obtained from igneous rocks within the study area can be used to show the various effects of the hydrothermal alteration, as well as segregating older and younger felsic intrusions. In comparing altered and unaltered samples from the same unit it can be demonstrated that the trace elements Nb, Zr, Ti, Y and Dy remain immobile in areas of intense hydrothermal alteration. As a result these elements are relied upon heavily from classifying the various altered units within the study area.

INTRUSIVE ROCKS (HIS, WHIS)

The geochemistry supports the field observations that hydrothermal alteration within the WHIS mainly affects Unit 7, which is characterized by highly variable mobile-element concentrations and local increases in SiO_2 due to silicification. The major-element geochemistry from the WHIS also demonstrates that Unit 7 and Unit 8 are chemical differentiates of Unit 6. The granitic rocks from the WHIS and HIS display very similar geochemical patterns. This suggests the WHIS, although more compositionally diverse than the Holyrood Granite, is actually comagmatic with the larger HIS. This is further supported by geochronology (Chapter 4). Geochemically, WHIS monzonite is like that of the Woodfords monzonite from the western side of the Holyrood Horst. In this instance, it is noted that the age of the units differ by 20 Ma (see O'Brien et al., 2001).

FESLIC VOLCANIC ROCKS (WMVS, MVS)

The geochemistry of the felsic volcanic units within the area displays very little variation, even when comparing units that have known age differences of at least 40 Ma. This chemical similarity between older and younger felsic volcanic rocks within the study area precludes inferring a co-magmatic source for the volcanic rocks. However, it also demonstrates that similar processes were ongoing throughout the same 40 Ma time span. The only variation observed within the geochemistry of the felsic volcanic rocks is induced by hydrothermal alteration. This alteration locally characterizes certain regions within the field area, for instances flow-banded rhyolites in the region of the Steep Nap prospect area characterized by Nb/La ratios >1. This is attributed to the mobility of La near the development of low-sulphidation veins and associated breccias. This mobility of

the LREE adjacent to low-sulphidation-related features is recognized in several areas and a number of units within the field area (Bergs and Steep Nap prospects). A detailed examination of this anomaly was carried out at the Steep Nap prospect, and it was demonstrated that the mobility of La and other LREE increased with decreasing distance from a large (approximately 1.9m) colloform-crustiform banded, low-sulphidation vein.

MAFIC VOLCANIC AND PLUTONIC ROCKS (WHPC)

In contrast to the felsic volcanic rocks, the mafic volcanic rocks and dykes within the study area do show chemical variations between the units. The mafic volcanic rocks included within the MVS can be separated from the mafic volcanic rocks of the WHPC using both major- and trace-element geochemistry. The chemistry of these mafic volcanic rocks record a transition from bimodal to predominantly mafic volcanism, suggesting a change in the overall tectonic environment. The major-element and trace-element geochemistry is also useful in identifying three separate groups of mafic dykes within the study area, although the trace-element variations are much more subtle.

This change in tectonic environment is also supported by the trace-element geochemistry of Unit 22, which plots outside of the volcanic-arc field on the Nb/Y tectonic plot of Pearce *et al.* (1984). This post-alteration porphyry represents the youngest magmatic event exposed within the field area and is chemically distinct from the pre-alteration quartz–feldspar porphyry of the WHIS. The geochemical data independently reflect the change in environment marked by the onset of sedimentation and marine mafic volcanicity and the possible transition into a back-arc type setting.

Table 3-1: Major-element contents of granite from the Holyrood Intrusive Suite.

Sample Number	Unit	Easting	Northing	Element	SiO2	TiO2	Al2O3	Fe2O3	FeO	MnO	MgO	CaO	Na2O	K2O	P2O5	LOI	Total
				Method	ICP-ES	ICP-ES	ICP-ES	ICP-ES	ICP-ES	ICP-ES	ICP-ES	ICP-ES	ICP-ES	ICP-ES	ICP-ES		
				Unit	%	%	%	%	%	%	%	%	%	%	%	%	%
				Limit	0.01	0.001	0.01	0.01	0.01	0.010	0.01	0.01	0.01	0.01	0.001		
Granite (HIS)																	
OB-97-033	N/A	347327	5257444		75.91	0.089	13.01	0.58	0.43	0.055	0.27	0.23	4.02	4.32	0.018	0.81	99.80
OB-97-035	N/A	348872	5255961		72.99	0.213	14.30	0.76	1.21	0.084	0.72	1.36	4.14	3.61	0.064	1.22	100.81
OB-97-039	5	351100*	5259850*		71.72	0.219	14.48	2.19	0.46	0.073	0.68	0.66	4.54	4.33	0.062	1.08	100.56
OB-97-045	N/A	344829	5255672		73.58	0.167	13.65	1.13	0.26	0.051	0.36	0.62	4.07	4.98	0.028	1.09	100.02
OB-97-047	N/A	342388	5255496		73.44	0.229	13.87	1.03	0.35	0.112	0.31	0.76	4.71	4.40	0.044	0.74	100.02
OB-97-068	N/A	345774	5255000		76.17	0.098	12.97	0.22	0.64	0.068	0.27	0.24	4.30	4.05	0.020	0.69	99.79
OB-97-070	N/A	345660	5255883		75.04	0.099	12.70	0.79	0.29	0.070	0.27	0.42	3.96	4.16	0.021	0.90	98.77
OB-97-309	N/A	348144	5247188		71.84	0.222	14.96	0.80	1.18	0.069	0.75	1.53	4.13	3.47	0.067	1.09	100.24
OB-97-313	N/A	349531	5246909		72.28	0.208	13.85	1.27	0.71	0.068	0.78	1.28	4.02	3.35	0.076	1.15	99.13
OB-97-317	N/A	349107	5245904		76.26	0.111	12.65	0.09	0.69	0.038	0.45	0.32	4.06	3.82	0.020	0.90	99.48
OB-00-067	N/A	350825	5237950		76.00	0.069	13.23	0.39	0.41	0.049	0.14	0.52	3.83	4.00	0.010	0.63	99.33
OB-00-094	N/A	350093	5235860		74.54	0.190	12.44	1.11	0.41	0.070	0.78	0.84	3.71	3.26	0.050	0.97	98.42
OB-00-095	N/A	348776	5234100		74.52	0.176	12.70	1.00	0.48	0.038	0.61	0.49	3.58	4.16	0.082	0.92	98.81
OB-00-103	N/A	347490	5231640		73.23	0.181	13.78	0.36	1.27	0.053	0.53	0.39	3.77	4.55	0.057	0.88	99.20
OB-00-115	N/A	347400*	5233500*		72.83	0.204	13.90	1.00	0.84	0.050	0.53	0.33	4.13	4.19	0.048	0.88	99.01
OB-00-123	N/A	348877	5251759		73.56	0.146	13.74	0.66	0.77	0.055	0.46	0.83	3.79	3.97	0.029	1.06	99.17
OB-00-124	N/A	350114	5250372		75.63	0.112	13.19	0.29	0.69	0.043	0.38	0.28	3.81	4.32	0.034	0.75	99.62
OB-00-125	N/A	350774	5248570		73.03	0.174	14.35	0.76	0.88	0.056	0.77	0.54	4.29	3.76	0.045	0.99	99.75
OB-00-127	N/A	350386	5249636		71.79	0.203	14.84	0.70	1.14	0.073	0.76	0.87	4.12	3.99	0.059	1.09	99.77
OB-00-159	N/A	346000*	5233900*		70.20	0.256	14.95	2.26	0.13	0.046	0.74	0.77	4.49	3.70	0.079	1.10	98.73
OB-00-257	N/A	348356	5251878		72.62	0.210	14.32	0.79	1.10	0.076	0.74	0.65	4.17	3.68	0.055	1.24	99.76
OB-00-258	N/A	348168	5250979		73.29	0.187	13.85	0.60	1.15	0.074	0.60	1.12	3.75	3.90	0.059	1.02	99.72
OB-00-261	N/A	347885	5251506		75.41	0.108	13.00	0.41	0.49	0.033	0.29	0.39	3.70	4.36	-	0.85	99.08
OB-00-262	N/A	346740	5238647		76.89	0.083	13.20	0.24	0.55	0.044	0.18	0.31	4.30	3.62	-	0.95	100.40
OB-00-266	N/A	345770	5236815		72.89	0.210	13.81	1.60	0.36	0.080	0.85	1.04	4.19	3.26	0.060	1.42	99.82
OB-00-304	N/A	345198	5233404		73.03	0.214	13.67	0.67	1.12	0.062	0.57	0.51	4.42	3.80	0.052	1.08	99.32
OB-03-037	5	350803	5261537		71.28	0.158	15.31	1.33	0.29	0.071	0.56	1.28	4.65	3.73	0.054	1.30	100.04
OB-03-042	N/A	353371	5256136		76.22	0.155	11.82	0.82	0.23	0.011	0.23	0.06	3.59	4.27	0.041	1.04	98.52
OB-03-044	N/A	349098	5253378		72.93	0.188	14.26	0.90	0.85	0.071	0.67	0.57	4.57	4.04	0.069	1.19	100.41
OB-03-045	N/A	347819	5252564		76.15	0.113	13.45	0.93	0.17	0.051	0.40	0.33	4.11	4.35	0.028	0.85	100.94
OB-03-047	N/A	345290	5246640		74.67	0.215	13.78	0.93	0.27	0.048	0.27	0.56	4.20	4.69	0.031	0.83	100.54
OB-03-048	N/A	342421	5255456		73.86	0.164	13.87	0.95	0.18	0.083	0.25	0.54	4.56	4.41	0.039	1.99	100.92
OB-03-052	N/A	341243	5256740		77.58	0.011	11.83	0.32	0.07	-	-	0.09	3.92	3.83	-	0.86	98.49
OB-03-053	N/A	341187	5256594		74.04	0.056	12.77	1.16	0.18	0.025	0.09	0.24	3.82	5.07	-	0.73	98.19
OB-03-054	N/A	341138	5256428		73.12	0.149	13.12	1.38	0.30	0.055	0.58	0.56	3.62	4.20	0.042	1.21	98.36
OB-03-057	N/A	349450	5253761		71.44	0.228	14.28	1.90	0.33	0.079	0.74	1.79	4.00	3.07	0.079	1.07	99.04
OB-03-058	N/A	350389	5254934		71.59	0.177	13.92	1.54	0.25	0.067	0.68	1.23	4.00	3.71	0.063	1.25	98.50
OB-03-059	N/A	350697	5255300		72.68	0.163	13.77	0.90	0.76	0.063	0.57	1.18	4.03	3.64	0.058	1.18	99.07

N/A = samples collected outside of field area

* samples with UTM's calculated from registered base map

Table 3-2: Major-element contents of intrusive rocks from the White Hills Intrusive Suite.

Sample Number	Unit	Easting	Northing	Element	SiO2	TiO2	Al2O3	Fe2O3	FeO	MnO	MgO	CaO	Na2O	K2O	P2O5	LOI	Total
				Method	ICP-ES	ICP-ES	ICP-ES	ICP-ES	ICP-ES	ICP-ES	ICP-ES	ICP-ES	ICP-ES	ICP-ES	ICP-ES		
				Unit	%	%	%	%	%	%	%	%	%	%	%	%	%
				Limit	0.01	0.001	0.01	0.01	0.01	0.010	0.01	0.01	0.01	0.01	0.001		
Monzonite (WHIS)																	
OB-97-376	6	352234	5262047		65.76	0.477	16.02	3.21	0.89	0.092	2.03	1.66	5.10	2.61	0.17	1.78	99.88
GS-02-081	6	351912	5262445		64.56	0.545	15.83	3.10	1.26	0.112	1.83	3.17	4.07	2.64	0.18	2.57	100.01
GS-03-030	6	352544	5261486		65.86	0.477	15.77	1.94	1.96	0.101	1.86	1.86	4.11	2.78	0.15	2.12	99.20
Medium- to Coarse-grained Equigranular Granite (WHIS)																	
OB-97-171	7	352686*	5261096*		75.38	0.185	13.29	1.30	0.34	0.011	0.12	0.33	7.27	0.17	0.050	0.54	99.03
OB-97-221	7	353072*	5263803*		74.70	0.181	13.44	1.11	0.44	0.041	0.63	0.19	3.39	4.69	0.050	1.14	100.06
OB-97-222	7	353068*	5263800*		76.74	0.178	12.04			0.045	0.59	0.24	2.98	3.69	0.054	1.39	99.73
OB-97-223	7	353052*	5263878*		77.70	0.177	11.39	.	.	0.041	0.41	0.28	3.83	3.28	0.050	1.02	100.09
OB-97-226	7	353045*	5263870*		78.43	0.164	11.25	.		0.027	0.30	0.27	4.72	1.98	0.044	0.82	99.41
OB-97-228	7	353048*	5263751*		80.58	0.084	9.55		.	0.011	0.09	0.09	2.25	4.29	0.008	0.82	98.55
OB-97-362	7	352644	5260024		75.33	0.209	13.57	0.66	0.26	0.003	0.24	0.10	3.00	5.43	0.038	1.31	100.20
OB-01-046	7	353476	5264601		73.03	0.205	13.78	0.98	1.14	0.139	1.29	0.25	3.33	3.48	0.030	1.83	99.61
OB-01-060	7	352837	5264286		78.75	0.068	11.23	0.22	0.23	.	0.08	0.05	3.05	4.73	-	0.79	99.21
OB-01-061	7	352899	5264199		73.70	0.168	13.79	0.87	0.69	0.022	0.43	0.08	3.43	4.32	0.040	1.50	99.12
OB-01-066	7	352951	5264145		73.17	0.188	13.94	0.28	1.06	0.042	0.43	0.23	4.25	4.51	0.145	1.22	99.58
GS-02-002	7	352931	5264192		73.63	0.263	12.95	0.36	1.76	0.092	0.79	0.52	3.90	3.78	0.086	1.29	99.60
GS-02-041	7	352988	5264573		75.29	0.190	11.83	1.52	0.34	0.091	1.05	0.49	1.46	4.50	0.033	1.91	98.74
GS-02-073	7	353043	5263806		77.78	0.179	11.85	0.65	0.59	0.046	0.44	0.24	4.01	2.98	0.055	0.75	99.63
GS-02-078	7	351766	5262510		72.79	0.265	14.42	1.82	0.43	0.072	0.99	1.05	4.25	3.40	0.088	1.34	100.95
GS-02-084	7	352615	5262019		72.91	0.223	14.38	1.57	0.57	0.063	0.76	0.38	4.17	3.90	0.081	1.05	100.12
GS-02-092	7	352863	5261776		76.55	0.195	12.44	1.60	0.13	0.014	0.31	0.31	3.91	3.35	0.067	0.81	99.70
OB-03-036	7	351263	5261891		71.24	0.283	14.33	1.78	0.42	0.091	0.78	0.64	4.86	3.44	0.072	1.44	99.42
GS-03-029	7	352415	5261390		74.55	0.123	13.17	0.73	0.52	0.044	0.39	0.38	3.49	4.97	0.038	0.85	99.31
GS-03-077	7	351867	5261012		70.30	0.284	14.37	2.20	0.35	0.082	0.88	1.03	4.24	3.46	0.098	1.12	98.45
GS-03-079	7	351985	5260927		73.80	0.205	13.75	1.42	0.47	0.033	0.44	0.29	4.30	3.74	0.052	1.07	99.63
GS-03-087	7	353340	5261029		71.66	0.195	14.03	1.28	0.58	0.051	0.60	0.34	3.70	4.66	0.061	1.14	98.38
GS-03-109	7	352027	5260759		74.89	0.152	13.21	0.99	0.33	0.024	0.35	0.22	3.79	3.68	0.048	1.03	98.74
GS-03-126	7	352730	5260152		75.07	0.198	13.03	1.17	0.30	0.017	0.40	0.13	2.98	4.29	0.060	1.64	99.33
GS-03-129	7	352158	5261691		71.38	0.212	13.99	1.69	0.42	0.042	0.59	0.31	4.06	4.20	0.060	1.15	98.16
Quartz-Feldspar Porphyry (WHIS)																	
OB-97-021	8	351844	5262640		73.17	0.260	14.18	1.92	0.43	0.058	0.83	0.83	4.86	3.25	0.079	0.99	100.90
OB-01-015	8	351917	5262653		72.71	0.247	13.47	1.86	0.40	0.055	0.92	0.48	4.82	3.10	0.094	0.94	99.12
OB-01-038	8	351957	5262613		74.40	0.151	13.67	0.97	0.09	0.017	0.37	0.98	4.36	3.70	0.043	0.74	99.48
GS-03-027	8	352371	5261328		72.75	0.165	13.96	1.02	0.45	0.054	0.49	1.02	4.22	3.77	0.050	1.44	99.44
GS-03-060	8	352053	5261835		72.57	0.199	14.24	1.29	0.68	0.049	0.67	0.70	5.13	3.06	0.064	0.94	99.66
GS-03-063	8	351824	5261603		74.04	0.161	13.66	0.99	0.48	0.055	0.51	0.36	4.05	4.03	0.049	0.86	99.30
GS-03-097	8	351945	5262660		71.10	0.261	14.15	2.14	0.29	0.064	0.94	0.72	4.62	3.14	0.093	1.15	98.72

* samples with UTM's calculated from registered base map

162

Table 3-3: Major-element contents of the rhyolitic volcanic rocks within the study area.

Sample Number	Unit	Easting	Northing	Element	SiO2	TiO2	Al2O3	Fe2O3	FeO	MnO	MgO	CaO	Na2O	K2O	P2O5	LOI	Total
				Method	ICP-ES	ICP-ES	ICP-ES	ICP-ES	ICP-ES	ICP-ES	ICP-ES	ICP-ES	ICP-ES	ICP-ES	ICP-ES		
				Unit	%	%	%	%	%	%	%	%	%	%	%	%	%
				Limit	0.01	0.001	0.01	0.01	0.01	0.010	0.01	0.01	0.01	0.01	0.001		
Minerals Road Rhyolite (WMVS)																	
OB-97-019	1	351957	5262683		75.67	0.141	12.79	0.68	0.25	0.013	0.08	0.12	1.83	7.88	0.008	0.42	99.90
OB-97-040	1	351799*	5260872*		79.89	0.113	10.89	0.38	0.23	0.003	0.04	0.08	3.29	4.02	0.004	0.49	99.46
OB-01-012	1	351843	5262605		77.29	0.117	11.26	0.66	0.10	0.022	0.15	0.10	3.05	5.05	-	0.40	98.19
OB-01-036	1	351888	5262516		77.38	0.118	11.41	0.63	0.10	0.009	0.13	0.08	0.72	8.77	-	0.39	99.73
OB-01-037	1	351897	5262608		72.68	0.130	13.46	0.88	0.13	0.023	0.28	0.11	1.68	8.80	-	0.61	98.79
GS-02-080	1	351787	5262498		77.38	0.158	13.00	0.86	0.35	0.042	0.62	0.21	4.96	2.33	-	0.59	100.54
OB-03-018	1	352986	5262305		79.33	0.132	11.90	0.12	0.32	0.004	0.14	0.13	6.68	0.10	-	0.45	99.32
OB-03-019	1	353049	5262262		76.80	0.159	13.24	0.77	0.17	0.014	0.32	0.17	5.74	2.25	-	0.50	100.14
GS-03-075	1	351926	5261343		76.48	0.130	12.19	0.75	0.19	0.014	0.15	0.18	3.18	5.25	-	0.41	98.93
Manuels River Rhyolite (WMVS)																	
OB-00-150	2	352865	5263152		79.57	0.115	11.84	0.22	0.22	-	0.03	0.09	3.90	3.73	-	0.46	100.19
OB-01-006	2	352971	5263209		81.41	0.087	10.50	0.05	0.10	-		0.03	3.75	3.43	-	0.45	99.80
OB-01-007	2	352931	5263179		78.84	0.102	12.12	0.30	0.08		0.02	0.10	4.70	3.13	-	0.35	99.74
OB-01-039	2	353111	5263779		69.28	0.581	14.85	2.70	0.15	0.043	0.37	0.57	4.46	4.58	0.139	0.77	98.51
OB-01-040	2	353125	5263815		67.87	0.780	16.19	3.41	0.42	0.046	0.49	0.91	5.33	3.82	0.202	0.91	100.42
OB-01-041	2	353503	5263791		74.19	0.267	13.35	0.93	0.42	0.065	0.58	0.38	5.56	2.01	0.012	0.68	98.49
OB-01-042	2	353553	5263767		73.76	0.278	12.75	0.10	1.08	0.037	0.29	0.33	5.47	2.16	-	0.68	97.06
OB-01-043	2	353893	5263644		77.52	0.171	12.97	0.59	0.19	0.020	0.31	0.25	5.46	2.01	0.016	0.53	100.07
GS-02-076	2	353976	5263545		74.04	0.232	14.57	1.10	0.28	0.055	0.43	0.46	4.71	3.92	0.041	0.71	100.58
GS-02-086	2	352905	5263070		81.24	0.110	10.77	0.60	0.09	0.021	0.22	0.06	1.05	5.10	0.014	0.99	100.26
OB-03-013	2	353107	5263281		76.02	0.153	14.04	0.85	0.10	-		0.20	7.98	0.14	-	0.26	99.74
OB-03-061	2	353272	5264249		76.25	0.222	11.32	0.97	0.36	0.010	0.17	0.12	0.15	9.17	0.012	0.52	99.31
GS-03-096	2	354138	5263257		69.32	0.496	15.44	2.26	0.30	0.074	1.31	0.43	6.26	2.12	0.122	1.06	99.22
Farmer's Field Rhyolite (MVS)																	
OB-97-176	9	353153	5261190		73.39	0.273	13.43	1.20	0.32	0.023	0.10	0.04	2.79	6.55	0.018	0.72	98.89
OB-97-178	9	353065	5261527		76.78	0.142	11.98	0.38	0.09	0.021	0.14	0.16	0.50	7.79	0.010	0.87	98.86
OB-00-087	9	352801	5259845		79.67	0.100	10.90	0.17	0.21	-	0.07	0.07	2.61	4.55	0.069	0.68	99.13
OB-03-017	9	353115	5262098		74.74	0.084	12.20	0.39	0.10	-	0.05	0.02	0.38	9.93	-	0.54	98.42
GS-03-053	9	353280	5261920		74.05	0.362	13.60	1.43	0.11	0.014	0.16	0.27	4.05	4.53	0.039	0.62	99.23
GS-03-058	9	353370	5261191		75.31	0.217	14.17	1.05	0.13	0.008	0.13	0.25	7.61	0.15	0.024	0.35	99.40
Pale Grey-Green, Moderately Porphyritic, Fine Rhyolite (MVS)																	
OB-97-010	11	353612*	5263724*		76.48	0.267	12.63	0.66	0.71	0.039	0.49	0.33	6.20	1.34	0.021	0.72	99.97
GS-02-071	11	353563	5263774		74.30	0.327	14.80	0.86	0.36	0.044	0.42	0.34	6.09	2.51	0.037	0.50	100.63
GS-02-072	11	353434	5263847		69.57	0.434	15.29	1.63	0.40	0.059	0.95	0.54	4.70	4.80	0.081	0.83	99.33

* samples with UTM's calculated from registered base map

163

Table 3-4: Major-element contents of ash-flow tuffs within the study area.

Sample Number	Unit	Easting	Northing	Element	SiO2	TiO2	Al2O3	Fe2O3	FeO	MnO	MgO	CaO	Na2O	K2O	P2O5	LOI	Total
				Method	ICP-ES	ICP-ES	ICP-ES	ICP-ES	ICP-ES	ICP-ES	ICP-ES	ICP-ES	ICP-ES	ICP-ES	ICP-ES		
				Unit	%	%	%	%	%	%	%	%	%	%	%	%	%
				Limit	0.01	0.001	0.01	0.01	0.01	0.010	0.01	0.01	0.01	0.01	0.001		
Welded, Fiamme-bearing Ash-Flow Tuff (WMVS)																	
OB-01-008	4	352913	5263846		73.99	0.338	13.91	1.50	0.13	0.012	0.20	0.41	5.01	3.59	0.033	0.52	99.67
OB-01-010	4	353404	5263833		72.58	0.353	14.11	1.75	0.10	0.021	0.28	0.45	5.67	2.88	0.040	0.71	98.95
OB-01-011	4	353421	5263842		74.22	0.332	13.82	1.55	0.20	0.037	0.46	0.42	5.32	2.98	0.072	0.78	100.22
Grey-Green, Pyritic, Pumiceous, Crystal-bearing, Ash-flow Tuff (MVS)																	
GS-02-074	12	353058	5264200		69.38	0.725	14.40	0.32	3.13	0.125	1.04	0.45	4.45	3.73	0.140	1.48	99.71
Dark Purple, Crystal-bearing, Ash-flow Tuff (MVS)																	
GS-02-009	13	352985	5264488		74.32	0.629	12.30	2.56	0.20	0.026	0.19	0.57	2.82	5.60	0.149	0.66	100.06
GS-02-087	13	352982	5264476		64.62	0.583	10.65	2.45	1.45	0.027	0.43	0.14	1.73	3.86	0.127	2.92	89.16
OB-03-060	13	352959	5264472		71.76	0.677	13.24	2.98	0.17	0.018	0.13	0.61	4.28	4.46	0.168	0.78	99.28
GS-03-052	13	353397	5262718		72.66	0.417	14.68	1.36	0.07	-	0.08	0.47	6.94	1.41	0.088	0.36	98.54

* samples with UTM's calculated from registered base map

Table 3-5: Major-element contents of the mafic rocks within the study area.

Sample Number	Unit	Easting	Northing	Element	SiO2	TiO2	Al2O3	Fe2O3	FeO	MnO	MgO	CaO	Na2O	K2O	P2O5	LOI	Total
				Method	ICP-ES	ICP-ES	ICP-ES	ICP-ES	ICP-ES	ICP-ES	ICP-ES	ICP-ES	ICP-ES	ICP-ES	ICP-ES		
				Unit	%	%	%	%	%	%	%	%	%	%	%	%	%
				Limit	0.01	0.001	0.01	0.01	0.01	0.010	0.01	0.01	0.01	0.01	0.001		
Mafic Volcanic/Intrusive Rocks (MVS)																	
OB-00-289	15	352722	5260727		56.79	2.158	16.06	7.45	2.43	0.228	2.85	1.98	5.03	1.77	1.118	2.41	100.55
GS-02-010	15	353005*	5264473*		47.15	1.326	17.28	1.76	8.99	0.321	10.18	1.17	0.98	3.59	0.169	6.55	100.45
GS-03-039	15	353534	5262310		56.02	0.977	17.12	5.17	1.55	0.137	3.02	4.47	7.79	0.14	0.237	4.13	100.94
GS-03-105	15	352660	5260024		47.25	2.381	18.77	6.68	6.45	0.281	4.11	2.46	5.01	1.18	0.493	3.69	99.49
Amygdaloidal Basalt/ Hyaloclastite (WHPC)																	
OB-00-280	21	354474	5263520		51.48	2.091	14.83	4.35	6.21	0.195	5.58	5.44	5.11	1.02	0.495	2.85	100.34
OB-01-001	21	354325	5263604		52.62	1.216	15.52	2.69	5.35	0.133	6.00	5.36	2.66	3.36	0.237	3.05	98.79
OB-01-003	21	354383	5263567		57.36	1.527	14.61	4.13	5.17	0.093	3.28	2.35	5.70	0.91	0.422	2.10	98.23
OB-01-004	21	354467	5263510		49.53	2.039	14.30	4.96	6.03	0.177	5.21	5.49	5.28	0.98	0.537	2.84	98.03
GS-03-033	21	352513	5262696		55.56	1.268	16.80	5.13	2.62	0.226	4.36	3.08	7.10	0.25	0.265	3.47	100.41
GS-03-034	21	352513	5262696		55.18	1.203	16.02	5.00	2.60	0.224	4.37	4.84	7.25	0.19	0.258	3.38	100.79
Mafic Dykes																	
OB-97-012	20a	353548	5264062		47.25	2.118	18.60	3.16	8.38	0.333	6.49	2.00	3.28	3.85	0.336	4.15	100.89
OB-00-276	20a	355302*	5263072*		51.75	1.801	15.77	3.98	5.80	0.291	6.11	3.04	5.17	0.70	0.495	3.94	99.48
GS-01-038	20a	352732	5260563		49.78	1.503	18.87	1.62	7.37	0.543	7.82	1.27	0.40	5.10	0.259	5.33	100.68
GS-02-007	20a	352931	5264192		57.43	2.086	12.98		-	0.411	3.52	1.97	3.44	1.31	0.436	4.44	100.33
GS-02-075	20a	352931	5264192		56.58	2.399	12.83	-	-	0.445	3.81	2.36	1.07	3.68	0.521	3.94	100.45
GS-03-122	20a	355039	5263253		52.80	1.903	15.72	7.83	2.63	0.317	6.32	3.12	4.76	0.57	0.513	4.02	100.79
GS-03-123	20a	354509	5263481		48.04	1.801	14.74	5.26	6.97	0.265	10.21	2.40	2.30	1.10	0.221	5.93	100.02
GS-03-127	20a	352744	5263061		48.79	1.989	20.09	5.55	6.60	0.600	4.25	0.50	1.33	3.86	0.414	5.24	99.95
GS-03-128	20a	352637	5263263		49.74	1.868	18.41	4.38	7.05	0.247	4.94	2.44	4.63	1.09	0.409	4.27	100.24
OB-01-002	20b	354371	5263576		43.33	1.532	14.89	3.16	6.32	0.197	7.01	7.47	4.31	1.21	0.470	7.83	98.42
OB-01-044	20b	353820	5263791		50.06	1.286	15.83	4.14	4.54	0.207	7.95	5.61	3.56	1.05	0.152	3.23	98.10
GS-03-124	20b	353395	5263847		54.34	1.183	16.12	6.05	2.02	0.143	6.03	5.57	4.40	1.57	0.219	2.94	100.81
GS-02-070	20c	353941	5263620		58.55	0.834	16.92	3.51	2.14	0.118	3.95	2.63	5.53	2.17	0.220	3.40	100.21
GS-03-074	20c	351892	5261238		60.71	0.612	17.37	2.92	2.15	0.128	2.72	1.50	6.44	2.41	0.152	2.34	99.69
GS-03-125	20c	351914	5262637		63.00	0.511	16.33	3.40	0.92	0.118	2.69	0.89	3.59	5.44	0.150	2.12	99.26

Table 3-6: Major-element contents of the Fowlers Road porphyry (Unit 22; Wych Hazel Pond Complex).

Sample Number	Unit	Easting	Northing	Element	SiO2	TiO2	Al2O3	Fe2O3	FeO	MnO	MgO	CaO	Na2O	K2O	P2O5	LOI	Total
				Method	ICP-ES	ICP-ES	ICP-ES	ICP-ES	ICP-ES	ICP-ES	ICP-ES	ICP-ES	ICP-ES	ICP-ES	ICP-ES		
				Unit	%	%	%	%	%	%	%	%	%	%	%	%	%
				Limit	0.01	0.001	0.01	0.01	0.01	0.010	0.01	0.01	0.01	0.01	0.001		
Fowler's Road Porphyry (WHPC)																	
OB-00-278	22	354539	5263455		70.20	0.249	13.46	-	-	0.038	1.15	0.26	6.14	0.40	0.010	1.50	97.08
OB-01-033	22	355290	5263150		72.57	0.163	13.25	0.98	0.18	0.024	0.55	0.09	1.10	9.59		0.64	99.14
GS-02-077	22	354574	5263452		73.59	0.268	13.40	1.93	1.17	0.080	1.85	0.31	5.77	0.47	0.026	1.31	100.32
GS-03-116	22	355311	5263097		77.24	0.151	12.84	0.88	0.15	0.018	0.47	0.20	5.01	2.70	0.019	0.63	100.32

* samples with UTM's calculated from registered base map

Table 3-7: Major-element contents of altered granite (White Hills Intrusive Suite) along the CBS By-Pass.

Sample Number	Unit	Easting	Northing	Element	SiO2	TiO2	Al2O3	Fe2O3	FeO	MnO	MgO	CaO	Na2O	K2O	P2O5	LOI	Total
				Method	ICP-ES	ICP-ES	ICP-ES	ICP-ES	ICP-ES	ICP-ES	ICP-ES	ICP-ES	ICP-ES	ICP-ES	ICP-ES		
				Unit	%	%	%	%	%	%	%	%	%	%	%	%	%
				Limit	0.01	0.001	0.01	0.01	0.01	0.010	0.01	0.01	0.01	0.01	0.001		
Silica-Sericite Altered Granite (WHIS)																	
OB-97-221	7	353072*	5263803*		74.70	0.181	13.44	1.11	0.44	0.041	0.63	0.19	3.39	4.69	0.050	1.14	100.06
OB-97-222	7	353068*	5263800*		76.74	0.178	12.04		-	0.045	0.59	0.24	2.98	3.69	0.054	1.39	99.73
OB-97-223	7	353052*	5263878*		77.70	0.177	11.39	-	-	0.041	0.41	0.28	3.83	3.28	0.050	1.02	100.09
OB-97-226	7	353045*	5263870*		78.43	0.164	11.25		-	0.027	0.30	0.27	4.72	1.98	0.044	0.82	99.41
OB-97-228	7	353048*	5263751*		80.58	0.084	9.55		-	0.011	0.09	0.09	2.25	4.29	0.008	0.82	98.55

Table 3-8: Trace-element contents of altered granite (White Hills Intrusive Suite) along the CBS By-Pass.

Sample Number	Unit	Easting	Northing	Element	Cr	Ni	Co	Sc	V	Cu	Pb	Zn	Cd	Mo	As	Ba	Sr
				Method	ICP-ES	ICP-ES	ICP-ES	ICP-ES	ICP-ES	ICP-ES	ICP-ES	ICP-ES	ICP-ES	ICP-ES	ICP-ES	ICP-ES	ICP-ES
				Unit	ppm	ppm	ppm	ppm	ppm	ppm	ppm	ppm	ppm	ppm	ppm	ppm	ppm
				Limit	1	1	1	0.1	1	1	1	1	1	0.1	1	2	1	1
Silica-Sericite Altered Granite (WHIS)																	
OB-97-221	7	353072*	5263803*		4	5	3	4.0	32	23	49	41	-	-		1013	104
OB-97-222	7	353068*	5263800*		3	2	2	4.0	36	189	26	45	-	-	-	793	82
OB-97-223	7	353052*	5263878*		3	1	3	3.8	22	8	108	37	-	-	-	953	98
OB-97-226	7	353045*	5263870*		3	2	3	3.4	18	25	103	23	-	-		707	84
OB-97-228	7	353048*	5263751*		3	2		3.0	8	30	255	228	-	3		1079	41

Table 3-8: cont'd

Sample Number	Unit	Easting	Northing	Element	Ga	Li	Nb	Zr	Ti	Y	La	Ce	Dy	Be	La/Dy	Nb/La	Ti/Zr	Zr/Nb	Zr/Y
				Method	ICP-ES	ICP-ES	ICP-ES	ICP-ES	ICP-ES	ICP-ES	ICP-ES	ICP-ES	ICP-ES	ICP-ES					
				Unit	ppm	ppm	ppm	ppm	ppm	ppm	ppm	ppm	ppm	ppm					
				Limit	1	0.1	1	1	1	1	1	1	1	0.1	0.1				
Silica-Sericite Altered Granite (WHIS)																				
OB-97-221	7	353072*	5263803*		8	8.5	9	149	1210	12	29	33	1.7	1.5	17.2	0.31	8.1	16.8	12.8
OB-97-222	7	353068*	5263800*		11	9.0	8	139	1267	19	29	57	2.8	1.6	10.6	0.29	9.1	16.6	7.2
OB-97-223	7	353052*	5263878*		11	4.5	9	139	1277	19	31	61	3.0	1.0	10.3	0.28	9.2	16.2	7.4
OB-97-226	7	353045*	5263870*		13	3.4	7	122	1178	13	17	29	1.9	0.9	8.9	0.41	9.7	17.7	9.3
OB-97-228	7	353048*	5263751*		5	2.5	8	112	606	16	10	25	2.3	1.0	4.3	0.79	5.4	14.4	7.2

* samples with UTM's calculated from registered base map

Table 3-9: Major-element contents of altered and unaltered samples from Unit 9 (Manuels Volcanic Suite).

Sample Number	Unit	Easting	Northing	Element	SiO2	TiO2	Al2O3	Fe2O3	FeO	MnO	MgO	CaO	Na2O	K2O	P2O5	LOI	Total
				Method	ICP-ES	ICP-ES	ICP-ES	ICP-ES	ICP-ES	ICP-ES	ICP-ES	ICP-ES	ICP-ES	ICP-ES	ICP-ES		
				Unit	%	%	%	%	%	%	%	%	%	%	%	%	%
				Limit	0.01	0.001	0.01	0.01	0.01	0.010	0.01	0.01	0.01	0.01	0.001		
Unaltered Farmer's Field Rhyolite (MVS)																	
OB-97-176	9	353153	5261190		73.39	0.273	13.43	1.20	0.32	0.023	0.10	0.04	2.79	6.55	0.018	0.72	98.89
GS-03-053	9	353280	5261920		74.05	0.362	13.60	1.43	0.11	0.014	0.16	0.27	4.05	4.53	0.039	0.62	99.23
GS-03-058	9	353370	5261191		75.31	0.217	14.17	1.05	0.13	0.008	0.13	0.25	7.61	0.15	0.024	0.35	99.40
Silica-Sericite-Pyrophyllite Alteration (MVS)																	
OB-97-277	17	352863*	5260708*		90.83	0.087	6.39	-	-	-	-	0.02	0.03	0.10	0.005	1.41	99.03
OB-97-290	17	352919*	5260723*		81.80	0.108	5.96	0.11	5.24	0.003	-	0.02	0.10	1.60	0.011	3.75	99.26
OB-97-291	17	352896*	5260666*		87.19	0.119	8.28	0.07	0.04	-	0.01	0.04	0.13	1.97	0.007	1.50	99.35

Table 3-10: Trace-element contents of altered and unaltered samples from Unit 9 (Manuels Volcanic Suite).

Sample Number	Unit	Easting	Northing	Element	Cr	Ni	Co	Sc	V	Cu	Pb	Zn	Cd	Mo	As	Ba	Sr
				Method	ICP-ES	ICP-ES	ICP-ES	ICP-ES	ICP-ES	ICP-ES	ICP-ES	ICP-ES	ICP-ES	ICP-ES	ICP-ES	ICP-ES	ICP-ES
				Unit	ppm	ppm	ppm	ppm	ppm	ppm	ppm	ppm	ppm	ppm	ppm	ppm	ppm
				Limit	1	1	1	0.1	1	1	1	1	0.1	1	2	1	1
Unaltered Farmer's Field Rhyolite (MVS)																	
OB-97-176	9	353153	5261190		3	-	-	3.8	34	3	5	35	-	-	-	1156	40
GS-03-053	9	353280	5261920		2	2	-	6.4	17	6	16	28	-	1	8	1199	97
GS-03-058	9	353370	5261191		1	1	-	3.1	5	2	16	18	-	2	-	48	28
				Average	2	2	-	4.4	18	3	12	27	-	2	8	801	55
Silica-Sericite-Pyrophyllite Alteration (MVS)																	
OB-97-277	17	352863*	5260708*		5	2	-	2.8	1	1	3	3	-	-	-	191	5
OB-97-290	17	352919*	5260723*		5	45	142	4.3	35	4	9	4	-	-	-	563	9
OB-97-291	17	352896*	5260666*		3	2	-	4.2	15	1	3	2	-	-	-	293	6

Table 3-10: cont'd

Sample Number	Unit	Easting	Northing	Element	Ga	Li	Nb	Zr	Ti	Y	La	Ce	Dy	Be	La/Dy	Nb/La	Ti/Zr	Zr/Nb	Zr/Y
				Method	ICP-ES	ICP-ES	ICP-ES	ICP-ES	ICP-ES	ICP-ES	ICP-ES	ICP-ES	ICP-ES	ICP-ES					
				Unit	ppm	ppm	ppm	ppm	ppm	ppm	ppm	ppm	ppm	ppm					
				Limit	1	0.1	1	1	1	1	1	1	0.1	0.1					
Unaltered Farmer's Field Rhyolite (MVS)																				
OB-97-176	9	353153	5261190		10	1.5	13	386	1898	44	45	99	6.9	1.8	6.5	0.28	4.9	30.5	8.7
GS-03-053	9	353280	5261920		-	3.1	13	339	2732	43	46	71	6.4	1.7	7.1	0.29	8.1	25.7	7.8
GS-03-058	9	353370	5261191		-	1.0	9	231	1564	44	38	63	6.4	2.5	5.8	0.25	6.8	24.7	5.3
				Average	10	1.8	12	319	2065	44	43	78	6.6	2.0	6.5	0.27	6.6	27.0	7.3
Silica-Sericite-Pyrophyllite Alteration (MVS)																				
OB-97-277	17	352863*	5260708*		6	116	6	105	478	12	3	11	1.4	0.3	1.8	2.16	4.6	19.0	8.8
OB-97-290	17	352919*	5260723*		10	0.6	3	76	653	13	5	13	1.5	0.5	3.5	0.55	8.6	26.1	6.0
OB-97-291	17	352896*	5260666*		3	1.2	5	168	587	18	10	22	2.4	0.8	4.0	0.53	3.5	33.1	9.5

* samples with UTM's calculated from registered base map

Table 3-11: Trace-element contents of granite from the Holyrood Intrusive Suite.

Sample Number	Unit	Easting	Northing	Element / Method / Unit / Limit	Cr ICP-ES ppm 1	Ni ICP-ES ppm 1	Co ICP-ES ppm 1	Sc ICP-ES ppm 0.1	V ICP-ES ppm 1	Cu ICP-ES ppm 1	Pb ICP-ES ppm 1	Zn ICP-ES ppm 1	Cd ICP-ES ppm 0.1	Mo ICP-ES ppm 1	As ICP-ES ppm 2	Ba ICP-ES ppm 1	Sr ICP-ES ppm 1
Pink-White-Green, Quartz-Phyric Granite (HIS)																	
OB-97-033	N/A	347327	5257444		-	-	-	2.5	5	-	14	28	-		-	790	62
OB-97-035	N/A	348872	5255961		-	-	3	3.6	18	3	14	42	-		-	1023	220
OB-97-039	5	351100*	5259850*		2	-	3	3.7	17	1	8	37	-		-	1229	135
OB-97-045	N/A	344829	5255672		-	-	1	4.0	8	1	11	28	-		-	1014	106
OB-97-047	N/A	342388	5255496		-	-		4.5	11	1	12	23	-		-	870	92
OB-97-068	N/A	345774	5255000		-	-	-	2.4	5	-	12	22			-	849	60
OB-97-070	N/A	345660	5255883		-	-	1	2.2	5	3	18	30	-		-	900	80
OB-97-309	N/A	348144	5247188			-	3	3.6	19	3	15	45			-	1291	271
OB-97-313	N/A	349531	5246909		-	-	3	3.7	19	2	14	42			-	1206	212
OB-97-317	N/A	349107	5245904		-	-	1	3.0	8	-	10	22	-		-	917	79
OB-00-067	N/A	350825	5237950		1	3	-	1.9	-	2	8	26	-	1	-	1144	117
OB-00-094	N/A	350093	5235860		2	2	3	4.6	13	41	13	60	-	-	4	1097	168
OB-00-095	N/A	348776	5234100		-	2	2	4.1	9	1	3	31	-	-	2	1042	125
OB-00-103	N/A	347490	5231640		1	3	3	4.2	11	4	5	35	-	1	3	976	121
OB-00-115	N/A	347400*	5233500*		-	2	3	4.8	9	2	-	32	-	-	4	1123	100
OB-00-123	N/A	348877	5251759		1	2	2	3.3	6	-	8	32	-	-	4	864	185
OB-00-124	N/A	350114	5250372		-	1	1	3.4	2	-	5	27	-	-	3	1105	106
OB-00-125	N/A	350774	5248570		1	2	2	3.7	8	-	-	37		-	5	975	151
OB-00-127	N/A	350386	5249636		1	2	3	4.0	10	-	2	43			-	1115	217
OB-00-159	N/A	346000*	5233900*		1	2	3	5.2	17	16		38	-		4	1003	214
OB-00-257	N/A	348356	5251878		1	2	3	3.8	13	1	4	44	-	3	5	1146	195
OB-00-258	N/A	348168	5250979		1	2	3	4.0	12	2	14	42	-		2	1189	202
OB-00-261	N/A	347885	5251506		-	1	1	3.4	4		14	27	-	-	4	965	109
OB-00-262	N/A	346740	5238647		-	1	-	1.9		1	12	25	-		-	1034	100
OB-00-266	N/A	345770	5236815		1	2	4	5.3	18	2	17	43	-	-	-	817	195
OB-00-304	N/A	345198	5233404		-	2	3	4.9	10	2	2	42	-	-	3	946	138
OB-03-037	5	350803	5261537		2	3	2	3.4	15	2	26	34	0.2	1.37	-	1505	282
OB-03-042	N/A	353371	5256136		2	1		3.6	14	28	140	20	0.1	5.82	-	1010	67
OB-03-044	N/A	349098	5253378		2	2	3	3.6	18	2	11	40	0.2	1.36		1089	114
OB-03-045	N/A	347819	5252564		1	3	1	3.6	.1	8	73	29	0.1	2.89	-	1079	98
OB-03-047	N/A	345290	5246640		2	2	1	6.0	15	2	18	32	0.1	-	-	1192	126
OB-03-048	N/A	342421	5255456		2	3		3.9	11		18	23	0.1	1.41		871	74
OB-03-052	N/A	341243	5256740		1	2	-	16.2	6	13	15	8	-	1.43	-	365	10
OB-03-053	N/A	341187	5256594		1	2		12.2	3	1	23	28	0.1	1.94	-	85	10
OB-03-054	N/A	341138	5256428		2	2	2	3.6	20		12	36	0.1		-	737	143
OB-03-057	N/A	349450	5253761		2	3	4	4.4	25	2	20	43	0.2	1.07		981	244
OB-03-058	N/A	350389	5254934		2	3	3	3.6	19		19	34	0.2	1.20		966	185
OB-03-059	N/A	350697	5255300		2	3	2	3.4	18	3	21	37	0.2	1.27		967	198

N/A = samples collected outside of field area

* samples with UTM's calculated from registered base map

Table 3-11: cont'd

Sample Number	Unit	Easting	Northing	Element	Ga	Li	Nb	Zr	Ti	Y	La	Ce	Dy	Be	La/Dy	Nb/La	Ti/Zr	Zr/Nb	Zr/Y
				Method Unit Limit	ICP-ES ppm 1	ICP-ES ppm 0.1	ICP-ES ppm 1	ICP-ES ppm 1	ICP-ES ppm 1	ICP-ES ppm 1	ICP-ES ppm 1	ICP-ES ppm 1	ICP-ES ppm 0.1	ICP-ES ppm 0.1					
Pink-White-Green, Quartz-Phyric Granite (HIS)																			
OB-97-033	N/A	347327	5257444		12	4.4	8.7	72	624	14	23	51	2.2	1.6	10.5	0.38	8.6	8.3	5.1
OB-97-035	N/A	348872	5255961		10	15.3	8.3	121	1492	15	33	61	2.1	1.8	15.6	0.25	12.4	14.5	8.2
OB-97-039	5	351100*	5259850*		15	6.5	8	130	1462	15	30	62	2.4	1.8	12.6	0.28	11.2	15.7	8.7
OB-97-045	N/A	344829	5255672		8	4.0	11.1	149	1121	22	30	61	2.9	2.0	10.4	0.36	7.5	13.4	6.9
OB-97-047	N/A	342388	5255496		14	3.6	17.9	180	1502	31	41	80	4.5	3.3	9.1	0.44	8.3	10.1	5.9
OB-97-068	N/A	345774	5255000		9	4.0	9.5	67	707	11	19	37	1.6	1.6	12.0	0.49	10.5	7.1	6.0
OB-97-070	N/A	345660	5255883		8	4.9	9.2	94	682	24	26	42	3.0	2.0	8.7	0.35	7.3	10.2	3.8
OB-97-309	N/A	348144	5247188		14	19.2	9.3	130	1613	13	31	52	1.8	1.7	17.3	0.30	12.4	14.1	9.9
OB-97-313	N/A	349531	5246909		15	9.2	9.5	99	1610	15	32	52	2.0	1.8	15.8	0.30	16.3	10.4	6.7
OB-97-317	N/A	349107	5245904		15	4.7	10.5	80	807	22	25	38	2.8	1.6	9.0	0.41	10.1	7.6	3.7
OB-00-067	N/A	350825	5237950		-	1.7	11	61	572	11	24	34	1.1	1.7	21.4	0.46	9.4	5.5	5.6
OB-00-094	N/A	350093	5235860		-	3.4	8	77	1328	12	21	29	1.5	1.4	14.2	0.38	17.3	9.5	6.5
OB-00-095	N/A	348776	5234100		-	3.6	7	121	1261	17	27	37	2.2	1.4	12.1	0.28	10.5	16.2	6.9
OB-00-103	N/A	347490	5231640		-	3.8	7	139	1300	14	23	36	2.0	1.5	11.7	0.33	9.3	18.6	10.2
OB-00-115	N/A	347400*	5233500*		-	3.7	10	170	1429	26	37	51	3.7	1.9	10.1	0.27	8.4	16.8	6.6
OB-00-123	N/A	348877	5251759		-	6.9	7	91	1073	13	22	30	1.5	1.7	14.1	0.33	11.8	12.5	6.8
OB-00-124	N/A	350114	5250372		-	2.6	10	74	847	10	20	30	1.1	1.6	18.3	0.50	11.5	7.4	7.2
OB-00-125	N/A	350774	5248570		-	5.4	8	106	1237	18	26	37	2.3	1.8	11.2	0.31	11.7	13.0	6.0
OB-00-127	N/A	350386	5249636		-	5.1	9	104	1427	17	28	38	2.3	2.1	11.9	0.33	13.7	11.6	6.1
OB-00-159	N/A	346000*	5233900*		-	5.1	9	225	1777	19	37	56	2.6	1.7	14.1	0.24	7.9	25.4	11.7
OB-00-257	N/A	348356	5251878		-	6.3	10	120	1512	14	31	43	1.8	2.2	17.2	0.32	12.6	12.1	8.7
OB-00-258	N/A	348168	5250979		-	7.5	8	130	1353	16	28	41	2.0	1.8	14.1	0.29	10.4	16.1	8.2
OB-00-261	N/A	347885	5251506		-	4.8	10	94	833	11	22	33	1.0	1.4	22.0	0.45	8.8	9.6	8.7
OB-00-262	N/A	346740	5238647		-	2.8	9	64	607	10	19	31	0.9	1.1	20.9	0.46	9.5	7.4	6.6
OB-00-266	N/A	345770	5236815		-	4.3	9	93	1455	16	25	35	2.0	1.9	12.9	0.34	15.6	10.9	5.7
OB-00-304	N/A	345198	5233404		-	2.7	12	174	1612	19	20	35	2.3	1.5	8.5	0.62	9.3	14.3	9.1
OB-03-037	5	350803	5261537		-	6.4	9.7	112	1232	18	21	30	2.3	2.0	9.0	0.47	11.0	11.6	6.4
OB-03-042	N/A	353371	5256136		-	1.5	7.2	124	1246	7	19	28	1.2	0.8	15.9	0.37	10.1	17.3	17.3
OB-03-044	N/A	349098	5253378		-	5.6	9.4	125	1442	14	24	35	1.7	1.6	14.4	0.38	11.5	13.4	9.3
OB-03-045	N/A	347819	5252564		-	4.6	11.0	85	924	14	22	32	1.8	1.7	11.9	0.51	10.9	7.7	6.3
OB-03-047	N/A	345290	5246640		-	3.1	14.5	166	1736	20	32	53	3.0	2.0	10.5	0.46	10.5	11.4	8.1
OB-03-048	N/A	342421	5255456		-	2.3	14.0	144	1222	23	37	56	3.2	2.9	11.4	0.38	8.5	10.3	6.2
OB-03-052	N/A	341243	5256740		-	4.8	33.5	71	190	94	18	37	14.0	6.8	1.3	1.84	2.7	2.1	0.7
OB-03-053	N/A	341187	5256594		-	1.9	26.3	98	525	33	31	53	5.2	2.7	5.9	0.85	5.4	3.7	3.0
OB-03-054	N/A	341138	5256428		-	6.1	8.2	97	1229	16	27	39	2.0	1.9	13.7	0.30	12.7	11.8	6.1
OB-03-057	N/A	349450	5253761		-	7.5	9.4	131	1688	15	32	45	2.0	1.8	16.0	0.30	12.9	14.0	8.6
OB-03-058	N/A	350389	5254934		-	6.0	9.2	120	1394	15	27	39	1.9	1.7	14.1	0.35	11.6	13.0	7.7
OB-03-059	N/A	350697	5255300		-	5.1	8.5	92	1310	15	28	41	1.7	1.6	16.0	0.31	14.2	10.8	6.2

N/A = samples collected outside of field area

* samples with UTM's calculated from registered base map

Table 3-12: Extended rare earth-element data for granite of the Holyrood Intrusive Suite.

Sample Number	Unit	Easting	Northing	Element	V	Cr	Co	Ni	Cu	Zn	Ga	Ge	As	Rb	Sr	Y	Zr	Nb	Mo
				Method	ICP-MS	ICP-MS	ICP-MS	ICP-MS	ICP-MS	ICP-MS	ICP-MS	ICP-MS	ICP-MS	ICP-MS	ICP-MS	ICP-MS	ICP-MS	ICP-MS	ICP-MS
				Unit	ppm	ppm	ppm	ppm	ppm	ppm	ppm	ppm	ppm	ppm	ppm	ppm	ppm	ppm	ppm
				Limit	5	20	1	20	10	30	1	1	5	2	2	1	5	1	2
Granite (HIS)																			
OB-00-127	5	350386	5249636		18		2			36	15	1	-	110	216	18	129	9	
OB-00-159	5	346000*	5233900*		24	.	3		21		15	1		76	211	20	207	9	.
OB-97-039	5	351100*	5259850*		15	-	2	.	.	39	13	1	.	107	145	15	129	9	

Table 3-12: cont'd

Sample Number	Unit	Easting	Northing	Element	Ag	In	Sn	Sb	Cs	Ba	La	Ce	Pr	Nd	Sm	Eu	Gd	Tb	Dy
				Method	ICP-MS	ICP-MS	ICP-MS	ICP-MS	ICP-MS	ICP-MS	ICP-MS	ICP-MS	ICP-MS	ICP-MS	ICP-MS	ICP-MS	ICP-MS	ICP-MS	ICP-MS
				Unit	ppm	ppm	ppm	ppm	ppm	ppm	ppm	ppm	ppm	ppm	ppm	ppm	ppm	ppm	ppm
				Limit	0.5	0.2	1.0	0.5	0.5	3	0.1	0.1	0.005	0.1	0.1	0.005	0.1	0.1	0.1
Granite (HIS)																			
OB-00-127	5	350386	5249636		-		1		2.3	1,050	26.4	45.3	5.13	16.1	3.1	0.81	2.7	0.5	2.7
OB-00-159	5	346000*	5233900*				-		1.5	947	33.7	63.2	7.08	23.1	4.5	1.15	3.6	0.6	3.4
OB-97-039	5	351100*	5259850*		-	-	1		1.8	1,250	28.1	55.2	5.42	16.9	3.2	0.77	2.6	0.4	2.4

Table 3-12: cont'd

Sample Number	Unit	Easting	Northing	Element	Ho	Er	Tm	Yb	Lu	Hf	Ta	W	Tl	Pb	Bi	Th	U
				Method	ICP-MS	ICP-MS	ICP-MS	ICP-MS	ICP-MS	ICP-MS	ICP-MS	ICP-MS	ICP-MS	ICP-MS	ICP-MS	ICP-MS	ICP-MS
				Unit	ppm	ppm	ppm	ppm	ppm	ppm	ppm	ppm	ppm	ppm	ppm	ppm	ppm
				Limit	0.1	0.1	0.05	0.1	0.04	0.2	0.1	1	0.1	5	0.4	0.1	0.1
Granite (HIS)																	
OB-00-127	5	350386	5249636		0.6	1.8	0.29	2.0	0.34	3.6	1.0	-	0.6	8	-	10.6	2.5
OB-00-159	5	346000*	5233900*		0.7	2.1	0.32	2.1	0.35	5.4	0.7	-	0.3	.	.	10.3	1.5
OB-97-039	5	351100*	5259850*		0.5	1.6	0.25	1.7	0.28	3.4	0.8		0.8	9	.	12.2	1.8

* samples with UTM's calculated from registered base map

170

Table 3-13: Trace-element contents of Unit 6 from the White Hills Intrusive Suite.

Sample Number	Unit	Easting	Northing	Element	Cr	Ni	Co	Sc	V	Cu	Pb	Zn	Cd	Mo	As	Rb	Ba	Sr
				Method	ICP-ES	ICP-ES	ICP-ES	ICP-ES	ICP-ES	ICP-ES	ICP-ES	ICP-ES	ICP-ES	ICP-ES	ICP-ES	ICP-ES	ICP-ES	ICP-ES
				Unit	ppm	ppm	ppm	ppm	ppm	ppm	ppm	ppm	ppm	ppm	ppm	ppm	ppm	ppm
				Limit	1	1	1	0.1	1	1	1	1	0.1	1	2	5	1	1
Monzonite (WHIS)																		
OB-97-376	6	352234	5262047		5	4	11	7.4	76	4	5	65	-	-		-	930	290
GS-02-081	6	351912	5262445		4	8	12	8.1	86	38	9	71	-	2	2	49	1143	321
GS-03-030	6	352544	5261486		3	6	11	7.7	76	90	18	67		-	.		1041	267

Table 3-13: cont'd

Sample Number	Unit	Easting	Northing	Element	Ga	Li	Nb	Zr	Ti	Y	La	Ce	Dy	Be	La/Dy	Nb/La	Ti/Zr	Zr/Nb	Zr/Y
				Method	ICP-ES	ICP-ES	ICP-ES	ICP-ES	ICP-ES	ICP-ES	ICP-ES	ICP-ES	ICP-ES	ICP-ES					
				Unit	ppm	ppm	ppm	ppm	ppm	ppm	ppm	ppm	ppm	ppm					
				Limit	1	0.1	1	1	1	1	1	1	0.1	0.1					
Monzonite (WHIS)																			
OB-97-376	6	352234	5262047		21	11.7	6	113	3311	11	22	39	1.9	1.5	11.5	0.28	29.3	18.7	10.5
GS-02-081	6	351912	5262445		-	10.9	9	114	3406	13	23	36	1.7	1.7	13.4	0.38	29.8	13.1	8.9
GS-03-030	6	352544	5261486		-	8.2	7	112	3049	12	25	39	1.8	1.6	14.4	0.29	27.1	15.4	9.5

Table 3-14: Trace-element contents of Woodford's monzonite.

Sample Number	Unit	Easting	Northing	Element	Cr	Ni	Co	Sc	V	Cu	Pb	Zn	Cd	Mo	As	Rb	Ba	Sr
				Method	ICP-ES	ICP-ES	ICP-ES	ICP-ES	ICP-ES	ICP-ES	ICP-ES	ICP-ES	ICP-ES	ICP-ES	ICP-ES	ICP-ES	ICP-ES	ICP-ES
				Unit	ppm	ppm	ppm	ppm	ppm	ppm	ppm	ppm	ppm	ppm	ppm	ppm	ppm	ppm
				Limit	1	1	1	0.1	1	1	1	1	0.1	1	2	5	1	1
Woodford's Monzonite (640 Ma)																		
OB-00-185		334725	5244830		150	44	29	21.5	191	52	3	88			5	-	1032	820
OB-00-235		336571	5251103		92	27	25	22.4	179	124	12	77	0.4	2	9		826	613
OB-00-236		336555	5251030		101	29	27	24.2	191	136	11	86	-	1	9	-	1084	610
OB-00-253		336932	5250153		66	23	24	21.2	171	67	12	74	-	2	9		1074	585

Table 3-14: cont'd

Sample Number	Unit	Easting	Northing	Element	Ga	Li	Nb	Zr	Ti	Y	La	Ce	Dy	Be	La/Dy	Nb/La	Ti/Zr	Zr/Nb	Zr/Y
				Method	ICP-AES	ICP-AES	ICP-AES	ICP-AES	ICP-AES	ICP-AES	ICP-AES	ICP-AES	ICP-AES	ICP-AES					
				Unit	ppm	ppm	ppm	ppm	ppm	ppm	ppm	ppm	ppm	ppm					
				Limit	1	0.1	1	1	1	1	1	1	0.1	0.1					
Woodford's Monzonite (640 Ma)																			
OB-00-185		334725	5244830			34.7	8	103	4393	18	41	63	3.2	1.9	12.8	0.19	42.8	12.8	5.6
OB-00-235		336571	5251103		-	26.8	10	168	4962	22	41	69	3.2	2.0	13.0	0.24	29.5	17.0	7.8
OB-00-236		336555	5251030		-	22.2	8	243	4898	23	42	71	3.6	2.1	11.7	0.19	20.6	29.4	10.7
OB-00-253		336932	5250153			17.0	12	319	5141	23	47	78	3.2	2.7	14.7	0.26	18.1	28.1	14.0

* samples with UTM's calculated from registered base map

Table 3-15: Trace-element contents of Unit 7 from the White Hills Intrusive Suite.

Sample Number	Unit	Easting	Northing	Element	Cr	Ni	Co	Sc	V	Cu	Pb	Zn	Cd	Mo	As	Rb	Ba	Sr
				Method Unit Limit	ICP-ES ppm 1	ICP-ES ppm 1	ICP-ES ppm 1	ICP-ES ppm 0 1	ICP-ES ppm 1	ICP-ES ppm 1	ICP-ES ppm 1	ICP-ES ppm 1	ICP-ES ppm 0 1	ICP-ES ppm 1	ICP-ES ppm 2	ICP-ES ppm 5	ICP-ES ppm 1	ICP-ES ppm 1
Medium- to Coarse-grained Equigranular Granite (WHIS)																		
OB-97-171	7	352686*	5261096*		5	3	1	3.4	16	19	2	18	-	-			68	109
OB-97-221	7	353072*	5263803*		4	5	3	40	32	23	49	41				-	1013	104
OB-97-222	7	353068*	5263800*		3	2	2	40	36	189	26	45	·			-	793	82
OB-97-228	7	353048*	5263751*		3	2	-	30	8	30	255	228		3			1079	41
OB-97-362	7	352644	5260024		3	1	-	44	39	5	26	11	-	4		-	1121	93
OB-01-046	7	353476	5264601		1	3	5	49	25	17	24	412		-	7	-	790	121
OB-01-060	7	352837	5264286			1	-	32	9	3	56	19		·	4	-	714	68
OB-01-061	7	352899	5264199		-	3	1	47	36	10	56	33		-	3	-	1214	113
OB-01-066	7	352951	5264145		3	3	2	45	22	8	13	33	·	-			1039	118
GS-02-002	7	352931	5264192		3	3	4	46	33	6	15	64		1	2	77	1134	103
GS-02-041	7	352988	5264573		4	5	4	43	44	8	8	128	0.1	1	7	130	1210	58
GS-02-073	7	353043	5263806		2	2	2	3.6	15	50	56	34	·	3	5	58	884	103
GS-02-078	7	351766	5262510		2	3	4	53	35	4	9	44		1	5	69	927	189
GS-02-084	7	352615	5262019		2	3	3	3.7	28	6	9	55		1	4	86	1165	131
GS-02-092	7	352863	5261776		3	3	2	42	22	3	8	30	-	1	5	70	983	131
OB-03-036	7	351263	5261891		2	2	3	44	28	6	10	31	0.1	1	4	-	1565	127
GS-03-029	7	352415	5261390		-	2	2	28	15	38	24	26		1	-	-	853	89
GS-03-077	7	351867	5261012		2	3	5	59	35	·	19	62		-		-	1203	199
GS-03-079	7	351985	5260927		1	2	2	45	28	1	15	29		1			1117	131
GS-03-087	7	353340	5261029		1	2	3	38	24	·	17	40	0.1	-	-	-	1072	124
GS-03-109	7	352027	5260759		1	2	3	35	17	8	15	26	-	1	-	-	1135	140
GS-03-126	7	352730	5260152		1	2		47	29	4	18	84	22	4	5	-	936	84
GS-03-129	7	352158	5261691		1	3	3	48	27	21	19	42	01	1			1075	116

* samples with UTM's calculated from registered base map

Table 3-15: cont'd.

Sample Number	Unit	Easting	Northing	Element	Ga	Li	Nb	Zr	Ti	Y	La	Ce	Dy	Be	La/Dy	Nb/La	Ti/Zr	Zr/Nb	Zr/Y
				Method Unit Limit	ICP-ES ppm 1	ICP-ES ppm 0.1	ICP-ES ppm 1	ICP-ES ppm 1	ICP-ES ppm 1	ICP-ES ppm 1	ICP-ES ppm 1	ICP-ES ppm 1	ICP-ES ppm 0.1	ICP-ES ppm 0.1					
Medium- to Coarse-grained Equigranular Granite (WHIS)																			
OB-97-171	7	352686*	5261096*		10	2.3	8	151	1297	19	22	50	2.7	1.2	8.4	0.34	8.6	19.7	8.1
OB-97-221	7	353072*	5263803*		8	8.5	9	149	1210	12	29	33	1.7	1.5	17.2	0.31	8.1	16.8	12.8
OB-97-222	7	353068*	5263800*		11	9.0	8	139	1267	19	29	57	2.8	1.6	10.6	0.29	9.1	16.6	7.2
OB-97-228	7	353048*	5263751*		5	2.5	8	112	606	16	10	25	2.3	1.0	4.3	0.79	5.4	14.4	7.2
OB-97-362	7	352644	5260024		3	3.6	9	173	1431	10	14	31	1.2	1.2	12.2	0.62	8.3	19.6	18.0
OB-01-046	7	353476	5264601			8.6	10	131	1400	20	33	60	3.4	2.1	9.8	0.31	10.7	12.6	6.4
OB-01-060	7	352837	5264286			2.3	13	89	647	12	8	16	1.8	1.1	4.6	1.62	7.3	6.8	7.3
OB-01-061	7	352899	5264199			10.4	14	143	1344	12	24	37	2.2	1.5	10.8	0.57	9.4	10.5	11.7
OB-01-066	7	352951	5264145		-	4.3	9	137	1422	13	17	28	1.3	1.4	13.9	0.50	10.4	15.9	10.8
GS-02-002	7	352931	5264192		-	4.3	8	157	1725	18	21	51	2.4	1.1	8.7	0.41	11.0	18.8	8.8
GS-02-041	7	352988	5264573		-	19.4	9	131	1381	10	28	41	1.5	1.9	18.9	0.33	10.6	14.1	13.1
GS-02-073	7	353043	5263806		-	3.5	8	141	1237	13	23	33	1.8	1.0	13.1	0.33	8.8	18.2	11.0
GS-02-078	7	351766	5262510		-	5.7	11	86	1768	15	19	27	1.8	1.4	10.7	0.54	20.6	8.1	5.6
GS-02-084	7	352615	5262019		-	5.5	8	124	1618	14	27	38	1.8	1.2	15.1	0.31	13.0	14.8	8.8
GS-02-092	7	352863	5261776			2.3	10	147	1453	17	17	29	2.3	1.3	7.4	0.55	9.9	15.5	8.5
OB-03-036	7	351263	5261891			6.6	11	216	2057	12	29	49	1.8	1.7	16.6	0.39	9.5	18.9	18.3
GS-03-029	7	352415	5261390		-	2.3	8	93	923	17	20	31	2.5	1.4	8.0	0.41	10.0	11.3	5.5
GS-03-077	7	351867	5261012		-	5.9	9	110	2009	16	28	45	2.0	1.6	14.4	0.32	18.2	12.4	7.1
GS-03-079	7	351985	5260927		-	3.2	9	162	1526	15	31	54	2.3	1.4	13.7	0.29	9.4	18.0	10.8
GS-03-087	7	353340	5261029		-	3.8	10	117	1434	16	22	34	1.8	1.3	12.1	0.44	12.3	12.0	7.4
GS-03-109	7	352027	5260759		-	2.8	9	75	1166	11	28	40	1.3	1.4	20.8	0.32	15.5	8.6	6.5
GS-03-126	7	352730	5260152		-	3.6	10	155	1485	11	19	31	1.5	1.2	12.7	0.54	9.6	15.2	14.7
GS-03-129	7	352158	5261691			4.0	11	152	1492	15	16	27	2.1	1.7	7.6	0.70	9.8	13.5	10.4

* samples with UTM's calculated from registered base map

173

Table 3-16: Extended rare earth element data for Unit 7 of the White Hills Intrusive Suite.

Sample Number	Unit	Easting	Northing	Element	V	Cr	Co	Ni	Cu	Zn	Ga	Ge	As	Rb	Sr	Y	Zr	Nb	Mo
				Method	ICP-MS	ICP-MS	ICP-MS	ICP-MS	ICP-MS	ICP-MS	ICP-MS	ICP-MS	ICP-MS	ICP-MS	ICP-MS	ICP-MS	ICP-MS	ICP-MS	ICP-MS
				Unit	ppm	ppm	ppm	ppm	ppm	ppm	ppm	ppm	ppm	ppm	ppm	ppm	ppm	ppm	ppm
				Limit	5	20	1	20	10	30	1	1	5	2	2	1	5	1	2
Medium- to Coarse-grained Equigranular Granite (WHIS)																			
OB-01-046	7	353476	5264601		22	-	4	-	25	401	14	1		118	120	22	172	10	
OB-01-061	7	352899	5264199		34		-		11	31	16	-		134	113	12	150	10	-
OB-97-221	7	353072*	5263803*		29	-	3	-	22	43	13	1	-	125	112	12	131	9	
OB-97-362	7	352644	5260024		36	-	-	-	-	-	15	1	5	134	103	11	157	10	4

Table 3-16: cont'd

Sample Number	Unit	Easting	Northing	Element	Ag	In	Sn	Sb	Cs	Ba	La	Ce	Pr	Nd	Sm	Eu	Gd	Tb	Dy
				Method	ICP-MS	ICP-MS	ICP-MS	ICP-MS	ICP-MS	ICP-MS	ICP-MS	ICP-MS	ICP-MS	ICP-MS	ICP-MS	ICP-MS	ICP-MS	ICP-MS	ICP-MS
				Unit	ppm	ppm	ppm	ppm	ppm	ppm	ppm	ppm	ppm	ppm	ppm	ppm	ppm	ppm	ppm
				Limit	0.5	0.2	1.0	0.5	0.5	3	0.1	0.1	0.005	0.1	0.1	0.005	0.1	0.1	0.1
Medium- to Coarse-grained Equigranular Granite (WHIS)																			
OB-01-046	7	353476	5264601		-		3	2.4	3.2	790	28.5	64.6	6.16	20.2	4.1	0.82	3.3	0.6	3.7
OB-01-061	7	352899	5264199		-	-	1	0.6	1.7	1170	21.0	39.4	4.47	14.7	2.9	0.61	2.3	0.4	2.1
OB-97-221	7	353072*	5263803*		0.6	-	1	-	1.8	1020	15.9	33.6	3.31	11.0	2.3	0.46	2.0	0.3	2.1
OB-97-362	7	352644	5260024		0.6	-	1	1.3	2.3	1140	17.7	34.3	3.63	11.0	2.0	0.45	1.5	0.3	1.7

Table 3-16: cont'd

Sample Number	Unit	Easting	Northing	Element	Ho	Er	Tm	Yb	Lu	Hf	Ta	W	Tl	Pb	Bi	Th	U
				Method	ICP-MS	ICP-MS	ICP-MS	ICP-MS	ICP-MS	ICP-MS	ICP-MS	ICP-MS	ICP-MS	ICP-MS	ICP-MS	ICP-MS	ICP-MS
				Unit	ppm	ppm	ppm	ppm	ppm	ppm	ppm	ppm	ppm	ppm	ppm	ppm	ppm
				Limit	0.1	0.1	0.05	0.1	0.04	0.2	0.1	1	0.1	5	0.4	0.1	0.1
Medium- to Coarse-grained Equigranular Granite (WHIS)																	
OB-01-046	7	353476	5264601		0.8	2.4	0.37	2.6	0.42	4.7	0.8	1	1.0	23	3.1	12.1	1.5
OB-01-061	7	352899	5264199		0.5	1.5	0.25	1.8	0.32	4.5	1.0	-	1.0	45	-	12.8	1.8
OB-97-221	7	353072*	5263803*		0.4	1.3	0.22	1.5	0.26	3.8	0.9		1.1	54	-	12.0	2.3
OB-97-362	7	352644	5260024		0.4	1.2	0.20	1.4	0.25	4.5	1.0	2	1.2	32	-	11.4	1.8

* samples with UTM's calculated from registered base map

Table 3-17: Trace-element contents of Unit 8 from the White Hills Intrusive Suite.

Sample Number	Unit	Easting	Northing	Element	Cr	Ni	Co	Sc	V	Cu	Pb	Zn	Cd	Mo	As	Rb	Ba	Sr
				Method	ICP-ES	ICP-ES	ICP-ES	ICP-ES	ICP-ES	ICP-ES	ICP-ES	ICP-ES	ICP-ES	ICP-ES	ICP-ES	ICP-ES	ICP-ES	ICP-ES
				Unit	ppm	ppm	ppm	ppm	ppm	ppm	ppm	ppm	ppm	ppm	ppm	ppm	ppm	ppm
				Limit	1	1	1	0.1	1	1	1	1	0.1	1	2	5	1	1
Quartz-Feldspar Porphyry (WHIS)																		
OB-97-021	8	351844	5262640		2	-	4	5.0	32	1	6	44			-	-	1148	158
OB-01-015	8	351917	5262653		1	4	5	5.4	35	-	5	51		-	3	-	1036	110
OB-01-038	8	351957	5262613		-	3	2	3.8	20	7	11	20			3	-	1347	195
GS-03-027	8	352371	5261328		1	2	2	3.6	18	2	20	34	0.1	1	-	-	1282	176
GS-03-060	8	352053	5261835		2	3	3	4.6	30	192	34	42	0.2	-		-	1096	129
GS-03-063	8	351824	5261603		1	2	2	4.0	18	5	22	31	0.2	2		-	1151	136
GS-03-097	8	351945	5262660		2	3	5	5.5	37	-	14	51	0.1	1	-	-	1149	146

Table 3-17: cont'd

Sample Number	Unit	Easting	Northing	Element	Ga	Li	Nb	Zr	Ti	Y	La	Ce	Dy	Be	La/Dy	Nb/La	Ti/Zr	Zr/Nb	Zr/Y
				Method	ICP-ES	ICP-ES	ICP-ES	ICP-ES	ICP-ES	ICP-ES	ICP-ES	ICP-ES	ICP-ES	ICP-ES					
				Unit	ppm	ppm	ppm	ppm	ppm	ppm	ppm	ppm	ppm	ppm					
				Limit	1	0.1	1	1	1	1	1	1	0.1	0.1					
Quartz-Feldspar Porphyry (WHIS)																			
OB-97-021	8	351844	5262640		14	6.5	7	110	1824	13	29	52	2.0	1.4	14.6	0.24	16.6	15.8	8.2
OB-01-015	8	351917	5262653		-	6.5	9	94	1812	13	24	41	2.5	1.2	9.5	0.37	19.3	10.6	7.2
OB-01-038	8	351957	5262613		-	3.0	10	111	1159	15	28	42	2.2	1.5	12.7	0.37	10.5	10.7	7.5
GS-03-027	8	352371	5261328		-	2.4	8	109	1101	13	29	40	1.7	1.5	16.7	0.26	10.1	14.4	8.2
GS-03-060	8	352053	5261835		-	4.8	10	113	1471	14	26	37	1.9	1.4	13.9	0.38	13.1	11.2	7.8
GS-03-063	8	351824	5261603		-	3.1	11	83	1180	15	22	35	1.8	1.6	12.2	0.49	14.3	7.8	5.7
GS-03-097	8	351945	5262660		-	6.4	9	115	1879	14	28	40	1.7	1.3	16.5	0.32	16.3	12.7	8.4

* samples with UTM's calculated from registered base map

Table 3-18: Trace-element contents of rhyolite successions within the study area.

Sample Number	Unit	Easting	Northing	Element	Cr	Ni	Co	Sc	V	Cu	Pb	Zn	Cd	Mo	As	Rb	Ba	Sr
				Method	ICP-ES	ICP-ES	ICP-ES	ICP-ES	ICP-ES	ICP-ES	ICP-ES	ICP-ES	ICP-ES	ICP-ES	ICP-ES	ICP-ES	ICP-ES	ICP-ES
				Unit	ppm	ppm	ppm	ppm	ppm	ppm	ppm	ppm	ppm	ppm	ppm	ppm	ppm	ppm
				Limit	1	1	1	0.1	1	1	1	1	0.1	1	2	5	1	1
Minerals Road Rhyolite (WMVS)																		
OB-97-019	1	351957	5262683		1	-	-	2.3	6	4	7	20	-		-	-	1983	83
OB-97-040	1	351799*	5260872*		1			3.6	12	7	3	13	-	-		-	727	29
OB-01-012	1	351843	5262605		1	1		3.7	8	-	4	30	0.1	-	4	-	1725	42
OB-01-036	1	351888	5262516			1	1	2.0	10		7	21	-	1	4	-	2460	83
OB-01-037	1	351897	5262608		-	2	1	2.5	10	-	8	38		2	2	-	2222	93
GS-02-080	1	351787	5262498		4	4	2	4.9	17	2	2	45	-	1	-	34	1029	67
OB-03-018	1	352986	5262305		2	1		2.9	5		2	21		3			27	36
OB-03-019	1	353049	5262262		2	1		3.5	4		11	25	0.1	3	2	-	779	99
GS-03-075	1	351926	5261343		1	-	-	2.3	5	1	17	22	0.1	2			1663	51
Manuels River Rhyolite (WMVS)																		
OB-00-150	2	352865	5263152		1	1		4.9	4	3		11	-	-	4	-	1041	21
OB-01-006	2	352971	5263209		-		-	3.0	7	9	3	7	-	-	-	-	1004	19
OB-01-007	2	352931	5263179		3		-	4.4	14	18	4	11	0.1	1			807	25
OB-01-039	2	353111	5263779		3	5	5	6.9	44	8	5	53	-	1	8	-	1203	111
OB-01-040	2	353125	5263815		5	7	7	10.0	57	2	3	55	0.1	-	5	-	1104	119
OB-01-041	2	353503	5263791		-	2	-	4.3	13	3	11	61	-	3	5	-	823	75
OB-01-042	2	353553	5263767		-	2	-	3.9	7	3	6	41	-	3	7		658	46
OB-01-043	2	353893	5263644		1	1		2.1	3		12	39		2			612	72
GS-02-076	2	353976	5263545		2	2	-	2.2	8		9	66	-	1	3	55	1464	85
GS-02-086	2	352905	5263070		2	1	-	5.0	14	5	13	21	-	2	-	124	1327	25
OB-03-013	2	353107	5263281		1	-	-	5.4	4	1	7	8	-	2	-		46	50
OB-03-061	2	353272	5264249		3	3		4.4	42	14	8	14	0.2	2	3	-	1706	28
GS-03-096	2	354138	5263257		2	4	2	7.0	24		12	97	-	2	-	-	708	113
Farmer's Field Rhyolite (MVS)																		
OB-97-176	9	353153	5261190		3	-	-	3.8	34	3	5	35	-	-	-	-	1156	40
OB-97-178	9	353065	5261527		3	2		3.7	3	2	11	19	-	-	-	-	1890	37
OB-00-087	9	352801	5259845		2	1	-	4.3	12	4	-	15	-		3	-	1153	30
OB-03-017	9	353115	5262098		1	1	-	2.8	5	2	5	16	0.2	1	3	-	1463	20
GS-03-053	9	353280	5261920		2	2		6.4	17	6	16	28	-	1	8	-	1199	97
GS-03-058	9	353370	5261191		1	1	-	3.1	5	2	16	18	-	2	-	-	48	28
Pale Grey-Green, Moderately Porphyritic, Fine, Rhyolite (MVS)																		
OB-97-010	11	353612*	5263724*		2		1	3.6	19	8	7	30	-	-	-	-	350	42
GS-02-071	11	353563	5263774		2	2	-	3.6	15	7	13	41	-	3	2	31	754	58
GS-02-072	11	353434	5263847		2	2	1	4.2	20		6	73	-	3	4	61	1152	74

* samples with UTM's calculated from registered base map

Table 3-18: cont'd

Sample Number	Unit	Easting	Northing	Element	Ga	Li	Nb	Zr	Ti	Y	La	Ce	Dy	Be	La/Dy	Nb/La	Ti/Zr	Zr/Nb	Zr/Y
				Method	ICP-ES	ICP-ES	ICP-ES	ICP-ES	ICP-ES	ICP-ES	ICP-ES	ICP-ES	ICP-ES	ICP-ES					
				Unit	ppm	ppm	ppm	ppm	ppm	ppm	ppm	ppm	ppm	ppm					
				Limit	1	0.1	1	1	1	1	1	1	0.1	0.1					
Minerals Road Rhyolite (WMVS)																			
OB-97-019	1	351957	5262683		15	1.6	12	163	1054	41	21	57	6.1	1.2	3.5	0.56	6.5	13.9	4.0
OB-97-040	1	351799*	5260872*		6	1.0	12	187	799	37	9	31	5.2	3.4	1.8	1.23	4.3	16.1	5.0
OB-01-012	1	351843	5262605			1.7	15	213	950	48	19	37	6.9	2.1	2.8	0.77	4.5	14.3	4.4
OB-01-036	1	351888	5262516			1.7	11	151	901	34	17	34	5.5	1.3	3.1	0.63	6.0	14.1	4.4
OB-01-037	1	351897	5262608		-	3.2	13	170	1009	36	20	38	5.8	1.3	3.5	0.65	6.0	12.7	4.7
GS-02-080	1	351787	5262498		-	4.1	13	140	1149	45	22	42	6.7	1.6	3.3	0.61	8.2	10.5	3.1
OB-03-018	1	352986	5262305		-	1.9	7	133	1071	29	9	18	3.9	0.8	2.3	0.78	8.1	19.0	4.6
OB-03-019	1	353049	5262262			2.3	8	161	1246	34	25	40	5.1	1.5	5.0	0.33	7.8	19.4	4.7
GS-03-075	1	351926	5261343		-	0.9	13	162	960	37	29	51	5.5	1.6	5.4	0.43	5.9	12.9	4.3
Manuels River Rhyolite (WMVS)																			
OB-00-150	2	352865	5263152		-	1.1	11	163	845	36	8	18	4.9	1.0	1.7	1.38	5.2	14.5	4.5
OB-01-006	2	352971	5263209		-	1.7	13	137	693	24	7	17	3.6	0.7	2.1	1.68	5.1	10.9	5.7
OB-01-007	2	352931	5263179		-	1.2	14	147	796	33	9	22	5.0	1.0	1.8	1.54	5.4	10.3	4.5
OB-01-039	2	353111	5263779		-	3.3	12	348	4279	37	30	50	5.5	1.9	5.5	0.38	12.3	30.2	9.4
OB-01-040	2	353125	5263815		-	4.0	12	362	5417	38	27	51	5.4	1.9	5.0	0.43	15.0	30.9	9.5
OB-01-041	2	353503	5263791		-	3.8	20	359	2051	50	45	77	7.2	2.6	6.3	0.43	5.7	18.2	7.1
OB-01-042	2	353553	5263767		-	1.7	18	345	1997	46	38	68	6.9	1.8	5.5	0.47	5.8	19.6	7.5
OB-01-043	2	353893	5263644			2.8	15	161	1299	38	46	72	5.6	1.7	8.2	0.32	8.0	11.0	4.3
GS-02-076	2	353976	5263545		-	3.3	15	195	1711	39	26	42	5.2	1.9	4.9	0.59	8.8	13.0	5.1
GS-02-086	2	352905	5263070		-	7.0	12	157	850	23	11	20	3.3	1.2	3.4	1.06	5.4	13.2	6.9
OB-03-013	2	353107	5263281		-	-	13	242	1214	46	44	74	7.4	1.6	6.0	0.29	5.0	18.9	5.3
OB-03-061	2	353272	5264249		-	2.0	15	364	1644	59	60	85	8.4	1.7	7.1	0.24	4.5	24.9	6.2
GS-03-096	2	354138	5263257		-	6.3	12	263	3240	40	29	50	5.9	1.3	4.9	0.41	12.3	22.7	6.6
Farmer's Field Rhyolite (MVS)																			
OB-97-176	9	353153	5261190		10	1.5	13	386	1898	44	45	99	6.9	1.8	6.5	0.28	4.9	30.5	8.7
OB-97-178	9	353065	5261527		12	3.9	12	176	994	37	35	76	5.7	1.6	6.2	0.33	5.6	15.0	4.7
OB-00-087	9	352801	5259845		-	1.3	11	145	768	33	16	30	4.3	1.3	3.9	0.64	5.3	13.6	4.4
OB-03-017	9	353115	5262098		-	0.8	11	136	740	29	24	37	4.6	1.5	5.2	0.46	5.4	12.5	4.7
GS-03-053	9	353280	5261920		-	3.1	13	339	2732	43	46	71	6.4	1.7	7.1	0.29	8.1	25.7	7.8
GS-03-058	9	353370	5261191		-	1.0	9	231	1564	44	38	63	6.4	2.5	5.8	0.25	6.8	24.7	5.3
Pale Grey-Green, Moderately Porphyritic, Fine, Rhyolite (MVS)																			
OB-97-010	11	353612*	5263724*		19	5.2	13	338	1888	41	38	96	5.9	1.5	6.5	0.34	5.6	26.2	8.2
GS-02-071	11	353563	5263774		-	3.7	12	304	2259	39	34	52	5.4	1.7	6.3	0.36	7.4	24.8	7.9
GS-02-072	11	353434	5263847		-	5.3	8	252	2836	29	35	55	4.0	1.6	8.8	0.22	11.2	32.3	8.8

* samples with UTM's calculated from registered base map

Table 3-19: Trace-element contents of ash-flow tuffs from within the study area.

Sample Number	Unit	Easting	Northing	Element	Cr	Ni	Co	Sc	V	Cu	Pb	Zn	Cd	Mo	As	Rb	Ba	Sr
				Method Unit Limit	ICP-ES ppm 1	ICP-ES ppm 1	ICP-ES ppm 1	ICP-ES ppm 0.1	ICP-ES ppm 1	ICP-ES ppm 1	ICP-ES ppm 1	ICP-ES ppm 1	ICP-ES ppm 0.1	ICP-ES ppm 1	ICP-ES ppm 2	ICP-ES ppm 5	ICP-ES ppm 1	ICP-ES ppm 1
Welded, Fiamme-bearing Ash-Flow Tuff (MVS)																		
OB-01-008	4	352913	5263846			3	1	4.8	14	-	8	35		1	4	-	1342	91
OB-01-010	4	353404	5263833		4	4	2	5.4	15		7	48	-	-	6		1018	91
OB-01-011	4	353421	5263842		2	4	2	4.9	10	.	5	64		1	7		1053	94
Grey-Green, Pyritic, Pumiceous, Crystal-bearing, Ash-flow Tuff (MVS)																		
GS-02-074	12	353058	5264200		2	4	2	10.8	40	3	17	113		2	64	85	997	135
Dark Purple, Crystal-bearing, Ash-flow Tuff (MVS)																		
GS-02-009	13	352985	5264488		3	3		9.6	35	-	6	25		1	13	130	1672	105
GS-02-087	13	352982	5264476		9	5	4	9.4	51	74	2	39		4	156	117	65100	188
OB-03-060	13	352959	5264472		3	3	-	10.8	39		8	24	0.1	1	8		1248	135
GS-03-052	13	353397	5262718		2	3	-	5.2	28	-	14	14		2	8		595	105

Table 3-19: cont'd

Sample Number	Unit	Easting	Northing	Element	Ga	Li	Nb	Zr	Ti	Y	La	Ce	Dy	Be	La/Dy	Nb/La	Ti/Zr	Zr/Nb	Zr/Y
				Method Unit Limit	ICP-ES ppm 1	ICP-ES ppm 0.1	ICP-ES ppm 1	ICP-ES ppm 1	ICP-ES ppm 1	ICP-ES ppm 1	ICP-ES ppm 1	ICP-ES ppm 1	ICP-ES ppm 0.1	ICP-ES ppm 0.1					
Welded, Fiamme-bearing Ash-Flow Tuff (MVS)																			
OB-01-008	4	352913	5263846		-	2.1	16	361	2440	45	43	74	7.2	2.0	5.9	0.38	6.8	22.3	8.0
OB-01-010	4	353404	5263833		-	3.5	15	368	2620	47	52	85	7.1	2.4	7.3	0.30	7.1	24.0	7.8
OB-01-011	4	353421	5263842		-	4.2	14	354	2470	46	45	77	6.9	2.3	6.6	0.30	7.0	25.7	7.6
Grey-Green, Pyritic, Pumiceous, Crystal-bearing, Ash-flow Tuff (MVS)																			
GS-02-074	12	353058	5264200		-	5.9	14	349	4903	44	31	59	6.7	2.0	4.6	0.44	14.1	25.2	7.9
Dark Purple, Crystal-bearing, Ash-flow Tuff (MVS)																			
GS-02-009	13	352985	5264488		-	5.7	12	310	4115	40	32	54	6.0	1.6	5.4	0.38	13.3	25.8	7.8
GS-02-087	13	352982	5264476		-	9.7	12	275	3815	29	7	19	3.7	2.1	1.9	1.69	13.8	23.3	9.6
OB-03-060	13	352959	5264472		-	4.4	13	322	4390	40	34	59	6.3	1.6	5.5	0.36	13.6	25.6	8.0
GS-03-052	13	353397	5262718		-	0.6	11	241	2847	31	37	60	4.4	1.4	8.4	0.29	11.8	22.1	7.7

* samples with UTM's calculated from registered base map

Table 3-20: Trace-element contents of mafic rocks from within the study area.

Sample Number	Unit	Easting	Northing	Element	Cr	Ni	Co	Sc	V	Cu	Pb	Zn	Cd	Mo	As	Rb	Ba	Sr
				Method Unit Limit	ICP-ES ppm 1	ICP-ES ppm 1	ICP-ES ppm 1	ICP-ES ppm 0.1	ICP-ES ppm 1	ICP-ES ppm 1	ICP-ES ppm 1	ICP-ES ppm 1	ICP-ES ppm 0.1	ICP-ES ppm 1	ICP-ES ppm 2	ICP-ES ppm 5	ICP-ES ppm 1	ICP-ES ppm 1
Mafic Volcanic/Intrusions (MVS)																		
OB-00-289	15	352722	5260727		1	5	11	29.5	98	-	2	160	-	-	4	-	355	141
GS-02-010	15	353005*	5264473*		141	145	53	29.8	225	32	2	140	-	-	3	116	799	59
GS-03-039	15	353534	5262310		13	17	23	20.8	157	53	15	91	-	-	-	-	77	191
GS-03-105	15	352660	5260024		20	66	58	26.8	227	96	12	190	-	-	2	-	373	114
Amygdaloidal Basalt/ Hyaloclastite (WHPC)																		
OB-00-280	21	354474	5263520		81	33	33	32.2	303	27	4	114	-	4	8	-	331	272
OB-01-001	21	354325	5263604		160	69	33	29.0	218	39	4	79	0.1	-	3	-	1406	306
OB-01-003	21	354383	5263567		12	20	25	25.1	274	19	1	98	0.2	-	2	-	288	165
OB-01-004	21	354467	5263510		73	34	33	31.8	326	14	7	108	0.1	-	3	-	380	332
GS-03-34	21	352513	5262696		67	57	33	24.8	194	38	13	99	-	-	5	-	94	123
GS-03-33	21	352513	5262696		65	55	29	23.5	203	36	13	80	-	-	-	-	76	115
Mafic Dykes																		
OB-97-012	20a	353548	5264062		4	10	34	31.9	394	50	1	142	-	-	-	-	1487	146
OB-00-276	20a	355302*	5263072*		19	27	26	26.6	201	23	-	113	-	-	4	-	150	152
GS-01-038	20a	352732	5260563		44	55	43	31.8	300	62	39	113	-	-	37	-	1668	20
GS-02-007	20a	352931	5264192		16	16	32	31.0	228	16	120	275	0.2	1	8	30	405	80
GS-02-075	20a	352931	5264192		14	13	32	34.9	266	14	74	276	-	1	6	85	1028	60
GS-03-122	20a	355039	5263253		18	30	25	27.2	228	29	11	110	-	-	-	-	189	180
GS-03-123	20a	354509	5263481		192	129	49	39.3	306	47	11	130	-	-	-	-	509	44
GS-03-127	20a	352744	5263061		30	27	37	35.7	309	68	73	311	-	-	10	-	316	13
GS-03-128	20a	352637	5263263		137	119	48	29.1	277	77	13	150	-	-	7	-	289	220
OB-01-002	20b	354371	5263576		176	73	40	29.8	265	66	1	116	0.1	-	3	-	441	203
OB-01-044	20b	353820	5263791		179	76	37	33.3	267	59	4	84	0.1	-	5	-	523	252
GS-03-124	20b	353395	5263847		66	56	32	25.7	211	53	15	78	-	-	2	-	563	437
GS-02-070	20c	353941	5263620		9	33	19	15.8	134	51	4	74	-	-	-	23	643	244
GS-03-074	20c	351892	5261238		48	52	18	13.1	112	4	15	108	-	-	-	-	671	175
GS-03-125	20c	351914	5262637		28	38	15	12.3	73	-	15	120	0.1	-	-	-	2465	96

* samples with UTM's calculated from registered base map

179

Table 3-20: cont'd

Sample Number	Unit	Easting	Northing	Element	Ga	Li	Nb	Zr	Ti	Y	La	Ce	Dy	Be	La/Dy	Nb/La	Ti/Zr	Zr/Nb	Zr/Y
				Method Unit Limit	ICP-ES ppm 1	ICP-ES ppm 0.1	ICP-ES ppm 1	ICP-ES ppm 1	ICP-ES ppm 1	ICP-ES ppm 1	ICP-ES ppm 1	ICP-ES ppm 1	ICP-ES ppm 0.1	ICP-ES ppm 0.1					
Mafic Volcanic/Intrusions (MVS)																			
OB-00-289	15	352722	5260727		-	21.5	14	268	13112	51	32	60	7.8	1.8	4.0	0.43	48.9	19.8	5.3
GS-02-010	15	353005*	5264473*		-	64.2	7	87	8323	17	5	16	2.8	2.2	1.9	1.36	95.5	12.6	5.0
GS-03-039	15	353534	5262310		-	13.7	6	120	6259	19	19	36	2.7	0.8	7.1	0.33	52.1	19.2	6.2
GS-03-105	15	352660	5260024		-	33.4	11	182	15051	28	24	52	4.5	1.4	5.3	0.47	82.7	15.9	6.6
Amygdaloidal Basalt/ Hyaloclastite (WHPC)																			
OB-00-280	21	354474	5263520		-	11.5	11	160	12996	35	20	41	5.5	1.2	3.7	0.55	81.1	14.3	4.6
OB-01-001	21	354325	5263604		-	20.1	7	125	8194	29	13	29	4.5	1.1	2.9	0.50	65.6	19.0	4.3
OB-01-003	21	354363	5263587		-	10.9	11	135	10506	29	17	37	4.8	1.1	3.6	0.66	77.8	12.1	4.7
OB-01-004	21	354467	5263510		-	10.4	11	148	13508	32	19	43	4.3	1.4	4.4	0.59	91.3	13.4	4.7
GS-03-34	21	352513	5262696		-	14.1	7	116	8097	21	10	26	3.2	0.8	3.2	0.67	69.8	16.6	5.5
GS-03-33	21	352513	5262696		-	12.7	6	110	7558	21	11	25	3.0	1.0	3.5	0.57	69.0	16.1	5.3
Mafic Dykes																			
OB-97-012	20a	353548	5264062		31	47.3	6	162	14249	31	18	40	5.2	2.8	3.4	0.33	88.0	27.5	5.3
OB-00-276	20a	355302*	5263072*		-	28.6	7	130	11058	32	16	33	4.9	1.2	3.3	0.45	85.0	17.6	4.1
GS-01-038	20a	352732	5260563		-	58.3	4	63	9671	24	6	18	1.8	4.1	3.3	0.67	154.6	15.6	2.6
GS-02-007	20a	352931	5264192		-	13.9	11	130	13343	44	12	35	6.4	1.8	2.0	0.85	102.7	12.3	2.9
GS-02-075	20a	352931	5264192		-	13.9	12	149	15185	64	28	57	7.8	1.6	3.7	0.41	101.7	12.8	2.3
GS-03-122	20a	355039	5263253		-	30.4	10	137	11965	29	16	35	4.8	1.2	3.5	0.64	87.3	13.5	4.7
GS-03-123	20a	354509	5263461		-	32.0	8	129	11677	38	9	26	5.8	1.2	1.5	0.86	90.3	16.9	3.4
GS-03-127	20a	352744	5263061		-	41.7	10	166	11995	28	18	39	4.0	3.4	4.4	0.54	72.4	17.3	5.9
GS-03-128	20a	352637	5263263		-	26.0	8	132	11705	23	13	32	3.4	1.8	3.7	0.66	88.7	15.9	5.7
OB-01-002	20b	354371	5263576		-	20.5	10	107	10343	22	24	52	3.7	1.1	6.3	0.41	96.5	11.1	4.8
OB-01-044	20b	353820	5263791		-	47.5	5	94	8628	25	7	21	3.7	1.4	2.0	0.73	93.5	17.3	3.8
GS-03-124	20b	353395	5263847		-	27.5	5	104	7409	23	13	29	3.0	0.7	4.4	0.41	70.9	19.1	4.5
GS-02-070	20c	353941	5263620		-	19.3	6	136	5311	19	18	31	2.7	1.5	6.7	0.35	39.0	21.5	7.1
GS-03-074	20c	351892	5261238		-	12.5	3	81	3981	11	13	25	1.4	1.0	9.6	0.26	49.0	23.5	7.1
GS-03-125	20c	351914	5262637		-	19.8	5	117	3303	16	16	31	2.0	1.5	8.0	0.32	28.3	22.9	7.2

* samples with UTM's calculated from registered base map

180

Table 3-21: Trace-element contents of Unit 22 (Wych Hazel Pond Complex).

Sample Number	Unit	Easting	Northing	Element	Cr	Ni	Co	Sc	V	Cu	Pb	Zn	Cd	Mo	As	Rb	Ba	Sr
				Method	ICP-ES	ICP-ES	ICP-ES	ICP-ES	ICP-ES	ICP-ES	ICP-ES	ICP-ES	ICP-ES	ICP-ES	ICP-ES	ICP-ES	ICP-ES	ICP-ES
				Unit	ppm	ppm	ppm	ppm	ppm	ppm	ppm	ppm	ppm	ppm	ppm	ppm	ppm	ppm
				Limit	1	1	1	0.1	1	1	1	1	0.1	1	2	5	1	1
Fowler's Road Porphyry (WHPC)																		
OB-00-278	22	354539	5263455		5	5		7.7	6	3	3	45		1	3	-	90	38
OB-01-033	22	353166	5264360			2	1	28	6	3	23	63	0.1	2	5	-	1642	29
GS-02-077	22	354574	5263452		-	4	-	7.7	12	2	2	88		2	3	3	243	59
GS-03-116	22	355311	5263097		1	1		2.8	5	2	14	32		1		-	961	62

Table 3-21: cont'd

Sample Number	Unit	Easting	Northing	Element	Ga	Li	Nb	Zr	Ti	Y	La	Ce	Dy	Be	La/Dy	Nb/La	Ti/Zr	Zr/Nb	Zr/Y
				Method	ICP-ES	ICP-ES	ICP-ES	ICP-ES	ICP-ES	ICP-ES	ICP-ES	ICP-ES	ICP-ES	ICP-ES					
				Unit	ppm	ppm	ppm	ppm	ppm	ppm	ppm	ppm	ppm	ppm					
				Limit	1	0.1	1	1	1	1	1	1	0.1	0.1					
Fowler's Road Porphyry (WHPC)																			
OB-00-278	22	354539	5263455		-	5.0	24	514	1723	63	28	49	8.6	1.7	3.3	0.85	3.4	21.4	8.1
OB-01-033	22	353166	5264360		-	2.2	20	199	1185	47	24	45	7.3	1.2	3.2	0.84	5.9	10.0	4.2
GS-02-077	22	354574	5263452		-	5.4	26	526	1746	51	43	70	8.3	1.6	5.2	0.61	3.3	20.0	10.2
GS-03-116	22	355311	5263097		-	2.7	20	198	1138	44	30	54	6.5	1.7	4.7	0.65	5.8	10.0	4.5

* samples with UTM's calculated from registered base map

Table 3-22: Major-element contents of Unit 3 from the White Mountian Volcanic Suite.

Sample Number	Unit	Easting	Northing	Element	SiO2	TiO2	Al2O3	Fe2O3	FeO	MnO	MgO	CaO	Na2O	K2O	P2O5	LOI	Total
				Method	ICP-ES	ICP-ES	ICP-ES	ICP-ES	ICP-ES	ICP-ES	ICP-ES	ICP-ES	ICP-ES	ICP-ES	ICP-ES		
				Unit	%	%	%	%	%	%	%	%	%	%	%	%	%
				Limit	0.01	0.001	0.01	0.01		0.010	0.01	0.01	0.01	0.01	0.001		
Massive, Lithic-Rich, Polymict, Lapilli Tuff (WMVS)																	
GS-02-085	3	352682	5263144		78.80	0.229	11.42	1.11	0.26	0.026	0.30	0.16	3.26	3.53	0.04	0.71	99.87
GS-03-100	3	352744	5263061		77.70	0.18	10.87			0.02	0.24	0.12	2.84	4.27	0.03	1.07	98.66
GS-03-130A	3	352614	5263218		76.42	0.149	12.67	0.53	0.47	0.029	0.43	0.09	2.93	4.16	0.03	1.10	99.05
GS-03-130B	3	352612	5263210		81.32	0.145	8.84	0.88	0.14	0.024	0.33	0.08	2.08	3.51	0.02	0.73	98.12
GS-03-130C	3	352614	5263224		81.30	0.183	9.47	0.89	0.17	0.024	0.30	0.10	2.24	3.70	0.03	0.72	99.14
GS-03-130G	3	352611	5263211		85.62	0.086	5.33	1.51	0.50	0.070	0.67	0.05	0.30	2.93	0.03	0.90	98.06
GS-03-130H	3	352612	5263214		78.77	0.179	10.04	1.02	0.38	0.054	0.46	0.14	2.65	3.71	0.03	0.73	98.22
GS-03-130I	3	352610	5263215		81.49	0.168	8.99	1.08	0.23	0.045	0.44	0.09	1.71	3.92	0.03	0.77	98.98

Table 3-23: Trace-element contents of two samples from Unit 3, collected distal from the roadside outcrop.

Sample Number	Unit	Easting	Northing	Element	Cr	Ni	Co	Sc	V	Cu	Pb	Zn	Cd	Mo	As	Ba	Sr
				Method	ICP-ES	ICP-ES	ICP-ES	ICP-ES	ICP-ES	ICP-ES	ICP-ES	ICP-ES	ICP-ES	ICP-ES	ICP-ES	ICP-ES	ICP-ES
				Unit	ppm	ppm	ppm	ppm	ppm	ppm	ppm	ppm	ppm	ppm	ppm	ppm	ppm
				Limit	1	1	1	0.1	1	1	1	1	0.1	1	2	1	1
Massive, Lithic-Rich, Polymict, Lapilli Tuff (WMVS)																	
GS-02-085	3	352682	5263144		10	5	2	5.9	30	7	7	34		1	3	857	54
GS-03-100	3	352744	5263061		5	7	3	5.3	21	6	17	20	-	8	5	161	52

Table 3-23: cont'd

Sample Number	Unit	Easting	Northing	Element	Li	Nb	Zr	Ti	Y	La	Ce	Dy	Be	La/Dy	Nb/La	Ti/Zr	Zr/Nb	Zr/Y
				Method	ICP-ES	ICP-ES	ICP-ES	ICP-ES	ICP-ES	ICP-ES	ICP-ES	ICP-ES	ICP-ES					
				Unit	ppm	ppm	ppm	ppm	ppm	ppm	ppm	ppm	ppm					
				Limit	0.1	1	1	1	1	1	1	0.1	0.1					
Massive, Lithic-Rich, Polymict, Lapilli Tuff (WMVS)																		
GS-02-085	3	352682	5263144		3.9	11	162	1703	34	22	36	4.9	1.7	4.5	0.5	10.5	14.6	4.7
GS-03-100	3	352744	5263061		2.1	11	164	1370	36	20	36	5.1	1.7	3.9	0.6	8.3	14.9	4.6

* samples with UTM's calculated from registered base map

Table 3-24: Extended rare earth element data for Unit 3 (White Mountian Volcanic Suite).

Sample Number	Unit	Easting	Northing	Element	V	Cr	Co	Ni	Cu	Zn	Ga	Ge	As	Rb	Sr	Y	Zr	Nb	Mo
				Method	ICP-MS	ICP-MS	ICP-MS	ICP-MS	ICP-MS	ICP-MS	ICP-MS	ICP-MS	ICP-MS	ICP-MS	ICP-MS	ICP-MS	ICP-MS	ICP-MS	ICP-MS
				Unit	ppm	ppm	ppm	ppm	ppm	ppm	ppm	ppm	ppm	ppm	ppm	ppm	ppm	ppm	ppm
				Limit	5	20	1	20	10	30	1	1	5	2	2	1	5	1	2
Massive, Lithic-Rich, Polymict, Lapilli Tuff (WMVS)																			
GS-03-130A	3	352614	5263218		34						15	-	-	138	50	35	200	10	-
GS-03-130B	3	352612	5263210		24	-					10		-	98	48	29	154	8	-
GS-03-130C	3	352614	5263224		22		1	-		-	10			102	50	27	163	8	-
GS-03-130D	3	352614	5263220		7		-	-	-		5			92	18	2	14	-	
GS-03-130E	3	352611	5263218		8		-	-	-	-	2			19	6	1	5		
GS-03-130F	3	352611	5263213		-		-				3		-	79	23	2	16	-	-
GS-03-130G	3	352611	5263211		27	-	3			87	8	-		85	23	15	84	4	
GS-03-130H	3	352612	5263214		21		2			36	11			89	59	29	147	8	
GS-03-130I	3	352610	5263215		32	-	2			44	11	1	-	109	48	27	163	8	

Table 3-24: cont'd

Sample Number	Unit	Easting	Northing	Element	Ag	In	Sn	Sb	Cs	Ba	La	Ce	Pr	Nd	Sm	Eu	Gd	Tb	Dy
				Method	ICP-MS	ICP-MS	ICP-MS	ICP-MS	ICP-MS	ICP-MS	ICP-MS	ICP-MS	ICP-MS	ICP-MS	ICP-MS	ICP-MS	ICP-MS	ICP-MS	ICP-MS
				Unit	ppm	ppm	ppm	ppm	ppm	ppm	ppm	ppm	ppm	ppm	ppm	ppm	ppm	ppm	ppm
				Limit	0.5	0.2	1	0.5	0.5	3	0.1	0.1	0.005	0.1	0.1	0.005	0.1	0.1	0.1
Massive, Lithic-Rich, Polymict, Lapilli Tuff (WMVS)																			
GS-03-130A	3	352614	5263218		2.2	-	3	1.7	1.4	995	21.9	53.4	6.26	25.4	5.8	1.01	5.1	0.9	5.4
GS-03-130B	3	352612	5263210		2.1	-	1	1.1	0.8	936	14.1	36.7	4.45	18.1	4.4	0.77	4.2	0.8	4.8
GS-03-130C	3	352614	5263224		3.3	-	2	1.1	0.8	840	12.8	31.2	4.01	16.1	3.9	0.73	3.8	0.7	4.4
GS-03-130D	3	352614	5263220		2.5	-		3.1	0.5	811	1.0	2.1	0.24	1.1	0.3	0.06	0.3		0.3
GS-03-130E	3	352611	5263218		1.6	-		8.7	0.8	116	1.6	3.4	0.44	1.9	0.4		0.3		0.2
GS-03-130F	3	352611	5263213		1.7	-		2.4		588	0.6	1.2	0.15	0.7	0.2		0.2	-	0.3
GS-03-130G	3	352611	5263211		5.6	-		1.3	0.6	753	5.2	11.6	1.63	6.9	1.8	0.40	1.8	0.4	2.2
GS-03-130H	3	352612	5263214		6.1		2			1000	21.5	46.8	5.44	21.1	4.4	1.00	4.4	0.8	4.7
GS-03-130I	3	352610	5263215		5.4		2	1.1	0.7	1020	29.9	68.3	7.89	28.1	4.8	0.86	4.2	0.7	4.1

Table 3-24: cont'd

Sample Number	Unit	Easting	Northing	Element	Ho	Er	Tm	Yb	Lu	Hf	Ta	W	Tl	Pb	Bi	Th	U
				Method	ICP-MS	ICP-MS	ICP-MS	ICP-MS	ICP-MS	ICP-MS	ICP-MS	ICP-MS	ICP-MS	ICP-MS	ICP-MS	ICP-MS	ICP-MS
				Unit	ppm	ppm	ppm	ppm	ppm	ppm	ppm	ppm	ppm	ppm	ppm	ppm	ppm
				Limit	0.1	0.1	0.05	0.1	0.04	0.2	0.1	1	0.1	5	0.4	0.1	0.1
Massive, Lithic-Rich, Polymict, Lapilli Tuff (WMVS)																	
GS-03-130A	3	352614	5263218		1.2	3.9	0.59	3.8	0.62	5.4	0.6	4	1.3			4.3	1.4
GS-03-130B	3	352612	5263210		1.0	3.4	0.50	3.2	0.52	4.5	0.6	-	1.2			4.3	1.4
GS-03-130C	3	352614	5263224		1.0	3.3	0.50	3.2	0.51	4.6	0.6	1	1.1			4.4	1.3
GS-03-130D	3	352614	5263220			0.1	-			0.3	-	-	1.1	-		-	-
GS-03-130E	3	352611	5263218			0.1	-			-	-	-	0.2	-		
GS-03-130F	3	352611	5263213			0.2		0.2		0.4	-	-	0.9		-	0.2	-
GS-03-130G	3	352611	5263211		0.5	1.7	0.27	1.7	0.29	2.3	0.3	-	1.1			2.3	0.9
GS-03-130H	3	352612	5263214		1.0	3.4	0.50	3.3	0.52	4.5	0.6	-	0.9		-	4.4	1.6
GS-03-130I	3	352610	5263215		0.9	3.1	0.51	3.3	0.57	4.7	0.6		1.4			4.6	1.6

* samples with UTM's calculated from registered base map

Table 3-25: Major- and trace-element XRF data for Unit 3 (White Mountain Volcanic Suite).

Sample Number	Unit	Easting	Northing	Element	SiO2	TiO2	Al2O3	Fe2O3T	MnO	MgO	CaO	Na2O	K2O	P2O5	S	Cl	Cr	Ni	Sc
				Method	XRF	XRF	XRF	XRF	XRF	XRF	XRF	XRF	XRF	XRF	XRF	XRF	XRF	XRF	XRF
				Unit	wt%	wt%	wt%	wt%	wt%	wt%	wt%	wt%	wt%	wt%	ppm	ppm	ppm	ppm	ppm
				Limit	0.01	0.003	0.012	0.005	0.002	0.012	0.003	0.008	0.003	0.005	25	41	8	4	10
Massive, Lithic-Rich, Polymict, Lapilli Tuff (WMVS)																			
GS-03-130A	3	352614	5263218		77.39	0.18	14.77	1.22	0.04	0.84	0.13	2.76	4.37	0.02	53	51			-
GS-03-130B	3	352612	5263210		84.67	0.18	10.27	1.19	0.04	0.71	0.11	2.1	3.57	0.02	57				
GS-03-130C	3	352614	5263224		82.38	0.21	10.15	1.3	0.04	0.57	0.13	2.15	3.59	0.03	72	47	14		
GS-03-130G	3	352611	5263211		87.43	0.11	6.55	2.35	0.09	1.41	0.09	0.31	2.98	0.03	75	62	12	6	
GS-03-130H	3	352612	5263214		82.31	0.22	11.03	1.7	0.07	0.96	0.19	2.71	3.57	0.04	62	45	9	6	
GS-03-130I	3	352610	5263215		82.73	0.19	9.89	1.55	0.06	0.81	0.13	1.71	3.77	0.03	46			10	-

Table 3-25: cont'd

Sample Number	Unit	Easting	Northing	Element	V	Cu	Pb	Zn	As	Ba	Rb	Sr	Ga	Nb	Zr	Y	Ce	Th	U
				Method	XRF	XRF	XRF	XRF	XRF	XRF	XRF	XRF	XRF	XRF	XRF	XRF	XRF	XRF	XRF
				Unit	ppm	ppm	ppm	ppm	ppm	ppm	ppm	ppm	ppm	ppm	ppm	ppm	ppm	ppm	ppm
				Limit	7	4	5	3	15	26	0.9	1.5	3	0.9	1.4	0.9	45	4	5
Massive, Lithic-Rich, Polymict, Lapilli Tuff (WMVS)																			
GS-03-130A	3	352614	5263218		43	-	-	9		922	127.7	47.3	12	11.2	183.4	29.2	61	-	-
GS-03-130B	3	352612	5263210		24	-	-	6		861	88.1	44.3	8	10.1	143.1	23.1	-	-	-
GS-03-130C	3	352614	5263224		29			6		786	96.2	48.3	9	10	160.3	22.6		4	
GS-03-130G	3	352611	5263211		33	-		37		675	75.5	22	6	5.2	80.4	10			
GS-03-130H	3	352612	5263214		22	-	-	25	-	966	88.6	59.9	11	10.8	156	25.7	72	6	
GS-03-130I	3	352610	5263215		37		5	19	-	941	100.4	46.1	9	10.9	153.5	21.5	88	5	

* samples with UTM's calculated from registered base map

Table 3-26: Comparison of common elements contained within the ICP-MS and XRF datasets.

Sample Number	Cr	Ni	V	Pb	Zn	As	Ba	Rb	Sr	Ga	Nb	Zr	Y	Ce	Th	U
	ppm	ppm	ppm	ppm	ppm	ppm	ppm	ppm	ppm	ppm	ppm	ppm	ppm	ppm	ppm	ppm
ICP-MS Dection Limit	20	20	5	5	30	5	3	2	2	1	1	5	1	0.1	0.1	0.1
XRF Dection Limit	8	4	7	5	3	15	26	0.9	1.5	3	0.9	1.4	0.9	45	4	5
ICP-MS-130A	-	-	34.34	-	-	-	995.08	137.81	49.55	15.36	9.78	200.28	34.69	53.40	4.26	1.41
XRF-130A	-	-	43.00	-	9.00	-	922.0	127.70	47.30	12.00	11.2	183.40	29.20	61	-	-
% Diff			20.14				7.93	7.92	4.76	28.00	12.68	9.20	18.80	12.46		
ICP-MS-130B	-	-	24.14	-		-	936.44	98.08	47.64	9.53	8.43	154.27	29.35	36.68	4.25	1.35
XRF-130B	-	-	24.00	-	6.00	-	861.0	88.10	44.30	8.00	10.1	143.10	23.10	-	-	-
% Diff			0.58				8.76	11.33	7.54	19.13	16.53	7.81	27.06			
ICP-MS-130C	-	-	22.12				840.21	102.08	49.52	10.09	7.81	163.43	26.97	31.22	4.42	1.33
XRF-130C	14.00		29.00	-	6.00	-	786.0	96.20	48.30	9.00	10	160.30	22.60	-	4	-
% Diff			23.72				6.90	6.11	2.53	12.11	21.90	1.95	19.34			
ICP-MS-130G	-	-	26.62	-	87.41	-	753.31	84.56	23.29	7.94	3.89	84.36	14.89	11.58	2.28	0.91
XRF-130G	12.00	6.00	33.00	-	37.00	-	675.0	75.50	22.00	6.00	5.2	80.40	10.00	-	-	-
% Diff			19.33		136.24		11.60	12.00	5.86	32.33	25.19	4.93	48.90			
ICP-MS-130H	-	-	20.82		36.48	-	1000.00	88.77	59.17	11.08	7.51	146.51	28.91	46.85	4.36	1.61
XRF-130H	9.00	6.00	22.00	-	25.00	-	966.0	88.60	59.90	11.00	10.8	156.00	25.70	72	6	-
% Diff			5.36		45.92		3.52	0.19	1.22	0.73	30.46	6.08	12.49	34.93		
ICP-MS-130I	-	-	32.30	-	43.55	-	1020.00	109.14	47.71	10.54	8.20	162.97	26.81	68.32	4.59	1.65
XRF-130I	10.00	-	37.00	5	19.00	-	941.0	100.40	46.10	9.00	10.9	153.50	21.50	88	5	
Average % Diff	N/A	N/A	12.70	N/A	129.21	N/A	8.40	8.71	3.49	17.11	24.77	6.17	24.70	22.36	N/A	N/A

Table 3-27: Comparison of common elements contained within the ICP-ES and XRF datasets.

Sample Number	SiO2 %	Al2O3 %	Fe2O3 Total %	MgO %	CaO %	Na2O %	K2O %	TiO2 %	MnO %	P2O5 %	Cr ppm	Zr ppm	Ba ppm
ICP-ES Dection Limit	0.01	0.01	0.01	0.01	0.01	0.01	0.01	0.001	0.01	0.001	1	1	1
XRF Dection Limit	0.01	0.012	0.005	0.012	0.003	0.008	0.003	0.003	0.002	0.005	8	1.4	26
ICP-ES-130A	76.42	12.67	1.05	0.43	0.09	2.93	4.16	0.15	0.03	0.03	-	164.5	1019
XRF-130A	77.39	14.77	1.22	0.84	0.13	2.76	4.37	0.18	0.04	0.02	-	183.4	922
% Diff	1.26	14.25	13.78	49.15	33.13	6.33	4.84	17.28	26.29	32.23		10.30	10.51
ICP-ES-130B	81.32	8.84	1.04	0.33	0.08	2.08	3.51	0.14	0.02	0.02	-	128.3	940
XRF-130B	84.67	10.27	1.19	0.71	0.11	2.10	3.57	0.18	0.04	0.02	-	143.1	861
% Diff	3.96	13.89	12.88	53.57	28.99	0.82	1.58	19.50	38.84	3.26		10.37	9.15
ICP-ES-130C	81.30	9.47	1.08	0.30	0.10	2.24	3.70	0.18	0.02	0.03	-	143.9	912
XRF-130C	82.38	10.15	1.30	0.57	0.13	2.15	3.59	0.21	0.04	0.03	14	160.3	786
% Diff	1.31	6.67	17.21	47.38	25.61	4.01	3.15	12.89	39.75	3.34		10.21	16.07
ICP-ES-130G	85.62	5.33	2.07	0.67	0.05	0.30	2.93	0.09	0.07	0.03	-	72.7	752
XRF-130G	87.43	6.55	2.35	1.41	0.09	0.31	2.98	0.11	0.09	0.03	12	80.4	675
% Diff	2.07	18.59	12.08	52.28	46.62	2.02	1.56	21.63	22.39	0.35		9.54	11.41
ICP-ES-130H	78.77	10.04	1.45	0.46	0.14	2.65	3.71	0.18	0.05	0.03		135.2	1096
XRF-130H	82.31	11.03	1.70	0.96	0.19	2.71	3.57	0.22	0.07	0.04	9	156.0	966
% Diff	4.30	8.95	14.93	52.07	25.40	2.06	3.85	18.53	22.97	15.71		13.30	13.51
ICP-ES-130I	81.49	8.99	1.33	0.44	0.09	1.71	3.92	0.17	0.04	0.03		135.1	1040
XRF-130I	82.73	9.89	1.55	0.81	0.13	1.71	3.77	0.19	0.06	0.03	10	153.5	941
Average % Diff	1.50	9.15	14.08	46.18	28.58	0.08	3.91	11.54	25.45	14.85		11.97	10.54

Table 3-28: Comparison of unaltered Unit 3 with samples collected at the roadside outcrop.

Sample Number	Unit	Easting	Northing	Element	SiO2	TiO2	Al2O3	Fe2O3	FeO	MnO	MgO	CaO	Na2O	K2O	P2O5	LOI	Zr	Ba
				Method Unit Limit	ICP-ES % 0.01	ICP-ES % 0.001	ICP-ES % 0.01	ICP-ES % 0.01	ICP-ES %	ICP-ES % 0.010	ICP-ES % 0.01	ICP-ES % 0.01	ICP-ES % 0.01	ICP-ES % 0.01	ICP-ES % 0.001	ICP-ES %	ICP-ES ppm 1	ICP-ES ppm 0.1
Massive, Lithic-Rich, Polymict, Lapilli Tuff (WMVS)																		
GS-02-085	3	352682	5263144		78.80	0.229	11.42	1.11	0.26	0.026	0.30	0.16	3.26	3.53	0.04	0.71	162	875
GS-03-130A	3	352614	5263218		76.42	0.149	12.67	0.53	0.47	0.029	0.43	0.09	2.93	4.16	0.03	1.10	165	1019
% Diff					3.02	34.86	10.93	52.40	79.44	13.95	44.51	44.07	9.89	17.82	40.94	55.29	1.57	16.50
GS-02-085	3	352682	5263144		78.80	0.229	11.42	1.11	0.26	0.026	0.30	0.16	3.26	3.53	0.04	0.71	162	875
GS-03-130I	3	352610	5263215		81.49	0.168	8.99	1.08	0.23	0.045	0.44	0.09	1.71	3.92	0.03	0.77	135	1040
% Diff					3.42	26.47	21.30	3.30	12.19	72.88	47.50	40.26	47.45	10.99	42.96	8.58	16.57	18.93

187

CHAPTER 4:

GEOCHRONOLOGY

4.1 INTRODUCTION

The geochronology presented herein combines new data generated during this study with previously unpublished geochronology on the MVS by Dr. John Ketchum on contract to the Geological Survey. The author collected a total of ten new samples for geochronological study, and from these samples, six well-defined U-Pb ages were established. In addition, the author collected and separated muscovite and adularia for ^{40}Ar-^{39}Ar work completed by Dr. M. Villeneuve (GSC), which resulted in one well defined ^{40}Ar-^{39}Ar age. One sample of aphanitic flow-banded rhyolite from the Farmer's Field region did not yield any zircon, and two of the three samples collected for ^{40}Ar-^{39}Ar dating produced disturbed patterns or anomalously young ages (written communication, M. Villeneuve, 2005).

Ketchum's previous U-Pb work established the age of the rhyolitic sequence hosting the advanced argillic alteration at the Oval Pit mine at 584 ± 2 Ma (J. Ketchum, 1998). More recent work by Dr. Greg Dunning has further refined this age, which is now defined at 584 ±1 Ma at a 95% confidence interval (C.I.). Recognition of the relatively young age of the hydrothermal alteration excluded the nearby HIS dated at 620 Ma (Krogh *et al.,* 1988; O'Brien *et al.,* 2001, Sparkes *et al.,* 2002) as a possible heat source for this event. Initial hypotheses identified rocks of the WHIS as a possible younger event related to the hydrothermal alteration of the MVS (O'Brien *et al.,* 2001). This was mainly

based on intrusive contacts with what was thought to be part of the 584 Ma volcanic sequence and the close spatial association between the WHIS and the advanced argillic alteration. It was also the aim of this study to identify possible age breaks within the previously unseparated MVS, which was known to contain older ash-flow tuff, dated at 616 ± 2 Ma (G. Dunning, unpublished data).

During this study, three separate samples of the WHIS were collected in order to determine the absolute age of the magmatism. A sample of silica–sericite–chlorite altered granite from the WHIS was sampled along the CBS By-Pass roadcut during previous work, however complications within the dataset prohibited an accurate age determination (J. Ketchum, 1998). Cathodoluminescence imaging of zircons and reexamination of the dataset was completed by the author as part of this study, with the aim of resolving the age of this unit.

A second aim of this study was to bracket the age of the high-sulphidation alteration. A pumiceous ash-flow tuff at the base of the sedimentary sequence, which unconformably overlies the rhyolitic rocks in the Oval Pit mine was sampled in order to establish a minimum age for the alteration. This ash-flow tuff also establishes the maximum age for the overlying sedimentary rocks of the WHPC.

The third aim of this study was to identify a maximum age limit for the development of low-sulphidation veins, which is currently unconstrained. Until recently low-sulphidation veins were not observed within rocks suitable for U-Pb geochronology. Recent construction work in the Manuels area uncovered stockwork style low-sulphidation veins hosted within a dark purple crystal-rich ash-flow tuff. Determination

of age constraints for the low-sulphidation system would allow comparison with the known ages of the high-sulphidation system. This dark purple crystal-rich ash-flow tuff was sampled to better constrain the maximum age limit of the low-sulphidation system. The younger limit for this system is provided by the unconformably overlying Paleozoic cover containing fossils of Lower Cambrian age (O'Brien, 2002).

The sedimentary rocks exposed in the eastern portion of the map area are correlated with the WHPC, which unconformably overlies the ca. 584 Ma felsic volcanic rocks in the area of the Oval Pit mine. In eastern portions of the map region the upper WHPC is intruded by feldspar porphyry. Field relationships identify this porphyry as, relatively, the youngest magmatic event exposed within the map area. The porphyry unit becomes brecciated upon intrusion into the sedimentary succession, suggesting the sediments were unconsolidated at the time of intrusion. Dating of this porphyry provides the age of the sedimentary host rock as well as the age for the youngest felsic magmatism within the region.

For a brief description of sample processing refer to Chapter 1 (a more detailed description is available in Appendix A). In the following discussion, all data points have 2σ uncertainties and the ages are cited at the 95% confidence interval. Age calculations of concordant points are weighted averages of the $^{206}Pb/^{238}U$ ages, while ages from discordant data points are calculated as the weighted averages of the $^{207}Pb/^{235}U$ ages. The letter preceding the name of the geochron samples is included for ease of reference to the corresponding sample in the data table and the associated concordia diagram.

4.2 GEOCHRONOLOGICAL DATA

The following discussion of the geochronology incorporates data from previous work and the current study. In the following discussion samples A, D, F and G are compiled from previous work and samples B, C, E, H, I and J were collected during the present study. All of the data is presented here to provide an accurate and detailed description of the geochronology within the eastern Avalon high-alumina belt (EAHB; Table 4.1). Samples containing "GS" in the beginning of the sample number represent samples collected by the author and other sample names not containing "GS" represent data compiled from previous work. Figure 4-1 contains sample locations and the absolute ages of the samples discussed below. Letters preceding unit names correspond with labeling within the data table and related concordia diagram.

4.2.1 Unit 5: Holyrood Intrusive Suite (HIS)

4.2.1.1 (A) Pink–White–Green Granite (PWG)

A sample of PWG Granite from the Holyrood Intrusive Suite was collected and analyzed during previous work by G.R. Dunning and S.J. O'Brien (see O'Brien *et al.,* 2001), which was collected outside of the current study area, approximately 5.5 km southwest of the Oval Pit mine (not shown in Figure 4-1). The sample displays alteration that is characteristic of the eastern margin of the Holyrood intrusion and is also similar to exposures within the field area. The dated sample consists of medium-grained, quartz-phyric, biotite-hornblende granite with extensive epidote and sericite alteration developed

Table 4-1: U–Pb zircon data for rocks of the eastern Avalon high-alumina belt.

Fraction	Weight (mg)	U (ppm)	Pb rad (ppm)	Total Common Pb (pg)	$^{206}Pb/^{204}Pb$	$^{208}Pb/^{206}Pb$	$^{206}Pb/^{238}U$	±	$^{207}Pb/^{235}U$	±	$^{207}Pb/^{206}Pb$	±	$^{206}Pb/^{238}U$	$^{207}Pb/^{235}U$	$^{207}Pb/^{206}Pb$
(A) Unit 5; PWG Granite, HIS (sample OBOD99GC-4) UTM: 350510E 5255190N															
Z1 10 lrg best	0.021	259	27.3	15	2353	0.1591	0.10036	22	0.8378	18	0.06055	6	617	618	623
Z2 sml best	0.021	313	33.1	17	2446	0.1627	0.10074	20	0.8408	18	0.06054	8	619	620	623
Z3 clr euh prms	0.034	302	31.9	2.4	26675	0.1628	0.10029	22	0.8366	18	0.06050	6	616	617	622
(B) Unit 6; Monzonite, WHIS (sample GS-GC-09) UTM: 351912E 5262445N															
Z1 1 lrg clr prms	0.003	99	11.6	2.7	717	0.2995	0.09965	48	0.8317	70	0.06053	46	612	615	623
Z2 1 lrg clr prms	0.003	61	6.6	2.8	415	0.2522	0.09649	68	0.8060	58	0.06059	28	594	600	625
Z3 2 clr prms abr	0.004	66	7.4	3.0	559	0.2599	0.09854	44	0.8232	42	0.06059	22	606	610	625
Z4 2 clr euh prms	0.003	193	20.8	1.8	2022	0.2362	0.09676	54	0.8076	32	0.06053	26	595	601	622
Z5 2 clr euh prms	0.003	186	20.2	3.2	1120	0.2001	0.09984	40	0.8333	32	0.06053	16	613	615	623
(C) Unit 7; Medium- to Coarse-grained Equigranular, Pyritic Granite, WHIS (sample GS-GC-05) UTM: 352730E 5260152N															
Z1 2 lrg clr euh	0.005	21	2.2	2.6	269	0.1676	0.10085	78	0.8453	88	0.06079	54	619	622	632
Z2 clr euh	0.005	30	3.3	1.2	817	0.2278	0.10082	96	0.8433	68	0.06067	36	619	621	627
Z3 clr euh	0.003	29	2.3	1.7	256	0.1607	0.07658	154	0.6523	82	0.06178	102	476	510	666
(D) Unit 7; Medium- to Coarse-grained Equigranular, Silica-Sericite-Chlorite Altered Granite, WHIS (sample SJOB97-GC-3) UTM: 353048E 5263751N															
Z1 lrg anh	0.039	184	19.6	30	1511	0.2006	0.09843	50	0.8172	38	0.06022	16	605	607	611
Z2 sml clr best prms	0.023	217	22.8	12	2549	0.1675	0.09954	34	0.8303	26	0.06050	14	612	614	621
Z3 clr anh	0.021	216	22.9	44	655	0.1892	0.09886	44	0.8232	36	0.06040	16	608	610	618
Z4 clr anh	0.022	232	24.7	8.9	3584	0.1905	0.09888	32	0.8218	24	0.06028	10	608	609	613
Z5 41 clr anh	0.036	254	27.0	69	845	0.1850	0.09896	40	0.8251	36	0.06047	14	608	611	620
Z6 euh clr sml prms	0.015	265	28.0	17	1490	0.1738	0.09960	40	0.8277	30	0.06027	18	612	612	613
Z7 6 clr euh	0.008	146	16.2	4.3	1679	0.2809	0.09645	62	0.7965	42	0.05989	26	594	595	600
(E) Unit 8; Quartz-Feldspar Porphyry, WHIS (sample GS-GC-02) UTM: 351945E 5262660N															
Z1 1 lrg clr euh	0.003	168	18.0	3.5	913	0.1886	0.09948	70	0.8317	50	0.06064	28	611	615	626
Z2 1 lrg clr euh	0.003	207	22.5	1.4	2755	0.2461	0.09652	46	0.8075	32	0.06068	20	594	601	628
Z3 2 clr euh abr	0.004	200	20.4	1.7	2874	0.1739	0.09572	44	0.7980	32	0.06046	22	589	596	620
Z4 4 clr euh prms	0.006	204	21.7	1.8	4255	0.1825	0.09942	52	0.8311	42	0.06063	14	611	614	626
Z5 2 clr euh prms	0.003	131	14.3	1.0	2556	0.2471	0.09696	56	0.9116	44	0.06071	22	597	603	629
Z6 2 clr euh prms	0.003	360	37.8	1.1	6251	0.1729	0.09899	44	0.8259	34	0.06051	14	608	611	622

*Corrected Atomic Ratios

Table 4-1: Continued

Fraction	Weight (mg)	U (ppm)	Pb rad (ppm)	Total Common Pb (pg)	206Pb/204Pb	208Pb/206Pb	206Pb/238U	±	207Pb/235U	±	207Pb/206Pb	±	206Pb/238U	207Pb/235U	207Pb/206Pb
(F) Unit 4; Welded, Fiamme-bearing Ash-Flow Tuff, WMVS (sample 99GC-5) UTM: 353270E 5263850N															
Z1 5 tiny frags	0.002	121	13.3	15	118	0.2166	0.10329	58	0.8402	116	0.06076	74	616	619	631
Z2 lrg prms	0.010	93	10.7	54	127	0.2649	0.10021	52	0.8333	74	0.06031	44	616	615	615
(G) Unit 9; Aphanitic Flow-Banded Rhyolite (Farmers Field Rhyolite), MVS (sample SJOB97-142) UTM: 352974E 5260702N															
Z1 16 clr euh prms	0.042	91	10.6	56	425	0.3663	0.09481	42	0.7814	48	0.05978	26	584	586	596
Z2 16 clr euh prms	0.052	75	8.6	99	251	0.3508	0.09482	36	0.7824	52	0.05985	30	584	587	598
Z3 6 clr coarse euh	0.018	78	8.8	4.0	2032	0.3368	0.09446	52	0.7722	42	0.05929	24	582	581	578
Z1 24 clr euh prms	0.040	126	14.1	26	1192	0.3065	0.09478	36	0.7788	32	0.05959	16	584	585	589
Z2 23 clr euh prms	0.039	122	14.2	25	1165	0.3571	0.09507	52	0.7809	42	0.05957	20	585	586	588
(H) Unit 13; Dark Purple, Crystal-bearing, Ash-flow Tuff, MVS (sample GS-GC-01) UTM: 352985E 5264488N															
Z1 2 lrg clr euh	0.005	63	6.1	2.8	660	0.1699	0.09106	60	0.7409	58	0.05902	42	562	563	568
Z2 2 sml clr euh	0.004	64	8.6	14	169	0.1057	0.13231	72	1.2364	142	0.06778	68	801	817	862
Z3 4 best sml clr	0.006	54	5.8	1.2	1667	0.2200	0.09788	40	0.8129	34	0.06024	16	602	604	612
Z4 3 sml clr	0.004	34	3.7	1.2	752	0.2004	0.10085	70	0.8457	62	0.06082	30	619	622	633
Z5 1 clr lrg euh	0.002	26	3.1	3.7	103	0.4135	0.09470	90	0.8045	482	0.06161	340	583	599	661
Z6 1 clr euh	0.002	22	2.6	13	38	0.4326	0.09456	134	0.7783	1216	0.05970	864	582	585	593
Z7 1 clr euh prm	0.002	32	3.7	3.9	113	0.4025	0.09339	194	0.7787	364	0.06048	252	576	585	621
(I) Unit 19a; Pumiceous Ash-flow Tuff, WHPC (sample GS-GC-03) UTM: 352850E 5260758N															
Z1 1 lrg clr euh	0.003	106	10.8	2.0	994	0.1597	0.09741	46	0.8108	42	0.06037	20	599	603	617
Z2 1 clr euh	0.003	85	9.0	2.1	764	0.2186	0.09643	48	0.7978	42	0.06001	18	593	596	604
Z3 1 clr euh	0.003	229	23.9	16	284	0.1838	0.09752	62	0.8183	94	0.06085	60	600	607	634
Z4 8 clr equ facet prms	0.015	31	3.5	3.8	765	0.2997	0.09523	52	0.7818	42	0.05954	24	586	586	587
Z5 10 clr equ facet	0.020	15	1.7	2.3	811	0.3065	0.09455	50	0.7767	46	0.05958	22	582	584	588
Z6 10 sml equ prms	0.010	37	4.0	2.1	1061	0.2632	0.09435	46	0.7779	52	0.05980	30	581	584	596
Z7 16 sml equ clr euh	0.016	35	3.8	1.7	1974	0.2622	0.09440	54	0.7778	38	0.05976	28	582	584	595
Z8 14 clr euh equ	0.014	32	3.4	1.6	1618	0.2594	0.09290	48	0.7690	46	0.06003	22	573	579	605
(J) Unit 22; Fowlers Road Porphyry, WHPC (sample GS-GC-06) UTM: 355311E 5263097N															
Z1 4 sml clr euh	0.008	69	7.6	9.1	369	0.3358	0.09238	68	0.7581	52	0.05952	32	570	573	586
Z2 4 clr euh prms	0.006	81	9.0	2.7	1091	0.3187	0.09307	46	0.7622	28	0.05939	28	574	575	582
Z3 2 lrg clr euh	0.004	48	5.4	2.0	583	0.3377	0.09398	54	0.7716	52	0.05955	32	579	581	587
Z5 clr euh prms	0.010	62	6.8	7.9	454	0.3829	0.08904	32	0.7363	44	0.05997	30	550	560	603
Z6 clr euh	0.011	174	18.7	7.3	1389	0.3511	0.08829	44	0.7240	40	0.05947	28	545	553	584
Z7 clr euh	0.020	31	3.4	12	310	0.3093	0.09276	42	0.7622	76	0.05959	52	572	575	589

Note: Z= zircon; clr=clear; lrg=large; sml=small; euh=euhedral; anh=anhedral; prms=prisms; prm=prism; frags=fragments; equ=equant; UTM=Universal Transverse Mercator Projection, NAD 27, Zone 22, NTS 1N/07 and 1N/10. All grains for all analyses were strongly abraded (cf. Krogh, 1982)

*Corrected for fraction, spike, laboratory blank of 1-3pg of common lead and initial common lead at the age of the sample calculated from the model of Stacey and Kramers (1975) and 1pg U blank. Two sigma uncertainties calculated with an error propagation program are reported after the ratios and refer to the final digits.
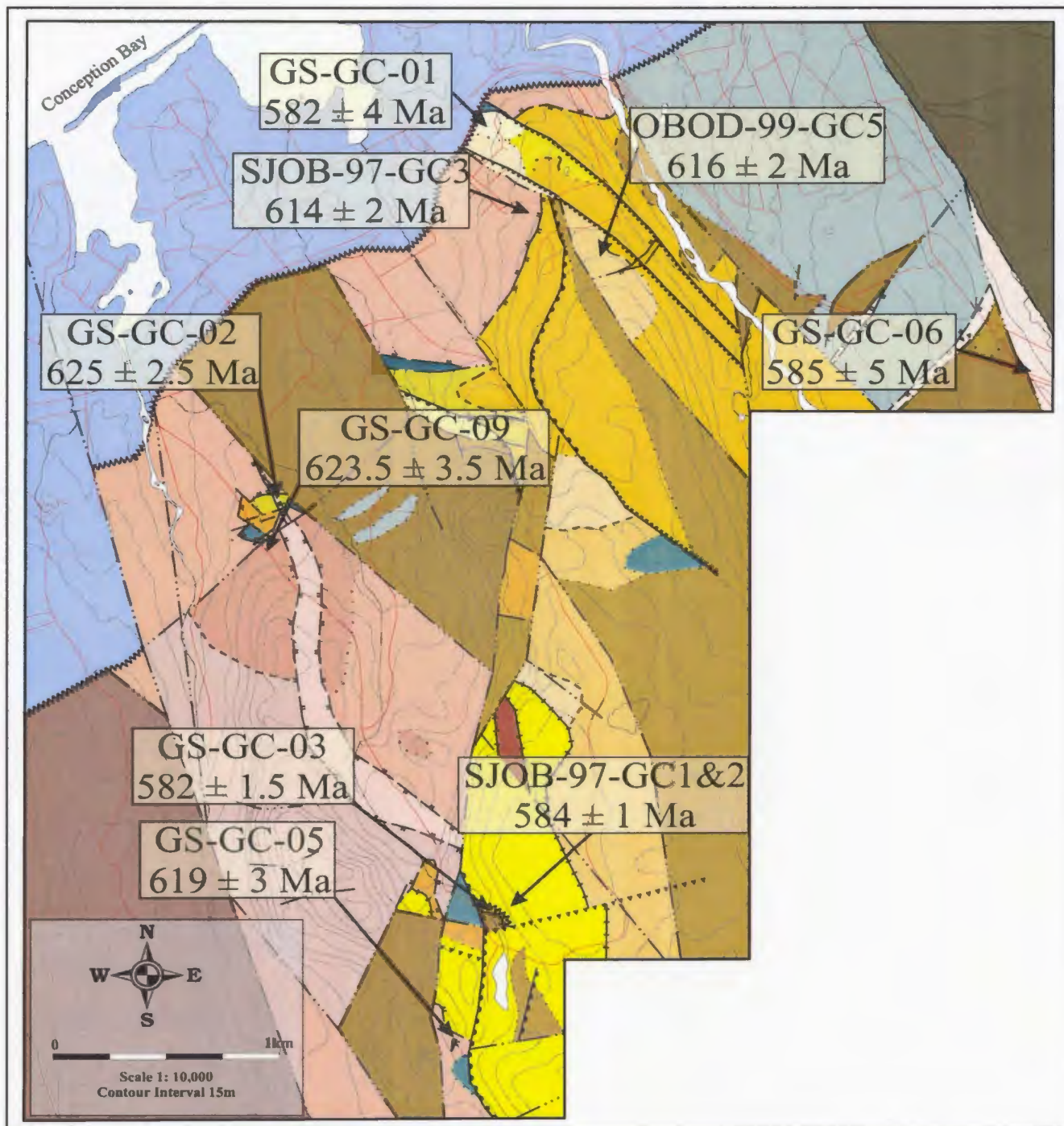
Figure 4-1: Simplified version of Map 1 showing the locations of dated samples and corresponding U-Pb zircon ages.

194

within the plagioclase. This granite is included as a representative of the regional scale HIS and is the closest dated sample to the current study area.

Three multiple-grain zircon fractions of abraded, clear, euhedral prisms were analyzed from this sample (Dunning, unpublished data). These fractions produced three points that are between 0.7% and 1.1% discordant. The weighted average of the $^{207}Pb/^{206}Pb$ ages of the three analyses is 622.5 ± 1.3 Ma (95% C.I; MSWD = 0.75; Figure 4-2).

This age is similar to other published ages of the HIS such as the 622 ± 2 Ma Butlers Pond porphyry (Sparks, B.A., *et al.,* 2002) and the 620 ± 2 Ma age from the central portion of the HIS (Krogh *et al.*, 1988). These ages represent the main period of magmatism of the HIS, which now dominates the central portion of the Holyrood Horst.

4.2.2 White Hills Intrusive Suite (WHIS)

4.2.2.1 (B) Unit 6: Monzonite

The inferred oldest unit within WHIS is Unit 6 (Chapter 3). This unit was sampled in the vicinity of Minerals Road Intersection (sample GS-GC-09; Figure 4-1). The dated sample consists of medium- to coarse-grained plagioclase and finer-grained chlorite, quartz and minor K-feldspar. When the sample was collected, care was taken as not to include any of the fine-grained dioritic xenoliths that are common throughout the unit.

This sample yielded abundant clear, euhedral prisms with length/width ratios approximately 3:1. A total of five analyses of the best abraded, euhedral prisms define a
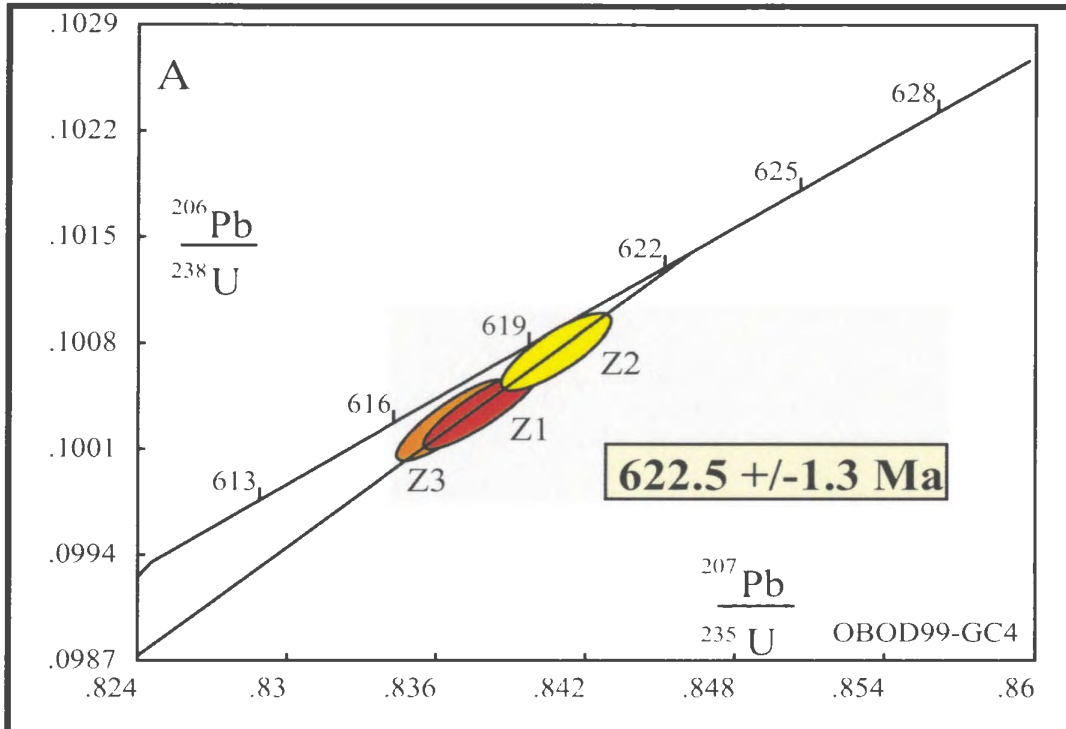
Figure 4-2: Concordia diagram for the PWG granite from the Holyrood Intrusive Suite (G.Dunning, unpublished data).
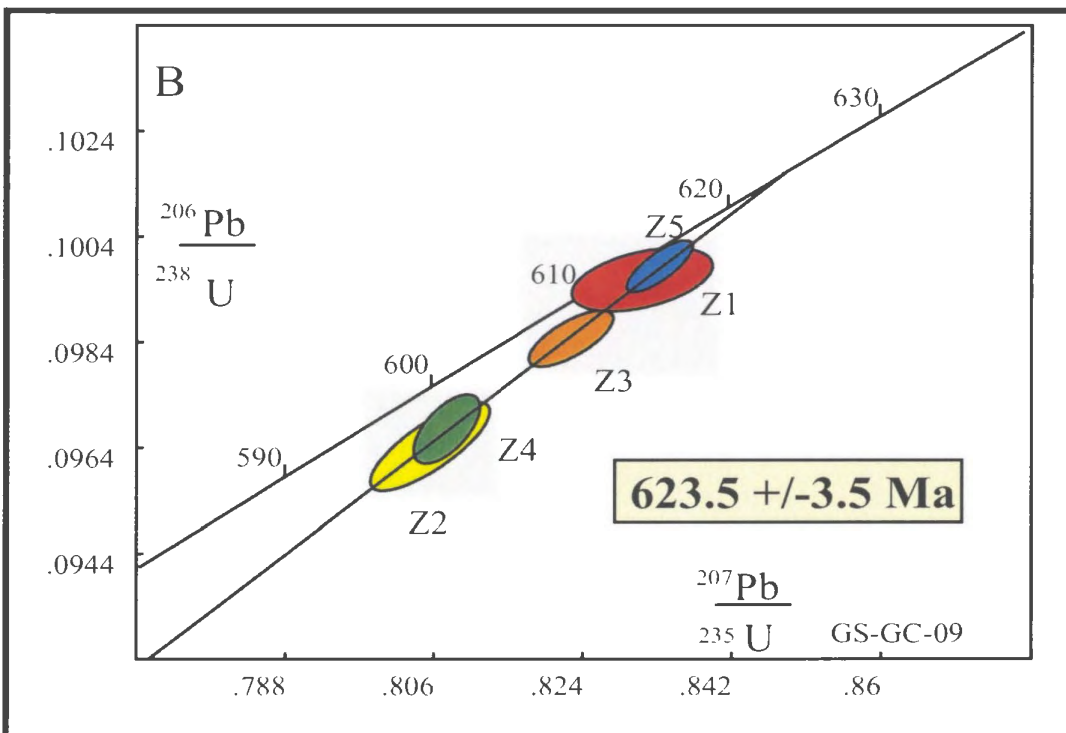
Figure 4-3: Concordia diagram for the monzonite from the White Hills Intrusive Suite.

line (99.1% probability of fit) with an upper intercept of 623.6 Ma. The five analyses are between 1.7 and 5.1% discordant along the line (Z5 and Z2, respectively; Figure 4-3). The weighted average of the $^{207}Pb/^{206}Pb$ ages provide an age of 623.5 ± 3.5 Ma (95% C.I.; MSWD 0.08).

4.2.2.2 (C) Unit 7: Medium- to Coarse-grained, Equigranular, Pyritic Granite

The second unit dated from the WHIS is pyritic granite located in the region of Mine Hill, immediately west of the Mine Hill Shear Zone (MHSZ; sample GS-GC-05). This granite was sampled because it contained a large (>8m diameter) raft of fine-grained silica–sericite altered felsic volcanic rock and therefore was initially thought to represent a younger intrusive event.

The pyritic granite yielded abundant clear, stubby, euhedral prisms, some of which contained tiny inclusions and moderate fracturing. Two multiple grain analyses of the best euhedral abraded grains produced concordant points, Z1 and Z2 respectively (Figure 4-4). The weighted average of the $^{206}Pb/^{238}U$ ages for the two analyses gives an age of 619 ± 3 Ma (95% C.I.).

4.2.2.3 (D) Unit 7: Medium- to Coarse-grained, Equigranular, Silica–Sericite–Chlorite Altered Granite

The silica–sericite–chlorite altered granite was initially collected during previous work by S.J. O'Brien and B. Dubé, however scattered data points complicated an age determination (see introduction; also Ketchum, 1998). Zircon separates from the sample were reexamined by the author during the current study. Fractions of euhedral grains
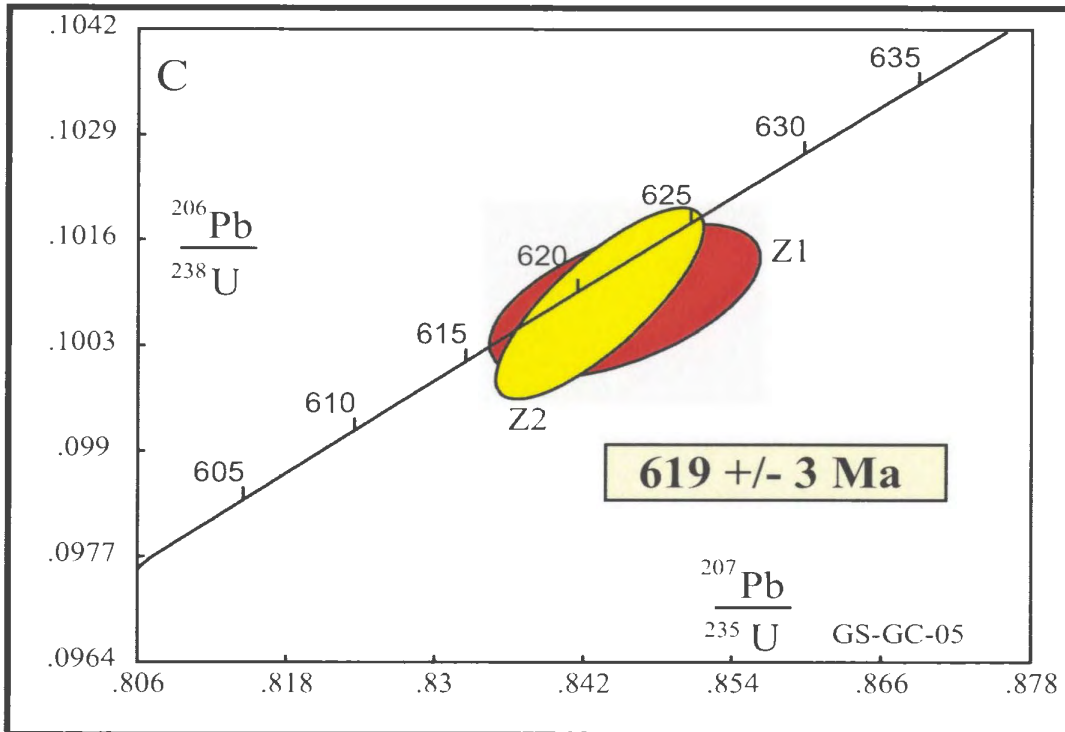
Figure 4-4: Concordia diagram for pyritic granite from the White Hills Intrusive Suite.
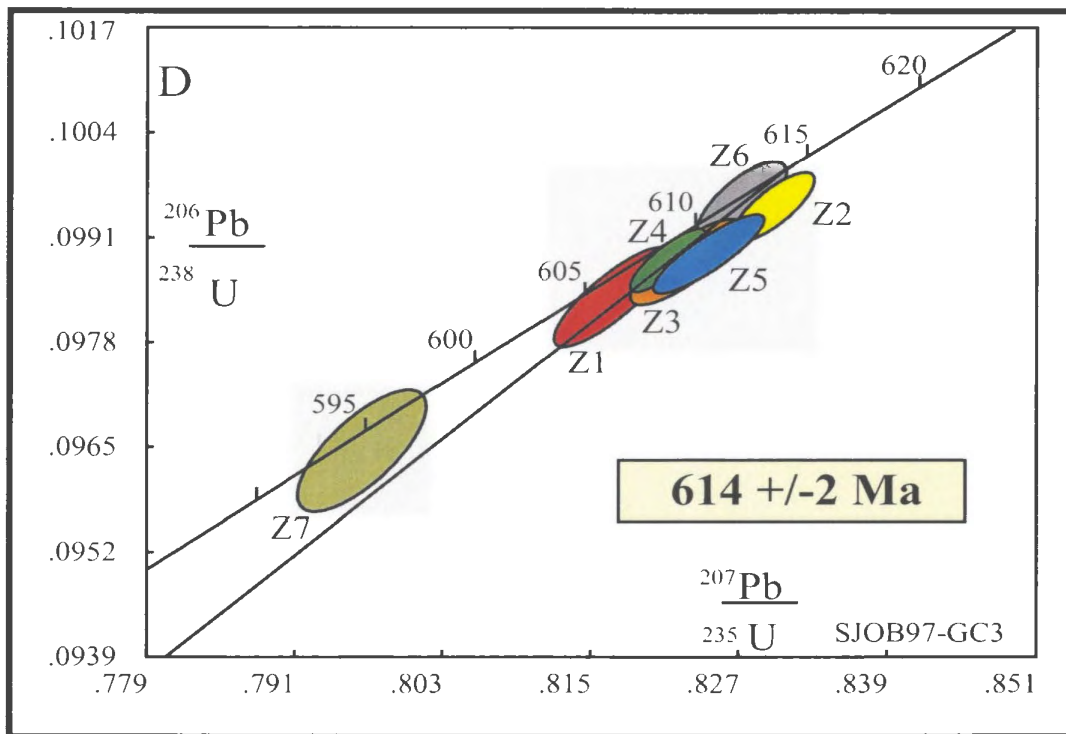
Figure 4-5: Concordia diagram for the silica-sericite-chlorite altered granite from the White Hills Intrusive Suite.

resembling the description of zircons included in previous analyses were selected for cathodoluminescence imaging. Images from these grains revealed relic cores within some of the euhedral zircons (Plate 4-1 and 4-2). Although this granite is geochemically similar to other granites within the WHIS, no other indication of inheritance was identified within this suite.

In total, seven analyses were carried out on zircon fractions from the silica–sericite–chlorite altered granite. This sample yielded abundant euhedral prisms, containing minor cracks and inclusions and length/width ratios approximately 2:1. The predominant portion of the data produced a cluster of points around 610 Ma, with one outlier at 595 Ma (Figure 4-5). All seven analyses consisted of multiple, euhedral, abraded grains and produced points between 0.3 and 2.1% discordant (Z6 and Z5, respectively). The ^{207}Pb/^{206}Pb ages for the five data points clustered around 610 Ma are: 1) Z1= 611.4 ± 5 Ma, 2) Z3= 617.8 ± 5 Ma, 3) Z4= 613.5 ±3 Ma, 4) Z5= 620.4 ± 4.5 Ma, 5) Z6= 613.4 ± 6 Ma. Z2 is not included as it is displaced to the right indicating possible inheritance. Analysis Z7, which has a ^{207}Pb/^{206}Pb age of 599.6 ± 9 Ma, is 1.05% discordant and is interpreted to have undergone Pb-loss. The weighted average of the ^{207}Pb/^{206}Pb ages for Z1, Z3, Z4, Z5 and Z6 gives an age of 615.5 ± 4 Ma at the 95% confidence interval (MSWD = 2.0; probability of fit = 0.089). The weighted average of the ^{207}Pb/^{206}Pb ages for Z1, Z3, Z4 and Z6 gives an age of 614 ± 2 Ma (95% C.I.; MSWD = 0.92; probability of fit = 0.43). The average of Z1, Z3, Z4 and Z6 gives a much more acceptable MSWD and since Z5 is slightly displaced to the right indicating possible

Plate 4-1: Transmitted light image of zircons from the silica-sericite-chlorite altered granite. Grains are less than 10 microns in length.
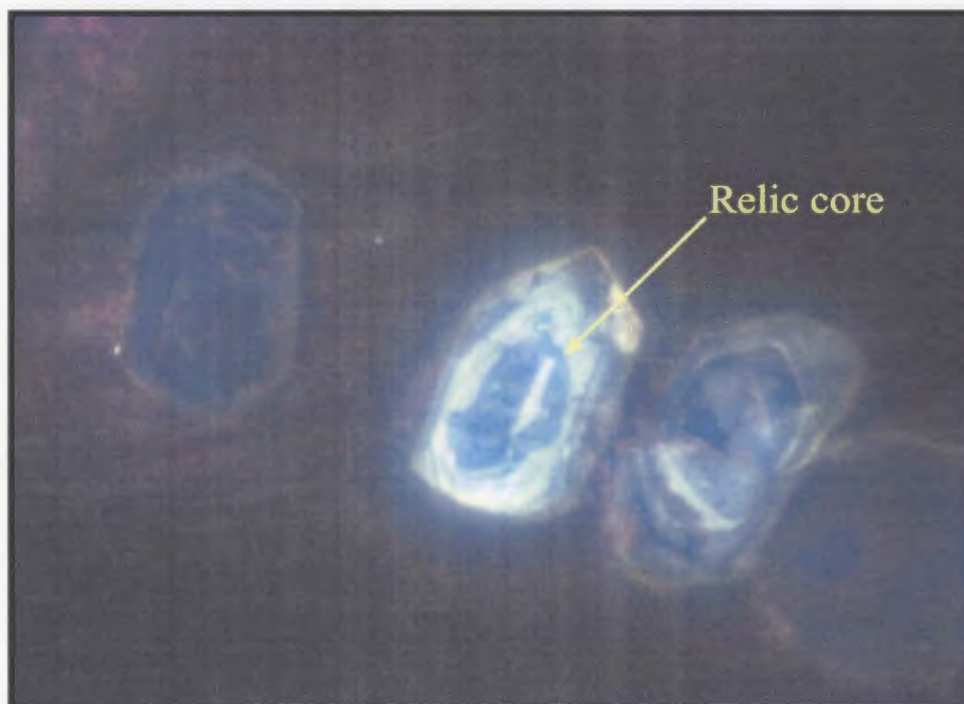
Plate 4-2: Cathodoluminescence image of zircons from the silica-sericite-chlorite altered granite displaying relic cores. Grains are less than 10 microns in length.

inheritance the age of 614 ± 2 Ma is interpreted as the absolute age for the silica–sericite–chlorite altered granite.

4.2.2.4 (E) Unit 8: Quartz–Feldspar Porphyry

The fourth sample collected for dating from WHIS is of quartz–feldspar porphyry that is inferred to be the youngest unit of the WHIS in the study area. This unit contains 2-4mm pale white plagioclase and pale pink K-feldspar crystals along with 3-4mm sub-rounded quartz crystals within a light purple aphanitic groundmass. The groundmass commonly contains fine-grained, dark green chlorite and typically consists of 40 to 60% phenocrysts. At the sample site near Minerals Road Intersection, this unit is intrusive into a volcaniclastic unit that contains fragments of earlier granitic and felsic porphyritic rocks. This volcaniclastic rock is also host to banded, colloform-crustiform, chalcedonic silica ± adularia low-sulphidation veins at the Steep Nap prospect.

The dated sample yielded abundant, predominantly clear, euhedral zircons, with a second more magnetic fraction of fractured, semi-clear prisms. Six analyses were carried out on clear, euhedral, abraded zircons with length/width ratios approximately 3:1. Two analyses consisted of single grains (Z1 and Z2), three analyses consisted of two clear, euhedral, abraded grains (Z3, Z5 and Z6) and one analysis consisted of four clear, euhedral, abraded grains (Z4). The resultant six analyses define a linear trend with analysis Z1 being closest to concordia and analysis Z3 being most discordant (Figure 4-6). The age of the porphyry is 625 ± 2.5 Ma, which is the weighted average of the $^{207}Pb/^{206}Pb$ ages of all six analyses (95% C.I.; MSWD = 1.0).
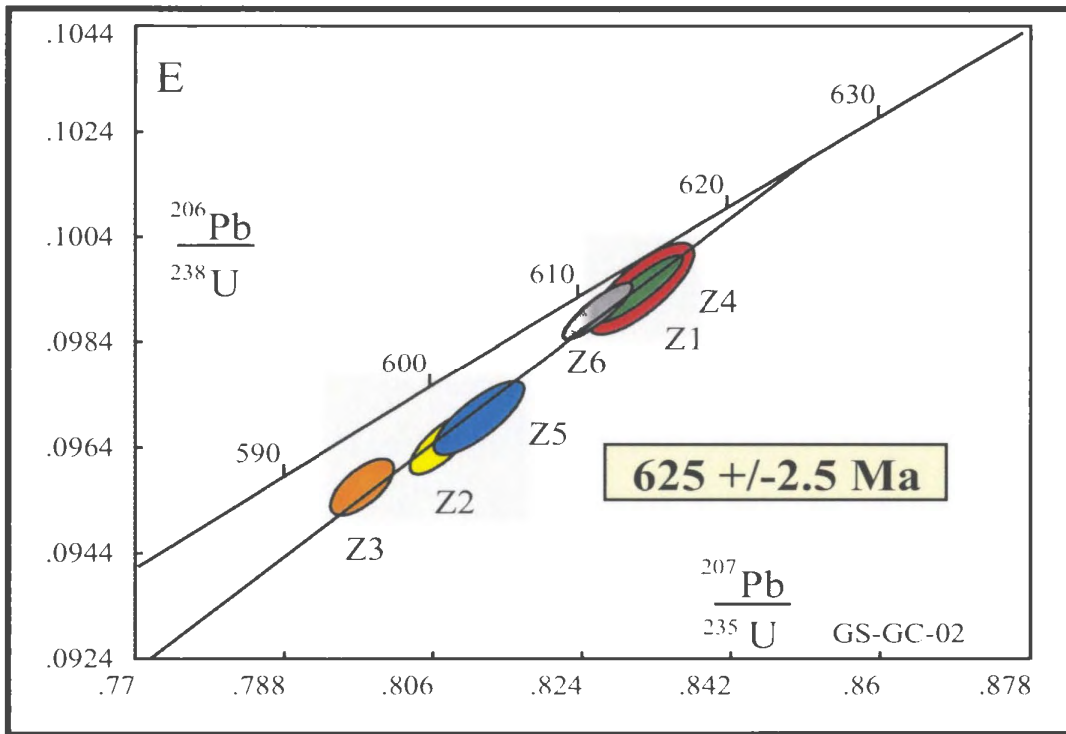
Figure 4-6: Concordia diagram for the quartz-feldspar porphyry from the White Hills Intrusive Suite.
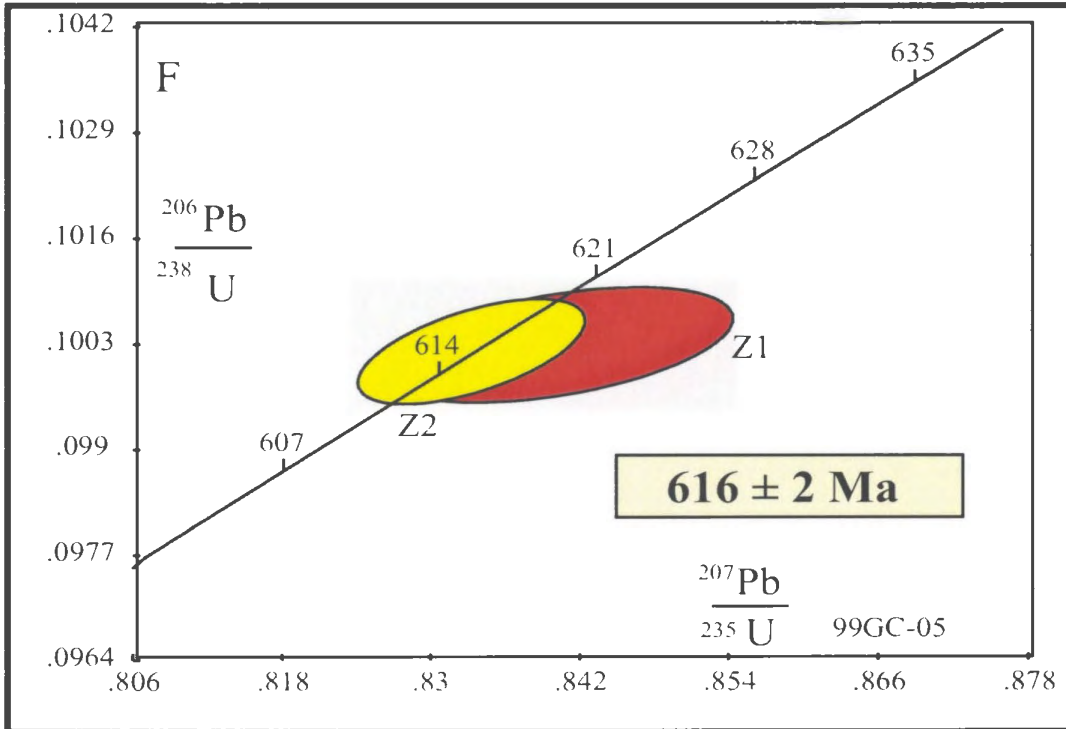
Figure 4-7: Concordia diagram for the welded ash-flow tuff from the White Mountain Volcanic Suite.

4.2.3 White Mountain Volcanic Suite (WMVS)

4.2.3.1 (F) Unit 4: Welded, Fiamme-bearing Ash-Flow Tuff

The oldest dated volcanic unit within the study area, as determined from previous work (Dunning, unpublished data), is a welded ash-flow tuff with well-developed eutaxitic foliation. This unit (Unit 4) is located in the north-central portion of the map area and is in faulted contact with adjacent units. The ash-flow tuff may represent the eastern equivalent of the Hawk Hills Tuff (O'Brien *et al.*, 2001), which is intruded by the HIS along the western and southern margins of the Holyrood Horst.

Two multiple grain fractions were analyzed from this sample; Z1 consisted of tiny abraded fragments and Z2 contained large abraded prisms. The two analyses produced concordant points at 616 Ma, analyses Z2 and Z1 respectively (Figure 4-7). The weighted average of the $^{206}Pb/^{238}U$ ages gives an age of 616 ± 2 Ma (95% C.I.).

4.2.4 Manuels Volcanic Suite (MVS)

4.2.4.1 (G) Unit 9: Aphanitic Flow-Banded Rhyolite and Ash-flow Tuff (Farmers Field Rhyolite)

These two samples of the MVS were collected by S.J. O'Brien and B. Dubé, and dated by J. Ketchum (J. Ketchum, 1998; see O'Brien *et al.*, 2001). The two samples are of the rhyolitic succession hosting the Oval Pit mine (pyrophyllite ± diaspore deposit) and were collected at the core of the advanced argillic alteration from the open pit. The first sample was collected from a zone of pyrophyllite–diaspore alteration (sample

SJOB97-GC-1) and the second is representative of low-strain and less-altered material in which relic flow banding and pumice fragments are well preserved (sample SJOBGC-97-2). Analyses Z1, Z2, Z1-2 and Z2-2 were carried out by J. Ketchum; a more recent analysis of SJOB97-GC-1 was conducted by G. R. Dunning in 2002 (Z3).

Sample SJOB97-GC-1 contained abundant small to large clear, euhedral prisms with minor cracks and inclusions. Three multiple-grain zircon fractions were analyzed for sample SJOB97-GC-1. The most recent fraction, Z3, consisted of 6 large clear, euhedral prisms and produced a concordant point at 582 Ma (Figure 4-8). The two remaining fractions Z1 and Z2 (analyzed in 1998) both consisted of 16 abraded, clear, euhedral zircons, and produced points that are displaced to the right of Z3 due to their higher proportion of common Pb. Also plotted are two analyses from sample SJOB97-GC-2, which contained zircons of similar morphology to those in SJOB97-GC-1. Two fractions Z1-2 and Z2-2, consisting of 24 and 23 grains respectively, produced two concordant points. All five analyses have $^{206}Pb/^{238}U$ ages in the range of 582 to 585 Ma and the weighted average of these analyses produces an age of 584 ± 1 Ma (95% C.I.).

4.2.4.2 (H) Unit 13: Dark Purple, Crystal-bearing, Ash-flow Tuff

The third sample collected from the MVS was a crystal-rich ash-flow tuff containing abundant stockwork style crustiform-colloform, chalcedonic silica ± adularia low-sulphidation veins and associated breccias (sample GS-GC-01). The dated ash-flow contains pale white 1-2mm crystals and crystal fragments within a dark purple hematite-rich groundmass.
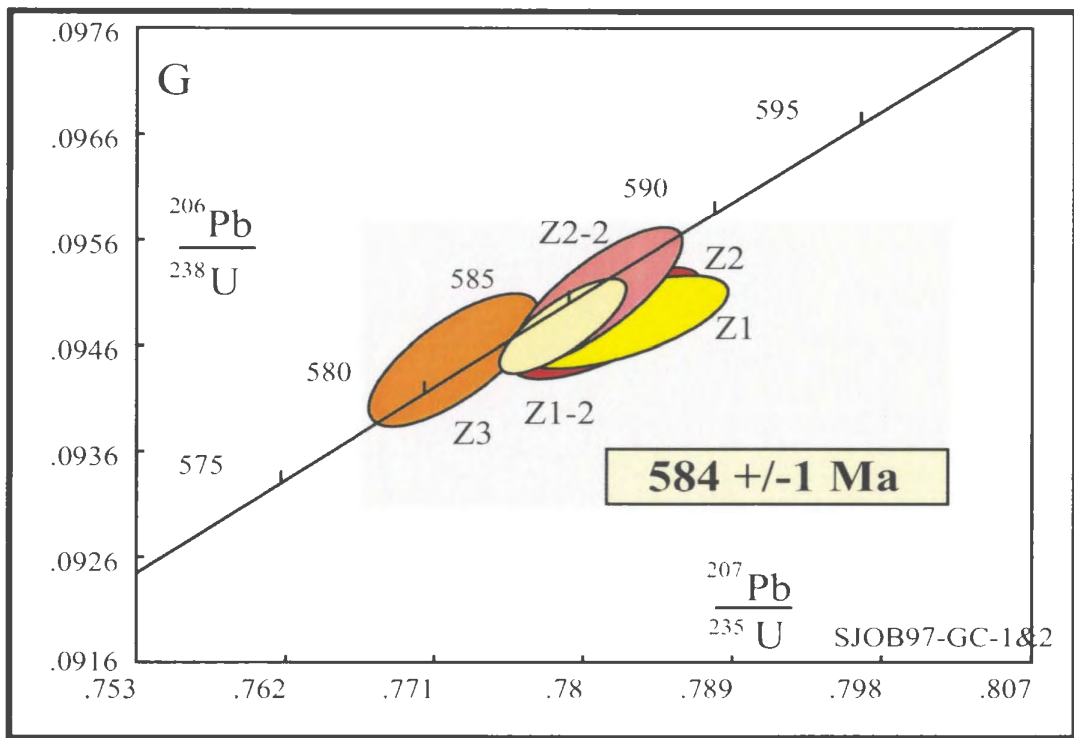
Figure 4-8: Concordia diagram for the rhyolite succession from the Manuels Volcanic Suite which hosts the advanced argillic alteration.
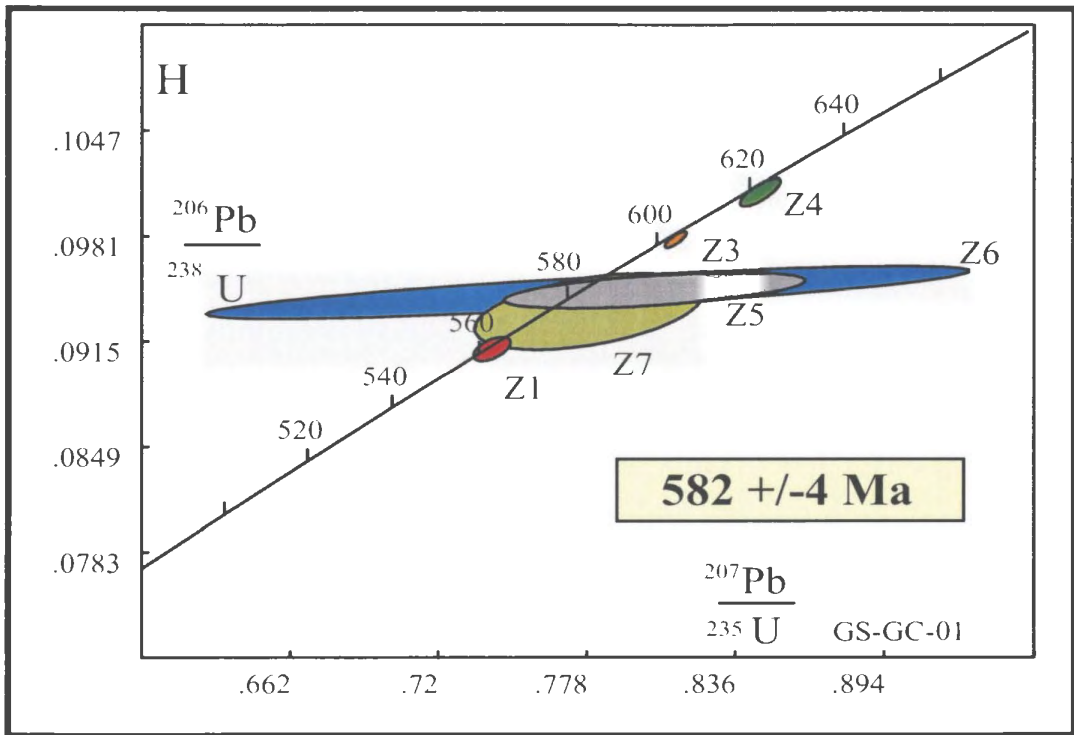
Figure 4-9: Concordia diagram for the dark purple crystal-rich ash-flow tuff.

The unit provided a very poor zircon yield, consisting of euhedral to sub-rounded grains, indicative of a potentially mixed-age population, resulting from the presence of detrital zircon. In total, seven fractions were analyzed. Three single grain analyses of the largest, clear, euhedral grains (Z5, Z6, Z7) provide the maximum age and possibly the eruption age of the ash-flow, at 582 ± 4 Ma (Figure 4-9). Z5 and Z6 have very low concentrations of ^{207}Pb, which accounts for the wide ellipses along the ^{207}Pb/^{235}U axis. Z7 has a higher concentration of common Pb, accounting for the larger ellipse. The 582 ± 4 Ma age is calculated from the weighted average of the ^{206}Pb/^{238}U ages of Z5, Z6 and Z7 and either represents the youngest age of detrital zircon present within the sample, or the actual eruption age of the ash-flow unit. Another concordant analysis consisting of two large, clear, euhedral, abraded zircons produced a point with a ^{207}Pb/^{206}Pb age of 568 Ma, and a ^{206}Pb/^{238}U age of 562 Ma (Z1: 1.1% discordant). One possible interpretation of this analysis is that it is the eruption age of the ash-flow. However, it has not been reproduced and thus is currently not incorporated into the age determination for this unit. Analyses Z2, Z3 and Z4, which consist of two small grains, four small grains and three small grains respectively, are 1.7 to 7.5% discordant. As these analyses did not contain any visible cores, they are presumed to represent a detrital component within the ash-flow.

4.2.5 Wych Hazel Pond Complex (WHPC)

4.2.5.1 (I) Unit 19a: Pumiceous Ash-flow Tuff

The pumiceous ash-flow tuff is located at the base of the sedimentary sequence in the Oval Pit mine, where it overlies silica–sericite–pyrite altered basal conglomerate of

the WHPC. The dated sample has a pale yellow-weathering and contains centimeter-scale pale to dark green collapsed pumice fragments (sample GS-GC-03). The ash-flow tuff caps the underlying silica–sericite–pyrite alteration, which is assumed to be associated with late-stage advanced argillic alteration.

This unit produced two distinct zircon populations, one consisting of moderately abundant, large, clear, euhedral zircons, and a second, more abundant, population of small, clear, euhedral zircon prisms with length/width ratios approximately 2-1:1. Four fractions consisting of 8,10, 16 and 14 abraded zircons, respectively, from the second population produced a cluster of points overlapping concordia at 583 Ma (Figure 4-10). The weighted average of the $^{206}Pb/^{238}U$ ages for Z5, Z6 and Z7 gives an age of 582 ± 1.5 Ma (95% C.I.; MSWD = 0.20). This is interpreted to be the age of eruption for this ash-flow tuff. The remaining analyses (Z1, Z2, Z3), which are discordant, are single grains from the larger less abundant zircon population. These grains, as indicated by the older ages, likely represent a detrital component contained within the tuff bed. Analysis Z8 is a multiple grain analysis from the younger grains, however this point is slightly displaced to the right which may imply that the analysis also included an older grain with the younger zircon population.

4.2.5.2 (J) Unit 22: Fowlers Road Porphyry

The second unit dated from the WHPC represents the youngest magmatic event yet documented within the field area. The Fowlers Road porphyry is confined to the northeastern portion of the map area, east of the Manuels River (Figure 4-1). The dated
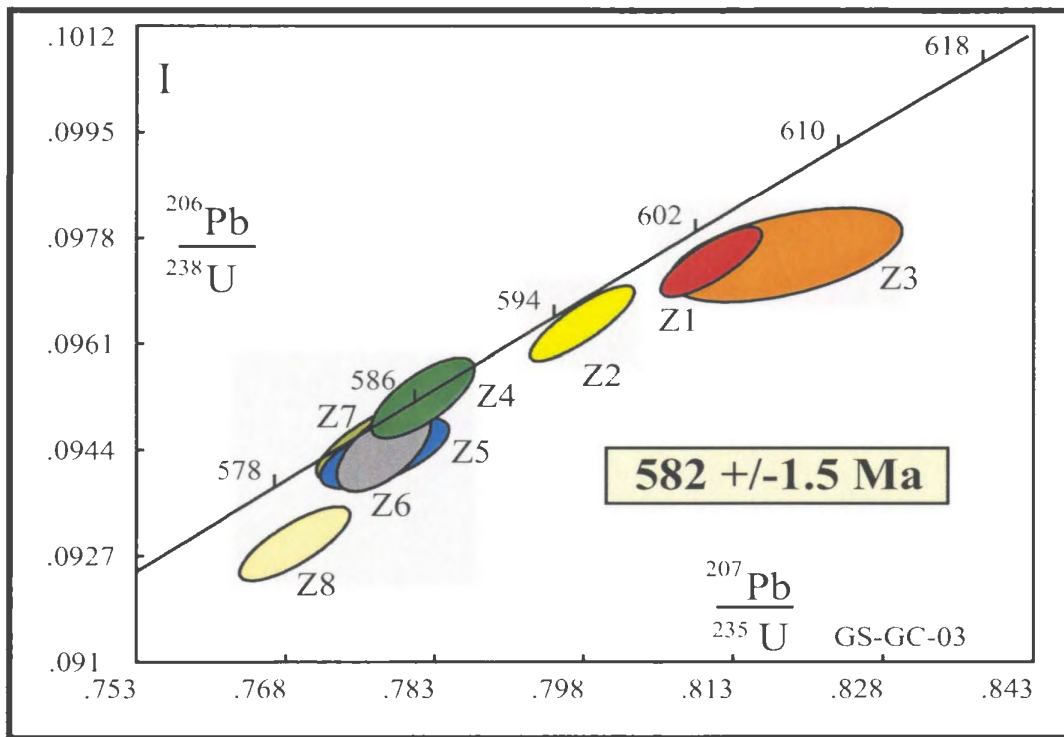
Figure 4-10: Concordia diagram for the pumiceous ash-flow tuff overlying the advanced argillic alteration.
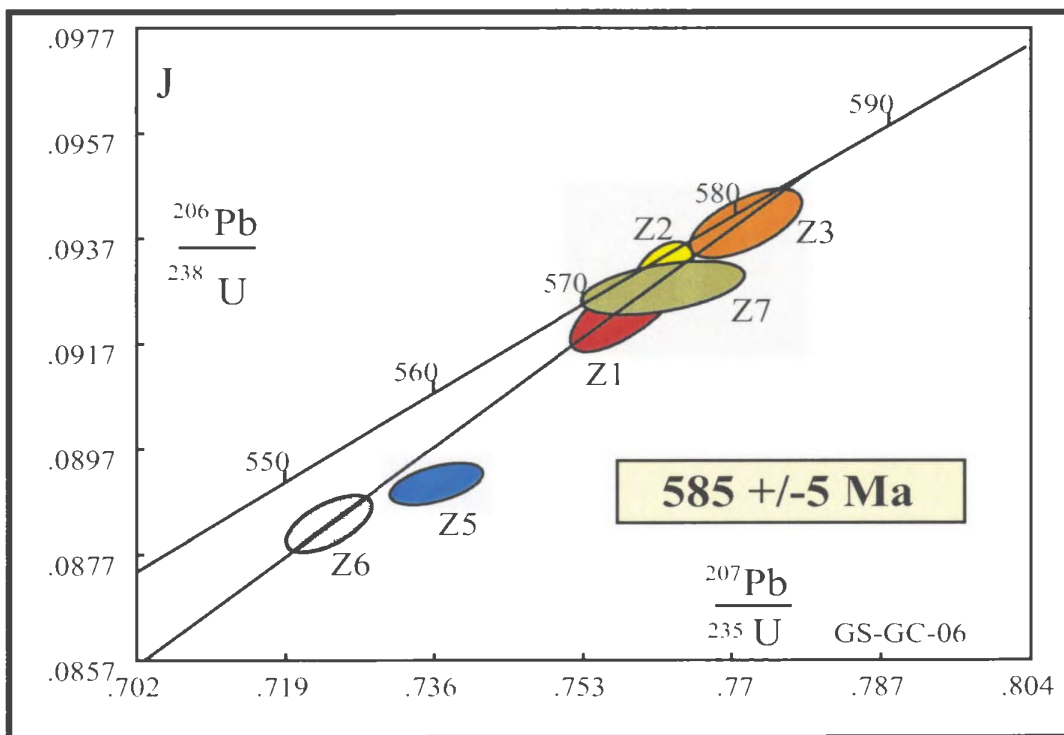
Figure 4-11: Concordia diagram for the Fowlers Road porphyry.

208

porphyry contains sub-to euhedral, white plagioclase phenocrysts (1-2mm in length) within a fine-grained, dark purple to pale grey groundmass (GS-GC-06). The porphyry unit was collected near its intrusive contact with thin- to medium-bedded, fine-grained, green siltstone of the upper WHPC, and is locally associated with the formation of a blocky peperite, which implies that the sediment was unconsolidated at the time of intrusion.

The sample produced abundant, clear, euhedral zircons with length/width ratios approximately 3:1, from which six fractions were analyzed; all of the analyses consisted of multiple, clear, euhedral grains (Figure 4-11). Analyses Z1, Z2, Z3, Z6 and Z7 define a line with Z6 being most discordant and Z3 being the least discordant along the line (0.94 probability of fit). Z5 is displaced to the right, suggesting that an older grain was included within the analysis. The weighted average of the ^{207}Pb/^{206}Pb ages of Z1, Z2, Z3, Z6 and Z7 at the 95% confidence interval is age of 585 ± 5 Ma (MSWD = 0.21).

4.3 ^{40}Ar-^{39}Ar ANALYSES

To further constrain the timing of events, including mineralization, three mineral separates were made as part of this study, and sent to the Geological Survey of Canada for ^{40}Ar-^{39}Ar analyses. A detailed description of sample processing and analytical methods is given in Appendix A and Villeneuve et al. (2000), respectively.

The ^{40}Ar-^{39}Ar samples were collected in an attempt to establish the absolute ages of the high- and low-sulphidation systems as well as the age of deformation along the MHSZ. The geochronology was done by M. Villeneuve of the GSC and provided an independent test on the timing of events as established by mapping and U-Pb

geochronology by the author and others in this area. One sample of fine-grained adularia (average grain size approximately 100 microns; sample GS-02-53) was collected from a well-developed crustiform-colloform, chalcedonic silica vein exposed in an exploration trench (Trench #3; Plate 4-3 and 4-4).

Two samples of sericite were collected in the region of the Oval Pit mine. The first was collected at the core of the advanced-argillic alteration within a large zone of massive silica alteration (average grain size approximately 50-75 microns; sample GS-GC-14). This sample was hand picked under a microscope, separating the long fibrous, possibly deformation related sericite, from the more sub-rounded grains (1:1 length/width ratio). The sub-rounded grains were selected to represent primary sericite associated with the formation of the advanced argillic alteration. The second sample of sericite was collected in the quarry located at Mine Hill (grain size approximately 50-100 microns; sample GS-GC-12). This sample was collected within a zone of intense shearing associated with post-mineral deformation. Long fibrous grains were selected from this sample under a microscope (4:1 length/width ratio) and are interpreted to represent deformation-related sericite.

Only the sericite from the MHSZ produced an undisturbed age plateau. The adularia sample collected at Steep Nap produced an anomalously young ^{40}Ar-^{39}Ar age of 278 ± 2 Ma (Figure 4-12). The presence of low-sulphidation detritus in Lower Cambrian rocks demonstrates the low-sulphidation system is pre-Cambrian (e.g. O'Brien, 2002), and therefore the adularia has undoubtedly been reset. The sericite separate from the Oval Pit mine did not produce an age, as the sample displays a partial-argon loss profile with
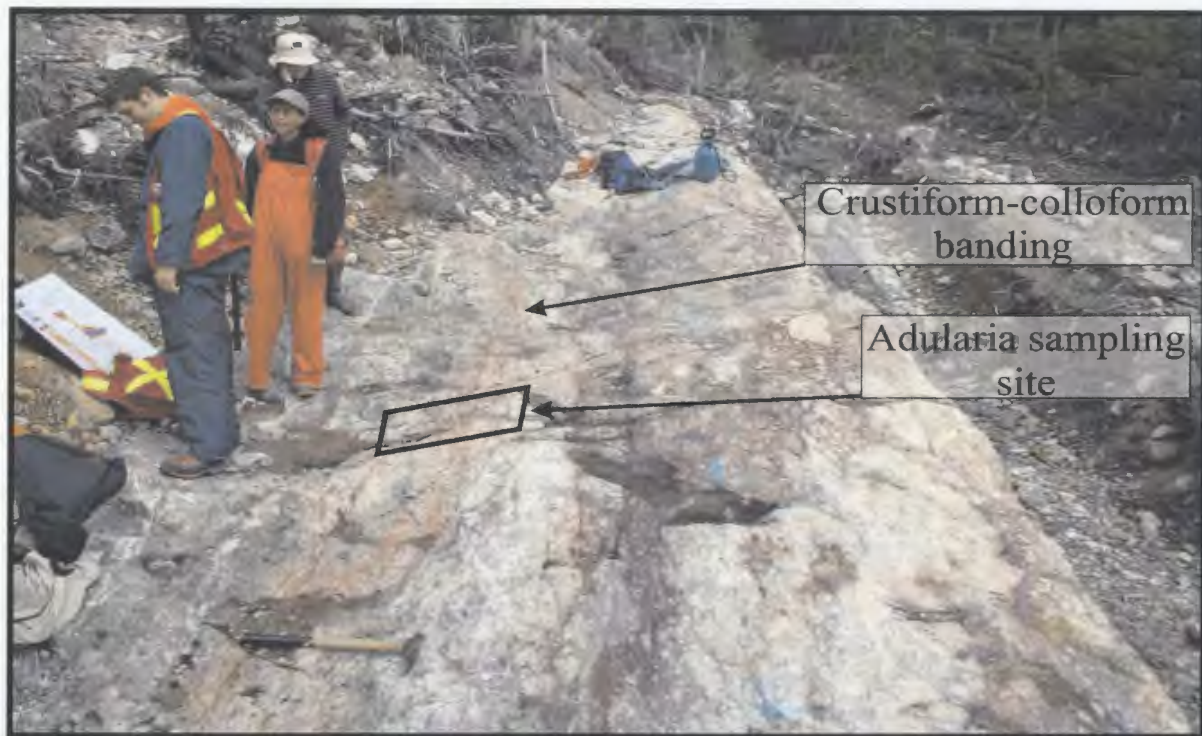
Plate 4-3: Trench #3 exposing a well developed crustiform-colloform, chalcedonic silica vein and associated breccias. Sampling site of adularia is outlined in box (Photo courtesy of Sean O'Brien, Department of Natural Resources, Geological Survey; Steep Nap prospect).

Plate 4-4: Close up photograph of adularia sampling site showing well-developed colloform textures (Trench #3; Steep Nap prospect).
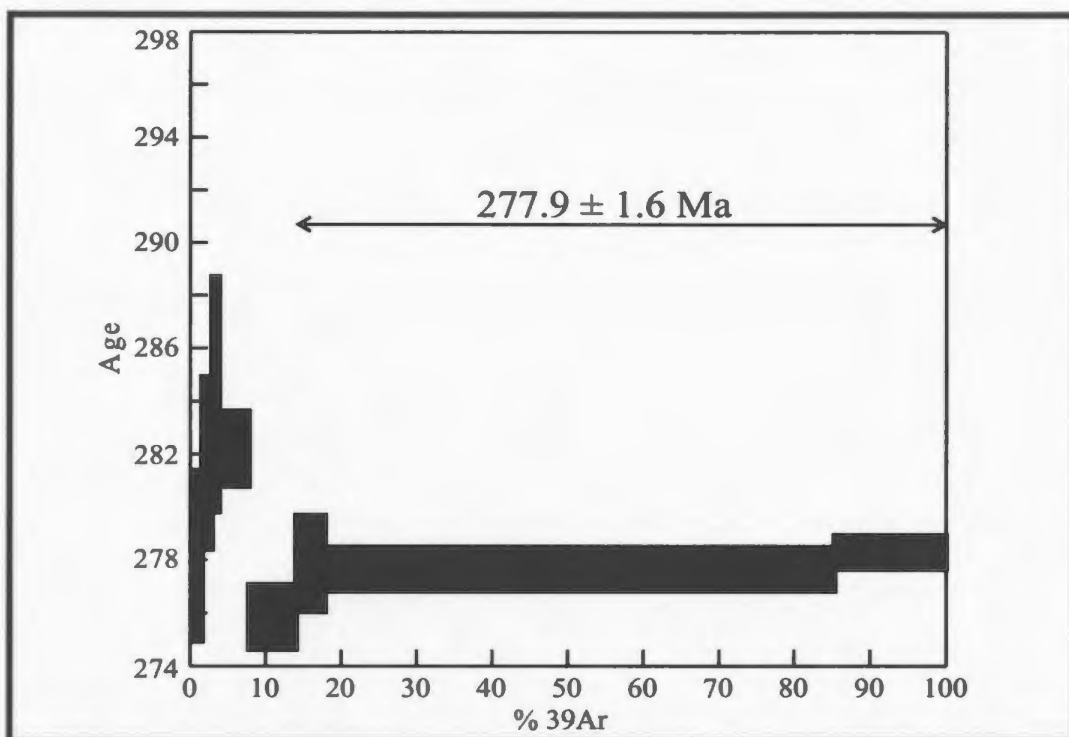
Figure 4-12: Step-heating ^{40}Ar-^{39}Ar spectra for adularia (GS-02-53) from gold-bearing low-sulphidation veins, Steep Nap prospect.
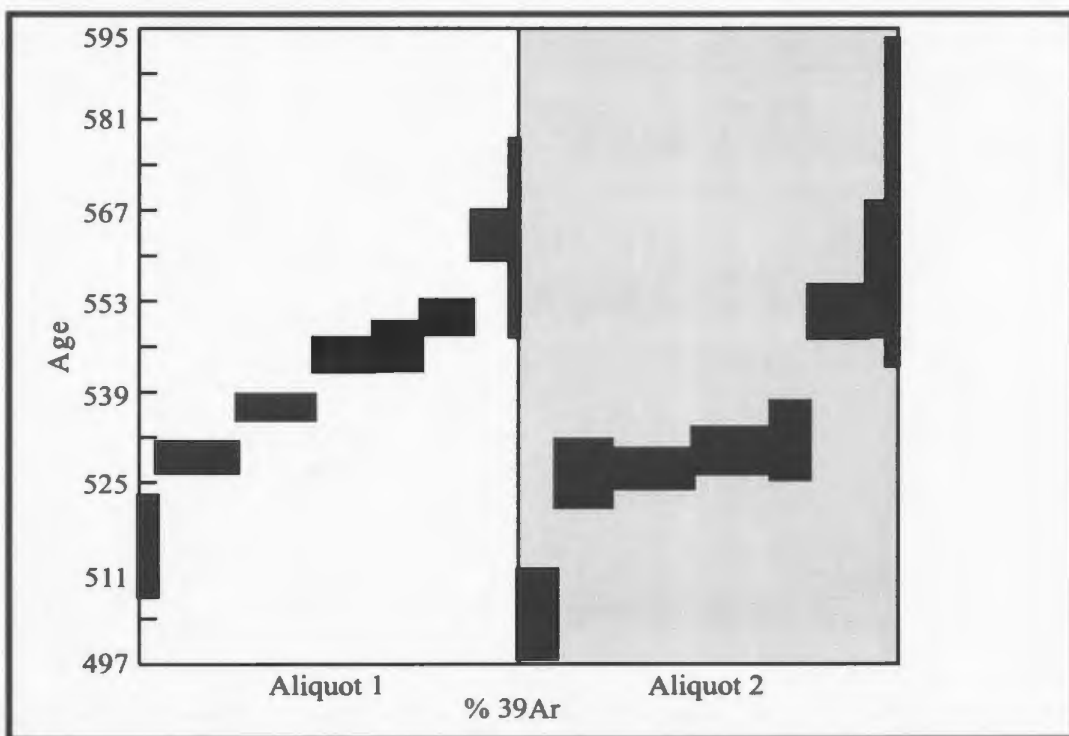
Figure 4-13: Step-heating ^{40}Ar-^{39}Ar spectra for two sericite separates (GS-GC-14) from the core of the advanced argillic alteration, Oval Pit mine.

no plateau (written communication, M. Villeneuve, 2005; Figure 4-13). The only age that falls within current field and U-Pb constraints is the sericite separate from the MHSZ. This sample produced a ^{40}Ar-^{39}Ar age plateau of 537 ± 3 Ma (Figure 4-14), which reflects the last period of deformation (as recorded by the sericite) along the MHSZ. This demonstrates that deformation within the region persisted until the end of the Neoproterozoic, with the upper limit defined by the relatively undeformed overlying Paleozoic platformal cover sequence, which contains Lower Cambrian age fossils (Boyce, 2001).

4.4 SUMMARY OF THE GEOCHRONOLOGICAL DEVELOPMENT OF THE EASTERN AVALON HIGH-ALUMINA BELT

The new and previously existing geochronology demonstrates a more complex and protracted igneous history within the EAHB than previously recognized. New U-Pb ages demonstrate the 625 to 620 Ma age of the WHIS. As a result many of the volcanic rocks originally thought to be part of the 584 Ma succession are now recognized as part of an older pre-625 Ma sequence. The 625 to 620 Ma age of the WHIS also conclusively demonstrates that this suite did not provide the heat source of hydrothermal fluids responsible for the development of the advanced argillic alteration. The similar age of the WHIS and HIS imply that the two are cogenetic, which is further supported by the geochemistry (as discussed in Chapter 3). From this new evidence it also becomes unclear whether the observed alteration within the WHIS is the result of intrusion-related alteration as observed elsewhere in the HIS, or if in fact the alteration is a result of the younger ca. 584 Ma epithermal alteration.
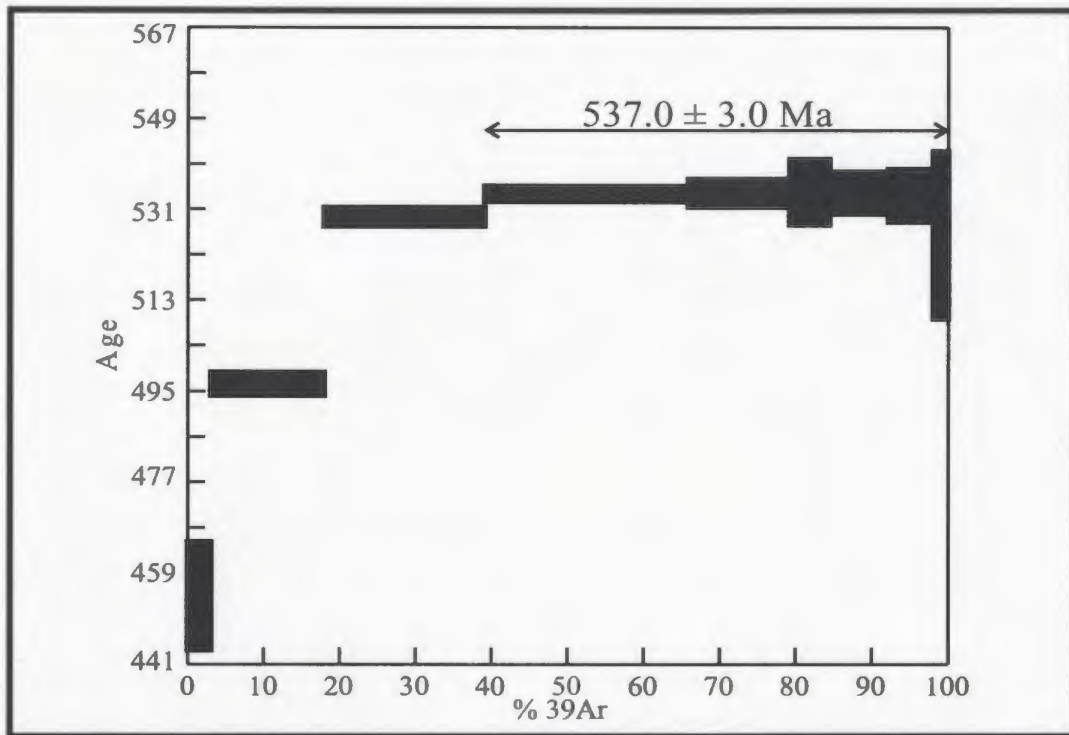
Figure 4-14: Step-heating ^{40}Ar-^{39}Ar spectra for sericite (GS-GC-12) from foliated advanced argillic alteration, Mine Hill.
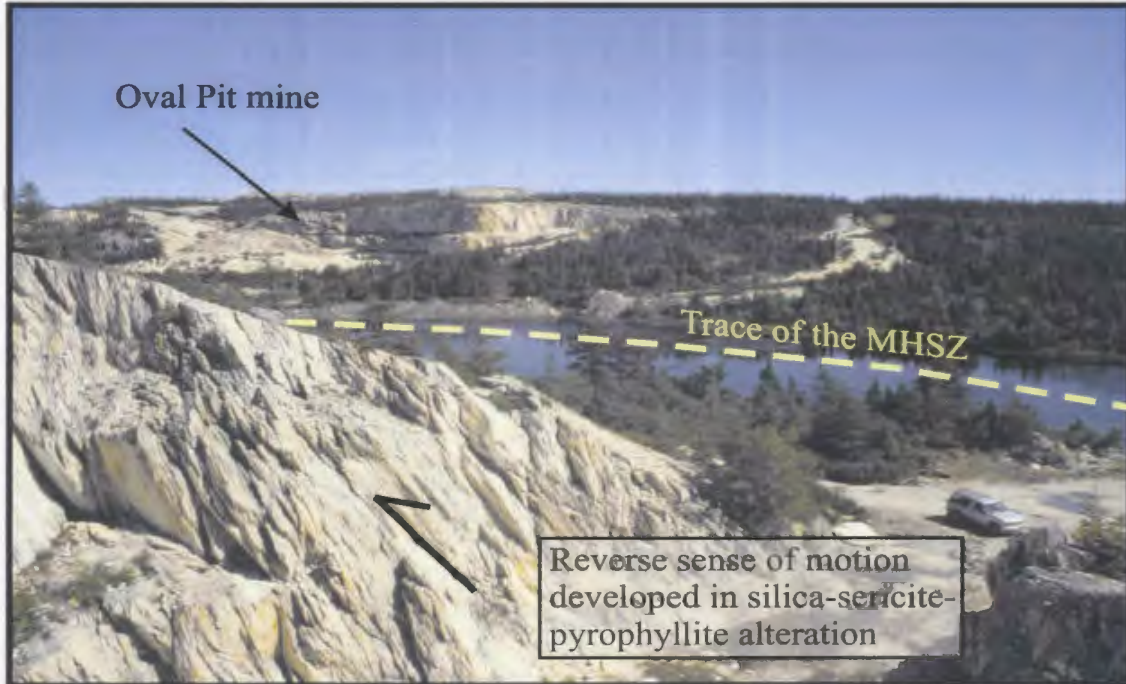
Plate 4-5: Mine Hill shear zone exposed in foreground with the Oval Pit mine in the background. Note the reverse sense of motion within the alteration. Viewed looking towards the northeast from Mine Hill. (Photo courtesy of Sean O'Brien, Department of Natural Resources, Geological Survey)

The older volcanic units identified within the study area may represent eastern equivalents of the Hawk Hills Tuff, which is intruded by the Holyrood Granite along the southern and western margins of the Holyrood Horst. Within the EAHB these older volcanic rocks are the primary host to the development of low-sulphidation veins at the Steep Nap prospect, yet these units are too old to be associated with the actual development of the epithermal system. Low-sulphidation veins are also locally observed crosscutting silica–sericite–chlorite altered granite of the WHIS in the vicinity of the Bergs prospect. The new geochronological data now demonstrates that the exposure of such granites does not imply deep erosion of the low-sulphidation system, rather that the granite and other intrusive rocks of the WHIS are actually basement to both epithermal systems. The preservation of felsic volcanic rafts, which are interpreted to represent roof pendants of the overlying volcanic carapace, along with the common development of tuffisite brecciation within the granite provide supporting evidence for relatively shallow levels of erosion within the WHIS.

The new U-Pb age determined for the ash-flow tuff from the base of the WHPC now brackets the age of the high-sulphidation system between 585 and 580.5 Ma. This time period is essentially coeval with the formation of the MVS, suggesting that the high-sulphidation system is related to the magmatism responsible for the formation of the 584 Ma volcanic sequence. The time of formation of the low-sulphidation veins with respect to the ages of the MVS and the high-sulphidation system remains poorly constrained, however limited field evidence suggests that the low-sulphidation system post-dates the high-sulphidation alteration (further discussed in Chapter 5). The new geochronology

from this study now brackets the age of the low-sulphidation system from 586 Ma to the base of the overlying Paleozoic cover (approximately 513 Ma). The one young analysis generated by the dark purple crystal-rich ash-flow tuff may suggest that the actual eruption age of the unit hosting the low-sulphidation veins at the Bergs prospect is as young as 568 Ma. This younger age would have significant ramifications as it would imply that the low-sulphidation system could affect the overlying WHPC, greatly increasing the exploration potential of the EAHB.

The age of the Fowlers Road porphyry, currently determined to be 585 ± 5 Ma, can be further constrained using field relationships observed within the map area. As mentioned-above the porphyry unit intrudes sedimentary rocks correlated with the WHPC, these sedimentary rocks are observed to unconformably overlie altered volcanic rocks in the Oval Pit mine. The base of the sequence within the Oval Pit mine has a defined age of 582 ± 1.5 Ma and therefore the porphyry must post-date the age of the ash-flow tuff at the base of the sequence. Using this lower time constraint the age of the porphyry falls within the time bracket of the high-sulphidation system. It is recognized that this porphyry is intrusive into sedimentary rocks that post-date the advanced argillic alteration. The Fowlers Road porphyry is interpreted to represent a late stage magmatic pulse associated with the main magmatic event responsible for the formation of the MVS and accompanying advanced argillic alteration. At the present time the 585 ± 5 Ma age makes the porphyry unit the best-known representative of a magmatic event that could have provided a heat source for the high-sulphidation system.

The new geochronological data also highlights a prominent divide between ca. 620 Ma intrusions and ca. 584 Ma volcanic rocks. This is most evident in the area of the Oval Pit mine and Mine Hill where dated samples of the MVS and WHIS, respectively are separated by just 700m. This region is the type locality of the MHSZ, which is taken to represent the major structural boundary between the older units to the west and the younger units to the east. In the area of Mine Hill this boundary is identified by an east-plunging, reverse-sense ductile fabric developed within silica–sericite–pyrophyllite alteration (Plate 4-5). Tracing this structure north of the Oval Pit mine is complicated by the development of post-mineralization deformation. The development of sericite-silica alteration within shear zones in the northern portion of the map region is interpreted to represent structures associated with the development of the main MHSZ. Regionally this zone is coincident with the development of advanced argillic alteration, and is interpreted to have played an important role in siting the development of the high-sulphidation system (Sparkes, *et al.,* 2004). Known occurrences of low-sulphidation veining also occur within close proximity to sericite–silica shear zones that are interpreted to be related to the larger-scale MHSZ. This evidence suggests that the shear zone may also have played a role in siting the development of low-sulphidation veins.

A summary diagram containing all of the geochronology and associated errors is presented in Figure 4-15. From this figure it is evident that there is a minimum of 26 Ma separating intrusive rocks of the WHIS and volcanic rocks of the MVS. It is also evident that the age bracket for the Late Neoproterozoic deformation is between 583.5 Ma and the base of the overlying Lower Middle Cambrian succession (approximately 513 Ma).
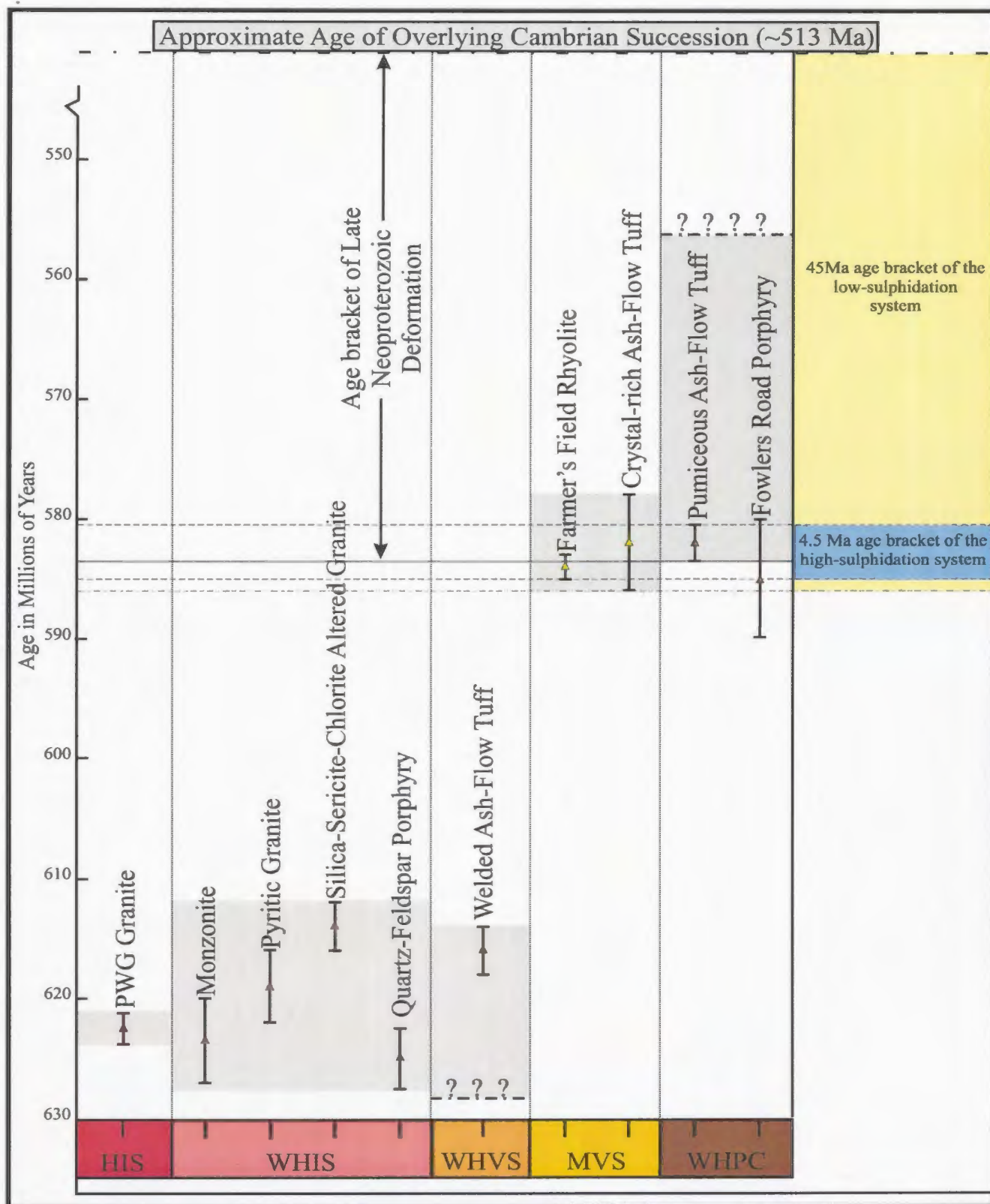
Figure 4-15: Diagram summarizing the geochronological data of the eastern Avalon high-alumina belt.

As indicated by the ^{40}Ar-^{39}Ar data, deformation persisted until at least 537 ± 3 Ma; this data demonstrates that there is a minimum of ca. 20 Ma separating the last known deformation and the deposition of the overlying Paleozoic cover sequence. In actual fact the deformation probably represents a continuum of events starting with arc-collapse around 582 Ma and ending during the beginning of the early Paleozoic.

CHAPTER 5:

FRACTURAL, ALTERATION AND THIN SECTION ANALYSES OF LOW-SULPHIDATION VEINS AND OBSERVED FIELD RELATIONSHIPS

5.1 FRACTURAL ANALYSIS OF LOW-SULPHIDATION VEINS

The distribution of low-sulphidation-style veins were analyzed in selected outcrops within the field area. These analyses were conducted on three planar outcrops and one vertical roadcut section. Each analysis involved measuring a taped section perpendicular to exposed low-sulphidation-style veins and recording the total number of veins that intersected the baseline. Limitations due to the small amount of outcrop exposure, lichen cover and chloritic fracture surfaces along the vertical section limited the total number of veins measured for each analysis. In general a minimum of 50 veins per analysis is necessary for the estimation of the power law exponent that is generally produced by the variation in vein thickness for robust vein populations (McCaffery and Johnston, 1996). Only one of the four analyses contained greater than 50 veins, however other important information can also be obtained from the smaller vein datasets. This information includes average vein thickness, average vein spacing, percent extension, the coefficient of variation (C_v), and vein densities for individual lines. The recorded information can be used to compare vein populations from different areas within the map region and can also be used to identify correlations between vein density or vein thickness and lithology.

5.1.1 Data Collection

The basic method used for collecting the vein data involves measuring a taped section perpendicular to exposures of low-sulphidation-style veins. For each line the recorded data includes, 1) the trend of the taped section, 2) total length of the line, 3) the point at which individual veins intersect the line, and 4) width of the veins and the trend and/or dip of the veins depending on whether the line is on a planar or vertical section. Veins >1mm in width were recorded, however due to lichen cover and poor outcrop exposure, veins ≥2-3mm are more representative for the lower limit of measured veins. For the data presented herein, vein widths are measured from wall to wall rather than from the center due to the asymmetry within some of the veins. The recorded vein information for horizontal sections was regenerated in CorelDraw, providing a visual representation of the vein distribution along the lines (note vein intersections are schematic and do not implying crosscutting relationships). This method of visual representation is not practical for larger vein datasets and can be substituted with plots of vein thickness versus distance along the line to show vein distribution.

Several important pieces of information can be determined from the above-mentioned data. As discussed in McCaffery and Johnston (1996) the sum of all vein thicknesses measured along a line can be used to calculate the percent extension over the length of the line. Vein densities also provide values that can be used in comparing various vein datasets, however as pointed out by Brathwaite *et al.* (2001), the total line length must be corrected for the increase in length due to veining. The line length is corrected by subtracting the sum of the vein thicknesses from the total line length, and

therefore, all comparisons of vein density are made with only the total length of host rock and not the length of host rock plus veins. Another important value used to compare various lines is the coefficient of variation (C_v), which is defined as the standard deviation of vein spacing divided by the mean of the spacing (Cox and Lewis, 1966; McCaffery and Johnston, 1996; Gillespie *et al.*, 1999; Brathwaite *et al.*, 2001). The values of the C_v can be used to demonstrate the degree of vein clustering within individual datasets. Vein populations that are anticlustered are defined by C_v values <1 and clustered veins are characterized by those datasets with C_v values >1; for perfectly regular vein sets $C_v = 0$ (McCaffery and Johnston, 1996). For a summary of the results from the four analyses refer to Table 5-1.

5.1.2 Fractural Analyses Data

One of the four vein analyses was carried out on outcrop #141, which is exposed immediately adjacent to a bonanza-grade low-sulphidation gold vein at the Bergs prospect (54.3 g/t Au; O'Brien and Sparkes, 2004). This analysis was restricted to a 4m-wide outcrop separated from the main bonanza-grade vein by approximately 3-4m of no exposure. The total line length measured was 3.64m along a trend of 272 degrees. In total 28 veins were measured, ranging from 1mm to 38mm in width. This line is characterized by a vein density of 8.1, 4.5 % extension over the 3.64m and a C_v value of 0.9, which suggests that these veins are anticlustered. From Figure 5-1 it is evident that the main vein population trends between 180 and 200 degrees. The data is also consistent with an increase in vein density with decreasing distance from the bonanza-grade vein, which is located to the west of the measured line.

Table 5-1: Summary of results from fractural analyses conducted within four separate areas of low-sulphidation vein exposures.

Location	Lithiology	Line Length (m)	No. of veins	Average spacing (mm)	Spacing Cv	Average thickness (mm)	Extension (%)	Vein density
Outcrop #42 Steep Nap South	Flow-banded rhyolite	28.00	27	67	1.0	77	7.2	1.0
Outcrop #77 Farmer's Field	Flow-banded rhyolite	12.30	30	38	1.0	6	1.4	2.5
Outcrop #141 Bergs prospect	Flow-banded rhyolite	3.64	28	12	0.9	6	4.5	8.1
Outcrop #18 Steep Nap main vein	Polymict lapilli tuff	40.87	136	28	1.4	25	8.4	3.6
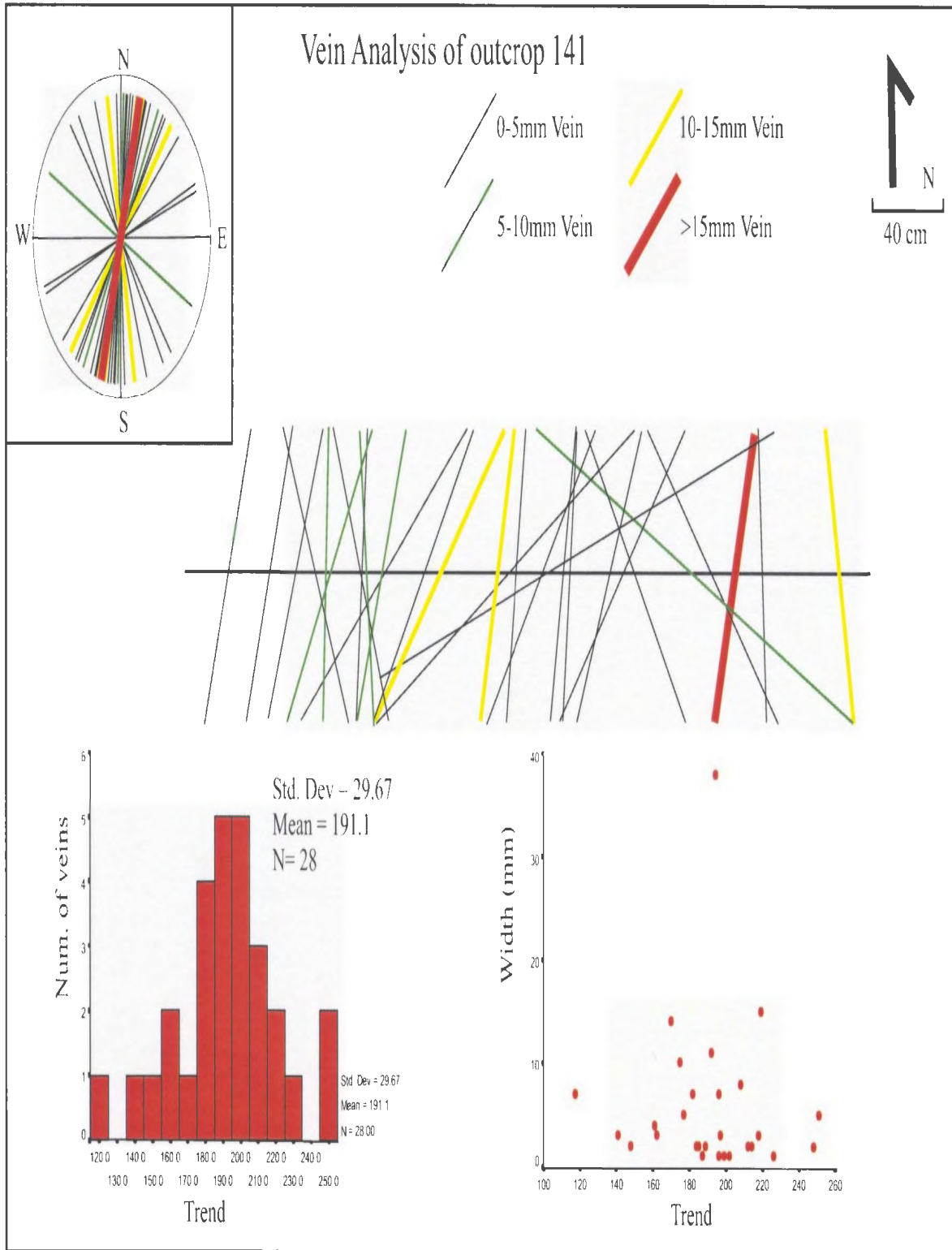
Figure 5-1: Schematic representation of vein distribution at outcrop #141 (Bergs prospect).

Two analyses of vein orientations were carried out on low-sulphidation-style veins within the Steep Nap prospect. The first was carried out at outcrop #18 along the vertical face of a roadside rockcut (elevation 50m a.b.s.). Due to the irregular shape of the vertical surface several short lines were measured and the total length presented here is the sum of six individual lines. The total length of this line is 40.87m along a trend of 30 degrees. A total of 136 veins intersected the line, however as mentioned above vein measuring was complicated by chloritic fracture surfaces that masked veins intersecting these surfaces. Vein widths range from 1mm to 1.900m, with the 1.900m vein representing the main colloform-crustiform, banded chalcedonic silica vein exposed along the roadside outcrop. This line has a vein density of 3.6, and is characterized by 8.4% extension over the 40.87m. The C_v value for this line is 1.4, which suggests that the line displays vein clustering; this is the only measured line that has a C_v value >1. Since this line was measured along a vertical plane it could not be illustrated as in Figure 5-1, however Figure 5-2 is a plot of vein thickness versus distance, and provides a graphical representation of vein distribution along the line. From this figure vein clustering is evident, and therefore, provides supporting evidence for the calculated C_v value. An analysis of vein orientation was carried out on this outcrop during previous work (refer Mills, 1998). From that analysis, 23 banded chalcedonic silica veins were measured and it was determined that the dominant trend was 128/59 NE (Mills, 1998).

The second line measurement was conducted on low-sulphidation veins exposed along a ridge approximately 340m SE of the roadside outcrop; outcrop #42 (elevation
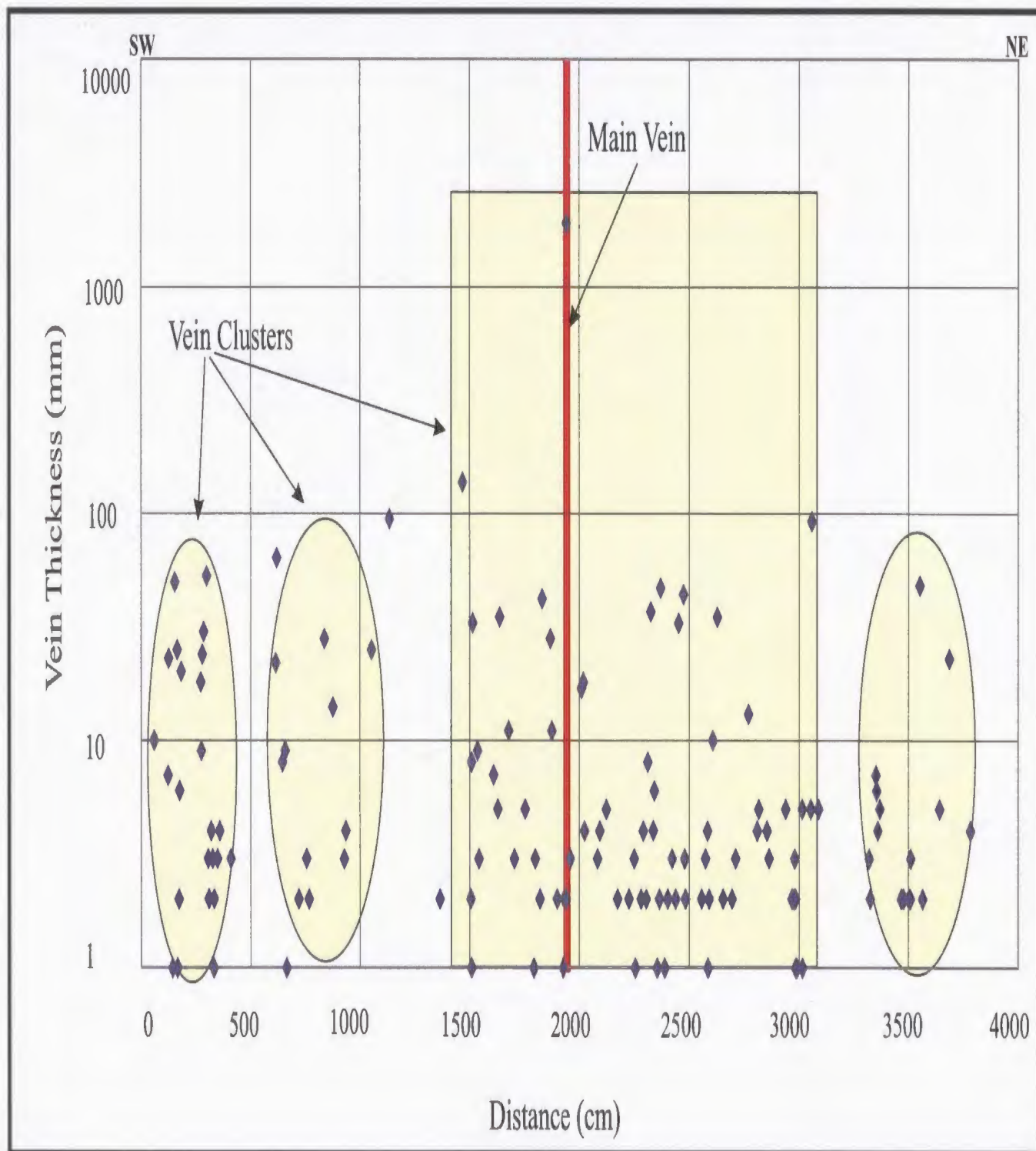
Figure 5-2: Log-norm plot of vein thickness versus distance along the line for vein measurements at outcrop #18 (Steep Nap prospect).

111m a.b.s.). A total of 27 veins occurred along a 28m line, trending 37 degrees. A planar view of the dataset collected at outcrop #42 is presented in Figure 5-3. Vein widths range from 1mm to 1.638m, with a total of 7.2% extension occurring over 28m. The vein density for this line was calculated to be 1.0 with an associated C_v value of 1.0. The C_v and Figure 5-3 show that the vein population is not clustered around the main vein and that the predominant portion of the vein population trends between 130 and 140 degrees. This trend is very similar to that described by Mills (1998) for the veins measured at outcrop #18. Figure 5-4 is a 3-D model of the elevation at the Steep Nap prospect showing the approximate locations of outcrops #18 and #42. From this figure it is evident that outcrop #42 is approximately 60m above outcrop #18. It should be noted that brecciation was common in outcrop #42 and was not taken into account in the calculation of percent extension.

The final vein measurement was conducted in an area of quartz-hematite and minor banded chalcedonic silica veins exposed in the of Farmer's Field area (approximately 240m a.b.s.; Figure 1-3). In this region a line was measured along a trend of 225 degrees. In total 30 veins ranging from 1mm to 52mm occurred over a 12m section (Figure 5-5). This region is characterized by the smallest percent extension, which was calculated to be 1.39% over 12m. The line contains a vein density of 2.5 and a corresponding C_v value of 1.0 suggesting randomly spaced veins. From Figure 5-5 it is evident that the predominant trend of the vein population is approximately 135 degrees, however the vein population as a whole has a mean orientation of 124 degrees and displays evenly distributed trends from 95 to 160 degrees.
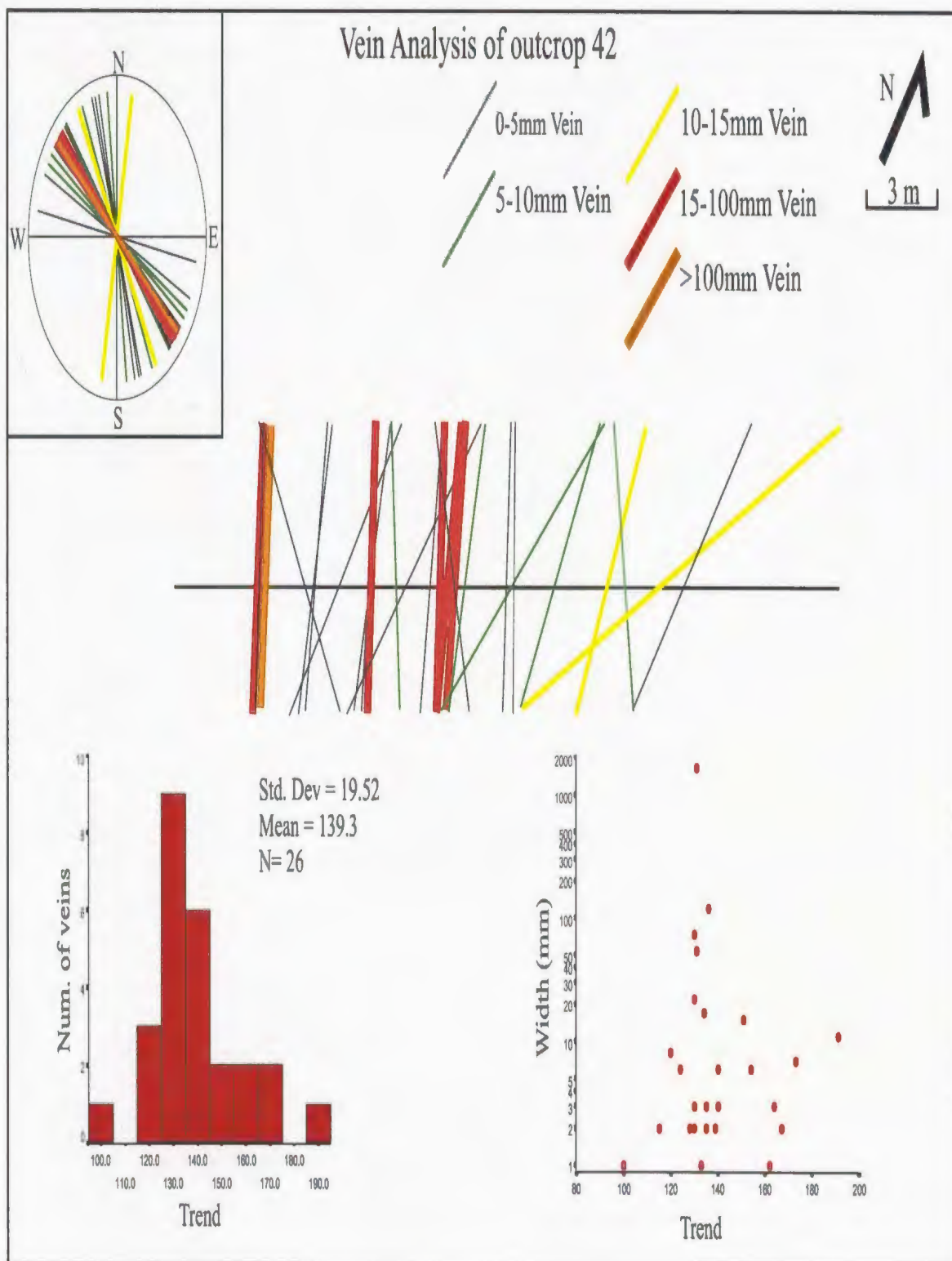
Figure 5-3: Schematic representation of vein distribution at outcrop #42 (Steep Nap prospect).
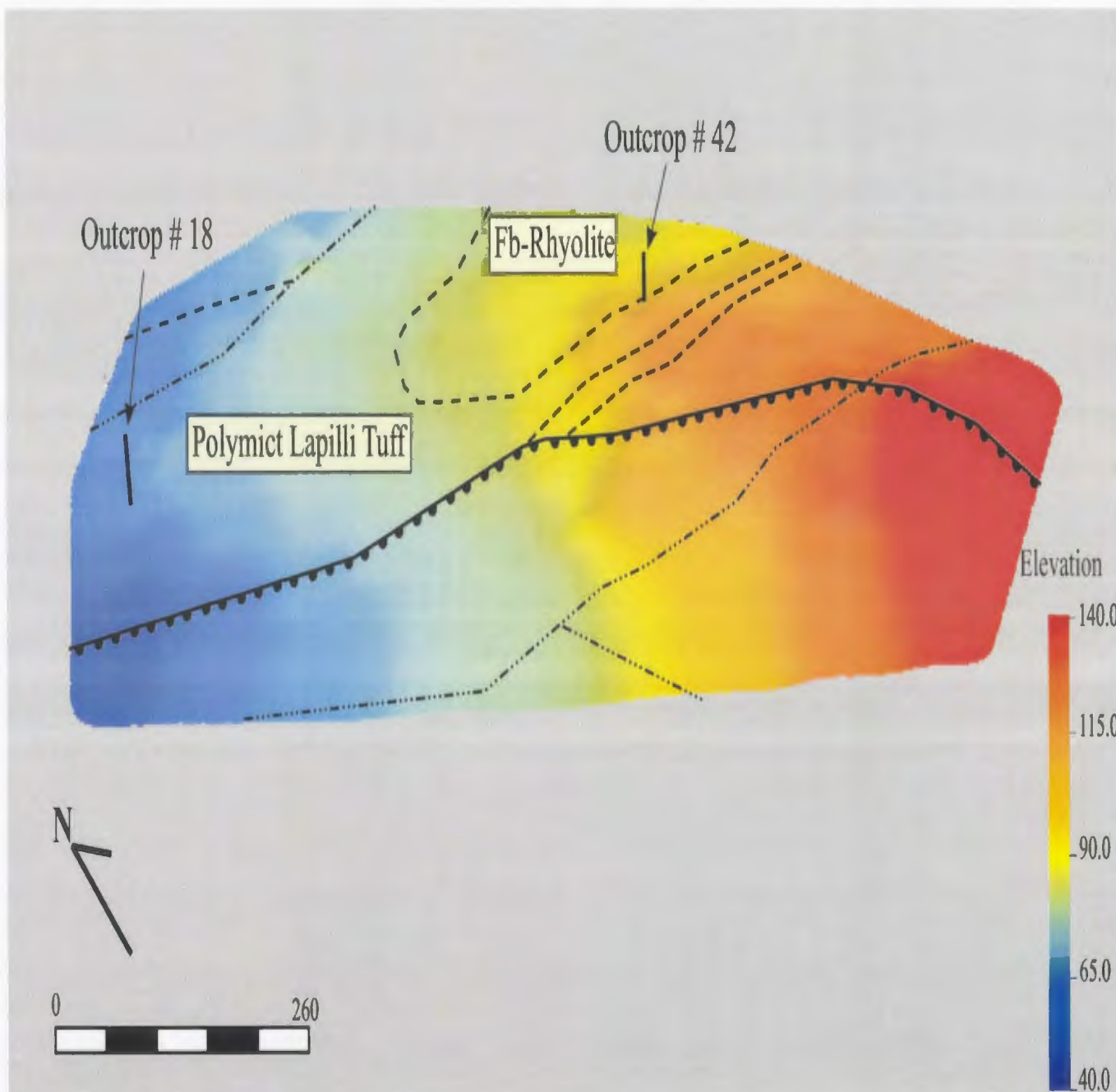
Figure 5-4: Elevation model of the Steep Nap prospect showing the location and elevation of the two measured lines discussed in the text. Note, location of contacts are approximated (elevation data courtesy of Rubicon Minerals Corporation).
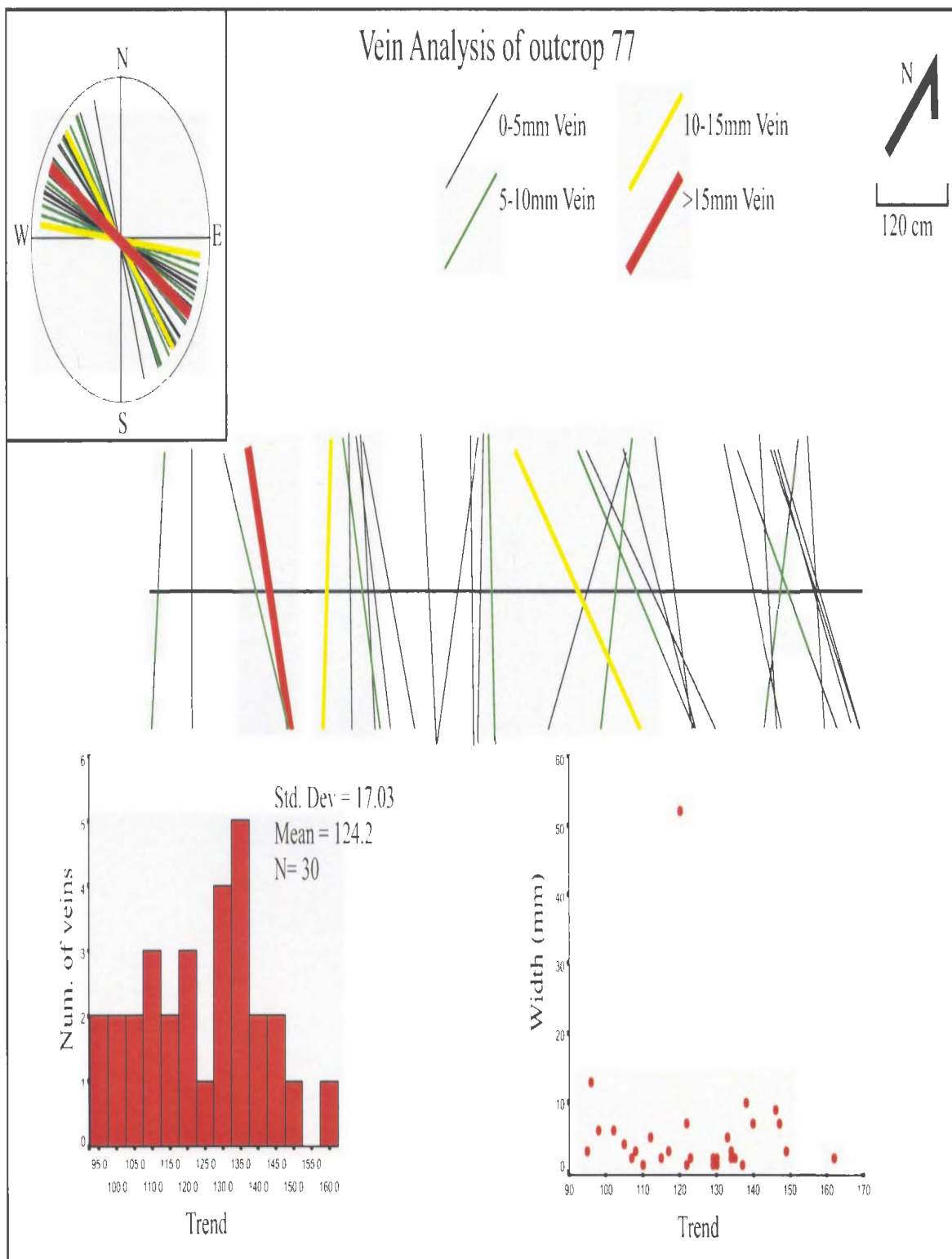
Figure 5-5: Schematic representation of vein distribution at outcrop #77 (Farmer's Field prospect).

<u>5.1.3 Summary of Results</u>

It has been demonstrated by Brathwaite *et al.* (2001) that lithology and the presence of primary structures such as jointing play an important role in the development and distribution of low-sulphidation veins. At this point no such primary control on vein development has been identified within the study area. This preliminary analysis lacks enough information from different lithologies to comment on the distribution of veins in relation to rock type. Average vein thickness, percent extension and C_v values increase with depth and proximity to major vein conduits (Brathwaite *et al.*, 2001). This also holds true for the two analyses carried out at the Steep Nap prospect as the two lines have the highest average vein thicknesses, percent extension and C_v values. These two lines intersect veins that are interpreted to represent the main fluid conduit within the prospect.

From these two analyses it is also evident that the percent extension and the C_v increase with depth. However, the average vein widths do not follow the expected trend and the section at the lower elevation has a smaller average vein thickness. It is possible that the higher average vein thickness for outcrop #42 is related to the host lithology. Flow-banded rhyolite dominates outcrop #42, whereas silicified lithic-rich lapilli tuff is the dominant host at outcrop #18. This information suggests that the rhyolite is characterized by fewer but thicker veins, while the lapilli tuff hosts more abundant but thinner veins. It is noted that this is a very preliminary assessment and requires more vein measurements in order to establish a more robust dataset.

5.2 ALTERATION ASSOCIATED WITH VEIN DEVELOPMENT

A detailed field examination supplemented by PIMA analysis performed by Alina Gaibor (IAMGOLD Corporation; personal communication, 2004) was carried out on a 10m section of wall rock adjacent to a well-developed vein and breccia zone exposed in an exploration trench (Steep Nap prospect; Trench #3; B. Sparkes, 2002). In this area, the low-sulphidation vein is hosted within the polymict lapilli tuff described in Chapter 2. For a schematic representation of results refer to Figure 5-6.

Beginning at the vein margin, the dominant form of alteration observed in the field is silica alteration with relic pale pink potassic-altered clasts in a pale green matrix; fracture hosted chlorite is also frequent. Plate 5-1 contains a representative chip sample from this locality along with a corresponding photomicrograph. PIMA analysis of a hand specimen from this location displayed predominantly silica with minor illite, chlorite and a very small amount of sericite alteration. At 0.5m from the vein there is less evidence of silica alteration, the matrix of the lapilli tuff is still pale green and hosts minor fracture hosted and disseminated pyrite. The matrix also appears to display selective replacement of clasts by a dark green alteration mineral (Plate 5-2). PIMA analysis from this area identified chlorite and hematite with minor amounts of illite.

From 1-1.8m the host rock is covered by overburden, at 2.0m from the vein the groundmass is again pale green with minor fracture-hosted and disseminated pyrite. Locally quartz-chlorite veins are crosscut by chlorite filled fractures. As evident from Plate 5-3 the matrix is predominantly pale green with only rare potassic altered clasts; also an unusual fan shaped silica texture was observed in a fragment within the matrix

Fractures/Veins

Chl
Qtz-Chl
Qtz-Hem

0m from vein: Banded vein, PIMA analysis consisting predominantly of silica with minor illite, chlorite and possible sericite.

0.5m from vein: Patchy pale green alteration within matrix, along with fracture hosted chlorite. PIMA analysis consists of chlorite, hematite and minor illite.

2.0m from vein: Fracture hosted and disseminated pyrite with pale green alteration in the matrix. Locally developed quartz-chlorite veins. PIMA analysis masked by too much background silica.

3.0m from the vein: Rare potassic-altered clasts, frequent quartz-chlorite veins and chlorite filled fractures. PIMA analysis shows predominantly silica with minor chlorite and hematite.

4.0m from vein: Pale pink groundmass with abundant potassic-altered clasts and patchy hematite. No longer see pale green groundmass alteration. PIMA analysis masked by excessive background silica.

5.0m from vein: Well-developed hematite halos, local quartz-hematite veins. PIMA analysis masked by excessive background silica.

8.0m from vein: Pale green groundmass alteration with disseminated pyrite and occasional quartz-hematite veins. PIMA analysis reveals illite, with possible minor sericite and smectite.

10m from vein: Pale pink groundmass with pale green illite. Local quartz-hematite veins and hematite filled fractures. PIMA analysis predominantly illite and hematite.

Proposed Vein Alteration
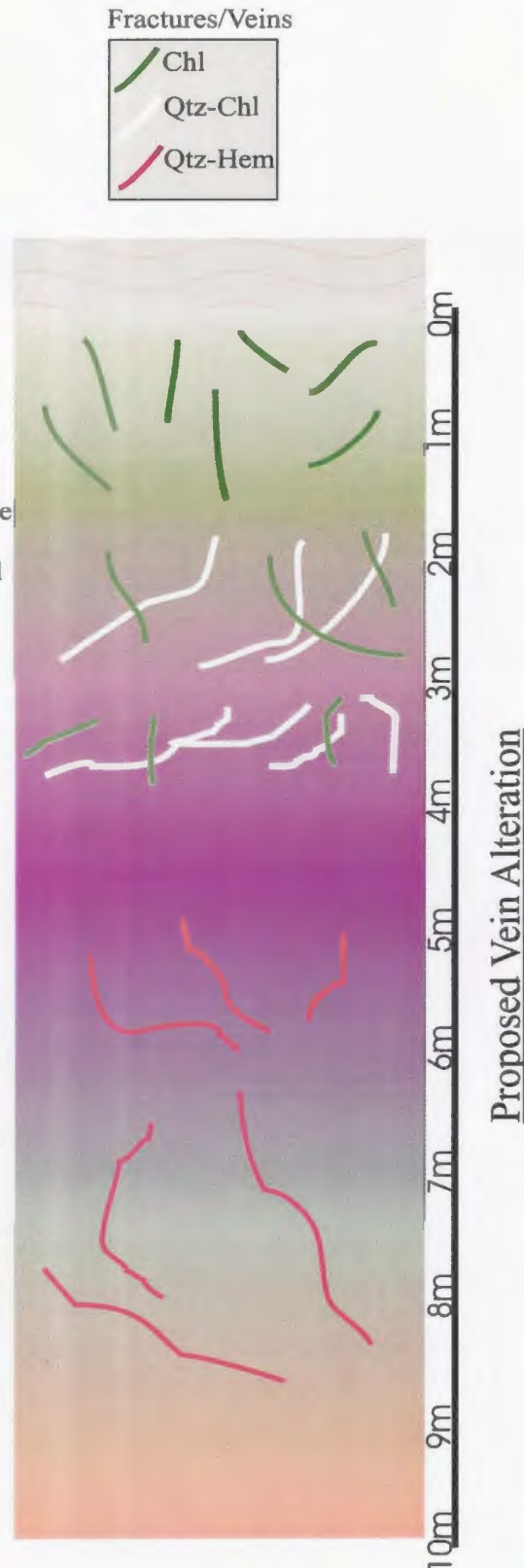
Figure 5-6: Proposed vein alteration for main low-sulphidation vein in exploration trench #3 (Steep Nap prospect).

Plate 5-1: Thin section chip and associated photomicrograph of sample GS-03-101A, collected at vein margin (Trench #3). The thin section chip is 2.7cm wide; photomicrograph in XPL, FOV ~4mm. Note the high birefringence mineral in upper left hand corner of photomicrograph and abundance of silica in the matrix of the chip sample.
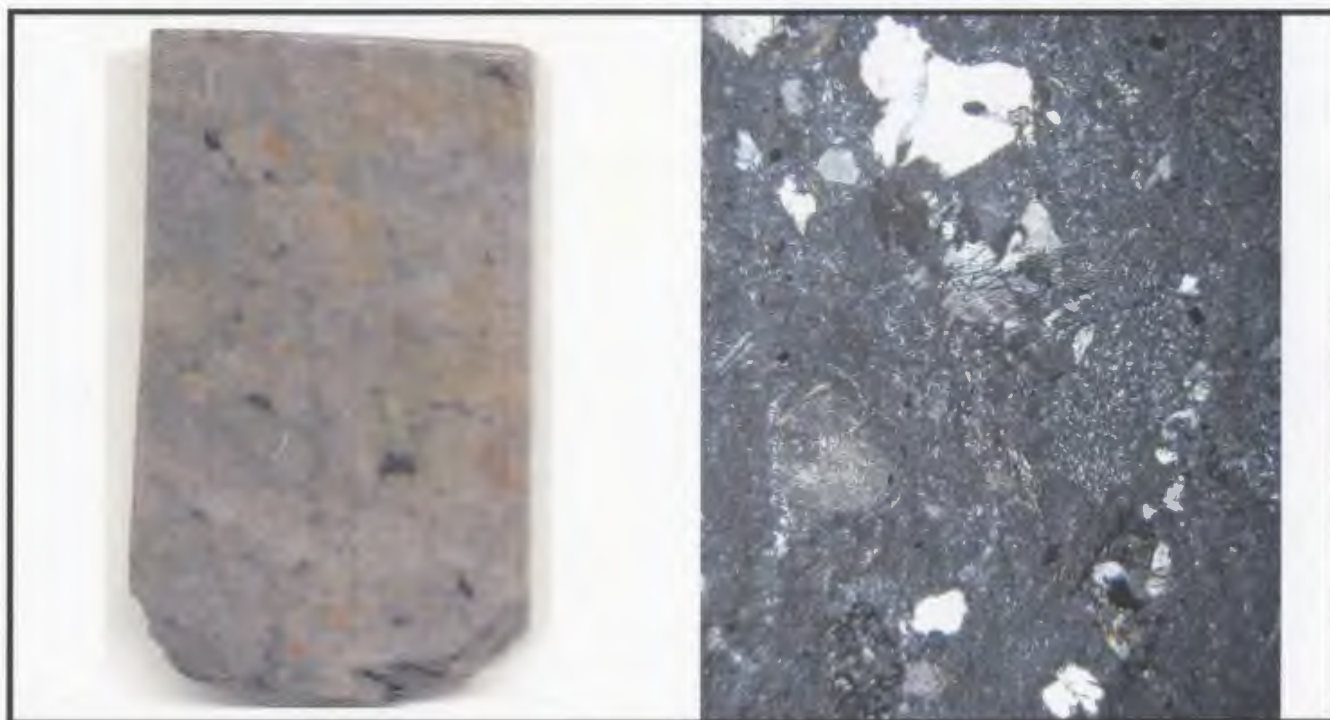
Plate 5-2: Thin section chip and associated photomicrograph of sample GS-03-101B, collected 0.5m from vein margin (Trench #3). The thin section chip is 2.2cm wide; photomicrograph in XPL, FOV ~4mm. Note increase in high birefringence clay mineral(s) in photomicrograph.
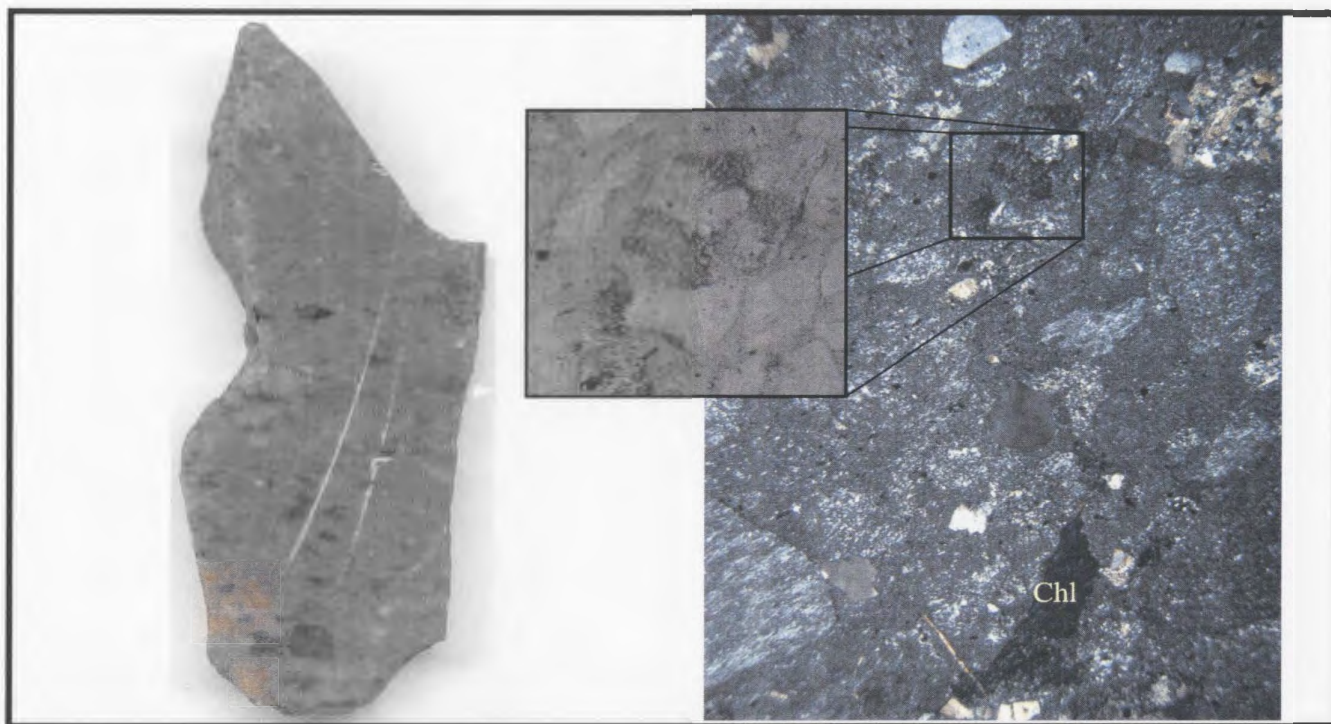
Plate 5-3: Thin section chip and associated photomicrograph of sample GS-03-101C, collected 2.0m from vein margin (Trench #3). The thin section chip is 2.3cm wide; photomicrograph in XPL, FOV ~4mm. Note decrease in abundance of potassic altered clasts in matrix of thin section chip. Insert of PPL enlargement of unusual silica texture from a clast within the matrix (Chl = chlorite).
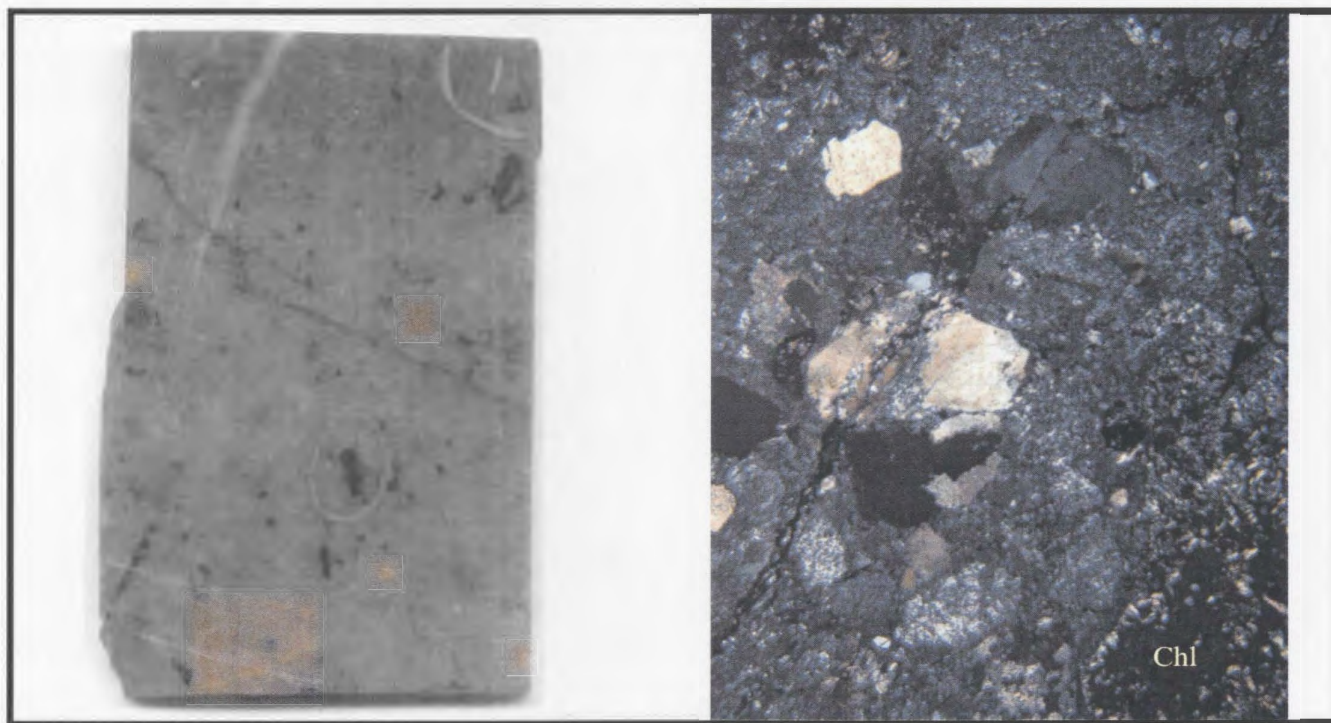
Plate 5-4: Thin section chip and associated photomicrograph of sample GS-03-101D, collected 3.0m from vein margin (Trench #3). The thin section chip is 2.3cm wide; photomicrograph in XPL, FOV ~4mm (Chl = chlorite). Chlorite in bottom right hand corner of photomicrograph may represent selective replacement of clasts.

(insert on photomicrograph). PIMA analysis from this region could not identify any clay minerals due to high background silica. The first evidence of hematite halos, as described by Mills (1998), are observed at 3.0m from the vein. At this point potassic-altered material is rare within the matrix (Plate 5-4). Again quartz-chlorite veins and chlorite filled fractures frequently crosscut the host rock. PIMA data from the hand sample is dominated by silica, with minor amounts of chlorite and hematite. Hematite haloes are well developed at 4.0m from the vein, and at this point, the matrix is pale pink and hosts abundant potassic-altered clasts (Plate 5-5). Quartz-chlorite veining and chlorite filled fractures are less frequent. PIMA analysis at 4.0m from the vein could not identify any clay minerals due to high background silica.

At 5.0m from the vein margin, minor occurrences of quartz-hematite veins are noted. This area contains abundant potassic-altered clasts within the matrix (Plate 5-6) and contains too much background silica to identify any clay minerals in the PIMA analysis. No outcrop is exposed from 5.5-8.0m. A pale green to pale pink matrix is predominant at 8.0m from the vein, along with selective replacement of clasts within the matrix by a dark green mineral; rare potassic-altered clasts are observed within the matrix (Plate 5-7). Quartz-hematite veins are still present, but hematite haloes are no longer present at 8.0m from the vein margin. PIMA data from this location identifies illite and possibly some sericite and smectite. At 10m from the vein margin the matrix is again pale pink in coloration and hosts abundant potassic-altered clasts (Plate 5-8). Locally, quartz-hematite veins and frequent hematite filled fractures crosscut the lapilli tuff. The main
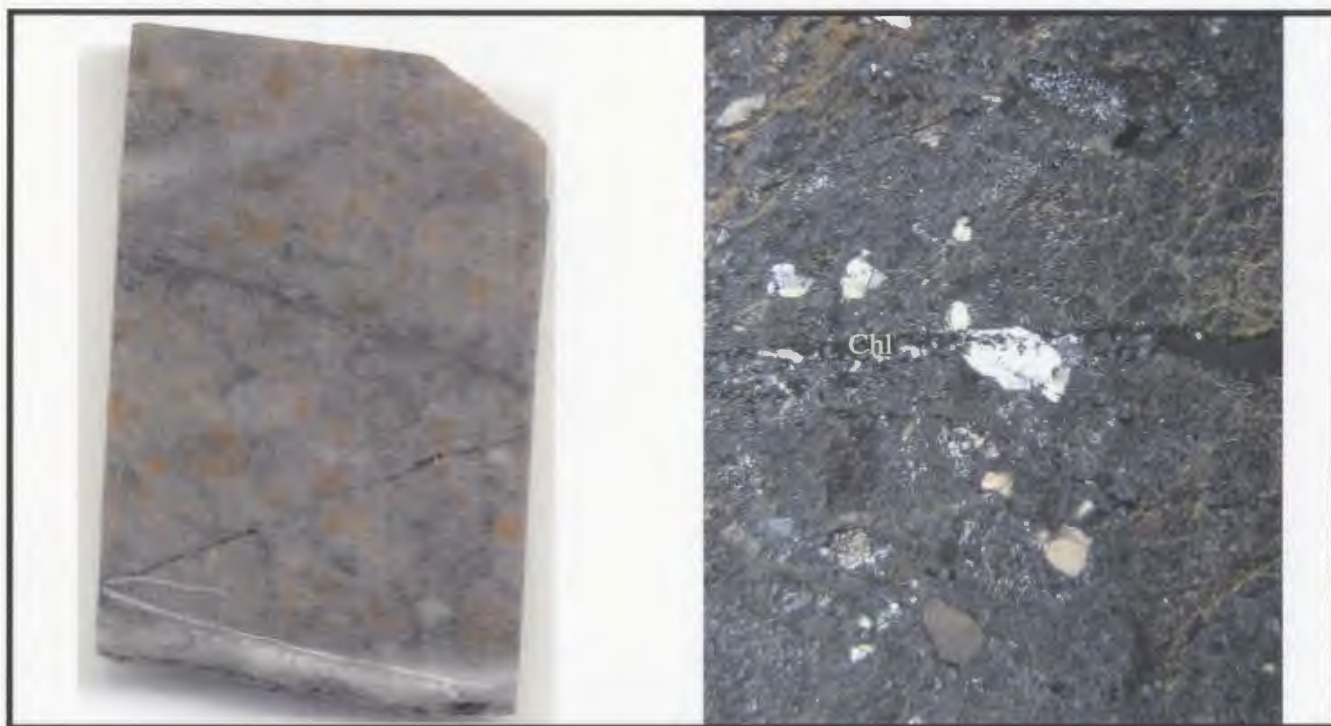
Plate 5-5: Thin section chip and associated photomicrograph of sample GS-03-101E, collected 4.0m from vein margin (Trench #3). The thin section chip is 2.3cm wide; photomicrograph in XPL, FOV ~4mm (Chl = chlorite). Note abundance of high birefringence mineral(s).
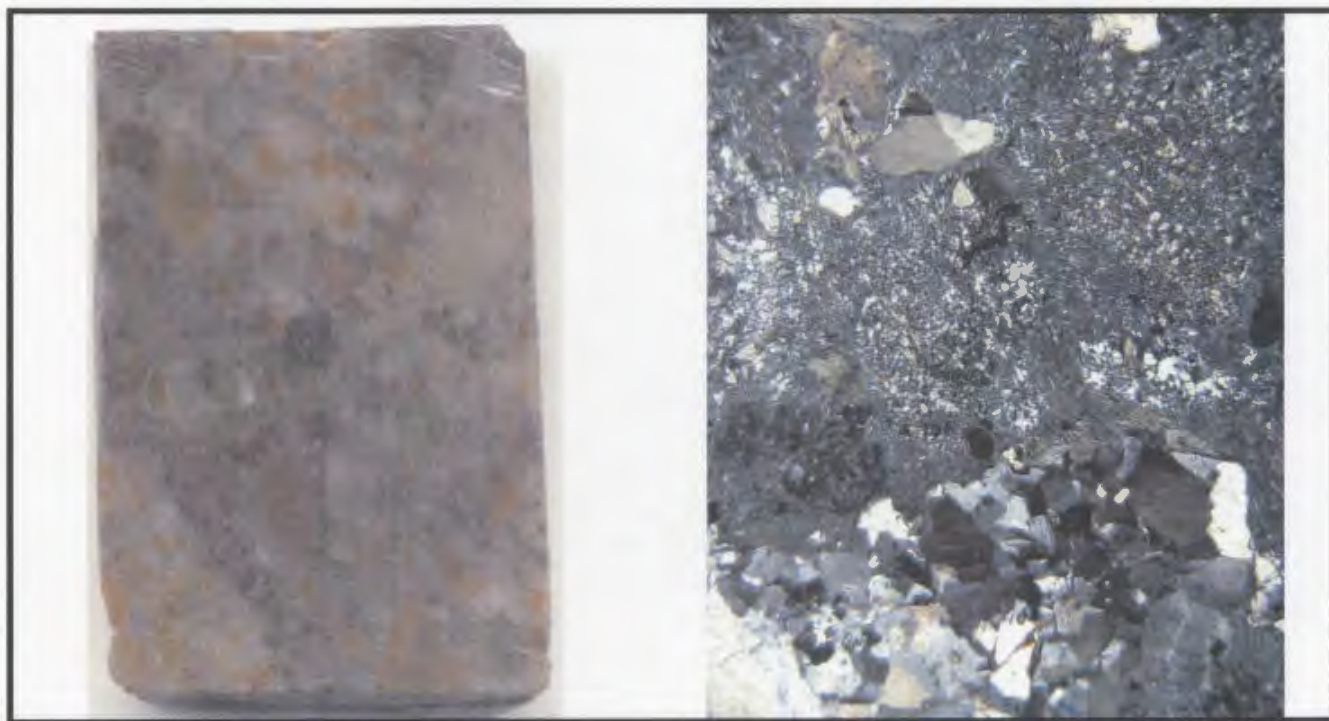
Plate 5-6: Thin section chip and associated photomicrograph of sample GS-03-101F, collected 5.0m from vein margin (Trench #3). The thin section chip is 2.3cm wide; photomicrograph in XPL, FOV ~4mm.

237
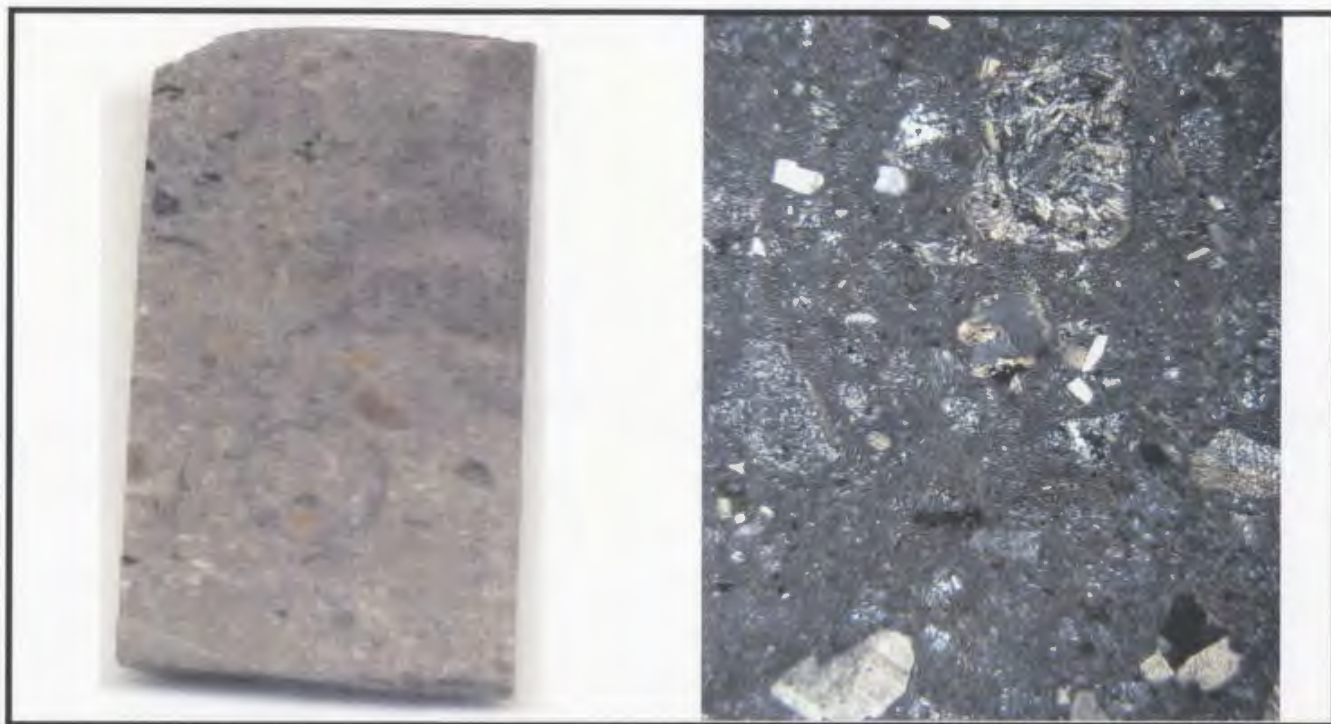
Plate 5-7: Thin section chip and associated photomicrograph of sample GS-03-101G, collected 8.0m from vein margin (Trench #3). The thin section chip is 2.1cm wide; photomicrograph in XPL, FOV ~4mm. Note primary textures in clasts are relatively unaffected by alteration.
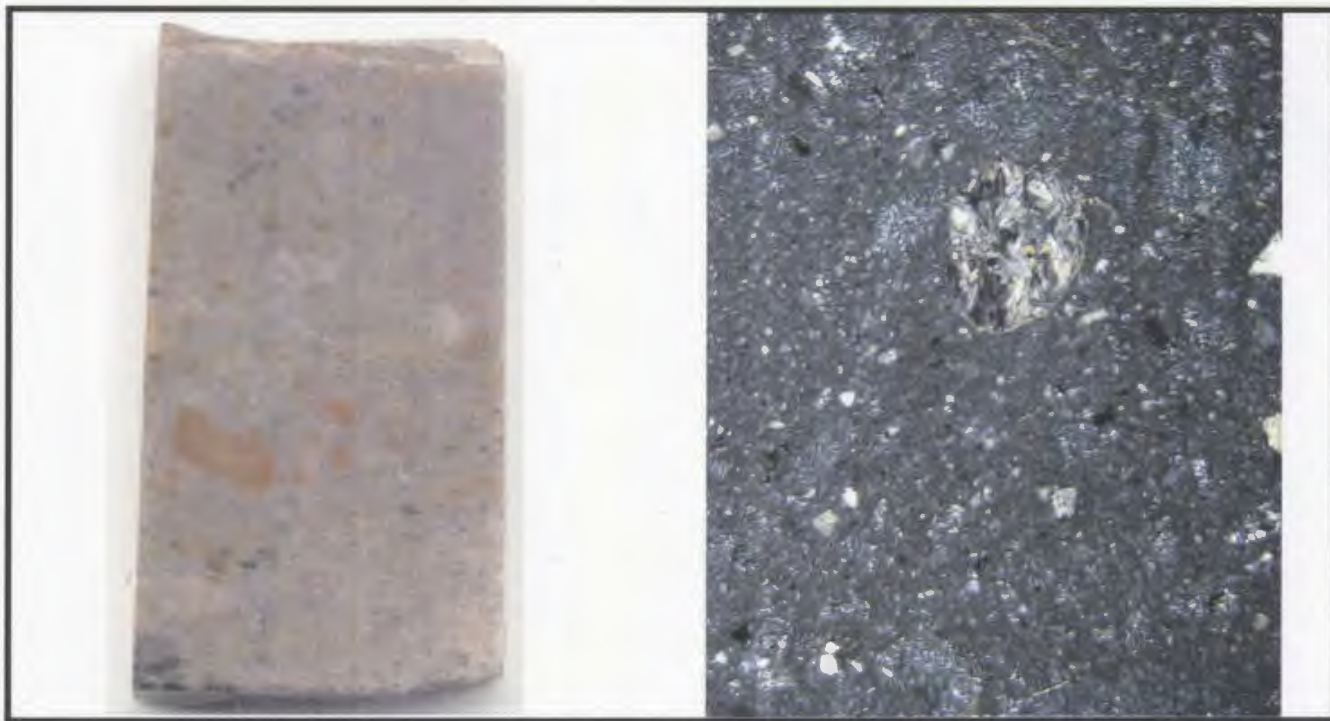
Plate 5-8: Thin section chip and associated photomicrograph of sample GS-03-101H, collected 10m from vein margin (Trench #3). The thin section chip is 2.2cm wide; photomicrograph in XPL, FOV ~4mm. Note primary textures in clasts are relatively unaffected by alteration.

two alteration minerals dominating this area, as identified with PIMA, are illite and hematite.

5.3 THIN SECTION ANALYSIS OF LOW-SULPHIDATION VEINS FROM THE BERGS PROSPECT

A detailed examination of vein textures from the Steep Nap prospect has been previously carried out by Mills (1998). The following discussion is a brief description of epithermal vein textures from the Bergs prospect. Textures observed within this area closely resemble those noted in the adjacent Steep Nap prospect. One exception is the abundance of hematite-dusted (orange) adularia, which appears to be confined to the region of the Steep Nap prospect. Recent feldspar staining of hand samples from the Bergs prospect has identified the occurrence of white adularia (Sparkes *et al.*, 2004). The examination of several thin sections courtesy of Rubicon Minerals Corporation shows a distinct correlation between gold grade and the abundance of epithermal textures. As displayed in Figures 5-7 to 5-10 the samples with more abundant colloform-crustiform banding are also associated with higher gold grades. In the following figures, thin sections were scanned in order to produce schematic drawings of vein textures. Photomicrographs of these textures are superimposed on the schematic drawings. The base of the drawings is shown as mosaic textured quartz, this is only a representation and does not reflect the actual abundance of this texture although it is the predominant texture in most of the thin sections. The dark to black patches within Figures 5-7 to 5-10 represent areas of hematite, which is intergrown with silica in the low-sulphidation veins.

The following discussion refers to common low-sulphidation vein textures as reported in Dong *et al.* (1995).

Sample 20856 is taken from a sample containing 9.6g/t gold (B. Sparkes, 2003). This section displays an abundance of hematite, which is associated with the well-developed crustiform banding and macro-scale colloform banding (Figure 5-7). The section is predominated by mosaic-textured quartz with local development of flamboyant extinction and ghost spheres. Vuggy zones are characterized by open-space infilling with subhedral quartz, hematite and clay minerals. This section contains multiple crustiform bands, which are locally crosscut by late-stage comb-textured quartz. The abundance of low-sulphidation vein textures in comparison with the other thin sections corresponds with the high gold-grade of this sample.

Sample 20857 contains a much lower gold-grade (607 ppb Au; B. Sparkes, 2003) in comparison to sample 20856 and displays a marked decrease in low-sulphidation-related textures as is evident in Figure 5-8. This section contains local development of feathery textured quartz around the terminations of comb-textured quartz crystals, as well as flamboyant extinctions. As evident from the photomicrograph in Figure 5-8 this sample contains parallel oriented quartz, which may represent a variation of parallel bladed quartz (Dong *et al.*, 1995). Also noted within this section are moderate amounts of chlorite. The chlorite appears to be late-stage, infilling open spaces and fractures. This sample again contains frequent hematite and only minor chalcedonic silica.

Sample 20860 represents a complicated section containing multiple generations of veining. The abundance of low-sulphidation-related textures again corresponds to higher
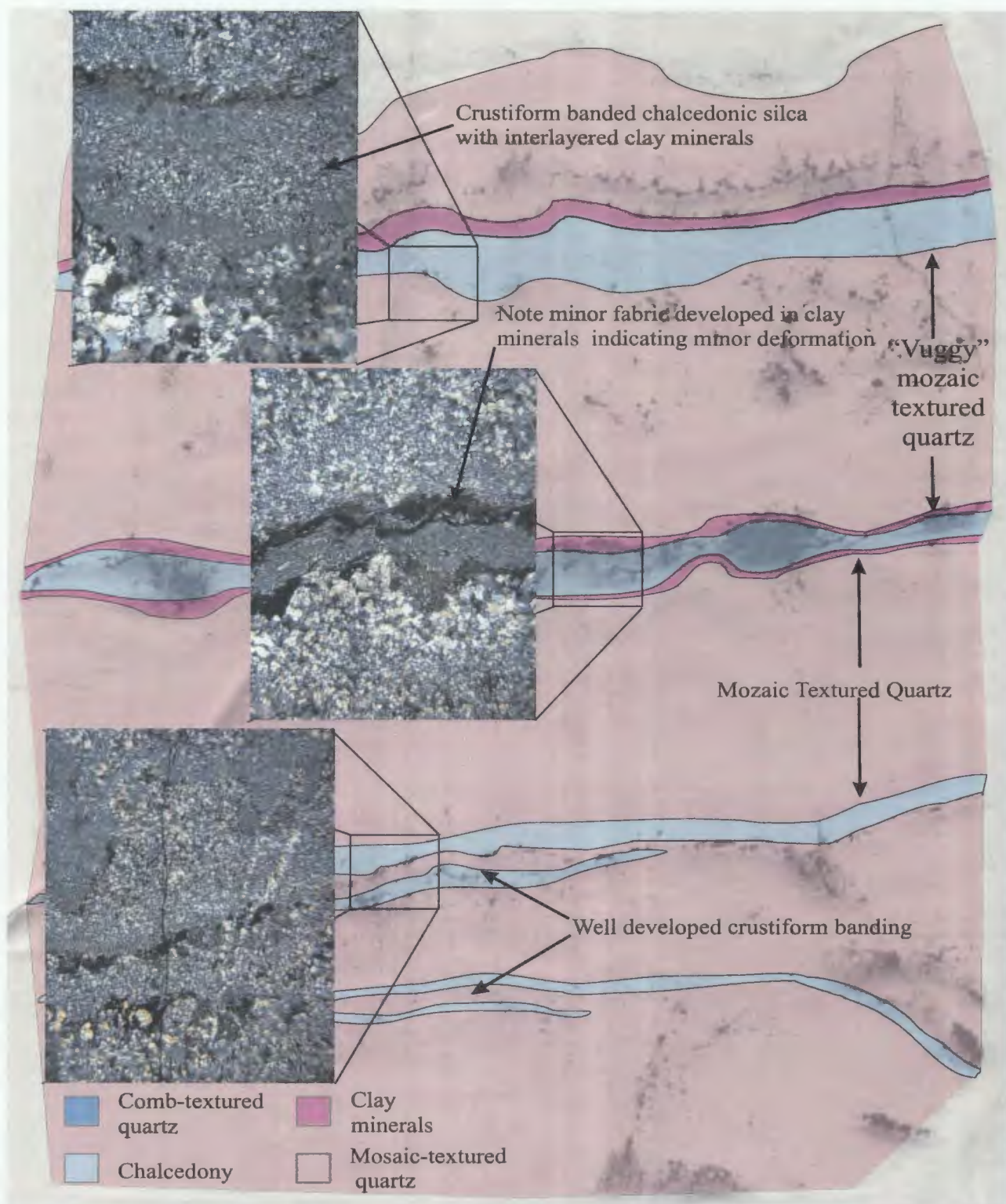
Figure 5-7: Schematic drawing of thin section 20856. Section is 33 x 50mm. Note photomicrographs displaying well-developed crustiform banding and chalcedonic silica (XPL, FOV ~3mm; thin section courtesy of Rubicon Minerals Corporation).
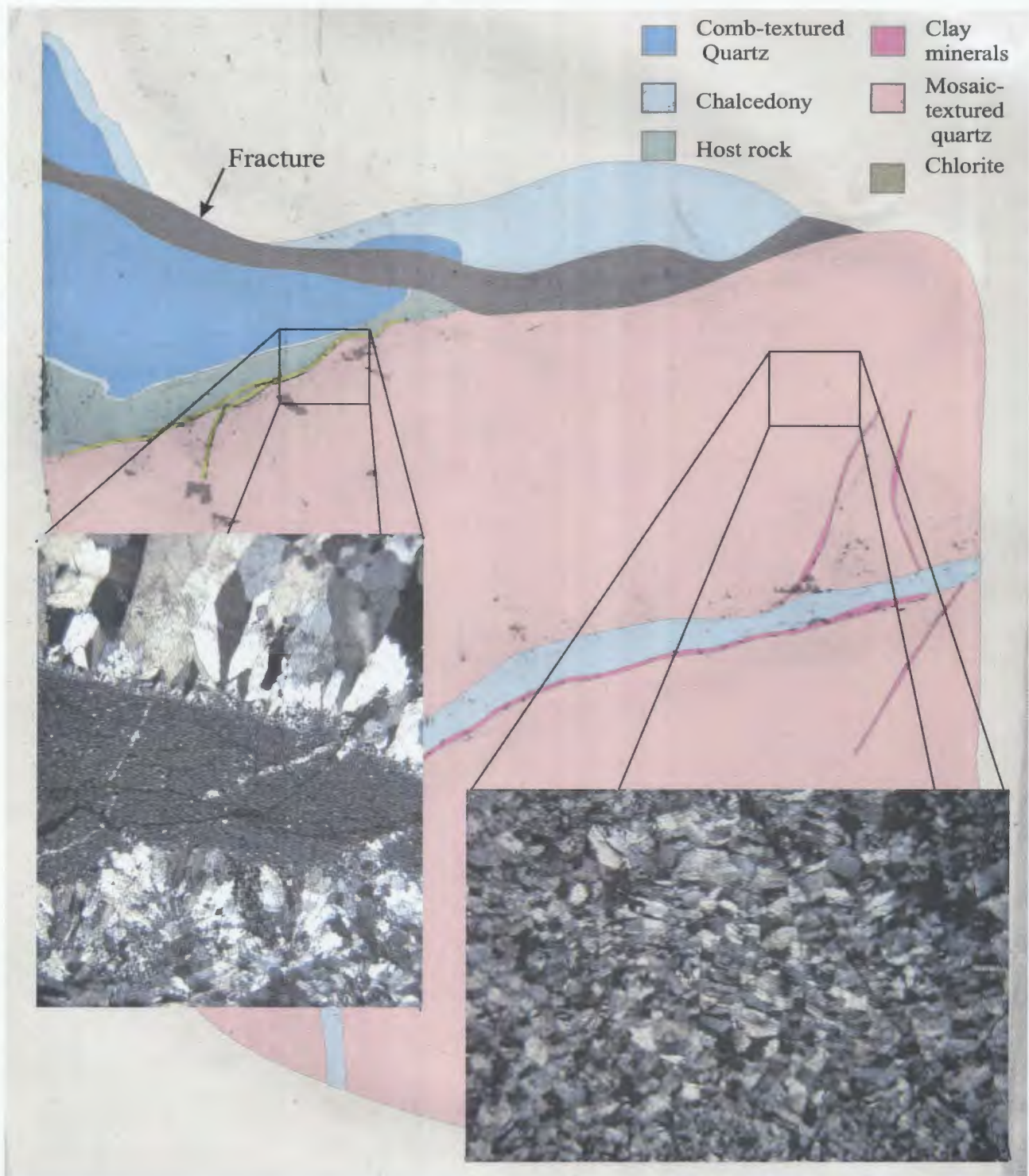
Figure 5-8: Schematic drawing of thin section 20857. Section is 29 x 40mm. Note photomicrographs displaying well-developed comb-textured quartz (left-hand photo) and possible parallel bladed quartz (right-hand photo; XPL, FOV ~3mm; thin section courtesy of Rubicon Minerals Corporation).

gold-grades within the sample (5.2 g/t Au; B. Sparkes, 2003). This section is noted to contain well-developed micro-scale colloform banding, which is composed of intergrown quartz and clay mineral(s). The section also contains well-developed comb-textured quartz with flamboyant extinctions. One area of the thin section appears to contain relic pesudo-bladed calcite in plane-polarized light (PPL), however there is no indication of this texture in cross-polarized light (XPL). In the lower section of Figure 5-9, the hematite-rich comb-textured quartz region contains well-developed botryoidal hematite.

Sample 20868 contains several distinct zones of chalcedonic silica along with the local development of flamboyant extinctions (Figure 5-10). This sample has a somewhat lower gold value (2.6 g/t Au; B. Sparkes, 2003), however the low-sulphidation vein textures are still more abundant than in sample 20857. In one location within this thin section an area containing a high relief, hematite-dusted mineral was identified. This mineral resembles the orange adularia from Steep Nap, however no distinctive rhomb-shapes could be identified.

The thin sections discussed above display similar textures to those described at Steep Nap by Mills (1998). It should be noted that this is not a detailed examination of the Bergs prospect and only represents a brief overview for comparison purposes. As mentioned previously, K-feldspar staining of samples from the Bergs area has identified the presence of white adularia; however as shown in the thin sections, hematite-dusted orange adularia does not appear to be present, despite the abundance of hematite within the veins at the Bergs prospect.

243
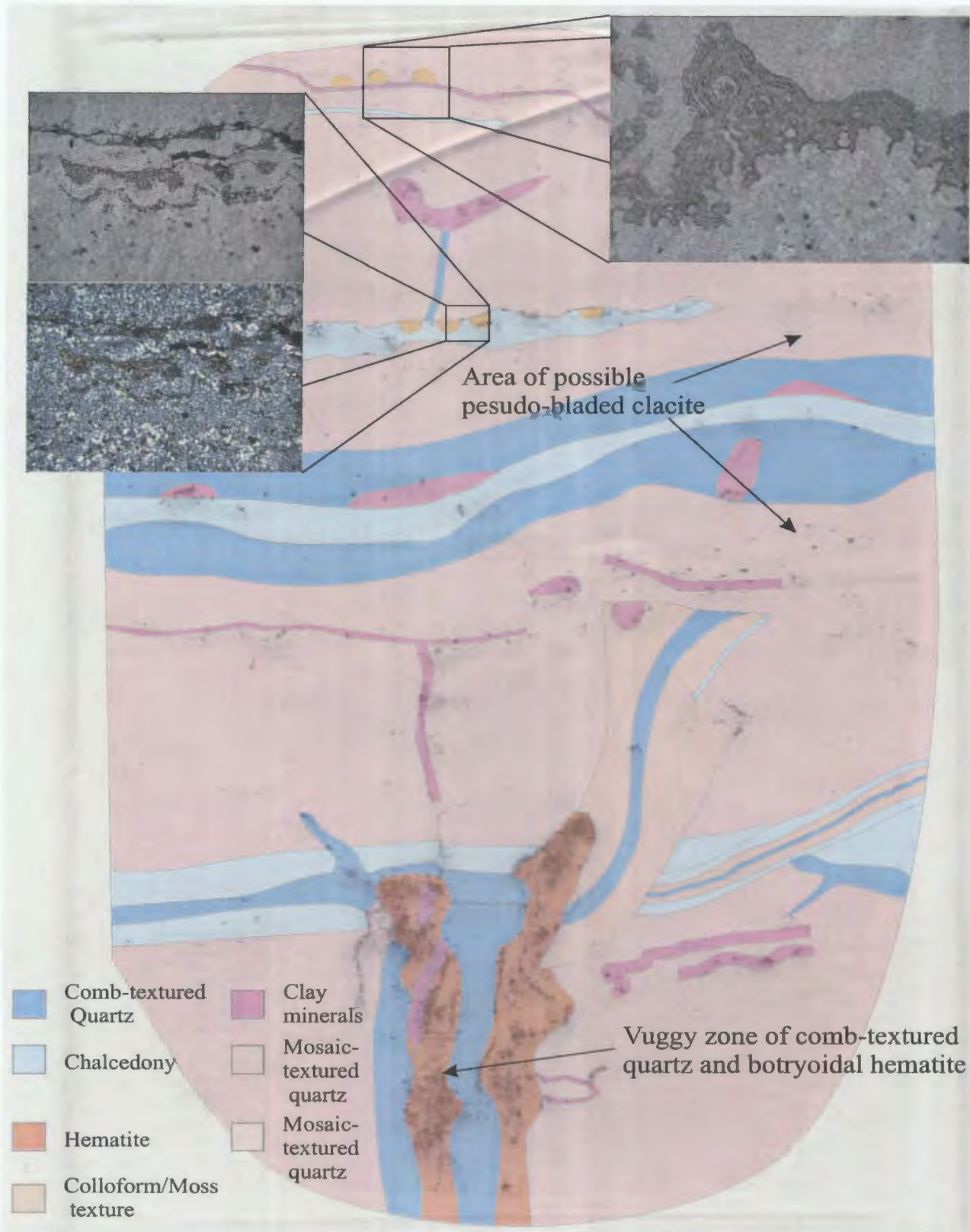
Figure 5-9: Schematic drawing of thin section 20860. Section is 33 x 53mm. Note photomicrographs displaying well-developed colloform textures (left-hand upper photo, PPL; FOV ~1mm, left-hand lower photo, XPL; FOV ~1mm; right-hand photo, PPL; FOV ~3 mm; thin section courtesy of Rubicon Minerals Corporation).

244
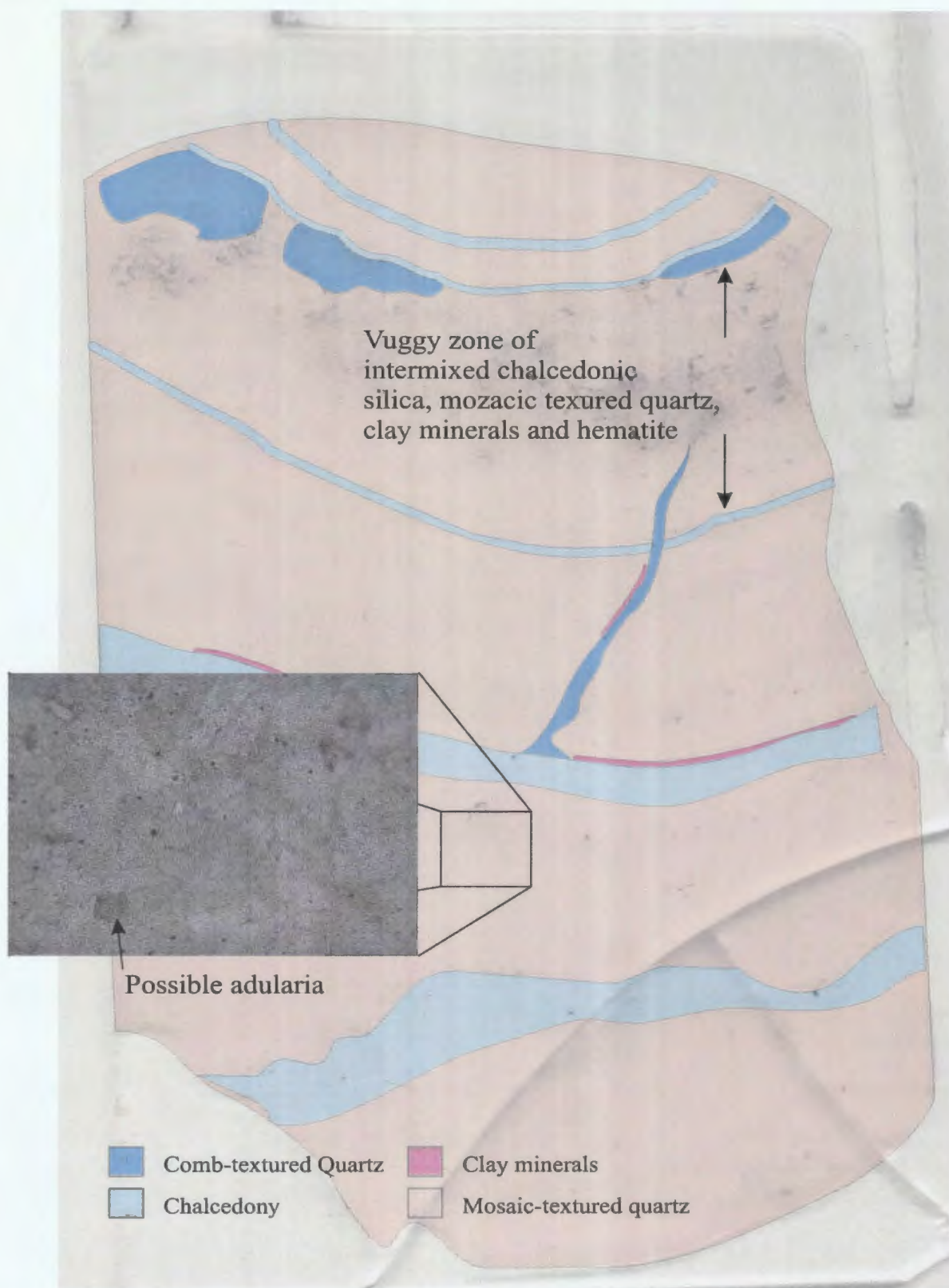
Figure 5-10: Schematic drawing of thin section 20868. Section is 30 x 42mm. Note photomicrograph displaying possible adularia (PPL, FOV ~3mm; thin section courtesy of Rubicon Minerals Corporation).

245

5.4 OBSERVED FIELD RELATIONSHIPS AFFECTING AND/OR RELATED TO LOW-SULPHIDATION VEINING AND ASSOCIATED BRECCIA DEVELOPMENT

The low-sulphidation veins within the current study area are hosted by rocks as old as pre-625 Ma and as young as ca. 582 Ma. New geochronological data combined with observed field relationships bracket the age of the low-sulphidation system between 586 Ma and the base of the overlying Paleozoic cover (Plate 5-9). No evidence was found that would suggest low-sulphidation veins affect the sedimentary rocks of the Wych Hazel Pond Complex (WHPC). However, coarse-grained red sandstones of the lower WHPC contain locally developed silica flooding immediately adjacent to a fault which separates low-sulphidation vein-bearing lapilli tuff (WMVS) from the lower WHPC at the Steep Nap prospect. An assay taken from the silica-flooded sedimentary rock did not contain anomalous gold. It is unknown whether the silica within the sedimentary rock is related to the low-sulphidation system or if it is just the result of late fluid flow along the structure. Basal conglomerates of the WHPC both immediately east of the Steep Nap prospect and within the Oval Pit mine were examined for fragments of low-sulphidation vein material, however no such material was found. One outcrop, which is located several meters stratigraphically above the silica-flooded sediment at Steep Nap, was found to contain subangular cobbles of silica altered material. It is uncertain whether this altered detritus is related to the high- or low-sulphidation system (Plate 5-10).

The low-sulphidation veins at the Bergs and Steep Nap prospects are also accompanied by hematite-rich breccias; the formation of which predominantly post-dates

Plate 5-9: Low-sulphidation vein unconformably overlain by Paleozoic cover (Photo courtesy of Sean O'Brien, Department of Natural Resources, Geological Survey).

Plate 5-10: Lower Wych Hazel Pond Complex (Unit 19a) containing silica-altered detritus (Steep Nap prospect).

vein development as is evident in Plate 5-11 (B. Sparkes, 2002). Breccias commonly contain fragments of low-sulphidation vein material along with rare fragments of underlying lithologies as indicted by Plate 5-12. The vein in Plate-5-11 is hosted within the polymict lapilli tuff at Steep Nap, however the hematite-rich breccias contain fragments of flow-banded rhyolite that is interpreted to underlie the tuff unit. Breccias similar to those in Plate 5-11 also occur in regions were low-sulphidation veins are not observed. In the area of Farmer's Field, gold-bearing hematite-rich breccia of an unknown affinity crosscut flow-banded rhyolite on the margin of the advanced argillic alteration (Plate 5-13). This breccia occurs approximately 500m from the core of the high-sulphidation system and may represent low-sulphidation related breccias overprinting high-sulphidation related alteration. A second example of a possible low-sulphidation related event overprinting high-sulphidation alteration occurs southeast of Mine Hill at the southern end of Johnnies Pond. In this area weakly crustiform-banded, chalcedonic silica veinlets of an unknown affinity crosscut advanced argillic alteration (Plate 5-14). These two examples may provide supporting evidence that the low-sulphidation system actually post-dates the high-sulphidation alteration.

Field evidence shows that the low-sulphidation veins are affected by variable amounts of post-mineralization deformation. Veins hosted within mafic volcanic rock of the MVS at the Bergs prospect are truncated by a NNW-SSE trending shear zone (Plate 5-15), which is later overlain by relatively undeformed basal conglomerate of Lower Middle Cambrian age (Plate 5-16). Plate 5-16 also demonstrates that the deformation within the region is pre-Lower Middle Cambrian in age. This structure is also intersected

248

Plate 5-11: Hematite-rich, matrix supported breccia sampling a colloform-crustiform, chalcedonic silica vein (Steep Nap; Trench #3; Photo courtesy of Sean O'Brien, Department of Natural Resources, Geological Survey).

Plate 5-12: Same hematite-rich breccia as in Plate 5-11. Note the flow-banded rhyolite fragments contained within the breccia (Photo courtesy of Sean O'Brien, Department of Natural Resources, Geological Survey).

249

Plate 5-13: Hematite-rich breccia of an unknown affinity, crosscutting margin of advanced argillic alteration (Farmer's Field; Photo courtesy of Sean O'Brien, Department of Natural Resources, GeologicalSurvey).

Plate 5-14: Weakly banded chalcedonic silica vein of an unknown affinity crosscutting advanced argillic alteration (area SE of Mine Hill; Photo courtesy of Sean O'Brien, Department of Natural Resources, Geological Survey).
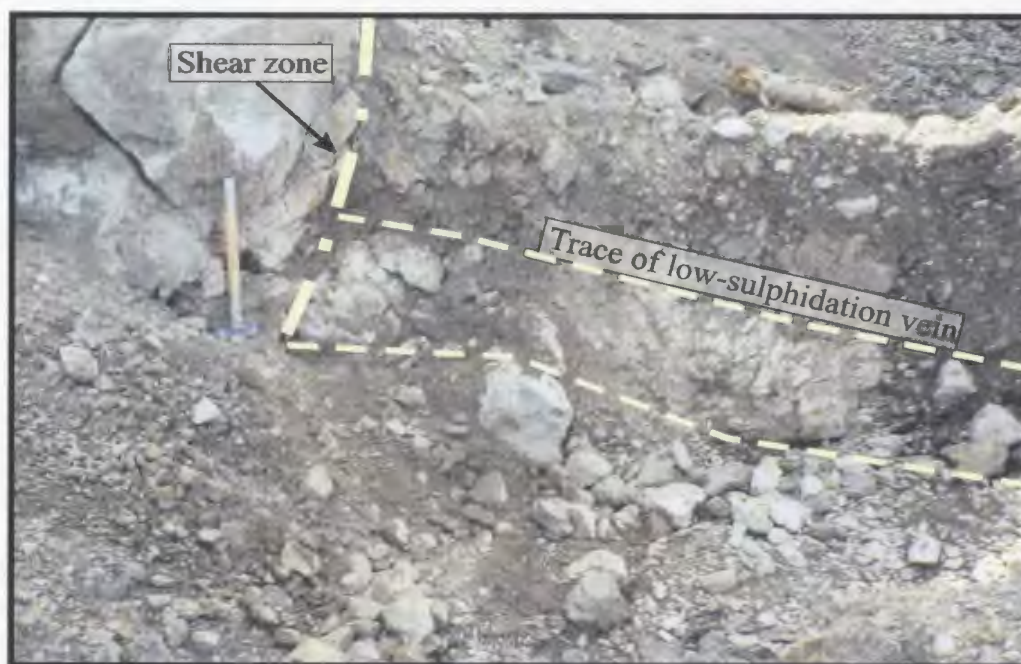
Plate 5-15: Low-sulphidation vein hosted within mafic volcanic rocks of the
Manuels Volcanic Suite; vein is truncated by a shear zone (Bergs
prospect).
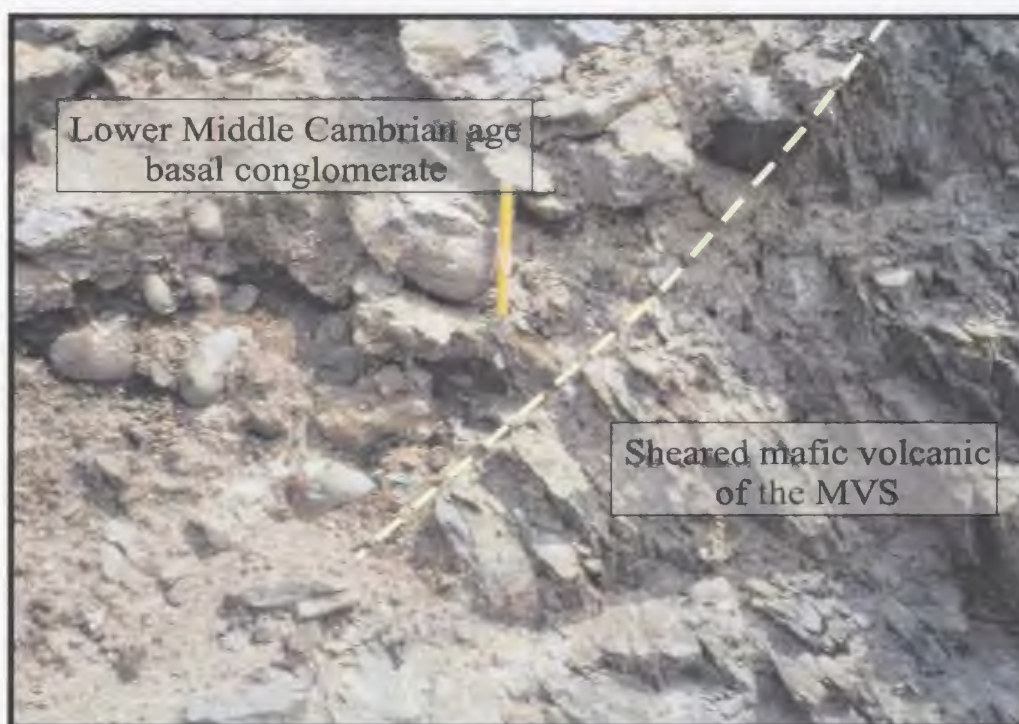
Plate 5-16: Same shear zone as in Plate 5-15, viewed ~20m N of point where shear
zone truncates low-sulphidation vein. Note shear zone is unconformably
overlain by undeformed Lower Middle Cambrian age basal
conglomerate.

in drill core from the Bergs prospect and again marks the termination point of low-sulphidation veining (B. Sparkes, 2003). At the Steep Nap prospect the main low-sulphidation vein is also affected by post-mineralization deformation (Plate 5-17; B. Sparkes, 2002, 2003, 2005). In this region meter-scale veining exposed in an exploration trench displays a sinistral offset along a post-mineralization fault. This is also evident in vein exposures along the ridge south of the main Steep Nap showing (Plate 5-18).

Across the down-dropped block of the lower WHPC (refer to Map 1; back pocket), weakly banded chalcedonic silica and quartz-hematite veins continue along strike from the Steep Nap showing. In this region low-sulphidation veins are observed to be syn-formational with quartz–K-feldspar tension gashes (Plate 5-19). These low-sulphidation-style veins crosscut deformation-related quartz–K-feldspar tension gashes and are deformed along the same structure.

From the above-mentioned field observations it is evident that the low-sulphidation system is affected by post-mineralization deformation. The low-sulphidation system may or may not postdate the high-sulphidation system, however the existing data is interpreted to represent low-sulphidation features overprinting high-sulphidation-style alteration. The relationship between the low-sulphidation veins and the overlying WHPC remains unclear, but the lack of detritus within the sedimentary rocks combined with the fact that no veins are observed crosscutting the WHPC suggests that the veins formed after the high-sulphidation alteration and prior to deposition of the WHPC.

Plate 5-17: N-S trending low-sulphidation vein offset by an E-W trending
fault (Steep Nap prospect; Trench #4).

Plate 5-18: Offset in a banded chalcedonic silica vein observed on the ridge south
of the Steep Nap prospect
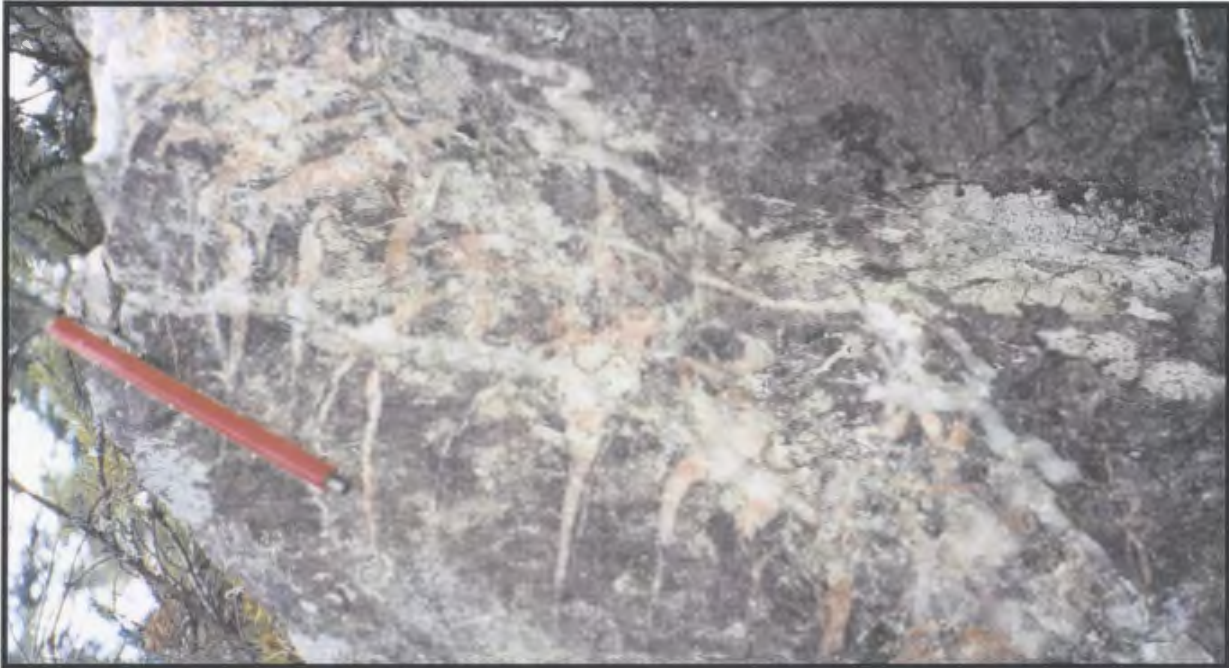
Plate 5-19: Chalcedonic silica and quartz-hematite veins crosscutting deformation related quartz-K-feldspar tension gashes. Note the low-sulphidation veins are also deformed.

5.5 SUMMARY

The various studies carried out on exposures of low-sulphidation veins provide several tools for vectoring in the region of low-sulphidation vein development. Detailed measurement of veins can provide useful data in the construction of elevation models for epithermal systems and for determining the relative location within the system at which the measurements were taken. For instance, vein measurements at outcrop #141 indicates an increase in vein density towards the west and also provides the predominant trend of veining at that location. Had the bonanza-grade vein not been exposed the measured data would still have indicated further exploration west of the measured line. The data collected within the Farmer's Field region could be interpreted to represent comparatively high levels within the system as indicated by the relatively low levels of percent extension. However it should also be noted that the same percentage extension could also be developed on the margin of a larger vein system at the same elevation, but no evidence of such veining is known within the Farmer's Field region. As mentioned above in the text, the datasets presented herein are preliminary and require further work to develop a more robust model for the vein systems.

As indicated from the alteration study, changes within the host rock can be recognized within the vicinity of vein development such as the mobilization of hematite, and the increased abundance of chlorite. These features involve very common minerals that could also be produced by many other events. Data supplied by PIMA analyses proves more useful in identifying less common minerals such as illite and smectite, and when combined with detailed field mapping, provides valuable information in vectoring

towards areas of low-sulphidation veining. It should be noted that this alteration analysis is only representative of one area; several more sections in various areas would be needed in order to generate a model of the vein alteration applicable across the whole system.

Observed field relationships conclusively demonstrate that the veins are affected by post-mineralization deformation, presumably of Late Neoproterozoic age. There is also some indication that the veins are associated with a syn-deformational event as indicated by banded chalcedonic veins crosscutting quartz–K-feldspar tension gashes and then being deformed along the same zone of structural weakness. The exposed field relationships between the high- and low-sulphidation systems are more ambiguous than the deformation relationships. Nowhere has it been observed conclusively that low-sulphidation-related features overprint elements of the high-sulphidation system. However, several examples of hematite-rich breccias and banded chalcedonic silica veins of possible low-sulphidation affinity are seen to crosscutting advanced argillic alteration associated with the development of the high-sulphidation system. So, from these examples, it could be interpreted that the low-sulphidation system is younger.

CHAPTER 6:

TECTONIC DEVELOPMENT OF THE NORTHERN PORTION OF

THE EASTERN AVALON HIGH-ALUMINA BELT

6.1 INTRODUCTION

This chapter provides a visual summary of the detailed field mapping and the known geochronology of the area covered during this study. Figures 6-2 to 6-3 represent a series of four E-W cross-sections through the study area. These cross-sections are vertically exaggerated in order to include all of the necessary details (approximate exaggeration is 2.4:1 for vertical versus horizontal). The cross-sections contain both known and possible occurrences of low-sulphidation vein development. All four sections are combined to show the spatial relationship between the known occurrences of low-sulphidation-style veins in Figure 6-4. Figure 6-5 presents a schematic summary of the geological and tectonic development of the eastern margin of the Holyrood Horst (this is an interpretive representation of the author's view on the formation of the northern portion of the high-alumina belt).

6.2 CROSS-SECTIONS OF THE NORTHERN HIGH-ALUMINA BELT

The following discussion is based on a series of four E-W cross-sections constructed for the northern portion of the high-alumina belt. These cross-sections have an approximate spacing of 1.25km, and intersect the three main occurrences of low-sulphidation veins and/or veins interpreted to have a low-sulphidation affinity. Figure 6-1
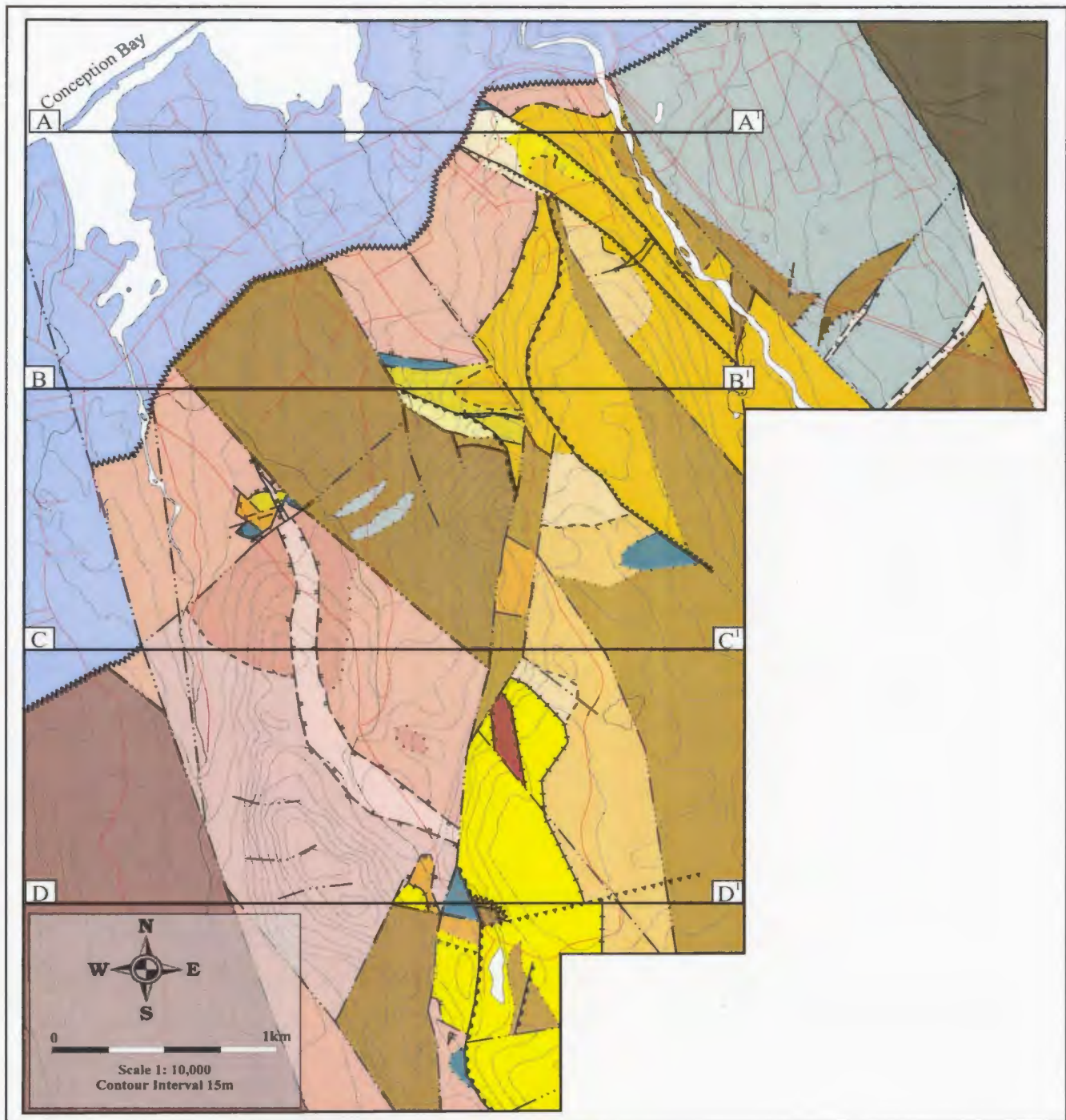
Figure 6-1: Simplified version of Map 1. Transects A-A¹, B-B¹, C-C¹ and D-D¹ are illustrated in Figures 6-2 and 6-3, respectively.

Legend
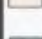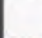
Cambrian
(24) Adeyton and Harcourt Groups (undivided)
- red and black siltstone with interbedded grey limestone; locally massive, poorly sorted boulder conglomerate at base

Late Neoproterozic
(23) Conception Group
- unseparated marine siliciclastic sedimentary rocks

Wych Hazel Pond Complex
(22) Fowlers Road Porphyry
-plagioclase-phyric, pale grey to green aphanitic rhyolite; unit associated with local development of a blocky peperite

(20) Amygdaloidal Basalt/Hyaloclastite
-moderately vesicular, locally amygdaloidal and pillowed dark purple basalt; associated with hyaloclastite containing irregularly shaped, dark purple basalt fragments in a dark grey-green, fine-grained matrix

(19b) Upper Wych Hazel Pond Complex
-thin- to medium-parallel-bedded, moderately to strongly siliceous, pale to dark green siltstone and interbedded medium- to coarse-grained, subarkosic sandstone; siltstone commonly displays soft sediment deformation

(19a) Lower Wych Hazel Pond Complex
-thin- to medium-bedded red siltstone; locally interbedded with medium- to coarse-grained red sandstone, pebbly conglomerate and pale yellow, chloritic-sericitic, massive pumiceous tuff

Manuels Volcanic Suite
(18) Hematite-Chlorite-rich Hydrothermal Breccia
-matrix supported, hematite-chlorite-rich breccia containing sub-rounded to subangular fragments of silicified rhyolite within a dark purple to green matrix; fragments generally 2-4cm in diameter

(17) Silica-Sericite-Pyrite-Pyrophyllite- Diaspore-Rutile Alteration
-pale white- to yellow-weathering alteration with varying proportions of silica-sericite-pyrite-pyrophyllite-diaspore-rutile

(16) Sericite-Silica ± Pyrite Alteration
-white- to pale yellow-weathering alteration with patchy pyrite development; alteration associated with prominent shear zones

(15) Mafic Volcanic/Intrusive Rocks
-fine-grained, dark brown- to dark green-weathering, moderate to weakly magnetic, locally amygdaloidal and plagioclase-phyric basalt

(14) Massive, Poorly-Sorted, Lithic-rich, Breccia
-matrix supported breccia containing sub-rounded to angular fragments of low-sulphidation vein material in a poorly sorted hematite-rich matrix

Silica Alteration
-pale white, pervasive silica alteration without pyrophyllite-diaspore-sericite (Bergs area)

(13) Dark Purple, Crystal-bearing, Ash-flow Tuff
-massive crystal-rich tuff, containing pale white mm-scale crystals within a dark purple, hematite-rich groundmass

(12) Grey-Green, Pyritic, Pumiceous, Crystal-bearing Ash-flow Tuff
-massive crystal-rich tuff, containing mm-scale white crystals, and cm-scale dark purple collapsed pumice fragments, in a dark green to grey groundmass; groundmass also contains minor fine-grained disseminated pyrite

(11) Pale Grey-Green, Moderately Porphyritic, Fine Rhyolite
-light grey- to green-weathering rhyolite, mm-scale white feldspar crystal and fine-grained disseminated pyrite in a fine-grained groundmass

(10) Aphanitic, Massive Rhyolite/Polymict Lithic Volcaniclastic Rock
-dark purple-weathering, massive volcanaiclastic containing subangular to sub-rounded fragments; fragments predominantly 5-10cm in diameter but locally up to 50cm

(9) Aphanitic Flow-Banded Rhyolite (Farmer's Field Rhyolite
-dark purple, pale white-weathering aphanitic rhyolite with local development of lithophysae

White Hills Intrusive Suite
(8) Quartz-Feldspar Porphyry
-pale purple-weathering porphyry containing 2-4mm phenocrysts of plagioclase, quartz and K-feldspar within a light purple aphanitic groundmass

Quartz-Feldspar Porphyry/Medium- to Coarse-grained Equigranular Granite
-unseparated quartz-feldspar porphyry/medium- to coarse-grained equigranular granite

(7) Medium- to Coarse-grained Equigranular Granite
-silica-sericite-chlorite-pyrite altered, grey-green- to pale pink-weathering, medium- to coarse-grained, equigranular, quartz-K-feldspar-plagioclase-rich granite

(6) Monzonite
-pale white-weathering monzonite with coarse-grained, pale green plagioclase and fine- to medium-grained chlorite, quartz and K-feldspar; locally contains 2-10cm diameter fine-grained dioritic xenoliths

Holyrood Intrusive Suite
(5) Pink-White-Green Granite
-propylitized granite with a pale pink-white-green-weathering, generally equigranular to quartz-phyric, with sub-equal amounts of plagioclase, K-feldspar and quartz

White Mountain Volcanic Suite
(4) Welded, Fiamme-Bearing Ash-flow Tuff
-dark purple, pale white-weathering tuff containing cm-scale, pale purple collapsed pumice within a pale white groundmass; unit displays well-developed eutaxitic foliation

(3) Massive, Lithic-rich, Polymict, Lapilli Tuff
-dark to pale green or pale pink, matrix supported tuff with sub-rounded to rounded fragments; fragments locally dominated by bright pink, potassic altered material

(2) Aphanitic, Flow-Banded Rhyolite (Manuels River Rhyolite
-purple to grey-green rhyolite with well developed flow banding and rare feldspar-phyric zones; unit is locally spherulitic

(1) Moderately, Feldspar-phyric, Flow-Banded Rhyolite (Minerals Road Rhyolite)
-pale pink to dark purple rhyolite with 2-4mm feldspar crystals within a dark purple, flow banded groundmass; groundmass is locally spherulitic

Symbols

Geological boundary (defined, approximated, assumed, gradational)

Fault (defined, approximated, assumed)

Shear zone (defined, approximated, assumed)

Reverse sense, brittle shear zone (defined and approximate)

Intrusive Contact (define, approximated)

Unconformity

Bedding

Cleavage

Hydrothemal vein

Road

259

is a simplified version of Map 1 and displays the orientation and location of the transect lines. Section A-A[1] (Figure 6-2) provides a cross-section of the Bergs prospect. Within this figure, the unconformable Cambrian succession overlies the dark-purple, crystal-rich ash-flow tuff, which is the main host to the low-sulphidation veins at the Bergs prospect. As mentioned in previous chapters this Cambrian succession contains detritus of low-sulphidation vein material and provides an upper time limit for the formation of these veins.

Fragments of both the crystal tuff and low-sulphidation vein material are contained in the poorly sorted lithic-rich breccia, which is thought to represent a surficial hydrothermal eruption breccia. Other world-wide examples of this type of breccia often displays a cone-like shape and is interpreted to transport material from up to 300m from below the paleosurface (Hedenquist and Henley, 1985). At the Bergs prospect this breccia is known to contain clasts of mineralized vein (up to 7.5g/t Au; O'Brien and Sparkes, 2004), which provides supporting evidence for mineralization at depth. Immediately west of the eruption breccia is a zone of predominantly massive silica-alteration, which locally contains minor disseminated pyrite and anomalous gold.

This zone of alteration is also host to bonanza-grade gold veins (up to 54.3g/t; O'Brien and Sparkes, 2004), which contain chalcedonic silica with white adularia (Sparkes *et al*, 2004). Microscopic gold is observed throughout the bands of chalcedonic silica within the high-grade sample, with the visible gold displaying a nugget effect. These bands of chalcedonic silica are crosscut by hematite-rich breccias, which contain moderate amounts of specular hematite (O'Brien and Sparkes, 2004). Insufficient data
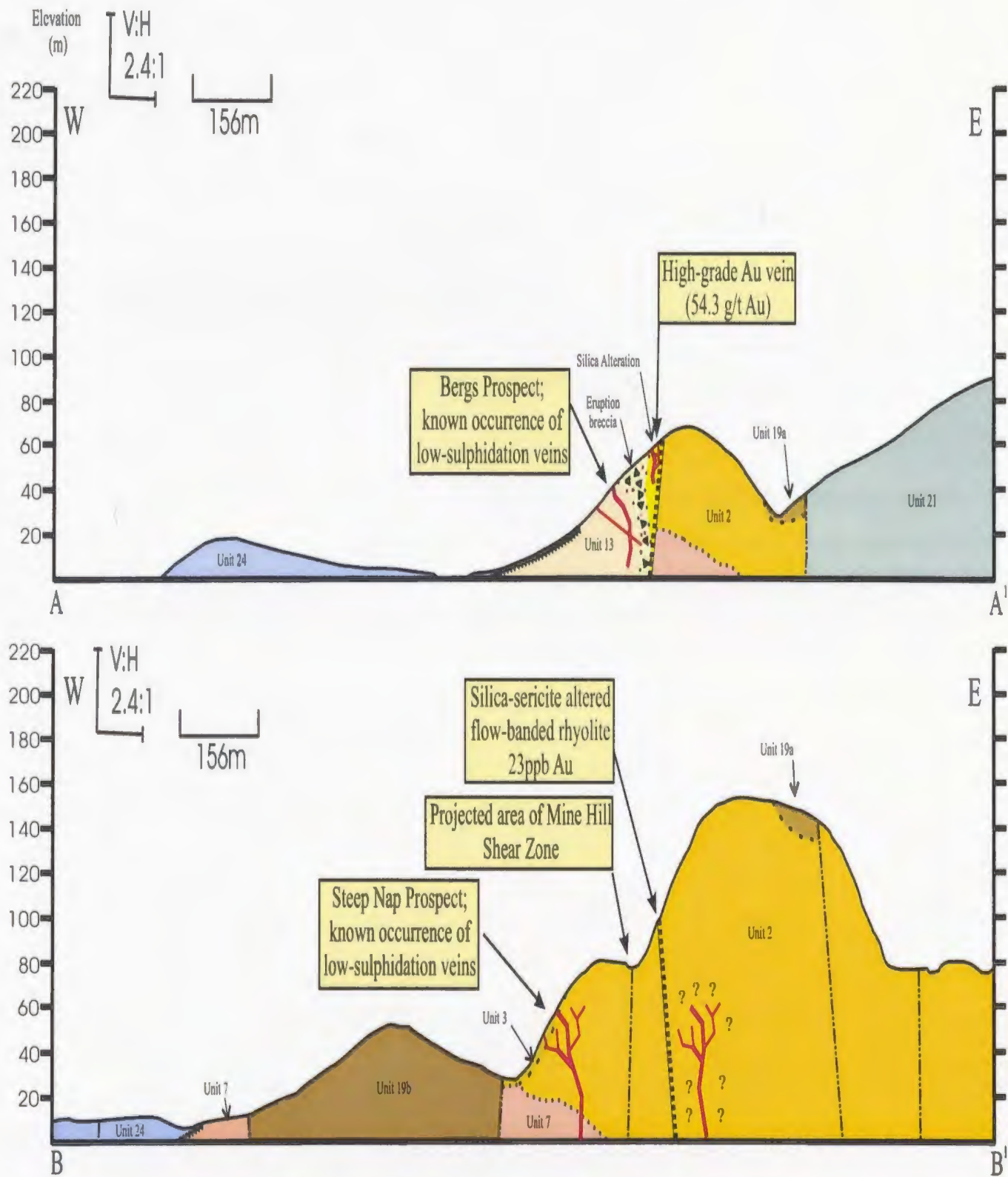
Figure 6-2: Cross-sections through the Bergs (A-A') and Steep Nap (B-B') prospects. Note vertical to horizontal exaggeration is approximately 2.4:1. Symbols and colors as per Figure 6-1.

exists to comment on the Ag/Au ratios from the Bergs prospect. Existing data demonstrates that gold-grades up to 5 g/t are associated with undetectable silver values (<5ppm). New exposures of banded chalcedonic silica veins ± adularia contain well-preserved examples of bladed calcite pseudomorphed by silica, demonstrating well-preserved boiling textures within the Bergs prospect (S.J. O'Brien, personal communication, 2005).

As indicated in Figure 6-2, a post-mineralization shear zone adjacent to the bonanza-grade vein is the eastern termination of known low-sulphidation veining. It should be noted however that there is very little outcrop east of this shear zone aside from that exposed in the Manuels River area (located in the region of the lower WHPC; Figure 6-2). An assumed fault east of the Manuels River defines the boundary between the felsic volcanic rocks to the west and the mafic volcanic rocks of the WHPC to the east.

In the second cross-section, Cambrian age sedimentary rock unconformably overlies granitic rocks of the White Hills Intrusive Suite (WHIS; Figure 6-2; B-B[1]). East of the granite is a down-dropped fault block of the upper WHPC, bedding in this block has a predominant south to southeast dip that ranges between 17 and 40 degrees. A prominent valley east of the sedimentary block defines the contact between sedimentary rocks of the WHPC and volcanic rocks of the White Mountain Volcanic Suite (WMVS). Immediately east of this contact are well-developed colloform-crustiform banded, chalcedonic silica ± adularia veins of the Steep Nap prospect. Drill hole data from Avalon Mines Limited (Pickett, W., 1995) indicates that granite of the WHIS underlies the Steep Nap prospect and is interpreted to intrude the volcanic rocks of the WMVS

based on field relationships seen in the area of Minerals Road Intersection. Known geochronological constraints on the formation of the low-sulphidation veins indicate that the vein system should crosscut the granitic rocks at depth.

Gold mineralization within the Steep Nap prospect shares a close association with the development of chalcedonic silica and adularia (Mills, 1998). Gold-grades up to approximately 9.2 g/t have been reported for the Steep Nap prospect (B.A. Sparkes, Rubicon Minerals, personal communication, 2003), however visible gold has yet to be identified. Again, insufficient data exists to comment on the Ag/Au with a great deal of certainty but existing data from this region suggests that the ratio ranges from 6-24 in samples containing detectable (>5ppm) amounts of Ag (ratio determined from three samples with detectable amounts of Ag). The region of the Steep Nap prospect also contains well-developed examples of bladed calcite pseudomorphed by silica, representing the preservation of boiling textures within the region (Mills, 1998; B. Sparkes, 2002).

East of the Steep Nap prospect is the projected trend of the regional Mine Hill Shear Zone (MHSZ). This structure is interpreted to represent a large-scale fault that may have focused fluids related to the low-sulphidation system and this region is marked by the development of silica–sericite alteration locally anomalous in gold (23ppb; O'Brien unpublished data). The area east of the projected MHSZ represents highly prospective ground, however there is very little outcrop within this region. A small outlier of the lower WHPC is located near the highest topographic elevation in the section. This sedimentary rock is assumed to unconformably overlie the rhyolitic volcanic rocks of the

263

WMVS. The relationship between these two units suggests that this area was at, or very near the paleosurface at approximately 582 Ma. The contacts in the valley east of the sedimentary outlier are poorly constrained due to very poor outcrop exposure.

The third section (Figure 6-3; C-C^1) contains the Farmer's Field prospect. This area contains centimeter-scale quartz–hematite and weakly banded chalcedonic silica veinlets, hosted within rhyolitic flows of the MVS. Also displayed along this section is the prominent divide between the older plutonic rocks of the WHIS and the younger volcanic rocks of the MVS. This region transects the highest elevations within the study area and the centimeter-scale quartz–hematite veinlets possibly represent the surficial expression of a deeper low-sulphidation system. The Farmer's Field prospect is approximately 100m above the highest exposure of well-developed low-sulphidation veins at the Steep Nap prospect, and therefore, holds the potential to host a more complete vein system. The Steep Nap prospect which displays well-preserved boiling textures at surface, suggesting partial erosion of the vein system.

Quartz–hematite veinlets occurring along the projected strike of the Steep Nap system, approximately 500m north of the cross-section are locally anomalous in gold. The same volcanic succession is also crosscut by gold-bearing, hematite-rich, hydrothermal breccias of an assumed low-sulphidation affinity approximately 700m south of the cross-section. The sedimentary rocks flanking the volcanic succession within the cross-section are interpreted to be younger than the development of the low-
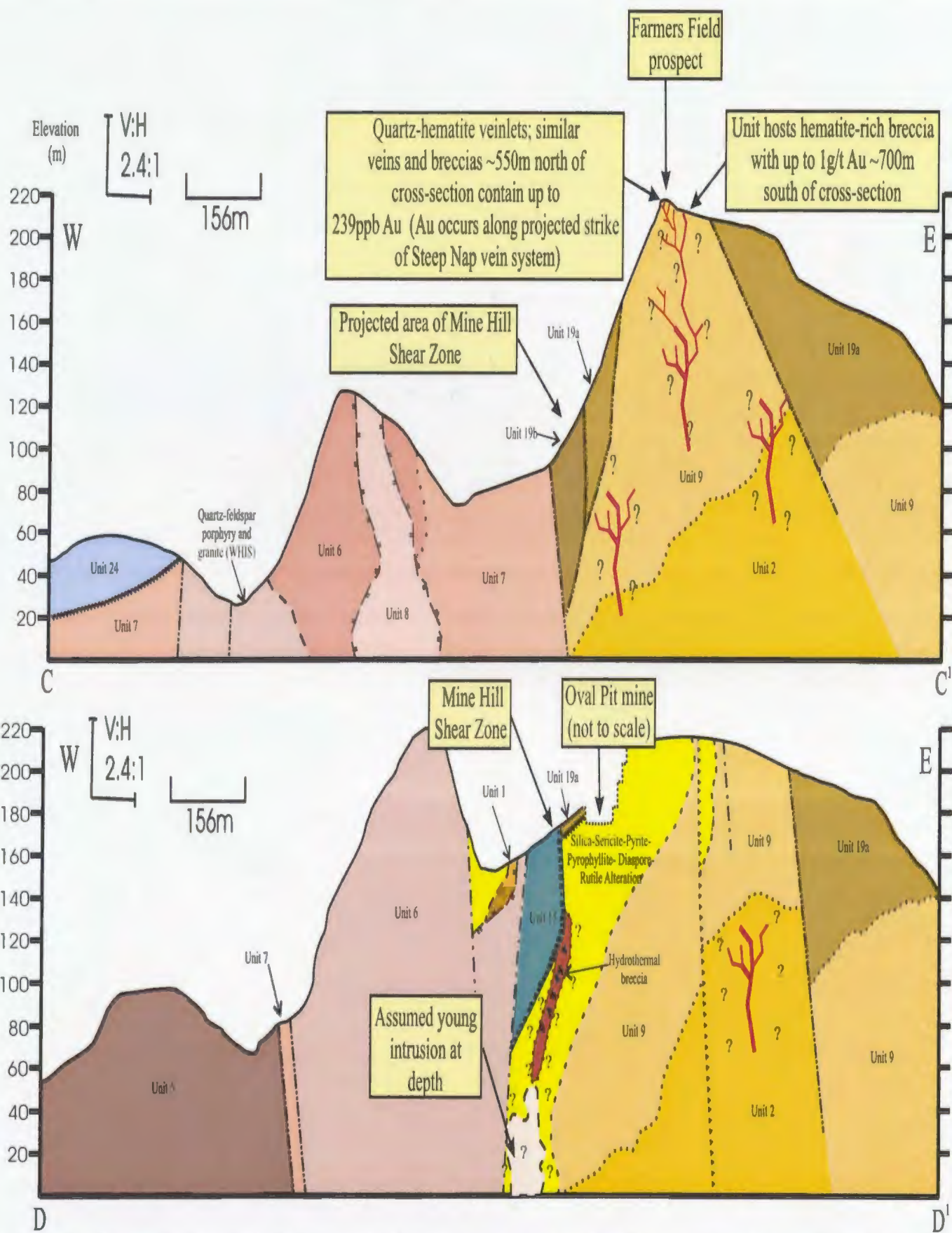
Figure 6-3: Cross-sections through the Farmer's Field prospect (C-C') and the Oval Pit mine (D-D'). Note vertical to horizontal exaggeration is approximately 2.4:1. Symbols and colors as per Figure 6-1.

sulphidation system and therefore would conceal any underlying evidence of low-sulphidation veins.

The final cross-section contains the Oval Pit mine and surrounding zone of advanced argillic alteration (Figure 6-3; D-D^1). The western portion of this section is dominated by plutonic rocks of the WHIS which display moderate amounts of patchy alteration in the region of the high-sulphidation system. Alteration of the volcanic raft contained within the WHIS may be syn-magmatic, or it may represent alteration associated with the formation of the high-sulphidation system. The mafic volcanic rocks adjacent to the WHIS contain minor amounts of pyritization and chloritization, but this alteration is not interpreted to be associated with the development of the high-sulphidation system. An outlier of the WHPC within the Oval Pit mine contains detrital advanced argillic alteration and provides the minimum time limit (582 ± 1.5 Ma) for the development of the high-sulphidation system. Located at depth below the Oval Pit mine is an assumed intrusion responsible for the development of the advanced argillic alteration. This intrusion may also be related to gold-bearing breccias similar to that exposed in the Mine By-Pass (O'Brien *et al*., 1998; G. Sparkes, 2002). East of the Oval Pit mine the relatively unaltered flows of the MVS could potentially host low-sulphidation vein systems at depth. Local evidence would suggest that the development of low-sulphidation veins overprints the advanced argillic alteration. The rheology of the pyrophyllite-rich altered rock within the Oval Pit mine may inhibit the development of low-sulphidation veins, which would explain why well-developed veins are not exposed within the open pit.

266

All four cross-sections are combined in Figure 6-4. From this diagram it is evident that three of the four cross-sections contain identified occurrences of low-sulphidation veins, which strongly suggests that there is great potential at depth within transect D-D[1]. The new geochronology demonstrates the significant break represented by the MHSZ. However, as shown in Figure 6-4 this break becomes hard to trace north of the Oval Pit mine due to later deformation.

6.3 TECTONIC DEVELOPMENT OF THE EASTERN MARGIN OF THE HOLYROOD HORST

Previous work has identified the environment of formation of the Harbour Main Group as an island-arc type setting (Hughes and Bruckner, 1971; King, 1990). Rocks of the Hawk Hills Tuff (previously part of the unseparated Harbour Main Group) are interpreted to represent the overlying volcanic carapace, which is locally intruded by plutonic rocks of the HIS (O'Brien *et al.*, 2001a). As illustrated in Figure 6-5 (Stage 1), 620 Ma ago the region of the Holyrood Horst was an active arc type setting (King, 1990). Volcanic rocks of the WMVS (this study) may possibly represent eastern equivalents of the Hawk Hills Tuff, and as demonstrated by U-Pb dating (e.g. 616 ± 2 Ma ash-flow tuff; Unit 4) some of the elements within this unit are known to have formed around 620 Ma. Associated with the intrusion of the Holyrood Intrusive Suite are auriferous syn-magmatic hydrothermal breccias (e.g. Butlers Pond; B. Sparkes, 2000), and associated regional-scale hydrothermal alteration (O'Brien *et al.,* 1998). This demonstrates that the region was a mineralizing environment prior to the development of the epithermal systems outlined in the current study.
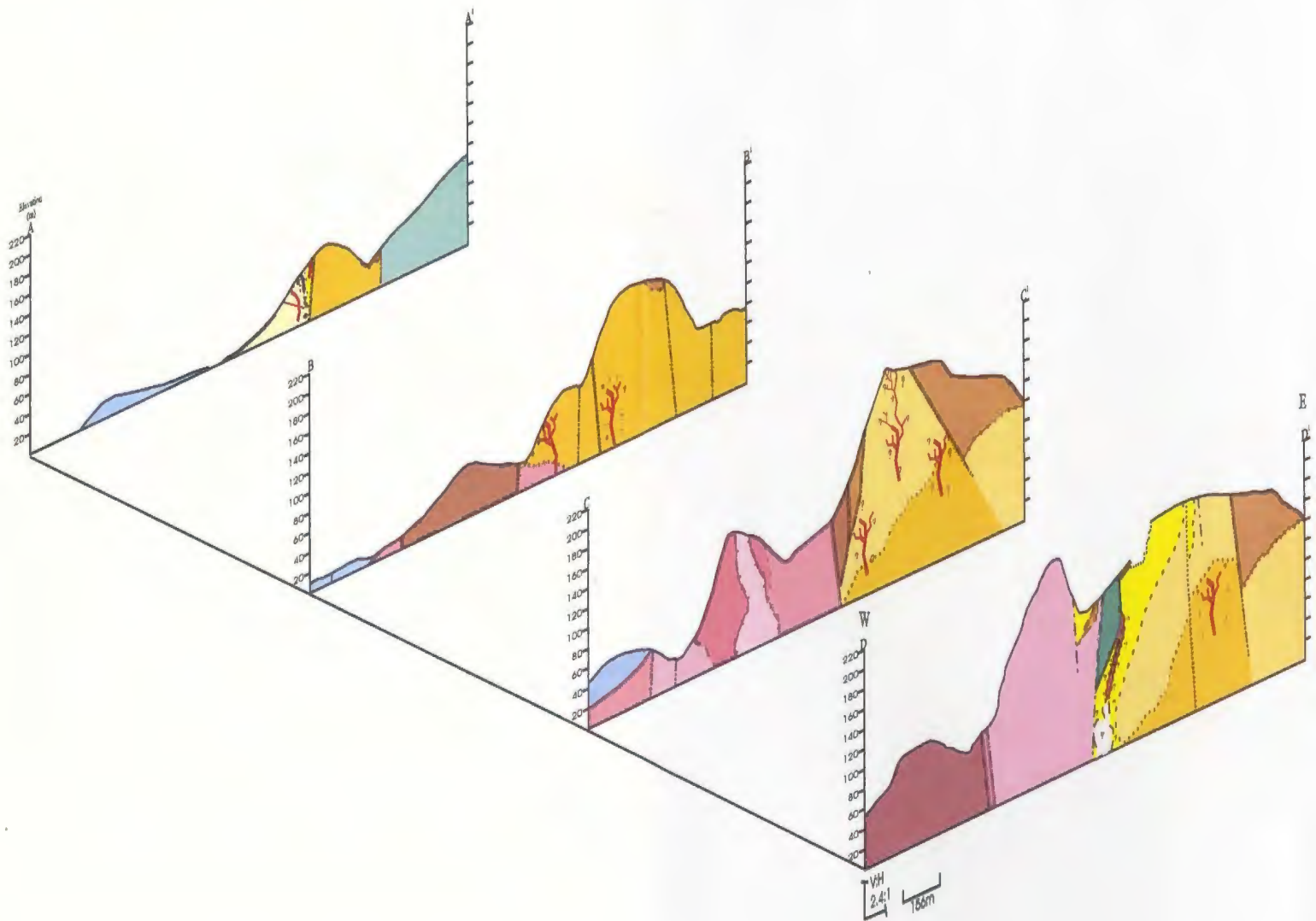
Figure 6-4: Schematic reconstruction of the four transects outlined in Figure 6-1.
Note vertical to horizontal exaggeration is approximately 2.4:1.
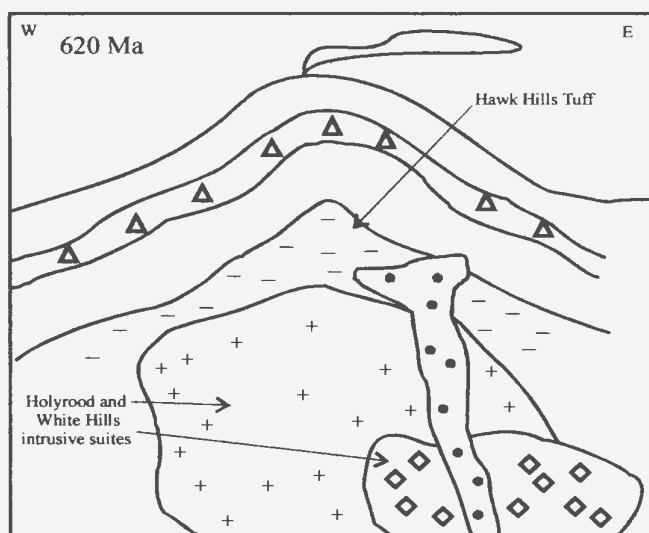
Stage 1: Continual development of the volcano-plutonic arc sequence. Intrusion of the HIS and cogenetic WHIS, along with the formation of coeval volcanic rocks.
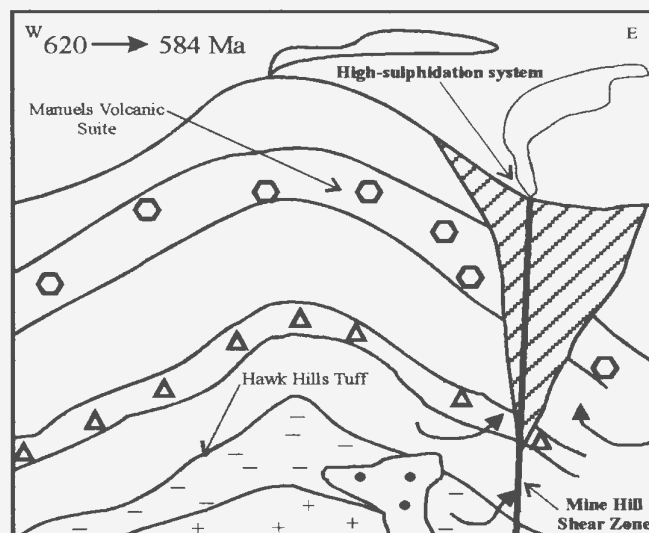
Stage 2: Volcanic activity associated with the intrusion of younger (ca. 584 Ma) intrusions; formation of the MVS. The development of large scale faults transport hydrothermal fluids to the paleosurface, resulting in the formation of vertically zoned advanced argillic alteration.
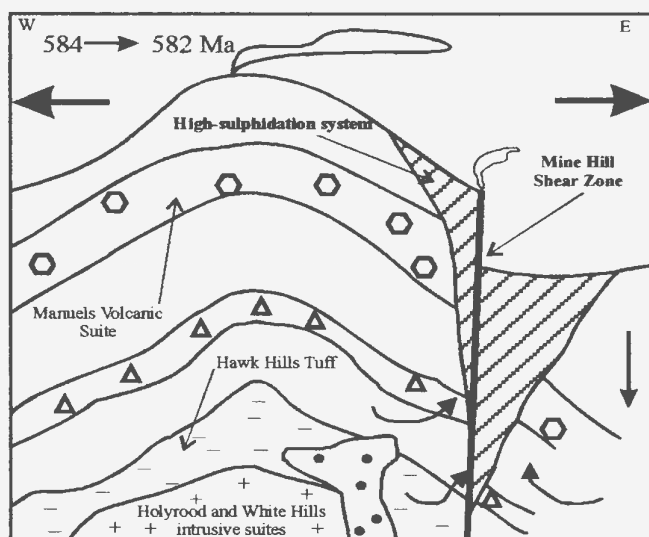
Stage 3: Development of normal faulting along the present-day MHSZ. Faulting offsets the eastern portion of the high-sulphidation system. Possibly some erosion of the high-sulphidation-style alteration.
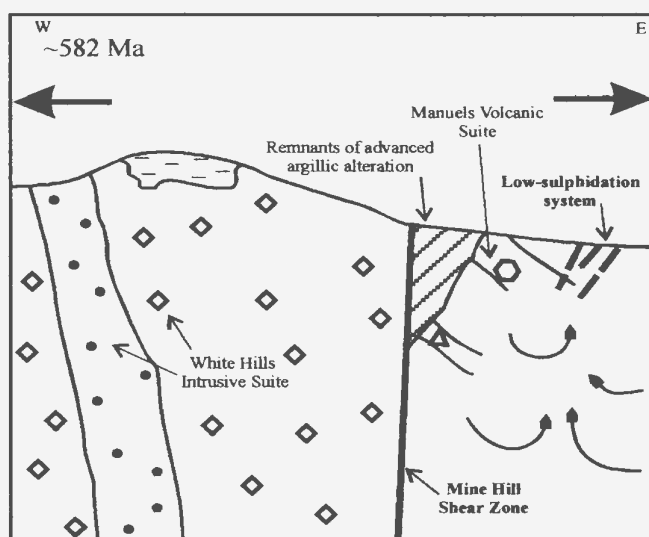
Stage 4: Erosion of the volcanic arc, with preservation of relatively deep alteration mineral assemblages in down-dropped portion of the alteration. As the high-sulphidation systems subsides, low-sulphidation veins develop on the margin of the advanced argillic alteration.

Figure 6-5: Schematic representation of the tectonic development for the northern portion of the eastern Avalon high-alumina belt.

269
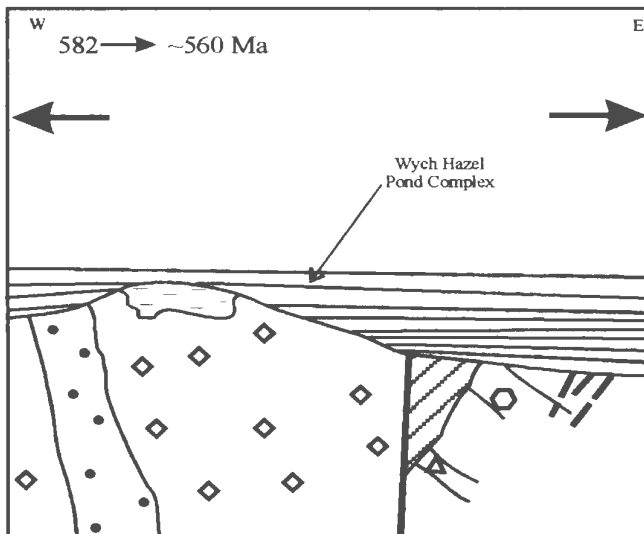
Stage 5: Continual subsidence of the arc complex. Onset of sedimentation, represented by siliciclastic rocks of WHPC, and transition into mafic dominated submarine volcanism. Collapse of hydrothermal system, followed by rapid burial, provides a protective cover sequence and prevents further erosion of the epithermal systems.
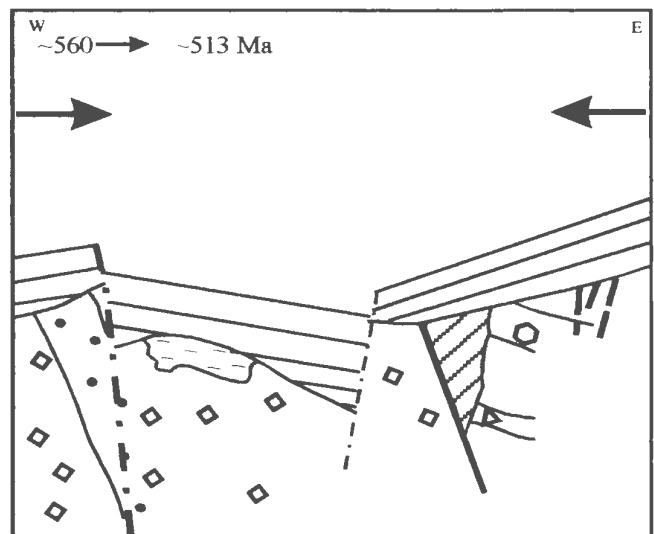
Stage 6: Folding and block faulting presumably associated with late stage deformation of the Avalonian Orogeny. Deformation causes re-exposure of the volcanic arc sequence, as demonstrated by the deposition of the Signal Hill Group (King, 1990).
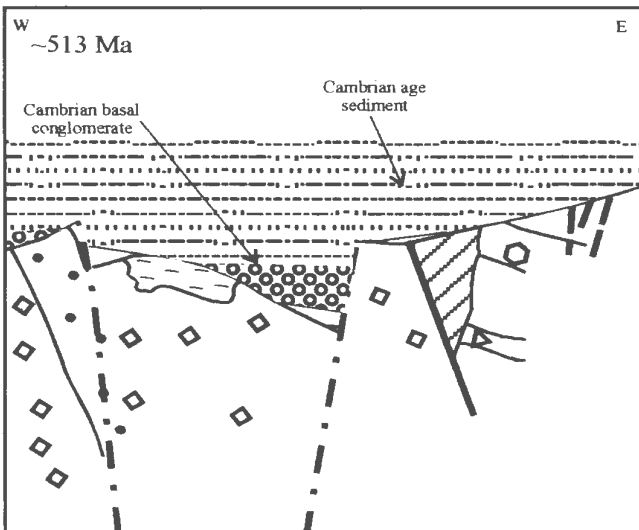
Stage 7: Deposition of Paleozoic cover sequence. Sequence unconformably overlies deformed volcanic arc material and deformed rocks of the WHPC.

Figure 6-5 cont'd: Schematic representation of the tectonic development for the northern portion of the eastern Avalon high-alumina belt.

A bimodal arc-type environment presumably existed until ca. 582 Ma with relatively little change in the overall tectonic setting, as indicated by the similar geochemistry of the volcanic rocks spanning this time period. Figure 6-5: (Stage 2) illustrates the increasing amount of arc-related volcanic material and the formation of the younger bimodal MVS. Prior to 584 Ma, tectonic activity resulted in the formation of large-scale faults, represented by the present day MHSZ. Young intrusions (ca. 584 Ma) in the vicinity of the present-day MHSZ initiate the convection of hydrothermal fluids which become focused along the crustal structures; this is supported by the close spatial association between the regional advanced argillic alteration and the MHSZ. These fluids migrate to paleosurface forming vertically zoned regions of advanced argillic alteration

Between 584 and 582 Ma, there was a decrease in the amount of volcanism and the region becomes dominated by erosion, which marks the onset of arc-collapse (Figure 6-5: Stage 3), during which time an extensional type environment dominated the region. The volcanic succession east of the MHSZ underwent normal faulting, while more western portions of the volcanic arc underwent more extensive erosion and degradation. The down-dropped portion of the eastern Avalon high-alumina belt was subjected to moderate amounts of erosion, which is interpreted to be on the order of 1.5-2km in the area of the Oval Pit mine (Sparkes *et al.*, 2005). The interpreted erosion of the advanced argillic alteration is further supported by the relatively deep alteration exposed within the Oval Pit mine. Removal of 1.5-2km of altered material in approximately 2 to 4.5 Ma requires erosional rates in the order of 375 to 1000 m/m.yr.. Calculated erosional rates for some tectonically active settings are comparable with the lower end of the erosional rates

listed above (e.g. 200-300 m/m.yr., Hulver, 1996). The altered material is generally predominated by clay minerals which would further assist in rapid erosion. By 582 Ma, the high-sulphidation system has subsided, the last stages of which affect the base of the juvenile lower WHPC. Around 582 Ma, convecting hydrothermal fluids result in the formation of low-sulphidation-style epithermal veins (Figure 6-5: Stage 4). These veins form during the onset of sedimentation and therefore do not affect sedimentary rocks of the WHPC, nor are the veins present as detrital material within the sedimentary sequence. The plutonic rocks west of the MHSZ possibly acted as an aquitard to the epithermal fluids and therefore influence the development of the low-sulphidation veins. Within this region the formation of the low-sulphidation system is interpreted to be relatively short-lived (ca. 1 Ma), and is inferred to have ended prior to the deposition of the upper WHPC.

From 582 to approximately 560 Ma there is continual submergence of the arc, which is supported by the deposition of the WHPC and Conception Group (Figure 6-5: Stage 5; King, 1990). A transition in the tectonic environment is supported by the change from bimodal volcanism to predominantly mafic volcanism with the deposition of the WHPC, possibly suggesting a transition into a back-arc type setting. With increasing time, the setting passes into a more pro-deltaic and then deep marine environment with the deposition of the Conception and St. John's groups, respectively (King, 1990).

Between approximately 560 to 513 Ma the region changes from an extensional to a compressional environment, which is marked by the deposition of the Signal Hill Group (Figure 6-5: Stage 6; King, 1990). The Signal Hill Group is interpreted to represent an

alluvial type environment and marks the re-exposure of arc material (King, 1990). This period of deformation is characterized by the development of open folds and block faulting (McCartney, 1967; Anderson *et al.,* 1975; King 1990, 1988b, 1980). Evidence obtained from the ^{40}Ar-^{39}Ar dating of sericite from the MHSZ indicates that the last recognized episode of deformation was around 537 ± 3 Ma, prior to the deposition of the Cambrian succession. Present day exposures of the Cambrian succession are relatively flat lying and generally follow present-day topography. The relatively undeformed Cambrian sedimentary succession demonstrates that the deformation within the eastern Avalon high-alumina belt occurred prior to ca. 513 Ma (age of base of Middle Cambrian currently defined by recent time scale studies, <www.stratigraphy.org>, April, 2005; Figure 6-5: Stage 7).

6.4 SUMMARY

The cross-sections constructed through the three main occurrences of low-sulphidation-style veins demonstrate that the veins have a close spatial association with altered granite of the WHIS and sericite-silica altered shear zones that are interpreted to be a part of, or related to, the regional-scale MHSZ. The granitic rocks are locally host to the development of low-sulphidation related veins, and their presence does not indicate deep erosion of the low-sulphidation system. In several regions of the field area weak surface anomalies containing anomalous gold-grades may be indicative of deeper, more extensive, low-sulphidation systems. The regionally developed MHSZ is interpreted to have been vital to the development of the high-sulphidation system (Sparkes *et al.*, 2005). The close spatial association between low-sulphidation veins and structures assumed to

be related to the MHSZ also suggests that these structures played a role in siting the development of low-sulphidation-style veins. It seems likely that the MHSZ has undergone multiple episodes of re-activation during the Late Neoproterozoic.

CHAPTER 7:

SUMMARY AND CONCLUSIONS

The following section presents, in point form, a review of the major conclusions stemming directly from this study. Some of these points have been presented in previous chapters but are again integrated in this final summary chapter. Areas for future research are also noted below.

1) New U-Pb ages from the White Hills Intrusive Suite (WHIS) range from 625 ± 2.5 Ma to 614 ± 2 Ma. This suite is geochemically similar to, and coeval with, the regionally developed Holyrood Intrusive Suite (HIS). Although spatially associated with both the high- and low-sulphidation systems, the new geochronological data demonstrates that the emplacement of the WHIS is not genetically associated with the development of either. At this point it is unclear whether the silica–sericite–pyrite alteration developed within the WHIS is associated with syn-magmatic alteration as seen elsewhere in the HIS, or if in fact it is related to the development of the epithermal systems, or possibly some combination of both.

2) New data now constrains the formation, uplift and erosion of the high-sulphidation system between 586 and 580.5 Ma. The maximum age limit is provided by the felsic succession hosting the alteration in the Oval Pit mine, which has been dated by previous work at 584 ± 1 Ma (G. Dunning, unpublished data). The minimum age limit is provided by an ash-flow tuff from the base of the

unconformably overlying Wych Hazel Pond Complex, which is dated at 582 ± 1.5 Ma.

3) New data provide the maximum age limit for the development of the low-sulphidation system. This limit is provided by a crystal-bearing ash-flow tuff from the Manuels Volcanic Suite, which is dated at 582 ± 4 Ma. The minimum limit is still defined by the base of the overlying Paleozoic cover, as identified by previous work (O'Brien, 2002).

4) The temporal relationship between the high- and low-sulphidation systems remain equivocal, however existing data is consistent with a younger age for the low-sulphidation system. The low-sulphidation system is interpreted to have formed after the collapse of the high-sulphidation system, but prior to the onset of sedimentation.

5) The new geochronological data identifies the presence of a pre-620 Ma volcanic sequence in this area, and therefore requires modification of the previously defined Manuels Volcanic Suite. These older volcanic rocks, herein defined as the White Mountain Volcanic Suite, are intruded by the 625 to 614 Ma White Hills Intrusive Suite, and includes previously dated volcanic rocks as young as 616 Ma (Dunning, unpublished data). The boundary between older magmatic rocks and younger volcanic rocks (post-584 Ma) is faulted, and defined by the regional-scale (post-alteration) Mine Hill Shear Zone. The old volcanic rocks are possibly correlative with the Hawk Hills Tuff, which is intruded by the Holyrood Intrusive Suite along the western margin of the Holyrood Horst (O'Brien, et al., 2001).

6) Felsic volcanic flows and ash-flow tuffs from the Manuels Volcanic Suite are chemically inseparable from older (ca. 616 ± 2 Ma) felsic volcanic rocks from the White Mountain Volcanic Suite. These data indicate little change in the overall tectonic environment and melting processes during the ca. 40 Ma time span represented by the felsic volcanic successions within the field area.

7) In the eastern portion of the field area, sedimentary rocks correlated with the Wych Hazel Pond Complex, are intruded by feldspar porphyry. Locally this porphyry is associated with the development of a blocky peperite, which indicates that the sediment was unconsolidated at the time of intrusion. The porphyry unit yielded a U-Pb zircon age of 585 ± 5 Ma and, based on field relationships, it is the youngest igneous rock exposed within the field area.

8) The post-alteration feldspar porphyry of the Wych Hazel Pond Complex is chemical distinct from older, pre-alteration quartz–feldspar porphyry of the White Hills Intrusive Suite (WHIS). The geochemical data is consistent with the feldspar porphyry forming in a somewhat different tectonic environment from the older WHIS.

9) Several groups of mafic dykes are recognizable using geochemistry and are interpreted as feeders to the mafic flows intercalated with the WHPC. The spatial and genetic association of mafic dykes with the occurrence of low-sulphidation veins is an interesting topic for further evaluation.

10) The new age data from the White Hills Intrusive Suite (ca. 620 Ma) in combination with the new age constraints on both the high- and low-sulphidation

systems (<585 Ma) indicates that the presence of granitic intrusions adjacent to the epithermal systems does not imply deep erosion, but rather that the intrusive rocks are basement to both systems.

11) The new age bracket for the high-sulphidation system requires a source of fluids and heat that is much younger than the Holyrood and White Hills intrusive suites. Intrusions such as the porphyry unit within the Wych Hazel Pond Complex may represent the final products of such a magmatic event.

12) The new geochronology demonstrates the rapid submersion and burial of the younger volcanic sequence following the end of the high-sulphidation-style alteration. This rapid burial plays a fundamental role in the preservation of old epithermal systems and is one of, if not the, key feature in the preservation of the high- and low-sulphidation systems exposed within the eastern Avalon high-alumina belt.

13) Chemical analyses from wall rock adjacent to low-sulphidation veins show the loss of mobile LREE, which is interpreted to be the result of the interaction between the wall rock and the epithermal fluids. This observation may have implications for gold exploration and requires further work.

14) The detailed measurement of veins adjacent to low-sulphidation systems provides useful information in modeling changes within the vein system with respect to changes in present-day elevation. Initial information gathered during this study also suggests that there may be a correlation between vein thickness and host rock.

15) Further work within the region should include a detailed analysis of the alteration mineralogy surrounding the Oval Pit mine and possibly fluid inclusion work to better constrain the depth of formation for the exposed alteration. Detailed analytical work may also provide clues as to the association of the Au-bearing breccias that are developed on the margin of the advanced argillic alteration.

REFERENCES

Anderson, M.M., Bruckner, W.D., King, A.F. and Maher,J.B.
    1975: The Late Proterozoic 'H.D. Lilly Unconformity' at Red Head, northeastern
    Avalon Peninsula, Newfoundland. American Journal of Science, vol.
    275, pages 1012-1027.

Arribas, Jr., A., Cunningham, C.G., Rytuba, J.J., Rye, R.O., Kelly, W.C., Podwysocki,
M.H., Mckee, E.H. and Tosdal, R.M.
    1995: Geology, geochronology, fluid inclusions, and isotope geochemistry of the
    Rodalquilar gold alunite deposit, Spain. Economic Geology vol. 90, pages 795-
    822.

Barrett, T.J. and MacLean, W.H.
    1994: Chemostratigraphy and hydrothermal alteration in exploration for VHMS
    deposits in greenstones and younger volcanic rocks, *In* Lentz, D.R, eds.,
    Alteration and Alteration Processes associated with Ore-forming Systems:
    Geological Association of Canada, Short Course Notes, vol. 11, pages 433-467.

Bergstrom, J. and Levi–Setti, R.
    1978: Phenotypic variation in the Middle Cambrian trilobite Paradoxides davidis
    Salter at Manuels, southeast Newfoundland. Geologica et Paleontologica, vol. 12,
    pages 1-40.

Boyce, W.D
    2001: Field Trip A3. Classic Cambrian trilobite localities of the
    Conception Bay South area, Avalon Peninsula, eastern Newfoundland.
    Geological Association of Canada-Mineralogical Association of Canada,
    Guidebook, 45 pages.

Brathwaite, R.L, Cargill, H.J., Christie, A.B. and Swain, A.
    2001: Lithological and spatial controls on the distribution of quartz veins in
    andesite- and rhyolite-hosted epithermal Au-Ag deposits of the Hauraki
    Goldfield, New Zealand. Mineralium Desposita, vol. 36, pages 1-12.

Bruckner, W. D.
    1969: Geology of Eastern Part of Avalon Peninsula, Newfoundland- A Summary,
    American Association of Petroleum Geology Memoir. 12, pages 130-138.

Buchanan, L.J.
    1981: Precious metal deposits associated with volcanic environments in the
    southwest. *In* Dickson, W.R. and Payne, W.D., eds., Relations of Tectonics to Ore
    Deposits in the Southern Cordillera: *Arizona Geological Society Digest*, vol. 14,
    pages 237-262.

Buddington, A.F.
　　1916: Pyrophyllitization, pinitization and silicification of rocks around
　　Conception Bay, Newfoundland. Journal of Geology, vol. 24, pages 130-152.

Calon, T.J.
　　1993: Stratigraphy and structure of Avalon Zone around Conception Bay. *In*
　　Atlantic Universities Geology Conference, Memorial University of
　　Newfoundland, St. John's. October, 1993, 24 pages.

Cox, D.R. and Lewis, P.A.W.
　　1966: The statistical analysis of series of events. Methuen, London.

Davis, D.W.
　　1982: Optimum linear regression and error estimation applied to U-Pb data.
　　Canadian Journal of Earth Sciences, vol. 19, pages 2141-2149.

Dawson, J.M.
　　1963: Regional geology of the Topsail-Foxtrap area. Unpublished M.Sc. thesis,
　　Memorial University of Newfoundland, St. John's, Newfoundland, 133 pages.

Dong, G., Morrison, G., and Jaireth, S.
　　1995: Quartz textures in epithermal veins, Queensland–classification, origin, and
　　implication. Economic Geology, vol. 90, pages 1841-1856.

Dubé, B., O'Brien, S.J., and Dunning, G.
　　2001: Gold deposits in deformed terranes: Examples of epithermal and
　　quartz-carbonate shear zone-related gold systems in the Newfoundland
　　Appalachians and their implications for exploration. North Atlantic Minerals
　　Symposium 2001, Extended Abstract vol., pages 31-35.

Dubé, B., Dunning, G, and Lauziere, K.
　　1995: Geology of the Hope Brook Mine, Newfoundland, Canada: A preserved
　　Late Proterozoic high-sulphidation epithermal gold deposit and its implications
　　for exploration. Economic Geology, vol. 93, pages 405-436.

Finch, C.J.
　　1998. Inductively coupled plasma-emission spectrometry (ICP-ES) at the
　　geochemical laboratory. *In* Current Research, Newfoundland Department of
　　Mines and Energy, Geological Survey, Report 98-1, pages 179-193.

Gillespie, P.A., Johnston, J.D., Lorgia, M.A., McCaffery, K.J.W., Walsh, J.J, Watterson, J.

    1999: Influence of layering on vein systematics in line samples. *In* McCaffery, K.J.W., Longergan, L., Wilkinson, J.J., eds.. Fractures, fluid flow and mineralization. Geological Society of London Special Publication, vol. 155, pages 35-36.

Goldstrand, P.M. and Schmidt, K.W.

    2000: Geology, mineralization, and ore controls at the Ken Snyder gold-silver mine, Elko Country, Nevada. *In* Cluer, J.K., Price, J.G., Struhsacker, E.M., Hardyman, R.F., and Morris, C.L., eds., Geology and Ore Deposits 2000: The Great Basin and Beyond: Geological Society of Nevada Symposium Proceedings, May 15-18, 2000, p. 265-287.

Haworth, R.T. and Le Forte, J.P.

    1979: Geophysical evidence for the extent of the Avalon Zone in Atlantic Canada, Canadian Journal of Earth Sciences, vol. 16, pages 552-567.

Hayes, J.P.

    1996: Geological setting and genesis of the eastern Avalon high-alumina belt. Unpublished M.Sc. thesis, Memorial University of Newfoundland, St. John's, Newfoundland, Canada, 172 pages.

Hayes, J.P. and O'Driscoll, C.F.

    1989a: Gold potential of the eastern Avalon high-alumina belt, Avalon Metallogeny Project-1989. *In* Report of Activities. Newfoundland Department of Mines and Energy, Mineral Development Division.

    1989b: The geology of the eastern Avalon high-alumina belt, Avalon Peninsula, Newfoundland. Newfoundland Department of Mine and Energy, Geological Survey Branch, Map 89-149.

    1990: Regional setting and alteration within the eastern Avalon high-alumina belt, Avalon Peninsula, Newfoundland. *In* Current Research. Newfoundland Department of Mines and Energy, Geological Survey Branch, Report 90-1, pages 145-155.

Hedenquist, J.W., Arribas, Jr., A. and Reynolds, T.J.

    1998: Evolution of an intrusion-centered hydrothermal system: far Southeast-Lepanto porphyry and epithermal Cu-Au deposits, Philippines. Economic Geology vol. 93, pages 373-404.

Hedenquist, J.W. and Henley, R.W.
 1985: Hydrothermal eruptions in the Waiotapu geothermal system, New Zealand: their origin, associated breccias, and relation to precious metal mineralization. Economic Geology, vol. 80, pages 1640-1668.

Hedenquist, J.W. and Lowenstern, J.B.
 1994: The role of magmas in the formation of hydrothermal ore deposits. Nature, vol. 370, pages 519-527.

Howell, B.F.
 1925: The faunas of the Cambrian Paradoxides beds at Manuels, Newfoundland. Bulletins of American Paleontology, 11 (43), 140 pages.

Hulver, M.L.
 1996: Post-orogenic denudation and mass-balanced topography of the Appalachian Mountain system from maturation indicators, thermochronology, and metamorphic petrology. Geological Society of America Abstracts with Programs, vol. 28, no. 7, 500 pages.

Howley, J.P.
 1907: Geological map of Newfoundland: Scale 1 inch to 17 miles, reprinted 1925.

Hughes, C.J.
 1970: The Late Precambrian Avalonian Orogeny in Avalon, southeast Newfoundland. American Journal of Science, vol. 269, pages 183-190.

Israel, S.
 1998: Geochronological, structural and stratigraphic investigation of a Precambrian unconformity between the Harbour Main Group and Conception Group, east coast Holyrood Bay, Avalon Peninsula, Newfoundland. Unpublished B.Sc. (Honors) thesis, Memorial University of Newfoundland, St. John's, Newfoundland, 78 pages.

Irvine, T.N. and Barager, W.R.A
 1971: A guide to the chemical classification of the common volcanic rocks. Canadian Journal of Earth Sciences, vol. 8, pages 523-548.

Izawa, E., Urashima, Y., Ibaraki, K., Suzuki, R., Yokoyama, T., Kawasaki, K., Koga, A. and Taguchi, S.
 1990: The Hishikari deposit: high grade epithermal veins in Quaternary volcanics of southern Kyushu, Japan. Journal of Geochemical Exploration, vol. 36, pages 1-56.

Jaffery, A.H, Flynn, K.F. Glendenin, L.E., Bentley, W.C. and Essling, A.M.
1971: Precision measurement of the half lives and specific activities of ^{235}U and ^{238}U. Physical Review, Section C, Nuclear Physics, vol. 4, pages 1889-1906.

Jukes, J.B.
1843: General Report of the Geological Survey of Newfoundland during the years 1839 and 1840. John Murray, London, 160 pages.

Keats, H.F.
1970: Geology and mineralogy of the pyrophyllite deposits south of Manuels, Avalon Peninsula, Newfoundland. Unpublished M.Sc. thesis, Memorial University of Newfoundland, St. John's, Newfoundland, 77 pages.

Ketchum, J.
1998: Report on U–Pb geochronology of hydrothermal altered volcanic and plutonic rocks on the Burin and central Avalon peninsulas, Newfoundland. Unpublished report on geochronology contract for the Newfoundland Department of Mines and Energy, Geological Survey, 4 pages.

King, A.F.
1980: The birth of the Caledonides: Late Precambrian rocks of the Avalon Peninsula, Newfoundland, and their correlatives in the Appalachian Orogen. *In* The Caledonides in the U.S.A. *Edited by* D. Wones. International Geological Correlation Project 27, Caledonide Orogen, 1979 meeting, Blacksburg, Virginia, pages 3-8.

King, A.F.
1982: Guidebook for Avalon and Meguma Zones of Atlantic Canada. IGCP Project 27, The Caledonide Orogen. Memorial University of Newfoundland, Department of Earth Sciences, Report 9, 308 pages.

1988a: Geology of the Avalon Peninsula, Newfoundland. Newfoundland Department of Mines and Energy, Geological Survey, Map 88-01, scale 1:250,000.

1988b: Late Precambrian sedimentation and related orogenesis of the Avalon Peninsula, Eastern Avalon Zone. Geological Association of Canada-Mineralogical Association of Canada-Canadian Society of Petroleum Geologists, Annual Meeting, Field Trip A-4, Guidebook. St. John's, Newfoundland, 84 pages.

1990: Geology of the St. John's area. Newfoundland Department of Mines and Energy, Geological Survey Branch, Report 90-2, 88 pages.

Krogh, T.E.

 1982: Improved accuracy of U-Pb zircon ages by the creation of more concordant systems using an air abrasion technique. Geochimica et Cosmochimica Acta, vol. 46: pages 637-649.

Krogh, T.E., Strong, D.F., O'Brien, S.J., and Papezik, V.S.

 1988: Precise U-Pb zircon dates from the Avalon Terrane in Newfoundland. Canadian Journal of Earth Sciences, vol.25, pages 442-453.

Landing, E., Bowring, S.A., Davidek, K.L., Westrop, S.R., Geyer, G., and Heldmaier, W.

 1998: Duration of the early Cambrian: U-Pb ages of volcanic ashes from Avalon and Gondwana. Canadian Journal of Earth Sciences, vol. 35, pages 329-338.

Lenters, M.H.

 1986: Report on geology, prospecting and geochemical sampling during May to August, 1986. Topsail claim group, licenses 2686 and 2773, NTS 1N/7, 10. Unpublished report, Esso Minerals Limited. Newfoundland and Labrador Geological Survey assessment file #1N/473.

Lewis, P.

 1999: Avalon Project. Eastern Newfoundland, NTS: 1N/07 & 1N/10, Report on Diamond Drilling Program, April 1999, Fort Knox Gold Resources, unpublished report.

Lilly, H.D.

 1966: Late Precambrian and Appalachian tectonics in the light of submarine exploration of the Grand Bank of Newfoundland in the Gulf of St. Lawrence: a preliminary view, American Journal of Science, vol. 264, pages 569-574.

Ludwig, K.R.

 1988: ISOPLOT for MS-DOS--A plotting and regression program for radiogenic-isotope data, for IBM-PC compatible computers, U.S. Geological Survey Open-File Report 87-601, 35 pp.

Maniar, P.D. and Piccoli, P.M.

 1989: Tectonic discrimination of granitoids. Geological Society of America Bulletin, vol. 101, pages 635-643.

McCaffrey, K.J.W. and Johnston, J.D.

 1996: Fractural analysis of a mineralized vein deposit: Curraghinalt gold deposit, Country Tyrone. Mineralium Deposita, vol. 13, pages 52-58.

McCartney, W.D.

    1967: Whitbourne map area. Geological Survey of Canada, Memoir 341, 135
    pages.

    1969: Geology of the Avalon Peninsula, southeast Newfoundland. American
    Association of Petroleum Geology Memoir 12, pages 115-129.

Meschede, M.

    1986: A method of discriminating between different types of mid-ocean ridge
    basalts and continental tholeiites with the Nb-Zr-Y diagram. *In* Chemical
    Geology, vol. 85, pages 207-218.

Mills, J.

    1998: A study of the late Neoproterozoic low-sulphidation (adularia-sericite)
    Steep Nap gold prospect, Avalon Zone, Newfoundland. Unpublished B.Sc.
    (Hons.) thesis, Memorial University of Newfoundland, St. John's,
    Newfoundland, Canada, 194 pages.

Mills, J., O'Brien, S.J., Dubé, B., Mason, R. and O'Driscoll, C.F.

    1999: The Steep Nap Prospect: A low-sulphidation, gold-bearing epithermal vein
    system of late Neoproterozoic age, Avalon Zone, Newfoundland Appalachians. *In*
    Current Research, Newfoundland Department of Mines and Energy, Geological
    Survey, report 99-1, pages 255-274.

Murray, A. and Howley, J.P.

    1881a: Reports of the Geological Survey of Newfoundland for 1864-1880.
    Stanford, London.
    1881b: Map of the Peninsula of Avalon. Geological Survey of Newfoundland.

O'Brien, S.J.

    2002: A Note on Neoproterozoic Gold, Early Paleozoic Copper and Basement-
    cover Relationships on the Margins of the Holyrood Horst, Southeastern
    Newfoundland. *In* Current Research. Newfoundland Department of Mines and
    Energy. Report 02-1, pages 219-227.

O'Brien, S.J. and Sparkes, G.

    2004: Bonanza-Grade Gold From Neoproterozoic Low-Sulphidation-Style
    Epithermal Veins and Breccias, Bergs Prospect, Avalon Zone, Eastern
    Newfoundland. Newfoundland Department of Mines and Energy, Geological
    Survey, Open File [001N/10/0742].

O'Brien, S.J, Dunning, G.R, Dubé, B., O'Driscoll, C.F., Sparkes, B., Israel, S. and Ketchum, J.
>2001a: New insights into the Neoproterozoic geology of the of the central Avalon Peninsula (parts of NTS map areas 1N/6, 1N/7 and 1N/3), eastern Newfoundland. *In* Current Research. Newfoundland Department of Mines and Energy, Geological Survey, Report 01-1, pages 169-189.

O'Brien, S.J., Dubé, B., and O'Driscoll, C.F.
>2001b: Epithermal-style hydrothermal systems in Late Neoproterozoic Avalonian rocks on the Avalon Peninsula, Newfoundland: Implications for gold exploration. Field Trip A-6 Guidebook. St. John's 2001 Geological Association of Canada - Mineralogical Association of Canada Annual Meeting, 29 pages.

O'Brien, S.J., Dubé, B., O'Driscoll, C.F.
>1999: Neoproterozoic epithermal gold–silver mineralization in the Newfoundland Avalonian belt. Geological Association of Canada, Mineral Deposits Section: Gangue Newsletter, Issue 62, pages 1-11.

O'Brien, S.J., Dubé, B., O'Driscoll, C.F. and Mills, J.
>1998: Geological setting of gold mineralization and related hydrothermal alteration in late Neoproterozoic (post-640 Ma) Avalonian rocks of Newfoundland, with a review of coeval gold deposits elsewhere in the Appalachian Avalonian belt. In Current Research. Newfoundland Department of Mines and Energy, Geological Survey, Report 98-1, pages 93-124.

O'Brien, S.J., King, A.F, and O'Driscoll, C.F.
>1997: Late Neoproterozoic geology of the central Avalon Peninsula, Newfoundland, with an overview of mineralization and hydrothermal alteration. *In* Current Research. Newfoundland Department of Mines and Energy, Geological Survey, Report 97-1, pages 257-282.

O'Brien, S.J., O'Brien, B.H., Dunning, G.R. and Tucker, R.D.
>1996: Late Neoproterozoic evolution of Avalonian and associated peri-Gondwanan rocks of the Newfoundland Appalachians. In: Avalonian and Related Terranes of the Circum-North Atlantic. Edited by M.D. Thompson and R.D. Nance. Geological Society of America, Special Paper 304, pages 9-28.

O'Brien, S.J. and O'Driscoll, C.F.,
>1996: Preliminary investigation of Neoproterozoic (Avalonian) rocks, northeastern Holyrood (NTS 1N/6) map area: notes on geology, mineralization and mineral exploration potential. *In* Current Research. Newfoundland Department of Mines and Energy, Geological Survey, pages 19-23.

O'Brien, S.J., Wardle, R.J. and King, A.F.
    1983: The Avalon Zone: A Pan-African terrane in the Appalachian Orogen of Canada. Geology Journal, vol. 18, pages 195-222.

O'Driscoll, C.F., Collins, C.J. and Tuach, J.,
    1988: Volcanic-hosted, high-alumina epithermal environments and the St. Lawrence fluorite deposit in the Avalon Zone, eastern Newfoundland. Geological Association of Canada- Mineralogical Association of Canada- Canadian Society of Petroleum Geologists, Trip A5, 82p.

Papezik, V.S.
    1972: Burial metamorphism of late Precambrian sediments near St. John's , Newfoundland. Canadian Journal of Earth Sciences, vol. 9, pages 1568-1572.

Papezik, V.S.
    1974: Prehnite-pumpellyite facies metamorphism of late Precambrian rocks of the Avalon Peninsula, Newfoundland. Canadian Mineralogist, vol. 12, pages 463-468.

Papezik, V. S., Keats, H F. and Vahtra, J.
    1978: Geology of the Foxtrap pyrophyllite deposit, Avalon Peninsula, Newfoundland; Canadian Institute of Mining Bulletin vol. 71, no. 791 pages 152-160. Geofile No.1N/10/0413

Pearce, J.A.
    1983: Role of the sub-continental lithosphere in magma genesis at active continental margins. *In* C.J. Hawkesworth and M.J. Norry eds., Continental Basalts and Mantle Xenoliths, Shiva Publishing Limited, pages 230-249.

Pearce, J.A., Harris, N.B.W. and Tindle, A.G.
    1984: Trace element discrimination diagrams for the tectonic interpretation of granitic rocks. Journal of Petrology, vol. 25, pages 956-983.

Pearce, J.A. and Norry, M.J.
    1979: Petrogenetic implications of Ti, Zr, Y, and Nb variations in volcanic rocks. *In* Contributions to Mineralogy and Petrology, vol. 69, pages 33-47.

Pickett, J.W.
    1995: Assessment report, geological mapping, lithogeochemical sampling, prospecting, soil sampling, ground magnetic and VLF electromagnetic surveying and diamond drilling, Dog Pond Property. Licence 4424, southeastern Newfoundland, NTS 1N/7. Newfoundland and Labrador Geological Survey assessment file # 001N/07/0648.

Pickett, J.W. and Jacobs, W.

    1995: First year assessment report on geological exploration for licence 4433 on claim block 7847 in the Hennesseys Pond and Jakes Pond areas, southeastern Newfoundland. Unpublished report, Avalon Mines Ltd., 11 pages. Newfoundland and Labrador Geological Survey assessment file # 001N/07/0563.

Porter, R.

    1988: The Pajingo gold mine: James Cook University of north Queensland. Economic Geology, Research Unit Contributions 29, pages 23-34.

Rose, E.R.

    1952: Torbay map area, Newfoundland. Geological Survey of a Canada Memoir 265, 64 pages.

Saunders, P.

    1986: Geological and rock geochemical surveys on the Foxtrap claims, Newfoundland, licences 2551, 2557, October 1985 to January 1986. Apex Geological Consultants Ltd, unpublished report. Newfoundland and Labrador Geological Survey assessment file # 001N/07/468.

    1991:Summary report on 1991 exploration on the Dog Pond Property (Licence 4112, NTS 1N/7) Avalon Peninsula, Newfoundland. Newfoundland and Labrador Geological Survey assessment file # 001N/07/0521.

Saunders, P. and Harris, J.

    1994: Summary report on the Dog Pond property, Avalon Peninsula, Newfoundland. NTS 1N/7, C.B. 7847, 7848. Unpublished report.

Shervais, J.W.

    1982: Ti-V plots in the petrogenesis of modern and ophiolitic lavas. Earth and Planetary Science Letters, vol. 59, pages 101-118.

Sillitoe, R. E. and Hedenquist, J.W.

    2001: Linkages between volcanotectonic settings, ore-fluid compositions, and epithermal precious metal deposits. Society of Economic Geologists, Special Publication 10, pages 1-29.

Sillitoe, R.H. and Lorson, R.C.

    1994: Epithermal gold-silver-mercury deposits at Paradise Peak, Nevada: ore controls, porphyry gold association, detachment faulting, and supergene oxidation. Economic Geology, vol. 89, pages 1228-1248.

Sparkes, B.A.
> 2002: First year assessment report on prospecting, geological mapping, grid cutting, soil geochemical sampling, trenching and channel sampling on the Steep Nap Property, License 8171M. Manuels area, eastern Newfoundland. NTS 1N/10. Rubicon Minerals Corporation, unpublished report. 41 pages plus appendices.

> 2003a: First year assessment report on prospecting, geological mapping, core logging and geochemistry on the Bergs Property, Licenses 8299M, 8452M,8466M, 8540M, 8541M and 8542M. Manuels area, eastern Newfoundland. NTS 1N/10 and 1N/07. Rubicon Minerals Corporation, unpublished report. 42 pages plus appendices.

> 2003b: Assessment report on prospecting and geochemical investigations on the Grog Pond Property, Licences 7371M (third year), and licenses 8564M, 8781M and 8782M (first year). Pouch Cove area, eastern Newfoundland. NTS 1N/10. Rubicon Minerals Corporation, unpublished report. 25 pages plus appendices.

> 2003c: First and ninth year assessment report on prospecting, soil and lake bottom sampling and geochemical investigations on the Bergs Property, Licenses 4822 (9th year), 8511M, 8524M, 8525M, 8526M, 8626M, 8627M, 8688, 8708M, 8709M, 8710M, 8711M, 8712M and 8713M (first year). Country Pond, Thousand Arc Marsh and TCH areas, eastern Newfoundland. NTS 1N/10 and 1N/07. Rubicon Minerals Corporation, unpublished report. 39 pages plus appendices.

> 2003d: Second year assessment report on channel sampling and geological mapping on the Steep Nap Property, License 8171M. Manuels area, eastern Newfoundland. NTS 1N/10. Rubicon Minerals Corporation, unpublished report. 28 pages plus appendices.

> 2004: Sixth year assessment report on lake bottom sampling, prospecting and geochemical investigations on the Pastureland Road Property, Licence 6127M. Pastureland Road area, eastern Newfoundland. NTS 1N/07. Rubicon Minerals Corporation, unpublished report. 19 pages plus appendices.

Sparkes, B.A., O'Brien, S.J., Wilson, M.R., and Dunning, G.R.
> 2002: The geological setting, geochemistry and age of Late Neoproterozoic intrusive rocks at the Butlers Pond Cu-Au prospect (NTS 1N/3), Avalon Peninsula, Newfoundland. *In* Current Research. Newfoundland Department of Mines and Energy, Geological Survey, Report 02-1, pages 245-264.

Sparkes, G

    2002: A comparison of the Mine By-Pass and Roadcut prospects: Two areas of breccia-hosted gold mineralization , Eastern Avalon Zone, Newfoundland. Unpublished B.Sc. (Hons) thesis, Memorial University of Newfoundland. 149 pages.

Sparkes, G.W., O'Brien, S.J., Dunning, G.R. and Dubé, B.

    2005: U-Pb geochronological constraints on the timing of magmatism, epithermal alteration and low-sulphidation gold mineralization, eastern Avalon Zone, Newfoundland. *In* Current Research. Newfoundland Department of Mines and Energy, Geological Survey, Report 05-1, pages 115-130.

Sparkes, G., O'Brien, S.J. and Dunning, G.R.

    2004: The setting and timing of epithermal alteration and gold mineralization in the eastern Avalon Zone; an update. *In* Report of Activities for 2004. Newfoundland Department of Natural Resources, Mines Branch, pages 24-26.

Stacy, J.S., and Kramers, J.D.

    1975: Approximation of terrestrial lead isotope evolution by a two stage model. Earth and Planetary Science Letters, 26, pages 207-221.

<www.Statigraphy.org>

    The Working Group on Stratigraphic Information System (SIS): Geological Time Scale – Paleozoic. Retrieved: 12 April, 2005 <http://www.stratigraphy.org/paleo.htm>

Stoffregen, R.E., and Alpers, C.N.

    1987: Woodhouseite and svanbergite in hydrothermal ore deposits: Products of apatite destruction during advanced argillic alteration; Canadian Mineralogist, vol. 25. pages 201-211.

Sun, S.S. and McDonough, W.F.

    1989: Chemical and isotopic systematics of oceanic basalts: Implications for mantle composition and processes. *In* Magmatism in the Ocean Basins. Geological Society, Special Publication 42, pages 313-345.

Vhay, J.S.

    1937: Pyrophyllite deposits of Manuels, Conception Bay, Newfoundland. Department of Natural Resources, Geological Section, Bulletin Number 7, 33 pages.

Villeneuve, M., Sandeman, H.A., and Davis, W.J.

    2000: A method for intercalibration of   U–Th–Pb and ^{40}Ar-^{39}Ar ages in the Phanerozoic. Geochimica et Cosmochimica Acta, vol. 64, no. 23, pages 4017-4030.

Walcott, C.D.

    1899: Precambrian fossiliferous formation. Geological Society of America Bulletin, vol. 10, pages 199-224.

White, N.C. and Hedenquist, J.W.

    1995: Epithermal gold deposits: styles, characteristics and exploration. Society of Economic Geologists Newsletter, Number 23, pages 9-13.

Williams, H.

    1964: The Appalachians in northeastern Newfoundland-A two-sided symmetrical system. American Journal of Science, vol. 262, pages 1137-1158.

    1979: Appalachian Orogen in Canada, Canadian Journal of Earth Sciences, vol. 16, pages 792-807.

Williams, H. and King, A.F.

    1979: Trepassey map area, Newfoundland. Geological Survey of Canada, Memoir 389, 24 pages.

Winchester, J.A. and Floyd, P.A.

    1977: Geochemical discrimination of different magma series and their differentiation products using immobile elements. *In* Chemical Geology, vol. 20, pages 325-343.

APPENDIX A

GEOCHRONOLOGICAL SAMPLE PREPARATION

<u>U-Pb Sample Preparation</u>

Samples collected for geochronological study were crushed using a 4x6 MASSCO crusher and then reduced to approximately <100 size mesh using a BRAUN direct drive pulverizer. From here the sample was concentrated further by passing it over a Wilfley table, which separated the heavy minerals from the lighter fraction. Following this, the sample was rinsed with alcohol to prevent oxidation and dried under a heat lamp.

After drying, the heavy fraction from the Wifley table was sieved using size 40 mesh, and passed under a magnet to remove metal fragments and highly magnetic material. The less than 40 mesh fraction was then put into a large separatory funnel with methylene iodide (MI), which has a known density of 3.32 g/cm^3. The separatory funnel was then shaken to mix the two materials and then left standing for approximately five minutes to allow the more dense material (including zircon) to settle to the bottom where it was drained from the MI. This procedure was repeated several times until the denser faction was removed. The denser fraction was then rinsed with acetone and dried under a heat lamp. After drying the material was passed through a Frantz Isodynamic Magnetic Separator, which allowed the separation of more magnetic minerals such as zircon, titanite and pyrite, from the remaining mineral fraction. The sample was passed through the Frantz Isodynamic Magnetic Separator several times varying the tilt angle and the voltage as listed; initial Frantz step 1) 10 degrees tilt at .25 amps, 2) 10 degrees tilt at .5 amps, 3) 10 degrees tilt at 1.0 amps, 4) 10 degrees tilt at 1.7 amps. For the final Frantz the

amps were set to 1.7, and the tilt was varied from 5, 3, 1, and 0 degrees. Finally zircon crystals were hand picked under a microscope from the remaining sample on basis of grain morphology, clarity and abundance. Selected grains were then abraded with pyrite to remove the outer portion of the crystals to reduce the effects of secondary Pb loss, and washed in hot nitric acid to dissolve the remaining pyrite.

Select abraded grains were then transferred into small beakers, washed with double distilled nitric acid and then placed on a hot plate for half an hour in double distilled nitric acid. After a half an hour, the zircons were removed from the hot plate and the remaining nitric acid decanted. The grains were then rinsed twice with double distilled water and covered with parafilm. Grains selected for individual analysis were pipetted into Teflon© bombs. Hydrofluoric acid was then added to the sample (approximately 15 drops, but varies in accordance with size of sample), along with the spike. The bombs were then sealed and placed in an oven at 210 degrees for 5 days.

^{40}Ar-^{39}Ar Sample Preparation

The adularia mineral separates were hand crushed, while the sericite samples were crushed the same as U-Pb samples. Both samples were sieved through size 40 and 70 mesh. After sieving the mineral fractions were then hand picked under a microscope where the best, euhedral grains were selected for analysis. The best fraction of adularia was found in the less than 70 mesh fraction, while the best fraction of sericite was chosen from the less than 40, greater then 70 mesh fraction. Only one morphology of adularia was identified within the sample, however the two sericite samples contained multiple generations of sericite. The sample collected within the Oval Pit mine (GS-GC-14)

contained fibrous looking sericite along with more subrounded pill shaped grains. For this sample, the goal was to separate sericite associated with the advanced argillic alteration and therefore the pill-shaped grains were selected and the fibrous grains were excluded. The second sample of sericite collected from the MHSZ was sampled in order to identify the age of deformation. For this reason fibrous sericite, assumed to be related to the deformation, was selected from this sample. The selected grains were packaged in glass vials and shipped to the Geological Survey of Canada in Ottawa to be analyzed.

Measurements by mass spectrometer were not carried out by the author for either U/Pb or Ar/Ar samples. U/Pb ages and uncertainties were calculated (at the 95% confidence interval) using the weighted average of the $^{207}Pb/^{206}Pb$ ages for discordant datasets, or the weighted average of the $^{206}Pb/^{238}U$ ages using ISOPLOT (Ludwig, 1988). Ages and uncertainties on the Ar/Ar data were calculated by M. Villeneuve (Geological Survey of Canada) using in house programs.

APPENDIX B

DUPLICATE AND STANDARD ANALYSIS FOR MAJOR-ELEMENT ICP-ES DATA FROM 1997 TO 2003

Duplicate and standard analyses presented here demonstrate the internal consistency in the ICP-ES major-element data. Common elements referred to in the text such as SiO_2, Al_2O_3, TiO_2, Na_2O and K_2O, are shown to have a common reproducibility of $\pm 10\%$. These elements were used to display the effects of hydrothermal alteration within the field area. Also contained within this dataset is the trace element Zr, which is relied upon heavily as an immobile element. Duplicate and standard analyses for Zr are all within $\pm 10\%$ error.

Appendix B: Duplicate and standard analyses for major-element ICP-ES data from 1997 to 2003.

Precision Lab #	Field #	Year	SiO2 %	Al2O3 %	Fe2O3 Total %	Fe2O3 %	FeO %	MgO %	CaO %	Na2O %	K2O %	TiO2 %	MnO %	P2O5 %	Cr ppm	Zr ppm	Ba ppm	L.O.I. %	Total
	Detection Limit		0.01	0.01	0.01	0.01	0.01	0.01	0.01	0.01	0.01	0.001	0.01	0.001	50	1	1		
1942373	OB970174	1997	57.35	32.73	0.26	Nd	Nd	Nd	0.02	0.14	3.60	0.379	Nd	0.026	Nd	476	372	5.29	99.77
1942390	OB970174	1997	57.81	33.25	0.26	Nd	Nd	Nd	0.02	0.14	3.69	0.381	Nd	0.030	Nd	477	375	5.23	100.80
	% Difference A		0.81	1.59	1.32	N/A	N/A	Nd	11.13	2.55	2.55	0.53	Nd	14.30	N/A	0.33	0.85	1.14	1.03
1942402	OB970363	1997	64.00	14.44	5.47	Nd	Nd	1.92	1.56	2.65	5.76	1.042	0.141	0.285	108	91	1897	2.38	99.65
1942410	OB970363	1997	63.86	14.93	5.55	Nd	Nd	2.01	1.54	2.77	6.08	1.063	0.145	0.294	Nd	88	1948	2.40	100.64
	% Difference B		0.22	3.35	1.53	N/A	N/A	4.65	1.56	4.60	5.49	2.01	2.51	3.34	N/A	3.13	2.71	0.88	0.99
	Average % Diff		0.51	2.47	1.43	N/A	N/A	4.65	6.36	3.68	4.02	1.27	2.51	8.82	N/A	1.73	1.78	1.01	1.01
1942704	OB-00-123	2000	73.56	13.74	1.51	0.66	0.77	0.46	0.83	3.79	3.97	0.146	0.055	0.03	Nd	91	864	1.06	99.17
1942710	1942704	2000	74.05	13.75	1.50	0.62	0.79	0.47	0.84	3.82	3.93	0.147	0.055	0.04	Nd	95	866	1.01	99.61
	% Difference A		0.66	0.07	1.09	6.26	2.93	1.79	1.16	0.72	1.06	0.58	1.54	29.73	N/A	4.47	0.31	4.58	0.44
1942725	OB-00-162	2000	61.56	17.31	5.99	4.01	1.79	2.64	1.12	3.78	3.97	0.629	0.147	0.37	Nd	139	970	2.47	99.99
1942730	1942725	2000	60.92	17.26	5.91	3.94	1.77	2.63	1.13	3.75	3.95	0.628	0.147	0.36	Nd	135	966	2.47	99.16
	% Difference B		1.04	0.18	1.46	1.66	1.11	0.47	0.81	0.71	0.59	0.25	0.43	3.06	N/A	2.93	0.45	0.05	0.83
1942787	OB-00-271	2000	52.50	17.29	7.19	2.60	4.13	4.92	5.35	5.38	0.52	0.917	0.119	0.16	Nd	86	127	3.09	97.44
1942790	1942787	2000	51.87	17.09	7.19	2.72	4.02	4.88	5.36	5.35	0.53	0.904	0.118	0.16	Nd	84	123	3.03	96.49
	% Difference C		1.20	1.17	0.01	4.59	2.58	0.71	0.18	0.45	2.02	1.48	1.38	0.38	N/A	1.57	2.90	1.88	0.97
1942787	OB-00-271	2000	52.51	17.31	7.49	2.90	4.13	4.90	5.27	5.70	0.27	0.929	0.117	0.18	Nd	78	126	3.09	97.77
1942790	1942787	2000	52.58	17.41	7.43	2.96	4.02	5.00	5.26	5.75	0.26	0.936	0.116	0.18	Nd	79	126	3.03	97.99
	% Difference D		0.13	0.60	0.85	1.88	2.58	2.17	0.20	0.89	0.69	0.73	0.56	1.15	N/A	1.33	0.42	1.88	0.23
1942828	OB-00-103	2000	74.26	13.06	1.59	0.57	0.93	0.51	0.30	3.45	4.57	0.164	0.048	0.03	Nd	138	1002	0.82	98.82
1942830	1942828	2000	74.30	13.09	1.57	0.62	0.86	0.50	0.30	3.41	4.57	0.168	0.048	0.04	Nd	131	1038	0.80	98.80
	% Difference E		0.05	0.25	1.45	8.76	7.61	2.25	1.41	1.03	0.05	2.17	0.00	23.01	N/A	5.02	3.58	2.57	0.01
	Average % Diff		0.62	0.45	0.98	4.83	3.36	1.48	0.75	0.76	0.88	1.04	0.78	11.47	N/A	3.06	1.53	2.19	0.50

Nd= Not detected
N/A= Not available

297

Appendix B: Cont'd

Precision Lab #	Field #	Year	SiO2 %	Al2O3 %	Fe2O3 Total %	Fe2O3 %	FeO %	MgO %	CaO %	Na2O %	K2O %	TiO2 %	MnO %	P2O5 %	Cr ppm	Zr ppm	Ba ppm	L.O.I. %	Total %
	Detection Limit		0.01	0.01	0.01	0.01	0.01	0.01	0.01	0.01	0.01	0.001	0.01	0.001	50	1	1		
1942839	OB-01-001	2001	52.62	15.52	8.63	2.69	5.35	6.00	5.36	2.66	3.36	1.216	0.133	0.24	137	125	1406	3.05	98.78
1942850	1942839	2001	53.57	15.87	8.74	2.80	5.34	6.16	5.48	2.81	3.46	1.243	0.135	0.24	138	125	1437	3.06	100.79
	% Difference A		1.82	2.25	1.32	4.30	0.03	2.67	2.16	5.30	2.88	2.20	1.39	1.96	0.77	0.17	2.21	1.09	2.02
1942851	OB-01-013	2001	78.87	12.53	0.38	0.26	0.11	0.17	0.17	5.05	3.12	0.109	0.011	Nd	Nd	163	1077	0.42	98.83
1942870	1942851	2001	78.46	12.72	0.33	0.23	0.09	0.17	0.17	4.74	3.16	0.113	0.011	Nd	Nd	176	1088	0.42	100.26
	% Difference B		2.06	1.53	14.77	11.56	21.70	2.38	1.93	6.29	1.30	3.58	3.57	N/A	N/A	8.96	0.97	0.00	1.47
1942878	OB-01-060	2001	78.75	11.23	0.48	0.22	0.23	0.08	0.05	3.05	4.73	0.068	Nd	Nd	Nd	89	714	0.79	99.21
1942890	1942878	2001	78.92	11.25	0.56	0.37	0.16	0.09	0.08	2.74	4.72	0.080	0.002	0.02	Nd	86	713	0.78	99.23
	% Difference C		0.22	0.11	15.10	69.48	30.95	24.23	70.49	10.18	0.19	16.62	N/A	N/A	N/A	3.23	0.17	1.44	0.02
	Average % Diff		1.37	1.30	10.40	28.45	17.56	9.76	24.86	7.26	1.46	7.46	N/A	N/A	N/A	4.12	1.12	0.84	1.17
1942965	GS-02-002	2002	73.63	12.95	2.31	0.36	1.76	0.79	0.52	3.90	3.78	0.26	0.09	0.09	Nd	167	1134	1.29	99.60
1942970	1942955	2002	73.10	13.38	2.19	1.03	1.04	0.76	0.49	3.86	3.74	0.25	0.09	0.08	Nd	163	1167	1.30	99.24
	% Difference A		0.72	3.30	5.16	190.87	40.75	3.38	5.87	1.07	1.00	3.47	2.21	2.52	N/A	4.06	2.94	0.62	0.36
1942974	GS-02-064	2002	72.91	14.38	2.20	1.57	0.57	0.76	0.38	4.17	3.90	0.22	0.08	0.08	Nd	124	1166	1.05	100.12
1942990	1942974	2002	72.53	14.28	2.18	1.72	0.42	0.76	0.39	4.15	3.92	0.22	0.08	0.08	Nd	138	1151	1.06	99.63
	% Difference B		0.52	0.74	0.74	9.48	26.24	0.24	3.46	0.47	0.63	1.53	1.54	0.90	N/A	11.15	1.24	0.76	0.49
Avg % Diff	Average % Diff		0.62	2.02	2.95	100.18	33.50	1.81	4.66	0.77	0.82	2.50	1.87	1.71	N/A	7.61	2.09	0.69	0.43
1943041	GS-03-34	2003	55.18	16.02	7.89	5.00	2.60	4.37	4.84	7.25	0.19	1.20	0.22	0.26	Nd	110	70	3.38	100.79
1943050	1943041	2003	54.84	16.06	7.85	4.95	2.61	4.35	4.84	7.22	0.19	1.19	0.22	0.26	Nd	110	69	3.63	100.65
	% Difference A		0.61	0.26	0.48	0.98	0.38	0.31	0.11	0.30	0.33	0.89	0.72	0.58	N/A	0.06	1.59	7.33	0.14
1943052	GS-03-77	2003	70.30	14.37	2.59	2.20	0.35	0.88	1.03	4.24	3.48	0.26	0.08	0.10	Nd	110	1229	1.12	98.45
1943070	1943052	2003	70.36	14.49	2.52	2.06	0.42	0.84	0.96	4.33	3.50	0.27	0.08	0.09	Nd	108	1240	1.19	98.63
	% Difference B		0.08	0.79	2.38	6.34	20.00	3.84	6.49	2.03	1.13	4.41	7.85	8.82	N/A	1.59	0.86	6.24	0.18
	Average % Diff		0.35	0.52	1.43	3.66	10.19	2.08	3.30	1.16	0.73	2.65	4.29	4.69	N/A	0.82	1.23	6.79	0.16

Nd= Not detected
N/A= Not available

Appendix B: Cont'd

Accuracy Lab #	Field #	Year	SiO2 %	Al2O3 %	Fe2O3 Total %	Fe2O3 %	FeO %	MgO %	CaO %	Na2O %	K2O %	TiO2 %	MnO %	P2O5 %	Cr ppm	Zr ppm	Ba ppm
	Detection Limit		0.01	0.01	0.01	0.01	0.01	0.01	0.01	0.01	0.01	0.001	0.01	0.001	50	1	1
STM-1	Standard	1997	59.94	18.39	5.22			0.1	1.09	8.94	4.28	0.14	0.22	0.18	4	1210	560
STM-1	Measured	1997	59.69	19.13	5.18	Nd	Nd	0.10	1.13	9.05	4.39	0.128	0.227	0.142	Nd	1315	607
	% Difference A		0.09	4.01	1.11	N/A	N/A	2.48	4.05	1.22	2.56	8.31	3.37	11.36	N/A	8.66	8.45
RGM-1	Standard	1997	73.45	13.72	1.86			0.28	1.15	4.07	4.3	0.27	0.04	0.05	4	219	807
RGM-1	Measured	1997	72.78	13.76	1.81	Nd	Nd	0.27	1.15	4.13	4.32	0.254	0.028	0.035	Nd	214	844
	% Difference B		0.91	0.32	2.42	N/A	N/A	2.79	0.34	1.55	0.55	5.87	29.68	29.86	N/A	2.44	4.57
Standard	Standard	1997	62.78	13.67	5.14			2.72	2.62	0.9	2.77	0.63	0.05	0.21	68	160	570
SCO-1	Measured	1997	63.51	13.89	5.17	Nd	Nd	2.77	2.58	0.95	2.81	0.569	0.046	0.200	Nd	167	600
	% Difference C		1.17	1.63	0.54	N/A	N/A	1.72	1.51	5.92	1.38	9.73	9.00	4.99	N/A	4.47	5.33
	Avg % Accuracy		0.72	1.99	1.35	N/A	N/A	2.33	1.97	2.89	1.50	7.97	14.01	15.41	N/A	5.19	6.12
Measured	VS-N	2000	55.73	13.26	4.04	N/A	N/A	4.28	4.36	5.90	8.03	1.021	0.096	-0.01	665	720	1009
Standard	VS-N	2000	55.57	13.44	4.14			4.51	4.53	5.95	8.12	1.08	0.10	0.00	700	700	1000
	% Difference A		0.29	1.31	2.31	N/A	N/A	5.06	3.77	0.77	1.11	5.50	3.99	N/A	5.04	2.82	0.94
Measured	STM-1	2000	59.71	18.48	5.30	N/A	N/A	0.07	1.11	7.89	4.20	0.114	0.219	0.14	Nd	1277	600
Standard	STM-1	2000	59.94	18.39	5.22			0.1	1.09	8.94	4.28	0.14	0.22	0.16	4	1210	560
	% Difference B		0.38	0.47	1.61	N/A	N/A	30.52	1.91	11.75	1.86	18.69	0.64	12.73	N/A	5.57	7.06
Measured	RGM-1	2000	72.89	13.77	1.74	N/A	N/A	0.25	1.19	3.86	4.38	0.244	0.027	0.02	Nd	215	866
Standard	RGM-1	2000	73.45	13.72	1.86			0.28	1.15	4.07	4.3	0.27	0.04	0.05	4	219	807
	% Difference C		0.76	0.34	6.34	N/A	N/A	11.42	3.23	5.08	1.76	9.55	31.34	51.44	N/A	1.73	7.25
	Avg % Accuracy		0.48	0.71	3.42	N/A	N/A	15.67	2.97	5.87	1.58	11.31	11.99	32.09	N/A	3.37	5.09
Measured	STM-1	2001	60.56	18.89	5.26	N/A	N/A	0.09	1.13	8.50	4.31	0.115	0.223	0.20	Nd	1282	610
Standard	STM-1	2001	59.94	18.39	5.22			0.1	1.09	8.94	4.28	0.14	0.22	0.16	4	1210	560
% Diff	% Difference A		1.03	2.70	0.85	N/A	N/A	7.29	3.77	4.92	0.62	17.52	1.43	22.03	N/A	5.92	8.99
Measured	RGM-1	2001	70.30	13.40	1.67	N/A	N/A	0.22	1.10	4.11	4.12	0.223	0.016	0.03	Nd	204	819
Standard	RGM-1	2001	73.45	13.72	1.86			0.26	1.15	4.07	4.3	0.27	0.04	0.05	4	219	807
	% Difference B		4.29	2.33	10.20	N/A	N/A	22.58	4.71	1.03	4.11	17.55	60.26	40.99	N/A	6.96	1.54
Measured	SCO-1	2001	62.83	13.68	5.19	N/A	N/A	2.64	2.56	1.06	2.64	0.548	0.044	0.22	Nd	162	594
Standard	SCO-1	2001	62.78	13.67	5.14			2.72	2.62	0.9	2.77	0.63	0.05	0.21	68	160	570
	% Difference C		0.09	0.08	0.96	N/A	N/A	2.76	2.34	17.36	2.43	12.99	12.29	4.70	N/A	1.40	4.19
	Avg % Accuracy		1.80	1.70	4.00	N/A	N/A	10.88	3.61	7.77	2.39	16.02	24.66	22.57	N/A	4.76	4.91
Measured	BHVO-1	2003	51.13	13.79	12.46	N/A	N/A	7.25	11.52	2.30	0.52	2.79	0.17	0.27	265.38	164	128
Standard	BHVO-1	2003	49.94	13.80	12.23			7.23	11.40	2.26	0.52	2.71	0.17	0.27	289.00	179	139
			1.19	0.01	0.23	N/A	N/A	0.02	0.12	0.04	0.00	0.06	0.00	0.00	N/A	15.34	10.75
	% Difference A		2.39	0.07	1.87	N/A	N/A	0.25	1.06	1.59	0.23	2.95	1.80	1.16	N/A	8.57	7.73

Nd= Not detected
N/A= Not available

APPENDIX C

DUPLICATE AND STANDARD ANALYSIS FOR TRACE-ELEMENT ICP-ES DATA FROM 1997 TO 2003

Duplicate and standard analyses presented here demonstrate the internal consistency in the ICP-ES trace-element analyses. This dataset contains the immobile trace elements that are used to classify many of the units within the field area. These elements include Ti, Nb, Dy, Sc, Y, La, and Ce; the following table illustrates that these trace elements generally have a reproducibility of ±10%.

Appendix C: Duplicate and standard analyses for trace-element ICP-ES data from 1997 to 2003

Precision Lab #	Field #	Year	Mo ppm	Cr ppm	Zn ppm	Pb ppm	Co ppm	Ni ppm	Fe %	Ga ppm	Tl ppm	V ppm	Be ppm	Nb ppm	Cu ppm	Dy ppm	Sc ppm	Y ppm	Mn %	Sr ppm	La ppm	Ce ppm	Ba ppm	Li ppm	As ppm
	Detection Limit		1	1	1	1	1	1	0.01	1	1	1	0.1	1	1	0.1	0.1	1	1	1	1	1	1	1	0.1
1942291	OB-97-140	1997	Nd	2	213	3	Nd	Nd	1.06	8	636	3	3.0	8	1	2.9	3.7	19	636	14	23	63	1585	20.6	N/A
1942310	1942291	1997	Nd	1	211	3	1	Nd	1.12	11	643	3	3.0	8	1	2.9	3.7	18	641	14	21	59	1564	20.4	N/A
	% Difference A		N/A	19.96	0.96	7.08	N/A	N/A	5.10	34.54	1.00	12.42	0.40	0.53	10.55	0.38	1.22	0.04	0.77	0.01	5.74	5.66	0.09	0.97	N/A
1942333	OB-97-137	1997	2	15	45	20	14	6	4.24	21	3135	116	1.5	6	19	1.7	12.5	10	640	129	18	36	636	25.1	N/A
1942350	1942333	1997	2	15	47	22	14	6	4.39	15	3317	117	1.6	6	20	1.8	12.7	11	676	135	19	33	668	25.6	N/A
	% Difference B		6.75	1.94	5.10	9.88	1.06	1.25	3.43	16.01	5.80	1.21	4.13	4.98	5.11	2.62	1.56	5.63	5.62	4.90	4.65	9.02	5.12	2.11	N/A
1942373	OB-97-174	1997	Nd	4	2	Nd	Nd	1	0.19	35	2867	5	0.8	31	1	6.9	12.1	52	Nd	15	39	114	353	7.8	N/A
1942390	1942373	1997	Nd	3	2	1	Nd	2	0.19	39	2800	5	0.8	31	1	6.8	12.0	51	4	16	43	115	344	7.8	N/A
	% Difference C		N/A	11.05	0.13	N/A	N/A	8.89	1.61	10.92	2.46	1.57	1.61	0.33	0.45	2.47	1.07	2.41	N/A	6.36	12.11	0.72	2.46	0.08	N/A
1942402	OB-97-363	1997	10	72	99	124	12	30	3.91	15	7229	105	1.1	4	63	3.8	18.2	20	1138	187	98	139	1732	14.1	N/A
1942410	1942402	1997	10	72	101	125	12	30	3.95	18	7325	106	1.1	3	63	4.1	18.4	20	1131	186	100	145	1730	14.2	N/A
	% Difference D		1.67	0.01	1.76	1.26	0.40	0.57	1.04	20.34	1.33	1.13	0.78	9.14	0.48	8.52	0.92	1.50	0.63	0.12	2.35	4.97	0.10	0.93	N/A
	Average % Diff		4.31	8.24	1.99	6.08	0.74	3.57	2.79	20.45	2.65	4.08	1.77	3.74	4.15	3.55	1.19	2.40	2.34	2.84	6.21	5.09	1.95	1.02	N/A
1942662	OB-00-023	2000	1	17	75	Nd	8	10	3.63	Nd	3847	77	1.8	10	1641	6.8	15.1	37	594	23	91	43	736	21.6	5
1942670	1942662	2000	1	16	76	Nd	9	10	3.65	Nd	3872	76	1.8	12	1672	7.1	15.3	37	598	24	91	43	738	21.3	5
	% Difference A		10.80	2.99	0.76	N/A	4.21	2.65	0.66	N/A	0.63	0.74	1.66	19.77	1.89	4.93	1.53	0.91	0.79	1.23	0.19	0.40	0.44	1.23	4.47
1942675	OB-00-076	2000	2	1	85	Nd	6	5	2.54	Nd	3109	40	1.1	6	3	2.1	9.2	18	1123	241	23	38	972	12.6	9
1942690	1942675	2000	2	2	91	2	6	5	2.53	Nd	3132	39	1.1	7	3	2.2	9.1	18	1135	237	23	36	970	12.6	9
	% Difference B		5.31	35.67	6.52	N/A	0.17	2.29	0.24	N/A	0.73	1.17	0.85	17.93	13.16	5.54	1.33	0.17	1.03	1.47	0.78	4.32	0.24	1.60	1.50
1942704	OB-00-123	2000	Nd	1	32	6	2	2	1.02	Nd	1073	6	1.7	7	Nd	1.5	3.3	13	551	185	22	30	833	6.9	4
1942710	1942704	2000	Nd	1	32	6	2	2	0.99	Nd	1049	6	1.7	7	Nd	1.4	3.2	13	537	180	22	30	813	6.6	6
	% Difference C		N/A	9.09	1.06	3.03	2.62	0.80	2.75	N/A	2.24	9.35	2.12	3.81	N/A	12.70	2.68	1.91	2.49	2.38	0.34	2.77	2.42	3.85	37.39
1942725	OB-00-162	2000	Nd	Nd	97	Nd	8	4	4.05	Nd	4079	57	1.9	8	2	3.3	13.7	22	1260	191	25	43	907	17.0	5
1942730	1942725	2000	Nd	Nd	97	Nd	8	4	4.05	Nd	4072	56	1.9	7	3	3.5	13.7	23	1267	192	25	42	910	16.9	3
	% Difference D		N/A	N/A	0.09	N/A	0.69	2.17	0.03	N/A	0.17	1.49	0.24	16.73	62.80	6.04	0.49	1.35	0.60	0.30	1.18	1.29	0.37	0.14	23.32
1942744	OB-00-193	2000	5	51	83	Nd	21	31	3.58	Nd	8340	113	2.8	14	2733	5.2	16.8	35	848	130	23	41	592	27.7	10
1942750	1942744	2000	5	49	84	Nd	21	31	3.59	Nd	8358	113	2.8	14	2728	5.7	16.8	36	852	130	24	43	586	28.1	8
	% Difference E		1.67	3.17	1.06	N/A	2.46	0.66	0.39	N/A	0.22	0.10	0.17	3.34	0.26	9.69	0.00	0.18	0.53	0.09	1.53	4.77	0.90	1.33	24.03
1942757	OB-00-305	2000	50	Nd	64	384	Nd	2	1.28	0.1	1572	12	1.5	11	9	0.8	4.5	8	247	99	9	13	948	1.3	29
1942770	1942757	2000	51	Nd	63	380	Nd	2	1.29	0.2	1564	13	1.5	10	10	0.4	4.5	8	246	100	9	16	959	1.5	34
	% Difference F		2.80	N/A	1.06	0.92	N/A	19.58	2.29	16.87	0.52	5.14	0.16	8.82	17.70	39.10	1.14	2.62	0.15	1.10	9.87	21.73	1.41	11.84	15.40
1942787	OB-00-271	2000	Nd	70	73	Nd	26	30	5.07	Nd	8022	162	0.7	4	47	3.3	25.0	24	989	310	11	19	135	20.3	3
1942790	1942787	2000	Nd	78	74	Nd	26	30	5.08	Nd	8013	165	0.7	4	46	2.8	25.1	24	994	312	12	21	134	20.0	3
	% Difference G		N/A	11.59	0.99	N/A	0.25	0.03	0.20	N/A	0.16	2.35	1.92	3.97	1.48	14.47	0.21	0.49	0.53	0.56	1.61	6.25	0.70	1.47	22.95
1942799	OB-00-279	2000	1	5	54	14	2	5	2.62	Nd	1724	7	2.1	25	29	9.3	8.1	68	460	62	43	73	383	6.5	4
1942810	1942799	2000	2	6	57	14	3	6	2.81	Nd	1776	8	2.1	25	33	9.2	8.3	68	483	64	46	73	345	6.9	5
	% Difference H		7.98	11.19	4.87	1.04	6.53	22.16	3.22	N/A	3.07	13.65	2.18	2.39	16.16	1.38	2.52	0.12	4.89	2.41	6.47	0.16	12.14	1.53	5.42
	Average % Diff		5.75	12.26	2.06	1.66	2.42	6.29	1.22	16.87	0.97	4.25	1.16	9.59	16.21	11.76	1.24	0.97	1.39	1.19	2.75	5.21	2.33	2.86	16.81

Nd= Not detected
N/A= Not available

Appendix C: Cont'd

Precision Lab #	Field #	Year	Mo ppm	Cr ppm	Zn ppm	Pb ppm	Co ppm	Ni ppm	Fe %	Cd ppm	Ti ppm	V ppm	Be ppm	Nb ppm	Cu ppm	Dy ppm	Sc ppm	Y ppm	Mn ppm	Sr ppm	La ppm	Ce ppm	Ba ppm	Li ppm	As ppm	Rb ppm
	Detection Limit		1	1	1	1	1	1	0.01	0.1	1	1	0.1	1	1	0.1	0.1	1	1	1	1	1	1	1	0.1	ppm
1942839	OB-01-001	2001	Nd	160	79	4	33	69	5.88	0.1	8194	218	1.1	7	39	4.5	29.0	29	1098	306	13	29	1295	20.1	3	N/A
1942850	1942839	2001	Nd	166	78	4	33	71	6.08	0.2	8462	221	1.1	8	43	4.7	29.1	29	1101	313	13	31	1333	20.6	3	N/A
	% Difference A		N/A	4.01	0.92	8.81	1.06	3.47	3.37	39.32	3.27	1.54	0.30	3.17	8.09	4.49	0.58	0.77	0.22	2.14	2.57	6.82	2.90	2.50	1.49	N/A
1942851	OB-01-013	2001	1	Nd	22	3	Nd	1	0.27	Nd	928	6	1.7	13	6	5.5	2.2	39	179	67	20	40	1108	2.2	4	N/A
1942870	1942851	2001	1	2	22	4	Nd	1	0.26	0.1	891	5	1.7	13	6	4.8	2.1	38	177	65	20	41	1076	2.0	Nd	N/A
	% Difference B		6.90	N/A	1.29	11.39	N/A	6.27	2.58	N/A	3.98	9.93	2.27	4.81	7.41	3.27	5.08	5.39	1.47	2.28	0.35	1.29	2.92	10.04	N/A	N/A
1942878	OB-01-080	2001	Nd	Nd	19	56	Nd	1	0.40	Nd	647	9	1.1	13	3	1.8	3.2	12	113	68	8	16	728	2.3	4	N/A
1942890	1942878	2001	Nd	Nd	19	54	Nd	1	0.39	Nd	636	11	1.1	10	6	1.5	2.9	13	112	68	9	18	720	2.3	3	N/A
	% Difference C		N/A	N/A	1.90	3.24	N/A	14.20	3.16	N/A	1.68	23.39	2.35	25.18	113.45	13.01	6.83	4.14	0.49	0.31	7.30	13.34	0.99	0.79	28.56	N/A
1942908	OB-01-050	2001	1	281	22	6	1	6	1.43	Nd	394	25	1.4	1	9	0.7	1.8	4	264	12	8	16	479	13.6	3	N/A
1942910	1942908	2001	1	280	21	6	1	6	1.41	Nd	403	27	1.5	Nd	9	0.9	1.7	4	262	12	8	13	480	13.8	3	N/A
	% Difference D		3.87	0.21	4.40	2.51	13.69	3.09	1.50	N/A	2.06	7.54	1.89	N/A	0.37	21.16	4.49	1.52	0.94	0.18	2.80	15.28	0.18	1.19	13.13	N/A
	Average % Diff		N/A	N/A	2.13	6.49	N/A	6.01	2.65	N/A	2.75	10.60	1.70	N/A	32.33	11.96	4.25	2.45	0.78	1.23	3.36	9.11	1.75	3.83	N/A	N/A
1942965	GS-02-002	2002	1.13	2.76	63.91	14.70	3.52	2.60	1.48	Nd	1725.24	32.52	1.07	8.36	5.90	2.37	4.64	17.74	749.40	103.15	20.60	51.05	238.57	4.27	2.47	77
1942970	1942965	2002	1.33	6.73	63.50	14.27	3.68	14.64	1.43	Nd	1753.51	33.06	1.08	8.16	5.90	2.39	4.70	18.30	760.32	104.17	20.94	52.21	278.27	4.35	3.79	79
	% Difference A		15.21	59.02	0.64	2.97	4.30	82.22	3.12	N/A	1.61	1.64	1.01	2.42	0.06	0.88	1.41	3.08	1.44	0.98	1.64	2.21	14.27	1.83	34.97	2.53
1942974	GS-02-084	2002	1.06	1.74	55.17	8.73	3.45	2.94	1.63	Nd	1617.53	28.39	1.24	8.37	5.55	1.77	3.71	14.06	548.36	130.68	26.81	37.84	1099.55	5.45	3.85	86
1942990	1942974	2002	1.19	2.23	54.55	8.86	3.54	3.55	1.54	Nd	1595.63	28.19	1.22	8.24	5.58	1.90	3.67	14.03	540.91	130.43	26.36	37.21	1084.34	5.38	3.81	85
	% Difference B		10.77	22.08	1.13	1.40	2.30	17.21	5.88	N/A	1.37	0.70	1.28	1.70	0.64	6.50	0.91	0.24	1.38	0.19	1.75	1.69	1.40	1.34	1.00	1.18
	Average % Diff		12.99	40.55	0.88	2.19	3.30	49.71	4.50	N/A	1.49	1.17	1.14	2.06	0.35	3.69	1.16	1.66	1.41	0.59	1.70	1.95	7.83	1.59	17.99	1.86
1943050	1943041	2003	Nd	64	79	13	29	54	5.19	Nd	7568	203	1.0	6	41	3.0	23.4	20	1733	113	10	25	75	12.9	4	N/A
1943041	GS-03-34	2003	Nd	65	80	13	29	55	5.27	Nd	7568	203	1.0	6	36	3.0	23.5	21	1735	115	11	25	76	12.7	Nd	N/A
	% Difference A		N/A	2.00	0.51	1.63	0.25	0.68	1.62	N/A	0.00	0.00	0.28	0.85	11.57	1.50	0.38	1.22	0.12	1.28	3.25	0.34	0.16	1.45	N/A	N/A
1943070	1943052	2003	Nd	2	61	18	5	3	1.90	Nd	1993	34	1.6	9	Nd	2.0	5.8	15	691	197	28	42	1195	5.8	Nd	N/A
1943052	GS-03-77	2003	Nd	2	62	19	5	3	2.00	Nd	2009	35	1.6	9	Nd	2.0	5.9	16	686	199	28	45	1203	5.9	Nd	N/A
	% Difference B		N/A	1.89	0.38	4.15	2.74	3.85	5.61	N/A	0.82	2.94	0.95	1.87	N/A	1.87	0.87	2.67	0.68	1.29	1.50	6.98	0.68	1.73	N/A	N/A
	Average % Diff		N/A	1.94	0.50	2.89	1.49	2.27	3.61	N/A	0.41	1.47	0.61	1.36	11.57	1.68	0.63	1.94	0.40	1.28	2.37	3.66	0.43	1.59	N/A	N/A

Nd= Not detected
N/A= Not available

Appendix C: Cont'd

Accuracy																								
	Year	Mo	Cr	Zn	Pb	Co	Ni	Fe	Ga	Ti	V	Be	Nb	Cu	Zr	Dy	Sc	Y	Mn	Sr	La	Ce	Ba	Li
		ppm	ppm	ppm	ppm	ppm	ppm	%	ppm	ppm	ppm	ppm	ppm	ppm	ppm	ppm	ppm	ppm	%	ppm	ppm	ppm	ppm	ppm
Detection Limit		1	1	1	1	1	1	0.01	1	1	1	0.1	1	1	0.1	0.1	1	1	1	1	1	1	1	0.1
Measured MRG-1	1997	Nd	284	214	3	N/A	N/A	12.08	23	24459	N/A	0.4	21	N/A	91	2.7	N/A	14	1276	261	13	31	48	3.8
Standard MRG-1	1997	1	430	191	10	87	193	12.55	N/A	22800	526	0.6	N/A	N/A	N/A	N/A	55.0	14	1300	266	10	26	61	4.2
% Diff		N/A	33.98	11.90	68.27	N/A	N/A	3.71	N/A	8.22	N/A	38.65	N/A	N/A	N/A	N/A	N/A	2.03	1.81	1.87	37.16	17.72	20.66	8.79
Measured SY-2	1997	Nd	6	N/A	N/A	9	5	N/A	N/A	N/A	53	N/A	N/A	5	N/A	N/A	6.8	N/A	N/A	N/A	N/A	N/A	N/A	N/A
Standard SY-2	1997	2	10	248	85	9	10	4.41	N/A	899	50	22.0	N/A	N/A	N/A	N/A	7.0	128	2500	271	75	175	460	95.0
% Diff		N/A	32.75	N/A	N/A	7.12	48.88	N/A	N/A	N/A	6.35	N/A	N/A	N/A	N/A	N/A	3.07	N/A	N/A	N/A	N/A	N/A	N/A	N/A
Measured MRG-1	1997	Nd	288	192	3	N/A	N/A	12.34	20	25162	N/A	0.4	21	N/A	92	2.8	N/A	14	1276	263	14	27	48	4.0
Standard MRG-1	1997	1	430	191	10	87	193	12.55	N/A	22800	526	0.6	N/A	N/A	N/A	N/A	55.0	14	1300	266	10	26	61	4.2
% Diff		N/A	33.08	0.57	68.12	N/A	N/A	1.70	N/A	11.34	N/A	38.48	N/A	N/A	N/A	N/A	N/A	0.40	1.86	1.09	45.15	2.13	19.07	5.60
Measured SY-2	1997	Nd	6	N/A	N/A	9	5	N/A	N/A	N/A	52	N/A	N/A	5	N/A	N/A	6.8	N/A	N/A	N/A	N/A	N/A	N/A	N/A
Standard SY-2	1997	2	10	248	85	9	10	4.41	N/A	899	50	22.0	N/A	N/A	N/A	N/A	7.0	128	2500	271	75	175	480	95.0
% Diff		N/A	34.66	N/A	N/A	6.38	46.11	N/A	N/A	N/A	3.29	N/A	N/A	N/A	N/A	N/A	3.57	N/A	N/A	N/A	N/A	N/A	N/A	N/A
Measured SY-2	1997	Nd	8	N/A	N/A	9	5	N/A	N/A	N/A	51	N/A	N/A	4	N/A	N/A	6.4	N/A	N/A	N/A	N/A	N/A	N/A	N/A
Standard SY-2	1997	2	10	248	85	9	10	4.41	N/A	899	50	22.0	N/A	N/A	N/A	N/A	7.0	128	2500	271	75	175	480	95.0
% Diff		N/A	19.72	N/A	N/A	1.60	49.99	N/A	N/A	N/A	1.99	N/A	N/A	N/A	N/A	N/A	9.07	N/A	N/A	N/A	N/A	N/A	N/A	N/A
Measured MRG-1	1997	Nd	283	196	4	N/A	N/A	12.74	29	26063	N/A	0.4	23	N/A	94	2.9	N/A	14	1343	265	16	31	50	4.1
Standard MRG-1	1997	1	430	191	10	87	193	12.55	N/A	22800	526	0.6	N/A	N/A	N/A	N/A	55.0	14	1300	266	10	26	61	4.2
% Diff		N/A	34.15	2.39	64.73	N/A	N/A	1.51	N/A	15.32		35.52	N/A	N/A	N/A	N/A	N/A	3.05	3.29	0.30	66.51	18.09	18.00	2.00
Measured SY-2	1997	Nd	6	N/A	N/A	9	6	N/A	N/A	N/A	51	N/A	N/A	4	N/A	N/A	6.5	N/A	N/A	N/A	N/A	N/A	N/A	N/A
Standard SY-2	1997	2	10	248	85	9	10	4.41	N/A	899	50	22.0	N/A	N/A	N/A	N/A	7.0	128	2500	271	75	175	480	95.0
% Diff		N/A	17.06	N/A	N/A	4.00	38.47	N/A	N/A	N/A	2.79	N/A	N/A	N/A	N/A	N/A	7.52	N/A	N/A	N/A	N/A	N/A	N/A	N/A
Measured MRG-1	1997	Nd	285	197	3	N/A	N/A	12.34	16	25833	N/A	0.4	22	N/A	90	2.8	N/A	14	1293	263	14	27	48	3.8
Standard MRG-1	1997	1	430	191	10	87	193	12.55	N/A	22800	526	0.6	N/A	N/A	N/A	N/A	55.0	14	1300	266	10	26	61	4.2
% Diff		N/A	33.78	3.10	68.19	N/A	N/A	1.70	N/A	13.42	N/A	37.75	N/A	N/A	N/A	N/A	N/A	0.99	0.54	1.04	40.05	4.11	21.00	8.37
Measured SY-2	1997	Nd	8	N/A	N/A	9	6	N/A	N/A	N/A	51	N/A	N/A	4	N/A	N/A	6.5	N/A	N/A	N/A	N/A	N/A	N/A	N/A
Standard SY-2	1997	2	10	248	85	9	10	4.41	N/A	899	50	22.0	N/A	N/A	N/A	N/A	7.0	128	2500	271	75	175	480	95.0
% Diff		N/A	14.54	N/A	N/A	7.09	36.06	N/A	N/A	N/A	2.38	N/A	N/A	N/A	N/A	N/A	6.94	N/A	N/A	N/A	N/A	N/A	N/A	N/A
Measured MRG-1	1997	Nd	286	187	4	N/A	N/A	12.43	24	25591	N/A	0.4	21	N/A	92	2.7	N/A	14	1295	261	13	27	48	3.8
Standard MRG-1	1997	1	430	191	10	87	193	12.55	N/A	22800	526	0.6	N/A	N/A	N/A	N/A	55.0	14	1300	266	10	26	61	4.2
% Diff			33.43	2.09	64.63	N/A	N/A	0.92	N/A	13.23	N/A	37.98	N/A	N/A	N/A	N/A	N/A	1.03	0.41	2.05	33.24	2.96	20.93	10.33
Measured SY-2	1997	Nd	8	N/A	N/A	9	7	N/A	N/A	N/A	50	N/A	N/A	4	N/A	N/A	6.4	N/A	N/A	N/A	N/A	N/A	N/A	N/A
Standard SY-2	1997	2	10	248	85	9	10	4.41	N/A	899	50	22.0	N/A	N/A	N/A	N/A	7.0	128	2500	271	75	175	480	95.0
% Diff		N/A	11.44	N/A	N/A	0.98	33.59	N/A	N/A	N/A	0.39	N/A	N/A	N/A	N/A	N/A	8.74	N/A	N/A	N/A	N/A	N/A	N/A	N/A
Avg % Accuracy		N/A	27.17	4.01	66.39	4.89	42.52	1.91	N/A	12.31	2.86	37.26	N/A	N/A	N/A	N/A	N/A	1.50	1.56	1.27	44.42	9.00	19.93	N/A

Nd= Not detected
N/A= Not available

303

Appendix C: Cont'd

Accuracy	Year	Mo ppm	Cr ppm	Zn ppm	Pb ppm	Co ppm	Ni ppm	Fe %	Cd ppm	Ti ppm	V ppm	Be ppm	Nb ppm	Cu ppm	Dy ppm	Sc ppm	Y ppm	Mn ppm	Sr ppm	La ppm	Ce ppm	Ba ppm	Li ppm	As ppm
Detection Limit		1	1	1	1	1	1	0.01	0.1	1	1	0.1	1	1	0.1	0.1	1	1	1	1	1	1	1	0.1
Measured WGB-1	2000	1	270	39	Nd	29	57	4.51	Nd	5036	215	0.4	9	103	2.2	41.4	17	1076	102	8	14	816	43.9	8
Standard WGB-1	2000	N/A	291	32	N/A	30	76	4.69	N/A	5040	222	N/A	N/A	N/A	N/A	44.0	15	1100	118	9	N/A	851	N/A	N/A
% Diff		N/A	7.36	23.36	N/A	3.89	25.56	3.90	N/A	0.04	3.35	N/A	N/A	N/A	N/A	6.00	16.00	2.17	13.83	12.44	N/A	4.25	N/A	N/A
Measured MRG-1	2000	Nd	270	187	6	N/A	N/A	12.02	Nd	21446	N/A	0.6	25	N/A	2.5	N/A	14	1261	251	9	28	48	5.2	3
Standard MRG-1	2000	1	430	191	10	87	193	12.55	N/A	22600	526	0.6	N/A	N/A	N/A	55.0	14	1300	266	10	26	61	4.2	N/A
% Diff		N/A	37.14	1.90	44.91	N/A	N/A	4.23	N/A	5.10	N/A	3.22	N/A	N/A	N/A	N/A	3.02	2.97	5.73	4.16	1.25	20.51	23.30	N/A
Measured SY-2	2000	1	7	N/A	N/A	9	10	N/A	Nd	N/A	43	N/A	N/A	3	N/A	7.3	N/A	N/A	N/A	N/A	N/A	N/A	N/A	18
Standard SY-2	2000	2	10	248	N/A	9	10	4.41	N/A	899	50	22.0	N/A	N/A	N/A	7.0	128	2500	271	75	175	460	95.0	N/A
% Diff		20.75	30.96	N/A	N/A	7.95	3.30	N/A	N/A	N/A	13.26	N/A	N/A	N/A	N/A	3.94	N/A	N/A	N/A	N/A	N/A	N/A	N/A	N/A
Measured WGB-1	2000	Nd	262	36	Nd	28	54	4.46	Nd	4995	205	0.4	9	103	2.3	41.1	17	1042	101	8	15	804	44.4	8
Standard WGB-1	2000	N/A	291	32	N/A	30	76	4.69	N/A	5040	222	N/A	N/A	N/A	N/A	44.0	15	1100	118	9	N/A	851	N/A	N/A
% Diff		N/A	9.91	21.77	N/A	4.41	28.33	4.93	N/A	0.88	7.66	N/A	N/A	N/A	N/A	6.67	13.64	5.23	14.30	6.09	N/A	5.47	N/A	N/A
Measured MRG-1	2000	Nd	284	179	2	N/A	N/A	12.22	Nd	21598	N/A	0.6	27	N/A	3.1	N/A	15	1278	253	9	29	48	5.1	6
Standard MRG-1	2000	1	430	191	10	87	193	12.55	N/A	22600	526	0.6	N/A	N/A	N/A	55.0	14	1300	266	10	26	61	4.2	N/A
% Diff		N/A	33.95	6.27	78.25	N/A	N/A	2.64	N/A	4.43	N/A	1.16	N/A	N/A	N/A	N/A	5.99	1.71	4.96	5.39	10.16	21.30	22.27	N/A
Measured SY-2	2000	Nd	6	N/A	N/A	9	9	N/A	Nd	N/A	47	N/A	N/A	4	N/A	7.4	N/A	N/A	N/A	N/A	N/A	N/A	N/A	17
Standard SY-2	2000	2	10	248	N/A	9	10	4.41	N/A	899	50	22.0	N/A	N/A	N/A	7.0	128	2500	271	75	175	460	95.0	N/A
% Diff		N/A	34.39	N/A	N/A	5.89	11.24	N/A	N/A	N/A	5.32	N/A	N/A	N/A	N/A	6.42	N/A	N/A	N/A	N/A	N/A	N/A	N/A	N/A
Measured WGB-1	2000	Nd	273	40	3	29	59	4.60	Nd	5039	214	0.4	9	106	2.3	42.3	17	1063	104	8	14	832	45.7	3
Standard WGB-1	2000	N/A	291	32	N/A	30	76	4.69	N/A	5040	222	N/A	N/A	N/A	N/A	44.0	15	1100	118	9	N/A	851	N/A	N/A
% Diff		N/A	6.20	26.42	N/A	3.81	22.76	1.86	N/A	0.02	3.40	N/A	N/A	N/A	N/A	3.86	16.06	3.37	11.50	2.66	N/A	2.28	N/A	N/A
Measured MRG-1	2000	Nd	282	186	2	N/A	N/A	12.15	Nd	21624	N/A	0.6	25		3.0	N/A	15	1285	252	10	28	49	5.1	-2
Standard MRG-1	2000	1	430	191	10	87	193	12.55	N/A	22600	526	0.6	N/A	N/A	N/A	55.0	14	1300	266	10	26	61	4.2	N/A
% Diff		N/A	34.36	2.39	83.41	N/A	N/A	3.18	N/A	4.32	N/A	3.72	N/A	N/A	N/A	N/A	4.73	0.97	5.32	2.91	7.02	20.22	22.14	N/A
Measured SY-2	2000	Nd	7	N/A	N/A	10	9	N/A	Nd		45	N/A	N/A	3	N/A	7.3	N/A	N/A	N/A	N/A	N/A	N/A	N/A	17
Standard SY-2	2000	2	10	248	N/A	9	10	4.41	N/A	899	50	22.0	N/A	N/A	N/A	7.0	128	2500	271	75	175	460	95.0	N/A
% Diff		N/A	27.35	N/A	N/A	14.68	6.24	N/A	N/A	N/A	10.87	N/A	N/A	N/A	N/A	3.92	N/A	N/A	N/A	N/A	N/A	N/A	N/A	N/A
Avg % Accuracy		20.75	24.63	13.69	66.85	6.75	16.57	3.46	N/A	2.47	7.26	2.71	N/A	N/A	N/A	5.14	9.91	2.84	9.26	5.61	6.15	12.34	22.57	N/A

Nd= Not detected

N/A= Not available

Appendix C: Cont'd

Accuracy	Year	Mo ppm	Cr ppm	Zn ppm	Pb ppm	Co ppm	Ni ppm	Fe %	Cd ppm	Ti ppm	V ppm	Be ppm	Nb ppm	Cu ppm	Dy ppm	Sc ppm	Y ppm	Mn ppm	Sr ppm	La ppm	Ce ppm	Ba ppm	Li ppm	As ppm
Detection Limit		1	1	1	1	1	1	0.01	0.1	1	1	0.1	1	1	0.1	0.1	1	1	1	1	1	1	1	0.1
Measured WGB-1	2001	Nd	268	42	5	29	60	4.52	0.2	5237	231	0.5	8	104	2.4	41.4	15	1065	103	7	18	839	46.2	2
Standard WGB-1	2001	N/A	291	31.5	N/A	29.8	76	4.69	N/A	5040	222	N/A	N/A	N/A	N/A	44	14.6	1100	118	8.7	N/A	851	N/A	N/A
% Diff		N/A	7.86	32.09	N/A	1.86	20.64	3.62	N/A	3.90	4.04	N/A	N/A	N/A	N/A	5.98	5.14	3.20	12.99	23.23	N/A	1.46	N/A	N/A
Measured SY-2	2001	Nd	6	N/A	N/A	10	11	N/A	0.1	N/A	53	N/A	N/A	5	N/A	7.3	N/A	N/A	N/A	N/A	N/A	N/A	N/A	18
Standard SY-2	2001	1.8	9.5	248	85	8.6	9.9	4.41	N/A	899	50	N/A	N/A	N/A	N/A	7	128	2500	271	75	175	460	95	N/A
% Diff		N/A	33.83	N/A	N/A	14.07	15.43	N/A	N/A	N/A	5.55	N/A	N/A	N/A	N/A	4.20	N/A	N/A	N/A	N/A	N/A	N/A	N/A	N/A
Measured WGB-1	2001	Nd	284	40	12	29	62	4.75	0.1	5298	233	0.7	9	106	2.4	41.3	17	1092	104	7	18	862	47.7	2
Standard WGB-1	2001	N/A	291	31.5	N/A	29.8	76	4.69	N/A	5040	222	N/A	N/A	N/A	N/A	44	14.6	1100	118	8.7	N/A	851	N/A	N/A
% Diff		N/A	2.45	27.36	N/A	2.10	18.62	1.27	N/A	5.09	5.15	N/A	N/A	N/A	N/A	6.21	13.69	0.71	12.03	19.90	N/A	1.25	N/A	N/A
Avg % Accuracy		N/A	14.71	29.72	N/A	6.01	18.23	2.45	N/A	N/A	4.91	N/A	N/A	N/A	N/A	5.46	9.41	1.95	12.51	21.57	N/A	1.35	N/A	N/A
Measured WGB-1	2002	1	274	40	7	29	69	4.34	Nd	5314	233	0.5	8	110	2.5	41.1	16	1063	105	8	14	799	45.4	5
Standard WGB-1	2002	N/A	291	31.5	N/A	29.8	76	4.69	N/A	5040	222	N/A	N/A	N/A	N/A	44	14.6	1100	118	8.7	N/A	851	N/A	N/A
% Diff		N/A	5.91	27.04	N/A	1.58	9.47	7.37	N/A	5.44	5.09	N/A	N/A	N/A	N/A	6.48	8.78	3.35	11.17	12.66	N/A	6.10	N/A	N/A
Measured SY-4	2002	Nd	9	100	10	2	10	4.44	Nd	1708	9	2.6	15	1	17.3	0.8	120	874	1051	62	96	349	38.7	3
Standard SY-4	2002	N/A	12	93	10	2.8	9	4.2	N/A	1720	8	2.6	N/A	N/A	N/A	1.1	119	819	1191	58	122	340	37	N/A
% Diff		N/A	26.62	7.46	4.45	20.98	7.56	5.60	N/A	0.68	9.48	1.33	N/A	N/A	N/A	29.34	0.46	6.72	11.76	6.41	21.44	2.68	4.51	N/A
Avg % Accuracy		N/A	16.27	17.26	N/A	11.23	8.51	6.59	N/A	3.06	7.29	N/A	N/A	N/A	N/A	17.91	4.63	5.04	11.46	9.54	N/A	4.39	N/A	N/A
Measured SY-4	2003	Nd	9	98	22	2	9	4.63	Nd	1750	10	2.7	14	2	16.8	0.8	123	847	1145	61	105	345	40.9	Nd
Standard SY-4	2003	N/A	12	93	10	2.8	9	4.2	N/A	1720	8	2.6	N/A	N/A	N/A	1.1	119	819	1191	58	122	340	37	1.38
% Diff		N/A	21.07	5.54	123.14	29.81	5.18	10.28	N/A	1.74	30.35	3.61	N/A	N/A	N/A	23.81	3.50	3.48	3.90	4.93	14.30	1.56	10.64	N/A
Measured MRG-1	2003	Nd	288	181	2	N/A	N/A	11.14	Nd	22516	N/A	0.4	23	N/A	1.7	N/A	13	1327	256	9	33	48	5.8	Nd
Standard MRG-1	2003	1	430	191	10	87	193	12.55	N/A	22600	526	0.6	N/A	N/A	N/A	55.0	14	1300	266	10	26	61	4.2	N/A
% Diff		N/A	32.93	5.21	79.52	N/A	N/A	11.26	N/A	0.37	N/A	29.20	N/A	N/A	N/A	N/A	6.91	2.06	3.62	11.75	26.10	21.49	37.65	N/A
Avg % Accuracy		N/A	27.00	5.37	101.33	N/A	N/A	10.77	N/A	1.05	N/A	16.40	N/A	N/A	N/A	N/A	5.20	2.77	3.76	8.34	20.20	11.53	24.14	N/A

Nd= Not detected
N/A= Not available

APPENDIX D

STANDARD ANALYSIS FOR XRF DATA

The following table contains standards analyzed with select samples from the field area. The major-elements such as SiO_2, Al_2O_3, Na_2O and K_2O all display errors less than 10%. Other elements, such as S, Cl and, to a lesser degree, V, have much more significant errors, but these elements were not applied to this study.

Appendix D: Standard analyses for XRF data

XRF Standard's data	Na2O	MgO	Al2O3	SiO2	P2O5	S	Cl	K2O	CaO	Sc	TiO2	V	Cr	MnO	Fe2O3T
	wt%	wt%	wt%	wt%	wt%	ppm	ppm	wt%	wt%	ppm	wt%	ppm	ppm	wt%	wt%
Detection Limit	0.008	0.012	0.012	0.01	0.005	25	41	0.003	0.003	10	0.003	7	8	0.002	0.005
Measured SY-2	4.22%	2.99%	12.78%	62.61%	0.42%	782	663	4.34%	7.99%	9	0.12%	49	3	0.31%	6.31%
Standard SY-2	4.31%	2.69%	12.04%	60.05%	0.43%	160	140	4.44%	7.96%	7	0.14%	50	10	0.32%	6.31%
% Diff	2.09	10.98	6.18	4.27	2.13	388.95	366.16	2.25	0.36	21.73	11.26	1.73	65.47	3.07	0.00
Measured SY-2	4.23%	2.98%	12.79%	62.67%	0.42%	800	665	4.37%	8.02%	11	0.12%	48	1	0.31%	6.31%
Standard SY-2	4.31%	2.69%	12.04%	60.05%	0.43%	160	140	4.44%	7.96%	7	0.14%	50	10	0.32%	6.31%
% Diff	1.82	10.94	6.22	4.36	1.80	400.18	374.97	1.49	0.73	53.75	11.45	4.45	89.21	3.21	0.07
Measured SY-2	4.20%	2.98%	12.74%	62.58%	0.43%	791	643	4.33%	7.98%	5	0.13%	52	Nd	0.31%	6.31%
Standard SY-2	4.31%	2.69%	12.04%	60.05%	0.43%	160	140	4.44%	7.96%	7	0.14%	50	10	0.32%	6.31%
% Diff	2.44	10.85	5.86	4.22	0.63	394.64	359.28	2.43	0.28	24.67	9.57	4.72	N/A	3.31	0.01
Measured SY-2	4.22%	2.99%	12.80%	62.61%	0.42%	792	678	4.31%	7.97%	15	0.12%	53	3	0.31%	6.31%
Standard SY-2	4.31%	2.69%	12.04%	60.05%	0.43%	160	140	4.44%	7.96%	7	0.14%	50	10	0.32%	6.31%
% Diff	2.00	11.32	6.34	4.26	1.95	394.93	384.27	2.84	0.14	118.49	11.33	6.51	65.94	2.91	0.06
Measured SY-3	4.12%	2.87%	12.55%	62.11%	0.52%	1093	710	4.17%	8.06%	10	0.12%	12	Nd	0.30%	6.16%
Standard SY-3	4.12%	2.67%	11.75%	59.62%	0.54%	510	150	4.23%	8.28%	7	0.15%	50	11	0.32%	6.49%
% Diff	0.10	7.43	6.83	4.18	3.29	114.27	373.63	1.32	2.37	38.36	17.44	75.57	N/A	5.73	5.11
Measured SY-3	4.11%	2.87%	12.54%	62.16%	0.53%	1085	732	4.19%	8.13%	Nd	0.13%	19	2	0.31%	6.19%
Standard SY-3	4.12%	2.67%	11.75%	59.62%	0.54%	510	150	4.23%	8.28%	7	0.15%	50	11	0.32%	6.49%
% Diff	0.36	7.39	6.76	4.30	2.69	108.92	388.23	0.93	1.53	N/A	11.40	61.98	86.21	3.84	4.68
Measured SY-3	4.11%	2.87%	12.52%	62.02%	0.53%	1100	760	4.21%	8.07%	Nd	0.13%	18	Nd	0.30%	6.17%
Standard SY-3	4.12%	2.67%	11.75%	59.62%	0.54%	510	150	4.23%	8.28%	7	0.15%	50	11	0.32%	6.49%
% Diff	0.25	7.52	6.53	4.03	2.00	115.60	406.43	0.38	2.34	N/A	14.11	84.24	N/A	6.47	4.95
Measured SY-3	4.11%	2.87%	12.51%	62.15%	0.53%	1104	700	4.19%	8.14%	11	0.12%	17	1	0.30%	6.17%
Standard SY-3	4.12%	2.87%	11.75%	59.62%	0.54%	510	150	4.23%	8.26%	7	0.15%	50	11	0.32%	6.49%
% Diff	0.22	7.49	6.44	4.24	2.34	116.42	366.67	0.92	1.39	62.73	17.81	66.92	93.76	6.64	4.90

Nd= Not detected

N/A= Not available

Appendix D: Cont'd

XRF Standard's data	Ni ppm	Cu ppm	Zn ppm	Ga ppm	As ppm	Rb ppm	Sr ppm	Y ppm	Zr ppm	Nb ppm	Ba ppm	Ce ppm	Pb ppm	Th ppm	U ppm
Detection Limit	4	4	3	3	15	0.9	1.5	0.9	1.4	0.9	26	45	5	4	5
Measured SY-2	18	5	201	29	24	219.8	271.0	118.4	293.9	38.0	450	173	85	348	292
Standard SY-2	10	5	248	29	17	217.0	271.0	128.0	280.0	29.0	460	175	85	379	284
% Diff	82.43	1.04	19.08	0.77	40.39	1.27	0.01	7.47	4.96	24.18	2.25	1.04	0.42	8.06	2.67
Measured SY-2	18	8	198	30	23	220.2	271.4	117.9	295.8	35.5	453	182	87	349	291
Standard SY-2	10	5	248	29	17	217.0	271.0	128.0	280.0	29.0	460	175	85	379	284
% Diff	84.05	60.11	20.06	3.68	34.54	1.47	0.14	7.89	5.63	22.32	1.49	3.84	2.43	7.85	2.43
Measured SY-2	16	8	200	28	19	220.2	270.5	117.2	296.5	35.2	451	204	85	345	290
Standard SY-2	10	5	248	29	17	217.0	271.0	128.0	280.0	29.0	460	175	85	379	284
% Diff	57.93	23.91	19.55	5.07	11.12	1.46	0.19	8.47	5.90	21.29	2.05	16.70	0.45	8.94	2.24
Measured SY-2	16	7	199	32	32	219.9	271.2	118.5	297.8	35.1	447	176	87	345	287
Standard SY-2	10	5	248	29	17	217.0	271.0	128.0	280.0	29.0	460	175	85	379	284
% Diff	59.80	42.10	19.86	9.07	86.07	1.33	0.07	7.42	6.37	21.16	2.91	0.47	2.24	8.93	1.11
Measured SY-3	62	Nd	235	28	7	203.2	296.5	606.9	347.3	253.6	421	2228	140	927	745
Standard SY-3	11	17	244	27	19	206.0	302.0	718.0	320.0	148.0	450	2230	133	1003	650
% Diff	459.53	N/A	3.88	4.76	62.42	1.36	1.83	15.48	8.52	71.34	6.37	0.17	5.40	7.54	14.66
Measured SY-3	68	Nd	236	25	27	202.3	296.2	604.6	345.4	253.3	425	2241	140	919	746
Standard SY-3	11	17	244	27	19	206.0	302.0	718.0	320.0	148.0	450	2230	133	1003	650
% Diff	517.37	N/A	3.39	7.49	40.78	1.79	1.91	15.80	7.94	71.13	5.60	0.49	4.90	8.39	14.70
Measured SY-3	73	Nd	234	26	11	202.5	297.9	609.0	347.0	251.3	439	2239	140	921	740
Standard SY-3	11	17	244	27	19	206.0	302.0	718.0	320.0	148.0	450	2230	133	1003	650
% Diff	568.53	N/A	4.14	1.92	43.16	1.68	1.36	15.19	8.44	69.79	2.43	0.39	5.13	8.13	13.81
Measured SY-3	69	Nd	236	25	9	202.4	297.0	607.4	348.0	253.8	433	2214	138	920	745
Standard SY-3	11	17	244	27	19	206.0	302.0	718.0	320.0	148.0	450	2230	133	1003	650
% Diff	524.30	N/A	3.40	6.80	52.99	1.73	1.65	15.41	8.76	71.52	3.78	0.71	3.81	8.28	14.55

Nd= Not detected

N/A= Not available

APPENDIX E

DUPLICATE AND STANDARD ANALYSIS FOR ICP-MS DATA

Duplicate and standard analyses presented here contain the immobile trace elements that are used to classify many of the units within the field area. Several of these elements display irregularities as element concentrations approach the lower limit of detection. However, for the main elements utilized such as Zr in the polymict lapilli tuff, the elements concentrations are generally well-above the lower limit of detection.

Appendix E: Duplicate and standard analyses for ICP-MS data.

Precision		V	Cr	Co	Ni	Cu	Zn	Ga	Ge	As	Rb	Sr	Y	Zr	Nb	Mo
Detection Limit		5	20	1	20	10	30	1	1	5	2	2	1	5	1	2
1943099	GS-03-130D	7.00	Nd	Nd	Nd	Nd	Nd	4.80	Nd	Nd	92.48	18.31	1.61	14.04	Nd	Nd
1943099	Repeat	5.76	Nd	Nd	Nd	11.77	Nd	4.69	Nd	Nd	92.84	17.91	1.59	7.15	Nd	Nd
% Difference A		21.53	N/A	N/A	N/A	N/A	N/A	2.26	N/A	N/A	0.40	2.21	1.58	96.32	N/A	N/A
1943097	GS-03-130B	24.14	Nd	Nd	Nd	Nd	Nd	9.53	Nd	Nd	98.08	47.64	29.35	154.27	8.43	Nd
1943106	Duplicate	19.80	Nd	1.07	Nd	Nd	Nd	9.65	Nd	Nd	93.86	45.89	27.94	156.48	7.64	Nd
% Difference B		21.88	N/A	N/A	N/A	N/A	N/A	1.29	N/A	N/A	4.50	3.81	5.04	1.41	10.32	N/A
1943101	GS-03-130E	7.85	Nd	Nd	Nd	Nd	Nd	2.45	Nd	Nd	19.37	5.93	1.33	5.25	Nd	Nd
1943107	Repeat	8.40	Nd	Nd	Nd	Nd	Nd	2.51	Nd	Nd	18.95	5.90	1.36	9.98	Nd	Nd
% Difference C		6.47	N/A	N/A	N/A	N/A	N/A	2.45	N/A	N/A	2.21	0.51	2.23	47.41	N/A	N/A

		Ag	In	Sn	Sb	Cs	Ba	La	Ce	Pr	Nd	Sm	Eu	Gd	Tb
Detection Limit		0.5	0.2	1	0.5	0.5	3	0.1	0.1	0.005	0.1	0.1	0.005	0.1	0.1
1943099	GS-03-130D	2.54	Nd	Nd	3.11	0.53	810.87	0.96	2.13	0.24	1.07	0.27	0.06	0.29	Nd
1943099	Repeat	2.58	Nd	Nd	3.76	0.57	806.65	0.93	2.09	0.25	1.06	0.28	0.05	0.32	Nd
% Difference A		1.51	N/A	N/A	17.13	5.61	0.52	3.30	1.76	4.02	0.87	1.69	16.34	10.45	N/A
1943097	GS-03-130B	2.14	Nd	1.46	1.06	0.77	936.44	14.07	36.68	4.45	18.13	4.41	0.77	4.24	0.82
1943106	Duplicate	4.48	Nd	1.26	1.02	0.64	893.53	15.30	39.49	4.66	19.30	4.68	0.75	4.45	0.81
% Difference B		52.23	N/A	15.79	3.12	8.36	4.80	8.07	7.11	4.53	6.09	5.71	2.59	4.73	1.46
1943101	GS-03-130E	1.63	Nd	Nd	8.69	0.79	115.90	1.57	3.38	0.44	1.91	0.35	-0.05	0.32	Nd
1943107	Repeat	2.81	Nd	Nd	10.70	0.77	119.55	1.60	3.40	0.44	1.84	0.35	-0.05	0.30	Nd
% Difference C		42.15	N/A	N/A	18.86	2.76	3.05	2.32	0.54	0.24	3.62	1.54	0.00	5.36	N/A

		Dy	Ho	Er	Tm	Yb	Lu	Hf	Ta	W	Tl	Pb	Bi	Th	U
Detection Limit		0.1	0.1	0.1	0.05	0.1	0.04	0.2	0.1	1	0.1	5	0.4	0.1	0.1
1943099	GS-03-130D	0.27	Nd	0.13	Nd	Nd	Nd	0.32	Nd	Nd	1.09	Nd	Nd	Nd	Nd
1943099	Repeat	0.26	Nd	0.13	Nd	Nd	Nd	Nd	Nd	Nd	1.25	Nd	Nd	Nd	Nd
% Difference A		1.29	N/A	4.68	N/A	N/A	N/A	N/A	N/A	N/A	13.06	N/A	N/A	N/A	N/A
1943097	GS-03-130B	4.80	1.01	3.37	0.50	3.18	0.52	4.47	0.61	Nd	1.20	Nd	Nd	4.25	1.35
1943106	Duplicate	4.71	0.99	3.14	0.48	3.05	0.50	4.44	0.57	Nd	1.11	Nd	Nd	4.20	1.31
% Difference B		1.83	1.41	7.08	4.93	3.72	4.07	0.63	8.50	N/A	7.87	N/A	N/A	1.29	3.37
1943101	GS-03-130E	0.25	Nd	0.13	Nd	Nd	Nd	Nd	Nd	Nd	0.18	Nd	Nd	Nd	Nd
1943107	Repeat	0.26	Nd	0.12	Nd	Nd	Nd	Nd	Nd	Nd	0.21	Nd	Nd	Nd	Nd
% Difference C		4.48	N/A	2.63	N/A	N/A	N/A	N/A	N/A	N/A	13.91	N/A	N/A	N/A	N/A

Nd= Not detected

N/A= Not available

Appendix E: Cont'd

Accuracy	V	Cr	Co	Ni	Cu	Zn	Ga	Ge	As	Rb	Sr	Y	Zr	Nb	Mo
Detection Limit	5	20	1	20	10	30	1	1	5	2	2	1	5	1	2
Measured WGB-1	219.15	273.99	24.00	77.14	104.07	Nd	12.03	2.13	Nd	18.57	113.15	15.15	56.70	5.09	Nd
Standard WGB-1	222.00	291.00	29.80	76.00	106.00	31.50	N/A	N/A	N/A	19.50	118.00	14.60	44.00	8.00	1.20
% Difference A	1.29	5.84	19.47	1.50	1.82	N/A	N/A	N/A	N/A	4.78	4.11	3.78	28.86	36.37	N/A

	Ag	In	Sn	Sb	Cs	Ba	La	Ce	Pr	Nd	Sm	Eu	Gd	Tb
Detection Limit	0.5	0.2	1	0.5	0.5	3	0.1	0.1	0.005	0.1	0.1	0.005	0.1	0.1
Measured WGB-1	2.38	Nd	4.44	1.22	Nd	822.62	7.67	16.03	2.12	9.62	2.70	1.24	2.82	0.49
Standard WGB-1	N/A	N/A	N/A	N/A	0.52	851.00	8.70	N/A	N/A	9.90	2.80	1.27	N/A	0.50
% Difference A	N/A	N/A	N/A	N/A	N/A	3.33	11.86	N/A	N/A	2.82	3.72	2.11	N/A	2.09

	Dy	Ho	Er	Tm	Yb	Lu	Hf	Ta	W	Ti	Pb	Bi	Th	U
Detection Limit	0.1	0.1	0.1	0.05	0.1	0.04	0.2	0.1	1	0.1	5	0.4	0.1	0.1
Measured WGB-1	2.73	0.55	1.55	0.22	1.41	0.21	1.48	0.35	Nd	0.49	Nd	Nd	0.95	0.67
Standard WGB-1	N/A	0.52	N/A	N/A	1.42	N/A	1.50	N/A	N/A	N/A	N/A	N/A	1.00	0.75
% Difference A	N/A	5.18	N/A	N/A	0.74	N/A	1.05	N/A	N/A	N/A	N/A	N/A	5.15	10.65

Nd= Not detected
N/A= Not available

311

APPENDIX F

The following table contains a list of mineralized samples referred to in the text. The majority of these samples are from the unpublished data of S. O'Brien, Newfoundland Geological Survey.
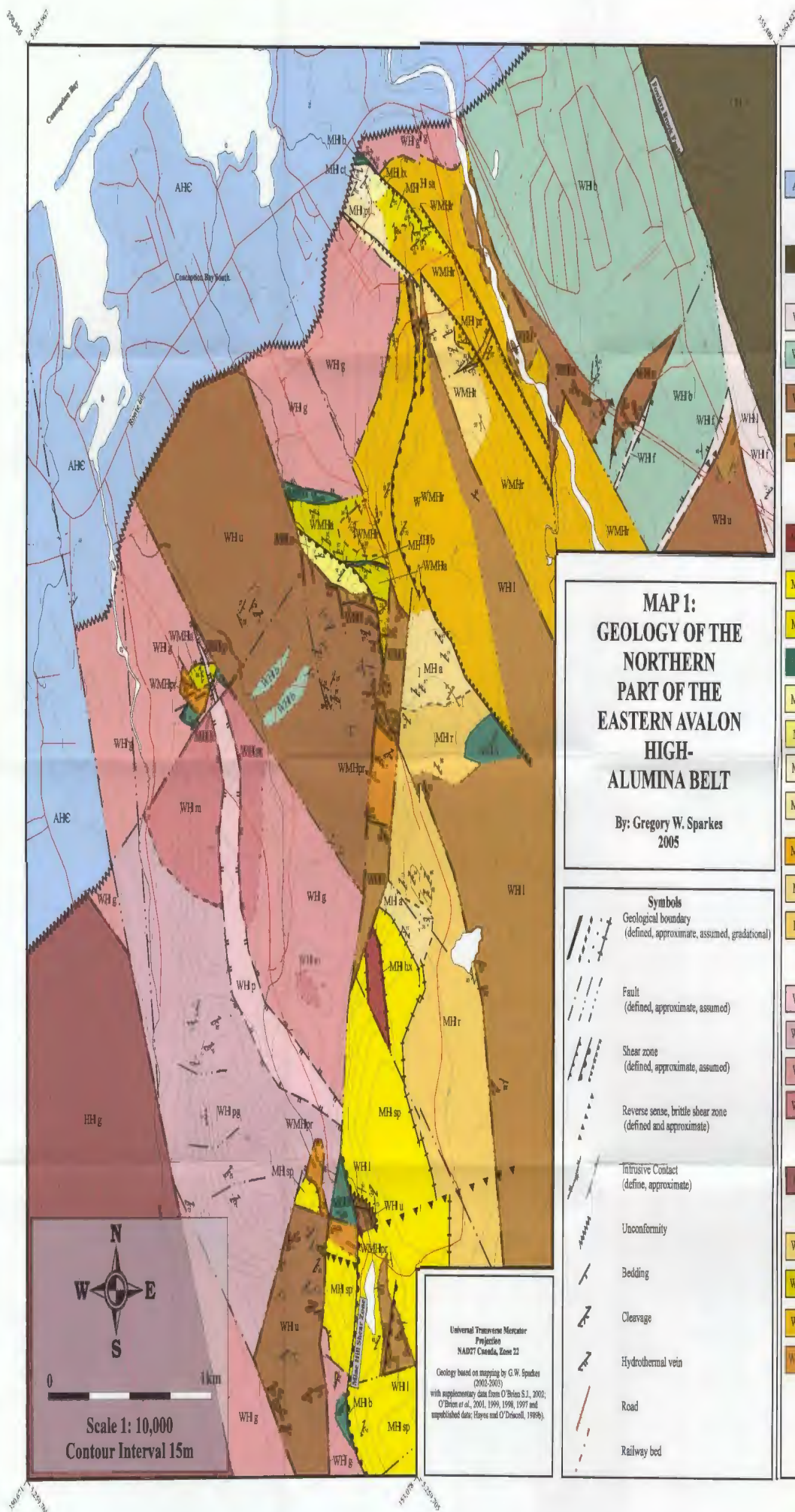
.

Appendix F: List of mineralized samples mentioned in text.

UTM E	UTM N	Field Number	YEAR	LAB	AU PPB	AG	AS	BA	CA %	CD	CO	CR	FE %	HG
352848	5263101	OB-97-233	1997	BECQ	12	Nd	6.4	470	Nd		Nd	Nd	0.74	Nd
352754	5262934	OB-97-433	1997	BECQ	21	Nd	32	990	Nd		2	Nd	1.67	Nd
352988	5264573	GS-02-51	2002	Eastern Anal.	27	0.2	5	63	0.16	0.5	1	390	0.62	1
353192	5264207	GS-03-01	2003	Eastern Anal.	74	N/A	N/A	N/A	N/A	N/A	N/A	N/A	N/A	N/A
352974	5262823	OB-03-011	2003	Eastern Anal.	398	9.6	5	36	0.01	0.5	1	146	0.61	1
352974	5262823	OB-03-012	2003	Eastern Anal.	640	12	5	101	0.01	0.5	1	224	0.86	1
353115	5262098	OB-03-016	2003	Eastern Anal.	46	0.2	5	41	0.04	0.5	1	231	0.90	1
352805	5260896	OB-03-024	2003	Eastern Anal.	65	0.2	5	226	0.01	1.2	1	135	0.55	1
352787	5260900	OB-03-025	2003	Eastern Anal.	112	0.2	8	186	0.01	0.5	1	87	0.92	1
352787	5260900	OB-03-026	2003	Eastern Anal.	122	0.2	5	86	0.01	0.5	1	57	0.72	1

UTM E	UTM N	Field Number	YEAR	LAB	MO	NA %	NI	RB	SB	SR %	W	ZN	LA	CE
352848	5263101	OB-97-233	1997	BECQ	9	0.03	Nd	75	0.7	Nd	Nd	Nd	17	34
352754	5262934	OB-97-433	1997	BECQ	4	0.31	Nd	190	10	Nd	7	52	21	40
352988	5264573	GS-02-51	2002	Eastern Anal.	22	0.22	6	N/A	5	0.2	10	23	10	29
353192	5264207	GS-03-01	2003	Eastern Anal.	N/A	N/A	N/A	N/A	N/A	N/A	N/A	N/A	N/A	N/A
352974	5262823	OB-03-011	2003	Eastern Anal.	11	0.08	9	20	5	0	10	6	10	49
352974	5262823	OB-03-012	2003	Eastern Anal.	14	0.12	6	20	5	0	10	3	10	28
353115	5262098	OB-03-016	2003	Eastern Anal.	15	0.18	9	20	5	0	10	11	11	19
352805	5260896	OB-03-024	2003	Eastern Anal.	8	0.18	1	20	5	0	14	6	19	35
352787	5260900	OB-03-025	2003	Eastern Anal.	19	0.13	2	20	5	0	21	4	10	10
352787	5260900	OB-03-026	2003	Eastern Anal.	15	0.1	2	20	5	0	10	5	10	10

UTM E	UTM N	Field Number	YEAR	LAB	P	Mg	V	Al %	Be	Cu	Pb	Bi	TI %	K %	Mn
352848	5263101	OB-97-233	1997	BECQ	N/A	N/A	N/A	N/A	N/A	N/A	N/A	N/A	N/A	N/A	N/A
352754	5262934	OB-97-433	1997	BECQ	N/A	N/A	N/A	N/A	N/A	N/A	N/A	N/A	N/A	N/A	N/A
352988	5264573	GS-02-51	2002	Eastern Anal.	0.01	0.07	3	0.36	0.5	8	7	2	0.01	0.17	188
353192	5264207	GS-03-01	2003	Eastern Anal.	N/A	N/A	N/A	N/A	N/A	N/A	N/A	N/A	N/A	N/A	N/A
352974	5262823	OB-03-011	2003	Eastern Anal.	0.01	0.05	4	0.2	0.5	5	2	2	0.01	0.09	60
352974	5262823	OB-03-012	2003	Eastern Anal.	0.01	0.01	2	0.16	0.5	8	2	2	0.01	0.12	14
353115	5262098	OB-03-016	2003	Eastern Anal.	0.01	0.06	5	0.3	1.5	2	3	2	0.03	0.16	114
352805	5260896	OB-03-024	2003	Eastern Anal.	0.01	0.01	1	0.53	0.5	2	11	4	0.01	0.21	27
352787	5260900	OB-03-025	2003	Eastern Anal.	0.01	0.01	2	0.18	0.5	3	8	10	0.01	0.04	5
352787	5260900	OB-03-026	2003	Eastern Anal.	0.01	0.01	1	0.16	0.5	2	2	2	0.01	0.04	5

Nd= Not detected
N/A= Not available

MAP 1:
GEOLOGY OF THE NORTHERN PART OF THE EASTERN AVALON HIGH-ALUMINA BELT

By: Gregory W. Sparkes
2005

Legend

Scale 1: 10,000
Contour Interval 15m

0   1km

Cambrian
(24) ADEYTON AND HARCOURT GROUPS (undivided) — AHЄ
- red and black siltstone with interbedded grey limestone; locally massive, poorly sorted boulder conglomerate at base

Late Neoproterozoic
(23) CONCEPTION GROUP
- unseparated marine siliciclastic sedimentary rocks

WYCH HAZEL POND COMPLEX
(22) Fowlers Road Porphyry — WHf
- plagioclase-phyric, pale grey to green aphanitic rhyolite; unit associated with local development of a blocky peperite

(21) Amygdaloidal Basalt/Hyaloclastite — WHb
- moderately vesicular, locally amygdaloidal and pillowed dark purple basalt; associated with hyaloclastite containing irregularly shaped, dark purple basalt fragments in a dark grey-green, fine-grained matrix

(19b) Upper Wych Hazel Pond Complex — WHu
- thin- to medium-parallel-bedded, moderately to strongly siliceous, pale to dark green siltstone and interbedded medium- to coarse-grained subarkosic sandstone, siltstone commonly displays soft sediment deformation

(19a) Lower Wych Hazel Pond Complex — WHl
- thin- to medium-bedded red siltstone; locally interbedded with medium- to coarse-grained red sandstone, pebbly conglomerate and pale yellow, chloritic-sericitic, massive pumiceous tuff

MANUELS VOLCANIC SUITE
(18) Hematite-Chlorite-rich Hydrothermal Breccia — MHhc
- matrix supported, hematite-chlorite-rich breccia containing sub-rounded to subangular fragments of silicified rhyolite within a dark purple to green matrix; fragments generally 2-4cm in diameter

(17) Silica-Sericite-Pyrite-Pyrophyllite- Diaspore-Rutile Alteration — MHsp
- pale white- to yellow-weathering alteration with varying proportions of silica-sericite-pyrite-pyrophyllite-diaspore-rutile

(16) Sericite-Silica ± Pyrite Alteration — MHsa
- white- to pale yellow-weathering alteration with patchy pyrite development; alteration associated with prominent shear zones

(15) Mafic Volcanic/Intrusive Rocks
- fine-grained, dark brown- to dark green-weathering, moderate to weakly magnetic, locally amygdaloidal and plagioclase-phyric basalt

(14) Massive, Poorly-Sorted, Lithic-rich, Breccia — MHlx
- matrix supported breccia containing sub-rounded to angular fragments of low-sulphidation vein material in a poorly sorted hematite-rich matrix

Silica Alteration — MHs
- pale white, pervasive silica alteration without pyrophyllite-diaspore-sericite (Bergs area)

(13) Dark Purple, Crystal-bearing, Ash-flow Tuff — MHct
- massive crystal-rich tuff, containing pale white mm-scale crystals within a dark purple, hematite-rich groundmass

(12) Grey-Green, Pyritic, Pumiceous, Crystal-bearing Ash-flow Tuff — MHpt
- massive crystal-rich tuff, containing mm-scale white crystals, and cm-scale dark purple collapsed pumice fragments, in a dark green to grey groundmass; groundmass also contains minor fine-grained disseminated pyrite

(11) Pale Grey-Green, Moderately Porphyritic, Fine, Rhyolite — MHpr
- light grey- to green-weathering rhyolite; mm-scale white feldspar crystals and fine-grained disseminated pyrite in a fine-grained groundmass

(10) Aphanitic, Massive Rhyolite/Polymict Lithic Volcaniclastic Rock — MHa
- dark purple-weathering, massive volcaniclastic containing subangular to sub-rounded fragments; fragments predominantly 5-10cm in diameter but locally up to 50cm

(9) Aphanitic Flow-Banded Rhyolite (Farmer's Field Rhyolite) — MHr
- dark purple, pale white-weathering aphanitic rhyolite with local development of lithophysae

WHITE HILLS INTRUSIVE SUITE
(8) Quartz-Feldspar Porphyry — WHp
- pale purple-weathering porphyry containing 2-4mm phenocrysts of plagioclase, quartz and K-feldspar within a light purple aphanitic groundmass

Quartz-Feldspar Porphyry/Medium- to Coarse-grained Equigranular Granite — WHpg
- unseparated quartz-feldspar porphyry/medium- to coarse-grained equigranular granite

(7) Medium- to Coarse-grained Equigranular Granite — WHg
- silica-sericite-chlorite-pyrite altered, grey-green- to pale pink-weathering, medium- to coarse-grained, equigranular, quartz-K-feldspar-plagioclase-bearing granite

(6) Monzonite — WHm
- pale white-weathering monzonite with coarse-grained, pale green plagioclase and fine- to medium-grained chlorite, quartz and K-feldspar; locally contains 2-10cm diameter fine-grained dioritic xenoliths

HOLYROOD INTRUSIVE SUITE
(5) Pink-White-Green Granite — HHg
- propylitized granite with a pale pink-white-green-weathering, generally equigranular to quartz-phyric, with sub-equal amounts of plagioclase, K-feldspar and quartz

WHITE MOUNTAIN VOLCANIC SUITE
(4) Welded, Fiamme-Bearing Ash-flow Tuff — WMHt
- dark purple, pale white-weathering tuff containing cm-scale, pale purple collapsed pumice within a pale white groundmass; unit displays well-developed eutaxitic foliation

(3) Massive, Lithic-rich, Polymict, Lapilli Tuff — WMHa
- dark to pale green or pale pink, matrix supported tuff with sub-rounded to rounded fragments; fragments locally dominated by bright pink, potassic altered material

(2) Aphanitic, Flow-Banded Rhyolite (Manuels River Rhyolite) — WMHr
- purple to grey-green rhyolite with well developed flow banding and rare feldspar-phyric zones; unit is locally spherulitic

(1) Moderately, Feldspar-phyric, Flow-Banded Rhyolite (Minerals Road Rhyolite) — WMHpr
- pale pink to dark purple rhyolite with 2-4mm feldspar crystals within a dark purple, flow handed groundmass; groundmass is locally spherulitic

*Note: Numbers preceding unit names refer to unit numbers as presented in the text. The numbering represents a best approximation of stratigraphic order.

Symbols

Geological boundary
(defined, approximate, assumed, gradational)

Fault
(defined, approximate, assumed)

Shear zone
(defined, approximate, assumed)

Reverse sense, brittle shear zone
(defined and approximate)

Intrusive Contact
(define, approximate)

Unconformity

Bedding

Cleavage

Hydrothermal vein

Road

Railway bed

N W S E